PHAGE BIOLOGY AND PHAGE THERAPY

EDITED BY: Shuai Le, Xuesong He and Yigang Tong
PUBLISHED IN: Frontiers in Microbiology

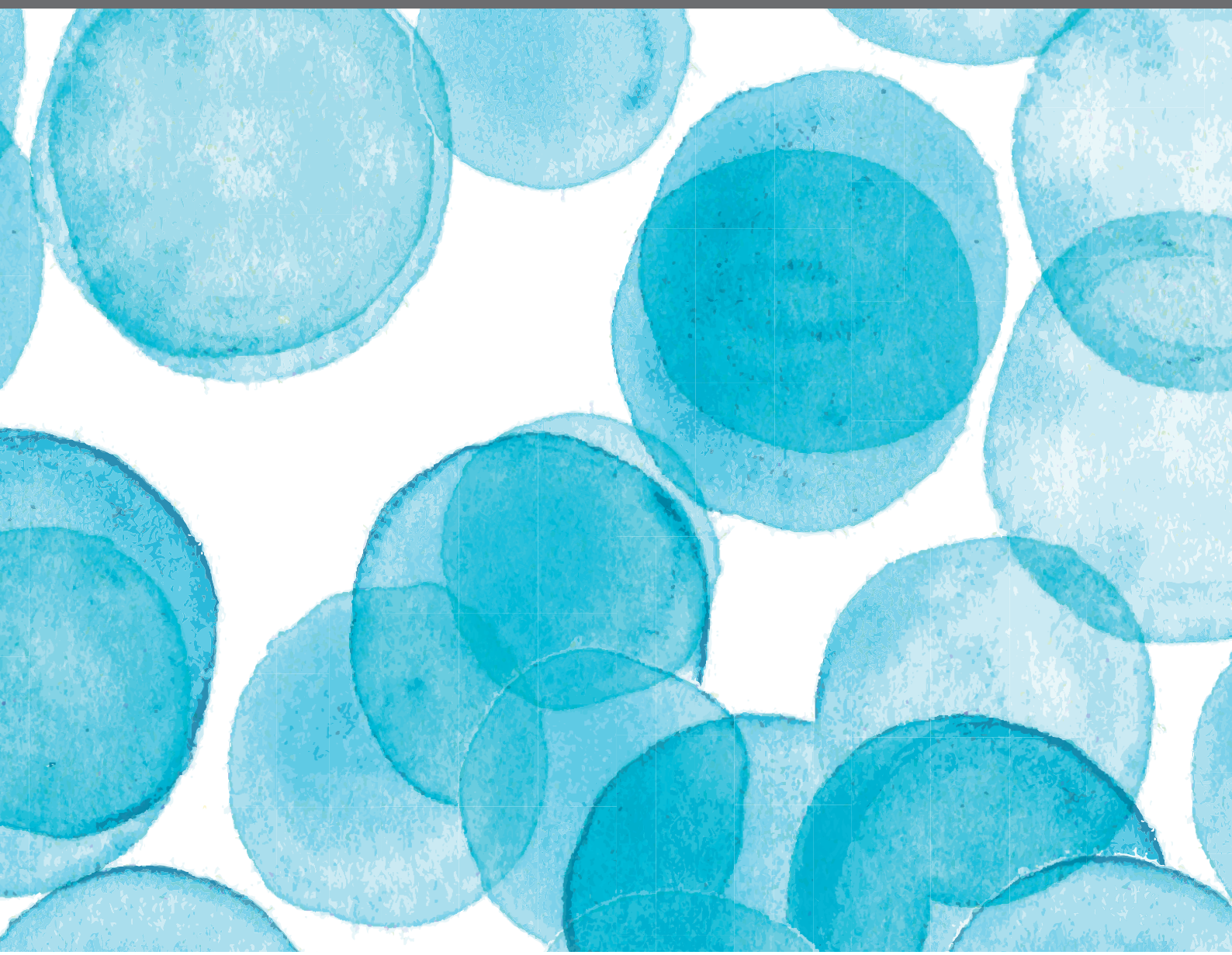

frontiers Research Topics

Frontiers eBook Copyright Statement

The copyright in the text of individual articles in this eBook is the property of their respective authors or their respective institutions or funders. The copyright in graphics and images within each article may be subject to copyright of other parties. In both cases this is subject to a license granted to Frontiers.

The compilation of articles constituting this eBook is the property of Frontiers.

Each article within this eBook, and the eBook itself, are published under the most recent version of the Creative Commons CC-BY licence. The version current at the date of publication of this eBook is CC-BY 4.0. If the CC-BY licence is updated, the licence granted by Frontiers is automatically updated to the new version.

When exercising any right under the CC-BY licence, Frontiers must be attributed as the original publisher of the article or eBook, as applicable.

Authors have the responsibility of ensuring that any graphics or other materials which are the property of others may be included in the CC-BY licence, but this should be checked before relying on the CC-BY licence to reproduce those materials. Any copyright notices relating to those materials must be complied with.

Copyright and source acknowledgement notices may not be removed and must be displayed in any copy, derivative work or partial copy which includes the elements in question.

All copyright, and all rights therein, are protected by national and international copyright laws. The above represents a summary only. For further information please read Frontiers' Conditions for Website Use and Copyright Statement, and the applicable CC-BY licence.

ISSN 1664-8714
ISBN 978-2-88976-143-2
DOI 10.3389/978-2-88976-143-2

About Frontiers

Frontiers is more than just an open-access publisher of scholarly articles: it is a pioneering approach to the world of academia, radically improving the way scholarly research is managed. The grand vision of Frontiers is a world where all people have an equal opportunity to seek, share and generate knowledge. Frontiers provides immediate and permanent online open access to all its publications, but this alone is not enough to realize our grand goals.

Frontiers Journal Series

The Frontiers Journal Series is a multi-tier and interdisciplinary set of open-access, online journals, promising a paradigm shift from the current review, selection and dissemination processes in academic publishing. All Frontiers journals are driven by researchers for researchers; therefore, they constitute a service to the scholarly community. At the same time, the Frontiers Journal Series operates on a revolutionary invention, the tiered publishing system, initially addressing specific communities of scholars, and gradually climbing up to broader public understanding, thus serving the interests of the lay society, too.

Dedication to Quality

Each Frontiers article is a landmark of the highest quality, thanks to genuinely collaborative interactions between authors and review editors, who include some of the world's best academicians. Research must be certified by peers before entering a stream of knowledge that may eventually reach the public - and shape society; therefore, Frontiers only applies the most rigorous and unbiased reviews.
Frontiers revolutionizes research publishing by freely delivering the most outstanding research, evaluated with no bias from both the academic and social point of view. By applying the most advanced information technologies, Frontiers is catapulting scholarly publishing into a new generation.

What are Frontiers Research Topics?

Frontiers Research Topics are very popular trademarks of the Frontiers Journals Series: they are collections of at least ten articles, all centered on a particular subject. With their unique mix of varied contributions from Original Research to Review Articles, Frontiers Research Topics unify the most influential researchers, the latest key findings and historical advances in a hot research area! Find out more on how to host your own Frontiers Research Topic or contribute to one as an author by contacting the Frontiers Editorial Office: frontiersin.org/about/contact

PHAGE BIOLOGY AND PHAGE THERAPY

Topic Editors:
Shuai Le, Army Medical University, China
Xuesong He, The Forsyth Institute, United States
Yigang Tong, Beijing University of Chemical Technology, China

Citation: Le, S., He, X., Tong, Y., eds. (2022). Phage Biology and Phage Therapy. Lausanne: Frontiers Media SA. doi: 10.3389/978-2-88976-143-2

Table of Contents

frontiers | Frontiers in Microbiology

EDITORIAL
published: 22 April 2022
doi: 10.3389/fmicb.2022.891848

Editorial: Phage Biology and Phage Therapy

Shuai Le[1], *Xuesong He*[2,3]* *and Yigang Tong*[4]*

[1] Department of Microbiology, Army Medical University, Chongqing, China, [2] The Forsyth Institute, Cambridge, MA, United States, [3] Department of Oral Medicine, Infection and Immunity, Harvard School of Dental Medicine, Boston, MA, United States, [4] College of Life Science and Technology, Beijing University of Chemical Technology, Beijing, China

Keywords: phage biology, phage therapy, phage resistance, animal models, nosocomial infection management

Editorial on the Research Topic

Phage Biology and Phage Therapy

Phage therapy is a promising approach for treating antibiotic resistant bacterial infections. As there is no remedy for everything, several limitations also restrict its large scale application, which include the specificity of phage host range, the resistance of the bacteria, and the manufacturing procedures of phage products. Thus, the continuous and collaborating efforts in phage biology are crucial in providing insights in designing improved phage therapy strategies.

In this Research Topic on *Phage Biology and Phage Therapy*, we selected 12 articles covering a wide range of topics, including phage isolation, phage resistance, animal models for evaluating the efficacy of phage therapy, as well as novel phage gene annotations through structural techniques.

Wu and Zhu reviewed the therapeutic bacteriophages in nosocomial infection management. To treat antibiotic resistant bacteria, the first step is to build an efficient and safe phage library. The key features of these phages, including complete genome sequence, host range and strict lytic activity, should be characterized. Though phages are abundant in nature, isolation of suitable phages for a specific pathogenic bacterial strain can be challenging, and is still an obstacle for building a high-quality phage library. A high-throughput study of the host specificity and phage engineering through synthetic biology is a promising approach to overcome these obstacles. The authors of this article provide a detailed discussion of the pros and cons of the two main methods in phage therapy, choosing a fixed composition (prêt-à-porter) or customized screened phage (sur-mesure). Finally, they summarize phage disinfection for nosocomial transmission control and provide a detailed workflow, which is currently applied at the Shanghai Public Health Clinical Center, China.

Animal model evaluation is essential for phage therapy before commencing human clinical trials. Penziner et al. report a detailed review of the animal models of phage therapy, that includes the selection of bacteria and phages, constructing the infection model and administering phage therapy, evaluation on the efficacy of phage therapy in diverse infection models, monitoring the phage pharmacokinetics and toxicity and immune response during phage therapy. They point out that, though animal studies could be used to monitor the efficacy and safety of phage therapy, there is still much to learn about standardization of the regimens, development of models that mimic the time course of infection, as well as the optimization of pharmacokinetic modeling. In a research article, Shi et al. evaluate the safety and efficacy of phage kpssk3 in treating *Klebsiella pneumoniae* bacteremia. Intraperitoneal injection with a single dose of phage (1×10^7 PFU/mouse) 3 h post infection rescues the mice from *Klebsiella pneumoniae* bacteremia without affecting the gut microbiome as revealed by high-throughput 16S rDNA sequence analysis of the stool samples, before and after phage therapy. Thus, this study provides direct evidence showing the minimal impact of phage therapy on the host's native microbiome, another advantage of phage therapy compared with conventional antibiotic-based treatment. Moreover, Wang, Cai et al. reported the

OPEN ACCESS

Edited and reviewed by:
Anna Kramvis,
University of the Witwatersrand, South Africa

***Correspondence:**
Xuesong He
xhe@forsyth.org
Yigang Tong
Tong.yigang@gmail.com

Specialty section:
This article was submitted to Virology, a section of the journal Frontiers in Microbiology

Received: *08 March 2022*
Accepted: *30 March 2022*
Published: *22 April 2022*

Citation:
Le S, He X and Tong Y (2022) Editorial: Phage Biology and Phage Therapy. Front. Microbiol. 13:891848. doi: 10.3389/fmicb.2022.891848

synergism of phage vB_KpnM_P-KP2 and gentamicin in combating acute pneumonia caused by *Klebsiella pneumoniae*. The phage-antibiotic combination treatment showed the best therapeutic efficiency than using single phage or antibiotics.

Bacteriophage resistance is a key factor that restricts bacteriophage therapy, and many phage-resistant mutants selected *in vitro* carry mutations in the phage receptor genes. Wei's group (Zhang X. et al.) reports the presence of the genetic polymorphism of minor alleles in the genomes of both *Staphylococcus aureus* AB91118 and its lytic phage, which may present a new mechanism to drive the co-evolution between host and phage. The authors establish a new method to identify the minor alleles in the genomes of bacteria and phages. Combined with other bioinformatics such as KEGG, they show that the minor alleles are mainly related to metabolic pathways, which could be inhibited by chloramphenicol (CHL). Interestingly, the phage-resistant bacteria could become sensitive to the phage again in the presence of CHL. They also demonstrate that the combined use of CHL and the evolved phage from 20 cycles in treating *S. aureus* AB91118 results in effective killing with the least bacterial resistance. This work provides a new mechanism that may explain the fast response to the selective pressure between host and phage. It also emphasizes the importance of identifying supplementary agents which could improve the outcome of phage therapy by reducing resistance.

Focusing on phage gene annotations, Liu's group described two interesting works. For *Escherichia coli* (*E. coli*) phage T4, arguably the most-studied model phage, Zhang K. et al. present their systemic studies on selected T4 gene products with only limited information or poorly characterized in the past. Combining the three major structural techniques: X-ray crystallography, NMR and Cryo-EM, the group performs initial analysis on some of the T4's overlooked proteins, including host RNA polymerase modifier (RpbA), Lon protease inhibitor (Pin) and host DNA exonuclease (ExoD). The Research Topic of data paves the way for the structural characterization of these interesting viral proteins, which have important roles in interplaying with *E. coli*. In a separate article, using the method developed in the aforementioned study, Liu's group report their finding on a specific gene product, Gp44 encoded by *Bacilis subitilis* phage SPO1 (Wang, Wang et al.). Gp44 is described as a non-specific bacterial RNA polymerase inhibitor for both *B. subtilis* and *E. coli*. Using NMR, bioinformation and other biochemical tools, the group reveal that Gp44 has a very unique structural arrangement: an N-terminal DNA binding motif, a middle single-strand DNA mimic region and a random-coiled C terminus. The model they propose could well explain the non-specificity of Gp44 in inhibiting both *E. coli and B. subtilis*. This rare and non-specific strategy employed by the phage protein sheds light on the development of broad range inhibitors targeting bacterial RNA polymerases for clinical applications.

The collection also includes papers reporting diverse phages from different environments and their ecological impact, including *Shigella* phages (Shahin et al.), *Enterococcus faecalis* phage EFA1 (Kabwe et al.), *Microcystis* phage PhiMa05 (Naknaen et al.) and *Escherichia coli* phage swi2 (Sui et al.). Moreover, Choua et al. presented an interesting mathematical model to reveal that viral plasticity and evolution influence the classic host quality-quantity trade-off, which could advance our understanding of the microbial response to changing environments.

Bacteria and phages are the most abundant biological entities. The significance of bacteria- phage interaction and its impact bacterial physiology as well as the application of phage therapy in targeting specific pathogen are yet to be fully appreciated. A comprehensive understanding of bacterial-phage interaction built upon basic research of phage biology, including the studied covered in this collection, is crucial in providing valuable insights into the translational potential and value of phage therapy.

AUTHOR CONTRIBUTIONS

All authors listed have made a substantial, direct, and intellectual contribution to the work and approved it for publication.

FUNDING

This research was supported by National Natural Science Foundation of China (NSFC, 31870167 to SL)

Conflict of Interest: The authors declare that the research was conducted in the absence of any commercial or financial relationships that could be construed as a potential conflict of interest.

Publisher's Note: All claims expressed in this article are solely those of the authors and do not necessarily represent those of their affiliated organizations, or those of the publisher, the editors and the reviewers. Any product that may be evaluated in this article, or claim that may be made by its manufacturer, is not guaranteed or endorsed by the publisher.

Copyright © 2022 Le, He and Tong. This is an open-access article distributed under the terms of the Creative Commons Attribution License (CC BY). The use, distribution or reproduction in other forums is permitted, provided the original author(s) and the copyright owner(s) are credited and that the original publication in this journal is cited, in accordance with accepted academic practice. No use, distribution or reproduction is permitted which does not comply with these terms.

frontiers in Microbiology

REVIEW
published: 28 January 2021
doi: 10.3389/fmicb.2021.631794

Animal Models of Phage Therapy

Samuel Penziner[1], Robert T. Schooley[1] and David T. Pride[1,2]*

[1] Department of Medicine, University of California, San Diego, San Diego, CA, United States, [2] Department of Pathology, University of California, San Diego, San Diego, CA, United States

Amidst the rising tide of antibiotic resistance, phage therapy holds promise as an alternative to antibiotics. Most well-designed studies on phage therapy exist in animal models. In order to progress to human clinical trials, it is important to understand what these models have accomplished and determine how to improve upon them. Here we provide a review of the animal models of phage therapy in Western literature and outline what can be learned from them in order to bring phage therapy closer to becoming a feasible alternative to antibiotics in clinical practice.

Keywords: phage therapy, phage, bacteriophage, animal models, bacterial infections

INTRODUCTION

The discovery of bacteriophages, viruses that infect bacteria, can be traced to the early 1900's when Frederick Twort and Félix d'Hérelle each observed unexplained clearings on agar plates of bacteria. Both men found that the clearings were transmissible, but it was d'Hérelle who postulated that they were caused by viruses and coined the term "bacteriophages," meaning "eaters of bacteria" (Chanishvili, 2012). D'Hérelle also saw the potential of bacteriophages (or "phages") as therapy against bacterial diseases. In 1919 he used them to cure a 12-year-old boy of Shigella dysentery, and eventually phage therapy was adopted around the world for the treatment of skin infections, diarrheal illnesses, and even the bubonic plague (Stone, 2002; Chanishvili, 2012; Myelnikov, 2018). However, following the development of antibiotics and concerns about inconsistent results, phage therapy waned in Western medicine in the 1940's (Eaton and Bayne-Jones, 1934; Chanishvili, 2012; Myelnikov, 2018). Countries in Eastern Europe continued to implement phage therapy in medical practice, though these studies were not conducted in such a way that would meet Western regulatory or pharmaceutical approval (Merril et al., 2003).

Antibiotics have served as the bedrock for the treatment of bacterial diseases and yet, due to the growing crisis of antibiotic resistance, routine infections are becoming difficult to treat (Lesho and Laguio-Vila, 2019). According to some estimates, by 2050 ten million people a year will die from multidrug resistant (MDR) bacterial infections (World Bank Group, 2017). Despite the critical need for new antibiotics, the antibiotic pipeline is not expected to keep pace with the rate of resistance (Årdal et al., 2020). This has led to a renewed interest in phage therapy. Phage therapy offers unique advantages over antibiotics such as the narrow specificity of each individual bacteriophage (allowing for preservation of the body's endogenous bacterial flora), ability to increase in number after administration (by replicating within the bacterial host), and capability to penetrate biofilms (Viertel et al., 2014; Rehman et al., 2019).

At present, phage therapy in humans has consisted of compassionate use cases (Schooley et al., 2017; Chan et al., 2018; Law et al., 2019; McCallin et al., 2019) and a few clinical trials hampered by small sample sizes or methodological issues (Wright et al., 2009; Sarker et al., 2016; Jault et al., 2019). The bulk of data on phage therapy lies in animal studies (**Table 1**). While these studies cannot replace human trials, they can impart valuable information about working with different

OPEN ACCESS

Edited by:
Shuai Le,
Army Medical University, China

Reviewed by:
William Calero-Cáceres,
Technical University of Ambato, Ecuador
Demeng Tan,
Fudan University, China

****Correspondence:***
Samuel Penziner
spenziner@health.ucsd.edu

Specialty section:
This article was submitted to Virology, a section of the journal Frontiers in Microbiology

Received: *20 November 2020*
Accepted: *11 January 2021*
Published: *28 January 2021*

Citation:
Penziner S, Schooley RT and Pride DT (2021) Animal Models of Phage Therapy. Front. Microbiol. 12:631794. doi: 10.3389/fmicb.2021.631794

infection models, bacterial species, phages, dosing strategies, and endpoints. They also provide data on the pharmacokinetics (absorption, metabolism, distribution, and elimination throughout the body), immunogenicity (interaction with the immune system), and safety of bacteriophages *in vivo*. This review describes how animal models of phage therapy have been constructed and what can be learned from their results in order to guide further work in the field.

BACTERIA AND PHAGES EMPLOYED IN ANIMAL MODELS

Since phages amount to the most abundant biological entity on earth with a population estimated at >10^30 (Hendrix, 2002), they infect many species of bacteria and can be studied in a variety of bacterial models. Bacteria used in animal studies tend to be those relevant in clinical practice, particularly with predilection for antibiotic resistance. Many studies have focused on the ESKAPE pathogens (*Enterococcus faecium*, *Staphylococcus aureus*, *Klebsiella pneumoniae*, *Acinetobacter baumannii*, *Pseudomonas aeruginosa*, and *Enterobacter cloacae*) (Debarbieux et al., 2010; Kumari et al., 2010; Chhibber et al., 2013; Jeon et al., 2016), a group of organisms designated by the World Health Organization as serious threats to global health based on high rates of multidrug resistance (Tacconelli et al., 2017). Animal studies have also used phage therapy to treat organisms such as *Escherichia coli* (Schneider et al., 2018), *Salmonella enterica* (Dallal et al., 2019), *Vibrio cholerae* (Bhandare et al., 2019), *Mycobacterium ulcerans* (Trigo et al., 2013), and *Burkholderia pseudomallei* (Guang-Han et al., 2016). Meanwhile, the relationship between antibiotic resistance and phage resistance (or sensitivity) in these organisms is a complex one. For example, while Chan et al. (2016) demonstrated an instance in which MDR *P. aeruginosa* exhibited a trade-off between antibiotic resistance and phage resistance through alterations in an efflux pump, work by Burmeister et al. (2020) provided an example where phage-resistant *E. coli* mutants exhibited increased resistance to tetracycline via changes to the bacterial lipopolysaccharide.

Phages kill bacteria in a process referred to as the lytic cycle where they adsorb to the bacterial surface, eject genetic material into the host, use bacterial replication machinery to generate phage progeny (and other proteins), and lyse the cell to release the newly generated virions (Gordillo Altamirano and Barr, 2019). Virulent phages are those which can only infect bacteria through the lytic cycle, whereas temperate phages can perform either the lytic cycle or an alternate process, the lysogenic cycle, in which phage DNA is integrated into the host's. Temperate phages are often considered unsuitable for phage therapy because lysogeny enables the transfer of genetic material (such as virulence factors or antibiotic resistance genes) to and between bacteria (Górski et al., 2018). As such, usually virulent phages are sought for use in phage therapy. Phages can be isolated from environments where the host bacteria can be found, such as sewage, soil, and river water (Smith and Huggins, 1982; Wang et al., 2006a). Alternatively, libraries of previously identified phages can be screened against the bacterial isolate of interest. *In vitro* phage-susceptibility testing is then performed with spot assays on agar plates (Chhibber et al., 2008; Heo et al., 2009) or with growth curves in liquid media which provide dynamic data on killing activity (Soothill, 1992; Tanji et al., 2005; Wang et al., 2006b). DNA sequencing provides phage characterization and is also essential to identify genes involved in lysogeny, such as integrases, which would implicate a phage as temperate. Unfortunately the functions of many phage genes remain unknown (Hatfull and Hendrix, 2011), and screening out phages based on putative gene functions does not always identify temperate phages.

The majority of virulent bacteriophages that have been discovered belong to the taxonomic order *Caudovirales*. *Caudovirales* are non-enveloped, tailed bacteriophages with icosahedral or elongated heads and genomes comprised of double-stranded DNA (Ackermann, 1998). Traditionally the order *Caudovirales* has been divided into three families—*Myoviridae*, *Siphoviridae*, and *Podoviridae*, though other families within the order have been discovered recently (Walker et al., 2019). *Siphoviridae* previously appeared to be the most abundant of the *Caudovirales*, but this varies from bacterial host to host (Ackermann, 1998). At present, there is insufficient evidence to indicate that one family of *Caudovirales* is more effective at killing bacteria than another.

CONSTRUCTING THE INFECTION MODEL AND ADMINISTERING PHAGE THERAPY

In the animal model of phage therapy, "infection" refers to the administration of bacteria. "Therapy" or "treatment" refers to the administration of phages *after* administration of bacteria and is distinct from phage "prophylaxis" in which phages are given *at or before* bacterial inoculation. To establish infection, the bacterial isolate is administered to the animal via the appropriate route (e.g., intranasally for pneumonia) at a known dose designated in colony-forming units (CFU) (Shivshetty et al., 2014). Investigators often set an endpoint (such as 100% animal fatality at 48 h) in order to determine the appropriate bacterial dose to employ in the subsequent phage therapy experiment (Biswas et al., 2002; Roach et al., 2017). This often requires trialing various doses before arriving at the desired infectious endpoint (Yang et al., 2015).

Bacteriophages require multiple steps of preparation before administration. Animals such as mice can only tolerate the administration of small volumes of liquid, especially when administered intravenously or intranasally; phages must therefore be concentrated to accommodate the necessary inoculum (Guang-Han et al., 2016; Roach et al., 2017). Inoculum size is dictated by the desired multiplicity of infection (MOI), which is the ratio of viral plaque forming units (PFU) to bacterial CFU. For example, if the animal receives 10^8 CFU of bacteria and an MOI of 100 is needed, then the volume that the animal receives must contain 10^10 PFU of bacteriophages. Once the bacteriophages have been concentrated, they are then purified further, often via ultracentrifugation using cesium chloride

TABLE 1 | Studies on phage therapy[a] according to organ system, bacteria, and animal model.

System	Bacteria	Animal Model	References
CNS	*Escherichia coli*	Rats	Pouillot et al., 2012
GI	*Escherichia coli*	Calves	Smith and Huggins, 1983; Smith et al., 1987
GI	*Escherichia coli*	Mice	Galtier et al., 2016
GI	*Escherichia coli*	Pigs	Smith and Huggins, 1983; Jamalludeen et al., 2009
GI	*Escherichia coli*	Sheep	Smith and Huggins, 1983; Raya et al., 2006
GI	*Salmonella enterica*	Chicken	Colom et al., 2015; Tie et al., 2018
GI	*Salmonella enterica*	Mice	Dallal et al., 2019
GI	*Salmonella enterica*	Quails	Ahmadi et al., 2016
GI	*Vibrio cholerae*	Mice	Jaiswal et al., 2014
GI	*Vibrio cholerae*	Rabbits	Bhandare et al., 2019
GI	*Vibrio parahaemolyticus*	Mice	Jun et al., 2014
Keratitis	*Pseudomonas aeruginosa*	Mice	Furusawa et al., 2016
Osteomyelitis	*Staphylococcus aureus*	Rabbits	Kishor et al., 2016
Otitis	*Pseudomonas aeruginosa*	Dogs	Hawkins et al., 2010
PNA	*Acinetobacter baumannii*	Mice	Jeon et al., 2016, 2019; Hua et al., 2017
PNA	*Burkholderia cenocepacia*	Mice	Carmody et al., 2010; Semler et al., 2014
PNA	*Burkholderia pseudomallei*	Mice	Guang-Han et al., 2016
PNA	*Escherichia coli*	Mice	Dufour et al., 2015, 2016, 2019
PNA	*Klebsiella pneumoniae*	Mice	Chhibber et al., 2008; Singla et al., 2015; Anand et al., 2020
PNA	*Pseudomonas aeruginosa*	Mice	Debarbieux et al., 2010; Morello et al., 2011; Alemayehu et al., 2012; Henry et al., 2013; Yang et al., 2015; Pabary et al., 2016; Roach et al., 2017; Waters et al., 2017; Chang et al., 2018; Forti et al., 2018; Abd El-Aziz et al., 2019
PNA	*Staphylococcus aureus*	Rats	Prazak et al., 2019
PNA	*Staphylococcus aureus*	Mice	Takemura-Uchiyama et al., 2014
Sinusitis	*Staphylococcus aureus*	Sheep	Drilling et al., 2014
SSTI	*Acinetobacter baumannii*	Mice	Regeimbal et al., 2016
SSTI	*Acinetobacter baumannii*	Pigs	Mendes et al., 2013
SSTI	*Acinetobacter baumannii*	Rats	Mendes et al., 2013; Shivaswamy et al., 2015
SSTI	*Klebsiella pneumoniae*	Mice	Kumari et al., 2010; Chadha et al., 2016
SSTI	*Mycobacterium ulcerans*	Mice	Trigo et al., 2013
SSTI	*Pseudomonas aeruginosa*	Rats	Mendes et al., 2013
SSTI	*Pseudomonas aeruginosa*	Pigs	Mendes et al., 2013
SSTI	*Staphylococcus aureus*	Mice	Capparelli et al., 2007; Chhibber et al., 2013
SSTI	*Staphylococcus aureus*	Rabbits	Wills et al., 2005
SSTI	*Staphylococcus aureus*	Rats	Mendes et al., 2013; Chhibber et al., 2017
SSTI	*Staphylococcus aureus*	Pigs	Mendes et al., 2013
Systemic	*Acinetobacter baumannii*	Galleria mellonella	Regeimbal et al., 2016; Jeon et al., 2019
Systemic	*Acinetobacter baumannii*	Mice	Leshkasheli et al., 2019
Systemic	*Burkholderia cenocepacia*	Galleria mellonella	Seed and Dennis, 2009
Systemic	*Citrobacter freundii*	Mice	Kaabi and Musafer, 2019
Systemic	*Clostridioides difficile*	Galleria mellonella	Nale et al., 2016a
Systemic	*Enterobacter cloacae*	Galleria mellonella	Manohar et al., 2018
Systemic	*Enterococcus faecalis*	Zebrafish	Al-Zubidi et al., 2019
Systemic	*Enterococcus faecalis*	Mice	Uchiyama et al., 2008
Systemic	*Enterococcus faecium*	Mice	Biswas et al., 2002
Systemic	*Escherichia coli*	Galleria mellonella	Manohar et al., 2018
Systemic	*Escherichia coli*	Mice	Smith and Huggins, 1982; Wang et al., 2006b; Pouillot et al., 2012; Dufour et al., 2016; Schneider et al., 2018; Kaabi and Musafer, 2019
Systemic	*Escherichia coli*	Quails	Naghizadeh et al., 2019
Systemic	*Haemophilus influenzae*	Mice	Kaabi and Musafer, 2019
Systemic	*Klebsiella pneumoniae*	Galleria mellonella	Manohar et al., 2018
Systemic	*Klebsiella pneumoniae*	Mice	Hung et al., 2011; Kaabi and Musafer, 2019
Systemic	*Moraxella catarrhalis*	Mice	Kaabi and Musafer, 2019
Systemic	*Pasteurella multocida*	Mice	Chen et al., 2019
Systemic	*Pseudomonas aeruginosa*	*Drosophila melanogaster*	Heo et al., 2009
Systemic	*Pseudomonas aeruginosa*	Galleria mellonella	Forti et al., 2018
Systemic	*Pseudomonas aeruginosa*	Mice	Wang et al., 2006a; Watanabe et al., 2007; Heo et al., 2009; Shivshetty et al., 2014;

TABLE 1 | Continued

System	Bacteria	Animal Model	References
			Kaabi and Musafer, 2019
Systemic	*Pseudomonas aeruginosa*	Zebrafish	Cafora et al., 2019
Systemic	*Salmonella enterica*	Caenorhabditis elegans	Tang et al., 2019
Systemic	*Salmonella enterica*	Mice	Capparelli et al., 2010; Tang et al., 2019
Systemic	*Staphylococcus aureus*	Mice	Capparelli et al., 2007; Takemura-Uchiyama et al., 2014; Oduor et al., 2016
Systemic	*Vibrio parahaemolyticus*	Mice	Jun et al., 2014
Systemic	*Vibrio vulnificus*	Mice	Cerveny et al., 2002
UTI	*Escherichia coli*	Mice	Dufour et al., 2016

CNS, central nervous system; GI, gastrointestinal; PNA, pneumonia; SSTI, skin and soft tissue infection; UTI, urinary tract infection.
[a]*Phage therapy refers to the administration of the first phage dose after the administration of bacteria (as opposed to phage prophylaxis which entails the first phage dose at or before the administration of bacteria). All of the studies listed include phage therapy as at least one component of their experiments conducted.*

(Biswas et al., 2002) followed by removal of the solvent with dialysis. Experiments usually take the additional step of removing endotoxin (Roach et al., 2017), a lipopolysaccharide released from the cell wall of Gram negative bacteria that can be extremely toxic. For phage therapy in human subjects, all of these steps are crucial to ensure purity, uniformity, and safety of bacteriophages prior to administration.

To initiate the phage therapy experiment, animals receive the bacterial isolate at the previously established dose. At a later time point the intervention group receives bacteriophages, and the control group receives buffer without phages, heat-inactivated phages (Wang et al., 2006a), or no treatment. Many proof-of-concept experiments have focused on phage monotherapy (Wang et al., 2006b; Capparelli et al., 2010; Carmody et al., 2010; Yang et al., 2015); however, since it is well established that phage-resistant bacterial variants emerge during treatment (Oechslin, 2018), studies have also examined phage cocktails, which contain mixtures of different bacteriophages (Forti et al., 2018; Seo et al., 2018; Naghizadeh et al., 2019). Cocktails provide a broader range of bacterial killing and may be able to mitigate the emergence of resistance by targeting different host receptors. For this reason, phage cocktails are used whenever possible in compassionate-use cases in humans.

The route of phage administration can be oral (Bhandare et al., 2019), intravenous (Capparelli et al., 2010), intraperitoneal (Biswas et al., 2002), subcutaneous (Capparelli et al., 2010), intramuscular (Naghizadeh et al., 2019), intranasal (Alemayehu et al., 2012), intratracheal (Chang et al., 2018), or topical (Mendes et al., 2013). For some models of infection, one route of phage administration fails even if adequate in other models or with other bacterial pathogens. For example, intravenous and intraperitoneal phages have not cured any animal models of *P. aeruginosa* pneumonia; only intranasal and intratracheal phages have worked (Debarbieux et al., 2010; Roach et al., 2017; Chang et al., 2018). Experiments may examine various MOIs of bacteriophages necessary to cure infection, which frequently lie between 1 and 1000 (Biswas et al., 2002; Jeon et al., 2016). Unsurprisingly, higher MOIs are more effective than lower MOIs at killing bacteria (Morello et al., 2011), though it is likely no further benefit exists after reaching a certain threshold.

A few points bear consideration on the limitations of experimental design and how animal work differs from clinical practice. First, *in vivo* animal experiments have the luxury of using bacterial isolates for which virulent phages have already been discovered. In human patients who require phage therapy, the bacterial isolate is obtained without *a priori* knowledge of any susceptibility to phages in a laboratory's phage library. In the critically ill, where delays in treatment are associated with decreased survival (Kumar et al., 2006), physicians cannot wait for isolate testing before initiating therapy. Phage cocktails, which could offer broad host-range empirically, may be a means of using phages when isolate susceptibility is not yet known. Models that use phage cocktails, such as those by Forti et al. (2018), Naghizadeh et al. (2019), and Prazak et al. (2019) warrant further attention.

Second, unlike in animal experiments in which the bacterial inoculum is known, human infections are caused by an amount of bacteria that often cannot be quantified, and applying accurate phage dosing by MOI in humans is difficult. It is also possible that the bacterial burden in a human infection could exceed the amount of bacteria used in any animal experiment by orders of magnitude; if attempting to mimic the MOIs of animal studies, this would call for larger doses of phages than implemented in any of these experiments. This still may be feasible based on the size of humans compared to mice, though interestingly, a number of case reports in humans have used phage inocula of comparable size to those used in animals. For example, in Schooley et al. (2017) treatment of a disseminated *A. baumannii* infection, intravenous phage doses each contained $5 \times 10\hat{}9$ PFU of virus, while Law et al. (2019) used phage doses of $4 \times 10\hat{}9$ PFU to successfully treat *P. aeruginosa* in a cystic fibrosis patient. In both cases, many doses of phages were given over a period of weeks, which may have compensated for the size of the individual doses. Nevertheless, it remains quite possible that high MOIs in humans may be unnecessary based on the self-amplifying nature of bacteriophages.

Finally, infections in animal studies compared to human infections also differ by their rates of progression. In most animal studies, experimentally induced infections progress rapidly, often killing animals within 48–72 h in the absence of phage treatment (Debarbieux et al., 2010; Roach et al., 2017; Schneider et al., 2018). As a result, phage therapy to treat these animal infections needs to be given immediately or soon after bacterial inoculation. Since human infections rarely progress as quickly as the infections in these animal models (e.g., a patient with pneumonia may wait a few days before even presenting to the hospital), phage therapy in humans will likely be administered after a delayed amount of time. Significant delays in treatment limit efficacy in animal models, though a theoretical benefit to a delay would be that phages could replicate to higher titers in the presence of a high bacterial burden. A few animal studies have managed

to recreate delayed conditions of human infections, notably the chronic *P. aeruginosa* pneumonia model established by Waters et al. (2017) and the non-lethal *S. aureus* bacteremia model constructed by Capparelli et al. (2007). More indolent infection models like these are needed, particularly of pneumonia and systemic infections, that allow animals to survive through at least 5 or 7 days without treatment and still can be cured when phage therapy is given after a delayed amount of time. Until then, it will remain unclear whether phages can reliably cure infections unless given soon after their onset.

EFFICACY OF PHAGE THERAPY IN ANIMAL MODELS

Research into phage therapy in the West laid relatively dormant from the 1940's onward but reappeared again in the 1980's with animal work conducted by Smith and Huggins (1982, 1983) and Smith et al. (1987). In one of their first experiments, they infected mice intramuscularly or intracerebrally with the bacterium *E. coli.* A single intramuscular dose of one phage with activity against the host bacteria reduced mortality more than multiple doses of various antibiotics (Smith and Huggins, 1982). A year later, they found that certain phages could treat *E. coli* diarrhea in calves, pigs, and lambs. They also found that phage-treated calves that survived *E. coli* infection continued to excrete phages in their feces, at least until the quantity of the pathogenic *E. coli* strain excreted was low (Smith and Huggins, 1983). Subsequent work demonstrated that phage cocktails could also be used in place of individual phages (Smith et al., 1987). Soothill was the next to examine phages in animals, albeit as prophylaxis rather than treatment. In their 1992 study (Soothill, 1992), phages prevented intraperitoneal *A. baumannii* and *P. aeruginosa* infections. Another study showed phages could prevent skin graft infections in guinea pigs if administered prior to the introduction of *P. aeruginosa* (Soothill, 1994).

While these studies were informative, there was little discussion in the early 1990's about the need for phage therapy in humans, so animal studies were not pursued robustly. However, as multidrug antibacterial resistance developed into a global crisis (Murray, 1994; Tenover and McGowan, 1996), the prospects of phage therapy attracted more attention (Alisky et al., 1998; Stone, 2002), prompting a new wave of animal studies.

Systemic Infections

Systemic infections are those that result in bacteremia and/or dissemination to multiple organs. The 1992 experiment by Soothill (1992) was a model of systemic infection but, as mentioned, it focused on prophylaxis. Cerveny et al. (2002) injected mice subcutaneously with *Vibrio vulnificus* to induce bacteremia and then administered phages intravenously. In this study, phages only had an effect when injected simultaneously as prophylaxis, whereas when given at 6 or 12 h after bacterial inoculation, they provided no mortality benefit. However, in the same year, Biswas et al. (2002) were able to successfully treat a systemic infection induced by intraperitoneal injections of vancomycin-resistant *E. faecium* in mice. Phages administered after 45 min at an MOI of 0.3 or 3.0 rescued 100% of the animals; when delayed until 5 h at an MOI of 3, 100% of mice still survived. Even with delays in treatment of 18 and 24 h, at which point all mice were quite ill, approximately 50% of the animals survived and recovered completely.

Most subsequent work has examined infections with *P. aeruginosa* and *E. coli*, though other studied bacterial species have included *S. aureus*, *A. baumannii, K. pneumoniae*, *S. enterica*, *Pasteurella multocida,* and *Vibrio parahaemolyticus* (Capparelli et al., 2007; Capparelli et al., 2010; Hung et al., 2011; Jun et al., 2014; Oduor et al., 2016; Chen et al., 2019; Leshkasheli et al., 2019). Studies often show that efficacy depends on the timing of administration. For example, in a study by Wang et al. (2006a) on imipenem-resistant *P. aeruginosa* infections, phages were 100% effective when administered 1 h after infection at an MOI of 200, but cure rates dropped to 50 and 20%, respectively, when treatment was delayed to 3 and 6 h. The same group studied drug-resistant *E. coli* infections and noted that all mice died when intraperitoneal phage treatment was delayed to 6 h (Wang et al., 2006b). Capparelli et al. (2007), however, showed that treatment could be quite delayed in the context of a more indolent infection; the investigators administered a low dose of $5 \times 10\hat{}6$ CFU of *S. aureus* intravenously and then at day 10 administered either no treatment or phages at an MOI of 1000. At day 20, phage-treated mice had sterilized their spleens, kidneys, hearts, and blood, whereas those tissues remain infected in the control mice.

The most common routes of phage administration for systemic infections entail intraperitoneal (Wang et al., 2006a; Uchiyama et al., 2008), intravenous (Oduor et al., 2016), oral (Jun et al., 2014), or intramuscular (Heo et al., 2009) dosing. For treatment of *P. aeruginosa*, Watanabe et al. (2007) determined that intravenous and intraperitoneal methods were superior to oral, and Heo et al. (2009) demonstrated that intraperitoneal was superior to intramuscular. In humans, phages for systemic infections will likely require intravenous or oral administration since these are the routes via which medications are typically administered in medical practice. More studies are needed to examine these routes of therapy.

Pneumonia

Pneumonia models of phage therapy initially lagged behind other models of infection but have since taken a prominent role in the literature. Chhibber et al. (2008) used *K. pneumoniae* at a concentration of $10\hat{}8$ CFU/ml to induce pneumonia in mice and simultaneously gave them phages intraperitoneally. As with the early systemic infection models (Soothill, 1992; Cerveny et al., 2002), phages successfully provided prophylaxis against infection but could not treat it. Nevertheless, this study helped set the stage for the other pneumonia models of phage therapy to come.

Studies have frequently focused on *P. aeruginosa*, a common culprit of hospital-acquired pneumonia and cystic fibrosis exacerbations. Additionally, mortality associated with MDR *P. aeruginosa* in ventilator-associated pneumonia exceeds 35% (Ramírez-Estrada et al., 2016). Debarbieux et al. (2010) demonstrated that pneumonia responded to phage treatment, but phage administration was intranasal, and timing of

administration was crucial. 100% of mice survived in the group treated with phages 2 h after bacterial inoculation, and 75% of mice survived when phages were given after 4 or 6 h. The study also examined various MOIs required to treat infection and found that an MOI of at least 10 was necessary. Unsurprisingly, other studies have found that higher MOIs are superior to lower ones (Morello et al., 2011). Administering phages early is also superior to waiting, even if by only an hour (Yang et al., 2015). There are two studies that capture efficacy of delayed treatment. Waters et al. (2017) established a chronic form of lung infection using a *P. aeruginosa* strain found in patients with cystic fibrosis. The study successfully cleared infection in mice with a phage at an MOI of 10 that was given as late as 48 h after bacterial inoculation. Abd El-Aziz et al. (2019) also treated pneumonia successfully at 12 h after infection using an MOI of 0.1. Only 60% of the control group developed severe disease, underscoring how interpretations of phage efficacy are dependent on the severity of the underlying bacterial infection.

In addition to treating *P. aeruginosa*, phages have shown efficacy in bacterial pneumonias caused by *S. aureus* (Prazak et al., 2019), *E. coli* (Dufour et al., 2016), *A. baumannii* (Jeon et al., 2016), *K. pneumoniae* (Anand et al., 2020), *B. pseudomallei* (Guang-Han et al., 2016), and *Burkholderia cenocepacia* (Carmody et al., 2010), all of which can cause MDR pneumonia in critically ill patients or those with cystic fibrosis. Dufour et al. (2015) found that bacteriophage treatment enabled 100% survival of mice infected with a highly virulent *E. coli* strain. A study of *A. baumannii* pneumonia observed that administration of phages at an MOI of 10 given 30 min after infection resulted in 100% survival (Jeon et al., 2016). In a *B. pseudomallei* study, phages in magnitude of 10^8 PFU rescued 1/3rd of the mice, which was superior to outcomes in control mice that were not given phages (Guang-Han et al., 2016).

Since some pathogens do not lead to rapidly progressive pneumonia, particularly those that form biofilms in the airways of patients with cystic fibrosis, investigators have also evaluated responses to phage therapy using quantitative microbial endpoints rather than simply assessing improvement in illness severity or mortality. Debarbieux, Roach, Forti, and others (Debarbieux et al., 2010; Henry et al., 2013; Dufour et al., 2015; Roach et al., 2017) infected mice with bioluminescent bacteria and used IVIS spectroscopy to display the decrease in luminescence that resulted from phage treatment. Pabary et al. (2016) administered phages 24 h after *P. aeruginosa* infection and then performed bronchoalveolar lavages (BALs) on mice at 48 h. There was complete clearance of bacteria in 6 of 7 phage-treated mice, and the median CFU/ml was significantly lower compared to controls that were not given phages. Another study found no bacteria detected in the lungs after lung extraction at 72 h (Abd El-Aziz et al., 2019), and the use of aerosolized phage by Chang et al. (2018) was able to decrease bacterial loads in lung homogenates at both 4 and 24 h compared to controls.

Synergy between the immune system and bacteriophages likely plays an important role in killing bacteria and has only partially been elucidated. Roach et al. (2017) showed that neutrophils are an essential part of controlling both phage-sensitive and emergent phage-resistant bacterial variants as a means of ensuring effective treatment. Work by Abd El-Aziz et al. (2019) showed that the addition of phages to a mixture of human serum and bacteria enhanced serum killing activity. Multiple studies provide evidence that the immune system generates antibodies against bacteriophages (Biswas et al., 2002; Wang et al., 2006a; Shivshetty et al., 2014), though this likely would impair rather than bolster activity against bacterial infection.

As with systemic models of infection, the efficacy of phage therapy is highly dependent on experimental conditions. Again, models are needed to prove phage efficacy when administered more than a few hours after infection.

Diarrheal Infections

Enteritis (infection of the small bowel) and colitis (infection of the large bowel) are common models of infection studied for the use of phage therapy. Because diarrheal infections primarily affect the lumen of the gastrointestinal tract, these studies allow for experimentation with oral phages (without requiring their systemic absorption), simplifying the administration of phage therapy.

Many studies have focused on *E. coli*, one of the most common causes of diarrheal illness in humans throughout the world (Leung et al., 2019). As mentioned earlier, Smith and Huggins (1983) looked at treatment of *E. coli* diarrhea in calves, pigs, and lambs. Raya et al. (2006) infected 8 sheep orally with *E. coli* strain O157:H7. Four of the sheep were given an oral phage at an MOI of 10, and 2 days later all eight sheep were euthanized. Bacterial counts in the colons of treated sheep were 2–3 $\log_{10}$ lower than the untreated ones. Jamalludeen et al. (2009) challenged pigs orally with 10^10 CFU of Enterotoxigenic *E. coli* (ETEC) and 24 h later administered a combination of two phages at a total of 10^8 PFU for three doses, separated 6 h apart. Compared to controls that did not receive phages, oral phage administration reduced the development of diarrhea and quantity of ETEC in pig feces.

Since *V. cholera* infects 3–5 million people annually and causes 21,000–143,000 deaths a year, studies have explored management with bacteriophages (Jaiswal et al., 2014; Yen et al., 2017; Bhandare et al., 2019). In a study by Jaiswal et al. (2014), mice received oral *V. cholerae* and then daily dosing of a phage cocktail (at an MOI of 0.5), the antibiotic ciprofloxacin, or oral rehydration. Phage cocktails reduced the burden of *V. cholerae* in tissue and blood by 3 $\log_{10}$ compared to rehydration, which provided no benefit, though ciprofloxacin produced superior results in reducing *V. cholerae* by 4 $\log_{10}$. Despite the inferiority of phages to ciprofloxacin in this study, the specificity of phages could preserve endogenous host flora compared to the broad host-range of antibiotics. In a cholera study in rabbits, animals were infected orally and then administered oral phages 6 h later. Eleven of 17 infected control rabbits developed symptoms of enteritis, whereas none of the nineteen phage-treated animals showed signs of disease. Phage treatment also significantly reduced the amount of *V. cholerae* recovered from the intestines of treated rabbits compared with untreated controls (Bhandare et al., 2019).

Other studies on infections of the lower gastrointestinal tract have examined enteric pathogens such as *S. enterica* and *V. parahaemolyticus*. A study of *S. enterica* serovar enteritidis in mice found that oral phages administered at an MOI of 10 1 day after gavage with the bacteria showed no signs of infection, and no bacteria were isolated from the liver; mice not administered phages all died at the end of the experiment and exhibited clear liver pathology associated with recovered Salmonella isolates (Dallal et al., 2019). In a model of *V. parahaemolyticus* enteritis, mortality rates were twice as high in control mice compared to mice treated intraperitoneally with phages (Jun et al., 2014).

While many studies focus on phages as prophylaxis, it is important to note that due to the unpredictability of infections in humans, some animal models of prophylaxis lack relevance to phage therapy in humans. An exception to this lies in the prophylaxis of bacterial diarrheal illnesses, which are widespread in developing countries due to contamination of water sources and are caused by a more limited range of bacterial species. In Eastern European literature, one of the largest human phage therapy studies conducted in the 1960's indicated that prophylactic tablets of oral phages could reduce the acquisition of Shigella dysentery (Chanishvili, 2012). In animal work on *V. cholera*, Yen et al. (2017) demonstrated that a cocktail of three phages reduced bacterial colonization of mice, optimally when given 6 h prior to bacterial inoculation, as opposed to 12 or 24 h prior. Apart from their experiment on cholera treatment, Bhandare et al. (2019) studied prophylaxis by giving rabbits oral phages at 10^9 PFU 6 h prior to infecting them with 5×10^8 CFU of bacteria; none of the rabbits developed diarrhea. Meanwhile, Nale et al. (2016b) studied the prevention of *Clostridioides difficile*, the most common culprit of hospital-acquired diarrhea. Hamsters received inoculation with *C. difficile* spores and a cocktail of phages simultaneously and every 8 h thereafter at an MOI of 10,000. At 36 h, phages reduced *C. difficile* bacterial counts in the GI lumen by at least 4 $\log_{10}$ and delayed mortality by greater than a day. Of note, this study used temperate phages rather than strictly lytic ones.

Other Infections

There are a number of models of skin and soft tissue infections. Wills et al. (2005) injected *S. aureus* subcutaneously into the flanks of rabbits. Phages administered subcutaneously simultaneously as prophylaxis prevented abscesses but when administered as treatment at 6, 12, or 24 h after infection, they did not. Kumari et al. (2010) examined murine wounds that were infected with *K. pneumoniae*. A single intraperitoneal injection of phages could rescue 73% of the animals when delayed to 6 h after burn/bacterial challenge. Delay in treatment resulted in lower survival, but even with delays of 12 and 18 h, at which point all the mice were ill, 46 and 26% of the animals, respectively, could be rescued and went on to recover completely. In a model of *S. aureus* foot infections in diabetic mice, phages were more effective than the antibiotic linezolid, though the two agents together showed superior efficacy (Chhibber et al., 2013). Shivaswamy et al. (2015) used topical phage treatments for infected wounds in both mice and pigs; phages were able to reduce bacterial counts caused by *P. aeruginosa* and *S. aureus*. Trigo et al. (2013) studied a slower form of skin/soft tissue infection caused by the bacteria *M. ulcerans*, waiting until 33 days post-infection to administer a single dose of bacteriophages. At day 68, footpads of non-treated mice started showing signs of ulceration, while in mycobacteriophage-treated mice the progression of swelling halted after day 91 post-infection.

Other models of infection include orthopedic, urinary tract, and CNS infections. Kishor et al. (2016) induced methicillin resistant *S. aureus* (MRSA) osteomyelitis of the distal femur in rabbits. Mice given phages in three doses every 2 days beginning in the 3rd week of infection were compared to phage treatment started in the 6th week of infection. All mice in the former group were cured based on microbiologic, radiologic, and histopathologic examinations. Those given phages starting in the 6th week showed some radiologic features of chronic osteomyelitis, but wounds healed, and the sites became sterile. Dufour et al. (2016) injected *E. coli* into the bladder of mice and the following day administered bacteriophage treatment intraperitoneally at an MOI of 200. At 48 h, bacterial loads in the kidneys decreased by 2 $\log_{10}$ compared to controls that received no phages. To treat a CNS infection in mice caused by ESBL *E. coli*, Pouillot et al. (2012) administered intraperitoneal phages 1 h later at a dose of 10^8 PFU. All animals survived to day 5. Phage concentration in the CSF was 10-fold higher than that in blood, demonstrating the capacity of phages to cross the blood-CSF barrier; work in humans by Ghose et al. (2019) has also recently confirmed this finding. Other studies have shown effective treatment of keratitis in mice (Furusawa et al., 2016), otitis media in dogs (Hawkins et al., 2010), sinusitis in sheep (Drilling et al., 2014), and systemic infections in zebrafish (Al-Zubidi et al., 2019; Cafora et al., 2019) and moth larvae (Hall et al., 2012; Augustine et al., 2014; Nale et al., 2016a; Manohar et al., 2018; Jeon et al., 2019), supporting the idea that phage therapy can be studied in a broad range of infection models and animal species.

The application of phage lysins (rather than the phages themselves) to fight infections is also an area of intense investigation. Ectolysins are structural enzymes on the phage virion that facilitate phage entry into bacterial cells, while endolysins are non-structural enzymes responsible for the release of phages after they have replicated within the cytoplasm (Kim et al., 2019). In both cases, lysins degrade the peptidoglycan of the bacterial cell wall. Endolysins have been found to kill bacteria effectively when they are applied extrinsically. Lysins have been studied most extensively with Gram positive bacteria where they can easily access the cell wall peptidoglycan; however, lysins active against Gram negative bacteria have also been found (Lood et al., 2015; Raz et al., 2019), and lysin-bacteriocin fusion molecules have been developed that can translocate the outer membrane of Gram negative organisms (Heselpoth et al., 2019), a technique that would allow lysins to gain access to the otherwise poorly accessible peptidoglycan protected by the Gram negative outer cell membrane. As with models of phage therapy, lysins have shown efficacy

in a variety of animal models of infection (Daniel et al., 2010; Vouillamoz et al., 2013; Schuch et al., 2014; Díez-Martínez et al., 2015; Lood et al., 2015; Raz et al., 2019), and a phase 3 clinical trial in humans studying a lysin for the treatment of *S. aureus* bacteremia is currently underway (Globe Newswire, 2020).

PHAGE PHARMACOKINETICS

The pharmacokinetics of bacteriophages are more complex than traditional antibiotics because they replicate after infecting their bacterial hosts. Thus, their behavior also differs depending on whether a bacterial host is present or absent, and the persistence of phages *in vivo* may suggest that infection has not been eradicated. Methods of characterizing phage kinetics have relied on serial blood and stool measurements (Cerveny et al., 2002; Seo et al., 2018), bronchoalveolar lavages (Morello et al., 2011), homogenizing organs after animal euthanasia at various time points (Chhibber et al., 2008; Takemura-Uchiyama et al., 2014), and in rare instances, phage labeling (Rusckowski et al., 2004, 2008).

Phages have been detected in all major organs following phage therapy, including the lungs, spleen, liver, kidney, stomach, and intestines (Carmody et al., 2010; Takemura-Uchiyama et al., 2014; Schneider et al., 2018). They have also been detected in brain tissue, indicating that they can pass through the blood-brain barrier (Pouillot et al., 2012; Ghose et al., 2019). When Pouillot et al. (2012) and Ghose et al. (2019) injected phages intraperitoneally, they found higher concentrations of phages in the spleen and kidney than compared to blood and concluded that this represented phage trapping by these organs.

Even in the absence of a host bacterial infection, phages persist in most body compartments for 2–3 days. Cerveny et al. (2002) initially estimated the half-life of phages in the blood of uninfected mice to be 2.2 h. In uninfected mice receiving intraperitoneal phage injections, Chhibber et al. (2008) found that maximum phage concentrations in blood, peritoneal fluid, and lungs occurred at 6 h and were negligible by 36 h. Jun et al. (2014) also found peak concentrations in blood occurred at 6 h following intraperitoneal injection, whereas after oral administration peak levels occurred at 12 h. Via both routes, no phages were detected at 48 h. Yen, Kumari, and others have arrived at similar results (Kumari et al., 2010; Yen et al., 2017). These data support the Uchiyama et al. (2009) two-compartment pharmacokinetic model where phages initially distribute to organs and then are slowly eliminated from the body. Interaction with the tissues of individual organ systems also likely contributes to these dynamics and is extremely complex. An example would be the subdiffusive movement of phages in mucous secretions which Barr et al. (2015) showed serves to increase the interactions between phages and bacteria.

Route of administration influences phage concentrations in various organs. For example, phage concentrations seem to achieve higher levels throughout the body when injected intramuscularly compared to intraperitoneally (Heo et al., 2009). Lungs contain higher concentrations following inhalational therapy compared to intraperitoneal therapy (Carmody et al., 2010). Subcutaneous administration results in lower and more delayed blood concentrations compared to intraperitoneal injection (Pouillot et al., 2012). Intravenous therapy functions similarly to intraperitoneal therapy, with the exception that the latter results in higher intraperitoneal phage concentrations.

In animals infected with bacteria that serve as hosts for bacteriophages, the persistence and concentration levels of phages also differ. When phages were administered in the presence of a systemic MRSA infection, phages could be detected for at least 96 h in the blood (Oduor et al., 2016). Watanabe et al. (2007) induced gut-derived sepsis with oral *P. aeruginosa*, which was followed by administration of oral phages. After 8 days, high concentrations of phages remained in the blood and liver when high levels of bacteria were still detected, demonstrating that phages continue to replicate as long the bacterial host remains present. Similarly, in an *E. coli* sepsis model in which IV phages were administered, they could be detected in the spleen up to 2 weeks after infection in the surviving mice (Schneider et al., 2018). Meanwhile, Takemura-Uchiyama et al. (2014) compared phage concentrations in mice with *S. aureus* sepsis and those that were not infected but given phages alone. Findings conveyed that phage concentrations in the blood, lung, and liver were 10^7, 10^5, and 10^3 times higher in the infected mice. In the Debarbieux et al. (2010) model of *P. aeruginosa* pneumonia, infected mice treated with phages demonstrated higher phage concentrations in their lungs by 1 $\log_{10}$ value compared to mice given only phages.

A couple of studies have labeled bacteriophages with technetium and administered them to infected animals (Rusckowski et al., 2004, 2008). These studies did not use phages intended to kill their bacterial host but instead focused on using the phages to locate the sites of the bacterial infection with imaging. These studies offer promise as an alternative means of assessing bacteriophage distribution within the body. Unfortunately, they only labeled parent phages (the directly administered phages) and were unable to characterize the distribution or behavior of progeny phages (phages produced after the parent phages replicated). Imaging techniques to detect both parent and progeny phages in phage therapy would offer valuable information moving forward.

TOXICITY AND IMMUNE RESPONSE

Phage therapy has proven safe in the many animal experiments thus far (Uchiyama et al., 2008; Shivshetty et al., 2014; Oduor et al., 2016). For example, Uchiyama et al. (2008) gave mice repeated intraperitoneal phage injections seven times a day every 4 days for 2 months and found this had no overt clinical effects. Chen et al. (2019) injected mice with 10^8 PFU of phages intraperitoneally and saw no abnormal histological changes in the main organs, and mice experienced no adverse health effects. Human studies have been equally reassuring (Sarker et al., 2016; Gindin et al., 2019; Ooi et al., 2019; Petrovic Fabijan et al., 2020).

Phages also do not induce significant amounts of inflammation. Dufour et al. (2019) found that phages could elicit cytokine production above baseline, but this was localized, phage dependent, and had no observable clinical consequences. Other work has shown that when uninfected mice were given inhalational or intraperitoneal phages, no appreciable levels of either TNF-α or MIP-2 were observed in the lungs (Carmody et al., 2010). In the study by Debarbieux et al. (2010), cytokine levels of IL-6 and TNF-α were as low in animals given phages as those given PBS solution. Roach et al. (2017) arrived at similar conclusions. These studies indicate that phage treatments alone do not result in significant inflammatory responses in the absence of host bacteria (Morello et al., 2011).

Nevertheless, phages do influence immune responses. Phages have served as antigenic stimuli in the evaluation of immunodeficiencies, and phage proteins have been used as vehicles for vaccine antigens (Górski et al., 2012). The immune response against phages results in their inactivation and clearance and has important implications in the efficacy of therapy. From an innate immunity standpoint, both the non-cellular complement system and phagocytosis lead to inactivation and clearance of phages from circulation (Dąbrowska, 2019; Hodyra-Stefaniak et al., 2019). Phagocytosis in the liver and spleen occurs rapidly (Inchley, 1969; Geier et al., 1973) and is also upregulated in the presence of concomitant systemic inflammation (such as that produced by a bacterial infection) (Hodyra-Stefaniak et al., 2015). In comparison to the liver, the spleen retains intact phages for longer periods by non-destructively capturing antigens using Schweigger-Seidel capillary sheaths (collections of macrophages in splenic capillary walls). This process may allow the spleen to serve as an ongoing source of antigens to stimulate antibody production (Geier et al., 1973), and in this way phagocytosis serves as the initial step leading to an adaptive immune response (Dąbrowska, 2019).

Adaptive immunity to phages is characterized by a strong humoral response. In one animal study, 1 dose of intraperitoneal phages caused anti-phage IgG titers to increase 26-fold, peaking at day 40 (Wang et al., 2006a). In another study, IgG titers rose 3,800-fold above baseline after phage administration (Biswas et al., 2002). In a study by Hodyra-Stefaniak et al. (2015), both IgM and IgG antibodies were able to neutralize phages rapidly in pre-immunized mice compared to those that were initially phage-naïve, and Huff et al. (2010) found that an increase in IgG titers from a prior phage exposure resulted in a 40% decrease in phage efficacy when treating colibacillosis in poultry. In a study using PEGylation to extend phage half-life, Kim et al. (2008) showed this was ineffective if given to animals already exposed to the same phage previously. This suggested that PEGylation could not prevent the adaptive immune response from rapidly eliminating the phage.

Interestingly, human studies have demonstrated low levels of phage-neutralizing antibodies in patient serum even prior to phage administration, likely due to pre-exposure from the ubiquity of phages in the environment (Górski et al., 2012). The clinical relevance of this remains to be determined, but it introduces the possibility that adaptive immunity could contribute to inactivation of phage therapy upon initial treatment administration. The rapid development of bacterial resistance is often pointed to as a source of potential phage treatment failure, but it is likely that the immune clearance and inactivation of phages will also play an important role.

CONCLUSION

Global antibiotic resistance has created urgency for phage therapy as an alternative to antibiotics. Studies in animals should serve as a guide to applying phage therapy in human diseases. The animal studies reviewed here reveal that phage therapy can work in all models of infection and on many species of bacteria. They have also demonstrated its safety. Nevertheless, there is still much to learn. Standardization of regimens, optimization of pharmacokinetic modeling, and development of models that mimic the time course of infection in human diseases are needed. Moving forward, animal models of phage therapy will need to address these issues if we hope to bring phage therapy into routine clinical practice in the 21st century.

AUTHOR CONTRIBUTIONS

SP wrote the review. DP and RS edited it. All the authors contributed to the article and approved the submitted version.

FUNDING

This research was supported by the Center for Innovative Phage Applications and Therapeutics (IPATH).

REFERENCES

Abd El-Aziz, A. M., Elgaml, A., and Ali, Y. M. (2019). Bacteriophage Therapy Increases Complement-Mediated Lysis of Bacteria and Enhances Bacterial Clearance After Acute Lung Infection With Multidrug-Resistant *Pseudomonas aeruginosa*. *J. Infect. Dis.* 219, 1439–1447. doi: 10.1093/infdis/jiy678

Ackermann, H. W. (1998). Tailed bacteriophages: the order caudovirales. *Adv. Virus Res.* 51, 135–201. doi: 10.1016/s0065-3527(08)60785-x

Ahmadi, M., Karimi Torshizi, M. A., Rahimi, S., and Dennehy, J. J. (2016). Prophylactic Bacteriophage Administration More Effective than Post-infection Administration in Reducing *Salmonella enterica* serovar Enteritidis Shedding in Quail. *Front. Microbiol.* 7:1253. doi: 10.3389/fmicb.2016.01253

Alemayehu, D., Casey, P. G., McAuliffe, O., Guinane, C. M., Martin, J. G., Shanahan, F., et al. (2012). Bacteriophages φMR299-2 and φNH-4 can eliminate *Pseudomonas aeruginosa* in the murine lung and on cystic fibrosis lung airway cells. *mBio* 3, 29–12 e. doi: 10.1128/mBio.00029-12

Alisky, J., Iczkowski, K., Rapoport, A., and Troitsky, N. (1998). Bacteriophages show promise as antimicrobial agents. *J. Infect.* 36, 5–15. doi: 10.1016/s0163-4453(98)92874-2

Al-Zubidi, M., Widziolek, M., Court, E. K., Gains, A. F., Smith, R. E., Ansbro, K., et al. (2019). Identification of Novel Bacteriophages with Therapeutic Potential That Target Enterococcus faecalis. *Infect. Immun.* 87, 512–519 e. doi: 10.1128/iai.00512-19

Anand, T., Virmani, N., Kumar, S., Mohanty, A. K., Pavulraj, S., Bera, B. C., et al. (2020). Phage therapy for treatment of virulent *Klebsiella pneumoniae* infection

in a mouse model. *J. Glob. Antimicrob. Resist.* 21, 34–41. doi: 10.1016/j.jgar.2019.09.018

Årdal, C., Balasegaram, M., Laxminarayan, R., McAdams, D., Outterson, K., Rex, J. H., et al. (2020). Antibiotic development - economic, regulatory and societal challenges. *Nat. Rev. Microbiol.* 18, 267–274. doi: 10.1038/s41579-019-0293-3

Augustine, J., Gopalakrishnan, M. V., and Bhat, S. G. (2014). Application of ΦSP-1 and ΦSP-3 as a therapeutic strategy against *Salmonella* Enteritidis infection using Caenorhabditis elegans as model organism. *FEMS Microbiol. Lett.* 356, 113–117. doi: 10.1111/1574-6968.12493

Barr, J. J., Auro, R., Sam-Soon, N., Kassegne, S., Peters, G., Bonilla, N., et al. (2015). Subdiffusive motion of bacteriophage in mucosal surfaces increases the frequency of bacterial encounters. *Proc. Natl. Acad. Sci. U. S. A.* 112, 13675–13680. doi: 10.1073/pnas.1508355112

Bhandare, S., Colom, J., Baig, A., Ritchie, J. M., Bukhari, H., Shah, M. A., et al. (2019). Reviving Phage Therapy for the Treatment of Cholera. *J. Infect. Dis.* 219, 786–794. doi: 10.1093/infdis/jiy563

Biswas, B., Adhya, S., Washart, P., Paul, B., Trostel, A. N., Powell, B., et al. (2002). Bacteriophage therapy rescues mice bacteremic from a clinical isolate of vancomycin-resistant Enterococcus faecium. *Infect. Immun.* 70, 204–210. doi: 10.1128/iai.70.1.204-210.2002

Burmeister, A. R., Fortier, A., Roush, C., Lessing, A. J., Bender, R. G., Barahman, R., et al. (2020). Pleiotropy complicates a trade-off between phage resistance and antibiotic resistance. *Proc. Natl. Acad. Sci. U. S. A.* 117, 11207–11216. doi: 10.1073/pnas.1919888117

Cafora, M., Deflorian, G., Forti, F., Ferrari, L., Binelli, G., Briani, F., et al. (2019). Phage therapy against *Pseudomonas aeruginosa* infections in a cystic fibrosis zebrafish model. *Sci. Rep.* 9:1527. doi: 10.1038/s41598-018-37636-x

Capparelli, R., Nocerino, N., Iannaccone, M., Ercolini, D., Parlato, M., Chiara, M., et al. (2010). Bacteriophage therapy of *Salmonella enterica*: a fresh appraisal of bacteriophage therapy. *J. Infect. Dis.* 201, 52–61. doi: 10.1086/648478

Capparelli, R., Parlato, M., Borriello, G., Salvatore, P., and Iannelli, D. (2007). Experimental phage therapy against Staphylococcus aureus in mice. *Antimicrob. Agents Chemother.* 51, 2765–2773. doi: 10.1128/aac.01513-06

Carmody, L. A., Gill, J. J., Summer, E. J., Sajjan, U. S., Gonzalez, C. F., Young, R. F., et al. (2010). Efficacy of bacteriophage therapy in a model of Burkholderia cenocepacia pulmonary infection. *J. Infect. Dis.* 201, 264–271. doi: 10.1086/649227

Cerveny, K. E., DePaola, A., Duckworth, D. H., and Gulig, P. A. (2002). Phage therapy of local and systemic disease caused by Vibrio vulnificus in iron-dextran-treated mice. *Infect. Immun.* 70, 6251–6262. doi: 10.1128/iai.70.11.6251-6262.2002

Chadha, P., Katare, O. P., and Chhibber, S. (2016). In vivo efficacy of single phage versus phage cocktail in resolving burn wound infection in BALB/c mice. *Microb. Pathog.* 99, 68–77. doi: 10.1016/j.micpath.2016.08.001

Chan, B. K., Sistrom, M., Wertz, J. E., Kortright, K. E., Narayan, D., and Turner, P. E. (2016). Phage selection restores antibiotic sensitivity in MDR *Pseudomonas aeruginosa*. *Sci. Rep.* 6, 26717. doi: 10.1038/srep26717

Chan, B. K., Turner, P. E., Kim, S., Mojibian, H. R., Elefteriades, J. A., and Narayan, D. (2018). Phage treatment of an aortic graft infected with *Pseudomonas aeruginosa*. *Evol. Med. Public Health* 2018, 60–66. doi: 10.1093/emph/eoy005

Chang, R. Y. K., Chen, K., Wang, J., Wallin, M., Britton, W., Morales, S., et al. (2018). Proof-of-Principle Study in a Murine Lung Infection Model of Antipseudomonal Activity of Phage PEV20 in a Dry-Powder Formulation. *Antimicrob. Agents Chemother.* 62, 1714–1717.e. doi: 10.1128/aac.01714-17

Chanishvili, N. (2012). Phage therapy–history from Twort and d'Herelle through Soviet experience to current approaches. *Adv. Virus Res.* 83, 3–40. doi: 10.1016/b978-0-12-394438-2.00001-3

Chen, Y., Guo, G., Sun, E., Song, J., Yang, L., Zhu, L., et al. (2019). Isolation of a T7-Like Lytic Pasteurella Bacteriophage vB_PmuP_PHB01 and Its Potential Use in Therapy against Pasteurella multocida Infections. *Viruses* 11:86. doi: 10.3390/v11010086

Chhibber, S., Kaur, S., and Kumari, S. (2008). Therapeutic potential of bacteriophage in treating *Klebsiella pneumoniae* B5055-mediated lobar pneumonia in mice. *J. Med. Microbiol.* 57, 1508–1513. doi: 10.1099/jmm.0.2008/002873-0

Chhibber, S., Kaur, T., and Sandeep, K. (2013). Co-therapy using lytic bacteriophage and linezolid: effective treatment in eliminating methicillin resistant Staphylococcus aureus (MRSA) from diabetic foot infections. *PLoS One* 8:e56022. doi: 10.1371/journal.pone.0056022

Chhibber, S., Shukla, A., and Kaur, S. (2017). Transfersomal Phage Cocktail Is an Effective Treatment against Methicillin-Resistant Staphylococcus aureus-Mediated Skin and Soft Tissue Infections. *Antimicrob. Agents Chemother.* 61, 2146–2116.e. doi: 10.1128/aac.02146-16

Colom, J., Cano-Sarabia, M., Otero, J., Cortés, P., Maspoch, D., and Llagostera, M. (2015). Liposome-Encapsulated Bacteriophages for Enhanced Oral Phage Therapy against *Salmonella* spp. *Appl. Environ. Microbiol.* 81, 4841–4849. doi: 10.1128/aem.00812-15

Dąbrowska, K. (2019). Phage therapy: What factors shape phage pharmacokinetics and bioavailability? Systematic and critical review. *Med. Res. Rev.* 39, 2000–2025. doi: 10.1002/med.21572

Dallal, M. M. S., Nikkhahi, F., Alimohammadi, M., Douraghi, M., Rajabi, Z., Foroushani, A. R., et al. (2019). Phage Therapy as an Approach to Control *Salmonella enterica* serotype Enteritidis Infection in Mice. *Rev. Soc. Bras. Med. Trop* 52:e20190290. doi: 10.1590/0037-8682-0290-2019

Daniel, A., Euler, C., Collin, M., Chahales, P., Gorelick, K. J., and Fischetti, V. A. (2010). Synergism between a novel chimeric lysin and oxacillin protects against infection by methicillin-resistant Staphylococcus aureus. *Antimicrob. Agents Chemother.* 54, 1603–1612. doi: 10.1128/aac.01625-09

Debarbieux, L., Leduc, D., Maura, D., Morello, E., Criscuolo, A., Grossi, O., et al. (2010). Bacteriophages can treat and prevent *Pseudomonas aeruginosa* lung infections. *J. Infect. Dis.* 201, 1096–1104. doi: 10.1086/651135

Díez-Martínez, R., De Paz, H. D., García-Fernández, E., Bustamante, N., Euler, C. W., Fischetti, V. A., et al. (2015). A novel chimeric phage lysin with high in vitro and in vivo bactericidal activity against Streptococcus pneumoniae. *J. Antimicrob. Chemother.* 70, 1763–1773. doi: 10.1093/jac/dkv038

Drilling, A., Morales, S., Boase, S., Jervis-Bardy, J., James, C., Jardeleza, C., et al. (2014). Safety and efficacy of topical bacteriophage and ethylenediaminetetraacetic acid treatment of Staphylococcus aureus infection in a sheep model of sinusitis. *Int. Forum Allergy Rhinol.* 4, 176–186. doi: 10.1002/alr.21270

Dufour, N., Clermont, O., La Combe, B., Messika, J., Dion, S., Khanna, V., et al. (2016). Bacteriophage LM33_P1, a fast-acting weapon against the pandemic ST131-O25b:H4 *Escherichia coli* clonal complex. *J. Antimicrob. Chemother.* 71, 3072–3080. doi: 10.1093/jac/dkw253

Dufour, N., Debarbieux, L., Fromentin, M., and Ricard, J. D. (2015). Treatment of Highly Virulent Extraintestinal Pathogenic *Escherichia coli* Pneumonia With Bacteriophages. *Crit. Care Med.* 43, 190–198.e. doi: 10.1097/ccm.0000000000000968

Dufour, N., Delattre, R., Chevallereau, A., Ricard, J. D., and Debarbieux, L. (2019). Phage Therapy of Pneumonia Is Not Associated with an Overstimulation of the Inflammatory Response Compared to Antibiotic Treatment in Mice. *Antimicrob. Agents Chemother.* 63, 379–319.e. doi: 10.1128/aac.00379-19

Eaton, M. D., and Bayne-Jones, S. (1934). Bacteriophage Therapy: Review of the Principles and Results of the Use of Bacteriophage in the Treatment of Infections. *J. Am. Med. Assoc.* 103, 1769–1776. doi: 10.1001/jama.1934.72750490003007

Forti, F., Roach, D. R., Cafora, M., Pasini, M. E., Horner, D. S., Fiscarelli, E. V., et al. (2018). Design of a Broad-Range Bacteriophage Cocktail That Reduces *Pseudomonas aeruginosa* Biofilms and Treats Acute Infections in Two Animal Models. *Antimicrob. Agents Chemother.* 62, 2573–2517 e. doi: 10.1128/aac.02573-17

Furusawa, T., Iwano, H., Hiyashimizu, Y., Matsubara, K., Higuchi, H., Nagahata, H., et al. (2016). Phage Therapy Is Effective in a Mouse Model of Bacterial Equine Keratitis. *Appl. Environ. Microbiol.* 82, 5332–5339. doi: 10.1128/aem.01166-16

Galtier, M., De Sordi, L., Maura, D., Arachchi, H., Volant, S., Dillies, M. A., et al. (2016). Bacteriophages to reduce gut carriage of antibiotic resistant uropathogens with low impact on microbiota composition. *Environ. Microbiol.* 18, 2237–2245. doi: 10.1111/1462-2920.13284

Geier, M. R., Trigg, M. E., and Merril, C. R. (1973). Fate of bacteriophage lambda in non-immune germ-free mice. *Nature* 246, 221–223. doi: 10.1038/246221a0

Ghose, C., Ly, M., Schwanemann, L. K., Shin, J. H., Atab, K., Barr, J. J., et al. (2019). The Virome of Cerebrospinal Fluid: Viruses Where We Once Thought There Were None. *Front. Microbiol.* 10:2061. doi: 10.3389/fmicb.2019.02061

Gindin, M., Febvre, H. P., Rao, S., Wallace, T. C., and Weir, T. L. (2019). Bacteriophage for Gastrointestinal Health (PHAGE) Study: Evaluating the Safety and Tolerability of Supplemental Bacteriophage Consumption. *J. Am. Coll. Nutr.* 38, 68–75. doi: 10.1080/07315724.2018.1483783

Globe Newswire (2020). *ContraFect Reports Fourth Quarter and Full Year 2019 Financial Results and Provides Business Update*. Available online at: https://www.globenewswire.com/news-release/2020/03/18/2002495/0/en/ContraFect-Reports-Fourth-Quarter-and-Full-Year-2019-Financial-Results-and-Provides-Business-Update.html (accessed on Dec 25, 2020).

Gordillo Altamirano, F. L., and Barr, J. J. (2019). Phage Therapy in the Postantibiotic Era. *Clin. Microbiol. Rev.* 32:30651225. doi: 10.1128/cmr.00066-18

Górski, A., Międzybrodzki, R., Borysowski, J., Dąbrowska, K., Wierzbicki, P., Ohams, M., et al. (2012). Phage as a modulator of immune responses: practical implications for phage therapy. *Adv. Virus Res.* 83, 41–71. doi: 10.1016/b978-0-12-394438-2.00002-5

Górski, A., Międzybrodzki, R., Łobocka, M., Głowacka-Rutkowska, A., Bednarek, A., Borysowski, J., et al. (2018). Phage Therapy: What Have We Learned? *Viruses* 10:288. doi: 10.3390/v10060288

Guang-Han, O., Leang-Chung, C., Vellasamy, K. M., Mariappan, V., Li-Yen, C., and Vadivelu, J. (2016). Experimental Phage Therapy for Burkholderia pseudomallei Infection. *PLoS One* 11:e0158213. doi: 10.1371/journal.pone.0158213

Hall, A. R., De Vos, D., Friman, V. P., Pirnay, J. P., and Buckling, A. (2012). Effects of sequential and simultaneous applications of bacteriophages on populations of *Pseudomonas aeruginosa* in vitro and in wax moth larvae. *Appl. Environ. Microbiol.* 78, 5646–5652. doi: 10.1128/aem.00757-12

Hatfull, G. F., and Hendrix, R. W. (2011). Bacteriophages and their genomes. *Curr. Opin. Virol.* 1, 298–303. doi: 10.1016/j.coviro.2011.06.009

Hawkins, C., Harper, D., Burch, D., Anggård, E., and Soothill, J. (2010). Topical treatment of *Pseudomonas aeruginosa* otitis of dogs with a bacteriophage mixture: a before/after clinical trial. *Vet. Microbiol.* 146, 309–313. doi: 10.1016/j.vetmic.2010.05.014

Hendrix, R. W. (2002). Bacteriophages: evolution of the majority. *Theor. Popul. Biol.* 61, 471–480. doi: 10.1006/tpbi.2002.1590

Henry, M., Lavigne, R., and Debarbieux, L. (2013). Predicting in vivo efficacy of therapeutic bacteriophages used to treat pulmonary infections. *Antimicrob. Agents Chemother.* 57, 5961–5968. doi: 10.1128/aac.01596-13

Heo, Y. J., Lee, Y. R., Jung, H. H., Lee, J., Ko, G., and Cho, Y. H. (2009). Antibacterial efficacy of phages against *Pseudomonas aeruginosa* infections in mice and Drosophila melanogaster. *Antimicrob. Agents Chemother.* 53, 2469–2474. doi: 10.1128/aac.01646-08

Heselpoth, R. D., Euler, C. W., Schuch, R., and Fischetti, V. A. (2019). Lysocins: Bioengineered Antimicrobials That Deliver Lysins across the Outer Membrane of Gram-Negative Bacteria. *Antimicrob. Agents Chemother.* 6:63. doi: 10.1128/aac.00342-19

Hodyra-Stefaniak, K., Lahutta, K., Majewska, J., Kaźmierczak, Z., Lecion, D., Harhala, M., et al. (2019). Bacteriophages engineered to display foreign peptides may become short-circulating phages. *Microb. Biotechnol.* 12, 730–741. doi: 10.1111/1751-7915.13414

Hodyra-Stefaniak, K., Miernikiewicz, P., Drapała, J., Drab, M., Jończyk-Matysiak, E., Lecion, D., et al. (2015). Mammalian Host-Versus-Phage immune response determines phage fate in vivo. *Sci. Rep.* 5:14802. doi: 10.1038/srep14802

Hua, Y., Luo, T., Yang, Y., Dong, D., Wang, R., Wang, Y., et al. (2017). Phage Therapy as a Promising New Treatment for Lung Infection Caused by Carbapenem-Resistant *Acinetobacter baumannii* in Mice. *Front. Microbiol.* 8:2659. doi: 10.3389/fmicb.2017.02659

Huff, W. E., Huff, G. R., Rath, N. C., and Donoghue, A. M. (2010). Immune interference of bacteriophage efficacy when treating colibacillosis in poultry. *Poult. Sci.* 89, 895–900. doi: 10.3382/ps.2009-00528

Hung, C. H., Kuo, C. F., Wang, C. H., Wu, C. M., and Tsao, N. (2011). Experimental phage therapy in treating *Klebsiella pneumoniae*-mediated liver abscesses and bacteremia in mice. *Antimicrob. Agents Chemother.* 55, 1358–1365. doi: 10.1128/aac.01123-10

Inchley, C. J. (1969). The actvity of mouse Kupffer cells following intravenous injection of T4 bacteriophage. *Clin. Exp. Immunol.* 5, 173–187.

Jaiswal, A., Koley, H., Mitra, S., Saha, D. R., and Sarkar, B. (2014). Comparative analysis of different oral approaches to treat *Vibrio cholerae* infection in adult mice. *Int. J. Med. Microbiol.* 304, 422–430. doi: 10.1016/j.ijmm.2014.02.007

Jamalludeen, N., Johnson, R. P., Shewen, P. E., and Gyles, C. L. (2009). Evaluation of bacteriophages for prevention and treatment of diarrhea due to experimental enterotoxigenic *Escherichia coli* O149 infection of pigs. *Vet. Microbiol.* 136, 135–141. doi: 10.1016/j.vetmic.2008.10.021

Jault, P., Leclerc, T., Jennes, S., Pirnay, J. P., Que, Y. A., Resch, G., et al. (2019). Efficacy and tolerability of a cocktail of bacteriophages to treat burn wounds infected by *Pseudomonas aeruginosa* (PhagoBurn): a randomised, controlled, double-blind phase 1/2 trial. *Lancet Infect. Dis.* 19, 35–45. doi: 10.1016/s1473-3099(18)30482-1

Jeon, J., Park, J. H., and Yong, D. (2019). Efficacy of bacteriophage treatment against carbapenem-resistant *Acinetobacter baumannii* in Galleria mellonella larvae and a mouse model of acute pneumonia. *BMC Microbiol.* 19:70. doi: 10.1186/s12866-019-1443-5

Jeon, J., Ryu, C. M., Lee, J. Y., Park, J. H., Yong, D., and Lee, K. (2016). In Vivo Application of Bacteriophage as a Potential Therapeutic Agent To Control OXA-66-Like Carbapenemase-Producing *Acinetobacter baumannii* Strains Belonging to Sequence Type 357. *Appl. Environ. Microbiol.* 82, 4200–4208. doi: 10.1128/aem.00526-16

Jun, J. W., Shin, T. H., Kim, J. H., Shin, S. P., Han, J. E., Heo, G. J., et al. (2014). Bacteriophage therapy of a Vibrio parahaemolyticus infection caused by a multiple-antibiotic-resistant O3:K6 pandemic clinical strain. *J. Infect. Dis.* 210, 72–78. doi: 10.1093/infdis/jiu059

Kaabi, S. A. G., and Musafer, H. K. (2019). An experimental mouse model for phage therapy of bacterial pathogens causing bacteremia. *Microb. Pathog.* 137:103770. doi: 10.1016/j.micpath.2019.103770

Kim, B. O., Kim, E. S., Yoo, Y. J., Bae, H. W., Chung, I. Y., and Cho, Y. H. (2019). Phage-Derived Antibacterials: Harnessing the Simplicity, Plasticity, and Diversity of Phages. *Viruses* 11:268. doi: 10.3390/v11030268

Kim, K. P., Cha, J. D., Jang, E. H., Klumpp, J., Hagens, S., Hardt, W. D., et al. (2008). PEGylation of bacteriophages increases blood circulation time and reduces T-helper type 1 immune response. *Microb. Biotechnol.* 1, 247–257. doi: 10.1111/j.1751-7915.2008.00028.x

Kishor, C., Mishra, R. R., Saraf, S. K., Kumar, M., Srivastav, A. K., and Nath, G. (2016). Phage therapy of staphylococcal chronic osteomyelitis in experimental animal model. *Indian J. Med. Res.* 143, 87–94. doi: 10.4103/0971-5916.178615

Kumar, A., Roberts, D., Wood, K. E., Light, B., Parrillo, J. E., Sharma, S., et al. (2006). Duration of hypotension before initiation of effective antimicrobial therapy is the critical determinant of survival in human septic shock. *Crit. Care Med.* 34, 1589–1596. doi: 10.1097/01.Ccm.0000217961.75225.E9

Kumari, S., Harjai, K., and Chhibber, S. (2010). Evidence to support the therapeutic potential of bacteriophage Kpn5 in burn wound infection caused by *Klebsiella pneumoniae* in BALB/c mice. *J. Microbiol. Biotechnol.* 20, 935–941. doi: 10.4014/jmb.0909.09010

Law, N., Logan, C., Yung, G., Furr, C. L., Lehman, S. M., Morales, S., et al. (2019). Successful adjunctive use of bacteriophage therapy for treatment of multidrug-resistant *Pseudomonas aeruginosa* infection in a cystic fibrosis patient. *Infection* 47, 665–668. doi: 10.1007/s15010-019-01319-0

Leshkasheli, L., Kutateladze, M., Balarjishvili, N., Bolkvadze, D., Save, J., Oechslin, F., et al. (2019). Efficacy of newly isolated and highly potent bacteriophages in a mouse model of extensively drug-resistant *Acinetobacter baumannii* bacteraemia. *J. Glob. Antimicrob. Resist.* 19, 255–261. doi: 10.1016/j.jgar.2019.05.005

Lesho, E. P., and Laguio-Vila, M. (2019). The Slow-Motion Catastrophe of Antimicrobial Resistance and Practical Interventions for All Prescribers. *Mayo. Clin. Proc.* 94, 1040–1047. doi: 10.1016/j.mayocp.2018.11.005

Leung, A. K. C., Leung, A. A. M., Wong, A. H. C., and Hon, K. L. (2019). Travelers' Diarrhea: A Clinical Review. *Rec. Pat. Inflamm. Aller. Drug Discov.* 13, 38–48. doi: 10.2174/1872213x13666190514105054

Lood, R., Winer, B. Y., Pelzek, A. J., Diez-Martinez, R., Thandar, M., Euler, C. W., et al. (2015). Novel phage lysin capable of killing the multidrug-resistant gram-negative bacterium *Acinetobacter baumannii* in a mouse bacteremia model. *Antimicrob. Agents Chemother.* 59, 1983–1991. doi: 10.1128/aac.04641-14

Manohar, P., Nachimuthu, R., and Lopes, B. S. (2018). The therapeutic potential of bacteriophages targeting gram-negative bacteria using Galleria mellonella infection model. *BMC Microbiol.* 18:97. doi: 10.1186/s12866-018-1234-4

McCallin, S., Sacher, J. C., Zheng, J., and Chan, B. K. (2019). Current State of Compassionate Phage Therapy. *Viruses* 11:343. doi: 10.3390/v11040343

Mendes, J. J., Leandro, C., Corte-Real, S., Barbosa, R., Cavaco-Silva, P., Melo-Cristino, J., et al. (2013). Wound healing potential of topical bacteriophage therapy on diabetic cutaneous wounds. *Wound Repair. Regen.* 21, 595–603. doi: 10.1111/wrr.12056

Merril, C. R., Scholl, D., and Adhya, S. L. (2003). The prospect for bacteriophage therapy in Western medicine. *Nat. Rev. Drug. Discov.* 2, 489–497. doi: 10.1038/nrd1111

Morello, E., Saussereau, E., Maura, D., Huerre, M., Touqui, L., and Debarbieux, L. (2011). Pulmonary bacteriophage therapy on *Pseudomonas aeruginosa* cystic fibrosis strains: first steps towards treatment and prevention. *PLoS One* 6:e16963. doi: 10.1371/journal.pone.0016963

Murray, B. E. (1994). Can antibiotic resistance be controlled? *N. Engl. J. Med.* 330, 1229–1230. doi: 10.1056/nejm199404283301710

Myelnikov, D. (2018). An Alternative Cure: The Adoption and Survival of Bacteriophage Therapy in the USSR, 1922-1955. *J. Hist. Med. Allied Sci.* 73, 385–411. doi: 10.1093/jhmas/jry024

Naghizadeh, M., Karimi Torshizi, M. A., Rahimi, S., and Dalgaard, T. S. (2019). Synergistic effect of phage therapy using a cocktail rather than a single phage in the control of severe colibacillosis in quails. *Poult. Sci.* 98, 653–663. doi: 10.3382/ps/pey414

Nale, J. Y., Chutia, M., Carr, P., Hickenbotham, P. T., and Clokie, M. R. (2016a). 'Get in Early'; Biofilm and Wax Moth (Galleria mellonella) Models Reveal New Insights into the Therapeutic Potential of Clostridium difficile Bacteriophages. *Front. Microbiol.* 7:1383. doi: 10.3389/fmicb.2016.01383

Nale, J. Y., Spencer, J., Hargreaves, K. R., Buckley, A. M., Trzepiński, P., Douce, G. R., et al. (2016b). Bacteriophage Combinations Significantly Reduce Clostridium difficile Growth In Vitro and Proliferation In Vivo. *Antimicrob. Agents Chemother.* 60, 968–981. doi: 10.1128/aac.01774-15

Oduor, J. M., Onkoba, N., Maloba, F., Arodi, W. O., and Nyachieo, A. (2016). Efficacy of lytic Staphylococcus aureus bacteriophage against multidrug-resistant Staphylococcus aureus in mice. *J. Infect. Dev. Ctries* 10, 1208–1213. doi: 10.3855/jidc.7931

Oechslin, F. (2018). Resistance Development to Bacteriophages Occurring during Bacteriophage Therapy. *Viruses* 10:351. doi: 10.3390/v10070351

Ooi, M. L., Drilling, A. J., Morales, S., Fong, S., Moraitis, S., Macias-Valle, L., et al. (2019). Safety and Tolerability of Bacteriophage Therapy for Chronic Rhinosinusitis Due to Staphylococcus aureus. *JAMA Otolaryngol. Head Neck Surg.* 145, 723–729. doi: 10.1001/jamaoto.2019.1191

Pabary, R., Singh, C., Morales, S., Bush, A., Alshafi, K., Bilton, D., et al. (2016). Antipseudomonal Bacteriophage Reduces Infective Burden and Inflammatory Response in Murine Lung. *Antimicrob. Agents Chemother.* 60, 744–751. doi: 10.1128/aac.01426-15

Petrovic Fabijan, A., Lin, R. C. Y., Ho, J., Maddocks, S., Ben Zakour, N. L., and Iredell, J. R. (2020). Safety of bacteriophage therapy in severe Staphylococcus aureus infection. *Nat. Microbiol.* 5, 465–472. doi: 10.1038/s41564-019-0634-z

Pouillot, F., Chomton, M., Blois, H., Courroux, C., Noelig, J., Bidet, P., et al. (2012). Efficacy of bacteriophage therapy in experimental sepsis and meningitis caused by a clone O25b:H4-ST131 *Escherichia coli* strain producing CTX-M-15. *Antimicrob. Agents Chemother.* 56, 3568–3575. doi: 10.1128/aac.06330-11

Prazak, J., Iten, M., Cameron, D. R., Save, J., Grandgirard, D., Resch, G., et al. (2019). Bacteriophages Improve Outcomes in Experimental Staphylococcus aureus Ventilator-associated Pneumonia. *Am. J. Respir. Crit. Care Med.* 200, 1126–1133. doi: 10.1164/rccm.201812-2372OC

Ramírez-Estrada, S., Borgatta, B., and Rello, J. (2016). *Pseudomonas aeruginosa* ventilator-associated pneumonia management. *Infect. Drug Resist.* 9, 7–18. doi: 10.2147/idr.S50669

Raya, R. R., Varey, P., Oot, R. A., Dyen, M. R., Callaway, T. R., Edrington, T. S., et al. (2006). Isolation and characterization of a new T-even bacteriophage, CEV1, and determination of its potential to reduce *Escherichia coli* O157:H7 levels in sheep. *Appl. Environ. Microbiol.* 72, 6405–6410. doi: 10.1128/aem.03011-05

Raz, A., Serrano, A., Hernandez, A., Euler, C. W., and Fischetti, V. A. (2019). Isolation of Phage Lysins That Effectively Kill *Pseudomonas aeruginosa* in Mouse Models of Lung and Skin Infection. *Antimicrob. Agents Chemother.* 63:31010858. doi: 10.1128/aac.00024-19

Regeimbal, J. M., Jacobs, A. C., Corey, B. W., Henry, M. S., Thompson, M. G., Pavlicek, R. L., et al. (2016). Personalized Therapeutic Cocktail of Wild Environmental Phages Rescues Mice from *Acinetobacter baumannii* Wound Infections. *Antimicrob. Agents Chemother.* 60, 5806–5816. doi: 10.1128/aac.02877-15

Rehman, S., Ali, Z., Khan, M., Bostan, N., and Naseem, S. (2019). The dawn of phage therapy. *Rev. Med. Virol.* 29:e2041. doi: 10.1002/rmv.2041

Roach, D. R., Leung, C. Y., Henry, M., Morello, E., Singh, D., Di Santo, J. P., et al. (2017). Synergy between the Host Immune System and Bacteriophage Is Essential for Successful Phage Therapy against an Acute Respiratory Pathogen. *Cell. Host. Microbe* 22, 38–47.e. doi: 10.1016/j.chom.2017.06.018

Rusckowski, M., Gupta, S., Liu, G., Dou, S., and Hnatowich, D. J. (2004). Investigations of a (99m)Tc-labeled bacteriophage as a potential infection-specific imaging agent. *J. Nucl. Med.* 45, 1201–1208.

Rusckowski, M., Gupta, S., Liu, G., Dou, S., and Hnatowich, D. J. (2008). Investigation of four (99m)Tc-labeled bacteriophages for infection-specific imaging. *Nucl. Med. Biol.* 35, 433–440. doi: 10.1016/j.nucmedbio.2008.02.011

Sarker, S. A., Sultana, S., Reuteler, G., Moine, D., Descombes, P., Charton, F., et al. (2016). Oral Phage Therapy of Acute Bacterial Diarrhea With Two Coliphage Preparations: A Randomized Trial in Children From Bangladesh. *EBioMedicine* 4, 124–137. doi: 10.1016/j.ebiom.2015.12.023

Schneider, G., Szentes, N., Horváth, M., Dorn, Á, Cox, A., Nagy, G., et al. (2018). Kinetics of Targeted Phage Rescue in a Mouse Model of Systemic *Escherichia coli* K1. *Biomed. Res. Int.* 2018:7569645. doi: 10.1155/2018/7569645

Schooley, R. T., Biswas, B., Gill, J. J., Hernandez-Morales, A., Lancaster, J., Lessor, L., et al. (2017). Development and Use of Personalized Bacteriophage-Based Therapeutic Cocktails To Treat a Patient with a Disseminated Resistant *Acinetobacter baumannii* Infection. *Antimicrob. Agents Chemother.* 61, 954–917.e. doi: 10.1128/aac.00954-17

Schuch, R., Lee, H. M., Schneider, B. C., Sauve, K. L., Law, C., Khan, B. K., et al. (2014). Combination therapy with lysin CF-301 and antibiotic is superior to antibiotic alone for treating methicillin-resistant Staphylococcus aureus-induced murine bacteremia. *J. Infect. Dis.* 209, 1469–1478. doi: 10.1093/infdis/jit637

Seed, K. D., and Dennis, J. J. (2009). Experimental bacteriophage therapy increases survival of Galleria mellonella larvae infected with clinically relevant strains of the Burkholderia cepacia complex. *Antimicrob. Agents Chemother.* 53, 2205–2208. doi: 10.1128/aac.01166-08

Semler, D. D., Goudie, A. D., Finlay, W. H., and Dennis, J. J. (2014). Aerosol phage therapy efficacy in Burkholderia cepacia complex respiratory infections. *Antimicrob. Agents Chemother.* 58, 4005–4013. doi: 10.1128/aac.02388-13

Seo, B. J., Song, E. T., Lee, K., Kim, J. W., Jeong, C. G., Moon, S. H., et al. (2018). Evaluation of the broad-spectrum lytic capability of bacteriophage cocktails against various *Salmonella* serovars and their effects on weaned pigs infected with *Salmonella* Typhimurium. *J. Vet. Med. Sci.* 80, 851–860. doi: 10.1292/jvms.17-0501

Shivaswamy, V. C., Kalasuramath, S. B., Sadanand, C. K., Basavaraju, A. K., Ginnavaram, V., Bille, S., et al. (2015). Ability of bacteriophage in resolving wound infection caused by multidrug-resistant *Acinetobacter baumannii* in uncontrolled diabetic rats. *Microb. Drug Resist.* 21, 171–177. doi: 10.1089/mdr.2014.0120

Shivshetty, N., Hosamani, R., Ahmed, L., Oli, A. K., Sannauallah, S., Sharanbassappa, S., et al. (2014). Experimental protection of diabetic mice against Lethal P. aeruginosa infection by bacteriophage. *Biomed. Res. Int.* 2014:793242. doi: 10.1155/2014/793242

Singla, S., Harjai, K., Katare, O. P., and Chhibber, S. (2015). Bacteriophage-loaded nanostructured lipid carrier: improved pharmacokinetics mediates effective resolution of *Klebsiella pneumoniae*-induced lobar pneumonia. *J. Infect. Dis.* 212, 325–334. doi: 10.1093/infdis/jiv029

Smith, H. W., and Huggins, M. B. (1982). Successful treatment of experimental *Escherichia coli* infections in mice using phage: its general superiority over antibiotics. *J. Gen. Microbiol.* 128, 307–318. doi: 10.1099/00221287-128-2-307

Smith, H. W., and Huggins, M. B. (1983). Effectiveness of phages in treating experimental *Escherichia coli* diarrhoea in calves, piglets and lambs. *J. Gen. Microbiol.* 129, 2659–2675. doi: 10.1099/00221287-129-8-2659

Smith, H. W., Huggins, M. B., and Shaw, K. M. (1987). The control of experimental *Escherichia coli* diarrhoea in calves by means of bacteriophages. *J. Gen. Microbiol.* 133, 1111–1126. doi: 10.1099/00221287-133-5-1111

Soothill, J. S. (1992). Treatment of experimental infections of mice with bacteriophages. *J. Med. Microbiol.* 37, 258–261. doi: 10.1099/00222615-37-4-258

Soothill, J. S. (1994). Bacteriophage prevents destruction of skin grafts by *Pseudomonas aeruginosa*. *Burns* 20, 209–211. doi: 10.1016/0305-4179(94)90184-8

Stone, R. (2002). Bacteriophage therapy. *Stalin's forgotten cure*. *Science* 298, 728–731. doi: 10.1126/science.298.5594.728

Tacconelli, E., Carrara, E., Savoldi, A., Harbarth, S., Mendelson, M., Monnet, D., et al. (2017). Discovery, research, and development of new antibiotics: The WHO priority list of antibiotic-resistant bacteria and tuberculosis. *Lancet Infect. Dis.* 18, 318–327. doi: 10.1016/S1473-3099(17)30753-3

Takemura-Uchiyama, I., Uchiyama, J., Osanai, M., Morimoto, N., Asagiri, T., Ujihara, T., et al. (2014). Experimental phage therapy against lethal lung-derived septicemia caused by Staphylococcus aureus in mice. *Microbes Infect.* 16, 512–517. doi: 10.1016/j.micinf.2014.02.011

Tang, F., Zhang, P., Zhang, Q., Xue, F., Ren, J., Sun, J., et al. (2019). Isolation and characterization of a broad-spectrum phage of multiple drug resistant *Salmonella* and its therapeutic utility in mice. *Microb. Pathog.* 126, 193–198. doi: 10.1016/j.micpath.2018.10.042

Tanji, Y., Shimada, T., Fukudomi, H., Miyanaga, K., Nakai, Y., and Unno, H. (2005). Therapeutic use of phage cocktail for controlling *Escherichia coli* O157:H7 in gastrointestinal tract of mice. *J. Biosci. Bioeng.* 100, 280–287. doi: 10.1263/jbb.100.280

Tenover, F. C., and McGowan, J. E. Jr. (1996). Reasons for the emergence of antibiotic resistance. *Am. J. Med. Sci.* 311, 9–16. doi: 10.1097/00000441-199601000-00003

Tie, K., Yuan, Y., Yan, S., Yu, X., Zhang, Q., Xu, H., et al. (2018). Isolation and identification of *Salmonella* pullorum bacteriophage YSP2 and its use as a therapy for chicken diarrhea. *Virus Gen.* 54, 446–456. doi: 10.1007/s11262-018-1549-0

Trigo, G., Martins, T. G., Fraga, A. G., Longatto-Filho, A., Castro, A. G., Azeredo, J., et al. (2013). Phage therapy is effective against infection by Mycobacterium ulcerans in a murine footpad model. *PLoS Negl. Trop Dis.* 7:e2183. doi: 10.1371/journal.pntd.0002183

Uchiyama, J., Maeda, Y., Takemura, I., Chess-Williams, R., Wakiguchi, H., and Matsuzaki, S. (2009). Blood kinetics of four intraperitoneally administered therapeutic candidate bacteriophages in healthy and neutropenic mice. *Microbiol. Immunol.* 53, 301–304. doi: 10.1111/j.1348-0421.2009.00125.x

Uchiyama, J., Rashel, M., Takemura, I., Wakiguchi, H., and Matsuzaki, S. (2008). In silico and in vivo evaluation of bacteriophage phiEF24C, a candidate for treatment of Enterococcus faecalis infections. *Appl. Environ. Microbiol.* 74, 4149–4163. doi: 10.1128/aem.02371-07

Viertel, T. M., Ritter, K., and Horz, H. P. (2014). Viruses versus bacteria-novel approaches to phage therapy as a tool against multidrug-resistant pathogens. *J. Antimicrob. Chemother.* 69, 2326–2336. doi: 10.1093/jac/dku173

Vouillamoz, J., Entenza, J. M., Giddey, M., Fischetti, V. A., Moreillon, P., and Resch, G. (2013). Bactericidal synergism between daptomycin and the phage lysin Cpl-1 in a mouse model of pneumococcal bacteraemia. *Int. J. Antimicrob. Agents* 42, 416–421. doi: 10.1016/j.ijantimicag.2013.06.020

Walker, P. J., Siddell, S. G., Lefkowitz, E. J., Mushegian, A. R., Dempsey, D. M., Dutilh, B. E., et al. (2019). Changes to virus taxonomy and the International Code of Virus Classification and Nomenclature ratified by the International Committee on Taxonomy of Viruses (2019). *Arch. Virol.* 164, 2417–2429. doi: 10.1007/s00705-019-04306-w

Wang, J., Hu, B., Xu, M., Yan, Q., Liu, S., Zhu, X., et al. (2006b). Use of bacteriophage in the treatment of experimental animal bacteremia from imipenem-resistant *Pseudomonas aeruginosa*. *Int. J. Mol. Med.* 17, 309–317.

Wang, J., Hu, B., Xu, M., Yan, Q., Liu, S., Zhu, X., et al. (2006a). Therapeutic effectiveness of bacteriophages in the rescue of mice with extended spectrum beta-lactamase-producing *Escherichia coli* bacteremia. *Int. J. Mol. Med.* 17, 347–355.

Watanabe, R., Matsumoto, T., Sano, G., Ishii, Y., Tateda, K., Sumiyama, Y., et al. (2007). Efficacy of bacteriophage therapy against gut-derived sepsis caused by *Pseudomonas aeruginosa* in mice. *Antimicrob. Agents Chemother.* 51, 446–452. doi: 10.1128/aac.00635-06

Waters, E. M., Neill, D. R., Kaman, B., Sahota, J. S., Clokie, M. R. J., Winstanley, C., et al. (2017). Phage therapy is highly effective against chronic lung infections with *Pseudomonas aeruginosa*. *Thorax* 72, 666–667. doi: 10.1136/thoraxjnl-2016-209265

Wills, Q. F., Kerrigan, C., and Soothill, J. S. (2005). Experimental bacteriophage protection against Staphylococcus aureus abscesses in a rabbit model. *Antimicrob. Agents Chemother.* 49, 1220–1221. doi: 10.1128/aac.49.3.1220-1221.2005

World Bank Group (2017). *Drug-resistant infections: a threat to our economic future*. Washington: World Bank.

Wright, A., Hawkins, C. H., Anggård, E. E., and Harper, D. R. (2009). A controlled clinical trial of a therapeutic bacteriophage preparation in chronic otitis due to antibiotic-resistant *Pseudomonas aeruginosa*; a preliminary report of efficacy. *Clin. Otolaryngol.* 34, 349–357. doi: 10.1111/j.1749-4486.2009.01973.x

Yang, M., Du, C., Gong, P., Xia, F., Sun, C., Feng, X., et al. (2015). Therapeutic effect of the YH6 phage in a murine hemorrhagic pneumonia model. *Res. Microbiol.* 166, 633–643. doi: 10.1016/j.resmic.2015.07.008

Yen, M., Cairns, L. S., and Camilli, A. (2017). A cocktail of three virulent bacteriophages prevents *Vibrio cholerae* infection in animal models. *Nat. Commun.* 8:14187. doi: 10.1038/ncomms14187

Conflict of Interest: The authors declare that the research was conducted in the absence of any commercial or financial relationships that could be construed as a potential conflict of interest.

Copyright © 2021 Penziner, Schooley and Pride. This is an open-access article distributed under the terms of the Creative Commons Attribution License (CC BY). The use, distribution or reproduction in other forums is permitted, provided the original author(s) and the copyright owner(s) are credited and that the original publication in this journal is cited, in accordance with accepted academic practice. No use, distribution or reproduction is permitted which does not comply with these terms.

frontiers in Microbiology

REVIEW
published: 28 January 2021
doi: 10.3389/fmicb.2021.638094

Potential of Therapeutic Bacteriophages in Nosocomial Infection Management

Nannan Wu[1]* *and Tongyu Zhu*[1,2]*

[1] Shanghai Institute of Phage, Shanghai Public Health Clinical Center, Fudan University, Shanghai, China, [2] Shanghai Key Laboratory of Organ Transplantation, Zhongshan Hospital, Fudan University, Shanghai, China

Nosocomial infections (NIs) are hospital-acquired infections which pose a high healthcare burden worldwide. The impact of NIs is further aggravated by the global spread of antimicrobial resistance (AMR). Conventional treatment and disinfection agents are often insufficient to catch up with the increasing AMR and tolerance of the pathogenic bacteria. This has resulted in a need for alternative approaches and raised new interest in therapeutic bacteriophages (phages). In contrast to the limited clinical options available against AMR bacteria, the extreme abundance and biodiversity of phages in nature provides an opportunity to establish an ever-expanding phage library that collectively provides sustained broad-spectrum and poly microbial coverage. Given the specificity of phage-host interactions, phage susceptibility testing can serve as a rapid and cost-effective method for bacterial subtyping. The library can also provide a database for routine monitoring of nosocomial infections as a prelude to preparing ready-to-use phages for patient treatment and environmental sterilization. Despite the remaining obstacles for clinical application of phages, the establishment of phage libraries, pre-stocked phage vials prepared to good manufacturing practice (GMP) standards, and pre-optimized phage screening technology will facilitate efforts to make phages available as modern medicine. This may provide the breakthrough needed to demonstrate the great potential in nosocomial infection management.

Keywords: antimicrobial resistance, nosocomial infections, phage library, phage therapy, disinfection

OPEN ACCESS

Edited by:
Xuesong He,
The Forsyth Institute, United States

Reviewed by:
Hang Yang,
Chinese Academy of Sciences, China
Paul Hyman,
Ashland University, United States

***Correspondence:**
Nannan Wu
wunannan@shphc.org.cn
Tongyu Zhu
tyzhu@shphc.org.cn

Specialty section:
This article was submitted to Virology, a section of the journal Frontiers in Microbiology

Received: *05 December 2020*
Accepted: *11 January 2021*
Published: *28 January 2021*

Citation:
Wu N and Zhu T (2021) Potential of Therapeutic Bacteriophages in Nosocomial Infection Management. Front. Microbiol. 12:638094. doi: 10.3389/fmicb.2021.638094

INTRODUCTION

Nosocomial infections (NIs), also known as hospital-acquired infections (HAI), are infections that are newly acquired in a hospital or other healthcare facility. They arise from various sources including healthcare staff, contaminated equipment, bed linen, and air droplets. NIs represent the most frequent adverse events during care delivery and typically result in prolonged hospital stays. There can be massive additional costs for health systems and patients, and unnecessary deaths (Allegranzi et al., 2011).

The misuse and overuse of antibiotics are accelerating the creation of antimicrobial resistance (AMR), which has become a major public health problem. In 2017, the World Health Organization (WHO) highlighted, as a global priority, a list of multidrug-resistant (MDR) bacterial pathogens (informally termed "superbugs") to help in prioritizing the research and development of new and effective antibiotic treatments (World Health Organization, 2017).

These healthcare-associated superbugs usually cause nosocomial outbreaks and opportunistic infections in hospitalized patients. The most prominent causative agents are carbapenem-resistant *Enterobacteriaceae* (CRE), carbapenem-resistant *Acinetobacter baumannii* (CRAB), MDR *Pseudomonas aeruginosa*, methicillin-resistant *Staphylococcus aureus* (MRSA), and vancomycin-resistant *Enterococcus* (VRE). In the absence of effective treatment for bacterial infections that have AMR, modern medical care becomes inadequate and the infections persist in the body, increasing the risk of spread to others. Even worse, increasing global connectivity facilitates the rapid transport of infectious agents and their resistance genes through the world (Mellon et al., 2020).

NIs pose a high healthcare burden in both developed and developing countries (Allegranzi et al., 2011), this problem is further aggravated by the global spread of multidrug-resistant organisms (MDROs), complicating infection management, limiting therapy options and resulting in poorer outcomes (Laxminarayan et al., 2013; Chng et al., 2020). The increasing AMR in bacteria has entailed a need for alternative approaches to therapy and prophylaxis of these infections and raised new interest in therapeutic bacteriophages (phages) for these purposes. Phages are viruses that exclusively infect bacteria and were used therapeutically against bacterial diseases almost immediately after their discovery. The extreme abundance and biodiversity of phages in our surroundings and inside our bodies constitute a source of natural precision agents for bactericidal use, which might play a major role in tackling the global AMR crisis. Despite the remaining obstacles for phage therapy such as regulatory issues and bacterial anti-phage resistance, efforts to make it available as modern medicine are ongoing. In fact, the potential of phages in clinical practice goes beyond therapeutic applications, it could be involved in the whole process of nosocomial infection management. In this review, we discuss the potential of therapeutic phages in nosocomial infection monitoring, phage therapy, and environmental disinfection. We also propose a practical model of nosocomial infection management that uses phages.

ESTABLISHING A PHAGE LIBRARY WITH BROAD-SPECTRUM AND POLY ANTIMICROBIAL COVERAGE

A key precondition in phage application is an eligible phage library (phage bank) with broad-spectrum, poly antimicrobial properties, where many well-characterized phages are constantly collected and arranged according to the host species. Although an increasing number of phage libraries has been established recently, the overall scale is small and the information in most of the existing phage collections is incomplete (**Table 1**) (Yerushalmy et al., 2020). This strongly limits wide access to phage therapy since not all patients can afford the time-consuming process of mailing pathogenic bacteria from a healthcare facility to a phage repository, followed by screening lytic phages and mailing therapeutic phages back; neither can they afford time for *de novo* phage screening from nature. For this reason, both the quantity and quality of phage libraries need enhancement.

A first step to build a phage library is to prepare a library of pathogenic bacteria that provides the baits for phage hunting. Phages can be isolated from diverse environmental samples, however, not all phages are useful for therapeutic use. Criteria of eligible phage candidates have been extensively discussed and, although estimates of index values vary among groups, there's a general consensus that the key features that must be characterized include: host species, complete genome sequence (to exclude or to allow modification of phages with known integration/toxic/resistance genes), host range testing, and high lytic activity (Gill and Hyman, 2010; Letarov and Kulikov, 2018; Merabishvili et al., 2018). Some other factors such as high yield, identified receptor, morphology, anti-biofilm activity, low resistance induction, stability during storage, and pre-clinical evaluation (e.g., safety, efficacy, pharmacodynamics and pharmacokinetics, human immune responses) are generally considered to be important during optimization of phages for therapeutics (Malik et al., 2017; D´abrowska and Abedon, 2019; Hesse and Adhya, 2019; Kortright et al., 2019; Yerushalmy et al., 2020).

In contrast to the limited number of antibiotics available, the extreme abundance and biodiversity of phages in nature make it possible to build an ever-expanding phage library that collectively provides sustained broad-spectrum and poly microbial coverage against the most common nosocomial pathogens such as the ESKAPE group (*E. faecium, S. aureus, K. pneumoniae, A. baumannii, P. aeruginosa*, and *Enterobacter* species) (Rice, 2008). However, given the diversity of phage-host interactions, isolation of suitable phages for some group of pathogenic bacteria has been found to be difficult (Mattila et al., 2015). For instance, almost all known phages against *Helicobacter Pylori* and *Clostridia difficile* are temperate (Hargreaves et al., 2015; Muñoz et al., 2020). Phage engineering and technical improvement on new phage isolation will be helpful to overcome these obstacles. The collaboration and sharing of phage libraries initiated by the Phage Directory (https://phage.directory) are also conducive to pool a global-scale phage library and to connect demands for therapeutic phages.

CONSTRUCTING A NOSOCOMIAL INFECTION MONITORING DATABASE BY USING PHAGE SUSCEPTIBILITY PROFILES

Rapid tracking of pathogen sources with appropriate subtyping tools and immediate initiation of appropriate antibacterial treatment are crucial in the management of nosocomial infections. However, conventional bacterial genotyping methods such as pulse-field gel electrophoresis (PFGE), multi-locus variable tandem repeat analysis (MLVA), multilocus-sequence typing (MLST), and whole-genome sequencing (WGS) are time-consuming, normally needing more than three workdays to yield results. In contrast, bacterial phenotypic technics

TABLE 1 | Phage libraries worldwide*.

Organization	Region	Size	Targets	References	Representative phage therapy reports	Clinical trial
Bioresource Centers						
The Felix d'Hérelle Reference Center for Bacterial Viruses	Canada	>400	A few dozen hosts	https://www.phage.ulaval.ca/en/phages-catalog/	Not applicable	Not applicable
German Collection of Microorganisms and Cell Cultures-Bacteriophages	Germany	415	A few dozen hosts	https://www.dsmz.de/collection/	Not applicable	Not applicable
The National Collection of Type Cultures-Bacteriophages	UK	>100	*Campylobacter, Staphylococcus, Streptococcus*	https://www.phe-culturecollections.org.uk/	Not applicable	Not applicable
American Type Culture Collection-Bacteriophages	US	~500	A few dozen hosts	https://www.atcc.org/	Not applicable	Not applicable
Non-profit organizations						
George Eliava Institute-Phage and Strain Collection	Georgia	>1000	180 bacterial species of 44 genera	http://eliava-institute.org/bacterial-strain-and-phage-collection/	Hoyle et al., 2018; Leitner et al., 2020	NCT03140085
Phage Therapy Unit-Bacteriophage Collection	Poland	>850	15 genera of the most common bacterial human pathogens	http://www.iitd.pan.wroc.pl/en/OTF/ZasadyTerapiiFagowej.html	Rostkowska et al., 2020; Żaczek et al., 2020	NCT00945087
Center for Phage Technology	US	Unknown	Unknown	https://cpt.tamu.edu/phage-therapy-projects/	Schooley et al., 2017	Not applicable
Pittsburgh Bacteriophage Institute-Actinobacteriophage Database	US	>15000	Species from *Actinobacteria* phylum	https://phagesdb.org/phages/	Dedrick et al., 2019	Not applicable
Yale University-Phage library	US	Unknown	11 species/genera of the most common bacterial human pathogens	http://www.benjaminchanphd.com/	Chan et al., 2018	NCT04636554
Fagenbank Phage Collection	Netherland	Unknown	9 species of the most common bacterial human pathogens	https://www.fagenbank.nl/	Not found	Not found
Bacteriophage Bank of Korea	Korea	>1000	21 species of the most common bacterial human pathogens	http://www.phagebank.or.kr/	Not found	Not found
Shanghai Institute of Phage-SIPhage Library	China	>600	ESKAPE, *Mycobacterium*	http://www.sipmed.cn/	Bao et al., 2020	ChiCTR1900020989, ChiCTR2000036801, ChiCTR2000037365
Hebrew University-Israeli Phage Bank	Israel	>300	16 different species	https://ronenhazanlab.wixsite.com/hazanlab/the-404-israeli-phage-bank	Nir-Paz et al., 2019	Not found
Phage companies						
Microgen-Bacteriophages Products	Russia	Unknown	The most common bacterial human pathogens	https://www.microgen.ru/en/products/bakteriofagi/	Sarker et al., 2017; McCallin et al., 2018	NCT04325685
Intralytix-Human phage therapy products	US	Unknown	*E. coli, Shigellosis,* Women's health associated bacteria, *Enterococcus*	http://intralytix.com/index.php?page = hum	Not found	NCT03808103
Armata Pharmaceuticals	US	Unknown	The most common bacterial human pathogens	https://www.armatapharma.com/pipeline/pipeline-overview/	Schooley et al., 2017; Aslam et al., 2019; Maddocks et al., 2019	NCT04596319, NCT03395769, NCT02757755, ACTRN12616000002482

(Continued)

TABLE 1 | Continued

Organization	Region	Size	Targets	References	Representative phage therapy reports	Clinical trial
Locus Biosciences	US	Unknown	Multiple bacterial human pathogens	https://www.locus-bio.com/#pipeline	Not found	NCT04191148
Adaptive phage therapy-Phage Bank	US	Unknown	ESKAPE, *Burkholderia cepacia*	https://www.aphage.com/science/	Schooley et al., 2017; Aslam et al., 2019; Duplessis et al., 2019	NCT04636554, NCT04287478
Pherecydes Pharma	France	Unknown	Multiple bacterial human pathogens	https://www.pherecydes-pharma.com/	Ferry et al., 2018; Jault et al., 2019; Ferry et al., 2020	NCT02116010, NCT02664740
BiomX	Israel	Unknown	*Cutibacterium acnes, K. pneumoniae, P. aeruginosa, S. aureus, F. nucleatum*	https://www.biomx.com/pipeline/	Not found	BX001 against acne Phase I completed under cosmetic route
Phagelux	China	Unknown	*K. pneumoniae, P. aeruginosa, Staphylococcus, P. Acnes*	http://www.phagelux.com/	Not found	NCT04287478

**Data isolated from the corresponding website up to 30th Nov, 2020; Armata Pharmaceuticals was merged between C3J and AmpliPhi in 2019.*
The Clinical trial numbers beginning with NCT refer to clinical trials registered on ClinicalTrials.gov (https://clinicaltrials.gov/), ChiCTR trials registered on Chinese Clinical Trial Registry (http://www.chictr.org.cn/), ACTRN trials registered on Australian New Zealand Clinical Trial Registry (https://www.anzctr.org.au/).

TABLE 2 | Overview of common bacterial subtyping methods*.

Method	Application scenarios	Subtype discrimination accuracy	Time to results from a colony	Commercial availability	Relative cost
Phenotypic subtyping					
Antibiotic susceptibility test	To select effective antimicrobial drugs.	Worse than DNA-based methods.	1–2 days	Yes (Laboratory medicine)	Low
Phage susceptibility test	To select effective lytic phages.	May perform better than PFGE/MLST for some bacteria but worse for others.	1–2 days	No*	Medium
Immunological test	To applied for the preliminary identification.	Typically worse than DNA-based methods.	<1 day	Yes (Laboratory medicine)	Medium
DNA-based subtyping					
Pulsed-field gel electrophoresis (PFGE)	To subtype bacterial species causing infection outbreaks	Gold-standard for many different bacteria	3–4 days	Yes	High
Multiple locus variable number of tandem repeats analysis (MLVA)	Usually been performed for more subtyping details after PFGE.	May perform better than PFGE for some bacteria but worse for others	1–2 days	No	Medium
Multilocus sequence typing (MLST)	To characterize bacterial populations at larger geographic and temporal scales	Typically worse than PFGE	>3 days (send out sequencing)	Yes	High
Whole-genome sequencing (WGS)	To cluster isolates for bacterial outbreak analysis.	Best discrimination among molecular subtyping approaches	2–4 weeks (send out sequencing)	Yes	High

**Mayo Clinic Laboratories (US) and Dr Dangs Lab (India) have announced to commercialize phage susceptibility test in 2020 (Adaptive Phage Therapeutics, 2020a; ANI, 2020).*

such as antibiotic susceptibility test, immunological methods (serotyping), or phage-typing are limited in discriminatory power but advantageous to save time (**Table 2**; Ferrari et al., 2017; Quainoo et al., 2017; Sloan et al., 2017; Vijayakumar et al., 2019). For the most common nosocomial pathogens which grow fast, a phage-typing can be achieved within six to eight hours by phage susceptibility testing.

A phage susceptibility test is a method followed by bacterial diagnosis, to simultaneously test the contents of a sub-library (specific to the target bacterial species) of

phage candidates against the bacteria isolated from a patient, thereby identifying phages for patient-specific precision therapy. Laboratory-developed phage susceptibility tests are widely used for therapeutic phage screening (Aslam et al., 2019; Dedrick et al., 2019; Kuipers et al., 2019; Nir-Paz et al., 2019; Bao et al., 2020; Petrovic Fabijan et al., 2020). Additionally, given the specificity of phage-host interactions, the distinguished phage susceptibility profiles can enable rapid fingerprinting of bacterial substrains. Several laboratories have applied this method to investigate outbreaks caused by nosocomial or foodborne bacterial pathogens (Demczuk et al., 2003; Boxrud et al., 2007; Cooke et al., 2010; Barco et al., 2013; Wuyts et al., 2015). However, due to the variable sizes and components among phage libraries, phage-typing is limited in discriminatory power than genotyping approaches. It needs standardization to guarantee comparability among laboratories, as well as methodology optimization to reduce labor costs (Ferrari et al., 2017).

Nevertheless, on the basis of known epidemiological situations and pre-established phage collections, phage susceptibility testing may serve as a rapid and cost-effective method for bacterial subtyping to routinely monitor nosocomial infections. It may also be a prelude to preparing ready-to-use phages for patient treatment and environmental sterilization. Data from several preliminary studies have shown good concordance of profiles between phage-typing and other subtyping methods in distinguishing bacterial isolates (Demczuk et al., 2003; Crabb et al., 2019; Sundell et al., 2019). However, the possibility of frequent shifts in phage susceptibility profiles of phage-resistant strains should be allowed for, especially by the medical establishments with an ongoing phage therapy practice. Nevertheless, a database of routine phage-typing profiles helps by providing an expandable reference map that can be adjusted based on conventional molecular genotyping methods. With further improvements in the phage library diversity and in understanding phage-bacteria interaction, hospital-wide surveys employing the phage-typing database will be increasingly feasible, providing valuable information for infection control and eventually becoming part of routine practice.

PHAGE THERAPY THAT TARGETS THE PROBLEMATIC BACTERIAL PATHOGENS

Fixed composition (*prêt-à-porter*) or customized screened (*sur-mesure*), that is the question for therapeutic phage selection (Pirnay et al., 2011). Fixed composition, which is a stable and widely distributed phage preparation, is more adaptive for the modern pharmaceutical regulations than a customized screened phage preparation (*sur-mesure*). However, due to the high species/strain specificity of phages and the frequently evolving phage resistance in bacteria, it is difficult for a fixed phage cocktail to provide broad coverage on clinical strains. There have been some well-conducted clinical trials on the effectiveness of fixed phage cocktails but they have failed to obtain positive results (Markoishvili et al., 2002; Wright et al., 2009; Gindin et al., 2019; Jault et al., 2019; Leitner et al., 2020).

In parallel with full-scale clinical trials, lessons learned from *sur-mesure* case studies have been reported by numerous groups all over the world. These efforts have advanced medicinal phage technologies and highlighted safety and efficacy of phage therapy (**Table 3**; Luong et al., 2020; Pires et al., 2020). However, the *sur-mesure* approach is not well compatible with modern licensing processes. The European Medicines Agency (EMA) and the US Food and Drug Administration (FDA) placed phages under the medicinal (biologicals) product regulation; this means that marketing a phage product requires proof of safety and efficacy, also of quality by manufacture under Good Manufacturing Practice (GMP) regulations (Pires et al., 2020).

The good news is that some small companies focused on phage-specific therapies are growing fast and some authorities have been open to rigorously controlled clinical phage applications. Despite the long way to go before general approval is reached for the use of phage therapy, recent progress in phage manufacturing and quality control has revitalized phage therapy worldwide. Notably, the FDA has approved several investigational phage therapy pipelines targeting prosthetic joint infection, urinary/genital tract infection, chronic wound infection, and secondary bacterial pneumonia under the Investigational New Drug (IND) allowance (Adaptive Phage Therapeutics, 2020b; Armata Therapeuticals, 2020; Intralytix, 2020; Phagelux, 2020).

PHAGE DISINFECTION FOR NOSOCOMIAL TRANSMISSION CONTROL

Good infection prevention practices such as hand hygiene, daily and terminal cleaning, and disinfection have been demonstrated to reduce the incidence of healthcare-associated infections (Ariza-Heredia and Chemaly, 2018; Mitchell et al., 2019). However, conventional disinfection methods such as ultraviolet and chemical agents (e.g., hydrogen peroxide, chlorine-derivatives) are often insufficient to cope with the increasing complexity and tolerance of the target bacteria. The application context and frequency are limited by the presence of the patient in the room. The concentration of chemical disinfectants needs to be constrained to a narrow range to balance the disinfection effectiveness and the level of harmful residuals and byproducts (Dong et al., 2019). In consequence, pathogenic bacteria can rapidly recolonize the environmental surface after disinfection (Laxminarayan et al., 2013; Weber et al., 2019).

Meanwhile, there has been great interest in developing novel sterilizing methods, such as "self-disinfecting" surfaces, continuous room disinfection with diluted chemical sterilant, and other reagents (Weber et al., 2019). Among these, the potential of phages in environmental disinfection has been long neglected but is now being applied in food processing workshops, livestock farms, and croplands (Holtappels et al., 2020; Pinto et al., 2020; Żbikowska et al., 2020). Phage disinfectants possess multiple advantages over conventional ones: first, phages are a very abundant microbial resource

TABLE 3 | Pros and cons of phage therapy.

	Antibiotic therapy	Phage therapy		
		Pros	**Cons**	**Solutions or optimizations**
Number of agents	Less than 30 antibiotics available	Expansible	Higher screening cost, Longer time between diagnosis and treatment	Pre-collected phage library and high-throughput screening technology
Antimicrobial spectrum	Broad spectrum	High species or strain specificity, limited impact on microbiome	Pathogenic bacterial strains are required to allow for a logical and customized phage screening	Phage cocktail, combined treatment with other antimicrobials
Anti-biofilms activity	Non/low effective	Some can penetrate and destroy biofilms	Phage's anti-biofilm activity is very specific and need to be pre-tested	Combined use of biofilm-destroyed phages with different depolymerases, as well as with other anti-biofilm agents
de novo resistance	Normally occurs slowly during antibiotic treatment	Phage can co-evolve to infect resistant bacteria	Rapid evolution of bacterial anti-phage resistance	Phage cocktail, combined treatment with other antimicrobials
Dosing	Constant dose and course of treatment	Self-amplifying in target bacteria	Floating dose and course of treatment	Need to be standardized and quantified
Safety	Safe under rational use	Generally recognized as safe, do not target eukaryotic cell and can be eradicated by immune system	Relatively fewer evidence from strict clinical trials, Phage-neutralizing antibody induced	Substitute new lytic phages for a new course of treatment
Adverse effect	Multiple side effects (e.g., intestinal disorders, allergies, organ toxicity) have been reported	Side effects attributed to phage therapy have rarely been described	Removal of bacterial debris and toxins during production is prerequisite	Phages need to be produced under Good Manufacturing Practices facilities with similar regulations for pharmaceutical products
Efficacy to sensitive bacteria	Supported by standard clinical trials	Adequate evidences from case studies	Lack of large-scale clinical investigations	Large-scale of standard clinical trials are needed.
Regulatory pathway	Slow but rules-based development process to ensure safety and efficacy	Rapid discovery process	Require innovative regulations for approving and manufacturing	Approve qualified phage collections as drug components
Clinical acceptability	Widely accepted for infection prophylaxis and treatment	Phage lysis capacity uncorrelated with bacterial drug-resistance level	Typically used only as a last-resort treatment	Mass education, apply phages to prophylaxis, early intervention and environmental sterilization

that holds great promise and options for targeting problematic bacteria such as those with multiple AMR or biofilm formation properties. Second, phages are species-specific viruses of prokaryotes and do not infect mammalian cells, which allows disinfection unlimited by frequency or by the presence of the patient in the room. Consequently, phage application has been proposed as a potential decontamination method for hospital surfaces and water systems (Jensen et al., 2015; Mathieu et al., 2019).

Recently, there has been a trickle of studies that demonstrated the efficacy of phages to rapidly decrease the load of pathogens commonly associated with nosocomial infections when they are present on different types of surfaces and aqueous systems in healthcare facilities (Ho et al., 2016; D'Accolti et al., 2019; Tseng et al., 2019). Ho et al reported an investigation of phage intervention in the intensive care unit (ICU) rooms. They applied 500 ml of customized phage-containing preparation with a concentration of 10^7 PFU (plaque forming unit)/ml for a $\sim$ 27m^3 room. A significant reduction in CRAB-associated NIs was observed when adding a single aerosolized phage treatment to the conventional chemical-based disinfection performed in ICU rooms at the patient discharge (Ho et al., 2016). D'Accolti et al added phages to probiotic-based sanitation (PCHS) in the Staphylococcal-contaminated bathrooms ($\sim$4.5 m^2, applied 2×10^8 PFU phages for a multiplicity of infection $\sim$1000) of General Medicine wards, reporting a rapid and significant decrease in *Staphylococcus spp.* load on treated surfaces, up to 97% more than PCHS alone (D'Accolti et al., 2019). Tseng et al developed a chamber study model to analyze the potential of aerosolized phage BTCU-1 in reducing airborne *Mycobacterium smegmatis* in different multiplicity of infection (MOI) and aerosol generation time. The result showed that, MOI of 10 000 for 10 seconds significantly blocked recovery of *M. smegmatis* colony from the culture medium (Tseng et al., 2019).

Notably, several challenges to balance between benefits and costs of implementing phage disinfection cannot be

neglected. In particular, storage condition and content of phage library depend on the stability and consumption of stocked phages; the absent of the quality control specification (QCS) for environmental applied phages should be addressed. It is certain that manufacture and QCS of phage disinfectants do not require as much as therapeutic phages (GMP-approved, endotoxin removal), however, this strategy needs mass consumption of phage and thus is production-capacity dependent. Although phages should not replace broad-spectrum agents in terminal disinfection, they offer great potential for continuous target-specific applications where the target is drug-resistant and antimicrobial chemicals are either relatively ineffective or their use would result in unintended detrimental consequences.

A PRACTICAL MODEL OF USING PHAGE IN NOSOCOMIAL INFECTION MANAGEMENT

The use of phages is consistent with the need of nosocomial infection control to diminish both bacterial infection and transmission, as well as to relieve the overuse of antibiotics. However, little has been described regarding the systemic application of phages in infection management. Nevertheless, a similar concept has been successfully practiced in several other settings (e.g., food, animals, crops) (Holtappels et al., 2020; Pinto et al., 2020; Żbikowska et al., 2020), where a few phage-based products have been approved by the supervisory authorities in the United States, Canada, Israel, Europe, Australia and New Zealand (Pinto et al., 2020).

How might phages be integrated into the clinical workflow at a healthcare establishment? First, a system of cooperation between different departments (e.g., clinical, infectious diseases, laboratory, infection control, phage, pharmacy, and GMP factory) is essential. Second, an established phage library is needed for screening lytic phages against a given pathogenic bacterium isolated from a patient or from a hospital surface. Third, ready-to-use phage vials need to be properly manufactured prior to application to humans (GMP-approved) or environments; qualified phage vials should be pre-stocked to accelerate phage delivery. In parallel to use in phage therapy, the same phage formula can be aerosol-applied to the room or even the entire ward of the treated patient to prevent nosocomial transmission. Fourth, the accumulated phage-typing database of many bacteria can serve to monitor nosocomial infection and as a prelude to preparing phage stocks for patient treatment and environmental sterilization. Fifth, both retrospective and prospective phage susceptibility tests can be united (adjusted by conventional bacterial-typing methods and epidemiological links) to design fixed-composition phage cocktails with broad-spectrum, poly antimicrobial properties against the epidemic strains; the fixed-composition cocktails could then be applied in routine environmental sterilization or in treatment of serious infections such as septic shock or severe pneumonia that call for rapid initiation of treatment (**Figure 1**).

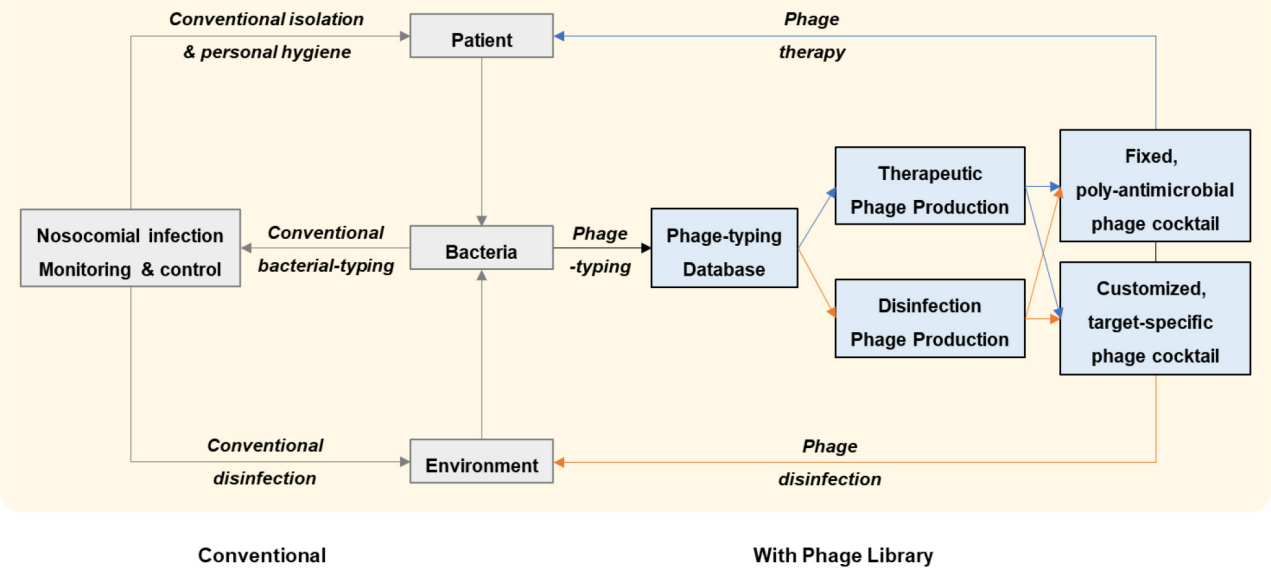

FIGURE 1 | Workflow of nosocomial infection management proposed in this study. With an established phage library, lytic phages against a given pathogenic bacterium that has been isolated from a patient or from a hospital surface are screened and pre-stocked phage vials are delivered for application to the patient or to the environment. Retrospective and prospective phage susceptibility tests on hospital bacterial isolates can be united in a phage-typing database which can be further adjusted by conventional bacterial-typing methods and epidemiological links. Engaging the phage-typing database serves as a complementary strategy to conventional nosocomial infection management. By monitoring nosocomial infections in this way, fixed-composition phage cocktails with broad-spectrum, poly antimicrobial properties against the epidemic strains can be rapidly applied to the patient or the environment.

CONCLUSION

The extreme abundance and biodiversity of phages in our surrounding environment and inside our body provides an opportunity to establish an ever-expanding phage library that collectively provides a sustainable broad-spectrum and poly microbial coverage. This library might play a major role in tackling the global AMR crisis. Whilst acknowledging the remaining obstacles for clinical phage application, we believe that by taking advantage of pre-established phage libraries, pre-stocked phage productions, and pre-optimized phage screening technology, phages can become available as modern medicine. This availability may constitute a breakthrough in both clinical treatment and environmental disinfection in the context of nosocomial infection management.

AUTHOR CONTRIBUTIONS

NW and TZ reviewed the literature, summarized the tables, conceptualized the figure, wrote the manuscript, and acquired funding. Both authors contributed to the article and approved the submitted version.

FUNDING

This work was financially supported by the National Major Science and Technology Projects of China (grant 2020ZX09201001-005-003 to NW), Natural Science Foundation of Shanghai (20Y11900300 to NW), National Natural Science Foundation of China (82070772 to TZ), and the Clinical Research Plan of SHDC (SHDC2020CR2028B to TZ).

ACKNOWLEDGMENTS

We thank all members from the Shanghai Institute of Phage for thoughtful discussions.

REFERENCES

Adaptive Phage Therapeutics (2020a). *Adaptive Phage Therapeutics Enters Agreement with Mayo Clinic to Commercialize a Phage Susceptibility Test*. Available online at: https://www.aphage.com/adaptive-phage-therapeutics-enters-agreement-with-mayo-clinic-to-commercialize-a-phage-susceptibility-test/ (accessed June 9, 2020).

Adaptive Phage Therapeutics (2020b). *Development Pipeline*. Available online at: https://www.aphage.com/science/pipeline/ (accessed December 3, 2020).

Allegranzi, B., Bagheri Nejad, S., Combescure, C., Graafmans, W., Attar, H., Donaldson, L., et al. (2011). Burden of endemic health-care-associated infection in developing countries: systematic review and meta-analysis. *Lancet* 377, 228–241. doi: 10.1016/s0140-6736(10)61458-4

ANI (2020). *In a first, Dr Dangs Lab begins bacteriophage susceptibility testing to combat antibiotic resistance*. Available online at: https://www.aninews.in/news/health/in-a-first-dr-dangs-lab-begins-bacteriophage-susceptibility-testing-to-combat-antibiotic-resistance20201022154604/ (accessed October 22, 2020).

Ariza-Heredia, E. J., and Chemaly, R. F. (2018). Update on infection control practices in cancer hospitals. *CA Cancer J. Clin.* 68, 340–355. doi: 10.3322/caac.21462

Armata Therapeuticals (2020). *Pipeline Overview*. Available online at: https://www.armatapharma.com/pipeline/pipeline-overview/ (accessed December 3, 2020).

Aslam, S., Courtwright, A. M., Koval, C., Lehman, S. M., Morales, S., Furr, C. L., et al. (2019). Early clinical experience of bacteriophage therapy in 3 lung transplant recipients. *Am. J. Transplant.* 19, 2631–2639. doi: 10.1111/ajt.15503

Bao, J., Wu, N., Zeng, Y., Chen, L., Li, L., Yang, L., et al. (2020). Non-active antibiotic and bacteriophage synergism to successfully treat recurrent urinary tract infection caused by extensively drug-resistant *Klebsiella pneumoniae*. *Emerg. Microbes Infect.* 9, 771–774. doi: 10.1080/22221751.2020.1747950

Barco, L., Barrucci, F., Olsen, J. E., and Ricci, A. (2013). *Salmonella* source attribution based on microbial subtyping. *Int. J. Food Microbiol.* 163, 193–203. doi: 10.1016/j.ijfoodmicro.2013.03.005

Boxrud, D., Pederson-Gulrud, K., Wotton, J., Medus, C., Lyszkowicz, E., Besser, J., et al. (2007). Comparison of multiple-locus variable-number tandem repeat analysis, pulsed-field gel electrophoresis, and phage typing for subtype analysis of *Salmonella enterica* serotype Enteritidis. *J. Clin. Microbiol.* 45, 536–543. doi: 10.1128/jcm.01595-06

Chan, B. K., Turner, P. E., Kim, S., Mojibian, H. R., Elefteriades, J. A., and Narayan, D. (2018). Phage treatment of an aortic graft infected with *Pseudomonas aeruginosa*. *Evol. Med. Public Health* 2018, 60–66. doi: 10.1093/emph/eoy005

Chng, K. R., Li, C., Bertrand, D., Ng, A. H. Q., Kwah, J. S., Low, H. M., et al. (2020). Cartography of opportunistic pathogens and antibiotic resistance genes in a tertiary hospital environment. *Nat. Med.* 26, 941–951. doi: 10.1038/s41591-020-0894-4

Cooke, F. J., Gkrania-Klotsas, E., Howard, J. C., Stone, M., Kearns, A. M., Ganner, M., et al. (2010). Clinical, molecular and epidemiological description of a cluster of community-associated methicillin-resistant *Staphylococcus aureus* isolates from injecting drug users with bacteraemia. *Clin. Microbiol. Infect.* 16, 921–926. doi: 10.1111/j.1469-0691.2009.02969.x

Crabb, H. K., Allen, J. L., Devlin, J. M., Firestone, S. M., Stevenson, M., Wilks, C. R., et al. (2019). Traditional *Salmonella* Typhimurium typing tools (phage typing and MLVA) are sufficient to resolve well-defined outbreak events only. *Food Microbiol.* 84:103237. doi: 10.1016/j.fm.2019.06.001

D´abrowska, K., and Abedon, S. T. (2019). Pharmacologically aware phage therapy: pharmacodynamic and pharmacokinetic obstacles to phage antibacterial action in animal and human bodies. *Microbiol. Mol. Biol. Rev.* 83:e00012-19.

D'Accolti, M., Soffritti, I., Lanzoni, L., Bisi, M., Volta, A., Mazzacane, S., et al. (2019). Effective elimination of Staphylococcal contamination from hospital surfaces by a bacteriophage-probiotic sanitation strategy: a monocentric study. *Microb. Biotechnol.* 12, 742–751. doi: 10.1111/1751-7915.13415

Dedrick, R. M., Guerrero-Bustamante, C. A., Garlena, R. A., Russell, D. A., Ford, K., Harris, K., et al. (2019). Engineered bacteriophages for treatment of a patient with a disseminated drug-resistant *Mycobacterium abscessus*. *Nat. Med.* 25, 730–733. doi: 10.1038/s41591-019-0437-z

Demczuk, W., Soule, G., Clark, C., Ackermann, H. W., Easy, R., Khakhria, R., et al. (2003). Phage-based typing scheme for *Salmonella enterica* serovar Heidelberg, a causative agent of food poisonings in Canada. *J. Clin. Microbiol.* 41, 4279–4284. doi: 10.1128/jcm.41.9.4279-4284.2003

Dong, F., Chen, J., Li, C., Ma, X., Jiang, J., Lin, Q., et al. (2019). Evidence-based analysis on the toxicity of disinfection byproducts in vivo and in vitro for disinfection selection. *Water Res.* 165:114976. doi: 10.1016/j.watres.2019.114976

Duplessis, C. A., Stockelman, M., Hamilton, T., Merril, G., Brownstein, M., Bishop-Lilly, K., et al. (2019). A case series of emergency investigational new drug applications for bacteriophages treating recalcitrant multi-drug resistant bacterial infections: confirmed safety and a signal of efficacy. *J. Intensive Crit. Care* 5:11.

Ferrari, R. G., Panzenhagen, P. H. N., and Conte-Junior, C. A. (2017). Phenotypic and genotypic eligible methods for *Salmonella* typhimurium source tracking. *Front. Microbiol.* 8:2587. doi: 10.3389/fmicb.2017.02587

Ferry, T., Batailler, C., Petitjean, C., Chateau, J., Fevre, C., Forestier, E., et al. (2020). The potential innovative use of bacteriophages within the DAC(®) hydrogel to treat patients with knee megaprosthesis infection requiring "debridement antibiotics and implant retention" and soft tissue coverage as salvage therapy. *Front. Med. (Lausanne)* 7:342. doi: 10.3389/fmed.2020.00342

Ferry, T., Boucher, F., Fevre, C., Perpoint, T., Chateau, J., Petitjean, C., et al. (2018). Innovations for the treatment of a complex bone and joint infection due to XDR *Pseudomonas aeruginosa* including local application of a selected cocktail of bacteriophages. *J. Antimicrob. Chemother.* 73, 2901–2903. doi: 10.1093/jac/dky263

Gill, J. J., and Hyman, P. (2010). Phage choice, isolation, and preparation for phage therapy. *Curr. Pharm. Biotechnol.* 11, 2–14. doi: 10.2174/138920110790725311

Gindin, M., Febvre, H. P., Rao, S., Wallace, T. C., and Weir, T. L. (2019). Bacteriophage for gastrointestinal health (PHAGE) study: evaluating the safety and tolerability of supplemental bacteriophage consumption. *J. Am. Coll. Nutr.* 38, 68–75. doi: 10.1080/07315724.2018.1483783

Hargreaves, K. R., Otieno, J. R., Thanki, A., Blades, M. J., Millard, A. D., Browne, H. P., et al. (2015). As clear as mud? determining the diversity and prevalence of prophages in the draft genomes of estuarine isolates of clostridium difficile. *Genome Biol. Evol.* 7, 1842–1855. doi: 10.1093/gbe/evv094

Hesse, S., and Adhya, S. (2019). Phage therapy in the twenty-first century: facing the decline of the antibiotic Era; is it finally time for the age of the phage? *Annu. Rev. Microbiol.* 73, 155–174. doi: 10.1146/annurev-micro-090817-062535

Ho, Y. H., Tseng, C. C., Wang, L. S., Chen, Y. T., Ho, G. J., Lin, T. Y., et al. (2016). Application of bacteriophage-containing aerosol against nosocomial transmission of carbapenem-resistant *Acinetobacter baumannii* in an intensive care unit. *PLoS One* 11:e0168380. doi: 10.1371/journal.pone.0168380

Holtappels, D., Fortuna, K., Lavigne, R., and Wagemans, J. (2020). The future of phage biocontrol in integrated plant protection for sustainable crop production. *Curr. Opin. Biotechnol.* 68, 60–71. doi: 10.1016/j.copbio.2020.08.016

Hoyle, N., Zhvaniya, P., Balarjishvili, N., Bolkvadze, D., Nadareishvili, L., Nizharadze, D., et al. (2018). Phage therapy against *Achromobacter xylosoxidans* lung infection in a patient with cystic fibrosis: a case report. *Res. Microbiol.* 169, 540–542. doi: 10.1016/j.resmic.2018.05.001

Intralytix (2020). *Human Therapeutics-Intralytix, A Pioneer In Phage-Based Regulatory Approvals*. Available online at: http://intralytix.com/index.php?page=hum (accessed December 3, 2020).

Jault, P., Leclerc, T., Jennes, S., Pirnay, J. P., Que, Y. A., Resch, G., et al. (2019). Efficacy and tolerability of a cocktail of bacteriophages to treat burn wounds infected by *Pseudomonas aeruginosa* (PhagoBurn): a randomised, controlled, double-blind phase 1/2 trial. *Lancet Infect. Dis.* 19, 35–45. doi: 10.1016/s1473-3099(18)30482-1

Jensen, K. C., Hair, B. B., Wienclaw, T. M., Murdock, M. H., Hatch, J. B., Trent, A. T., et al. (2015). Isolation and host range of bacteriophage with lytic activity against methicillin-resistant *Staphylococcus aureus* and potential use as a fomite decontaminant. *PLoS One* 10:e0131714. doi: 10.1371/journal.pone.0131714

Kortright, K. E., Chan, B. K., Koff, J. L., and Turner, P. E. (2019). Phage therapy: a renewed approach to combat antibiotic-resistant bacteria. *Cell Host Microbe* 25, 219–232. doi: 10.1016/j.chom.2019.01.014

Kuipers, S., Ruth, M. M., Mientjes, M., De Sévaux, R. G. L., and Van Ingen, J. (2019). A dutch case report of successful treatment of chronic relapsing urinary tract infection with bacteriophages in a renal transplant patient. *Antimicrob. Agents Chemother.* 64:e01281-19.

Laxminarayan, R., Duse, A., Wattal, C., Zaidi, A. K., Wertheim, H. F., Sumpradit, N., et al. (2013). Antibiotic resistance-the need for global solutions. *Lancet Infect. Dis.* 13, 1057–1098.

Leitner, L., Ujmajuridze, A., Chanishvili, N., Goderdzishvili, M., Chkonia, I., Rigvava, S., et al. (2020). Intravesical bacteriophages for treating urinary tract infections in patients undergoing transurethral resection of the prostate: a randomised, placebo-controlled, double-blind clinical trial. *Lancet Infect. Dis.* S1473-3099(20)30330-3. doi: 10.1016/S1473-3099(20)30330-3

Letarov, A. V., and Kulikov, E. E. (2018). Determination of the bacteriophage host range: culture-based approach. *Methods Mol. Biol.* 1693, 75–84. doi: 10.1007/978-1-4939-7395-8_7

Luong, T., Salabarria, A. C., and Roach, D. R. (2020). Phage therapy in the resistance Era: where do we stand and where are we going? *Clin. Ther.* 42, 1659–1680. doi: 10.1016/j.clinthera.2020.07.014

Maddocks, S., Fabijan, A. P., Ho, J., Lin, R. C. Y., Ben Zakour, N. L., Dugan, C., et al. (2019). Bacteriophage therapy of ventilator-associated pneumonia and empyema caused by *Pseudomonas aeruginosa*. *Am. J. Respir. Crit. Care Med.* 200, 1179–1181. doi: 10.1164/rccm.201904-0839le

Malik, D. J., Sokolov, I. J., Vinner, G. K., Mancuso, F., Cinquerrui, S., Vladisavljevic, G. T., et al. (2017). Formulation, stabilisation and encapsulation of bacteriophage for phage therapy. *Adv. Colloid Interface Sci.* 249, 100–133. doi: 10.1016/j.cis.2017.05.014

Markoishvili, K., Tsitlanadze, G., Katsarava, R., Morris, J. G. Jr., and Sulakvelidze, A. (2002). A novel sustained-release matrix based on biodegradable poly(ester amide)s and impregnated with bacteriophages and an antibiotic shows promise in management of infected venous stasis ulcers and other poorly healing wounds. *Int. J. Dermatol.* 41, 453–458. doi: 10.1046/j.1365-4362.2002.01451.x

Mathieu, J., Yu, P., Zuo, P., Da Silva, M. L. B., and Alvarez, P. J. J. (2019). Going viral: emerging opportunities for phage-based bacterial control in water treatment and reuse. *Acc. Chem. Res.* 52, 849–857. doi: 10.1021/acs.accounts.8b00576

Mattila, S., Ruotsalainen, P., and Jalasvuori, M. (2015). On-Demand isolation of bacteriophages against drug-resistant bacteria for personalized phage therapy. *Front. Microbiol.* 6:1271. doi: 10.3389/fmicb.2015.01271

McCallin, S., Sarker, S. A., Sultana, S., Oechslin, F., and Brüssow, H. (2018). Metagenome analysis of Russian and Georgian Pyophage cocktails and a placebo-controlled safety trial of single phage versus phage cocktail in healthy *Staphylococcus aureus* carriers. *Environ. Microbiol.* 20, 3278–3293. doi: 10.1111/1462-2920.14310

Mellon, G., Turbett, S. E., Worby, C., Oliver, E., Walker, A. T., Walters, M., et al. (2020). Acquisition of antibiotic-resistant bacteria by U.S. International Travelers. *N. Engl. J. Med.* 382, 1372–1374. doi: 10.1056/nejmc1912464

Merabishvili, M., Pirnay, J. P., and De Vos, D. (2018). Guidelines to compose an ideal bacteriophage cocktail. *Methods Mol. Biol.* 1693, 99–110. doi: 10.1007/978-1-4939-7395-8_9

Mitchell, B. G., Hall, L., White, N., Barnett, A. G., Halton, K., Paterson, D. L., et al. (2019). An environmental cleaning bundle and health-care-associated infections in hospitals (REACH): a multicentre, randomised trial. *Lancet Infect. Dis.* 19, 410–418. doi: 10.1016/s1473-3099(18)30714-x

Muñoz, A. B., Stepanian, J., Trespalacios, A. A., and Vale, F. F. (2020). Bacteriophages of *Helicobacter* pylori. *Front Microbiol* 11:549084. doi: 10.3389/fmicb.2020.549084

Nir-Paz, R., Gelman, D., Khouri, A., Sisson, B. M., Fackler, J., Alkalay-Oren, S., et al. (2019). Successful treatment of antibiotic-resistant, poly-microbial bone infection with bacteriophages and antibiotics combination. *Clin. Infect. Dis.* 69, 2015–2018. doi: 10.1093/cid/ciz222

Petrovic Fabijan, A., Lin, R. C. Y., Ho, J., Maddocks, S., Ben Zakour, N. L., and Iredell, J. R. (2020). Safety of bacteriophage therapy in severe *Staphylococcus aureus* infection. *Nat. Microbiol.* 5, 465–472.

Phagelux (2020). *Summary of Clinical Trials*. Available online at: http://en.phageluxbio.com/phageluxbioen/vip_doc/22746970_0_0_1.html (accessed December 3, 2020).

Pinto, G., Almeida, C., and Azeredo, J. (2020). Bacteriophages to control Shiga toxin-producing E. coli - safety and regulatory challenges. *Crit. Rev. Biotechnol.* 40, 1081–1097. doi: 10.1080/07388551.2020.1805719

Pires, D. P., Costa, A. R., Pinto, G., Meneses, L., and Azeredo, J. (2020). Current challenges and future opportunities of phage therapy. *FEMS Microbiol. Rev.* 44, 684–700. doi: 10.1093/femsre/fuaa017

Pirnay, J. P., De Vos, D., Verbeken, G., Merabishvili, M., Chanishvili, N., Vaneechoutte, M., et al. (2011). The phage therapy paradigm: prêt-à-porter or sur-mesure? *Pharm. Res.* 28, 934–937. doi: 10.1007/s11095-010-0313-5

Quainoo, S., Coolen, J. P. M., Van Hijum, S., Huynen, M. A., Melchers, W. J. G., Van Schaik, W., et al. (2017). Whole-Genome sequencing of bacterial pathogens: the future of nosocomial outbreak analysis. *Clin. Microbiol. Rev.* 30, 1015–1063. doi: 10.1128/cmr.00016-17

Rice, L. B. (2008). Federal funding for the study of antimicrobial resistance in nosocomial pathogens: no ESKAPE. *J. Infect. Dis.* 197, 1079–1081. doi: 10.1086/533452

Rostkowska, O. M., Miêdzybrodzki, R., Miszewska-Szyszkowska, D., Górski, A., and Durlik, M. (2020). Treatment of recurrent urinary tract infections in a 60-year-old kidney transplant recipient. The use of phage therapy. *Transpl. Infect. Dis.* e13391. doi: 10.1111/tid.13391

Sarker, S. A., Berger, B., Deng, Y., Kieser, S., Foata, F., Moine, D., et al. (2017). Oral application of *Escherichia coli* bacteriophage: safety tests in healthy and diarrheal children from Bangladesh. *Environ. Microbiol.* 19, 237–250. doi: 10.1111/1462-2920.13574

Schooley, R. T., Biswas, B., Gill, J. J., Hernandez-Morales, A., Lancaster, J., Lessor, L., et al. (2017). Development and use of personalized bacteriophage-based therapeutic cocktails to treat a patient with a disseminated resistant *Acinetobacter baumannii* infection. *Antimicrob. Agents Chemother.* 61: e00954-17.

Sloan, A., Wang, G., and Cheng, K. (2017). Traditional approaches versus mass spectrometry in bacterial identification and typing. *Clin. Chim. Acta* 473, 180–185. doi: 10.1016/j.cca.2017.08.035

Sundell, K., Landor, L., Nicolas, P., Jørgensen, J., Castillo, D., Middelboe, M., et al. (2019). Phenotypic and genetic predictors of pathogenicity and virulence in *Flavobacterium psychrophilum*. *Front. Microbiol.* 10:1711. doi: 10.3389/fmicb.2019.01711

Tseng, C. C., Chang, D. C., and Chang, K. C. (2019). Development of a biocontrol method applying bacteriophage-containing aerosol against *Mycobacterium tuberculosis* using the bacteriophage BTCU-1 and M. smegmatis as models. *Microorganisms* 7:237. doi: 10.3390/microorganisms7080237

Vijayakumar, S., Veeraraghavan, B., Pragasam, A. K., and Bakthavachalam, Y. D. (2019). Genotyping of *Acinetobacter baumannii* in nosocomial outbreak and surveillance. *Methods Mol. Biol.* 1946, 17–22. doi: 10.1007/978-1-4939-9118-1_2

Weber, D. J., Rutala, W. A., Sickbert-Bennett, E. E., Kanamori, H., and Anderson, D. (2019). Continuous room decontamination technologies. *Am. J. Infect. Control* 47s, A72–A78.

World Health Organization (2017). *Global Priority List of Antibiotic-Resistant Bacteria to Guide Research, Discovery, and Development of New Antibiotics*. Available online at: https://www.who.int/medicines/publications/global-priority-list-antibiotic-resistant-bacteria/en/ (accessed February 27, 2017).

Wright, A., Hawkins, C. H., Anggård, E. E., and Harper, D. R. (2009). A controlled clinical trial of a therapeutic bacteriophage preparation in chronic otitis due to antibiotic-resistant *Pseudomonas aeruginosa*; a preliminary report of efficacy. *Clin. Otolaryngol.* 34, 349–357. doi: 10.1111/j.1749-4486.2009.01973.x

Wuyts, V., Denayer, S., Roosens, N. H., Mattheus, W., Bertrand, S., Marchal, K., et al. (2015). Whole genome sequence analysis of *salmonella* enteritidis PT4 outbreaks from a national reference laboratory's viewpoint. *PLoS Curr.* 7, 1–14. doi: 10.1371/currents.outbreaks.aa5372d90826e6cb0136ff66bb7a62fc

Yerushalmy, O., Khalifa, L., Gold, N., Rakov, C., Alkalay-Oren, S., Adler, K., et al. (2020). The israeli phage bank (IPB). *Antibiotics (Basel)* 9:269. doi: 10.3390/antibiotics9050269

Żaczek, M., Weber-Dąbrowska, B., Miêdzybrodzki, R., Łusiak-Szelachowska, M., and Górski, A. (2020). Phage therapy in poland – a centennial journey to the first ethically approved treatment facility in Europe. *Front. Microbiol.* 11:1056. doi: 10.3389/fmicb.2020.01056

Żbikowska, K., Michalczuk, M., and Dolka, B. (2020). The use of bacteriophages in the poultry industry. *Animals (Basel)* 10:872. doi: 10.3390/ani10050872

Conflict of Interest: The authors declare that the research was conducted in the absence of any commercial or financial relationships that could be construed as a potential conflict of interest.

Copyright © 2021 Wu and Zhu. This is an open-access article distributed under the terms of the Creative Commons Attribution License (CC BY). The use, distribution or reproduction in other forums is permitted, provided the original author(s) and the copyright owner(s) are credited and that the original publication in this journal is cited, in accordance with accepted academic practice. No use, distribution or reproduction is permitted which does not comply with these terms.

frontiers in Microbiology

ORIGINAL RESEARCH
published: 17 February 2021
doi: 10.3389/fmicb.2021.619323

Biodiversity of New Lytic Bacteriophages Infecting *Shigella* spp. in Freshwater Environment

*Khashayar Shahin[1], Mohadeseh Barazandeh[1], Lili Zhang[1], Abolghasem Hedayatkhah[2], Tao He[1], Hongduo Bao[1], Mojtaba Mansoorianfar[3], Maoda Pang[1], Heye Wang[1], Ruicheng Wei[1] and Ran Wang[1]**

[1]Key Lab of Food Quality and Safety of Jiangsu Province-State Key Laboratory Breeding Base, Jiangsu Academy of Agricultural Sciences, Institute of Food Safety and Nutrition, Nanjing, China, [2]Curtin Medical School, Curtin University, Perth, WA, Australia, [3]Suzhou Institute of Nano-Tech and Nano-Bionics, Chinese Academy of Sciences, Suzhou, China

Bacteriophages, viruses that infect and replicate within prokaryotic cells are the most abundant life forms in the environment, yet the vast majority of them have not been properly reported or even discovered. Almost all reported bacteriophages infecting the *Enterobacteriaceae* family, with *Escherichia coli* being the major subject of studies, have been isolated from wastewater, sewage, and effluent resources. In the present study, we focused on the distribution and biodiversity of *Shigella* phages in an aquatic ecosystem. While no *Shigella* bacteria was recovered from the Yangtze River, three lytic phages were isolated from this ecosystem and were subjected to biological, morphological, and genomic characteristics. Comparative genomics and phylogenetic analyses demonstrated that vB _SflM_004 isolate belongs to *Myoviridae* family, *Felixounavirus* genus of *Ounavirinae* subfamily, vB_SdyM_006 was classified under the same family, however, it is suggested to be in a new genus under *Tevenvirinae* subfamily with some other related bacteriophages. vB_SsoS_008 phage belongs to the *Siphoviridae* family, *Tunavirus* genus, *Tunavirinae* subfamily. The phages did not harbor any genes involved in the lysogenic cycles and showed a high temperature and pH stability. The biodiversity of the isolated phages highly suggests that continued isolation on non-model members of *Enterobacteriaceae* family is necessary to fully understand bacteriophage diversity in aquatic environments.

Keywords: water, phage, biodiversity, bacteriophage, *Shigella*, *Enterobacteriaceae*

OPEN ACCESS

Edited by:
Shuai Le,
Army Medical University, China

Reviewed by:
Ji Hyung Kim,
Korea Research Institute of Bioscience and Biotechnology (KRIBB), South Korea
Ahmed Askora,
Zagazig University, Egypt

***Correspondence:**
Ran Wang
ranwang@jaas.ac.cn

Specialty section:
This article was submitted to Virology, a section of the journal Frontiers in Microbiology

Received: *20 October 2020*
Accepted: *11 January 2021*
Published: *17 February 2021*

Citation:
Shahin K, Barazandeh M, Zhang L, Hedayatkhah A, He T, Bao H, Mansoorianfar M, Pang M, Wang H, Wei R and Wang R (2021) Biodiversity of New Lytic Bacteriophages Infecting Shigella spp. in Freshwater Environment. Front. Microbiol. 12:619323. doi: 10.3389/fmicb.2021.619323

INTRODUCTION

Bacteria-infecting viruses or bacteriophages (phages) are the most abundant biological entities on planet earth (Suttle, 2005). With an estimated minimum number of 10^{31} bacteriophages have the highest diversity with respect to genetics, morphology, host range, and infection cycles (Hendrix et al., 2002). Our knowledge on bacteriophages is extremely limited for three main reasons. First, in theory, each and every bacterial species is a host for at least a phage. With our current knowledge on the field and the state of the art and technology, only a small percentage of bacteria can be grown *in vitro* thus the majority of the microorganisms are uncultivated (or yet-to-be-cultivated; Hatfull and Hendrix, 2011). Second, of the cultured one,

only very few numbers have been used as hosts for phage isolation (Hatfull and Hendrix, 2011). Finally, even with this limited number of host cells, almost all of the phages reported so far have been isolated from environments such as untreated sewage and hospital wastewater or wound since there is a higher chance of isolating bacteriophages using such resources due to these resources being the most contaminated ecosystem containing a high number of pathogens. Considering the above facts, isolation of phages from other aquatic environments such as freshwater resources and reservoirs like rivers and lakes is of particular importance in view of their impact on both the microbial diversity and the ecological fate of photogenic bacteria.

Shigella is a gram-negative bacterial genus including four species: *Shigella boydii*, *Shigella dysenteriae*, *Shigella flexneri*, and *Shigella sonnei* (Shahin et al., 2019c), all causing shigellosis with hundreds of millions of food/water-borne infections annually (WHO, 2005). Although shigellosis can be usually treated with antibiotics, propagation of antibiotic-resistant strains has created many serious health problems in recent years (Baker et al., 2018), for example over the past few decades several shigellosis outbreaks have been reported in the geographical regions (Löfdahl et al., 2009; He et al., 2012; Abaidani et al., 2015; Puzari et al., 2018).

As an alternative to antibiotic, lytic bacteriophages can be used to control or to treat bacterial infections, a process is known as phage therapy (Shahin et al., 2019d; Bao et al., 2020). Despite the worldwide distribution of *Shigella* species, the high number of infected cases, and the great importance of food safety, only very few *Shigella*-infecting phages have been identified, studied, and reported so far. Almost all of these reported phages have been isolated from raw sewage samples. *Myoviridae* phages (pSs-1 and WZ1; Jamal et al., 2015; Jun et al., 2016a), *Siphoviridae* phages (vB_SflS-ISF001, vB_SsoS-ISF002, vB-SdyS-ISF003, SH6, Shfl1, and pSf-2; Jun et al., 2013, 2016b; Hamdi et al., 2017; Shahin et al., 2018, 2019a,b), and *Podoviridae* phages (pSb-1 and Sf6; Casjens et al., 2004; Jun et al., 2014) are among the phages that infect different species of *Shigella*. Moreover, although phage therapy for controlling *Shigella* has a long history as the first phage research was done by Felix d'Herelle in the 1910s (Duckworth, 1976), nevertheless there is no comprehensive research on the abundance, distribution, and diversity of *Shigella* in natural aquatic environments yet.

Hence, in this study, we focused on isolation and subsequent morphological, biological and genomic characterization of *Shigella*-infecting phages from Yangtze River as one of the biggest freshwater resources on the planet earth.

MATERIALS AND METHODS

Bacterial Stains and Growth Condition

All the *Shigella* bacteria used in the present study (**Supplementary Table S1**) have been previously isolated. They were all stored in tryptic soy broth (TSB; Merck, Germany) containing 30% glycerol and kept at −70°C in the central bacterial strains collection of International Phage Research Center (IPRC) containing 30% glycerol at 70°C. In addition to these isolates, the type-stains of *S. sonnei* (ATCC 9290), *S. flexneri* (ATCC 12022), *S. dysenteriae* (PTCC 1188), *S. boydii* (ATCC 9207), and *Escherichia coli* (ATCC 25922) were used for the determination of the bacteriophages host range. All the isolates were cultured routinely on brain heart infusion (BHI) agar (Merck, Germany) or in BHI broth (Merck, Germany) with constant shaking at 200 rpm and 37°C.

Bacteriophages Isolation and Morphology Analysis

Four *Shigella* isolates including *S. flexneri* (w7) and *S. sonnei* (w44) which had been isolated earlier from other freshwater sources and also showed the highest antibiotic resistance, as well as *S. dysenteriae* (s.d.f1) and reference strain *S. boydii* (ATCC 9207), were used individually as the host bacteria for phages isolation following the previously described method with a slight modification (Yazdi et al., 2020). Briefly, 100 ml of Yangtze River water samples [GPS coordinates of sampling locations include: (1) latitude: 32°06′37.8″N and longitude: 118°44′56.1″E; (2) latitude: 32°09′25.9″N and longitude: 118°50′48.8″E; **Supplementary Figure S1**] was centrifuged (10 min at 6,000 × g) and filtrated through 0.45 μm sterile syringe filters (JinTeng, China). The filtrate was used for phage isolation with pre-enrichment (method I) or without pre-enrichment (method II) pre-enrichment. In method I, 50 ml of the filtrate water was added to 50 ml of the early-exponential culture of the host bacteria and incubated overnight with constant shaking (200 rpm). After centrifugation (10 min, 8,000 × g) and filtration (0.45-μm), 20 μl of the filtrate was spotted on BHI plates overlaid with the individual strain. In method II, 20 μl of the filtrate water sample was dropped directly onto the surface of lawn cultures of the host bacteria and incubated at 37°C for at least 24 h. Emergence of clear plaques either in method I or method II were considered primary as the presence of a lytic phage. Then a single plaque was picked up carefully for phage purification procedure using three repeats of single plaque isolation, elution, and re-plating. Phage propagation and phage titers determination were carried out regularly according to Clokie and Kropinski's (2009) protocols.

Phages Transmission Electron Microscopy

The phage lysates (10^9 PFU ml^{-1}) were precipitated using NaCl (0.5 M) and PEG 8000 (10%, Amresco, Solon, United States) and then highly purified using centrifugation on cesium chloride gradient as described by Clokie and Kropinski (2009). The phages were negatively stained with 2% phosphotungstic acid (PTA) for 1 min and left to dry for 30 min and finally, the grids were analyzed in a Hitachi HT7700 transmission electron microscope at an operating voltage of 100 kV at Nanjing Agricultural University (NAU), Nanjing, China.

Host Range

The host ranges of the phages were determined using spot assays (Shahin and Bouzari, 2018). Ten microliters of the phage suspension (10^9 PFU ml^{-1}) was spotted onto double-layered BHI agar plates of each host strains (**Supplementary Table S1**). After an overnight incubation, the plates were checked for the

appearance of clear plaque (++), turbid plaque (+), or no plaque (−). The efficiency of plating assay (EOP) was carried out against the phages-sensitive isolates of *Shigella* spp. as described previously (Shahin et al., 2020). The EOP of the phage on their primary host strain (reference host) was considered as 1 and EOP of each strain were calculated as the ratio of phage titer on the tested bacterium to the phage titer on the reference host.

The Phages Biological Characterizations

Shigella flexneri (w7), *S. dysenteriae* (s.d.f1), and *S. sonnei* (w44) were used as host bacteria in all the experiments. The thermostability and pH stability of the phages were evaluated by incubation of the phages lysate (10^9 PFU ml^{-1}) at wide range of temperatures (−20 to 80°C) and pH (2–12) as previously described (Shahin et al., 2018). Briefly, 1 ml of phage solution (10^9 pfu/ml) was incubated at −20 to 70°C individually for 1 h to evaluate the bacteriophage stability to different temperatures. Moreover, to measure the tolerance of isolated phages to different pH values, they were added to microtubes containing sterile SM buffer at pH values of 3−12 and then incubated for 1 h. The survival phages in both examinations were measured using the overlay method and the titer is reported as a percentage of the control sample titers. The phages adsorption rates to the surface of their bacterial hosts were determined as previously described (Kropinski et al., 2009). Moreover, one-step growth experiments were done to determine phages burst size and latent periods (Shahin et al., 2018). The bacteriolytic potential of the phages were evaluated by monitoring the changes in OD_{600} absorbance of the phage/host mixture at different MOI as described previously (Shahin and Bouzari, 2018). The assays were performed in triplicate.

DNA Extraction, DNA Fingerprinting, and Whole Genome Sequencing

The stocks of purified phages were condensed using ultracentrifugation at 105,000 × g for 3 h at 4°C (Beckman Optima L-80 XP ultracentrifuge, TYPE 45 Ti rotor). The pellet was diluted in SM buffer and treated by 10 µg/ml DNase I and RNase I (Sigma, China) to digest any free DNA and RNA. The genomic DNA of phages was then extracted using phenol/chloroform/isoamyl alcohol protocol as described previously by Sambrook and Russell (2001). Finally, the quality and quantity of the extracted DNA were examined using agarose gel electrophoresis and NanoDrop (Thermo Scientific, United States).

The digestion patterns produced by *EcoRI*, *EcoRV*, and *HindIII* restriction enzymes (Thermo Fisher Scientific, United States) were used for DNA fingerprinting analysis. The phage DNA and the endonuclease were mixed individually according to the manufacturer's protocol. After the incubation period, the DNA fragments were separated by 1% agarose gel electrophoresis at 90 V for 60 min. The DNA libraries and whole-genome sequences were obtained using Illumina HiSeq NGS DNA sequencing system (TGS, Shenzhen, China). The raw sequencing data were assembled using SOAPdenovo (v2.04) at the default setting and the assembled sequences were deposited at DDBJ/EMBL/GenBank (**Table 1**).

Bioinformatic Analysis

Open reading frames (ORFs) were detected using Prokaryotic GeneMark.hmm version 3.25[1] (Besemer et al., 2001) and NCBI ORF Finder[2] and translated to protein sequences using ExPASy translate tool.[3] Molecular weight and isoelectric pH of the predicted ORF were estimated using ExPASy compute pI/Mw tool[4] (Gasteiger et al., 2005). tRNAscan-SE was used to find any tRNA sequence (Schattner et al., 2005). Functional and conserved domains of the predicted ORFs proteins were analyzed using a couple of software and online tools including Basic Local Alignment Search Tool (BLASTp),[5] HHpred[6] (Zimmermann et al., 2018), Pfam[7] (Finn et al., 2015), and InterProScan[8] (Altschul et al., 1997). The promoter sequences were identified using BPROM program of the Softberry website with the maximum allowable distance from the starting codon of a gene at 100 bp (Salamov and Solovyevand, 2011).

Comparative Genomic Analysis and Phylogeny

The whole-genome sequences of the taxonomically close and related phages were obtained from NCBI database[9] and were used for comparison of the sequences at both genome and proteome levels using EasyFig v 2.2.3 (Sullivan et al., 2011). In addition,

[1]http://opal.biology.gatech.edu/genemark/gmhmmp.cgi
[2]https://www.ncbi.nlm.nih.gov/orffinder/
[3]http://web.expasy.org/translate/
[4]http://web.expasy.org/compute_pi/
[5]https://blast.ncbi.nlm.nih.gov/Blast.cgi
[6]https://toolkit.tuebingen.mpg.de/#/tools/hhpred
[7]http://pfam.xfam.org/search#tabview=tab1
[8]http://www.ebi.ac.uk/interpro/search/sequence-search
[9]https://ncbi.nlm.nih.gov

TABLE 1 | Morphologic and genomic characteristics of the isolated phages in current study.

	vB_SfIM_004	vB_SdyM_006	vB_SsoS_008
Host	*Shigella flexneri*	*Shigella dysenteriae*	*Shigella sonnei*
Isolation method	II	I	I
Plaque size	1.5–2 mm	2 mm	2.5–2.7 mm
Head diameter	99.6 ± 8 nm	92.7 ± 2 nm	59.2 ± 2 nm
Tail length (relaxed form)	107.2 ± 6 nm	106.2 ± 4	171.9 ± 5
Width (relaxed form)	15.5 ± 1 nm	15.5 nm	6.9 ± 1 nm
Tail length (contracted form)	50.2 ± 2 nm	54.1 ± 1 nm	–
Width (contracted form)	15.8 ± 1 nm	15 ± 1 nm	–
Family	*Myoviridae*	*Myoviridae*	*Siphoviridae*
Sequencing platform	Illumina HiSeq	Illumina HiSeq	Illumina HiSeq
Fold coverage	4,115×	3,247×	1,405×
Genome length	85,887 bp	166,138 bp	50,414 bp
G+C%	38.6	31.5	45.6
No. of coding sequences	135	252	83
tRNA	0	9	0
GenBank ID	MK295205	MK295204	MK335533

CoreGenes 3.5 was used for core gene analysis (Zafar et al., 2002). The phylogenetic tree was constructed using Mega 7.0 based on unweighted pair group method with arithmetic mean (UPGMA) with 2,000 bootstrap replication (Kumar et al., 2016).

RESULTS

Phages Isolation and Morphology

Phages were isolated from Yangtze River according to their ability to lyse and generate clear plaques with or without hallow zones using several *Shigella* species as the host cells. The transmission electron microscopy micrographs show that the isolated phages for *S. flexneri* and *S. dysenteriae* have an icosahedral head, contractile tail, collar, and base plate, the typical properties *Myoviridae* family of bacteriophages (**Figures 1A-D**). Moreover, the TEM micrograph of the isolated phage for *S. sonnei* shows that it has an icosahedral head and a non-contractile tail, a similar structure to that of the *Siphoviridae* phages (**Figures 1E,F**). The head diameter, tail length, and width of the phages are summarized in **Table 1**. The phages were designated as vB_SflM_004, vB_SdyM_006, and vB_SsoS_008 according to their host species and phage family.

Bacteriophages Host Ranges

The host range of the isolated phages were tested on a wide range of bacteria including *Shigella* isolates, as well as standard strains of gram-negative and gram-positive bacteria.

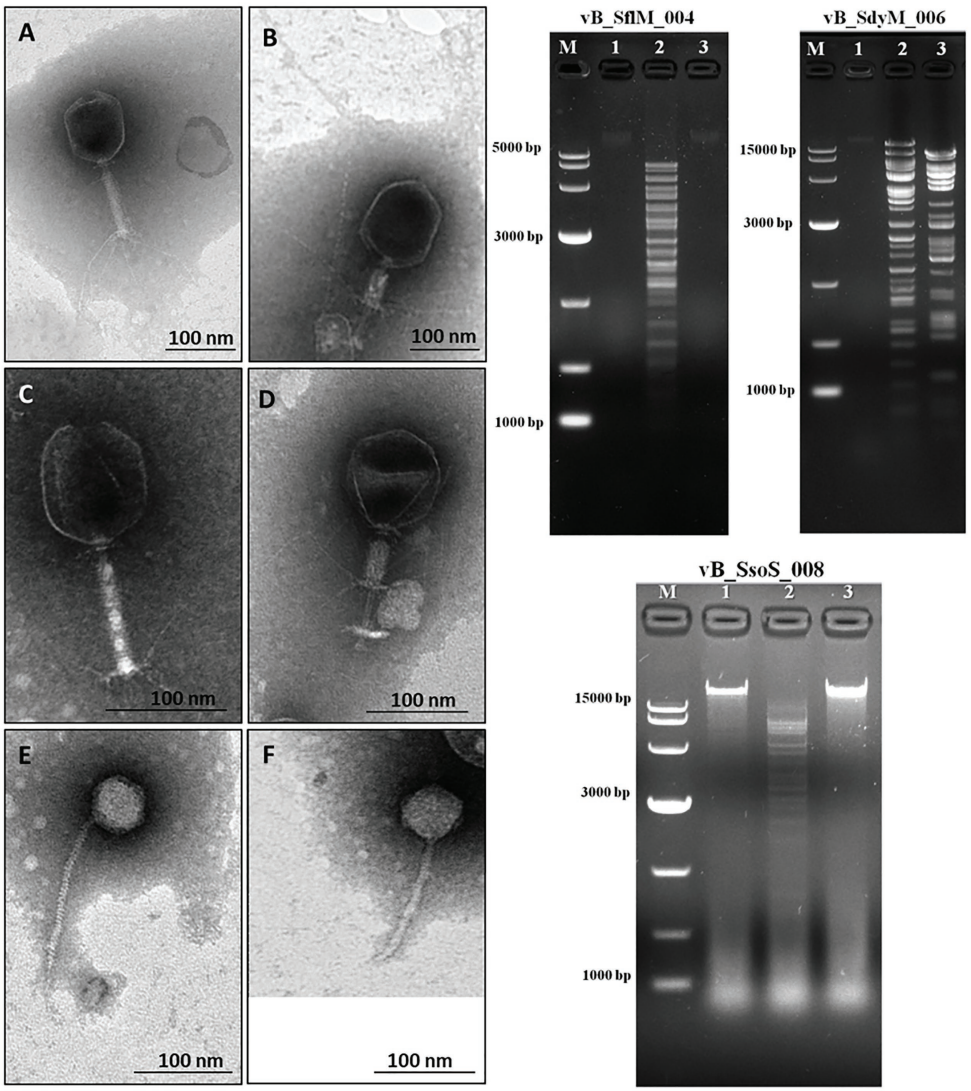

FIGURE 1 | (Left side) The electron micrograph of phages vB _SflM_004 **(A,B)**, vB_SdyM_006 **(C,D)**, and vB_SsoS_008 **(E,F)**. The samples were negatively stained with 2% phosphotungstic acid (PTA). Scale bars 100 nm. (Right side) The DNA fingerprinting analysis of the genomic DNA of phage vB _SflM_004, vB_SdyM_006, and vB_SsoS_008. The genome was digested with *EcoRI* (line1), *EcoRV* (line2), and *HindIII* (line3). M line represents the DNA marker.

The vB_SdyM_006 phage was capable of producing clear plaque only on *S. dysenteriae* isolates (3/3 isolates), while vB_SflM_004 and vB_SsoS_008 produced either clear or cloudy plaques on most of the tested *S. flexneri* and *S. sonnei* isolates (**Supplementary Table S1**). A relatively wide range of EOP (0.12 ± 0.07 ~ 1) of the phages was observed against different isolates of *Shigella* spp. (**Supplementary Table S2**).

DNA Fingerprinting

The DNA fingerprinting of the isolated phages were obtained using restriction endonucleases *EcoRI*, *EcoRV*, and *HindIII*. The obtained restriction pattern revealed that the genome of the phages vB _SflM_004 and vB_SsoS_008 were digested only with *EcoRV* and the genome of phage vB_SdyM_006 was digested with *EcoRV* and *HindIII*. The observed differences in the DNA fingerprints in terms of size and pattern (**Figure 1**) imply that the genome size and sequence of the isolated phages were different from each other.

Basic Biological Characteristics

The thermo- and pH-stability of the phages were tested at a wide range of temperatures and pH values (**Figure 2**). Titer of all the three phages were stable (>90%) at −20 to 40°C, but it started to decrease when incubated at 50°C for 1 h. While by further increase in the temperature to 80°C, vB_SdyM_006 and vB_SsoS_008 could not be recovered, the vB _SflM_004 phage was still recovered at this temperature, but lost its activity when incubated at 90°C (**Figure 2A**). In the case of pH stability, the highest activity was observed at pHs ranging from 6 to 8. Incubation at basic pH of 12 (for all phages) and acidic pHs of 4 (for vB_SsoS_008) and 3 (for vB_SdyM_006 and vB _SflM_004) led to deactivation of the phages (**Figure 2B**). The one-step growth curves demonstrated that the phages vB _SflM_004, vB_SdyM_006, and vB_SsoS_008 were started to release from their host cells after 30, 50, and 15 min, respectively. Moreover, the burst sizes were estimated to be about 139 ± 29, 93 ± 15, and 94 ± 9 virions per single bacterium for vB _SflM_004, vB_SdyM_006, and vB_SsoS_008, respectively (**Figure 2C**). Additionally, as shown in **Figure 2D** the phages particles were absorbed immediately after incubation where vB _SflM_004, vB_SdyM_006, and vB_SsoS_008 phages were fully absorbed on their host cell after 12, 6, and 10 min, respectively.

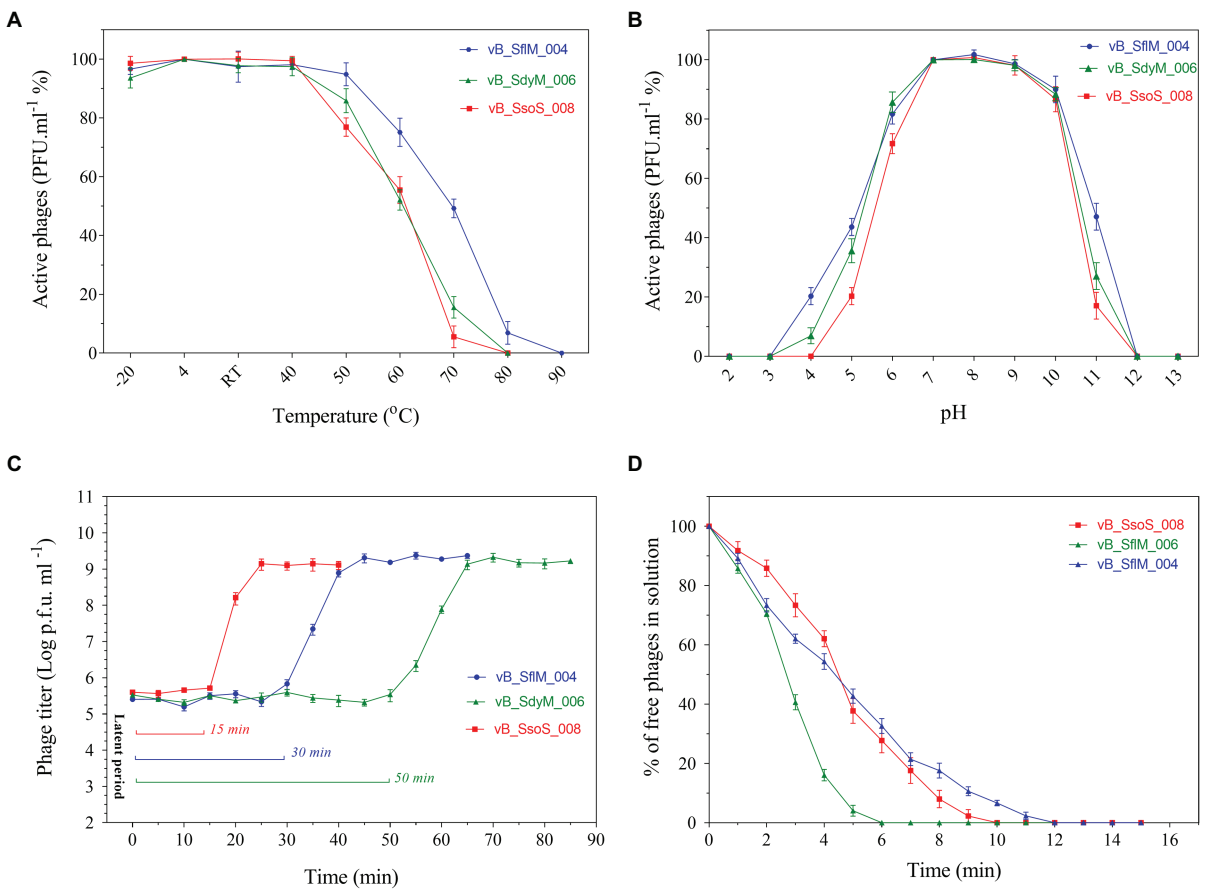

FIGURE 2 | The thermostability **(A)**, pH stability **(B)**, one-step growth curve **(C),** and adsorption rate **(D)** of vB _SflM_004, vB_SdyM_006, and vB_SsoS_008. The error bars indicate standard deviations (SD).

Genome Analysis

The fold coverage, genome size, G+C contents, and other general genome features of the phages vB_SflM_004, vB_SdyM_006, and vB_SsoS_008 are presented in **Table 1**.

Genome Analysis of vB_SflM_004

ATG was detected as the start codon in all of the ORFs. The Opal (TGA), Ochre (TAA), and Amber (TAG) stop codons were presented in 59, 49, and 20 ORFs, respectively. The BPROM search detected 16 promoters (**Supplementary Data 1**) with consensus sequences at −10 (tttTAtaaT) and −35 (TTcAca; the capital letters indicated conserved nucleotides). Nine Rho-factor independent termination sites were also detected in the vB_SflM_004 genome with FindTerm online software (**Figure 3**).

In general, the genomic organization and genetic analysis of the phage vB_SflM_004 demonstrated that the genome contained 135 possible ORFs including 20 ORFs encoding structural proteins, 25 ORFs for metabolism-related proteins, four ORFs associated with bacterial lysis-like proteins, 83 ORFs encoding hypothetical proteins which showed relatively high similarity to the previously described phage hypothetical proteins with no clear understanding of their functions yet, and the three remaining ORFs which showed no similarity to any known proteins in the databases (**Figure 3**). The list of 135 ORFs, as well as their details and annotation, is provided in **Supplementary Data 2**. The detected genes involved in the bacterial cell lysis were lysozyme (*gp111*), holin (*gp79*), and two spanin (o-spanin, *gp28* and i-spanin, *gp29*) which are similar to the previously reported genes in the *Ounavirinae* subfamily including *Felixounavirus* (*gp28* and *gp29*), *Mooglevirus* (*gp111*), and *Suspvirus* (*gp79*). In addition, two pairs of rIIA/rIIB proteins were also detected at the semi-beginning (*ORF32* and *ORF33*) and the end (*ORF134* and *ORF135*) of vB_SflM_004 genome which could play role in regulation of bacterial lysis (**Supplementary Data 2**). The gene products involved in the metabolism/regulation pathways of vB_SflM_004 were identified as different types of DNA polymerases, kinases, reductases, protease, nucleases, hydrolysis, and regulatory proteins with relatively high similarity to those of *Ounavirinae* subfamily (check **Supplementary Data 2** for more detail). The structural and assembly genes were encoding the tail fiber proteins, tail sheath, tail protein, tail tube protein, minor tail protein, tail assembly protein, major capsid, pro-head assembly scaffold protein, and a head maturation protease. Some of these proteins were similar to those available in the GenBank database. For instance, tail tube, major capsid, and tail protein were almost identical (≥97%) to the respective predicted gene products of phages vB_EcoM_Alf5, SF19, Meda, and SF13. On the other hand, the tail proteins and the major capsid protein represented a low identity (≤55%) to the previously reported phage proteins. The gene distribution pattern (**Figure 3** and **Supplementary Data 2**) shows that about half of the gene products of ORF81 to ORF110 were identified as structural proteins. Same as other viruses, bacteriophages tend to have the genes with similar function close to each other in a compact arrangement (Bardina et al., 2016). Thus, it is possible that the

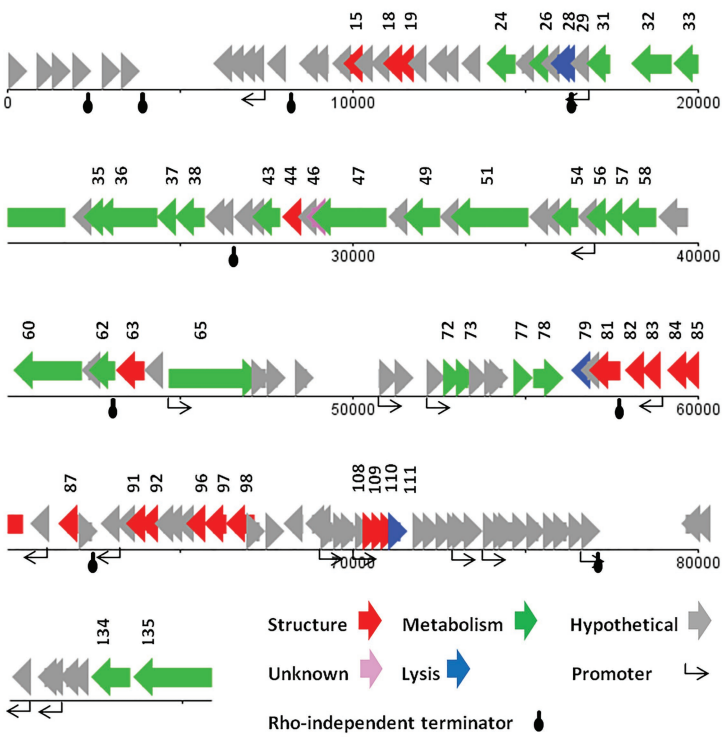

FIGURE 3 | The linear genome map of phage vB_SflM_004.

remaining ORFs (which have been considered as hypothetical proteins) in this region of the genome may have a structural function.

The highest similarity of the hypothetical proteins was to those of phage SF13 (13 out of 83 ORF) with a clear concordant relation in their gene products function and their respective identified conserved domains. However, in the case of conserved domains of DUF3277 and DUF3383 no clear relations were found (**Supplementary Data 2**).

BLASTN analysis of the phage vB_SflM_004 genome revealed that the genome of the phage was highly similar (~94% similarity with >75% query coverage) to *E. coli* phage 11, phage 12, *Enterobacteria* phage WV8, and *Salmonella* phage BPS15Q2. As shown in (**Figure 4**) the dot plot analysis of these bacteriophages using Gepard demonstrated a considerable sequence similarity between vB_SflM_004 and the other related phages with a few remarkable differences such as deletion of an ~10 kb region at position around 18,000. Comparison of the genome with other close phages using CoreGenes showed that 68% of the proteins were shared with *Ounavirinae* subfamily in which the entire lysis group proteins, some genes with structural or regulatory functions, as well as some of the hypothetical proteins were conserved (**Figure 4** and **Supplementary Data 3**). **Supplementary Table S4** summarized the comparison of the basic genomic properties and **Supplementary Figure S2** depicts the relatedness of vB_SflM_004 and other phages with high homology using Easyfig software.

Genome Analysis of vB_SdyM_006

The genome of vB_SdyM_006 contains 252 ORFs (**Supplementary Data 2**) and nine tRNA coding regions (**Supplementary Table S3**). The only identified start codon was ATG. Ocher, Amber, and Opal stop codons were identified in 91, 50, and 111 ORFs, respectively. A BPROM search identified

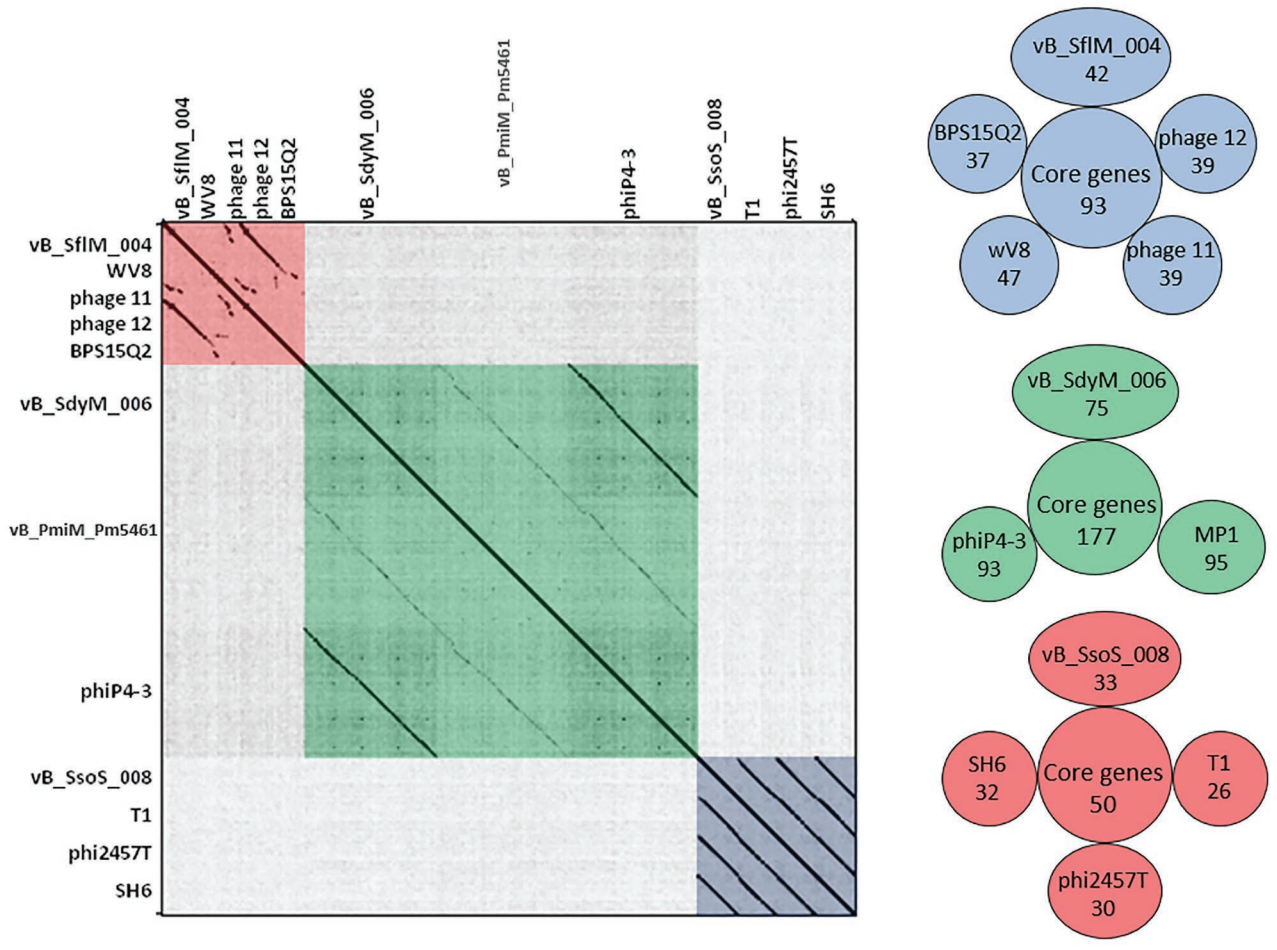

FIGURE 4 | (Left side) Dot plot alignment of the nucleotide sequences of the isolated phages vB _SflM_004, vB_SdyM_006, and vB_SsoS_008 with that of the close related phages. The FASTA file of 1,300,800 bp file was compared to itself using GEPARD. Dark diagonal lines parallel to the main diagonal shows strong and continuous sequence similarity, while pale lines indicate weaker sequence relationships due to interruptions that result in a discontinuous line. The red, green, and blue boxes were added to illustrate the phage sequences related to vB _SflM_004, vB_SdyM_006, and vB_SsoS_008. (Right side) The shared conserved proteins of vB _SflM_004, vB_SdyM_006, and vB_SsoS_008 phages with their close related phages (SH6, Shfl1, ADB-2, JMPW2). Only the gene products with >75 score in CoreGenes analysis were considered as a homolog.

31 promoters, with the consensus sequences of ATGTATAAT and TTTAAT at the −10 and −35 positions, respectively (the conserved bases were presented in bold; **Supplementary Data 1**). In addition, the only identified potential Rho-factor independent termination site was located after the gene encoding the inhibitor of the prohead protease (*gp187*; **Figure 5**).

With regard to the comprehensive genetic analysis of vB_SdyM_006 and the homology-based search of its 252 ORFs, the predicted ORFs could be clustered into five groups. Forty-five ORFs were predicted as structure proteins, nearly from *ORF133* to *ORF182* (**Supplementary Data 2**). Tail completion and sheath stabilizer protein, head completion protein, baseplate wedge subunit, baseplate wedge tail fiber connector, baseplate wedge subunit and tail pin, short tail fibers, fibritin, neck protein, tail sheath stabilization protein, tail sheath protein, tail tube protein, portal vertex of head, prohead core protein, prohead core scaffold protein, major capsid protein, capsid vertex protein, membrane protein, baseplate tail tube initiator, baseplate tail tube cap, baseplate hub subunit, and baseplate hub distal subunit all were detected in this region and have a high similarity rate to the respective predicted gene products of phages vB_PmiM_Pm5461, PM2, phiP4-3, and vB_MmoM_MP1 (Männistö et al., 1999; Oliveira et al., 2017; Morozova et al., 2018; Gkoutzourelas et al., 2020). Moreover, a small group of five genes was detected close to the end of the genome (from *ORF233* to *ORF237*) encoding different parts of the tail structure including long tail fiber proximal subunit, long tail fiber proximal connector, long tail fiber distal connector, long tail fiber distal subunit, and distal long tail fiber assembly catalyst which had 100% similarity to vB_PmiM_Pm5461 and phiP4-3 (**Supplementary Data 2**; Morozova et al., 2018; Gkoutzourelas et al., 2020).

Within the lysis functions, the *ORF98* encodes an endolysin with peptidase activity (conserved domain pfam13539).

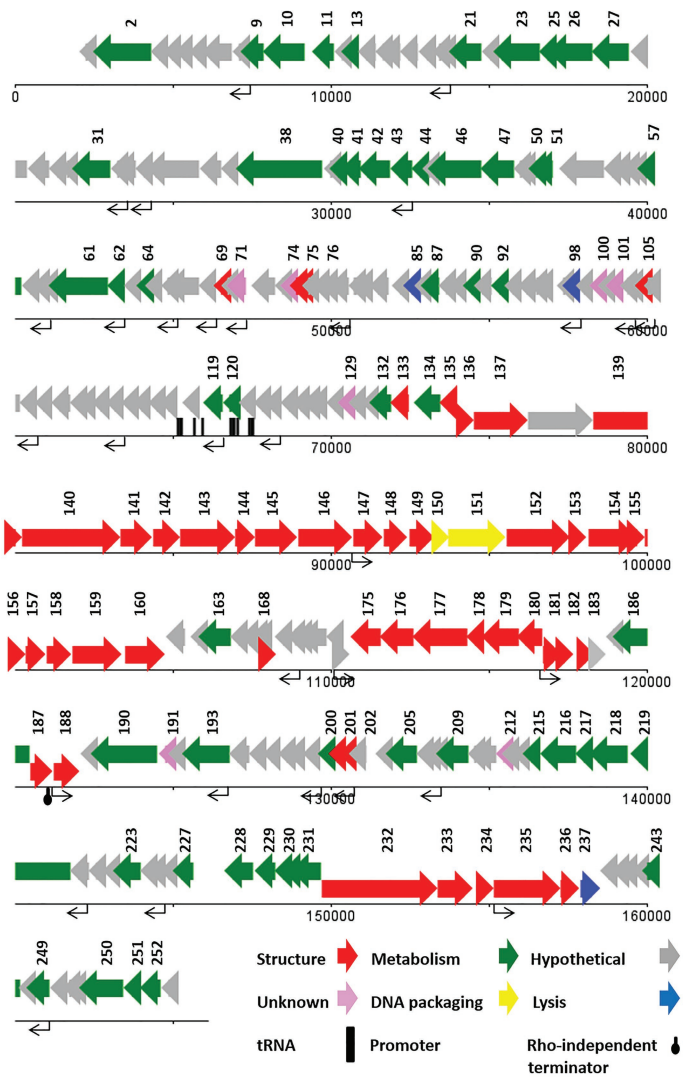

FIGURE 5 | The linear genome map of phage vB_SdyM_006.

The *gp238* was identified as a Holin lysis mediator due to its high similarity to the respective predicted gene product of phage vB_PmiM_Pm5461. The *gp85* (lysis inhibition regulator) and *gp200* (rIII lysis inhibition accessory protein) are predicted to have the regulatory roles in the lysis pathway. It is worth mentioning that *ORF137* (baseplate hub + tail lysozyme) and *ORF157* (head core scaffold protein + protease) encodes bifunctional proteins whose contain either C- or N-terminal sequences and showed a relatively high similarity with those of the cell wall lysozymes.

Terminases, the proteins responsible for packaging the phage genome were detected almost in the middle of the genome (*ORF150* and *ORF151*), showing a ≥94% similarity to the small and large subunits of phage vB_MmoM_MP1 terminase (**Figure 5** and **Supplementary Data 2**). Furthermore, the conserved domains of DNA_Packaging (pfam11053) and Terminase_6 (pfam03237) were identified in the small and large subunits of the terminase, respectively.

The predicted genes involved in the metabolic and regulatory functions were including several DNA-associated genes (DNA polymerase, helicase, primase, ligase, topoisomerase, and endonuclease proteins), RNA-associated genes (RNA polymerase, tRNA synthetase, ligase, endonuclease, and RNaseH proteins), different types of exonuclease, recombinase, anti-sigma factors, sigma factors, anaerobic NTP reductase, thioredoxin, kinase, host translation inhibitors, and several other genes. Most of the predicted proteins showed a high identity (≥90%) with the counterpart proteins of *Tevenvirinae* subfamily of phages while some others had no similarity (*gp71*, *gp74*, *gp100*, *gp129*, *gp191*, and *gp212*; **Supplementary Data 2**).

Based on the BLASTN analysis, the genome sequence of vB_SdyM_006 had 98% (97% query coverage) and 97% (73% query coverage) similarity to the genome sequences of *Proteus* phages, phiP4-3 and vB_PmiM_Pm5461, respectively. Moreover, the sequences alignment of these three phages using Gepard software showed a higher similarity between vB_SdyM_006 and phiP4-3 than vB_SdyM_006 and vB_PmiM_Pm5461 (**Figure 4**). Furthermore, the relatedness of vB_SdyM_006 and other phages with a high degree of homology was determined using Easyfig software (**Supplementary Figure S3**) and comparison of the basic genomic properties of the isolated phage of vB_SdyM_006 with other phages were summarized in **Supplementary Table S4**.

The CoreGene analysis showed that vB_SdyM_006 shared ~84% similarity with that of the encoded proteins of the mentioned phages above (score >70), including 111 hypothetical proteins and 101 known proteins with different functions. These protein-coding genes were spread out all along the genome and were not restricted to any particular region (**Figure 4** and **Supplementary Data 3**).

Genome Analysis of vB_SsoS_008

The genome of vB_SsoS_008 contained 83 putative ORFs, of which the function of 33 ORFs were predicted (**Supplementary Data 2**), and the other 50 ORFs were assigned as hypothetical proteins in which 47 ORFs had similarities with the hypothetical proteins of bacteriophages vB_EcoS_SH2, Sfin-1, T1, SH6, and phi2457T while the other 3 ORFs were evidently unique to UAB_Phi87 and showed no similarity with the already deposited sequences. Twelve sequences with conserved consensus sequences of gTtTAatAT (−10) and TTgCaA (−35) were identified as promoter and were distributed throughout the phage genome (the conserved bases were presented in capital letter; **Supplementary Data 1**). All of the ORFs started with an ATG codon, with Opal (36 ORFs), Ochre (30 ORFs), and Amber (17 ORFs) stop codons. Only one Rho-independent terminator was identified by FindTerm (**Figure 6**). The genome of vB_SsoS_008 contained no tRNA or pseudo-tRNA genes.

The vB_SsoS_008 ORFs were encoding known protein that can be classified into five functional groups. The structural group contained 21 proteins including portal protein (gp26), capsid proteins (gp28-31), tail proteins (gp41, 43–55, 61, and 62). All of the structural proteins showed a relatively high to high similarity (85–100%) with the respective predicted gene products of phages B_EcoS_SH2, Sfin-1, T1, SH6, and phi2457T, except *gp46* in which only 58% similarity was observed to the tail fibers protein of *Shigella* phage Sfin-1. Detection of pfam05939 conserved domain (Phage_min_tail) in this gene approved the function of *gp46* as the tail fibers. The second group includes eight proteins predicted to be associated with nucleotide metabolism and its regulation. The product of these genes facilitate genome replication, transcription, and translation. These proteins are DNA methylase (gp3), kinase (gp17), nuclease (gp58), recombination protein (gp59), DNA primase (gp63) and primase (gp64), helicase (gp66), and methyltransferase (gp68) which showed ≥80% similarity to the counterpart proteins of phages Sfin-1, T1, and phi2457T (**Supplementary Data 2**). The third group includes the necessary protein involved in the bacterial cell lysis process. The two genes, 76 and 77, are predicted to encode endolysin and spanin, respectively, and had 90% (query coverage of 65%) and 84% (query coverage of 79%) identity with their counterpart proteins of *Shigella* phage Sfin-1and *Shigella* phage SH6, respectively. Interestingly, holin gene was found neither close nor far from the lysine gene. The DNA packaging complex consisted of large (gp25) and small (gp24) subunits of terminase was categorized as the fourth group. The large subunit of this complex had a high identity (96%, query coverage of 100) while the small subunit had only 73% similarity (query coverage of 90%) with the counterpart proteins of the related phages (**Supplementary Data 2**).

BLASTN analysis of the phage vB_SsoS_008 genome showed ~91.2% (query coverage 90%), 91.7% (query coverage 84), and 90.5% (query coverage 96%) similarity with *Shigella* phage SH6, *Enterobacteria* phage T1, and *Shigella* phage Sfin-1, respectively. The CoreGenes analysis (score >70) revealed that vB_SsoS_008, *Shigella* phage SH6, *Enterobacteria* phage T1, and *Shigella* phage phi2457T had ~60% proteins in common including the structural, DNA packaging, metabolic, endolysin and hypothetical proteins (**Figure 4** and **Supplementary Data 3**). In addition, the alignment of nucleotide sequences using Gepard software showed a high similarity between vB_SsoS_008 with *Shigella* phage SH6, *Enterobacteria* phage T1, and *Shigella* phage phi2457T (**Figure 4**). Furthermore, the relatedness of the vB_SsoS_008 and other phages with high homology was determined using the Easyfig (**Supplementary Figure S4**). The basic genomic properties of the isolated phage vB_SsoS_008 were compared to other phages and were summarized in **Supplementary Table S4**.

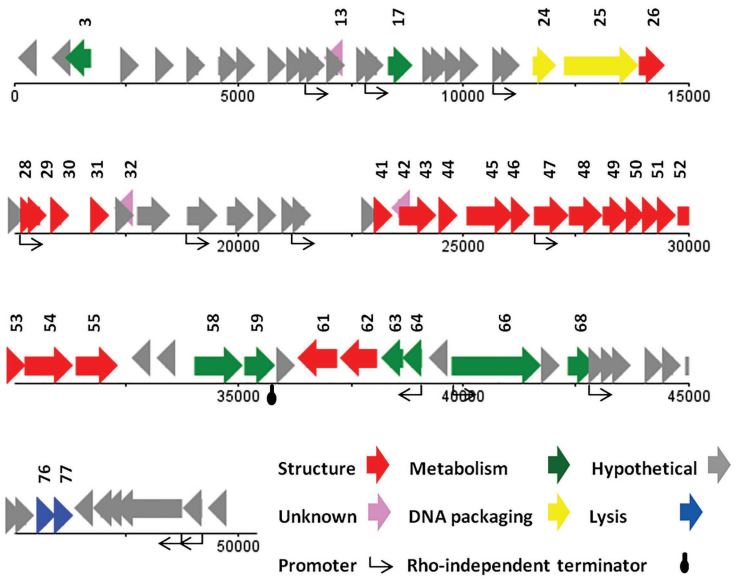

FIGURE 6 | The linear genome map of phage vB_SsoS_008.

Phylogenetic Analysis

The phylogenetic relationship between the isolated phages and other similar phages available in online databases was studied using the construction of the phylogenic tree based on major capsid sequences that were identified in all of these phages (**Figure 7**). Both vB _SflM_004 and vB_SdyM_006 were clustered as a member of the *Myoviridae* family. However, their major capsid sequences were different enough to classify them into lower taxa levels in which vB _SflM_004 was clustered into *Felixounavirus* genus of *Ounavirinae* and vB_SdyM_006 was only classifiable to a subfamily level and as a member of the *Tevenvirinae*. The constructed phylogenic tree based on the major capsid sequences suggests that vB_SdyM_006 along with phiP4-3, PM2, and vB_PmiM_Pm5461 phages could be considered as a new genus in *Tevenvirinae* subfamily due to the considerable phylogenic distance with other related members such as those of *Tequatrovirus* genus. Moreover, the phylogenic analysis indicated that phage vB_SsoS_008 should be added to *Tunavirus* genus, *Tunavirinae* subfamily of *Siphoviridae* family.

DISCUSSION

Independent Distribution of *Shigella* Phages From *Shigella* Bacterial Cells

There are many reports concerning isolation of *Shigella* phages from sources such as municipal wastewater, drainage ponds, and surface runoff after the regional occurrence of shigellosis, which could be due to the contact of *Shigella*-contaminated resource (such as the municipal wastewaters) with other water resources that usually are *Shigella* free (such as the runoff waters; Egoz et al., 1991; Barnell et al., 1996; Arias et al., 2006; He et al., 2012; Garner et al., 2017; Shahin et al., 2019c). In the present study, a number of *Shigella*-infecting phages were isolated from a large freshwater resource, the Yangtze River, and in an area with no prevalence of *Shigella*. This is especially interesting and important because no *Shigella* bacteria were recovered during the entire sampling period. Therefore, the relatively high abundance and diversity of *Shigella* phages could be an indication of their omnipresence in environments, especially in aquatic environments.

In general, the lipopolysaccharides of gram-negative bacteria include the O-antigen as the source of the bacterial diversity at the serotypes level, and the outer core as the source of diversity at the species level (Kropinski et al., 2007). In *Shigella* spp. the inner core is conserved (Brooke and Valvano, 1996). Since both vB _SflM_004 and vB_SsoS_008 phages infected all of the tested *S. sonnei* and *S. flexneri* isolates (with the exception of three isolates) in this study, it can be said that their function was independent of the O-antigen. The vB_SdyM_006 phage, however, only lysed *S.dysenteriae* isolates and had no effect on the isolates of other genera. Based on these observations, it can be inferred that the vB _SflM_004 and vB_SdyM_006 phages act as O-antigen-independent phages and are capable of lysing various species and serotypes, while vB_SdyM_006 is more specific and may only work on the serotypes of a certain species.

The presence of *Shigella* bacteria in various water resources has been recorded in different parts of the world. Connor et al. (2015) and Shahin et al. (2019c) acknowledged that neither *S. boydii* nor *S. dysenteriae* was the dominant endemic species in any country. However, *S. sonnei* is the dominant species in industrialized countries (WHO, 2005). *Shigella flexneri*, which has had a longer and more frequent history of presence, is also distributed worldwide (Shahin et al., 2019c). We expected in our observations to see coordination between the distribution and presence of the bacteria and of their infecting phages.

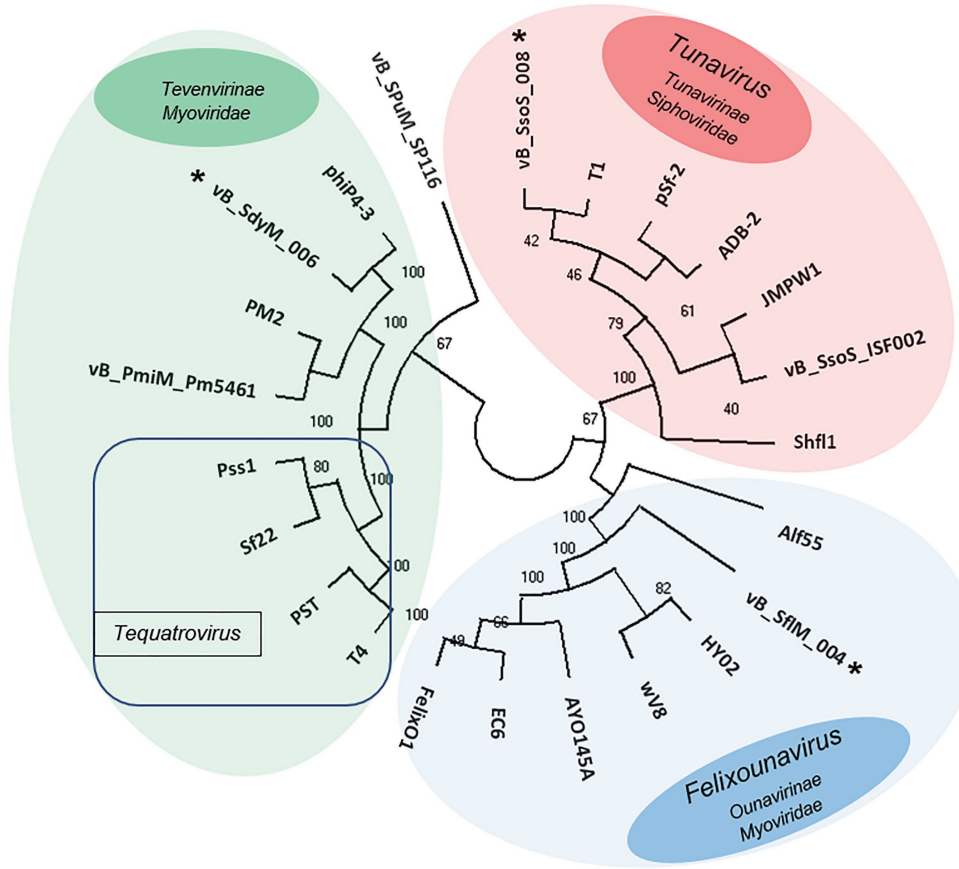

FIGURE 7 | Unweighted pair group method with arithmetic mean (UPGMA) tree phylogenic analysis of the major capsids of phages vB _SflM_004, vB_SdyM_006, and vB_SsoS_008. The tree was rooted using the major capsid of *Salmonella enterica* serovar Pullorum lytic phage vB_SPuM_SP116 (Bao et al., 2019) as the out-group. The bootstrap percentages are shown next to each node. Phage groups as defined in the ICTV virus taxonomy (https://talk.ictvonline.org/taxonomy/) release are represented by different colors.

Therefore, at first glance, it was expected that the frequency of *S. sonnei* and *S. flexneri* would be high in the studied aqueous environment (at least at the time of phage isolation). Nevertheless, despite using an enrichment step no *Shigella bacteria* were recovered during this research. Considering the proven specific nature of the phage-host interaction in many cases, a plausible hypothesis is that these phages have high stability in such environmental conditions and therefore remained dormant in the environment until the proper host reappears. In other words, *Shigella* and their infecting phages entered the environment and after a while, with the destruction of the bacterial host, the phages remained in the environment. However, given the very high abundance of the phages (estimated at 10^{31}) on our planet and the bacteria in natural environment (Hendrix et al., 2002), as well as the culturability of only a very small percentage of bacterial species under laboratory conditions (Buchanan and Gibbons, 1974), another improbable but possible hypothesis is that there are other host(s) for vB _SflM_004, vB_SdyM_006, and vB_SsoS_008 phages. In other words, these phages may have infected some of the yet-to-be-cultivated bacteria.

Doore et al. (2019) hypothesized that *S. flexneri* might be the dominant species in the studied environment (water resources of Michigan, United States) in view of a high abundance of *S. flexneri* phages in those ecosystems. In our study, isolation of vB _SflM_004 without pre-enrichment (method II) indicates its higher frequency than that of the other two phages. The higher structural, host, and biological diversity in the isolated phages of the present study than the *Shigella* phages isolated from the Michigan and Nebraska aquatic environments could be justified due to the size of the studied water resource (the Yangtze River) and the repeated sampling at different times in the present investigation.

Suitable Biological Properties for Stability in the Environmental

The thermos- and pH-stability tests demonstrated that for all of three phases (vB _SflM_004, vB_SdyM_006, and vB_SsoS_008) more than 50% of the infectivity was preserved at temperatures of −20 to 60°C and pHs of 6−10. Similar to our observation, it was reported frequently that *Shigella* phages have higher stability under alkaline conditions compared to acidic conditions (Jun et al., 2013; Hamdi et al., 2017; Shahin and Bouzari, 2018;

Shahin et al., 2018; Doore et al., 2019). The absence of any significant changes in the phage titers at −20 to 40°C and in neutral to somewhat alkaline pH is an indication of the high stability of the phages in normal environments (neutral or slightly acidic/alkaline pH and ambient temperatures of ≤40°C).

One-step growth curve analysis and phage adsorption rate provide a comprehensive perspective of phage interactions with their bacterial host. In general, short adsorption time indicates a more powerful initial attachment behavior of a phage to its host surface, while shorter latent period and larger burst size are indications of a higher of lytic potency of a phage (Shahin et al., 2018). Therefore, in the case of the isolated *Shigella* phages in this study, it can be assumed that almost immediately after the introduction of an appropriate host cell to the environment, these phages identify the host cells, get attached, then replicate very fast and keep their titer high in the environment.

The Isolated *Shigella* Phages Have Unique DNA Fingerprints

The use of restriction enzymes to determine the genome size of bacteriophages and to differentiate them from each other has a long history (Braun et al., 1989). The obtained DNA fingerprint profiles indicated that vB _SflM_004 and vB_SdyM_006 phages were different from each other and belong to two different groups despite both of them being a member of *Myoviridae* phages as it proved through the whole genome sequencing. Moreover, a comparison of these profiles with the already reported *Shigella* phages such as pSf-1, pSf-2, Shfl1, vB_SflS-ISF001, vB_SsoS-ISF002, and vB-SdyS-ISF003 shows a clear difference. Therefore, it can be concluded that the DNA fingerprint profiles can be used as a genome-based typing method to identify similar phages. Our results demonstrate that rapidness, cost-effectiveness, proper degree of sensitivity, in addition to not using any sophisticated laboratory equipment are the advantages of this test and makes it an appropriate method for preliminary analysis of phage diversity.

High Diversity of *Shigella* Phages

Although vB _SflM_004 and vB_SdyM_006 phages were both of the *Myoviridae* family, there were substantial phylogenetic differences to placed vB _SflM_004 in the *Felixounavirus* genus, *Ounavirinae* subfamily of *Myoviridae* family. Moreover, although vB_SdyM_006 together with Phi4-3, PM2, Pm5461, CGG4-1, PEi20, and PST, and T4 phages were phylogenetically placed in the *Tevenvirinae* subfamily, these phages were sufficiently different from Pss1, Sf 22, PST14 phages (of the *Tequatrovirus* genus) to be clustered in a new genus together with phages closely related to it such as Phi4-3, PM2, and PM5461 (Männistö et al., 1999; Oliveira et al., 2017; Morozova et al., 2018; Gkoutzourelas et al., 2020). Several phage families are capable of infecting *Shigella* bacteria. According to the latest online version of the ICTV (2018), totally there are 24 *Shigella*-infecting phages in the *Siphoviridae* (5 phages), *Podoviridae* (5 phages), *Myoviridae* (13 phages), and *Ackermannviridae* (1 phage) families. Through searching the public databases, a total 35 phages were found as the *Shigella*-infecting phages between 2016 and 2018. However, since then until January 2020, another 73 complete sequences of *Shigella* phages (39 *Myoviridae*, 24 *Siphoviridae*, 8 *Podoviridae*, and 2 *Ackermannviridae*) were registered at NCBI.[10] In the present study, isolation of more phages from *Myoviridae* family and even without using pre-enrichment in the case of vB_SflM_004, is in agreement with the general pattern mentioned above, that is a higher frequency of bacteriophages from *Myoviridae* family in the previous studies.

In conclusion, isolation of the three types of lytic phages while no *Shigella* bacteria were recovered implies that the presence of phages in an environment could be completely independent of the presence of their target host bacteria. Such observation is highly likely due to a high level of stability of these phages in the environment, or in a less-likely hypothesis, due to the phages having other host(s) among the yet-to-be-cultivated bacteria. Furthermore, *Shigella* phage isolation using methods with or without enrichment also demonstrated coordination in the distribution of these phages in freshwater and other environments. The genomic and bioinformatics analyses did not identify any genes involved in the lysogenic cycles in the genome sequences of the three isolated phages, and no plaques suspected of harboring lysogenic phages were detected during the tests. Both of these observations indicate the absolute linearity of these phages and, given the desirability of their other biological properties, they can be introduced as suitable antibacterial candidates for bio-control of *Shigella* in different conditions.

DATA AVAILABILITY STATEMENT

The datasets presented in this study can be found in online repositories. The names of the repository/repositories and accession number(s) can be found in the article/**Supplementary Material**.

AUTHOR CONTRIBUTIONS

KS and RWa designed the research. KS, MB, and AH contributed to data analysis and drafted the manuscript. MB, LZ, HB, MM, MP, and TH performed the laboratory phage works, DNA extraction and sequencing. All authors contributed to the article and approved the submitted version.

FUNDING

This study was supported by funds from the National Natural Science Foundation of China (NSFC No. 31950410562, 31602078, and 31702297) and Natural Science Foundation of Jiangsu Province (BK20180054).

SUPPLEMENTARY MATERIAL

The Supplementary Material for this article can be found online at: https://www.frontiersin.org/articles/10.3389/fmicb.2021.619323/full#supplementary-material

[10]https://www.ncbi.nlm.nih.gov/nuccore

REFERENCES

Abaidani, I., Raju, P. A., Al-Shualli, I., Al-Sa'di, K., Al-Shaqsi, N., and Al-Khatri, A. (2015). Shigellosis outbreak in Al Batinah south governorate, Oman: case-control study. *Sultan Qaboos Univ. Med. J.* 15, 382–389. doi: 10.18295/squmj.2015.15.03.013

Altschul, S. F., Madden, T. L., Schäffer, A. A., Zhang, J., Zhang, Z., Miller, W., et al. (1997). Gapped BLAST and PSI-BLAST: a new generation of protein database search programs. *Nucleic Acids Res.* 25, 3389–3402. doi: 10.1093/nar/25.17.3389

Arias, C., Sala, M., Domínguez, A., Bartolomé, R., Benavente, A., Veciana, P., et al. (2006). Waterborne epidemic outbreak of *Shigella sonnei* gastroenteritis in Santa Maria de Palautordera, Catalonia, Spain. *Epidemiol. Infect.* 134, 598–604. doi: 10.1017/S0950268805005121

Baker, K. S., Dallman, T. J., Field, N., Childs, T., Mitchell, H., Day, M., et al. (2018). Horizontal antimicrobial resistance transfer drives epidemics of multiple *Shigella* species. *Nat. Commun.* 9:1462. doi: 10.1038/s41467-018-03949-8

Bao, H., Shahin, K., Zhang, Q., Zhang, H., Wang, Z., Zhou, Y., et al. (2019). Morphologic and genomic characterization of a broad host range *Salmonella enterica* serovar Pullorum lytic phage vB_SPuM_SP116. *Microb. Pathog.* 136:103659. doi: 10.1016/j.micpath.2019.103659

Bao, H., Zhou, Y., Shahin, K., Zhang, H., Cao, F., Pang, M., et al. (2020). The complete genome of lytic *Salmonella* phage vB_SenM-PA13076 and therapeutic potency in the treatment of lethal *Salmonella Enteritidis* infections in mice. *Microbiol. Res.* 237:126471. doi: 10.1016/j.micres.2020.126471

Bardina, C., Colom, J., Spricigo, D. A., Otero, J., Sánchez-Osuna, M., Cortés, P., et al. (2016). Genomics of three new bacteriophages useful in the biocontrol of *Salmonella*. *Front. Microbiol.* 7:545. doi: 10.3389/fmicb.2016.00545

Barnell, A., Bennet, J., Chehey, R., and Greenblatt, J. (1996). *Shigella sonnei* outbreak associated with contaminated drinking water--Island Park, Idaho, August 1995. *MMWR Morb. Mortal. Wkly Rep.* 45, 229–231.

Besemer, J., Lomsadze, A., and Borodovsky, M. (2001). GeneMarkS: a self-training method for prediction of gene starts in microbial genomes. Implications for finding sequence motifs in regulatory regions. *Nucleic Acids Res.* 29, 2607–2618. doi: 10.1093/nar/29.12.2607

Braun, V. Jr., Hertwig, S., Neve, H., Geis, A., and Teuber, M. (1989). Taxonomic differentiation of bacteriophages of *Lactococcus lactis* by electron microscopy, DNA-DNA hybridization, and protein profiles. *Microbiology* 135, 2551–2560.

Brooke, J. S., and Valvano, M. A. (1996). Biosynthesis of inner core lipopolysaccharide in enteric bacteria identification and characterization of a conserved phosphoheptose isomerase. *J. Biol. Chem.* 271, 3608–3614. doi: 10.1074/jbc.271.7.3608

Buchanan, R. E., and Gibbons, N. E. (1974). *Bergey's manual of determinative bacteriology*. Baltimore: Williams and Wilkins.

Casjens, S., Winn-Stapley, D. A., Gilcrease, E. B., Morona, R., Kühlewein, C., Chua, J. E., et al. (2004). The chromosome of *Shigella flexneri* bacteriophage Sf6: complete nucleotide sequence, genetic mosaicism, and DNA packaging. *J. Mol. Biol.* 339, 379–394. doi: 10.1016/j.jmb.2004.03.068

Clokie, M. R., and Kropinski, A. M. (2009). *Bacteriophages*. Totowa, NJ: Springer.

Connor, T. R., Barker, C. R., Baker, K. S., Weill, F. -X., Talukder, K. A., Smith, A. M., et al. (2015). Species-wide whole genome sequencing reveals historical global spread and recent local persistence in *Shigella flexneri*. *eLife* 4:e07335. doi: 10.7554/eLife.07335

Doore, S. M., Schrad, J. R., Perrett, H. R., Schrad, K. P., Dean, W. F., and Parent, K. N. (2019). A cornucopia of *Shigella* phages from the cornhusker state. *Virology* 538, 45–52. doi: 10.1016/j.virol.2019.09.007

Duckworth, D. H. (1976). Who discovered bacteriophage? *Bacteriol. Rev.* 40, 793–802.

Egoz, N., Shmilovitz, M., Kretzer, B., Lucian, M., Porat, V., and Raz, R. (1991). An outbreak of *Shigella sonnei* infection due to contamination of a municipal water supply in northern Israel. *J. Infect.* 22, 89–93. doi: 10.1016/0163-4453(91)91122-e

Finn, R. D., Clements, J., Arndt, W., Miller, B. L., Wheeler, T. J., Schreiber, F., et al. (2015). HMMER web server: 2015 update. *Nucleic Acids Res.* 43, W30–W38. doi: 10.1093/nar/gkv397

Garner, E., Benitez, R., von Wagoner, E., Sawyer, R., Schaberg, E., Hession, W. C., et al. (2017). Stormwater loadings of antibiotic resistance genes in an urban stream. *Water Res.* 123, 144–152. doi: 10.1016/j.watres.2017.06.046

Gasteiger, E., Hoogland, C., Gattiker, A., Duvaud, S'e., Wilkins, M. R., Appel, R. D., et al. (2005). *Protein identification and analysis tools on the ExPASy server*. Totowa, NJ: Springer.

Gkoutzourelas, A., Barmakoudi, M., and Bogdanos, D. P. (2020). A bioinformatics analysis reveals novel pathogens as molecular mimicry triggers of systemic sclerosis. *Mediterr. J. Rheumatol.* 31, 50–70. doi: 10.31138/mjr.31.1.50

Hamdi, S., Rousseau, G. M., Labrie, S. J., Tremblay, D. M., Kourda, R. S., Slama, K. B., et al. (2017). Characterization of two polyvalent phages infecting *Enterobacteriaceae*. *Sci. Rep.* 7:40349. doi: 10.1038/srep40349

Hatfull, G. F., and Hendrix, R. W. (2011). Bacteriophages and their genomes. *Curr. Opin. Virol.* 1, 298–303. doi: 10.1016/j.coviro.2011.06.009

He, F., Han, K., Liu, L., Sun, W., Zhang, L., Zhu, B., et al. (2012). Shigellosis outbreak associated with contaminated well water in a rural elementary school: Sichuan Province, China, June 7–16, 2009. *PLoS One* 7:e47239. doi: 10.1371/journal.pone.0047239

Hendrix, R. W., Hatfull, G. F., Ford, M. E., Smith, M. C., and Burns, R. N. (2002). "Evolutionary relationships among diverse bacteriophages and prophages: all the world's a phage" in *Horizontal gene transfer.* eds. M. Syvanen and C. Kado (Elsevier), 133–VI.

Jamal, M., Chaudhry, W. N., Hussain, T., Das, C. R., and Andleeb, S. (2015). Characterization of new *Myoviridae* bacteriophage WZ1 against multi-drug resistant (MDR) *Shigella dysenteriae*. *J. Basic Microbiol.* 55, 420–431. doi: 10.1002/jobm.201400688

Jun, J. W., Giri, S. S., Kim, H. J., Yun, S. K., Chi, C., Chai, J. Y., et al. (2016a). Bacteriophage application to control the contaminated water with *Shigella*. *Sci. Rep.* 6:22636. doi: 10.1038/srep22636

Jun, J. W., Kim, J. H., Shin, S. P., Han, J. E., Chai, J. Y., and Park, S. C. (2013). Characterization and complete genome sequence of the *Shigella* bacteriophage pSf-1. *Res. Microbiol.* 164, 979–986. doi: 10.1016/j.resmic.2013.08.007

Jun, J. W., Kim, H. J., Yun, S. K., Chai, J. Y., Lee, B. C., and Park, S. C. (2016b). Isolation and comparative genomic analysis of T1-like *Shigella* bacteriophage pSf-2. *Curr. Microbiol.* 72, 235–241. doi: 10.1007/s00284-015-0935-2

Jun, J. W., Yun, S. K., Kim, H. J., Chai, J. Y., and Park, S. C. (2014). Characterization and complete genome sequence of a novel N4-like bacteriophage, pSb-1 infecting *Shigella boydii*. *Res. Microbiol.* 165, 671–678. doi: 10.1016/j.resmic.2014.09.006

Kropinski, A. M., Mazzocco, A., Waddell, T. E., Lingohr, E., and Johnson, R. P. (2009). Enumeration of bacteriophages by double agar overlay plaque assay. *Methods Mol. Biol.* 501, 69–76. doi: 10.1007/978-1-60327-164-6_7

Kropinski, A. M., Sulakvelidze, A., Konczy, P., and Poppe, C. (2007). "*Salmonella* phages and prophages—genomics and practical aspects" in *Salmonella.* eds. H. Schatten and A. Eisenstark (Totowa, NJ: Springer), 133–175.

Kumar, S., Stecher, G., and Tamura, K. (2016). MEGA7: molecular evolutionary genetics analysis version 7.0 for bigger datasets. *Mol. Biol. Evol.* 33, 1870–1874. doi: 10.1093/molbev/msw054

Löfdahl, M., Ivarsson, S., Andersson, S., Långmark, J., and Plym-Forshell, L. (2009). An outbreak of *Shigella dysenteriae* in Sweden, May-June 2009, with sugar snaps as the suspected source. *Eur. Secur.* 14, 29–35. doi: 10.2807/ese.14.28.19268-en

Männistö, R. H., Kivelä, H. M., Paulin, L., Bamford, D. H., and Bamford, J. K. (1999). The complete genome sequence of PM2, the first lipid-containing bacterial virus to be isolated. *Virology* 262, 355–363. doi: 10.1006/viro.1999.9837

Morozova, V., Kozlova, Y., Shedko, E., Babkin, I., Kurilshikov, A., Bokovaya, O., et al. (2018). Isolation and characterization of a group of new *Proteus* bacteriophages. *Arch. Virol.* 163, 2189–2197. doi: 10.1007/s00705-018-3853-3

Oliveira, H., Pinto, G., Oliveira, A., Noben, J. -P., Hendrix, H., Lavigne, R., et al. (2017). Characterization and genomic analyses of two newly isolated *Morganella* phages define distant members among *Tevenvirinae* and *Autographivirinae* subfamilies. *Sci. Rep.* 7:46157. doi: 10.1038/srep46157

Puzari, M., Sharma, M., and Chetia, P. (2018). Emergence of antibiotic resistant *Shigella* species: a matter of concern. *J. Infect. Public Health* 11, 451–454. doi: 10.1016/j.jiph.2017.09.025

Salamov, V. S. A., and Solovyevand, A. (2011). "Automatic annotation of microbial genomes and metagenomic sequences" in *Metagenomics and its applications in agriculture.* ed. R. W. Li (Hauppauge: Nova Science Publishers), 61–78.

Sambrook, J., and Russell, D. W. (2001). *Molecular cloning: A laboratory manual*. NY: Cold Spring Harbor Laboratory.

Schattner, P., Brooks, A. N., and Lowe, T. M. (2005). The tRNAscan-SE, snoscan and snoGPS web servers for the detection of tRNAs and snoRNAs. *Nucleic Acids Res.* 33, W686–W689. doi: 10.1093/nar/gki366

Shahin, K., Bao, H., Komijani, M., Barazandeh, M., Bouzari, M., Hedayatkhah, A., et al. (2019a). Isolation, characterization, and PCR-based molecular identification of a *siphoviridae* phage infecting *Shigella dysenteriae*. *Microb. Pathog.* 131, 175–180. doi: 10.1016/j.micpath.2019.03.037

Shahin, K., and Bouzari, M. (2018). Bacteriophage application for biocontrolling *Shigella flexneri* in contaminated foods. *J. Food Sci. Technol.* 55, 550–559. doi: 10.1007/s13197-017-2964-2

Shahin, K., Bouzari, M., Komijani, M., and Wang, R. (2020). A new phage cocktail against multidrug, ESBL-producer isolates of *Shigella sonnei* and *Shigella flexneri* with highly efficient Bacteriolytic activity. *Microb. Drug Resist.* 26, 831–841. doi: 10.1089/mdr.2019.0235

Shahin, K., Bouzari, M., and Wang, R. (2018). Isolation, characterization and genomic analysis of a novel lytic bacteriophage vB_SsoS-ISF002 infecting *Shigella sonnei* and *Shigella flexneri*. *J. Med. Microbiol.* 67, 376–386. doi: 10.1099/jmm.0.000683

Shahin, K., Bouzari, M., and Wang, R. (2019b). Complete genome sequence analysis of a lytic *Shigella flexneri* vB_SflS-ISF001 bacteriophage. *Turk. J. Biol.* 43, 99–112. doi: 10.3906/biy-1808-97

Shahin, K., Bouzari, M., Wang, R., and Khorasgani, M. R. (2019c). Distribution of antimicrobial resistance genes and integrons among *Shigella* spp. isolated from water sources. *J. Glob. Antimicrob. Resist.* 19, 122–128. doi: 10.1016/j.jgar.2019.04.020

Shahin, K., Bouzari, M., Wang, R., and Yazdi, M. (2019d). Prevalence and molecular characterization of multidrug-resistant *Shigella* species of food origins and their inactivation by specific lytic bacteriophages. *Int. J. Food Microbiol.* 305:108252. doi: 10.1016/j.ijfoodmicro.2019.108252

Sullivan, M. J., Petty, N. K., and Beatson, S. A. (2011). Easyfig: a genome comparison visualizer. *Bioinformatics* 27, 1009–1010. doi: 10.1093/bioinformatics/btr039

Suttle, C. A. (2005). Viruses in the sea. *Nature* 437, 356–361. doi: 10.1038/nature04160

WHO (2005). Shigellosis: disease burden, epidemiology and case management. *Wkly Epidemiol. Rec.* 80, 94–99.

Yazdi, M., Bouzari, M., Ghaemi, E. A., and Shahin, K. (2020). Isolation, characterization and genomic analysis of a novel bacteriophage VB_EcoS-Golestan infecting multidrug-resistant *Escherichia coli* isolated from urinary tract infection. *Sci. Rep.* 10:7690. doi: 10.1038/s41598-020-63048-x

Zafar, N., Mazumder, R., and Seto, D. (2002). CoreGenes: a computational tool for identifying and cataloging "core" genes in a set of small genomes. *BMC Bioinformatics* 3:12. doi: 10.1186/1471-2105-3-12

Zimmermann, L., Stephens, A., Nam, S. -Z., Rau, D., Kübler, J., Lozajic, M., et al. (2018). A completely reimplemented MPI bioinformatics toolkit with a new HHpred server at its core. *J. Mol. Biol.* 430, 2237–2243.

Conflict of Interest: The authors declare that the research was conducted in the absence of any commercial or financial relationships that could be construed as a potential conflict of interest.

Copyright © 2021 Shahin, Barazandeh, Zhang, Hedayatkhah, He, Bao, Mansoorianfar, Pang, Wang, Wei and Wang. This is an open-access article distributed under the terms of the Creative Commons Attribution License (CC BY). The use, distribution or reproduction in other forums is permitted, provided the original author(s) and the copyright owner(s) are credited and that the original publication in this journal is cited, in accordance with accepted academic practice. No use, distribution or reproduction is permitted which does not comply with these terms.

frontiers in Microbiology

ORIGINAL RESEARCH
published: 24 March 2021
doi: 10.3389/fmicb.2021.627897

Genetic Polymorphism Drives Susceptibility Between Bacteria and Bacteriophages

Xiaoxu Zhang[1,2†], Dongyan Xiong[1,2†], Junping Yu[1], Hang Yang[1], Ping He[1,2] and Hongping Wei[1]*

[1] Key Laboratory of Emerging Pathogens and Biosafety, Centre for Biosafety Mega-Science, Wuhan Institute of Virology, Chinese Academy of Sciences, Wuhan, China, [2] College of Life Science, University of Chinese Academy of Sciences, Beijing, China

Phage therapy has attracted much attention for the treatment of antibiotic-resistant bacteria in recent years. However, it is common for bacteria to obtain resistance capability in short time after interaction with a lytic phage, as observed in phage therapy and co-culture of host and phage in a lab. In order to understand the mechanisms behind resistance, *Staphylococcus aureus* AB91118 and its lytic phage LQ7 were studied as a model system. A mutant strain named R1-3-1 resistant to the ancestral phage LQ7 was isolated, and then phages experimentally evolved from LQ7 were able to kill R1-3-1. Genomes of the two bacterial strains and the three phages (LQ7, ELQ7P-10, and ELQ7P-20) were analyzed based on deep sequencing data of NGS. Analyses showed that a few mutations could be identified in R1-3-1 and the evolved phages. Instead, in all the genomes of the bacteria and the phages, there exists genetic polymorphism of minor alleles, which distributes in many functional genes. Specifically, in the AB91118-LQ7 system it was found that the unique polymorphism sites in R1-3-1 associated to metabolic pathways could be inhibited by chloramphenicol (CHL). The resistant mutant R1-3-1 could become sensitive to the phage LQ7 in the presence of CHL. Combined use of CHL and the evolved phage from 20 cycles (ELQ7P-20) could produce the least resistance when killing the bacteria AB91118. The genetic polymorphism of minor alleles would be a new mechanism to drive the co-evolution between a phage and its host, which may enable the phage and the host get ready and fast response to the selective pressure from one to the other.

Keywords: bacteriophage, *Staphylococcus aureus*, experimental evolution, genetic polymorphism, minor alleles

OPEN ACCESS

Edited by:
Yigang Tong,
Beijing University of Chemical Technology, China

Reviewed by:
Hidetomo Iwano,
Rakuno Gakuen University, Japan
Jingmin Gu,
Jilin University, China

***Correspondence:**
Hongping Wei
hpwei@wh.iov.cn

† These authors have contributed equally to this work

Specialty section:
This article was submitted to Virology, a section of the journal Frontiers in Microbiology

Received: *10 November 2020*
Accepted: *28 February 2021*
Published: *24 March 2021*

Citation:
Zhang X, Xiong D, Yu J, Yang H, He P and Wei H (2021) Genetic Polymorphism Drives Susceptibility Between Bacteria and Bacteriophages. Front. Microbiol. 12:627897. doi: 10.3389/fmicb.2021.627897

INTRODUCTION

With the emergence of antibiotic-resistant bacteria such as methicillin-resistant *S. aureus* (MRSA) and vancomycin-resistant *S. aureus* (VRSA), the treatment of bacterial infections through antibiotics has become increasingly problematic (Sakoulas et al., 2005; Senok et al., 2019). As an alternative, phage therapy has attracted new interest for the treatment of antibiotic-resistant bacteria in recent years (Levin and Bull, 2004; Lyon, 2017). Normally lytic bacteriophages were used for phage therapy (Sulakvelidze et al., 2001). For example, phage therapy has been found to be effective for treatment of staphylococcal infections in animals (Garcia et al., 2019;

Lehman et al., 2019). Clinical trials in human (Kishor et al., 2016; Ooi et al., 2019; Prazak et al., 2019) are also in progress. However, like antibiotic resistance, the use of phages can lead to the emergence of phage-resistant strains, which would be a significant obstacle for phage therapy (Denes et al., 2015; El Haddad et al., 2018). It is important to understand how bacteria and bacteriophage evolve in the presence of the other.

Previous studies have shown that the interaction between a phage and a bacterium is a co-evolutionary arms race. Bacteria could resist the infections of phages by a range of antiviral mechanisms such as adsorption-blocking systems, blocking phage DNA entry, restriction–modification (R/E) systems, CRISPR Cas systems, and abortive infection (Abi), etc (Labrie et al., 2010; Safari et al., 2020). Phages, in response, can evolve multiple tactics to overcome these defensive strategies in order to thrive in most environments (Labrie et al., 2010). For example, phages can evolve by specifically modifying their genomes to gain increased capability such as a broader host range, a faster adsorption or a more effective bactericidal capacity to defeat bacterial defense (Samson et al., 2013). Coevolution between bacteria and bacteriophages can be characterized as an infinitive constant evolutionary battle (phage-host arms race) (Golais et al., 2013). However, most of the current studies have mainly focused on the mutations or indels of genes in bacterial and phage genomes. For example, Denes et al. (2015) revealed that mutations associated with phage resistance in *Listeria monocytogenes* were found primarily in two loci, which link to phage adsorption. The phage resistant mutants of *Acinetobacter baumannii* had a single-nucleotide deletion resulting in a frameshift in a gene within the K locus (Gordillo Altamirano et al., 2021). Another lytic phage SPO1 could gain a broader host range against *Bacillus subtilis* after having mutations in two genes, encoding the baseplate, and the fiber proteins required for host attachment (Habusha et al., 2019). It needs more studies to understand how these mutations were generated. It is also not clear if a phage could evolve further to obtain the capability to kill the phage-resistant bacteria. Finding the mechanisms behind will be important not only to understand the co-evolution between host and phage, but also to find the solutions to overcome phage resistance during phage therapy.

In present study, we try to understand how bacteria evolve resistance in the presence of a lytic phage, which is normally chosen for phage therapy, and if the phage could evolve further experimentally to overcome the developed resistant bacteria. *Staphylococcus aureus* AB91118 strain and its novel lytic dsDNA phage LQ7, a natural isolate from a raw river sample (Yan et al., 2017), were studied as an example. The results showed that besides mutations, a new mechanism, minor alleles in the genomes of the bacteria and the phages, would be important factors contributing to the resistance of the host to the phage and vice versa.

MATERIALS AND METHODS

The design for the overall experiment is shown in **Figure 1**. Briefly, *S. aureus* AB91118 was cultured with a lytic phage LQ7 for more than 24 h on an agar plate and then a colony named R1-3-1 resistant to the phage LQ7 were isolated. After that, LQ7 were experimentally evolved with R1-3-1 for 20 rounds. Genomes of *S. aureus* AB91118 and mutant R1-3-1 were sequenced and analyzed to find their difference. Genome sequences of LQ7 and the evolved phages at 10th and 20th round were also analyzed and compared with each other to find the possible changes in their genomes.

Strains and Culture Conditions

Staphylococcus aureus AB91118 was bought from China Microbe Collection Center (CMCC) and cultured at 37°C with shaking (180 rpm) in Luria-Bertani (LB) broth. Phage LQ7 was previously isolated from a raw river sample (Yan et al., 2017). Plaque purification and enumeration of phage titers were all performed using the double-layer overlay method (0.7% agar for the top layer and 1.5% agar for the LB layer).

Isolation of Phage-Resistant Bacterial Mutant R1-3-1

Isolation of a phage-resistant mutant was performed as described in previous studies (Habusha et al., 2019). Briefly, a single colony of *S. aureus* AB91118 formed on agar plate was inoculated into LB broth and cultivated at 37°C with shaking at 180 rpm. After cultivation for 8 h to exponential growth phase, the suspension containing 5×10^8 CFU/mL ($OD_{600} \approx 0.45$) of *S. aureus* AB91118 was mixed with phage LQ7 at a multiplicity of infection (MOI) of 100. The mixture was left at 37°C for 10 min for the adsorption and infection of the phage. Then the infected culture was poured on a double-layer plate and incubated until form of some phage-resistant bacterial colonies (in about 24 h) as shown in **Figure 1A**. After that, a single colony was picked up and inoculated onto a phage containing semisolid plate for further culture to obtain resistant mutants. After repeating this process for five times, a phage-resistant mutant named as R1-3-1 was isolated.

Growth Rate of Bacteria

Growth rates of *S. aureus* AB91118 and R1-3-1 were measured by adding 200 μL of the bacteria solution in fresh LB medium ($OD_{600} \approx 0.45$) into a 96-well plate for 10 h using a microplate reader (Biotek, US), which tracks optical density at 600 nm (OD_{600}). The growth rates were also measured in the presence of phage LQ7 at MOI ≈ 10. At the same time, 200 μL of LB liquid medium without bacteria and phage buffer (50 mM Tris-Cl, pH 7.5, containing 150 mM NaCl, 10 mM $MgCl_2 \cdot 6H_2O$ and 2 mM $CaCl_2$) were used as blank controls. The experiments were performed in triplicate.

The Experimental Evolution of Phage LQ7

The experimental evolution of phage LQ7 was conducted as reported previously (Akusobi et al., 2018). Briefly, phage-resistance bacterial mutant R1-3-1 at stationary-phase were stored at −80°C to keep them stable in aliquots and one aliquot was used for each round of the phage evolution experiment.

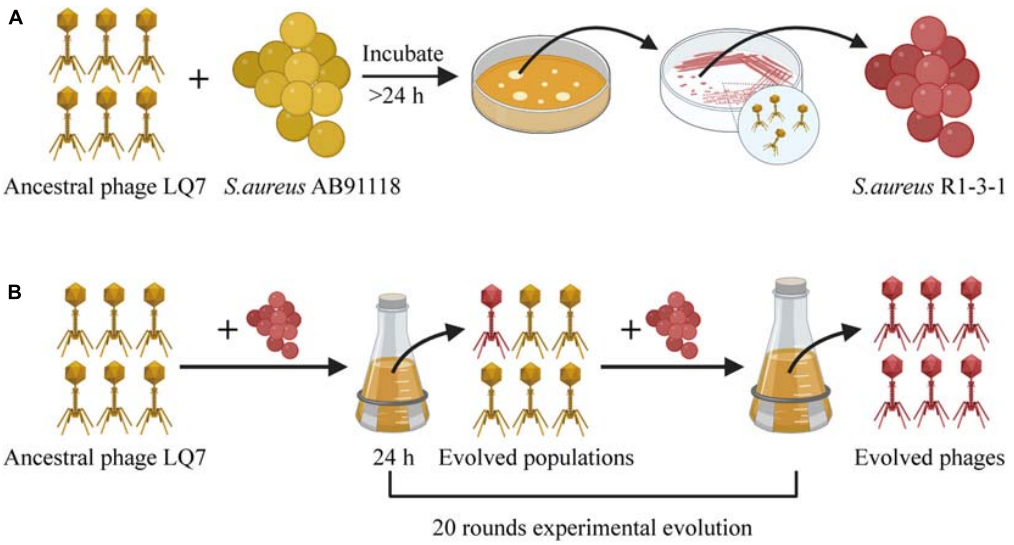

FIGURE 1 | The overall experiment design for studying the evolution between *S. aureus* AB91118 and lytic phage LQ7. **(A)** Phage-resistant mutant isolation. **(B)** Experimental evolution of phages.

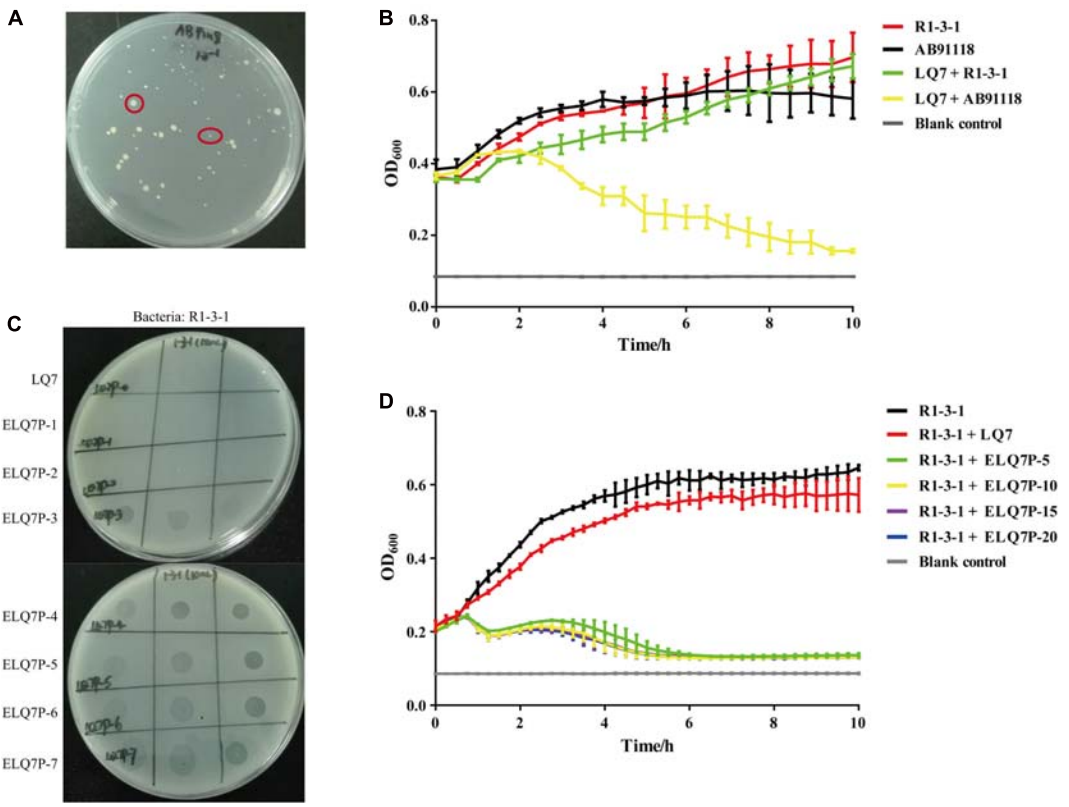

FIGURE 2 | Isolation of *S. aureus* mutants resistant to lytic phage LQ7 and evolution of phage LQ7 against phage-resistant mutant R1-3-1. **(A)** Phage-resistant mutants on the double-layer plate show varied sizes after 24 h incubation of *S. aureus* AB91118 and LQ7. **(B)** Growth curves of R1-3-1 and AB91118 in presence of LQ7 at MOI = 10. Error bars show average values and SD of three independent experiments. **(C)** Spots formed on the double-layer plates by the evolved phages after different rounds of evolution against R1-3-1. **(D)** Growth curves of R1-3-1 in presence of LQ7 or evolve phages (ELQ7P-5, ELQ7P-10, ELQ7P-15, ELQ7P-20) at MOI = 1. Error bars show average values and SD of three independent experiments.

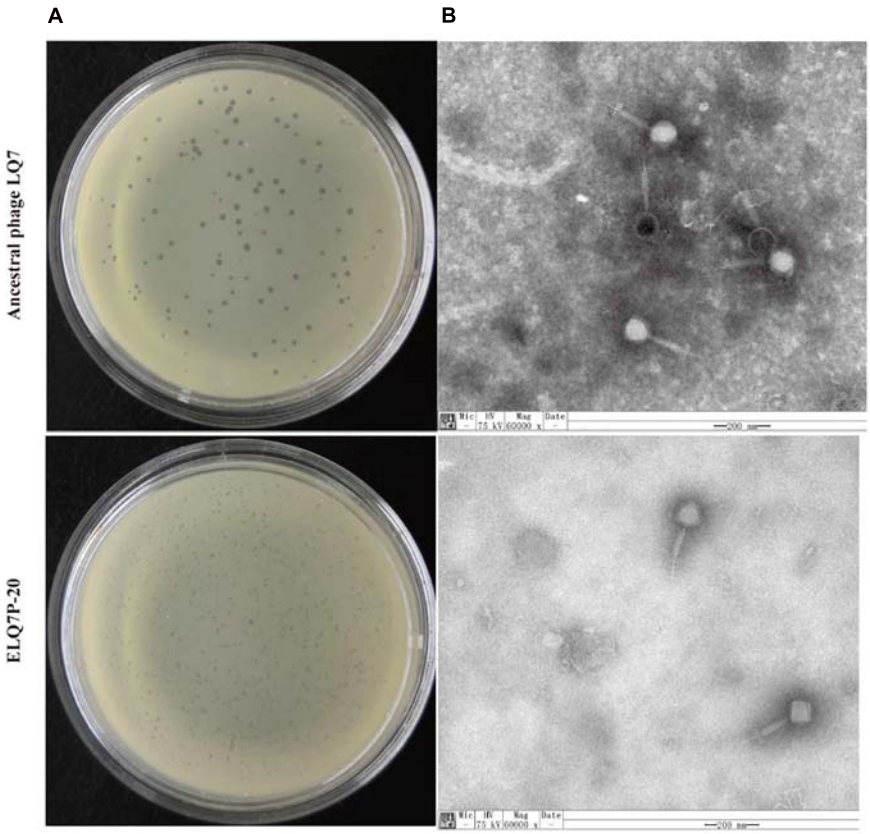

FIGURE 3 | Plaques of LQ7 and ELQ7P-20 formed on lawns of AB91118 **(A)** and TEM images **(B)** of phage LQ7 and ELQ7P-20 stained negatively with freshly prepared 2% phosphor tungstic acid. Scale bar = 200 nm.

At the start of the experiment, 20 μL of ancestral phage LQ7 (1×10^9 PFU/mL) and 200 μL of the stationary-phase R1-3-1 were added to a conical flask containing 20 mL LB. The mixture was incubated at 37°C for 24 h with shaking. After that, the mixture was centrifuged with 16,000 × *g* for 10 min at 4°C. Then the lysate in the supernatant was filtered through a 0.22 μm sterile filter. 20 μL of the filtered lysate was mixed with 200 μL of the stationary-phase bacteria R1-3-1 again to perform the next round. This process was repeated for 20 successive rounds. The lysate of each round, containing evolved phages, was collected and stored at 4°C until use.

CHARACTERIZATION OF ANCESTRAL PHAGE LQ7 AND EVOLVED PHAGES

Infection Activity Test

A total of 500 μL of R1-3-1 in exponential growth phase with a concentration of 5×10^8 CFU/mL was mixed with melted semisolid agar (0.7% top agar) and poured onto solid Luria Bertani agar plate first. Then 2.5 μL of ancestral phage LQ7 and the evolved phages were dripped into the soft agar containing R1-3-1, respectively. After overnight incubation, spot formation was examined.

Effects on Bacterial Growth

Growth of R1-3-1 infected with either the ancestral phage LQ7 or the evolved phages from different rounds of evolution (ELQ7P-5, ELQ7P-10, ELQ7P-15, and ELQ7P-20) were measured in a 96 well plate as described above. Each well was added with 100 μL LB medium, 50 μL bacteria (5×10^8 CFU/mL) and 50 μL phage (5×10^8 PFU/mL) at MOI = 1. LB medium was used as the blank control. The experiments were performed in triplicate.

Transmission Electron Microscope (TEM)

The phage LQ7 and four evolved phages (ELQ7P-5, ELQ7P-10, ELQ7P-15, and ELQ7P-20) was analyzed using transmission electron microscopy (TEM). Briefly, the amplified phages were concentrated at 4°C using CsCl density gradient ultracentrifugation at 2,10,000 × *g* for 2 h in a Beckman SW 41 Ti rotor. The phage collected was dialyzed using a cellulose membrane in phage buffer for 12 h. Then 20 μL of the phage suspension was dripped on a carbon-coated copper grid and allowed to adsorb for 10 min. Excess liquid was drawn off carefully by touching the side of the grid with filter paper. The grid was allowed to dry in air. Phages were negatively stained with freshly prepared 2% (wt/vol) phosphor tungstic acid (PTA) for 3 min. The copper grids were air dried for 2 h and then

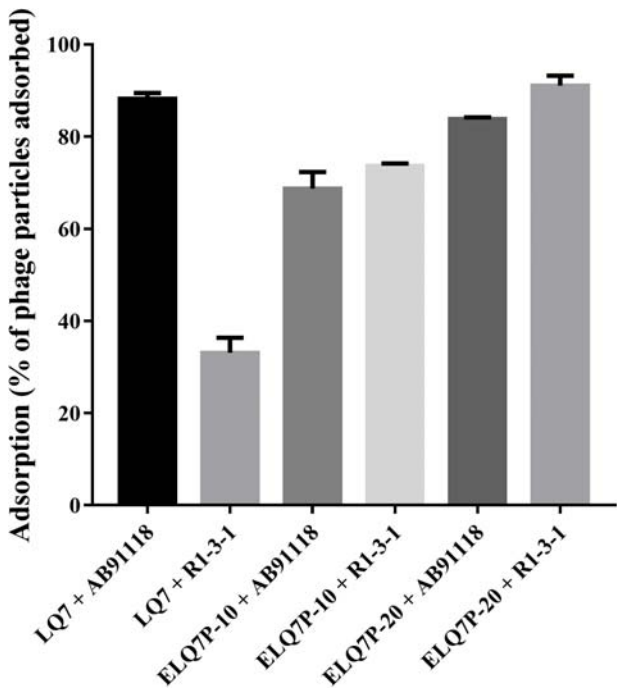

FIGURE 4 | Adsorption rates (percentage of phage particles adsorbed) of evolved and ancestral phage against wild type *S. aureus* AB91118 and phage-resistance mutant *S. aureus* R1-3-1. Error bars show average values and SD of three independent experiments.

observed under a transmission electron microscope (Hitachi H-7000FA, Japan) at an operating voltage of 75 kV.

Adsorption Assay

Adsorption rate of phages to bacteria was determined as described previously (Uchiyama et al., 2017). Mixture containing 200 μL of bacteria (OD_{600} = 0.6), 100 μL of phage (1×10^4 PFU/mL) and 200 μL of LB medium was incubated for 7.5 min at 37°C. Respective phages in LB medium were used as the control groups. After pelleting the bacterial cells by centrifugation (21,000 × *g*, 1 min), the concentration of the unbound phages in the supernatant was measured using a plaque assay. The experiments were performed in triplicate.

GENOME SEQUENCING AND ANALYSIS

DNA Extraction and Sequencing

To extract DNA from *S. aureus*, *S. aureus* cells were harvested by centrifuging 5 mL of bacteria in exponential growth phase at 14,000 × *g* for 5 min. The pellets were re-suspended in 500 μL TE buffer (10 mM Tris–HCl, 1 mM EDTA, pH 7.6) and lysed with lysostaphin (1mg/mL, Sigma-Aldrich, Saint-Louis, MO, United States) at 37°C for 1 h. The cell lysate was then treated with 5 μL RNase A (10 mg/mL) (Thermo Fisher Scientific) at 37°C for 1 h to remove RNA, followed by adding 0.5 mg/mL proteinase-K and incubation at 56°C for 1 h. Finally, bacteria genomic DNA was extracted using the phenol-chloroform protocol as described previously (Sun, 2010).

To extract phage DNA, a single plaque of LQ7 were picked and propagated to obtain 20 mL of phage lysate for the final DNA preparation. Genomic DNA of the evolved phages at round 10th and 20th (ELQ7P-10 and ELQ7P-20) were extracted from 20 mL of the lysates directly (Kering et al., 2020). The quality and quantity of the DNA obtained were determined using a NanoDrop spectrophotometer (ND-2000, Thermo Fisher Scientific, Waltham, MA, United States). Genome high-throughput sequencing was done by Benagen Inc (Wuhan, Hubei, China) using Illumina NovaSeq 6000 sequencer for the phages and the bacteria and 150 bp pair-end reads were generated. Furthermore, Nanopore PromethION platform was performed on the machine of Oxford Nanopore Technologies, ONT for the bacteria.

Variation and Polymorphism Analyses of Bacteria and Phage Genomes

The bacterial genome sequences were obtained by the Nanopore platform sequencing data using software Wtdbg2 and Minimap (Li, 2016; Ruan and Li, 2020) and errors were corrected using the high quality NGS data (> Q30) on the base-level through Nanopolish software (Loman et al., 2015). The phage LQ7 genome was *de novo* assembled from the NGS data by SPAdes v3.13.0 (Bankevich et al., 2012) with the default parameters. During the genome assembling, each base with major allele frequency was also analyzed. In addition, the software Prokka[1]was used to annotate the bacteria and phage genes.

For the genetic variation analysis of the bacteria and the phages, the clean reads of the NGS data were aligned to the reference genomes (AB91118 genome for the bacteria and LQ7 phage genome for the phages) using BWA software (Li and Durbin, 2009). The sequencing depth was calculated by the aligned reads using SAMtools and Bedtools (Li et al., 2009; Quinlan, 2014). Mutation information was archived by software Bcftools (Narasimhan et al., 2016).

For the genetic polymorphism analysis of the bacteria and the phages, the sequencing error rates of NGS were estimated using Jellyfish software with the default options (Marçais and Kingsford, 2011). The genetic polymorphisms were identified based on the minor allele frequency (MAF). The minor allele frequency (MAF) was calculated by the VarScan software (Koboldt et al., 2012) (version: 2.3.9, with the default options chose) and confirmed by the IGV software (Thorvaldsdóttir et al., 2013) (version 2.7.2). According to the sequencing error rates and related studies (Broniewski et al., 2020), the sites with the both minor allele frequency (MAF) greater than 0.03 and sequencing depth at least 100 were considered as polymorphism sites to minimize sequencing errors and noises. This approach may inevitably underestimate the true number of the polymorphism sites since the sites with lower MAF were filtered out to limit the noise caused by sequencing errors.

Finally, genes with polymorphism sites as well as mutations in the genomes were identified by a R script. Five identified

[1]http://www.vicbioinformatics.com/software.prokka.shtml

polymorphism sites with higher MAF and the mutations were verified by PCR and Sanger sequencing using the designed primers based on the genome sequences. Gene Ontology (GO) (Gene Ontology Consortium, 2015) enrichment analysis was performed through the R package ClusterProfiler; Yu et al. (2012) with default options based on the genes with the polymorphism sites that occurred only in the R1-3-1 genome. All statistical analysis was performed by the R program (version 3.5.3)[2].

EFFECTS OF BACTERIOSTATIC ANTIBIOTICS AND PHAGES ON THE GROWTH OF R1-3-1 AND MUTANT FREQUENCY OF AB91118

Minimum Inhibitory Concentration (MIC) of Chloramphenicol

The stock solution of chloramphenicol (CHL) (Sigma Chemical Co., St. Louis, MO, United States) was prepared by dissolving CHL in ethyl alcohol to a final concentration of 1.024 mg/mL. The MICs of CHL against *S. aureus* AB91118 and R1-3-1 were determined using a broth dilution method (Wiegand et al., 2008). Briefly, bacteria (10^5 CFU/mL) were inoculated into LB medium with serial two-fold dilution CHL from concentration of 256 μg/mL. After incubation for 20 h at 37°C, minimum inhibitory concentration (MIC) was determined as the CHL concentration at which no visible growth of *S. aureus* was observed.

Growth Rate of *S. aureus* R1-3-1

The antimicrobial activity of chloramphenicol alone, phage alone, and the combination of the two was evaluated against *S. aureus* R1-3-1 as described previously (Jo et al., 2016). R1-3-1 prepared in LB to a concentration of 10^6 CFU/mL was incubated in a 96-well plate for 16 h in the presence of CHL (1/4 MIC or 1/2 MIC; 1 μg/mL or 2 μg/mL), LQ7 phage (10^6 PFU/mL), or the combination (1 μg/mL or 2 μg/mL of CHL and 10^6 PFU/mL of the phage). LB medium was used as a blank control and R1-3-1 without chloramphenicol and phage was used as a growth control. The optical density of the wells at 600 nm (OD_{600}) was tracked using a microplate reader (Biotek, United States). The experiments were performed in triplicate.

Mutant Rates Assay

The mutant rates of *S. aureus* AB91118 resistant to CHL, LQ7 or ELQ7P-20 were estimated, in triplicate, according to the method described previously (Jo et al., 2016; Valério et al., 2017). *S. aureus* AB91118 (5×10^6 CFU/mL) was cultured in presence of CHL (at the concentration of 1/2 MIC), LQ7 (5×10^6 PFU/mL), ELQ7P-20 (5×10^6 PFU/mL), or different combinations of the three for 48 h first. A control was set by culturing *S. aureus* AB91118 (5×10^6 CFU/mL) alone simultaneously. After the incubation, the bacteria was collected by centrifuge, washed with phosphate buffered saline (PBS: 137 mM NaCl, 2.7 mM KCl, 10 mM Na_2HPO_4, 2 mM KH_2PO_4) once, and then resuspended in PBS. The concentration of the bacteria in the suspensions were determined by plating serial dilutions onto LB agar plates. Finally, the mutant rates of *S. aureus* AB91118 after the 48 h incubation were determined by adjusting the bacterial concentration to 1×10^5 CFU/mL and culturing on LB agar plates for 16 h at 37°C with CHL at the concentration of 1 MIC and individual phages at MOI of 1,000, respectively. The numbers of surviving colonies on the LB with and without CHL or phages were counted as resistant mutant numbers and total numbers, individually. Finally, the rates of mutants were calculated by dividing the number of mutants by the total number of bacteria.

[2]https://cran.r-project.org/bin/windows/base/old/3.5.3/

RESULTS

Isolation and Growth Rate of *S. aureus* Phage-Resistant Mutant

After incubation of *S. aureus* AB91118 and the lytic phage LQ7 on the double-layer plate for more than 24 h, some colonies were formed with varied sizes as shown in **Figure 2A**. These colonies are phage-resistant, which could not be killed by LQ7. After five repeats of incubation of a selected single resistant colony with phage LQ7, a resistant mutant was isolated and named as R1-3-1.

Although R1-3-1 showed resistance to LQ7, the presence of LQ7 at MOI of 10 could retard the growth rate of R1-3-1 compared with that of R1-3-1 without LQ7 (**Figure 2B**). Moreover, in the first one hour after mixing LQ7 and R1-3-1, the OD_{600} of the bacteria suspension did not increase, which indicated that R1-3-1 did not grow or grew very slowly in the first one hour.

Comparing the growth curve of AB91118 with that of R1-3-1, it could find that after 6 h the growth rate of R1-3-1 was significantly higher than that of AB91118. Even in the presence of LQ7, the growth rate of R1-3-1 from 8 to 10 h was higher than that of AB91118.

Increased Killing Efficiency of the Evolved Phages on the Phage-Resistant Mutant

Experimental phage evolution using R1-3-1 as the host and LQ7 as the ancestral phage showed that after three rounds of evolution, the evolved phages started to show spots to R1-3-1 on the double-layer plates and the bactericidal activity of the evolved phages was retained for the subsequent rounds (**Figure 2C**). The growth curves in **Figure 2D** indicated that the evolved phages (ELQ7P-5, ELQ7P-10, ELQ7P-15, and ELQ7P-20) obtained the bactericidal activity to R1-3-1. The curves also showed that the initial bactericidal activity of the evolved phages was increased gradually as the evolution round increased. Moreover, consistent with the above results, the growth rate of R1-3-1 in the presence of LQ7 at MOI of 1 was lower than that of R1-3-1 in the absence of LQ7.

The Morphology of Phages

On the double-layer plates, the single plaque sizes of the ancestral phage LQ7 were approximately 1 mm in diameter on a lawn

of *S. aureus* AB91118, and the single plaque size of the evolved phages (ELQ7P-20) were a little smaller than that of LQ7 (**Figure 3A**). TEM analysis revealed there was no obvious change in the phage morphology between LQ7 and ELQ7P-20, and they all belong to *Myoviridae* family (**Figure 3B**). Ancestral phage LQ7 has an icosahedral capsid (88 ± 3 nm, n = 5) with a long contractile tail (200 ± 10 nm, n = 5) and evolved phage population ELQ7P-20 has an icosahedral capsid (97 ± 8 nm, n = 5) with a long contractile tail (197 ± 10 nm, n = 5). Other three evolved phages (ELQ7P-5, ELQ7P-10, ELQ7P-15) are almost identical to that of ELQ7P-20 (Figures didn't show).

Enhanced Adsorption of the Evolved Phages to Phage-Resistant R1-3-1

As shown in **Figure 4**, ancestral phage LQ7 demonstrated 88.2% adsorption rate to *S. aureus* AB91118 and 33.1% adsorption rate to *S. aureus* R1-3-1, suggesting the adsorption ability of LQ7 to phage-resistant R1-3-1 has decreased significantly. In comparison, the evolved phages ELQ7P-20 showed 83.8% adsorption rate to AB91118 and 91.0% adsorption rate to R1-3-1. The adsorption rates of the evolved phage ELQ7P-10 to both bacteria were between that of LQ7 and ELQ7P-20.

GENOME ANALYSIS

Mutations in the Genomes of Bacteria and Phages

Both genomes of *S. aureus* AB91118 and R1-3-1 were found having a size of 2,852,442 bp, including 2,654 genes, 19 rRNA, 61 tRNA, and 1 tmRNA. The average sequencing depths of *S. aureus* AB91118 and R1-3-1 were 1,516 and 1,239, respectively (**Supplementary Figure 1A**). There is only one mutation at site 2,48,520 (non-coding region) in the genome of R1-3-1, compared with that of AB91118.

The complete genome of the ancestral LQ7 is 138,579 bp in size containing 193 genes. The average sequencing depths of LQ7, ELQ7P-10 and ELQ7P-20 were 24,530, 25,737, and 23,930, respectively (**Supplementary Figure 1B**). Compared with the genome of LQ7, there are five mutations in the evolved phages ELQ7P-10 and ELQ7P-20 (**Table 1**). These mutations caused four amino acid non-synonymous substitutions.

TABLE 1 | Mutations in the evolved phage populations.

Mutation site in the genome	CDs	Encoded protein	Protein length (aa)	Amino acid change (position)
54,927	LQ7_57	Capsid and scaffold protein (contain carbohydrate binding domain)	637	Asp → Asn (577)
91,133				
91,137				
91,140	LQ7_103	Sigma factor	219	Asn → Tyr (93) Ser → Val (94)
91,141				

Analysis of Polymorphism Sites in the Genomes of Bacteria and Bacteriophage

Although the genomes of the bacteria and the phage LQ7 were determined by extracting genomic DNA from bacteria and phages growing from single colony of the bacteria and the phage, respectively, there were some polymorphism sites found to exist in the genomes, i.e., there are alternative bases with minor frequencies at certain sites of the genomes. The detailed four base frequency information on polymorphism sites in the genomes of the bacteria and the phages are listed in the **Supplementary Table 1**. Existence of some of the polymorphism sites with high MAF were verified by PCR-Sanger sequencing as shown in **Supplementary Figure 3**.

Using the criteria of MAF larger than 0.05 (which is more than 7 times of the sequencing errors 0.58% for AB91118 and 0.72% for R1-3-1) in the sequencing reads for bacteria to identify the polymorphism, there were 175 and 196 nucleotide polymorphism sites found in the genomes of AB91118 and R1-3-1, respectively (**Figures 5A,B**). Most of these sites exist more than 3 different bases (**Figures 5A,B**). Among them, there were 139 polymorphism sites existing in the both genomes of AB91118 and R1-3-1 (**Figure 5C**). Based on the unique polymorphism sites in the 38 functional genes of R1-3-1, 59 biological processes were identified by gene ontology enrichment analysis (**Figure 5D**). Most of the biological processes are related to nucleotide metabolism, energy metabolism and biomass synthesis. In particular, a biological process that responded to xenobiotic stimuli was enriched. The complete information of GO enrichment was given in the **Supplementary Table 2**.

Polymorphism sites in the genomes of the phages were also identified. Using the criteria of MAF larger than 0.03, which is more than 9 times of the sequencing errors 0.35% for LQ7, 0.34% for ELQ7P-10 and 0.17% for ELQ7P-20, in the sequencing reads for the phages to identify the polymorphism, there were 30, 31, and 29 nucleotide polymorphism sites found in the genomes of LQ7, ELQ7P-10, and ELQ7P-20, respectively (**Figures 5E–G**). For the most of these sites, 2 different bases existed (**Figures 5E–G**). Among them, there were 14 polymorphism sites existing in all the three genomes of the phages (**Figure 5H**). The phage ELQ7P-10 has 7 polymorphism sites different from LQ7, while ELQ7P-20 has 15 polymorphism sites different from LQ7. From the Venn diagram shown in **Figure 5H**, ELQ7P-10 looks like a transition from LQ7 to ELQ7P-20. Particularly, there are three common polymorphism sites at position 4,783, 4,785, and 49,236 in the genomes of ELQ7P-10 and ELQ7P-20, which belong to two different CDs encoding terminase large subunit and baseplate morphogenetic protein, causing two non-synonymous amino acids change (terminase large subunit: M25V, baseplate morphogenetic protein: K83N). The detailed base frequencies of the polymorphism sites in the genomes of phages are listed in the **Supplementary Table 3**. These polymorphism sites mainly existed in the functional genes encoding terminase large subunit, baseplate morphogenetic protein and tail lysin (at position 33,966). Further analysis showed that it was almost base A

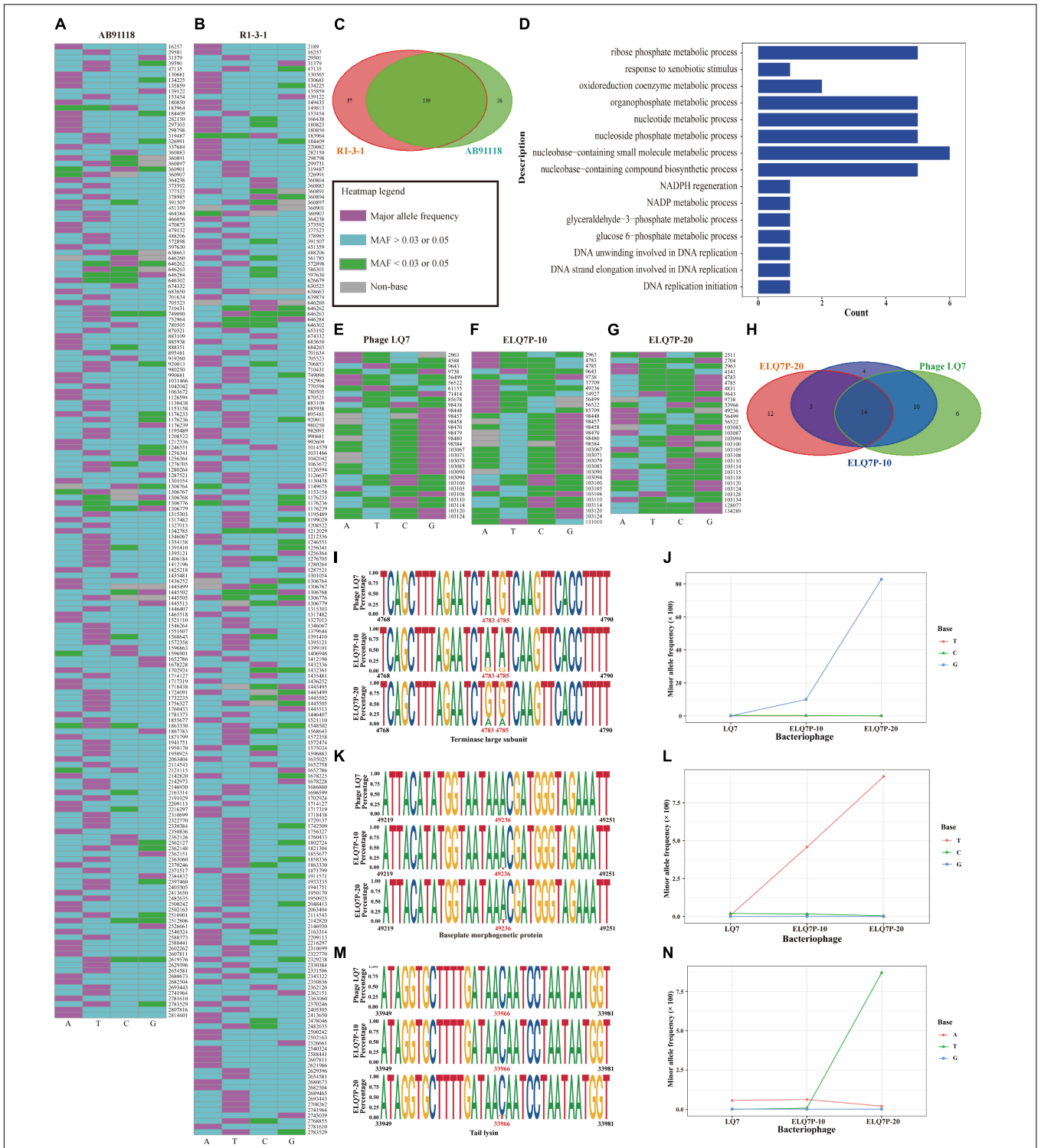

FIGURE 5 | Genetic polymorphism sites in the genomes of bacteria and phages. **(A)** Polymorphisms heatmap of bacteria AB91118. **(B)** Polymorphisms heatmap of bacteria R1-3-1. **(C)** Venn diagram of polymorphism sites in the genomes of bacteria. **(D)** Fifteen of fifty-nine enriched biological process based on the 38 genes with unique polymorphism sites in R1-3-1. **(E)** Heatmap of polymorphism sites in the genome of phage LQ7. **(F)** Heatmap of polymorphism sites in the genome of phage ELQ7P-10. **(G)** Heatmap of polymorphism sites in the genome of phage ELQ7P-20. **(H)** Venn diagram of polymorphism sites in the genomes of phages. **(I)** Polymorphism sites at position 4,783 and 4,785 in the terminase large subunit gene. **(J)** Frequency changes of 3 minor bases at the polymorphism site 4,783 in the genomes of the phages. **(K)** Polymorphism site at position 49,236 in the baseplate morphogenetic gene. **(L)** Frequency changes of 3 minor bases at the polymorphism site 49,236 in the genomes of the phages. **(M)** Polymorphism site at position 33,966 in the tail lysin gene. **(N)** Frequency changes of 3 minor bases at the polymorphism site 33,966 in the genomes of the phages.

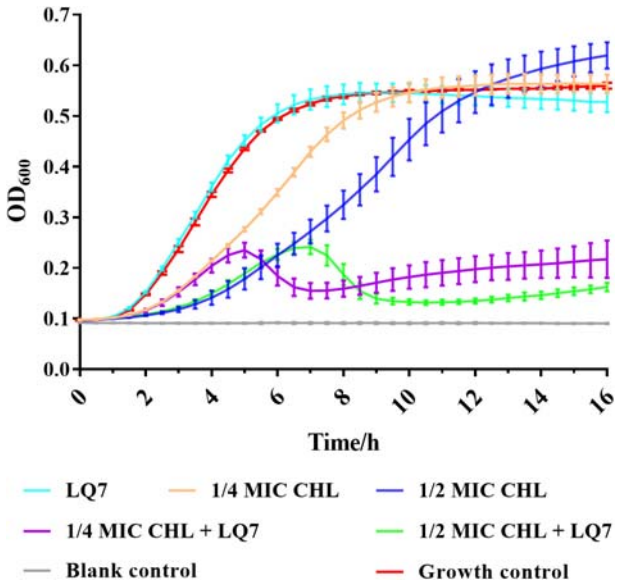

FIGURE 6 | Effects of bacteriostatic antibiotic chloramphenicol and phage on the growth of R1-3-1.

at 4,783 position in the terminase large subunit gene in the ancestral phage LQ7, but the frequency of G base, which was very low in LQ7, increased by about 290 times in ELQ7P-10, and further increased by about eight times in ELQ7P-20 during the evolution process (**Figures 5I,J**). The other two polymorphism sites at position 49,236 and 33,966 showed similar base frequency changes during the evolution (**Figures 5K–N**).

EFFECTS OF BACTERIOSTATIC ANTIBIOTICS AND PHAGE ON SUSCEPTIBILITY OF BACTERIA TO PHAGES AND ANTIBIOTICS

Since the genome comparison between AB91118 and R1-3-1 revealed that there was only one mutation in the non-coding region, it was suspected that the polymorphism sites unique in R1-3-1 would contribute to the resistance of R1-3-1 to phage LQ7 also. Because the unique polymorphism sites in R1-3-1 mainly affect the biological processes related to nucleotide metabolism, energy metabolism and biomass synthesis (**Figure 5D**), chloramphenicol, an antibiotic inhibiting metabolism, was tested to see how it would affect susceptibility of the bacteria to the phage.

The MIC of chloramphenicol was determined to be 4 μg/mL against both *S. aureus* AB91118 and mutant R1-3-1. From the growth curves in **Figure 6**, the growth of R1-3-1 could not be inhibited by LQ7 or chloramphenicol at 1/2 and 1/4 of MIC alone. However, the growth of R1-3-1 could be inhibited in the presence of both LQ7 and sublethal levels of chloramphenicol.

Further testing the growth of *S. aureus* AB91118 after 48 h incubation under different combinations of CHL and phages showed that AB91118 was inhibited most by the combination of CHL and ELQ7P-20, and followed by the combination of CHL and LQ7 (**Table 2**). At the same time, much less inhibition was observed by CHL alone or the phages alone. Comparing the phage groups without CHL, ELQ7P-20 showed better inhibition to AB91118 than LQ7. However, the combination of LQ7 and ELQ7P-20 did not improve the inhibition further.

After the 48 h incubation, the bacterial resistance frequencies (the number of the mutant resistant to CHL, LQ7 or ELQ7P-20 over that of the total bacteria in the solution) were determined (**Table 2**). Generally, the bacterial resistance frequencies in all treatment groups became higher than that for the control. Treating the bacteria with CHL could significantly increase the resistance frequency to CHL, but not to the phages. While treating the bacteria with LQ7 or ELQ7P-20 alone could induce similar resistance frequencies to both phages, LQ7 treatment developed higher resistance frequency to CHL than the ELQ7P-20 treatment, and 10 folds lower frequencies to both phages than the ELQ7P-20 treatment. Treatments by combining any two of them showed that the combination of CHL and LQ7 developed the highest resistance frequency to CHL, and the combination of LQ7 and ELQ7P-20 induced the highest resistance frequencies to both phages and the lowest to CHL. Interestingly, the combination of CHL and ELQ7P-20 showed low resistance frequency to CHL and both phages. Further combining the three of them demonstrated slightly higher frequencies to CHL, but lower frequencies to both phages than the CHL and ELQ7P-20 combination.

DISCUSSION

It is quite common in lab to observe that there will be some resistant colonies shown after incubation of host bacterium and its lytic phage on agar plate for about 1 day. Because there exist only the host and the phage in the plate, it seems not possible for the host to obtain external genetic elements to obtain resistance. Therefore, there is an interesting question: how are the resistant colonies generated?

In the current study, by isolating a single colony from the agar plate after culturing the host with the ancestral phage LQ7, mutant R1-3-1 resistant to LQ7 could be obtained. Comparing the genome of R1-3-1 with that of AB91118, only one mutation at position 248,520 in the non-coding region could be identified, which is quite surprised if the resistance of R1-3-1 is exclusively due to this mutation. Fortunately, due to the enormous reads obtained during the genome sequencing, re-analyzing them revealed there exist many minor alleles in the genomes of both AB91118 and R1-3-1 (**Figures 5A,B**). The GO enrichment results showed that the polymorphism sites unique in the R1-3-1 genome distributed in thirty-eight functional genes, which were involved in biosynthesis, nucleotide metabolism and energy metabolism of the bacterium (**Figure 5D**). Coincidently the growth rate of R1-3-1 was found significantly higher than that of AB91118 (**Figure 2B**). Normally, high growth rates indicate high levels of biomass synthesis, which agrees with the GO enrichment results. These results reminded us that these unique

TABLE 2 | Changes of bacterial quantity and the rates of mutant resistant to CHL and phages after 48 h incubation with AB91118 under different treatments.

Treatment	Bacterial quantity after 48 h incubation	Mutant rates		
		Resistant to CHL (1 MIC)	Resistant to LQ7 (MOI 1000)	Resistant to ELQ7P-20 (MOI 1000)
CHL (1/2 MIC)	$2.70 \pm 0.99 \times 10^{9}$	0.55 ± 0.03	$4.50 \pm 0.71 \times 10^{-5}$	$8.50 \pm 0.71 \times 10^{-5}$
LQ7 (MOI 1)	$1.45 \pm 0.21 \times 10^{9}$	0.40 ± 0.11	$6.10 \pm 1.55 \times 10^{-4}$	$2.80 \pm 1.41 \times 10^{-4}$
ELQ7P-20 (MOI 1)	$1.65 \pm 1.52 \times 10^{8}$	0.12 ± 0.07	$8.70 \pm 0.42 \times 10^{-3}$	$6.65 \pm 0.35 \times 10^{-3}$
CHL + LQ7	$1.30 \pm 0.42 \times 10^{6}$	0.93 ± 0.01	$2.25 \pm 0.35 \times 10^{-2}$	$2.92 \pm 1.29 \times 10^{-3}$
CHL + ELQ7P-20	$4.05 \pm 1.70 \times 10^{5}$	0.03 ± 0.01	$5.96 \pm 0.21 \times 10^{-3}$	$1.37 \pm 0.11 \times 10^{-3}$
LQ7 + ELQ7P-20	$5.65 \pm 1.62 \times 10^{8}$	0.02 ± 0.01	$8.50 \pm 0.71 \times 10^{-2}$	$3.60 \pm 0.57 \times 10^{-2}$
CHL + LQ7 + ELQ7P-20	$3.10 \pm 1.27 \times 10^{6}$	0.07 ± 0.01	$3.75 \pm 0.35 \times 10^{-3}$	$7.72 \pm 0.71 \times 10^{-4}$
Control	$4.00 \pm 0.01 \times 10^{9}$	0	$3.00 \pm 1.41 \times 10^{-5}$	$7.00 \pm 1.41 \times 10^{-5}$

polymorphism sites may contribute to the resistance of R1-3-1 to LQ7. More interestingly, R1-3-1 became sensitive to LQ7 in the presence of chloramphenicol at concentrations of 1/2 or 1/4 MIC (**Figure 6**). Previous studies have shown that bacteriostatic antibiotics chloramphenicol (CHL) could result in accumulation of amino acid, ATP, as well as NADH, due to reduced energy utilization and macromolecule biosynthesis of *S. aureus* (Lobritz et al., 2015; Stokes et al., 2019), which led us to try if CHL could be used to suppress the higher metabolic activity of R1-3-1 so that to reverse its resistance to the phage LQ7. As expected, the results in **Figure 6** showed that nucleotide polymorphisms (minor alleles) that occurred in thirty-eight genes of R1-3-1 were not accidental and it is highly possible that the metabolic activity of R1-3-1 conferred partially its resistance to LQ7. It is worthy of note that there is a report having a similar postulate that the metabolic state of bacteria could influence their susceptibility to antibiotics (Stokes et al., 2019). Compare with other resistance mechanisms, the naturally existing minor alleles in the genome of the bacteria would provide the host a fast response to the selective pressure of the phage.

By the experimental evolution of LQ7 against R1-3-1, phages sensitive to R1-3-1 could be obtained as the plaques shown in **Figure 3**. Genome sequencing analysis showed that both mutation and the polymorphism of minor alleles would contribute to the susceptibility during the evolution process. Compared with the genome of LQ7, the evolved phage ELQ7P-10 and ELQ7P-20 showed five mutations causing three non-synonymous substitutions of amino acids (**Table 1**). Due to the capsid and scaffold protein in LQ7 containing the carbohydrate-binding domain, the mutation in this protein might contribute to the higher absorption rate of ELQ7P-10 to R1-3-1 (**Figure 4**). Previous studies reported that the widely existed carbohydrate-binding modules domain in phage can present in the tail protein to adsorb to its host (Dieterle et al., 2017; Hayes et al., 2018). At the same time, the polymorphism of minor alleles was also identified in the genomes of the ancestral phage LQ7 and the two evolved phages (**Figures 5E–G**). Based on the distribution of the minor alleles (**Figure 5H**), it was clearly shown that ELQ7P-10 was a transit between LQ7 and ELQ7P-20 during the evolution process. Specifically, there are six polymorphism sites associated with terminase large subunit gene, the baseplate morphogenetic gene and the tail lysin gene (**Supplementary Table 3**). The bacteriophage terminase consists of a small terminase subunit and a large terminase subunit, the latter possesses the ATPase and nuclease activities for packaging the DNA in the phage head, which is important in phage maturation (Weiditch et al., 2019). The increased proportion of non-synonymous polymorphism site on the baseplate morphogenetic protein (**Figures 5K,L** and **Supplementary Figure 2B**) might contribute to the higher adsorption capacity of ELQ7P-20 than that of ELQ7P-10 (**Figure 4**) since previous reports revealed that some phages in *Myoviridae* phage family evolved on baseplate and fibers genes associated with host recognition and adsorption (Akusobi et al., 2018; Habusha et al., 2019; Kizziah et al., 2020). Tail lysin participates in the digestion of bacterial cell walls and aids in the injection of phage DNA during infection Lavigne and Ceyssens (2012), but the polymorphism of minor allele occurred in this gene causes no amino acid change (**Supplementary Figure 2C**). Because none of the above polymorphism sites have been reported with the functions directly related to the metabolic activity of *S. aureus*, we believe other polymorphism sites in the genome of ELQ7P-10, which has 7 polymorphism sites different from LQ7, and ELQ7P-20, which has 15 polymorphism sites different from LQ7, might contribute its sensitivity to R1-3-1 also.

The arms race seems endless between phages and bacteria (Safari et al., 2020), which is true in the simplified system in the current study. As shown in **Table 2**, AB91118 was inhibited most by the combination of CHL and ELQ7P-20, and followed by the combination of CHL and LQ7 (**Table 2**). Therefore, it is beneficial to combine use of both CHL and phage to kill the bacteria. However, even with the combination of CHL and the phages, there are always some resistant mutants remained after the treatment. Actually, it could generally find the resistant mutant ratios became higher after the interaction of bacteria with either CHL or phages. It is quite interesting to find that treatments by combining CHL and LQ7 developed the highest mutant ratios resistant to CHL, but much smaller ratios resistant to CHL and both phages were observed after the treatment by the combination of CHL and ELQ7P-20. These results show that there are complementary effects between CHL and ELQ7P-20 to develop fewer mutants resistant to CHL and phages, but synergic effects between CHL and LQ7 to promote more mutants resistant to CHL and phages. Therefore, it may be case-by-case whether the combination of antibiotics and phages could produce less

resistance while killing bacteria effectively (Valério et al., 2017). All these results hinted that it might be generally beneficial to combine antibiotic and phage for phage therapy, but complicated outcomes might be generated.

To be concluded, we found that the genetic polymorphism of minor alleles exists in the genomes of both bacteria and phages, which may be a new mechanism to enable host and phage get ready and have a fast response to the selective pressure by one to the other. Specifically, in the AB91118-LQ7 system studied here, it was found that the metabolic pathways involved in the genes with some unique polymorphic sites could be inhibited by CHL and make the resistant mutant R1-3-1 become sensitive to LQ7. Combination of CHL and ELQ7P-20 could produce less resistance and killing bacteria effectively. The polymorphism of minor alleles would open new clues to elucidate the interactions between bacteria and phages. But it needs further study to prove whether this is applicable to the complicated systems in nature, where host and phage exist with many other bacteria and phages.

DATA AVAILABILITY STATEMENT

The datasets presented in this study can be found in the Genome Warehouse in the National Genomics Data Center (National Genomics Data Center Members and Partners, 2020), Beijing Institute of Genomics (China National Center for Bioinformation), Chinese Academy of Sciences. The names of the repository/repositories and accession number(s) can be found below: https://bigd.big.ac.cn/gwh, GWHAOOZ00000000, https://bigd.big.ac.cn/gwh, GWHAOOY00000000, and https://bigd.big.ac.cn/gwh, CRA003040.

AUTHOR CONTRIBUTIONS

XZ designed and performed all experiments and wrote the manuscript. DX performed all the bioinformatics data analysis and wrote the manuscript. JY and HY attended the results discussion. PH performed the isolation of resistant R1-3-1. HW generated the idea, analyzed the results, and wrote the manuscript. All authors read and approved the final manuscript.

ACKNOWLEDGMENTS

We thank the financial supports from the Chinese Academy of Sciences (Project Numbers: 153211KYSB20160001 and SAJC201605). We are grateful to Bi-Chao Xu, Pei Zhang, and Anna Du of Core Facility and Technical Support, Wuhan Institute of Virology for the technical support in transmission electron microscopy. We also thank the Benagen Inc., (Wuhan, Hubei, China) for the genome high-throughput sequencing.

SUPPLEMENTARY MATERIAL

The Supplementary Material for this article can be found online at: https://www.frontiersin.org/articles/10.3389/fmicb.2021.627897/full#supplementary-material

Supplementary Figure 1 | The sequencing depth of *Staphylococcus aureus* and phages.

Supplementary Figure 2 | Changes in the amino acid sequence of terminal large subunit, baseplate morphogenetic protein and tail lysin caused by polymorphisms among phages.

Supplementary Figure 3 | The evidence of Sanger sequencing data for five polymorphism sites.

Supplementary Table 1 | Detailed four base frequency information on polymorphism sites in the genomes of the bacteria and the phages.

Supplementary Table 2 | Fifty-nine biological processes identified by gene ontology enrichment analysis based on the unique polymorphism sites in the 38 functional genes of R1-3-1.

Supplementary Table 3 | The protein information encoded by the gene with the polymorphic sites in the phage genomes and the numbers of four bases mapped to these sites.

REFERENCES

Akusobi, C., Chan, B. K., Williams, E., Wertz, J. E., and Turner, P. E. (2018). Parallel evolution of host-attachment proteins in phage pp01 populations adapting to *Escherichia coli* O157:H7. *Pharmaceuticals* 11:60. doi: 10.3390/ph11020060

Bankevich, A., Nurk, S., Antipov, D., Gurevich, A. A., Dvorkin, M., Kulikov, A. S., et al. (2012). SPAdes: a new genome assembly algorithm and its applications to single-cell sequencing. *J. Comput. Biol.* 19, 455–477. doi: 10.1089/cmb.2012.0021

Broniewski, J. M., Meaden, S., Paterson, S., Buckling, A., and Westra, E. R. (2020). The effect of phage genetic diversity on bacterial resistance evolution. *ISME J.* 14, 828–836. doi: 10.1038/s41396-019-0577-7

Denes, T., den Bakker, H. C., Tokman, J. I., Guldimann, C., and Wiedmann, M. (2015). Selection and characterization of phage-resistant mutant strains of *Listeria monocytogenes* reveal host genes linked to phage adsorption. *Appl. Environ. Microbiol.* 81, 4295–4305. doi: 10.1128/AEM.00087-15

Dieterle, M. E., Spinelli, S., Sadovskaya, I., Piuri, M., and Cambillau, C. (2017). Evolved distal tail carbohydrate binding modules of *Lactobacillus* phage J-1: a novel type of anti-receptor widespread among lactic acid bacteria phages. *Mol. Microbiol.* 104, 608–620. doi: 10.1111/mmi.13649

El Haddad, L., Harb, C. P., Gebara, M. A., Stibich, M. A., and Chemaly, R. F. (2018). A Systematic and critical review of bacteriophage therapy against multidrug-resistant ESKAPE organisms in humans. *Clin. Infect. Dis.* 69, 167–178. doi: 10.1093/cid/ciy947

Garcia, R., Latz, S., Romero, J., Higuera, G., Garcia, K., and Bastias, R. (2019). Bacteriophage production models: an overview. *Front. Microbiol.* 10:1187. doi: 10.3389/fmicb.2019.01187

Gene Ontology Consortium, (2015). Gene ontology consortium: going forward. *Nucleic Acids Res.* 43, D1049–D1056. doi: 10.1093/nar/gku1179

Golais, F., Holly, J., and Vitkovska, J. (2013). Coevolution of bacteria and their viruses. *Folia Microbiol.* 58, 177–186. doi: 10.1007/s12223-012-0195-5

Gordillo Altamirano, F., Forsyth, J. H., Patwa, R., Kostoulias, X., Trim, M., Subedi, D., et al. (2021). Bacteriophage-resistant *Acinetobacter baumannii* are resensitized to antimicrobials. *Nat. Microbiol.* 6, 157–161. doi: 10.1038/s41564-020-00830-7

Habusha, M., Tzipilevich, E., Fiyaksel, O., and Ben-Yehuda, S. (2019). A mutant bacteriophage evolved to infect resistant bacteria gained a broader host range. *Mol. Microbiol.* 111, 1463–1475. doi: 10.1111/mmi.14231

Hayes, S., Vincentelli, R., Mahony, J., Nauta, A., Ramond, L., Lugli, G. A., et al. (2018). Functional carbohydrate binding modules identified in evolved dits from siphophages infecting various Gram-positive bacteria. *Mol. Microbiol.* 110, 777–795. doi: 10.1111/mmi.14124

Jo, A., Kim, J., Ding, T., and Ahn, J. (2016). Role of phage-antibiotic combination in reducing antibiotic resistance in *Staphylococcus aureus*. *Food Sci. Biotechnol.* 25, 1211–1215. doi: 10.1007/s10068-016-0192-6

Kering, K. K., Zhang, X., Nyaruaba, R., Yu, J., and Wei, H. (2020). Application of adaptive evolution to improve the stability of bacteriophages during storage. *Viruses* 12:423. doi: 10.3390/v12040423

Kishor, C., Mishra, R. R., Saraf, S. K., Kumar, M., Srivastav, A. K., and Nath, G. (2016). Phage therapy of staphylococcal chronic osteomyelitis in experimental animal model. *Indian J. Med. Res.* 143, 87–94. doi: 10.4103/0971-5916.178615

Kizziah, J. L., Manning, K. A., Dearborn, A. D., and Dokland, T. (2020). Structure of the host cell recognition and penetration machinery of a *Staphylococcus aureus* bacteriophage. *PLoS Pathog.* 16:e1008314. doi: 10.1371/journal.ppat.1008314

Koboldt, D. C., Zhang, Q., Larson, D. E., Shen, D., McLellan, M. D., Lin, L., et al. (2012). VarScan 2: somatic mutation and copy number alteration discovery in cancer by exome sequencing. *Genome Res.* 22, 568–576. doi: 10.1101/gr.129684.111

Labrie, S. J., Samson, J. E., and Moineau, S. (2010). Bacteriophage resistance mechanisms. *Nat. Rev. Microbiol.* 8, 317–327. doi: 10.1038/nrmicro2315

Lavigne, R., and Ceyssens, P.-J. (2012). "Family - Myoviridae," in *Virus Taxonomy*, eds A. M. Q. King, M. J. Adams, E. B. Carstens, and E. J. Lefkowitz, (San Diego: Elsevier), 46–62.

Lehman, S. M., Mearns, G., Rankin, D., Cole, R. A., Smrekar, F., Branston, S. D., et al. (2019). Design and preclinical development of a phage product for the treatment of antibiotic-resistant *Staphylococcus aureus* infections. *Viruses* 11:88. doi: 10.3390/v11010088

Levin, B. R., and Bull, J. J. (2004). Population and evolutionary dynamics of phage therapy. *Nat. Rev. Microbiol.* 2, 166–173. doi: 10.1038/nrmicro822

Li, H. (2016). Minimap and miniasm: fast mapping and de novo assembly for noisy long sequences. *Bioinformatics* 32, 2103–2110. doi: 10.1093/bioinformatics/btw152

Li, H., and Durbin, R. (2009). Fast and accurate short read alignment with Burrows-Wheeler transform. *Bioinformatics* 25, 1754–1760. doi: 10.1093/bioinformatics/btp324

Li, H., Handsaker, B., Wysoker, A., Fennell, T., Ruan, J., Homer, N., et al. (2009). The Sequence Alignment/Map format and SAMtools. *Bioinformatics* 25, 2078–2079. doi: 10.1093/bioinformatics/btp352

Lobritz, M. A., Belenky, P., Porter, C. B. M., Gutierrez, A., Yang, J. H., Schwarz, E. G., et al. (2015). Antibiotic efficacy is linked to bacterial cellular respiration. *Proc. Natl. Acad. Sci. U.S.A.* 112:8173. doi: 10.1073/pnas.1509743112

Loman, N. J., Quick, J., and Simpson, J. T. (2015). A complete bacterial genome assembled de novo using only nanopore sequencing data. *Nat. Methods* 12, 733–735. doi: 10.1038/nmeth.3444

Lyon, J. (2017). Phage Therapy's role in combating antibiotic-resistant pathogens. *JAMA* 318, 1746–1748. doi: 10.1001/jama.2017.12938

Marçais, G., and Kingsford, C. (2011). A fast, lock-free approach for efficient parallel counting of occurrences of k-mers. *Bioinformatics* 27, 764–770. doi: 10.1093/bioinformatics/btr011

Narasimhan, V., Danecek, P., Scally, A., Xue, Y., Tyler-Smith, C., and Durbin, R. (2016). BCFtools/RoH: a hidden Markov model approach for detecting autozygosity from next-generation sequencing data. *Bioinformatics* 32, 1749–1751. doi: 10.1093/bioinformatics/btw044

National Genomics Data Center Members and Partners, (2020). Database resources of the national genomics data center in 2020. *Nucleic Acids Res.* 48, D24–D33. doi: 10.1093/nar/gkz913

Ooi, M. L., Drilling, A. J., Morales, S., Fong, S., Moraitis, S., Macias-Valle, L., et al. (2019). Safety and tolerability of bacteriophage therapy for chronic rhinosinusitis due to *Staphylococcus aureus*. *JAMA Otolaryngol. Head Neck Surg.* 145, 723–729. doi: 10.1001/jamaoto.2019.1191

Prazak, J., Iten, M., Cameron, D. R., Save, J., Grandgirard, D., Resch, G., et al. (2019). Bacteriophages improve outcome in experimental *Staphylococcus aureus* ventilator associated pneumonia. *Am. J. Respir. Crit. Care Med.* 200, 1126–1133. doi: 10.1164/rccm.201812-2372OC

Quinlan, A. R. (2014). BEDTools: the swiss-army tool for genome feature analysis. *Curr. Protoc. Bioinform.* 47, 11.12.11–11.12.34. doi: 10.1002/0471250953.bi1112s47

Ruan, J., and Li, H. (2020). Fast and accurate long-read assembly with wtdbg2. *Nat. Methods* 17, 155–158. doi: 10.1038/s41592-019-0669-3

Safari, F., Sharifi, M., Farajnia, S., Akbari, B., Karimi Baba Ahmadi, M., Negahdaripour, M., et al. (2020). The interaction of phages and bacteria: the co-evolutionary arms race. *Crit. Rev. Biotechnol.* 40, 119–137. doi: 10.1080/07388551.2019.1674774

Sakoulas, G., Eliopoulos, G. M., Fowler, V. G. Jr., Moellering, R. C. Jr., Novick, R. P., Lucindo, N., et al. (2005). Reduced susceptibility of *Staphylococcus aureus* to vancomycin and platelet microbicidal protein correlates with defective autolysis and loss of accessory gene regulator (agr) function. *Antimicrob. Agents Chemother.* 49, 2687–2692. doi: 10.1128/AAC.49.7.2687-2692.2005

Samson, J. E., Magadan, A. H., Sabri, M., and Moineau, S. (2013). Revenge of the phages: defeating bacterial defences. *Nat. Rev. Microbiol.* 11, 675–687. doi: 10.1038/nrmicro3096

Senok, A., Somily, A. M., Nassar, R., Garaween, G., Kim Sing, G., Müller, E., et al. (2019). Emergence of novel methicillin-resistant *Staphylococcus aureus* strains in a tertiary care facility in Riyadh, Saudi Arabia. *Infect. Drug Resist.* 12, 2739–2746. doi: 10.2147/IDR.S218870

Stokes, J. M., Lopatkin, A. J., Lobritz, M. A., and Collins, J. J. (2019). Bacterial metabolism and antibiotic efficacy. *Cell Metab.* 30, 251–259. doi: 10.1016/j.cmet.2019.06.009

Sulakvelidze, A., Alavidze, Z., and Morris, J. G. Jr. (2001). Bacteriophage therapy. *Antimicrob. Agents Chemother.* 45, 649–659. doi: 10.1128/AAC.45.3.649-659.2001

Sun, W. (2010). "Chapter 4 - Nucleic extraction and amplification," in *Molecular Diagnostics*, eds W. W. Grody, R. M. Nakamura, C. M. Strom, and F. L. Kiechle, (San Diego: Academic Press), 35–47.

Thorvaldsdóttir, H., Robinson, J. T., and Mesirov, J. P. (2013). Integrative Genomics Viewer (IGV): high-performance genomics data visualization and exploration. *Brief. Bioinform.* 14, 178–192. doi: 10.1093/bib/bbs017

Uchiyama, J., Taniguchi, M., Kurokawa, K., Takemura-Uchiyama, I., Ujihara, T., Shimakura, H., et al. (2017). Adsorption of *Staphylococcus* viruses S13' and S24-1 on *Staphylococcus aureus* strains with different glycosidic linkage patterns of wall teichoic acids. *J. Gen. Virol.* 98, 2171–2180. doi: 10.1099/jgv.0.000865

Valério, N., Oliveira, C., Jesus, V., Branco, T., Pereira, C., Moreirinha, C., et al. (2017). Effects of single and combined use of bacteriophages and antibiotics to inactivate *Escherichia coli*. *Virus Res.* 240, 8–17. doi: 10.1016/j.virusres.2017.07.015

Weiditch, S. A., Seraphim, T. V., Houry, W. A., and Kanelis, V. (2019). Strategies for purification of the bacteriophage HK97 small and large terminase subunits that yield pure and homogeneous samples that are functional. *Protein Express. Purif.* 160, 45–55. doi: 10.1016/j.pep.2019.03.017

Wiegand, I., Hilpert, K., and Hancock, R. E. W. (2008). Agar and broth dilution methods to determine the minimal inhibitory concentration (MIC) of antimicrobial substances. *Nat. Protoc.* 3, 163–175. doi: 10.1038/nprot.2007.521

Yan, C., Zhang, Y., Yang, H., Yu, J., and Wei, H. (2017). Combining phagomagnetic separation with immunoassay for specific, fast and sensitive detection of *Staphylococcus aureus*. *Talanta* 170, 291–297. doi: 10.1016/j.talanta.2017.04.007

Yu, G., Wang, L. G., Han, Y., and He, Q. Y. (2012). clusterProfiler: an R Package for comparing biological themes among gene clusters. *OMICS J. Integr. Biol.* 16, 284–287. doi: 10.1089/omi.2011.0118

Conflict of Interest: The authors declare that the research was conducted in the absence of any commercial or financial relationships that could be construed as a potential conflict of interest.

Copyright © 2021 Zhang, Xiong, Yu, Yang, He and Wei. This is an open-access article distributed under the terms of the Creative Commons Attribution License (CC BY). The use, distribution or reproduction in other forums is permitted, provided the original author(s) and the copyright owner(s) are credited and that the original publication in this journal is cited, in accordance with accepted academic practice. No use, distribution or reproduction is permitted which does not comply with these terms.

frontiers in Microbiology

ORIGINAL RESEARCH
published: 31 March 2021
doi: 10.3389/fmicb.2021.650849

Lytic Bacteriophage EFA1 Modulates HCT116 Colon Cancer Cell Growth and Upregulates ROS Production in an *Enterococcus faecalis* Co-culture System

*Mwila Kabwe[1], Terri Meehan-Andrews[1], Heng Ku[1], Steve Petrovski[2], Steven Batinovic[2], Hiu Tat Chan[2,3] and Joseph Tucci[1]**

[1] Department of Pharmacy and Biomedical Sciences, La Trobe Institute for Molecular Science, La Trobe University, Bendigo, VIC, Australia, [2] Department of Physiology, Anatomy and Microbiology, La Trobe University, Melbourne, VIC, Australia, [3] Department of Microbiology, Royal Melbourne Hospital, Melbourne, VIC, Australia

OPEN ACCESS

Edited by:
Shuai Le,
Army Medical University, China

Reviewed by:
Alan J. Wolfe,
Loyola University Chicago, United States
Mengjun Cheng,
Fudan University, China

***Correspondence:**
Joseph Tucci
j.tucci@latrobe.edu.au

Specialty section:
This article was submitted to Virology, a section of the journal Frontiers in Microbiology

Received: *08 January 2021*
Accepted: *08 March 2021*
Published: *31 March 2021*

Citation:
Kabwe M, Meehan-Andrews T, Ku H, Petrovski S, Batinovic S, Chan HT and Tucci J (2021) Lytic Bacteriophage EFA1 Modulates HCT116 Colon Cancer Cell Growth and Upregulates ROS Production in an Enterococcus faecalis Co-culture System. Front. Microbiol. 12:650849. doi: 10.3389/fmicb.2021.650849

Enterococcus faecalis is an opportunistic pathogen in the gut microbiota that's associated with a range of difficult to treat nosocomial infections. It is also known to be associated with some colorectal cancers. Its resistance to a range of antibiotics and capacity to form biofilms increase its virulence. Unlike antibiotics, bacteriophages are capable of disrupting biofilms which are key in the pathogenesis of diseases such as UTIs and some cancers. In this study, bacteriophage EFA1, lytic against *E. faecalis,* was isolated and its genome fully sequenced and analyzed *in silico*. Electron microscopy images revealed EFA1 to be a *Siphovirus*. The bacteriophage was functionally assessed and shown to disrupt *E. faecalis* biofilms as well as modulate the growth stimulatory effects of *E. faecalis* in a HCT116 colon cancer cell co-culture system, possibly via the effects of ROS. The potential exists for further testing of bacteriophage EFA1 in these systems as well as *in vivo* models.

Keywords: *Enterococcus faecalis*, bacteriophage, genomics, biofilm, colon cancer proliferation, reactive oxygen species

INTRODUCTION

Understanding the interactions between host and microbe is cardinal to the development of treatment modalities to curb pathogen associated disease. In the human body, the number of bacteria cells is relatively similar to that of human cells (Sender et al., 2016), with the gut being the largest reservoir (Kho and Lal, 2018). *Enterococcus* species which are Gram-positive facultative anaerobes form approximately 1% of all microbiota in the gut and are readily isolated from human and animal feces as well as from the environment (Dubin and Pamer, 2014). Enterococci, including *E. faecium* and *E. faecalis* are the most predominant species and have traditionally been considered normal flora and sometimes used as probiotics to treat gut infections (Franz et al., 2003). Previous recommendations for use as probiotics stemmed from studies that explored the capacity for *Enterococcus* spp. to attach to epithelial cells thereby preventing colonization of more pathogenic bacteria (Kropec et al., 2005; Nueno-Palop and Narbad, 2011; Tinrat et al., 2018;

Wang J. et al., 2020). However, emerging trends show that *Enterococcus* spp. are a major cause of a range of difficult to treat nosocomial infections, with implicated isolates displaying both acquired and intrinsic multi-antibiotic resistance (Franz et al., 2003; Hollenbeck and Rice, 2012). *Enterococcus* spp. survive on inanimate objects (e.g., intravenous catheters, handrails and bed frames) as fomites (Zervos et al., 1987; Hota, 2004) creating an opportunity for the transmission of antibiotic resistant Enterococci among patients in hospitals via their attending health workers (Dubin and Pamer, 2014; Drees et al., 2008). Although both *E. faecium* and *E. faecalis* are predominant Enterococci in the normal gut microbiota (De Lastours et al., 2017), the latter has been implicated in a higher frequency of Hospital Acquired Infections (HAI) (Weiner-Lastinger et al., 2020). In the American national surveillance program report from 2015 to 2017 involving more than 2,400 hospitals, *E. faecalis* was the fifth most common cause of HAI after *Escherichia coli*, *Staphylococcus aureus*, *Klebsiella* spp. and *Pseudomonas aeruginosa* while it was the most frequently reported pathogen in oncology units (Weiner-Lastinger et al., 2020).

Although *E. faecalis* has traditionally been considered a normal constituent of the gut microbiome, recent data suggests that it is intrinsically linked to colorectal cancer (CRC) (Lennard et al., 2016). A study quantifying bacterial prevalence in feces of CRC patients found an increased level of *E. faecalis* compared to normal controls (Balamurugan et al., 2008) while transcriptional modeling of host genes expressed in *E. faecalis* colonized CRC showed activation of pathways related to tumor invasion and cancer metastasis (Lennard et al., 2016). Further, *E. faecalis* has been shown to colonize the murine gastrointestinal tract by formation of bacterial biofilms (Barnes et al., 2017), promote aneuploidy and tetraploidy, induce colonic epithelial DNA double-strand breaks and arrest cell cycle (Wang et al., 2008) via increased reactive oxygen species (ROS) production (Huycke et al., 2002; Wang and Huycke, 2007; Wang et al., 2008). The bacterial microbiome is now considered an important aspect of the tumor microenvironment. The recent highlighting of the role of oncobacteria in tumorigenesis has added weight to the argument that tumor microbiota manipulation could be key to unlocking the potential of cancer chemotherapy and immunotherapy (Bhatt et al., 2017; Rajagopala et al., 2017; Helmink et al., 2019; Parhi et al., 2020).

The abundance of bacteria in humans and the environment pales in comparison to their viral predators, the bacteriophages. For instance, bacterial numbers are estimated at 10^{11} cells per gram weight of fecal material compared to approximately 10^{12} bacteriophages in the same amount (Cani, 2018). Bacteriophages have been shown to drive the composition of the gut microbiome (Moreno-Gallego et al., 2019) by specifically targeting gut bacteria and creating an evolutionary arms race between bacterial host and virus (Azam and Tanji, 2019; Wang G. et al., 2020). Further, studies have shown the capacity of bacteriophages to disrupt biofilms (Hansen et al., 2019; Lusiak-Szelachowska et al., 2020), kill intracellular bacteria (Jonczyk-Matysiak et al., 2015), and modulate the immune system (Van Belleghem et al., 2018), all key to counteracting virulence mechanisms that oncobacteria use to promote tumor growth (Holt and Cochrane, 2017). Bacteriophage against *Fusobacterium nucleatum*, a classic oncobacterium implicated in various cancers (Mitsuhashi et al., 2015; Yamamura et al., 2016; Al-Hebshi et al., 2017; Zhao et al., 2017; Yang S. F. et al., 2018; Gaiser et al., 2019; Kharrat et al., 2019; Yachida et al., 2019), have shown the potential to augment chemotherapy in the treatment of *F. nucleatum* associated CRC (Zheng et al., 2019). In this study, we demonstrate the augmentation of CRC cell growth *in vitro* by *E. faecalis,* and how these effects can be modulated by treatment with the *E. faecalis* specific bacteriophage EFA1, possibly via an increase of ROS production. Bacteriophage EFA1 was isolated from wastewater, phenotypically characterized and its whole genome sequenced. The whole genome sequence of EFA1 bacteriophage has been deposited in GenBank® (Benson et al., 2000) under accession number MT857001.

MATERIALS AND METHODS

Ethics Statement

Study protocols were approved by the La Trobe University Ethics Committee under reference number S17-112 and all methods performed in accordance with the La Trobe University Ethics, Biosafety and Integrity guidelines, and regulations.

HCT116 Human Colon Cancer Cell Culture and Bacterial Culture Conditions

Human colonic HCT116 cells (ATCC CCL-247) were maintained in RPMI-1640 medium with L-glutamine and sodium bicarbonate (Sigma-Aldrich®, Australia) that was supplemented with 10% fetal bovine serum (FBS; Sigma-Aldrich®, Australia) and passaged by detachment using 0.5% trypsin (Sigma-Aldrich®, Australia). HCT116 cells were maintained in humidified 5% CO_2 at 37°C.

The *E. faecalis* strains used in these experiments were isolated from wastewater. They were cultured at 37°C in Brain-Heart infusion media (BHI; Oxoid™, Australia) under anaerobic conditions. Anaerobic conditions were generated using the AnaeroGen pack (Oxoid™, Australia). For confirmation of *E. faecalis* strain identity, 16s rRNA PCR gene amplification was performed and the amplicons purified using the QIAquick® PCR purification kit (Qiagen, Australia) before Sanger sequencing at the Australian Genome Research Facility. The primers used for the 16s rRNA PCR and sequencing were U27F: 5′AGAGTTTGATCMTGGCTCAG3′ and U492R: 5′AAGGAG GTGWTCCARCC 3′ under thermocycling conditions: 95°C for 3 min, 32 cycles of 95°C for 30 s, 60°C for 30 s, and 72°C for 90 s, with a final extension at 72°C for 10 min (Kabwe et al., 2019).

Bacteriophage Isolation and One-Step Growth Curve Determination

Bacteriophage isolation was carried out as previously described (Kabwe et al., 2020). Wastewater from Victoria, Australia was collected and filtered using 0.2 μm cellulose acetate filters (Advantec, Australia). Filtered wastewater was then added to 10^8 colony forming units/mL (CFU/mL) of *E. faecalis* in BHI

broth at 1% (v/v). The *E. faecalis*-wastewater enrichment culture was then incubated at 37°C anaerobically for 4 d before 0.2 μm cellulose acetate filtration. Serially diluted enrichment filtrates (10 μL) were placed on fresh lawns of *E. faecalis* on BHI containing 1% agar and plates incubated for 24 h. Any potential bacteriophage clearing was excised (along with a portion of agar) and resuspended in 500 μL of media, before centrifugation (12,000 × *g* for 5 min) and a 10-fold serial dilution was completed. Then 10 μL of each dilution was placed on a bacterial lawn such that plaques could be observed after an overnight anaerobic incubation at 37°C. This serial dilution purification was repeated five times to ensure single virion infection. The concentration of the bacteriophage suspensions was determined and calculated as number of plaque forming units (PFU)/mL.

Host range was assessed by making 10-fold serial dilutions of the bacteriophage stock (1×10^8 PFU/mL) and spotting 10 μL of the serial dilution aliquots onto freshly plated lawns of oral and enteric bacteria including, *F. nucleatum*, *Solobacterium moorei*, *Streptococcus mutans*, *Lactobacillus Casei*, *Aeromonas hydrophila*, and *Escherichia coli*. All plates were incubated at 37°C under anaerobic conditions except for *E. coli* and *A. hydrophila* that were incubated under aerobic conditions. A lack of individual plaques indicated that the bacteriophage EFA1 did not target these strains.

To determine the one-step growth curve (OSGC), 1 mL of *E. faecalis* in exponential growth phase at the concentration of 1×10^8 CFU/mL was centrifuged at 12,000 × *g* for 5 min. The cell pellet was then resuspended in 900 μL of cold BHI broth before adding 100 μL of EFA1 bacteriophage at multiplicity of infection (MOI) of 0.1 as previously described (Kabwe et al., 2020). The bacteria-bacteriophage mixture was incubated at 4°C for 5 min to allow for bacteriophage adsorption onto bacteria. The mixture was then centrifuged at 12,000 × *g* for 10 min and unadsorbed bacteriophages assayed. Adsorbed bacteriophage were together collected with bacteria in a pellet and resuspended in BHI broth at 50 × dilution, incubated anaerobically at 37°C and bacteriophage concentration determined every 5 min. A graph of bacteriophage concentration (*y*-axis) against time (*x*-axis) was plotted and burst size (PFU/bacterial cell) calculated as a fraction of burst of newly released bacteriophage out of the total number of infecting bacteriophages.

Transmission Electron Microscopy

Visualization of the bacteriophage phenotype was achieved using a JEOL JEM-2100 transmission electron microscope (TEM) operated at 200 kV as previously described (Kabwe et al., 2020). Using a 400-mesh formvar and carbon copper grids (ProScieTech, Australia), EFA1 bacteriophage particles were adsorbed for 1 min before rinsing the grids with milli-Q water and negatively staining for 20 s with 2% (w/v) uranyl acetate (Sigma-Aldrich®, Australia). Excess uranyl acetate was removed, and the copper grids allowed to air dry at room temperature for 30 min. The Gatan Orius SC200D 1 wide-angle camera coupled to the Gatan Microscopy Suite and Digital Micrograph Imaging software (Version 2.3.2.888.0) was used to take the TEM images before being exported to Image J (Version 1.8.0_112) for further analysis.

Bacteriophage DNA Extraction

Using an established method (Kabwe et al., 2019), 10 mL of 1×10^8 PFU/mL bacteriophage solution in phosphate buffered saline (PBS, pH 7.4) was prepared for genomic DNA extraction. In brief, the bacteriophage solution was treated for 30 min at room temperature with 5 mmol/L of $MgCl_2$ (Sigma-Aldrich®, Australia), and 10 μg/mL RNAse A and DNAse I (Promega, Australia). Bacteriophage particles were then precipitated at 4°C with 10% (w/v) Polyethylene glycol (PEG-8000) and 1 g/L sodium chloride, and resuspended in 50 μL nuclease-free water (Promega, Australia) before viral proteins were digested with 50 μg/mL of proteinase K, 20 mmol/L EDTA (Sigma-Aldrich®, Australia) and 0.5% (v/v) of sodium dodecyl sulfate (Sigma-Aldrich®, Australia) for 1 h at 55°C. An equal volume of phenol-chloroform-isoamyl alcohol (29:28:1) (Sigma-Aldrich®, Australia) was added to the DNA/bacteriophage protein mixture and their columns separated by centrifugation at 12,000 × *g* for 10 min to collect an aqueous phase with bacteriophage DNA. The bacteriophage DNA was then precipitated out using 70% ethanol and collected by 12,000 × *g* centrifugation before resuspension in 30 μL nuclease-free water (Promega, Australia).

Bacteriophage Whole Genome Sequencing and *in silico* Analysis

Bacteriophage whole genome sequencing was performed on the Illumina MiSeq® technology using the NEBNext® Ultra™ II DNA Library Prep Kit (NEB) and a MiSeq® V3 600 cycle reagent kit (Illumina, Australia) according to manufacturer's instructions. Generated reads were trimmed using Trim Galore v0.6.4 with the default settings (Q scores of ≥ 20, with automatic adapter detection) and assembled using the Unicycler *de novo* assembly pipeline (Wick et al., 2017). PhageTerm was used to reorient the phage genome to begin at its pac site (Garneau et al., 2017) before exporting to Geneious (Version 11.0.5)[1]. Translated open reading frames (ORFs) were mapped onto the National Centre for Biotechnology Institute (NCBI) database using BLASTP (Mount, 2007) and annotated sequence submitted to GenBank®. To allocate taxa for bacteriophage EFA1, Viral Proteomic Tree (ViPTree) webserver was used to construct a viral proteomic tree with other related bacterial viral genomes in the reference database (Nishimura et al., 2017). The generated proteomic tree was annotated using the Interactive Tree of Life (iTOL) (Letunic and Bork, 2019). Amino acids of putative beta-lactamase protein in bacteriophage EFA1 and bacteria (*E. faecalis*) were aligned by a pair-wise progressive alignment in CLC genomics workbench version 9.5.4.

[1]http://www.geneious.com/

Biofilm Growth Analysis

The *E. faecalis* mono-biofilms were grown in 96 well polystyrene plates as described previously (Kabwe et al., 2020). Briefly, 100 μL of 10^8 CFU/mL *E. faecalis* in BHI broth supplemented with 5% glucose (Sigma-Aldrich®, Australia) was added to sterile BHI (100 μL) and incubated anaerobically for 4 d at 37°C and 120 rpm shaking (Ratek Medium Orbital shaking incubator). Bacteriophage was added at concentration 10^8 PFU/mL and biofilm bacteriophage mixture allowed to incubate anaerobically at 37°C. The biofilm mass was determined at 2, 4, 6, 8, and 24 h post bacteriophage treatment (Merritt et al., 2005). Biofilms were rinsed in milli-Q water for 5 min and stained with 200 μL of 1% aqueous crystal violet for 10 min. Excess crystal violet was rinsed off in milli-Q water. Adherent crystal violet was solubilized in 70% ethanol and absorbance read on the FlexStation 3 plate reader (Molecular Devices, United States) at 600 nm wavelength.

In order to visualize the *E. faecalis* biofilm and the disruptive effects of bacteriophage EFA1, the biofilms were cultured on glass slides and stained with SYBR® gold (Eugene, United States) and Propidium Iodide (PI), each at final concentration of 2 μg/mL. The biofilms were visualized on the Olympus Fluoview Fv10i-confocal laser-scanning microscope (Olympus Life Science, Australia). The excitation wavelength was 485 nm, and emission wavelengths of 535 nm (green) and 635 nm (red) to indicate membrane intact and compromised cells, respectively.

HCT116 Colon Cancer Cell, Bacteria, and Bacteriophage Co-culture System

For the HCT116 and *E. faecalis* co-culture experiments, *E. faecalis* in exponential growth phase was resuspended in RPMI 1640 media with 10% FBS (Sigma-Aldrich, Australia) before adding to a suspension of HCT116 cells at MOI of 10. For treatment with bacteriophages, a single plaque was purified and concentrated to make a working stock that was further purified by removing lipoteichoic acid and other cell debris as performed by Branston and colleagues (Branston et al., 2015) with minor modification. Briefly, after treating with 10 μg/mL DNase I and RNase A to digest any naked nucleic acids, bacteriophage was precipitated in PEG and NaCl at 4°C for 10 min. Precipitated bacteriophage particles were treated with 2% v/v Triton® X-100 (Sigma-Aldrich®, Australia) and washed 3 times in PBS (pH 7.4) by centrifugation at 12,000 × *g* for 15 min. The precipitation, Triton® X-100 treatment and PBS (pH 7.4) wash steps were repeated 3 times before precipitated bacteriophage was resuspended in RPMI 1640. *E. faecalis* present in HCT116 co-cultures were treated with the bacteriophage at an MOI of 0.1 and incubated for 48 h in humidified 5% CO_2 at 37°C.

HCT116 Cancer Cell Proliferation Assay

Colon cancer cells and co-cultures were incubated at 37°C for 48 h in humidified 5% CO_2 and proliferation determined by Sulforhodamine B (SRB) assay (Skehan et al., 1990). Briefly, cells were fixed in 10% (w/v) trichloroacetic acid (Thermo Fisher Scientific, Australia) for 30 min at 4°C. Fixed cells were then washed in milli-Q water 5 times before staining with 1% (w/v) SRB (Sigma-Aldrich®) in glacial acetic acid (Thermo Fisher Scientific, Australia). Excess SRB was washed off in 1% (v/v) glacial acetic acid before using 10 mM of unbuffered TRIS base to bring the cell associated SRB into solution. Absorbance at 540 nm was measured using the FlexStation 3 plate reader (Molecular Devices, United States).

Reactive Oxygen Species Determination

Reactive oxygen species activity was evaluated using the ROS-Glo™ Hydrogen Peroxide (H_2O_2) assay kit (Promega, Australia), according to the manufacturer's instructions. Briefly, 48 h co-cultures in 96-well plates were treated with H_2O_2 substrate solution at a final concentration of 25 μM. The treated co-cultures were then further incubated at 37°C, 5% CO_2 for 6 h before adding an equal volume of ROS-Glo™ detection solution. This was then incubated for 20 min before reading relative luminescence units (RLU) on the FlexStation 3 plate reader (Molecular Devices, United States).

Statistical Analysis

To assess bacteriophage capacity to disrupt biofilms and to modulate *E. faecalis* effects on the colon cancer cell line, Shapiro-Wilk was used to test for the normality of the data. For data that were determined to be normally distributed, the means between two groups were compared using paired *T*-test whilst one-way analysis of variance (ANOVA) was used to compare means of more than two groups. Data on biofilms and cell proliferation were normally distributed while luminescence data were not. In this case, median of two different groups were compared using the Mann-Whitney U test. All data were visualized as box plots illustrating the five-number statistic comprising median, 25th, 75th percentile and upper (Q3 + 1.5 × IQR) and lower limit (Q1-1.5 × IQR). All statistical analysis was performed using the Statistical Package for Social Sciences (SPSS, Inc., United States) with *P*-values less than 0.05 considered statistically significant.

RESULTS

Isolation and Phenotypic Characterization of *E. faecalis* Bacteriophage EFA1

After combining the filtrate of the wastewater and *E. faecalis* 4 d enrichment, pinprick-sized plaques were visualized on agar plates. Image analysis revealed plaques to be approximately 0.3 mm in diameter (**Figure 1A**). A concentrated bacteriophage stock assessed by TEM indicated *Siphoviridae* viral particles with a tail length approximately 223 ± 7 nm and capsid diameter approximately 58 ± 3 nm (**Figure 1B**). The host range of EFA1 extended to both of the *E. faecalis* strains isolated in this study but not other oral/enteric bacteria such as *F. nucleatum*, *Solobacterium moorei*, *Streptococcus mutans*, *Lactobacillus Casei*, *Aeromonas hydrophila*, or *Escherichia coli*. The OSGC analysis revealed EFA1 on the host *E. faecalis* to have a latent period of 20 min. Initial release up to the point where no new bacteriophage were released (burst) took 10 min with each bacterium releasing 120 plaque forming units (PFU)/cell (**Figure 1C**).

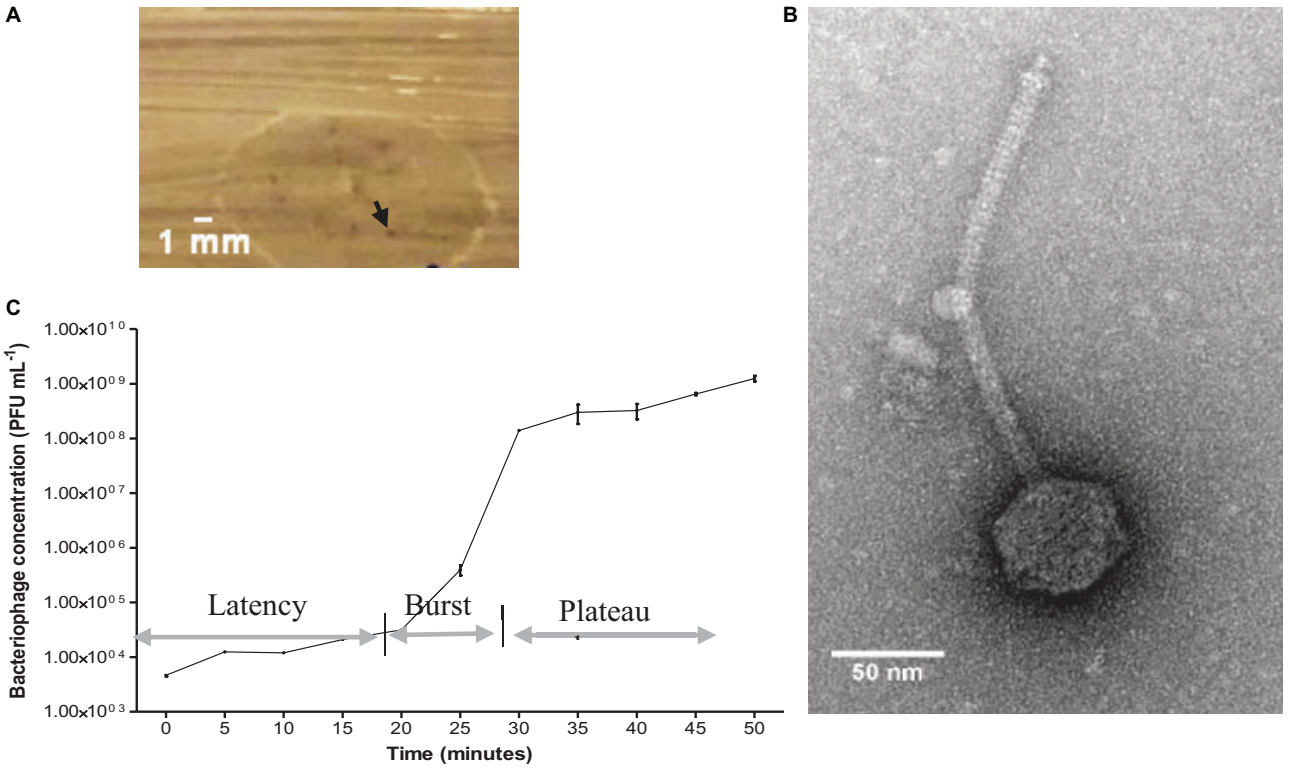

FIGURE 1 | EFA1 plaque morphology, TEM image and growth kinetics. Pin prick plaques with diameter approximately 0.3 mm on *E. faecalis* host **(A)**. TEM revealed *Siphoviridae* morphology with capsid diameter of 58 ± 3 nm and tail length of 223 ± 7 nm **(B)**. EFA1 OSGC: latent phase of 20 min; burst lasting 10 min; plateau phase occurs after approximately 30 min **(C)**.

EFA1 Whole Genome Analysis

Whole genome sequencing revealed a linear dsDNA genome of 40,454 bp with GC content of 34.8% and 68 predicated ORFs. The ORFs were bi-directional with the predicted genes encoding packaging, structural and lysis putative proteins orientated from left to right and putative genes encoding DNA manipulation functions orientated in the opposite direction (**Figure 2**). After arrangement of the genome so that the putative terminase gene marked the start (Garneau et al., 2017), putative terminase and portal proteins were followed by putative capsid genes then genes predicated to connect the capsid to tail and putative tail genes. The putative autolysin was located after the putative tail genes and was the last gene in the left-to-right orientation, before putative glutaredoxin in the opposite direction (**Figure 2**). The putative Glutaredoxin was then followed by putative DNA modification, DNA polymerase and interestingly, a putative beta-lactamase superfamily domain in ORF 33 (**Figure 2**). However, alignment of the putative protein sequence of ORF 33 and the *E. faecalis* metallo-beta-lactamase protein, revealed low homology (**Figure 3**). Analysis of the EFA1 genome using InterProScan (Mitchell et al., 2019) and Prosite (Sigrist et al., 2013) did not reveal any active sites or beta-lactamase domains required for catalysis (Moali et al., 2003). These findings were confirmed by the Comprehensive Antibiotic Resistance Database (CARD) (Jia et al., 2017) program, which predicted that the EFA1 genome did not carry any functional antibiotic resistance genes. The EFA1 genome also contained genes coding for putative DNA manipulation enzymes including putative endonucleases, NUMOD4 motif protein, helicase and primase. Putative hypothetical genes made up 57.4% (39/68) of EFA1 ORFs. There were no tRNAs, tmRNAs (Laslett and Canback, 2004; Lowe and Chan, 2016), CRISPR sequences (Grissa et al., 2007), or genes predicted to code for integrase found in the bacteriophage EFA1 genome.

Bacteriophage Phylogeny

Using the ViPTree server, bacteriophages that clustered with EFA1 were selected to generate a proteomic tree based on genome wide sequence similarities. This was comprised of bacteriophages targeting *Enterococcus, Lactobacillus, Streptococcus, Oenococcus*, and *Staphylococcus* bacteria. Proteomic analysis revealed that EFA1 is part of a monophyletic group with the *E. faecalis* bacteriophage SANTOR1 (Subfamily *Efquatrovirus*), with which it is most closely related (nucleotide similarity of 93.42% over 79% of the whole genome and 87% amino acid similarity). These two are part of a clade of 11 *Enterococcus* bacteriophages which target *E. faecalis* or *E. faecium*, and which also form a larger clade with bacteriophages infecting *Lactobacillus* and *Streptococcus* hosts, but cluster more distantly from other *Siphoviridae*,

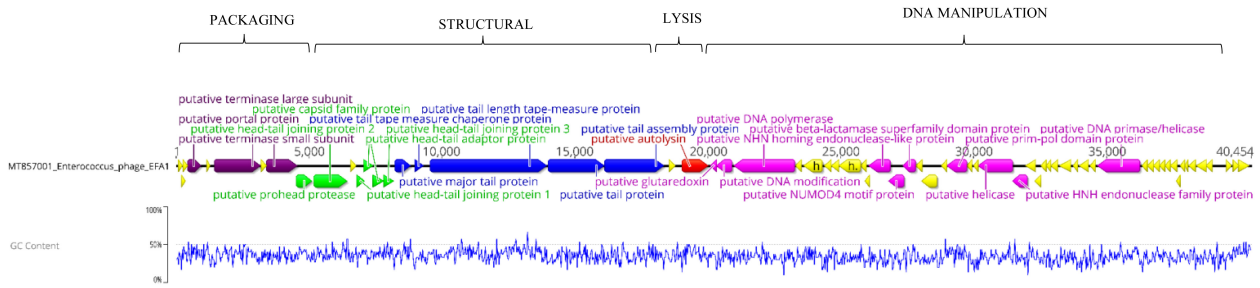

FIGURE 2 | Bacteriophage EFA1 genome orientated according to bacteriophage termini (PAC site). Putative genes coding for DNA packaging (purple), capsid genes (green), tail genes (blue) and putative endolysin (red) are orientated in the left-to-right direction, while putative DNA manipulation genes (pink) are in the opposite direction. Other putative genes whose functionality could not be predicted were considered hypothetical genes (yellow).

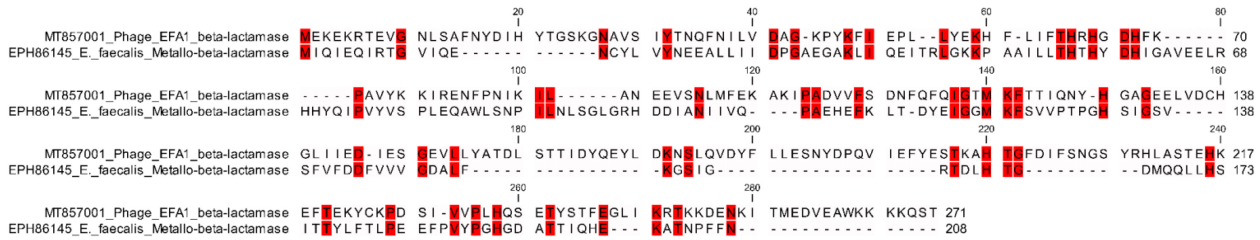

FIGURE 3 | Amino acid alignment of the *E. faecalis* beta-lactamase protein (EPH86145) with EFA1 bacteriophage putative beta-lactamase protein (ORF number 33). Red colored regions highlight areas of identical amino acids [47/272 (17.3%)] between the bacterial and bacteriophage putative beta-lactamase proteins, whereas the non-colored areas define regions where amino acids were non-identical.

Herelleviridae and *Podoviridae* bacteriophages which target *E. faecalis* hosts (**Figure 4**).

Disruption of *E. faecalis* Mono-Biofilm by Bacteriophage EFA1

Viability of Biofilm

To demonstrate the capacity of bacteriophage EFA1 to disrupt *E. faecalis* biofilms, confocal imaging was used to visualize biofilm mass on glass slides. Untreated *E. faecalis* biofilm mass (**Figure 5A**) and that with 2 h bacteriophage EFA1 treatment (**Figure 5B**) were stained with SYBR Gold® and PI to indicate membrane intact bacterial cells (green color) as proxy for live cells and dead/membrane compromised cells indicated by the red color. Images indicated a densely populated biofilm mass in the untreated control (**Figure 5A**) with both live and dead cells remaining attached to the glass slide while a sparse population of membrane intact bacteria remained on the EFA1 treated biofilm (**Figure 5B**).

Quantification of Biofilm Mass

In order to quantify the effect of bacteriophage EFA1 on *E. faecalis* mono-biofilms, these were grown in polystyrene 96 well plates (Greiner Bio-one, Australia) for 4 d to yield biofilm mass of mean absorbance (SE) at OD_{600nm} of 0.86 (0.05). The bacteriophage EFA1 significantly lowered the mean biofilm mass at all treatments from 2 to 24 h ($p < 0.001$) (**Figure 5C**). The mean (SE) biomass following treatment with EFA1 bacteriophage ranged from 0.47 (0.02) for a 2 h treatment to 0.6 (0.07) for a 24 h treatment. While there was a significant reduction in biofilm following treatments at all time points, exposure to EFA1 for 2 h resulted in the greatest decrease in biofilm mass, and the biofilm mass was shown to increase with the length of EFA1 treatment ($p < 0.001$). Paired *T*-tests revealed statistically increased mean (SE) absorbance of biofilm mass between EFA1 treatments for 2 h [0.47 (0.02)] and 6 h [0.52 (0.02)], 4 h [0.48 (0.02)] and 8 h [0.58 (0.02)]; 6 h [0.52 (0.02)] and 24 h [0.6 (0.07)], 8 h [(0.58 (0.02)], and 24 h [0.6 (0.07)]. In order to assess whether the bacteria was developing resistance to EFA1 with the longer treatments, a 5 days biofilm was exposed to EFA1 for (a) 24 h (b) 2 h, and (c) 24 h + 2 h (where after 24 h, media was replaced with fresh media and EFA1, then left for a further 2 h). In these experiments, the biofilm reduction with the 24 h + 2 h treatment was similar to that for 2 h, suggesting that *E. faecalis* had not developed resistance to EFA1 (**Figure 5D**).

EFA1 Effect on the Proliferation and ROS Production of HCT116 Colon Cancer Cell Line Co-cultured With *E. faecalis*

HCT116 Colon Cancer Cell Proliferation in *E. faecalis* Co-culture

As SRB stoichiometrically binds to protein under mild acidic conditions, the absorbance of bound SRB is proportional to cell mass and hence used as proxy for cell proliferation (Orellana and Kasinski, 2016). The greatest proliferation of HCT116 colon cancer cells was seen when co-cultured with *E. faecalis* (**Figure 6A**). The crudely prepared bacteriophage EFA1 caused

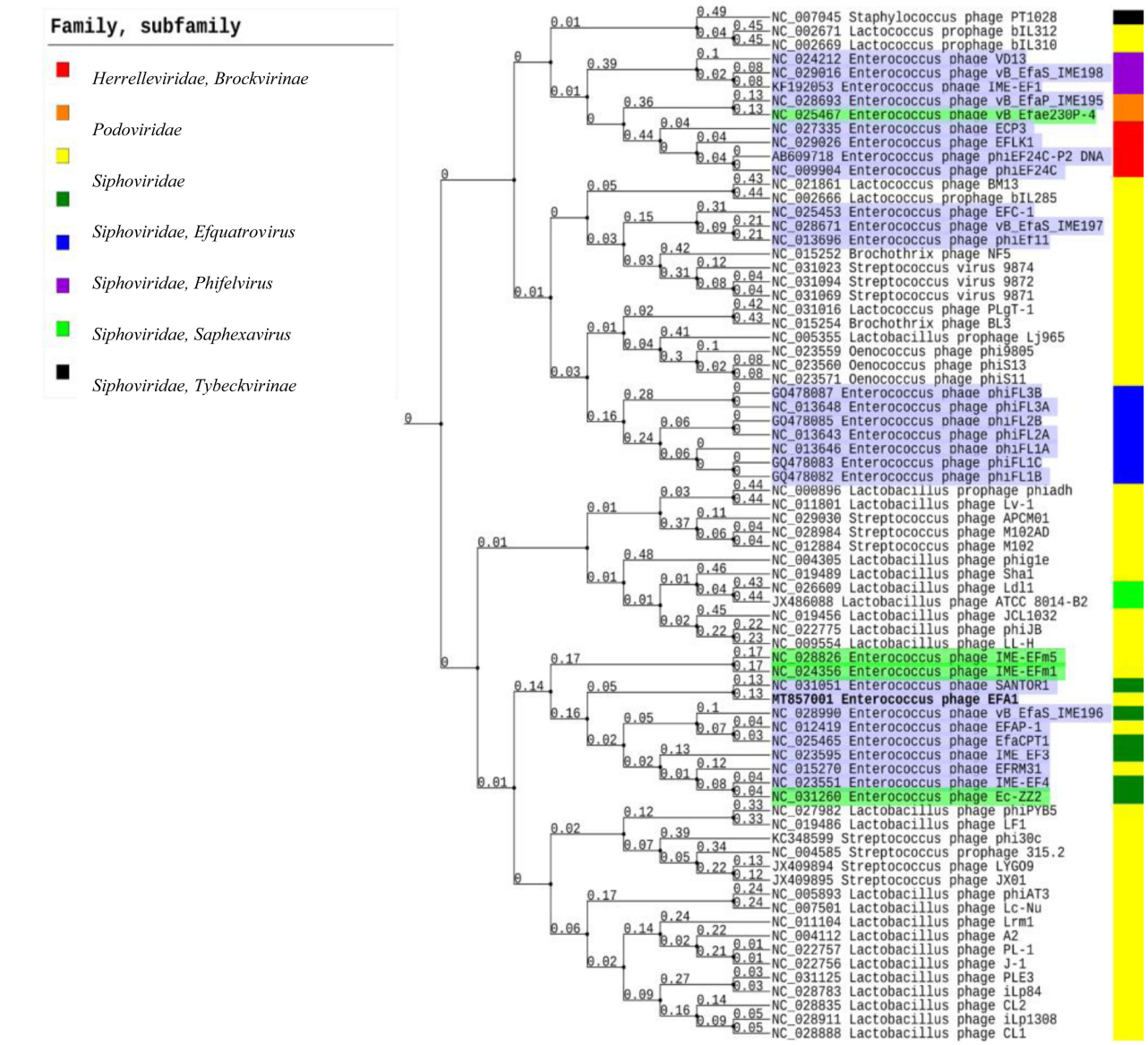

FIGURE 4 | Proteomic tree showing the genome-wide proteomic diversity between bacteriophage EFA1 (highlighted in bold font) and related bacteriophage genomes. Bacteriophages targeting *E. faecalis* are highlighted in purple while those targeting *E. faecium* are highlighted in green. Color coded bar represents the family and subfamily of the bacteriophage (key is at top left).

an increased proliferation of HCT116 cells with mean (SE) SRB absorbance of 0.46 (0.02), $p < 0.001$ (**Figure 6A**), while the mean (SE) SRB absorbance of purified EFA1 treated HCT116 colon cancer cells of 0.31 (0.02) was comparable to that of untreated cells: 0.34 (0.01) ($p = 0.709$). Both the untreated HCT116 cells and those treated with purified EFA1 had significantly less proliferation than HCT116 treatment with unpurified EFA1 and the *E. faecalis*/HCT116 colon cancer cell co-culture [0.57 (0.02), $p < 0.001$] (**Figure 6A**). The least cell proliferation was seen in HCT116 cells that were co-cultured with *E. faecalis* and purified bacteriophage EFA1 with mean (SE) SRB absorbance of 0.13 (0.02) equivalent to a 77.2% reduction in cell proliferation ($p < 0.001$) (**Figure 6A**). The RPMI growth media and *E. faecalis* growing in RPMI showed minimal SRB absorbance.

ROS Production in the *E. faecalis*/HCT116 Colon Cancer Cell Co-culture

To investigate the ROS production in co-culture, RLU as proxy for ROS production were compared between HCT116 colon cancer cells alone and those in co-culture with *E. faecalis*

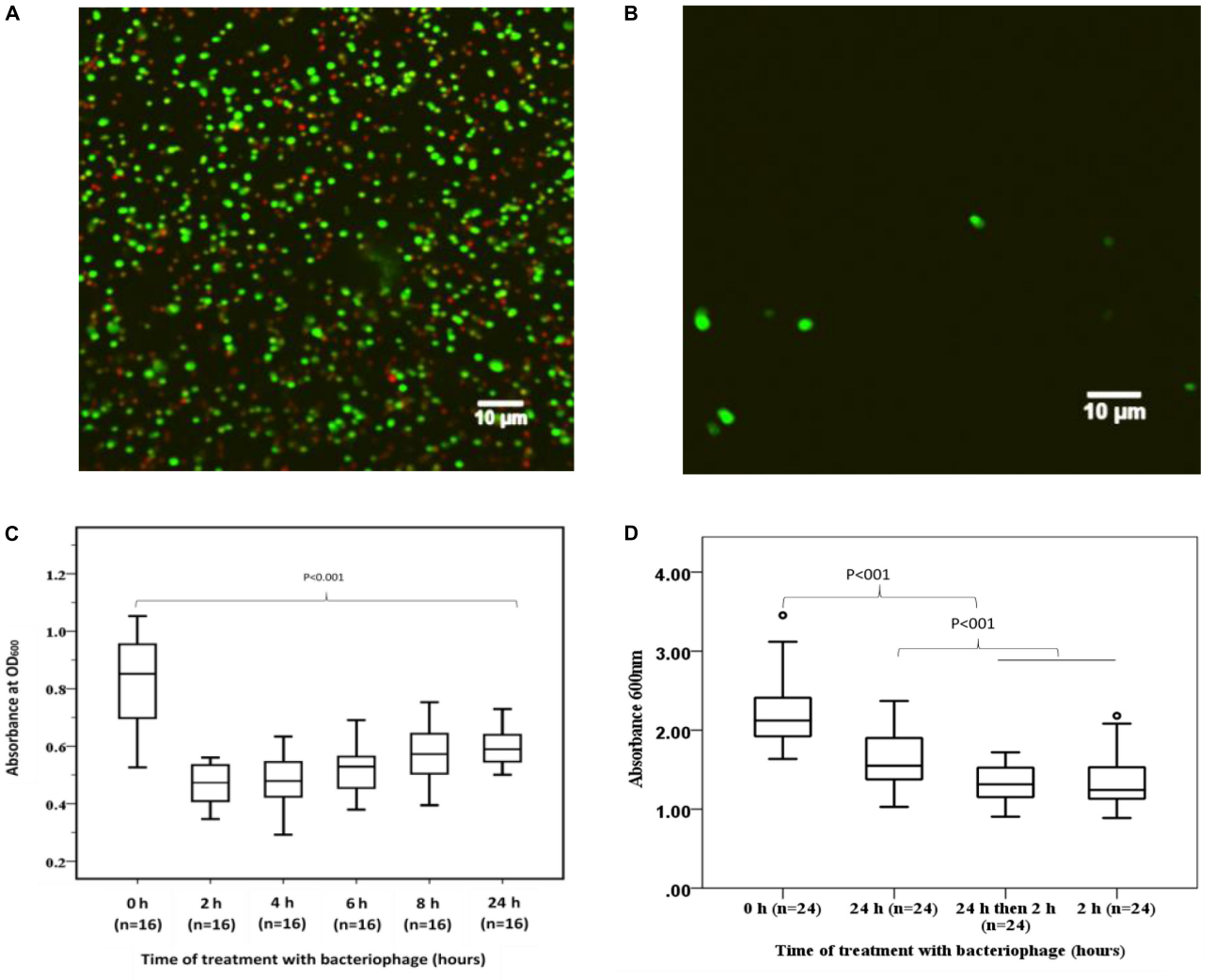

FIGURE 5 | Effects of EFA1 bacteriophage on *E. faecalis* biofilm viability and mass. **(A)** Untreated *E. faecalis* biofilm showing bacteria attached to slide were predominantly membrane intact cells (green), with some bacteria with leaky membranes (red/brown). **(B)** Bacteriophage EFA1 treated biofilm with scant cells remaining attached to slide. **(C)** Quantification of biofilm at time 0 h (without EFA1 treatment) is significanlty greater than any other biofilm treated with bacteriophage EFA1. The lowest amount of biofilm mass was seen after 2 h treatment. Biofilm mass steadly increased with exposure to EFA1. **(D)** 5 days biofilm treated with EFA1 for 24, 2, and 24 h + 2 h, showing similar disruption at 24 + 2 h exposure as that for 2 h.

(**Figure 6B**). HCT116 colon cancer cells alone had similar RLU to HCT116 colon cancer cells with added purified bacteriophage EFA1 ($P = 0.200$). The median (Q1–Q3) RLU for HCT116 cells and the HCT116 with EFA1 were 45.2 (31.2–106.1) and 59.5 (45.5–65.7), respectively. The HCT116 colon cancer cells that were co-cultured with *E. faecalis* had higher RLU than both non-treated HCT116 cancer cells and those with purified EFA1 ($P < 0.001$) (**Figure 6B**). The median (Q1–Q3) RLU for HCT116 co-cultured with *E. faecalis* was 467.0 (365.7–662.3). The RLU of HCT116 colon cancer cells co-cultured with *E. faecalis* and purified bacteriophage EFA1 was significantly increased over that of the HCT116 colon cancer cell pure culture, HCT116 colon cancer cells with EFA1 ($P < 0.001$), and HCT116 colon cancer cells co-cultured with *E. faecalis* ($p = 0.007$) (**Figure 6B**). The mean (Q1-Q3) RLU of the HCT116 colon cancer cells co-cultured with *E. faecalis* and bacteriophage EFA1 was 748.8 (643.8–1475.1).

DISCUSSION

In this study we describe the isolation and characterization of the lytic bacteriophage EFA1 which targets *E. faecalis*. We also describe its modulation of the growth stimulating effects of *E. faecalis* in a colon cancer cell co-culture. There have not been any other studies investigating the actions of *Enterococcus* bacteriophages in colon cancer cells and *E. faecalis* bacterial co-cultures. EFA1 belongs to the family *Siphoviridae*. The bacteriophage host range did not extend to the other bacterial species tested. As such, EFA1 has the potential to

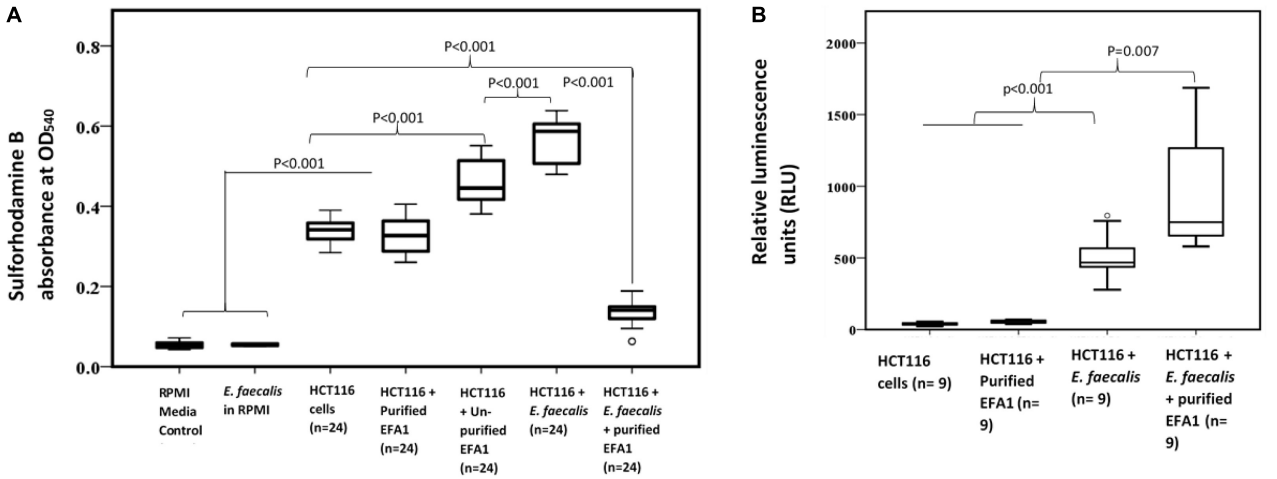

FIGURE 6 | Bacteriophage EFA modulates the effects of *E. faecalis* on HCT116 cancer cell line by increasing ROS production and attenuating cancer cell proliferation. **(A)** Cancer cell proliferation was significantly increased in *E. faecalis* co-cultured HCT116 cells compared to all other cultures. The RPMI growth media and *E. faecalis* growing in RPMI showed minimal SRB absorbance. HCT116 cells grown with purified bacteriophage EFA1, and the HCT116 cells grown on their own, had similar levels of proliferation. Treatment of the HCT116 cells/*E. faecalis* co-culture with purified bacteriophage EFA1 resulted in significant reduction of cancer cell growth, to levels below those of the control HCT116 culture. **(B)** ROS production was significantly increased in the HCT116/*E. faecalis* co-culture with purified EFA1, and to a lesser extent in the HCT116/*E. faecalis* co-culture, compared to HCT116 cells on their own. There was no statistical difference in ROS production between untreated HCT116 and those grown with purified bacteriophage EFA1.

minimize impact on other microbes if used in a diverse microbial environment. In terms of its replication kinetics, the bacteriophage had a latency of 20 min, and a burst size of 120 PFU/bacterial cell. This compares to a latency of 30 min and burst size of 116 for the *E. faecium* bacteriophage IME-Efm1 (Wang et al., 2014), which is the closest related bacteriophage whose replication kinetics are known. To date there are at least 80 *Enterococcus* bacteriophage genomic sequences deposited in NCBI GenBank (Accessed 31 July 2020). The diversity among these viruses is very broad. EFA1 is most closely related to the *E. faecalis* bacteriophage Santor1. These two are part of a monophyletic group of 11 bacteriophages which target *E. faecalis* or *E. faecium*, and which also form a larger clade with bacteriophages infecting *Lactobacillus* and *Streptococcus* hosts, but which cluster more distantly from other bacteriophages which target *E. faecalis* hosts. The genomic arrangement and predicted putative genes found in the bacteriophage EFA1 genome infers a lytic bacteriophage lifestyle and therefore supports its potential suitability to be used in therapy. This was further supported by the lack of toxins or factors that may enhance bacterial virulence such as antibiotic resistance (Mathew, 2016). Some bacteriophages have been shown to carry antibiotic resistant genes that may be transferred between biomes (Muniesa et al., 2013). While genomic analysis of EFA1 did not show any putative genes coding for such bacterial virulence enhancing proteins, ORF33 in EFA1 coded for a putative beta-lactamase protein. However, amino-acid alignment with the bacterial beta-lactamase sequence showed very little identity between the two proteins. Further, screening with the antibiotic resistance CARD database did not show any positive hits for putative antibiotic resistance genes (Jia et al., 2017) in the EFA1 genome. The InterProScan (Mitchell et al., 2019) and Prosite (Sigrist et al., 2013) did not reveal any active sites or beta-lactamase domains required for catalysis (Moali et al., 2003) in the EFA1 genome either. While the ORF 33 genetic element is currently apparently non-functional as a beta-lactamase, it may have allowed the transfer of *E. faecalis* antibiotic resistance by bacteriophages in the past. ORF33 is located among genes coding for putative DNA manipulation, and it is possible its function is in this area, or otherwise unknown, rather than that of a bacterial beta-lactamase. Most of the *Enterococcus* bacteriophages that form a clade with EFA1 also contain a genetic element with some similarity to ORF 33, and so this may represent an evolutionary link between closely related viruses.

Functionally, bacteriophage EFA1 was capable of disrupting *E. faecalis* biofilms within 2 h of treatment. This was evidenced using confocal microscope imaging that revealed sparse cells on bacteriophage treated biofilm compared to untreated biofilm. Quantification of the biofilm mass supported these findings. With increased exposure to the bacteriophage, the biofilm mass began to steadily increase. However, it is likely that this consistent increase was not due to bacterial resistance to EFA1, as adding fresh media and EFA1 after 24 h resulted in biofilm reduction similar to that seen after exposure for 2 h. In this connection, studies with the *E. coli* bacteriophage T4 in *E. coli* mono-biofilms revealed increased bacterial growth after prolonged treatment from 4 to 6 h (Corbin et al., 2001). This phenomenon was not seen in planktonic cultures but considered to be unique to biofilms and suggested to be important in maintenance of the bacteria and bacteriophage ecosystem (Sutherland et al., 2004). These findings raise important issues with respect to potential applications of bacteriophages such as EFA1 in therapy. For instance, they highlight the need for further experiments to more precisely define these host-parasite interactions and kinetics,

so that timing of bacteriophage treatment regimens results in optimal biofilm degradation.

Since *E. faecalis* has been shown to be closely linked to CRC, we investigated the effect of this bacteria on the proliferation of HCT116 colon cancer cells. Similar to the effects of oncobacteria such as *F. nucleatum* (Rubinstein et al., 2013, 2019), *E. faecalis* increased the proliferation of HCT116 colon cancer cells. We found that when we exposed HCT116 cells to unpurified EFA1 (which did not have treatment to rid remnant lipoteichoic acid and/or other cell debris), there was a mitogenic effect and stimulation of cancer cell growth. This effect was lost when EFA1 was purified to remove bacterial cell debris. When treated with purified bacteriophage EFA1, *E. faecalis* induced HCT116 colon cancer cell proliferation was significantly attenuated to levels below that of untreated HCT116 colon cancer cells. To investigate this further we assayed for ROS production. In HCT116 cells co-cultured with *E. faecalis* there was a significant increase, while exposure of HCT116 to purified EFA1 alone resulted in no change, in ROS levels. Our findings also showed significantly increased ROS production, to levels higher than in the HCT116/*E. faecalis* co-culture, when purified bacteriophage EFA1 was added to the HCT116/*E. faecalis* co-culture. We could not find any reports investigating the effects of bacteriophage and associated bacteria on ROS production in cancer cells or mammalian cells other than in leukocytes (Przerwa et al., 2006; Miedzybrodzki et al., 2008; Miernikiewicz et al., 2013). In these studies, there was a decrease in ROS when bacteriophage T4 treated granulocytes were co-cultured with *E. coli*, in contrast with our findings. Therefore, it may be that this difference in ROS induction is dependent on cell type.

The role of ROS in cancer (Liou and Storz, 2010) and in cancer therapy (Trachootham et al., 2009) has been reviewed. It is known that cells express antioxidants that neutralize ROS while maintaining sufficient levels needed for cellular signaling (Gonzalez et al., 2002). In some tumorigenic events, increased intracellular ROS promotes tumor progression (Jackson, 1994). However, high and excessive ROS levels are induced by chemotherapy agents leading to cell cycle arrest and cell death (Yang H. et al., 2018). Although the exact mechanism and effect of ROS production in our system is unknown, and requires further investigation, the excessive ROS production could contribute to the significantly lower cancer cell proliferation seen when the HCT116/*E. faecalis* co-culture was treated with EFA1.

CONCLUSION

The bacteriophage EFA1 isolated from wastewater was fully characterized and its whole genome sequenced. EFA1 was capable of disrupting *E. faecalis* mono-biofilms. Further, while *E. faecalis* enhanced the proliferation of HCT116 colon cancer cells, in the presence of EFA1 the proliferation was significantly inhibited with an associated increase in ROS production. EFA1 alone did not significantly alter the proliferation or ROS production of HCT116 cells. Such findings may lead to further testing of bacteriophages such as EFA1 in the control of oncobacteria induced cancer cell growth.

DATA AVAILABILITY STATEMENT

The authors declare that all relevant data supporting the findings of the study are available in this article and the **Supplementary Figure** file, or from the corresponding author upon reasonable request. The complete genome sequence of bacteriophage EFA1 has been submitted to NCBI GenBank under accession number MT857001.

AUTHOR CONTRIBUTIONS

JT and MK: conceptualization, data analysis, and writing—original draft. MK and TM-A: mammalian cell and bacterial co-culture. MK and SB: genomic. MK and HK: electron microscope imaging and biofilm. JT, HC, and SP: supervision. All authors contributed to writing, reviewing, and editing of the manuscript.

ACKNOWLEDGMENTS

We would like to acknowledge La Trobe University, the Olivia Newton John Cancer Research Institute, and the La Trobe Institute for Molecular Science Bioimaging facility.

SUPPLEMENTARY MATERIAL

The Supplementary Material for this article can be found online at: https://www.frontiersin.org/articles/10.3389/fmicb.2021.650849/full#supplementary-material

REFERENCES

Al-Hebshi, N. N., Nasher, A. T., Maryoud, M. Y., Homeida, H. E., Chen, T., Idris, A. M., et al. (2017). Inflammatory bacteriome featuring *Fusobacterium nucleatum* and *Pseudomonas aeruginosa* identified in association with oral squamous cell carcinoma. *Sci. Rep.* 7:1834.

Azam, A. H., and Tanji, Y. (2019). Bacteriophage-host arm race: an update on the mechanism of phage resistance in bacteria and revenge of the phage with the perspective for phage therapy. *Appl. Microbiol. Biotechnol.* 103, 2121–2131. doi: 10.1007/s00253-019-09629-x

Balamurugan, R., Rajendiran, E., George, S., Samuel, G. V., and Ramakrishna, B. S. (2008). Real-time polymerase chain reaction quantification of specific butyrate-producing bacteria, desulfovibrio and *Enterococcus faecalis* in the feces of patients with colorectal cancer. *J. Gastroenterol. Hepatol.* 23, 1298–1303.

Barnes, A. M. T., Dale, J. L., Chen, Y., Manias, D. A., Greenwood Quaintance, K. E., Karau, M. K., et al. (2017). *Enterococcus faecalis* readily colonizes the entire gastrointestinal tract and forms biofilms in a germ-free mouse model. *Virulence* 8, 282–296. doi: 10.1080/21505594.2016.1208890

Benson, D. A., Karsch-Mizrachi, I., Lipman, D. J., Ostell, J., Rapp, B. A., and Wheeler, D. L. (2000). GenBank. *Nucleic Acids Res.* 28, 15–18.

Bhatt, A. P., Redinbo, M. R., and Bultman, S. J. (2017). The role of the microbiome in cancer development and therapy. *Ca Cancer J. Clin.* 67, 326–344. doi: 10.3322/caac.21398

Branston, S. D., Wright, J., and Keshavarz-Moore, E. (2015). A non-chromatographic method for the removal of endotoxins from bacteriophages. *Biotechnol. Bioeng.* 112, 1714–1719. doi: 10.1002/bit.25571

Cani, P. D. (2018). Human gut microbiome: hopes, threats and promises. *Gut* 67, 1716–1725. doi: 10.1136/gutjnl-2018-316723

Corbin, B. D., Mclean, R. J., and Aron, G. M. (2001). Bacteriophage T4 multiplication in a glucose-limited *Escherichia coli* biofilm. *Can. J. Microbiol.* 47, 680–684. doi: 10.1139/w01-059

De Lastours, V., Maugy, E., Mathy, V., Chau, F., Rossi, B., Guerin, F., et al. (2017). Ecological impact of ciprofloxacin on commensal enterococci in healthy volunteers. *J. Antimicrob. Chemother.* 72, 1574–1580. doi: 10.1093/jac/dkx043

Drees, M., Snydman, D. R., Schmid, C. H., Barefoot, L., Hansjosten, K., Vue, P. M., et al. (2008). Prior environmental contamination increases the risk of acquisition of vancomycin-resistant enterococci. *Clin. Infect. Dis.* 46, 678–685. doi: 10.1086/527394

Dubin, K., and Pamer, E. G. (2014). Enterococci and their interactions with the intestinal microbiome. *Microbiol. Spectr.* 5:10.1128/microbiolsec.BAD–0014–2016. doi: 10.1128/microbiolspec.BAD-0014-2016

Franz, C. M., Stiles, M. E., Schleifer, K. H., and Holzapfel, W. H. (2003). Enterococci in foods–a conundrum for food safety. *Int. J. Food. Microbiol.* 88, 105–122. doi: 10.1016/s0168-1605(03)00174-0

Gaiser, R. A., Halimi, A., Alkharaan, H., Lu, L., Davanian, H., Healy, K., et al. (2019). Enrichment of oral microbiota in early cystic precursors to invasive pancreatic cancer. *Gut* 68, 1–9. doi: 10.1007/978-1-62703-287-2_1

Garneau, J. R., Depardieu, F., Fortier, L. C., Bikard, D., and Monot, M. (2017). PhageTerm: a tool for fast and accurate determination of phage termini and packaging mechanism using next-generation sequencing data. *Sci. Rep.* 7:8292.

Gonzalez, C., Sanz-Alfayate, G., Agapito, M. T., Gomez-Nino, A., Rocher, A., and Obeso, A. (2002). Significance of Ros in oxygen sensing in cell systems with sensitivity to physiological hypoxia. *Respir Physiol. Neurobiol.* 132, 17–41. doi: 10.1016/s1569-9048(02)00047-2

Grissa, I., Vergnaud, G., and Pourcel, C. (2007). Crisprfinder: a web tool to identify clustered regularly interspaced short palindromic repeats. *Nucleic Acids Res.* 35, W52–W57.

Hansen, M. F., Svenningsen, S. L., Røder, H. L., Middelboe, M., and Burmølle, M. (2019). Big impact of the tiny: bacteriophage–bacteria interactions in biofilms. *Trends Microbiol.* 27, 739–752. doi: 10.1016/j.tim.2019.04.006

Helmink, B. A., Khan, M. A. W., Hermann, A., Gopalakrishnan, V., and Wargo, J. A. (2019). The microbiome, cancer, and cancer therapy. *Nat. Med.* 25, 377–388.

Hollenbeck, B. L., and Rice, L. B. (2012). Intrinsic and acquired resistance mechanisms in enterococcus. *Virulence* 3, 421–433. doi: 10.4161/viru.21282

Holt, R. A., and Cochrane, K. (2017). Tumor potentiating mechanisms of *fusobacterium nucleatum*, a multifaceted microbe. *Gastroenterology* 152, 694–696. doi: 10.1053/j.gastro.2017.01.024

Hota, B. (2004). Contamination, disinfection, and cross-colonization: are hospital surfaces reservoirs for nosocomial infection? *Clin. Infect. Dis.* 39, 1182–1189. doi: 10.1086/424667

Huycke, M. M., Abrams, V., and Moore, D. R. (2002). *Enterococcus faecalis* produces extracellular superoxide and hydrogen peroxide that damages colonic epithelial cell Dna. *Carcinogenesis* 23, 529–536. doi: 10.1093/carcin/23.3.529

Jackson, J. H. (1994). Potential molecular mechanisms of oxidant-induced carcinogenesis. *Environ. Health Perspect.* 102(Suppl. 10), 155–157. doi: 10.2307/3432232

Jia, B., Raphenya, A. R., Alcock, B., Waglechner, N., Guo, P., Tsang, K. K., et al. (2017). Card 2017: expansion and model-centric curation of the comprehensive antibiotic resistance database. *Nucleic Acids Res.* 45, D566–D573.

Jonczyk-Matysiak, E., Lusiak-Szelachowska, M., Klak, M., Bubak, B., Miedzybrodzki, R., Weber-Dabrowska, B., et al. (2015). The effect of bacteriophage preparations on intracellular killing of bacteria by phagocytes. *J. Immunol. Res.* 2015:482863.

Kabwe, M., Brown, T., Speirs, L., Ku, H., Leach, M., Chan, H. T., et al. (2020). Novel bacteriophages capable of disrupting biofilms from clinical strains of *Aeromonas hydrophila*. *Front. Microbiol.* 11:194. doi: 10.3389/fmicb.2020.00194

Kabwe, M., Brown, T. L., Dashper, S., Speirs, L., Ku, H., Petrovski, S., et al. (2019). Genomic, morphological and functional characterisation of novel bacteriophage Fnu1 capable of disrupting *Fusobacterium nucleatum* biofilms. *Sci. Rep.* 9:9107.

Kharrat, N., Assidi, M., Abu-Elmagd, M., Pushparaj, P. N., Alkhaldy, A., Arfaoui, L., et al. (2019). Data mining analysis of human gut microbiota links *Fusobacterium* spp. with colorectal cancer onset. *Bioinformation* 15, 372–379. doi: 10.6026/97320630015372

Kho, Z. Y., and Lal, S. K. (2018). The human gut microbiome - a potential controller of wellness and disease. *Front. Microbiol.* 9:1835. doi: 10.3389/fmicb.2018.01835

Kropec, A., Hufnagel, M., Zimmermann, K., and Huebner, J. (2005). In vitro assessment of the host response against *Enterococcus faecalis* used in probiotic preparations. *Infection* 33, 377–379. doi: 10.1007/s15010-005-5063-7

Laslett, D., and Canback, B. (2004). Aragorn, a program to detect tRNA genes and tmRNA genes in nucleotide sequences. *Nucleic Acids Res.* 32, 11–16. doi: 10.1093/nar/gkh152

Lennard, K. S., Goosen, R. W., and Blackburn, J. M. (2016). Bacterially-associated transcriptional remodelling in a distinct genomic subtype of colorectal cancer provides a plausible molecular basis for disease development. *PLoS One* 11:e0166282. doi: 10.1371/journal.pone.0166282

Letunic, I., and Bork, P. (2019). Interactive tree of life (iTOL) v4: recent updates and new developments. *Nucleic Acids Res.* 47, W256–W259.

Liou, G. Y., and Storz, P. (2010). Reactive oxygen species in cancer. *Free Radic Res.* 44, 479–496.

Lowe, T. M., and Chan, P. P. (2016). tRNAscan-Se On-line: integrating search and context for analysis of transfer Rna genes. *Nucleic Acids Res.* 44, W54–W57.

Lusiak-Szelachowska, M., Weber-Dabrowska, B., and Gorski, A. (2020). Bacteriophages and lysins in biofilm control. *Virol Sin.* 35, 125–133. doi: 10.1007/s12250-019-00192-3

Mathew, S. (2016). A need for careful consideration of bacteriophage therapy. *Indian J. Med. Res.* 144, 482–483. doi: 10.4103/0971-5916.198691

Merritt, J. H., Kadouri, D. E., and O'toole, G. A. (2005). Growing and analyzing static biofilms. *Curr. Protoc. Microbiol.* 1, Unit 1B.1.

Miedzybrodzki, R., Switala-Jelen, K., Fortuna, W., Weber-Dabrowska, B., Przerwa, A., Lusiak-Szelachowska, M., et al. (2008). Bacteriophage preparation inhibition of reactive oxygen species generation by endotoxin-stimulated polymorphonuclear leukocytes. *Virus Res.* 131, 233–242. doi: 10.1016/j.virusres.2007.09.013

Miernikiewicz, P., Dabrowska, K., Piotrowicz, A., Owczarek, B., Wojas-Turek, J., Kicielinska, J., et al. (2013). T4 phage and its head surface proteins do not stimulate inflammatory mediator production. *PloS One* 8:e71036. doi: 10.1371/journal.pone.0071036

Mitchell, A. L., Attwood, T. K., Babbitt, P. C., Blum, M., Bork, P., Bridge, A., et al. (2019). InterPro in 2019: improving coverage, classification and access to protein sequence annotations. *Nucleic Acids Res.* 47, D351–D360.

Mitsuhashi, K., Nosho, K., Sukawa, Y., Matsunaga, Y., Ito, M., Kurihara, H., et al. (2015). Association of *Fusobacterium* species in pancreatic cancer tissues with molecular features and prognosis. *Oncotarget* 6, 7209–7220. doi: 10.18632/oncotarget.3109

Moali, C., Anne, C., Lamotte-Brasseur, J., Groslambert, S., Devreese, B., Van Beeumen, J., et al. (2003). Analysis of the importance of the metallo-beta-lactamase active site loop in substrate binding and catalysis. *Chem. Biol.* 10, 319–329. doi: 10.1016/s1074-5521(03)00070-x

Moreno-Gallego, J. L., Chou, S. P., Di Rienzi, S. C., Goodrich, J. K., Spector, T. D., Bell, J. T., et al. (2019). Virome diversity correlates with intestinal microbiome diversity in adult monozygotic twins. *Cell Host. Microbe.* 25, 261e5–272e5.

Mount, D. W. (2007). Using the basic local alignment search tool (blast). *CSH Protoc.* 2007:dbto17.

Muniesa, M., Colomer-Lluch, M., and Jofre, J. (2013). Could bacteriophages transfer antibiotic resistance genes from environmental bacteria to human-body associated bacterial populations? *Mob. Genet. Elements* 3:e25847. doi: 10.4161/mge.25847

Nishimura, Y., Yoshida, T., Kuronishi, M., Uehara, H., Ogata, H., and Goto, S. (2017). Viptree: the viral proteomic tree server. *Bioinformatics* 33, 2379–2380. doi: 10.1093/bioinformatics/btx157

Nueno-Palop, C., and Narbad, A. (2011). Probiotic assessment of Enterococcus faecalis Cp58 isolated from human gut. *Int. J. Food Microbiol.* 145, 390–394. doi: 10.1016/j.ijfoodmicro.2010.12.029

Orellana, E. A., and Kasinski, A. L. (2016). Sulforhodamine B (Srb) assay in cell culture to investigate cell proliferation. *Bio. Protoc.* 6:e1984.

Parhi, L., Alon-Maimon, T., Sol, A., Nejman, D., Shhadeh, A., Fainsod-Levi, T., et al. (2020). Breast cancer colonization by *Fusobacterium nucleatum* accelerates tumor growth and metastatic progression. *Nat. Commun.* 11:3259.

Przerwa, A., Zimecki, M., Switala-Jelen, K., Dabrowska, K., Krawczyk, E., Luczak, M., et al. (2006). Effects of bacteriophages on free radical production and phagocytic functions. *Med. Microbiol. Immunol.* 195, 143–150. doi: 10.1007/s00430-006-0011-4

Rajagopala, S. V., Vashee, S., Oldfield, L. M., Suzuki, Y., Venter, J. C., Telenti, A., et al. (2017). The human microbiome and cancer. *Cancer Prev. Res. (Phila)* 10, 226–234.

Rubinstein, M. R., Baik, J. E., Lagana, S. M., Han, R. P., Raab, W. J., Sahoo, D., et al. (2019). *Fusobacterium nucleatum* promotes colorectal cancer by inducing Wnt/beta-catenin modulator Annexin A1. *Embo Rep.* 20:e47638.

Rubinstein, M. R., Wang, X., Liu, W., Hao, Y., Cai, G., and Han, Y. W. (2013). *Fusobacterium nucleatum* promotes colorectal carcinogenesis by modulating E-cadherin/beta-catenin signaling via its FadA adhesin. *Cell Host. Microbe.* 14, 195–206. doi: 10.1016/j.chom.2013.07.012

Sender, R., Fuchs, S., and Milo, R. (2016). Are we really vastly outnumbered? revisiting the ratio of bacterial to host cells in humans. *Cell* 164, 337–340. doi: 10.1016/j.cell.2016.01.013

Sigrist, C. J., De Castro, E., Cerutti, L., Cuche, B. A., Hulo, N., Bridge, A., et al. (2013). New and continuing developments at Prosite. *Nucleic Acids Res.* 41, D344–D347.

Skehan, P., Storeng, R., Scudiero, D., Monks, A., Mcmahon, J., Vistica, D., et al. (1990). New colorimetric cytotoxicity assay for anticancer-drug screening. *J. Natl. Cancer Inst.* 82, 1107–1112. doi: 10.1093/jnci/82.13.1107

Sutherland, I. W., Hughes, K. A., Skillman, L. C., and Tait, K. (2004). The interaction of phage and biofilms. *Fems Microbiol. Lett.* 232, 1–6. doi: 10.1016/s0378-1097(04)00041-2

Tinrat, S., Khuntayaporn, P., Thirapanmethee, K., and Chomnawang, M. T. (2018). In vitro assessment of Enterococcus faecalis Mtc 1032 as the potential probiotic in food supplements. *J. Food Sci. Technol.* 55, 2384–2394. doi: 10.1007/s13197-018-3155-5

Trachootham, D., Alexandre, J., and Huang, P. (2009). Targeting cancer cells by Ros-mediated mechanisms: a radical therapeutic approach? *Nat. Rev. Drug Discov.* 8, 579–591. doi: 10.1038/nrd2803

Van Belleghem, J. D., Dabrowska, K., Vaneechoutte, M., Barr, J. J., and Bollyky, P. L. (2018). Interactions between bacteriophage, bacteria, and the mammalian immune system. *Viruses* 11:10. doi: 10.3390/v11010010

Wang, G., Liu, Q., Pei, Z., Wang, L., Tian, P., Liu, Z., et al. (2020a). The diversity of the Crispr-cas system and prophages present in the genome reveals the co-evolution of *Bifidobacterium pseudocatenulatum* and phages. *Front. Microbiol.* 11:1088. doi: 10.3389/fmicb.2020.01088

Wang, J., Da, R., Tuo, X., Cheng, Y., Wei, J., Jiang, K., et al. (2020b). Probiotic and safety properties screening of *Enterococcus faecalis* from healthy chinese infants. *Probiotics Antimicrob. Proteins* 12, 1115–1125. doi: 10.1007/s12602-019-09625-7

Wang, X., Allen, T. D., May, R. J., Lightfoot, S., Houchen, C. W., and Huycke, M. M. (2008). *Enterococcus faecalis* induces aneuploidy and tetraploidy in colonic epithelial cells through a bystander effect. *Cancer Res.* 68, 9909–9917. doi: 10.1158/0008-5472.can-08-1551

Wang, X., and Huycke, M. M. (2007). Extracellular superoxide production by *Enterococcus faecalis* promotes chromosomal instability in mammalian cells. *Gastroenterology* 132, 551–561. doi: 10.1053/j.gastro.2006.11.040

Wang, Y., Wang, W., Lv, Y., Zheng, W., Mi, Z., Pei, G., et al. (2014). Characterization and complete genome sequence analysis of novel bacteriophage Ime-Efm1 infecting *Enterococcus faecium*. *J. Gen. Virol.* 95, 2565–2575. doi: 10.1099/vir.0.067553-0

Weiner-Lastinger, L. M., Abner, S., Edwards, J. R., Kallen, A. J., Karlsson, M., Magill, S. S., et al. (2020). Antimicrobial-resistant pathogens associated with adult healthcare-associated infections: summary of data reported to the national healthcare safety network, 2015-2017. *Infect. Control Hosp. Epidemiol.* 41, 1–18. doi: 10.1086/668770

Wick, R. R., Judd, L. M., Gorrie, C. L., and Holt, K. E. (2017). Unicycler: resolving bacterial genome assemblies from short and long sequencing reads. *PLoS Comput. Biol.* 13:e1005595. doi: 10.1371/journal.pcbi.1005595

Yachida, S., Mizutani, S., Shiroma, H., Shiba, S., Nakajima, T., Sakamoto, T., et al. (2019). Metagenomic and metabolomic analyses reveal distinct stage-specific phenotypes of the gut microbiota in colorectal cancer. *Nat. Med.* 25, 968–976. doi: 10.1038/s41591-019-0458-7

Yamamura, K., Baba, Y., Nakagawa, S., Mima, K., Miyake, K., Nakamura, K., et al. (2016). Human microbiome *Fusobacterium Nucleatum* in esophageal cancer tissue is associated with prognosis. *Clin. Cancer Res.* 22, 5574–5581. doi: 10.1158/1078-0432.ccr-16-1786

Yang, H., Villani, R. M., Wang, H., Simpson, M. J., Roberts, M. S., Tang, M., et al. (2018a). The role of cellular reactive oxygen species in cancer chemotherapy. *J. Exp. Clin. Cancer Res.* 37:266.

Yang, S. F., Huang, H. D., Fan, W. L., Jong, Y. J., Chen, M. K., Huang, C. N., et al. (2018b). Compositional and functional variations of oral microbiota associated with the mutational changes in oral cancer. *Oral Oncol.* 77, 1–8. doi: 10.1016/j.oraloncology.2017.12.005

Zervos, M. J., Terpenning, M. S., Schaberg, D. R., Therasse, P. M., Medendorp, S. V., and Kauffman, C. A. (1987). High-level aminoglycoside-resistant enterococci. Colonization of nursing home and acute care hospital patients. *Arch. Intern. Med.* 147, 1591–1594. doi: 10.1001/archinte.147.9.1591

Zhao, H., Chu, M., Huang, Z., Yang, X., Ran, S., Hu, B., et al. (2017). Variations in oral microbiota associated with oral cancer. *Sci. Rep.* 7:11773.

Zheng, D. W., Dong, X., Pan, P., Chen, K. W., Fan, J. X., Cheng, S. X., et al. (2019). Phage-guided modulation of the gut microbiota of mouse models of colorectal cancer augments their responses to chemotherapy. *Nat. Biomed. Eng.* 3, 717–728. doi: 10.1038/s41551-019-0423-2

Conflict of Interest: The authors declare that the research was conducted in the absence of any commercial or financial relationships that could be construed as a potential conflict of interest.

Copyright © 2021 Kabwe, Meehan-Andrews, Ku, Petrovski, Batinovic, Chan and Tucci. This is an open-access article distributed under the terms of the Creative Commons Attribution License (CC BY). The use, distribution or reproduction in other forums is permitted, provided the original author(s) and the copyright owner(s) are credited and that the original publication in this journal is cited, in accordance with accepted academic practice. No use, distribution or reproduction is permitted which does not comply with these terms.

frontiers in Microbiology

ORIGINAL RESEARCH
published: 13 April 2021
doi: 10.3389/fmicb.2021.674415

Systemic Expression, Purification, and Initial Structural Characterization of Bacteriophage T4 Proteins Without Known Structure Homologs

Kaining Zhang[1†], Xiaojiao Li[1†], Zhihao Wang[1,2†], Guanglin Li[1], Biyun Ma[1], Huan Chen[1], Na Li[3], Huaiyu Yang[4], Yawen Wang[1] and Bing Liu[1,2*]*

[1] BioBank, The First Affiliated Hospital of Xi'an Jiaotong University, Xi'an, China, [2] Department of Life Sciences, Faculty of Natural Sciences, Imperial College London, London, United Kingdom, [3] Department of Laboratory Medicine, The First Affiliated Hospital of Xi'an Jiaotong University, Xi'an, China, [4] Department of Chemical Engineering, University of Loughborough, Leicestershire, United Kingdom

OPEN ACCESS

Edited by:
Shuai Le,
Army Medical University, China

Reviewed by:
Jianfeng Yu,
Shenzhen University, China
Nan Hou,
Chinese Academy of Medical Sciences, China

***Correspondence:**
Yawen Wang
wangyawen@xjtu.edu.cn
Bing Liu
bliu2018@xjtu.edu.cn

[†] These authors have contributed equally to this work

Specialty section:
This article was submitted to Virology, a section of the journal Frontiers in Microbiology

Received: 01 March 2021
Accepted: 22 March 2021
Published: 13 April 2021

Citation:
Zhang K, Li X, Wang Z, Li G, Ma B, Chen H, Li N, Yang H, Wang Y and Liu B (2021) Systemic Expression, Purification, and Initial Structural Characterization of Bacteriophage T4 Proteins Without Known Structure Homologs. Front. Microbiol. 12:674415. doi: 10.3389/fmicb.2021.674415

Bacteriophage T4 of *Escherichia coli* is one of the most studied phages. Research into it has led to numerous contributions to phage biology and biochemistry. Coding about 300 gene products, this double-stranded DNA virus is the best-understood model in phage study and modern genomics and proteomics. Ranging from viral RNA polymerase, commonly found in phages, to thymidylate synthase, whose mRNA requires eukaryotic-like self-splicing, its gene products provide a pool of fine examples for phage research. However, there are still up to 130 gene products that remain poorly characterized despite being one of the most-studied model phages. With the recent advancement of cryo-electron microscopy, we have a glimpse of the virion and the structural proteins that present in the final assembly. Unfortunately, proteins participating in other stages of phage development are absent. Here, we report our systemic analysis on 22 of these structurally uncharacterized proteins, of which none has a known homologous structure due to the low sequence homology to published structures and does not belong to the category of viral structural protein. Using NMR spectroscopy and cryo-EM, we provided a set of preliminary structural information for some of these proteins including NMR backbone assignment for Cef. Our findings pave the way for structural determination for the phage proteins, whose sequences are mainly conserved among phages. While this work provides the foundation for structural determinations of proteins like Gp57B, Cef, Y04L, and Mrh, other *in vitro* studies would also benefit from the high yield expression of these proteins.

Keywords: bacteriophage, T4, NMR, cryo-EM, Mrh, Cef, Y04L and Gp57B

INTRODUCTION

With an estimated population of 10^{31}, the bacteriophage—a type of virus preying on a bacterium—is the most abundant organism in the Earth's biosphere (Clokie et al., 2011). It is believed that every bacterial strain hosts at least one type of phage, making the phage the most diversified organism (Keen, 2015). With such complexity, phage research has been focused on a few model phages

that infect the most-studied bacteria like *Escherichia coli* and *Bacillus subtilis* (Miller et al., 2003). *Escherichia* virus T4 is one such example upon which studies have contributed to various aspects of viral biology since its discovery in the 1940s (Gamkrelidze and Dabrowska, 2014; Taj et al., 2014). As a member of the viral subfamily *Tevenvirinae*, T4 is also one of the seven known coliphages that specifically target *E. coli* and are lethal to cells (Yap and Rossmann, 2014). Along with other *E. coli* phages, it has provided instrumental tools for developing many fundamental biological concepts and applications. Some of the most significant discoveries in modern biology were aided by T4 phages, including the recognition of nucleic acids as genetic material, the demonstration that genetic codons are triplets, the discovery of mRNA, DNA restriction and modification, and self-splicing of intron/exon arrangements in prokaryotes (Kutter et al., 1995; Miller et al., 2003).

The double-stranded DNA genome of T4 is about 169 kbp in length, encoding about 289 proteins and bearing three eukaryotic-like introns (Comeau et al., 2007). T4-related phages exist in almost every ecosystem and represent a large portion of the tailed phages known to date (Amarillas et al., 2016). The functional annotations for the genes in these phages are mainly based on studies from T4, usually without any further verification. After years of effort, the majority of T4 gene products have been assigned to various functions, some of which have unique structures and features. Analysis of the sequential events during T4 infection has revealed the interactions between phage and the host, the strategies that phage employed to modulate host molecular machinery, as well as the specific function of individual proteins (Gamkrelidze and Dabrowska, 2014). For example, gene products of asiA have been characterized and determined to be anti-sigma factors in a wide range of phages (Sharma and Chatterji, 2008), including *Shigella* and *Acinetobacter* phages, thanks to studies into T4.

Although T4 is considered to be one of the best-known phages, approximately 130 out of its 289 proteins are still poorly described (Miller et al., 2003). For example, Y04L coded by the *y04L* gene in the pin-nrdC intergenic region is an example of proteins whose biological function and mechanism are yet to be addressed (Zhang et al., 2019). On the other hand, Cef is known to play a role in the maturation of viral tRNAs, a process that is still poorly characterized in phages (Pulitzer et al., 1985). Its molecular mechanism remains elusive, partially due to the absence of a relevant structure. Other examples include Mrh, which is a transcriptional regulator of late T4 genes that modulates the phosphorylation status of host heat shock sigma factor rpoH and thus promotes the attachment of host RNA polymerase to specific initiation sites (Mosig et al., 1998). The molecular basis remains unclear without structural interpretation on the Mrh protein and its binding partner. Thus, it is essential to study these poorly characterized proteins in order to further understand T4 phage biology. As phage study is gaining popularity due to the challenge from antibiotic-resistant bacteria (Lin et al., 2017), it is essential to assess the safety of phages in therapeutic applications. Without a fully annotated genome and functional interpretation of individual phage gene products, it is difficult to validate the safety of T4 related phages to be used in humans (Loc-Carrillo and Abedon, 2011).

This study attempts to express some of these proteins recombinantly in *E. coli* and in a cell-free system, as obtaining correctly folded proteins is the foundation for structure determination and *in vitro* functional analysis. We systemically screened the T4 genome and specifically looked for proteins with no homologous structure deposited in the Protein Data Bank (PDB). Finally, we selected 22 proteins for preliminary structural analysis. While some of these 22 proteins could be expressed as soluble proteins, others were found primarily in the inclusion body, possibly due to the toxicity to its native host *E. coli* or the lack of auxiliary T4 proteins that essential for proper folding. We applied two types of N-terminal fusion tags, SUMO and Msyb, to these proteins to improve the solubility and folding, with success in some cases (Marblestone et al., 2006; Yang et al., 2020). Using the Nuclear Magnetic Resonances (NMR) spectroscopy and Cryogenic electron microscopy, we provided an initial assessment for the folding and oligomeric states for soluble proteins and made progress on the structural determinations. Our systematic study provided preliminary data on expression conditions of the candidate proteins and shed light on the potential choice of techniques (solution NMR, X-ray crystallography, or Cryo-electron microscopy) for their structure determinations.

MATERIALS AND METHODS

Plasmid Construction

The coding sequence of the candidate proteins was amplified from genomic DNA of the T4 phage using PCR. The PCR products were examined by agarose gel electrophoresis and further purified before being cloned into respective vectors to recombinantly attach the N-terminal His-tag (in-house modified pET-28 vector), His-SUMO tags (pET-SUMO vector), or His-Msyb tags (in-house modified from pET-SUMO), respectively. All primers and plasmids used are available in **Supplementary Table 2**. The resultant plasmids were transformed into *E. coli* DH5α cells. At least five independent clones of each plasmid were sequenced.

Recombinant Protein Expression in *E. coli*

The expression vector was transformed into BL21(DE3) pLysS *E. coli* for protein expression. LB medium, supplemented with selected antibiotics (350 μg/mL of ampicillin, 485 μg/mL of kanamycin, or 378 μg/mL of carbenicillin) was used for the cultivation of *E. coli* strains. Minimal medium containing ^{15}N-labeled ammonium chloride as the sole source of nitrogen and ^{13}C-labeled glucose as the sole source of carbon were used to obtain uniformly ^{15}N and ^{13}C-enriched protein for structural determination using NMR.

The starting cultures were incubated overnight at 37°C with compatible antibiotics in a 50 ml centrifuge tube containing 30 ml of LB medium by inoculating a single colony from the plates. The starting cultures were then transferred into 1 L of fresh LB media

or minimal media supplemented with the appropriate antibiotic. The cultures were incubating at 37℃ until an optical density at 600 nm (OD_{600}) of 0.6 was reached followed by the addition of 1 mM of IPTG to induce the expression. The cultures were then incubated overnight at 18℃ before being harvested.

Cell-Free Protein Expression

The coding sequence of Cef was coding optimized using the manufacturer's online tool (Kangma-Healthcode, Shanghai). The *cef* gene was cloned into the cloned pD_2P vector and amplified using DNA rolling circle amplification. The plasmid was then added into a 10 ml ProteinFactory fast reaction system. The reaction mixture was incubated for 3 h under room temperature with gentle shaking. The reaction mixture was then subjected to standard His-tagged protein purification or magnetic bead purification.

Protein Purification

The culture was harvested by centrifugation at 5,000 rpm for 10 min at 4℃, resuspended in binding buffer (50 mM NaH_2PO_4, 300 mM NaCl, 10 mM imidazole, and pH 8.0), and lysed by sonication. Cell lysate was then centrifuged at 20,000 rpm for 30 min at 4℃. The supernatant or cell-free mixture was subjected to immobilized metal affinity chromatography (IMAC) and applied to the pre-equilibrated Ni-NTA resin (Qiagen). The resin was then washed with 5× wash buffer (50 mM NaH_2PO_4, 300 mM NaCl, 20 mM imidazole, and pH 8.0) before being eluted using an elution buffer (50 mM NaH_2PO_4, 300 mM NaCl, 250 mM imidazole, and pH 8.0) and dialyzed into respective buffers at 4℃ overnight. The dialysis buffers used are detailed in **Supplementary Table 3**. Fractions were collected at each step, and aliquots were taken for Sodium dodecyl sulfate–polyacrylamide gel electrophoresis (SDS-PAGE). Cell debris was further resolubilized in denaturing buffer (8 M urea, 50 mM NaH_2PO_4, 300 mM NaCl, 10 mM imidazole, and pH 8.0), and an aliquot was taken for SDS-PAGE.

The SUMO tag was removed using SUMO protease, and the MysB tag was removed using TEV protease. The reaction mixtures were passed through the His-Trap column at least twice to remove the residual His-SUMO or His-Msyb.

Size Exclusion Chromatography

Proteins were further purified and analyzed using an automated Äkta pure system in respective dialysis buffers. Different HiLoad columns were selected based on the molecular weight and the multimeric states of the proteins. Superdex 75 pg column was designed for proteins with smaller molecular weight (3–70 kDa), and Superdex 200 pg column was designed for protein polymers and proteins with large molecular weight (10–600 kDa).

Sodium Dodecyl Sulfate–Polyacrylamide Gel Electrophoresis (SDS-PAGE)

The 12 μL protein samples were mixed with 3 μL 5× loading buffer and heated at 95°C for 5 min. The 10 μL mixtures were loaded in each lane of 20% polyacrylamide gels in the Mini Trans-Blot Cell system (BIO-RAD) running at 210 V for 1 h. Gels were stained with Coomassie brilliant blue for no less than 10 min followed by destaining in water overnight.

Western Blot

Purified Y00G protein was loaded and separated by SDS-PAGE, and the gel was then transferred to the PVDF membrane. After blocking non-specific binding sites with 5% (w/v) BSA in buffer [10 mM Tris-HCl (pH 7.6), 100 mM NaCl, and 0.1% (v/v) Tween-20] for 2 h at room temperature (25°C), the primary antibody [His-tag antibody (2365S, CST)] was added overnight to the shaker at 4°C. Then, PVDF membranes were incubated with secondary antibodies (bs-40295G-HRP, Bioss, Beijing) for 1 h at room temperature. Western blot images were captured with the Amersham Imager 680 (GE).

NMR Data Acquisition and Analysis

Size exclusion chromatography purified proteins were concentrated to at least 0.1 mM for 1D analysis and 0.5 mM for 2D and 3D NMR analysis. All NMR experiments were collected on a Bruker 600 MHz (Avance III) equipped with a cryoprobe. The water resonance was pre-saturated during the relaxation delay, and the chemical shift of the signal peak was determined with reference to D_2O (4.72 ppm). The spectra were acquired using Topspin 10, processed using NmrPipe, and analyzed in NmrDraw. The phase and baseline of the spectra were corrected manually.

Resonance Assignments for Cef

The near-complete backbone assignment was achieved by using NmrView5 with an in-house add-on script. Except for the first lysine and two proline residues, all of the 68 other crosspeaks in the 2D ^{1}H–^{15}N HSQC spectrum have been assigned. In total, 98% of all ^{1}H, ^{15}N, $^{13}C'$, $^{13}C\alpha/\beta$, 97% Hα, and 96% Hβ resonances were assigned. For sidechain resonances, 95.1% of aliphatic and aromatic sidechains (96.1% for H and 94.3% for C) were assigned, providing the basis for further structure determination.

Cryo-EM Data Acquisition

The sample was diluted at a final concentration of around 0.3 mg/mL. A total of 3 mL of the sample were applied onto glow-discharged 200-mesh R2/1 Quantifoil copper grids. The grids were blotted for 4 s and rapidly cryocooled in liquid ethane using a Vitrobot Mark IV (Thermo Fisher Scientific) at 4°C and 100% humidity. The samples were imaged in a Titan Krios cryo-electron microscope (Thermo Fisher Scientific) operated at 300 kV with a GIF energy filter (Gatan) at a magnification of 105,000× (corresponding to a calibrated sampling of 0.82 Å per pixel). Micrographs were recorded by EPU software (Thermo Fisher Scientific) with a Gatan K3 Summit direct electron detector, where each image was composed of 30 individual frames with an exposure time of 2.5 s and an exposure rate of 22.3 electrons per second per $Å^2$.

RESULTS

Target Protein Selection

The primary selection criterion for our proteins of interest is the absence of published homologous structure due to low sequence homology. On top of this, we filtered out small peptides with fewer than 50 amino acids in sequence, membrane proteins that may require bespoke protocols, and viral structural proteins that appear in the final virion assembly. After applying this filter, we selected 22 proteins from 268 reviewed T4 proteins listed in UniProt for our initial analysis (**Table 1** and **Supplementary Table 1**). Using BLAST (Altschul et al., 1997) and Jpred (Cuff et al., 1998) for homology comparisons, we confirmed that the 22 proteins have no known structure homologs in PDB. In fact, all the amino acid sequences of these proteins are only conserved among bacteriophages, as seen from the multiple sequence alignments (**Figure 1** and **Supplementary Figure 1**).

We then categorized the 22 proteins into three groups based on our current understanding (groups illustrated in **Table 1**). Y00H, Y00G, Y02D, Y00E, Y01A, Y00F, and Y04L fall into the first group, as none of its members have the function assigned. However, the genetic neighbors of these gene products may offer glimpses of their potential functions. For example, gene *y04L*, located in the pin-nrdC intergenic region, may have a role in blocking host Lon protease or phage ribonucleotide reducing reaction (Zhang et al., 2019). Y00E is another example of one whose neighboring genes are in the motB-dexA intergenic region. As the *dexA* gene (Gruber et al., 1988) codes for an exodeoxyribonuclease and the *motB* gene (Uzan et al., 1985) codes for a transcription regulatory protein, Y00E is likely to have a role in nucleic acids regulation.

The second category includes 11 proteins—Cef, Pin, MRH, DexA, ComCα, MotB, SegA, SegE, SegF, Gp57B, and MobE. These proteins are shown to participate in certain biological processes, and yet the exact binding partners or precise steps of the biological reaction involved remain inconclusive. For example, MRH was considered to play a role in regulating host heat-shock sigma factor RpoH and prevent phage progeny production in the ΔrpoH *E. coli* strain under high temperatures (Frazier and Mosig, 1990). ComCα was shown in regulating the expression of some T4 genes involved in DNA synthesis, such as the helicase Gp41, and was proposed to be a Rho-dependent transcriptional anti-termination factor. Cef (Stitt and Mosig, 1989) is responsible for the maturation of some of the phage tRNAs (Pulitzer et al., 1985), yet the exact function remains unclear.

The four remaining proteins fall in the last category. RpbA, alc, Valyl, and Gp64 are better understood among our selection, and their functions are assigned to specific events during phage invasion. Both RpbA and alc are involved in regulating host transcription—RpbA was shown to bind tightly to the *E.coli* RNA polymerase core (Herendeen et al., 1990), and protein alc is a site-specific transcription terminator that only inhibits transcriptional elongation on cytosine-containing DNA but not on the 5-hydroxymethyl cytosine present in the phage DNA (Kashlev et al., 1993). Valyl was shown to bind to host valyl-tRNA ligase and modifies its biochemical property (Müller and Marchin, 1977), and Gp64 is a DNA binding protein that binds to the termini of phage DNA, protecting it against host recBCD mediated degradation (Wang et al., 2000).

TABLE 1 | Summary of the 22 proteins selected for the initial studies presented in this study, including their respective lengths and known functions.

Groups	Proteins	Length	Function
1	Y00H	81 aa	In dexA-dda intergenic region, function unknown
	Y00G	80 aa	Function unknown
	Y02D	125 aa	In imm-Gp43 intergenic region, function unknown
	Y00E	119 aa	In motB-dexA intergenic region, function unknown
	Y01A	103 aa	In dda-modA intergenic region, function unknown
	Y00F	166 aa	In motB-dexA intergenic region, function unknown
	Y04L	102 aa	In pin-nrdC intergenic region, function unknown (Zhang et al., 2019)
2	Cef	71 aa	Plays a role in the processing of a cluster of viral tRNAs (Pulitzer et al., 1985)
	Pin	161 aa	Plays a role in the inhibition of bacterial toxin-antitoxin system (Skorupski et al., 1988)
	MRH	161 aa	Plays a role in transcriptional regulation of late T4 genes (Mosig et al., 1998)
	DexA	227 aa	May play a role in the final step of host DNA degradation; Huang et al., 1999
	ComCα	141 aa	May act as a transcriptional antitermination factor (Stitt and Mosig, 1989)
	Motb	162 aa	Plays a role in the transcriptional regulation of middle promoters (Uzan et al., 1985)
	SegA	221 aa	Probably involved in the movement of the endonuclease-encoding DNA (Sharma and Hinton, 1994)
	segE	205 aa	Probably involved in the movement of the endonuclease-encoding DNA (Kadyrov et al., 1997)
	SegF	224 aa	Homing endonuclease (Belle et al., 2002)
	Gp57B	152 aa	Chaperones for tail fiber assembly include gp57A, gp57B, and Gp38 (Mosig and Eiserling, 2006)
	MobE	141 aa	Probable mobile endonuclease E (Wilson and Edgell, 2009)
3	RpbA	129 aa	Binds to host RNA polymerase core (Herendeen et al., 1990)
	alc	167 aa	Participates in the host transcription shutoff by causing premature termination of transcription from host DNA (Drivdahl and Kutter, 1990)
	Valyl	115 aa	Binds to the host valyl—tRNA ligase and thereby changes several of its physicochemical properties (Müller and Marchin, 1975)
	Gp64	274 aa	Binds to the viral DNA ends and protects the viral DNA against recBCD mediated degradation (Wang et al., 2000)

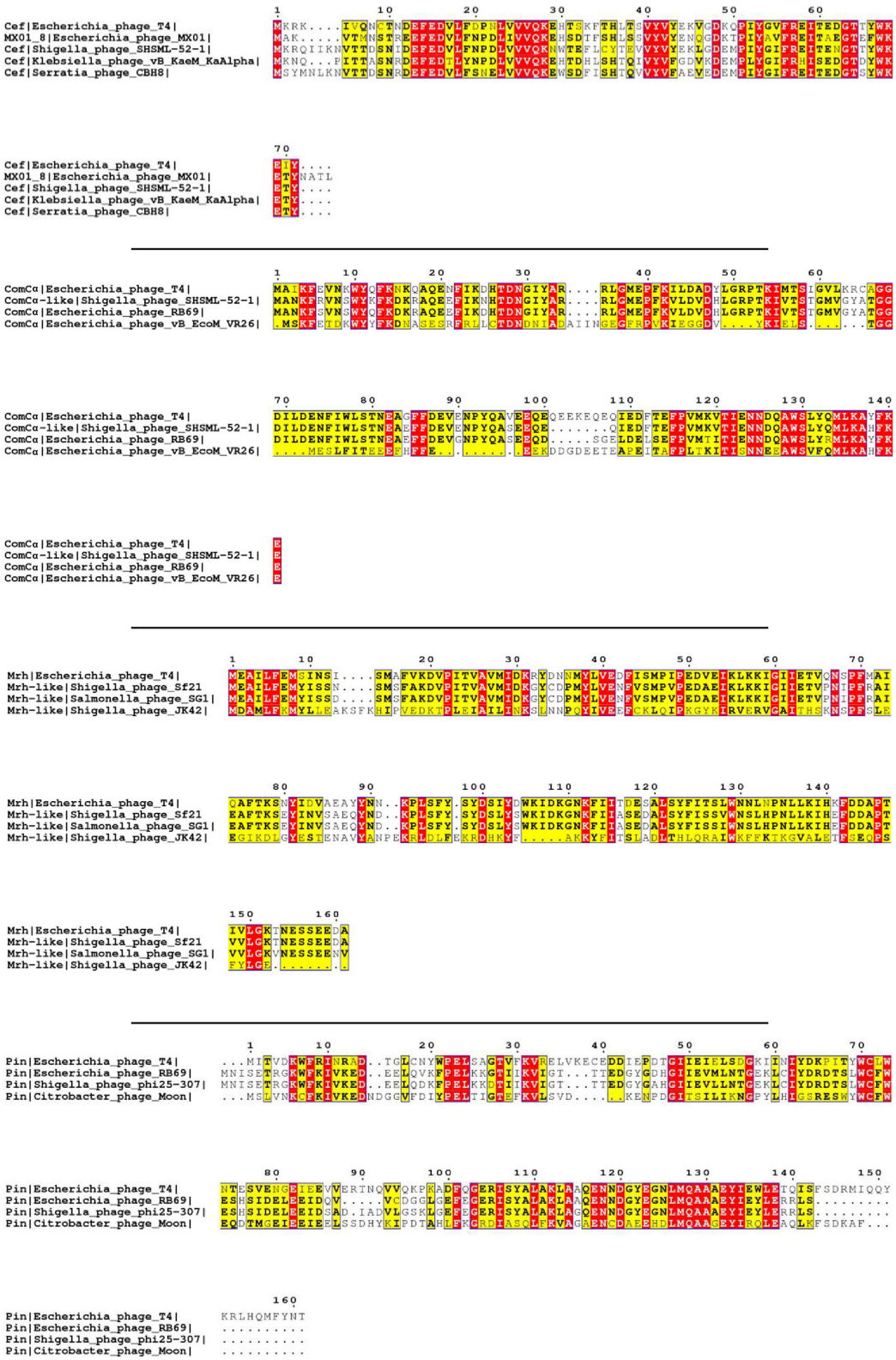

FIGURE 1 | Multiple sequence alignment of selected T4 proteins. The multiple sequence alignments of Cef, ComCα, Mrh, and Pin of T4 showing the conserved regions of each viral protein with that of other phages. The purification and characterization of these proteins could provide a solid basis for future studies on these homologs of other phages. The red and yellow color is the visualization of "*," which represents the fully conserved amino acid amongst all the sequences, and ":," which represents amino acids with high similarities amongst the sequences (>0.5 in the Gonnet Pam 250 Matrix) used in the ClusterW alignment format.

His-Tagged Protein Expression and Purification

We subjected the 22 selected candidates to recombinant protein expression using the standard N-terminal His-tag. Expression trials were set up in different *E.coli* strains under various induction temperatures, times, and ITPG concentrations. To generalize the protocol, we chose the *E. coli* (pLyss) strain that was induced with 1mM IPTG and overnight induction at 18°C as the general protocol. In summary, MRH, Pin, MRH, Y00H, Y00G, and DexA had good yield in the soluble fraction (**Figure 2A**)

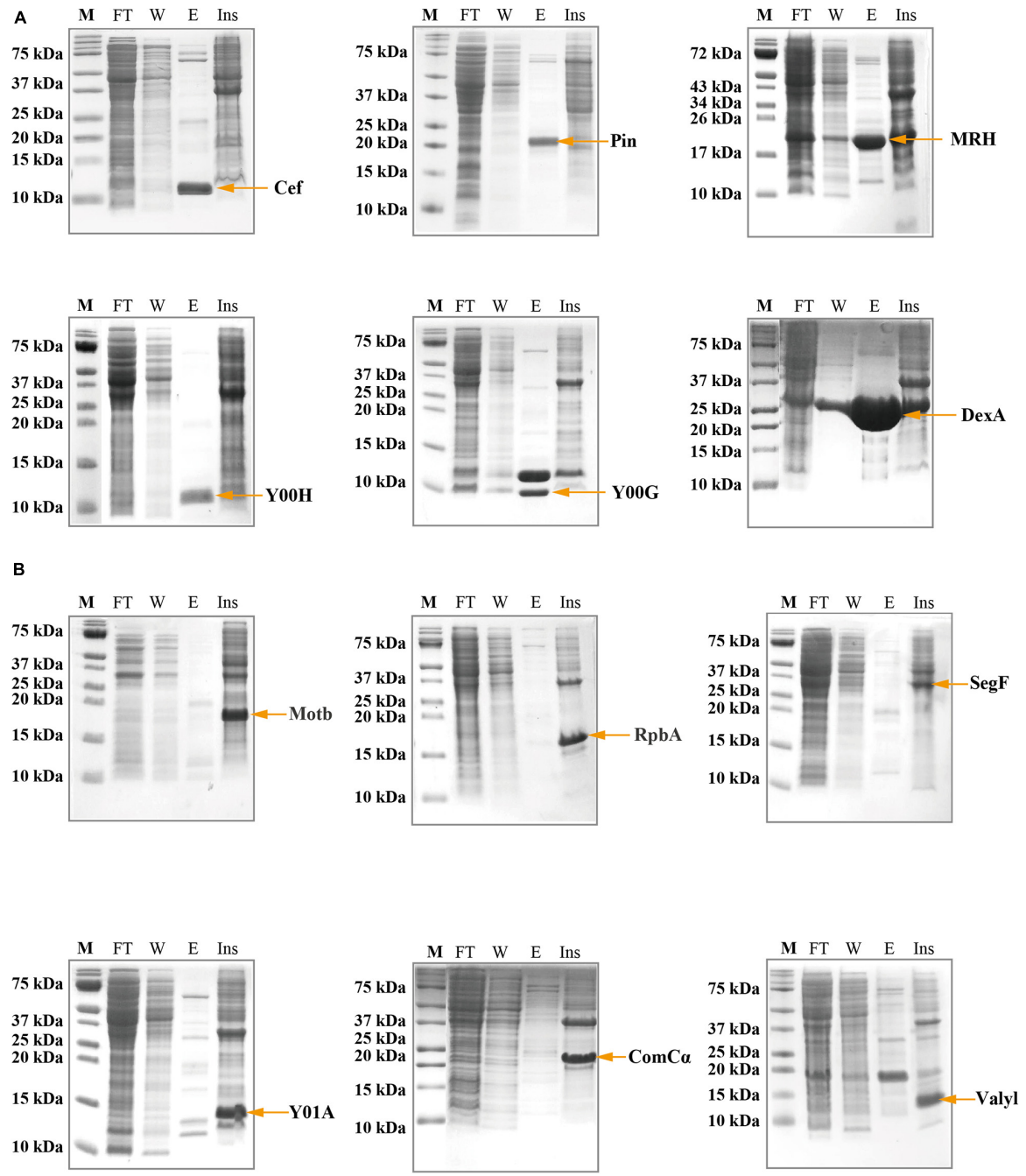

FIGURE 2 | Sodium dodecyl sulfate–polyacrylamide gel electrophoresis (SDS-PAGE) showing the expression and the purification of the viral proteins using N-terminal His-tag. **(A)** Cef, Pin, MRH, Y00H, Y00G, and DexA proteins were collected in the soluble fraction, evident by the presence of bands of correct molecular weight in the elusion fraction. **(B)** MotB, RpbA, SegF, Y01A, ComCα, and ValyI proteins were expressed into the inclusion body, evident by the absence of bands of correct molecular weight in the elusion fraction and the presence of the bands in the insoluble fraction. M, Marker; FT, Flow-through fraction; W, Wash fraction; E, elusion fraction; Ins, Resolublized cell debris containing insoluble protein.

while ComCα, RpbA, SegF, MotB, Valyl, SegE, MobE, alc, and Gp64 appeared in insoluble fraction (**Figure 2B**). Interestingly, two bands (approximately at 12 and 9 kDa) appeared in the gel of Y00G. Western blot using the anti-6X His tag antibody suggested that the 12 kDa band belonged to Y00G and the other might be an *E. coli* protein coeluted with the phage protein (**Supplementary Figure 2**). In contrast, Y02D, Y00E, Y04L, Gp57B, SegA, and Y00F had no success in recombination expression under the conditions we tested (data not shown). Thus, six proteins that could be expressed as soluble proteins were subjected to further purification and structural analysis. Furthermore, nine proteins that could be expressed as insoluble proteins were then tested for expression with protective tags and/or denature-refold preparation strategies (data not shown).

Solubility Tag Expression: Sumo and Msyb

The SUMO tag fusion system can help recombinant proteins be expressed efficiently in *E. coli*, and SUMO can later be cleaved using SUMO-specific protease (Ulp1) to ensure the native activity of the target protein. The Msyb tag is a small acidic protein naturally found in *E.coli*, and it is another tag used to improve the solubility of the target protein (Yang et al., 2020). We constructed a plasmid (pET-Msyb) by replacing the gene encoding SUMO protein with the Msyb gene and a TEV cleavage site. As the SUMO tag can be removed without any extra residue left while TEV protease would leave an extra G, we chose the SUMO tag and presented our results. Strikingly, the yield of Gp57B and Y04L

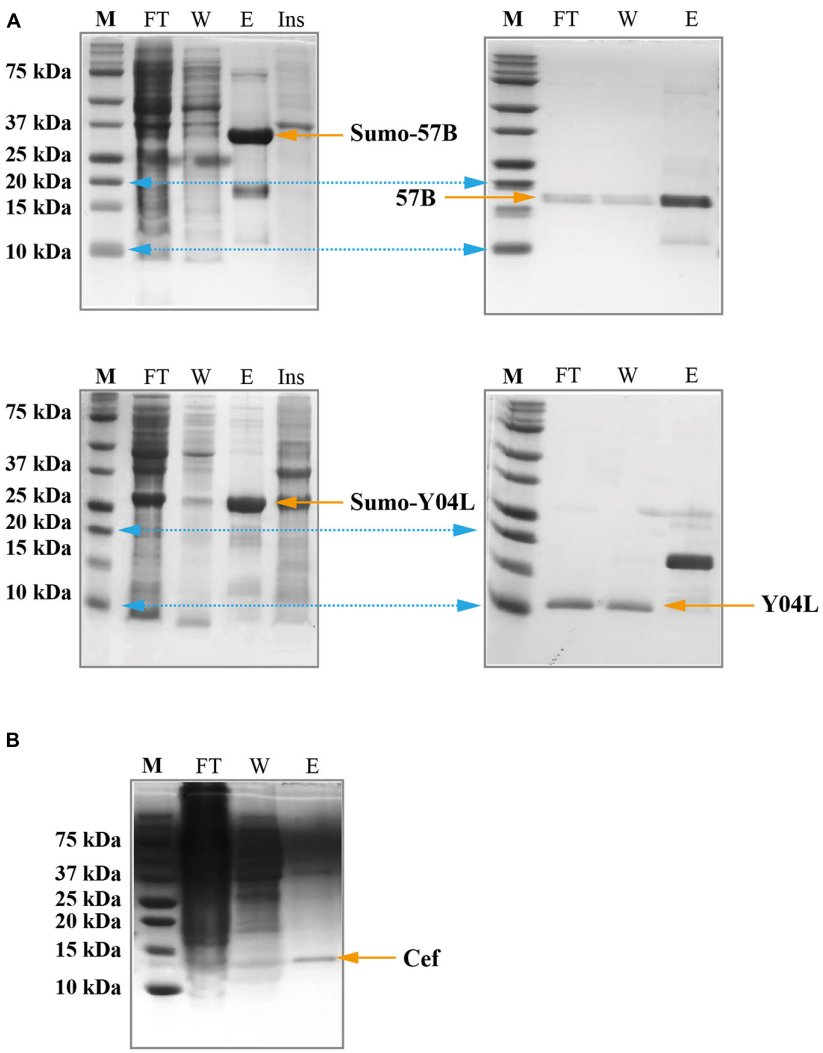

FIGURE 3 | SDS-PAGE showing the expression and the purification of viral proteins using solubilization tags and the cell-free expression system. **(A)** SUMO-Gp57B and SUMO-Y04L were expressed and collected in the soluble fraction, evident by the presence of bands of correct molecular weight in the elusion fraction (left). The native proteins were collected after SUMO cleavage, evident by the bands in the flow-through and wash fraction (right). M, Marker; FT, Flow-through fraction; W, Wash fraction; E, Elusion fraction; Ins, Resolublized cell debris containing insoluble protein. **(B)** Cef protein was expressed and collected in the soluble fraction, using the cell-free expression system, evident by the presence of a sharp band at the corresponding size in the elution fraction. M, Marker; FT, Flow-through fraction; W, Wash fraction; E, Elusion fraction.

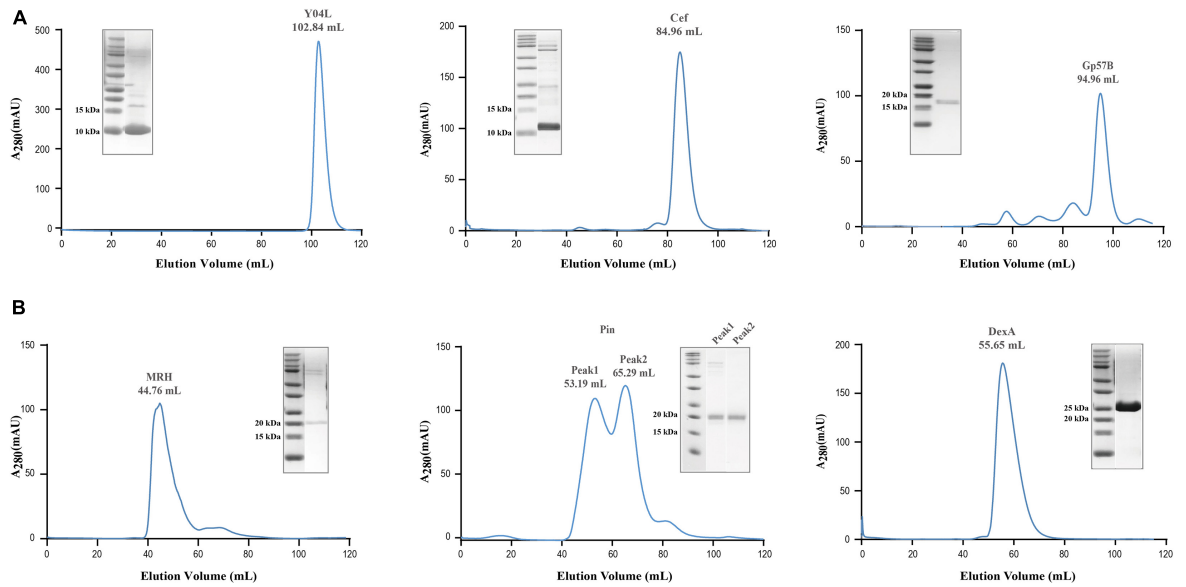

FIGURE 4 | Size exclusion chromatography of soluble viral proteins for assessment of multimeric state in solution. **(A)** Size exclusion chromatography of Pin, Y04L, Cef, and Gp57B demonstrated the viral proteins existed as a homogenous monomeric state in solution, shown by the absorption peak at the volume of the expected molecular weight. **(B)** Size exclusion chromatography of MRH and DexA demonstrated a homogenous multimeric state in solution, as the proteins eluted at a lower volume, indicating a larger molecular weight. The chromatographies of Y04L and Gp57B were performed using HiLoad 16/600 Superdex 200 pg while the experiments of Cef, MRH, Pin, and DexA were using HiLoad 16/600 Superdex 75 pg.

had improved considerably using the SUMO tag, and the fusion tag was removed using Ulp1 (**Figure 3A**).

Cell-Free Expression

As *E. coli* is the native host of the T4 phage, recombination T4 proteins that are not expressed or appear in the inclusion body may have toxic effects and are thus guided away from the host's soluble protein production (Ramón et al., 2014). To address this issue, we subjected the insoluble or unexpressed proteins (with or without fusion tags) to a yeast-based (*Kluyveromyces lactis*) cell-free expression system (Kangma-Healthcode, Shanghai). After codon optimization, the plasmid carrying the gene was added to the reaction mixture and harvested in 3 h under room temperature. Strikingly, Cef had reached a 5 mg yield in the 10 ml cell-free system (**Figure 3B**) and produced an almost identical spectrum as its counterparts produced in *E. coli* in ^{1}H NMR analysis (**Supplementary Figure 3**).

Size Exclusion Chromatography

The recombinantly expressed soluble proteins Pin, MRH, Y04L, DexA, Gp57B, and Cef underwent size exclusion chromatography to further purify and multimeric states analysis. While Pin, Y04L, Cef, and Gp57B appeared at expected elution volumes in the chromatograms (**Figure 4A**), DexA and MRH appeared at positions for protein with larger molecular weights (MW) (**Figure 4B**). Interestingly, the 25 kDa DexA likely exists as a dimer and the 19 kDa Mrh appears to be assembled into a large megadalton complex (**Figure 4B**). The results provide us with important information for further structural analysis and functional predictions of these proteins.

Nuclear Magnetic Resonance Spectroscopy (NMR) Analysis

Using ^{1}H NMR, we conducted an initial structural analysis of Cef, Y04L, Gp57B, MRH, and DexA. The spectra of Cef, Y04L, and Gp57B have good dispersion of peaks with upfield peaks around 0 ppm for aliphatic protons and downfield peaks around 10 ppm for amide protons, suggesting these protein are well-folded (**Figure 5A**). Meanwhile, MRH and DexA are in line with the characteristics of larger protein complexes in solution, with the former having characteristic dispersion of peaks for large protein and the latter has limited peaks in the 0 ppm region for folded protein. We then proceed to 2D ^{1}H-^{15}N HSQC experiments and structural determination for Cef, Y04L, and Gp57B. The HSQC spectra of all three proteins are as expected for the well-folded proteins of their respective MWs (**Figure 5B**). While we have demonstrated our work on Y04L (Zhang et al., 2019), the backbone assignments and structural calculations of Cef and Gp57B are currently in progress.

Backbone Assignment of Cef

Using a standard multidimensional NMR technique, we started structural determination of Y04L and Cef. Except for the first two residues, four proline residues, all 96 other crosspeaks in the 2D ^{1}H-^{15}N HSQC spectrum have been assigned for Y04L (Zhang et al., 2019). For Cef, 68 residues, except for the first Methonine and two proline restudies, were assigned to the 2D ^{1}H-^{15}N HSQC spectrum (**Figure 5C**).

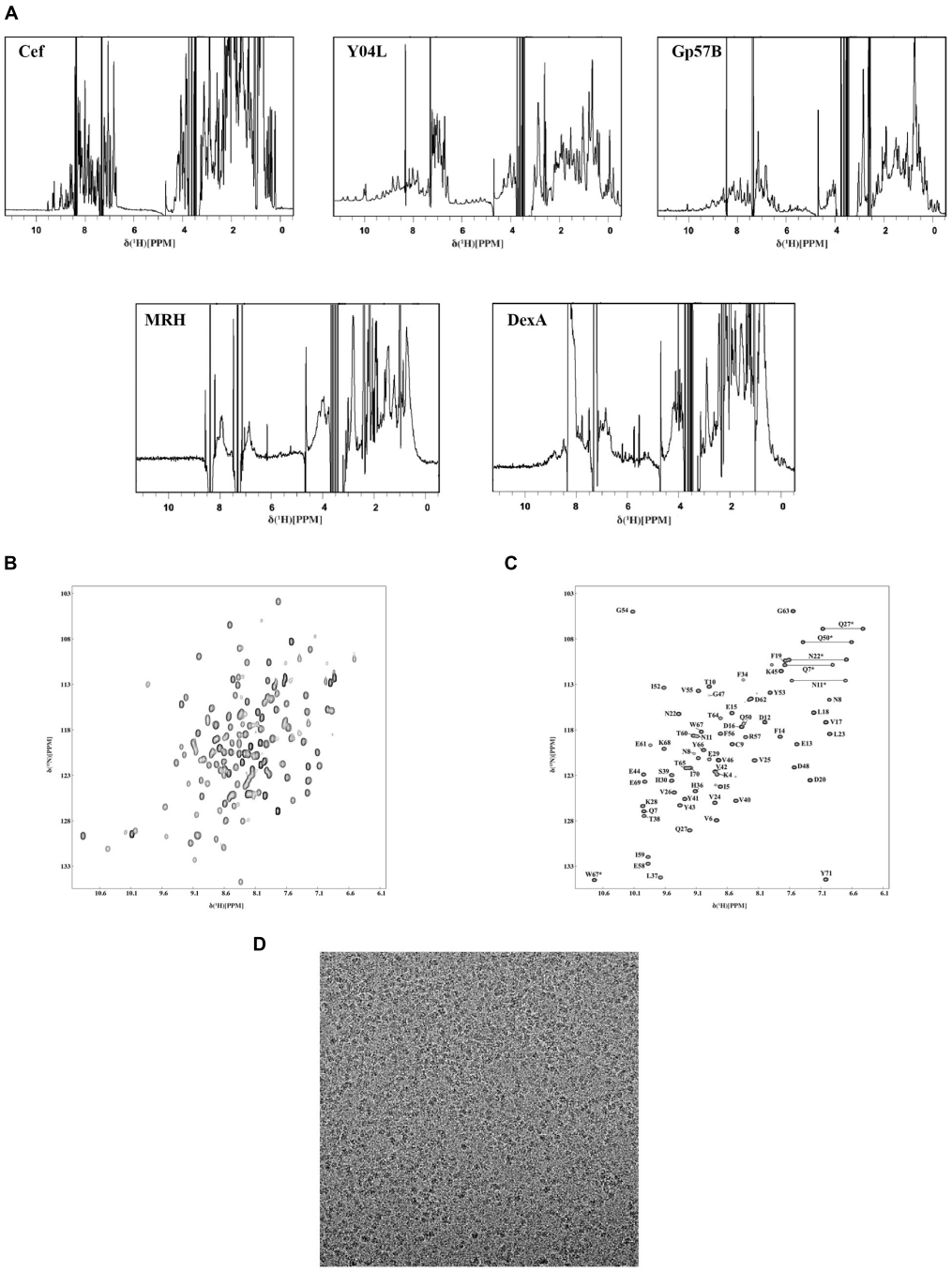

FIGURE 5 | Characterization of the soluble phage proteins using NMR and Cryo-EM. **(A)** 1D ^{1}H-NMR spectra of Cef, Y04L, and Gp57B showed characteristics of folded structural features, such as the presence of the sharp peaks below 1.0 ppm as well as the dispersion of peaks between 6.0 and 11.0 ppm. The ^{1}H-NMR spectra of MRH and DexA showed the characteristics of a large multimeric protein, such as broad peak caused by the higher molecular weight, which was in agreement with the size exclusion chromatograms of MRH and DexA. **(B)** The 2D ^{1}H-^{15}N HSQC spectra of Y04L showed crosspeaks that were dispersed, indicating a folded structure in solution. **(C)** The assigned 2D ^{1}H-^{15}N HSQC spectra of Cef showed crosspeaks that were dispersed, indicating a folded structure in solution. The crosspeaks were assigned with the corresponding amino acid number and type. **(D)** The representative motion-corrected cryo-EM micrograph of DexA.

Cryo-EM Single-Particle Analysis

To further understand the DexA and MRH complex, we performed cryogenic electron microscopy (cryo-EM) single-particle analysis of this complex obtained from size-exclusion chromatography. The samples produced optimal grids at a concentration of ∼0.5 mg/ml. We then solved the structure of MRH at 3.3 Å, which revealed a novel mechanism that the phage protein used to respond to heat shock (data not shown). While

we continued the refinement of the structure of MRH, the images of DexA also show promising results, and the putative dimer is subjected to further structure analysis (**Figure 5D**).

DISCUSSION

Phages are very simple organisms. Of these, T4 is the most studied and has continuously provided discoveries for modern biology. Despite the numerous efforts since its discovery, 45% of T4 phage genes remain poorly characterized. Many of these genes could be functionally assigned using sequence homology comparison with the development of molecular and structural biology. For example, *segA* is predicted to code for an endonuclease that is probably involved in the movement of the endonuclease-encoding DNA, based on domain conservation. In contrast, the gene product of *mrh* was shown to play a role in transcriptional regulation of T4 late genes, yet its function remains elusive. Phage proteins like Mrh with no reported structure homologs are generally very poorly described even within this less characterized protein category. Our systemic work attempts to functionally assign some of these proteins through structural studies, thus complementing the current effects to annotate these genes in phage biology.

Using the conventional recombinant expression in *E. coli*, we found that a protein was coeluted with Y00G. Mass spectroscopy analysis suggested this protein belongs to *E. coli*, revealing the potential host binding partner of Y00G. In order to express soluble proteins for subsequent structural studies, the feasibility of using soluble tags and a cell-free expression system was explored in addition to routine His-tagged protein expression. SUMO and Msyb tags are relatively small tags that might facilitate a high yield of these small phage proteins without bringing a burden to the protein production system of *E. coli*. Indeed, proteins like Y04L benefitted greatly from the fusion tag with a high yield at 100 mg/L. Meanwhile, some phage proteins were still found in the inclusion body, and this is likely because these phage proteins are naturally interferers for *E. coli*. Thus, the cell-free system, yeast-based in particular, is ideal for expressing T4 proteins like RbpA, which interacts with *E. coli* RNA polymerase. We have demonstrated that Cef produced in the cell-free system had structural features identical to the one expressed in *E. coli*.

After the recombination proteins were crude purified using standard His-tag purification, size exclusion chromatography was applied for another purification and assessment of the potential multimeric states. Characterization tools, such as NMR or Cryo-EM, were utilized for the initial structural characterization of the proteins. Furthermore, proteins like Gp57B, Cef, and Y04L were subjected to structural determination by NMR, and the initial structures of Cef and Y04L (unpublished) suggested that these proteins adopt novel folds and are likely to have unique functions. Meanwhile, proteins like DexA and Mrh are in the structure determination using cryo-EM. These structures in the pipeline could provide molecular explanations for the observation in other biological experiments. Currently, structural prediction software relies heavily on the available structure templates, and the gene annotation of other phages is mainly relying on the understanding of proteins from model phages like T4 or λ. These structures, which do not have significant sequence homologs to published structures, would enrich the current pool of the protein structure database and provide templates for annotating other phage proteins.

DATA AVAILABILITY STATEMENT

The original contributions presented in the study are included in the article/**Supplementary Material**, further inquiries can be directed to the corresponding author/s.

AUTHOR CONTRIBUTIONS

KZ, XL, ZW, BM, HC, and NL performed the experiments. YW and BL designed the experiments. HY and BL analyzed the data. KZ, ZW, and BL wrote the manuscript. All authors contributed to the article and approved the submitted version.

FUNDING

This project was supported by the National Natural Science Foundation of China (81871662), National Scientific and Technological Major Special Project for Significant Creation of New Drugs (2020ZX09201020), and EPSRC (EP/T005378/1).

SUPPLEMENTARY MATERIAL

The Supplementary Material for this article can be found online at: https://www.frontiersin.org/articles/10.3389/fmicb.2021.674415/full#supplementary-material

REFERENCES

Amarillas, L., Chaidez, C., González-Robles, A., and León-Félix, J. (2016). Complete genome sequence of new bacteriophage phiE142, which causes simultaneously lysis of multidrug-resistant *Escherichia coli* O157: H7 and *Salmonella enterica*. *Stand. Genomic Sci.* 11:89.

Altschul, S. F., Madden, T. L., Schäffer, A. A., Zhang, J., Zhang, Z., Miller, W., et al. (1997). Gapped BLAST and PSI-BLAST: a new generation of protein database search programs. *Nucleic Acids Res.* 25, 3389–3402. doi: 10.1093/nar/25.17.3389

Belle, A., Landthaler, M., and Shub, D. A. (2002). Intronless homing: site-specific endonuclease SegF of bacteriophage T4 mediates localized marker exclusion analogous to homing endonucleases of group I introns. *Genes Dev.* 16, 351–362. doi: 10.1101/gad.960302

Clokie, M. R., Millard, A. D., Letarov, A. V., and Heaphy, S. (2011). Phages in nature. *Bacteriophage* 1, 31–45.

Comeau, A. M., Bertrand, C., Letarov, A., Tétart, F., and Krisch, H. (2007). Modular architecture of the T4 phage superfamily: a conserved core genome and a plastic periphery. *Virology* 362, 384–396. doi: 10.1016/j.virol.2006.12.031

Cuff, J. A., Clamp, M. E., Siddiqui, A. S., Finlay, M., and Barton, G. J. (1998). JPred: a consensus secondary structure prediction server. *Bioinformatics* 14, 892–893. doi: 10.1093/bioinformatics/14.10.892

Drivdahl, R. H., and Kutter, E. M. (1990). Inhibition of transcription of cytosine-containing DNA in vitro by the alc gene product of bacteriophage T4. *J. Bacteriol.* 172, 2716–2727. doi: 10.1128/jb.172.5.2716-2727.1990

Frazier, M. W., and Mosig, G. (1990). The bacteriophage T4 gene mrh whose product inhibits late T4 gene expression in an *Escherichia coli* rpoH (σ32) mutant. *Gene* 88, 7–14. doi: 10.1016/0378-1119(90)90053-t

Gamkrelidze, M., and Dabrowska, K. (2014). T4 bacteriophage as a phage display platform. *Arch. Microbiol.* 196, 473–479. doi: 10.1007/s00203-014-0989-8

Gruber, H., Kern, G., Gauss, P., and Gold, L. (1988). Effect of DNA sequence and structure on nuclease activity of the DexA protein of bacteriophage T4. *J. Bacteriol.* 170, 5830–5836. doi: 10.1128/jb.170.12.5830-5836.1988

Herendeen, D. R., Williams, K. P., Kassavetis, G. A., and Geiduschek, E. P. (1990). An RNA polymerase-binding protein that is required for communication between an enhancer and a promoter. *Science* 248, 573–578. doi: 10.1126/science.2185541

Huang, Y.-J., Parker, M. M., and Belfort, M. (1999). Role of exonucleolytic degradation in group I intron homing in phage T4. *Genetics* 153, 1501–1512.

Kadyrov, F. A., Shlyapnikov, M. G., and Kryukov, V. M. (1997). A phage T4 site-specific endonuclease, SegE, is responsible for a non-reciprocal genetic exchange between T-even-related phages. *FEBS Lett.* 415, 75–80. doi: 10.1016/s0014-5793(97)01098-3

Kashlev, M., Nudler, E., Goldfarb, A., White, T., and Kutter, E. (1993). Bacteriophage T4 Alc protein: a transcription termination factor sensing local modification of DNA. *Cell* 75, 147–154. doi: 10.1016/s0092-8674(05)80091-1

Keen, E. C. (2015). A century of phage research: bacteriophages and the shaping of modern biology. *Bioessays* 37, 6–9. doi: 10.1002/bies.201400152

Kutter, E., Gachechiladze, K., Poglazov, A., Marusich, E., Shneider, M., Aronsson, P., et al. (1995). Evolution of T4-related phages. *Virus Genes* 11, 285–297. doi: 10.1007/bf01728666

Lin, D. M., Koskella, B., and Lin, H. C. (2017). Phage therapy: an alternative to antibiotics in the age of multi-drug resistance. *World J. Gastrointest. Pharmacol. Ther.* 8:162. doi: 10.4292/wjgpt.v8.i3.162

Loc-Carrillo, C., and Abedon, S. T. (2011). Pros and cons of phage therapy. *Bacteriophage* 1, 111–114. doi: 10.4161/bact.1.2.14590

Marblestone, J. G., Edavettal, S. C., Lim, Y., Lim, P., Zuo, X., and Butt, T. R. (2006). Comparison of SUMO fusion technology with traditional gene fusion systems: enhanced expression and solubility with SUMO. *Protein Sci.* 15, 182–189. doi: 10.1110/ps.051812706

Miller, E. S., Kutter, E., Mosig, G., Arisaka, F., Kunisawa, T., and Ruger, W. (2003). Bacteriophage T4 genome. *Microbiol. Mol. Biol. Rev.* 67, 86–156.

Mosig, G., and Eiserling, F. (2006). "T4 and related phages: structure and development," in *The Bacteriophages*, 2nd Edn, ed. R. Calendar (Oxford: Oxford University Press), 225–267.

Mosig, G., Colowick, N. E., and Pietz, B. C. (1998). Several new bacteriophage T4 genes, mapped by sequencing deletion endpoints between genes 56 (dCTPase) and dda (a DNA-dependent ATPase-helicase) modulate transcription. *Gene* 223, 143–155. doi: 10.1016/s0378-1119(98)00238-8

Müller, U., and Marchin, G. (1977). Purification and properties of a T4 bacteriophage factor that modifies valyl-tRNA synthetase of *Escherichia coli*. *J. Biol. Chem.* 252, 6640–6645. doi: 10.1016/s0021-9258(17)39895-2

Müller, U., and Marchin, G. L. (1975). Temporal appearance of bacteriophage T4-modified valyl tRNA synthetase in *Escherichia coli*. *J. Virol.* 15, 238–243. doi: 10.1128/jvi.15.2.238-243.1975

Pulitzer, J. F., Colombo, M., and Ciaramella, M. (1985). New control elements of bacteriophage T4 pre-replicative transcription. *J. Mol. Biol.* 182, 249–263. doi: 10.1016/0022-2836(85)90343-2

Ramón, A., Señorale, M., and Marín, M. J. F. I. M. (2014). Inclusion bodies: not that bad.… *Front. Microbiol.* 5:56. doi: 10.3389/fmicb.2014.00056

Sharma, M., and Hinton, D. M. (1994). Purification and characterization of the SegA protein of bacteriophage T4, an endonuclease related to proteins encoded by group I introns. *J. Bacteriol.* 176, 6439–6448. doi: 10.1128/jb.176.21.6439-6448.1994

Sharma, U. K., and Chatterji, D. (2008). Differential mechanisms of binding of anti-sigma factors *Escherichia coli* Rsd and bacteriophage T4 AsiA to E. coli RNA polymerase lead to diverse physiological consequences. *J. Bacteriol.* 190, 3434–3443. doi: 10.1128/jb.01792-07

Skorupski, K., Tomaschewski, J., Rüger, W., and Simon, L. (1988). A bacteriophage T4 gene which functions to inhibit *Escherichia coli* Lon protease. *J. Bacteriol.* 170, 3016–3024. doi: 10.1128/jb.170.7.3016-3024.1988

Stitt, B. L., and Mosig, G. (1989). Impaired expression of certain prereplicative bacteriophage T4 genes explains impaired T4 DNA synthesis in *Escherichia coli* rho (nusD) mutants. *J. Bacteriol.* 171, 3872–3880. doi: 10.1128/jb.171.7.3872-3880.1989

Taj, M. K., Samreen, Z., Taj, I., Hassani, T. M., Ling, J., and Yunlin, W. (2014). T4 bacteriophage as a model organism. *IMPACT Int. J. Res. Appl. Nat. Soc. Sci.* 2, 19–24.

Uzan, M., d'Aubenton-Carafa, Y., Favre, R., de Franciscis, V., and Brody, E. (1985). The T4 mot protein functions as part of a pre-replicative DNA-protein complex. *J. Biol. Chem.* 260, 633–639. doi: 10.1016/s0021-9258(18)89779-4

Wang, G., Vianelli, A., and Goldberg, E. (2000). Bacteriophage T4 self-assembly: in vitro reconstitution of recombinant gp2 into infectious phage. *J. Bacteriol.* 182, 672–679. doi: 10.1128/jb.182.3.672-679.2000

Wilson, G. W., and Edgell, D. R. (2009). Phage T4 mobE promotes trans homing of the defunct homing endonuclease I-TevIII. *Nucleic Acids Res.* 37, 7110–7123. doi: 10.1093/nar/gkp769

Yang, Y., Ke, Z., Wang, Z., Li, Y., Li, Y., Wang, Y., et al. (2020). 1H, 13C and 15 N NMR assignments of solubility tag protein Msyb of *Escherichia coli*. *Biomol. NMR Assign.* 14, 251–254. doi: 10.1007/s12104-020-09955-6

Yap, M. L., and Rossmann, M. G. (2014). Structure and function of bacteriophage T4. *Future Microbiol.* 9, 1319–1327. doi: 10.2217/fmb.14.91

Zhang, K., Wang, Z., Chang, G., Wang, H., Wang, Y., and Liu, B. (2019). Resonance assignments of bacteriophage T4 Y04L protein. *Biomol. NMR Assign.* 14, 51–54. doi: 10.1007/s12104-019-09919-5

Conflict of Interest: The authors declare that the research was conducted in the absence of any commercial or financial relationships that could be construed as a potential conflict of interest.

Copyright © 2021 Zhang, Li, Wang, Li, Ma, Chen, Li, Yang, Wang and Liu. This is an open-access article distributed under the terms of the Creative Commons Attribution License (CC BY). The use, distribution or reproduction in other forums is permitted, provided the original author(s) and the copyright owner(s) are credited and that the original publication in this journal is cited, in accordance with accepted academic practice. No use, distribution or reproduction is permitted which does not comply with these terms.

frontiers in Microbiology

ORIGINAL RESEARCH
published: 20 April 2021
doi: 10.3389/fmicb.2021.660351

A Novel Jumbo Phage PhiMa05 Inhibits Harmful *Microcystis* sp.

*Ampapan Naknaen[1], Oramas Suttinun[1,2], Komwit Surachat[3,4], Eakalak Khan[5] and Rattanaruji Pomwised[6]**

[1] *Environmental Assessment and Technology for Hazardous Waste Management Research Center, Faculty of Environmental Management, Prince of Songkla University, Hat Yai, Thailand,* [2] *Center of Excellence on Hazardous Substance Management (HSM), Bangkok, Thailand,* [3] *Division of Computational Science, Faculty of Science, Prince of Songkla University, Hat Yai, Thailand,* [4] *Molecular Evolution and Computational Biology Research Unit, Prince of Songkla University, Hat Yai, Thailand,* [5] *Department of Civil and Environmental Engineering and Construction, University of Nevada, Las Vegas, United States,* [6] *Division of Biological Science, Faculty of Science, Prince of Songkla University, Hat Yai, Thailand*

Microcystis poses a concern because of its potential contribution to eutrophication and production of microcystins (MCs). Phage treatment has been proposed as a novel biocontrol method for *Microcystis*. Here, we isolated a lytic cyanophage named PhiMa05 with high efficiency against MCs-producing *Microcystis* strains. Its burst size was large, with approximately 127 phage particles/infected cell, a short latent period (1 day), and high stability to broad salinity, pH and temperature ranges. The PhiMa05 structure was composed of an icosahedral capsid (100 nm) and tail (120 nm), suggesting that the PhiMa05 belongs to the *Myoviridae* family. PhiMa05 inhibited both planktonic and aggregated forms of *Microcystis* in a concentration-dependent manner. The lysis of *Microcystis* resulted in a significant reduction of total MCs compared to the uninfected cells. A genome analysis revealed that PhiMa05 is a double-stranded DNA virus with a 273,876 bp genome, considered a jumbo phage. Out of 254 predicted open reading frames (ORFs), only 54 ORFs were assigned as putative functional proteins. These putative proteins are associated with DNA metabolisms, structural proteins, host lysis and auxiliary metabolic genes (AMGs), while no lysogenic, toxin and antibiotic resistance genes were observed in the genome. The AMGs harbored in the phage genome are known to be involved in energy metabolism [photosynthesis and tricarboxylic acid cycle (TCA)] and nucleotide biosynthesis genes. Their functions suggested boosting and redirecting host metabolism during viral infection. Comparative genome analysis with other phages in the database indicated that PhiMa05 is unique. Our study highlights the characteristics and genome analysis of a novel jumbo phage, PhiMa05. PhiMa05 is a potential phage for controlling *Microcystis* bloom and minimizing MC occurrence.

Keywords: *Microcystis*, jumbo phage, cyanophage, aggregation, genome analysis, auxiliary metabolic genes, efficiency of phage killing (EOK)

OPEN ACCESS

Edited by:
Shuai Le,
Army Medical University, China

Reviewed by:
Alon Philosof,
California Institute of Technology, United States
Ahmed Askora,
Zagazig University, Egypt

****Correspondence:***
Rattanaruji Pomwised
rattanaruji.p@psu.ac.th

Specialty section:
This article was submitted to Virology, a section of the journal Frontiers in Microbiology

Received: *29 January 2021*
Accepted: *29 March 2021*
Published: *20 April 2021*

Citation:
Naknaen A, Suttinun O, Surachat K, Khan E and Pomwised R (2021) A Novel Jumbo Phage PhiMa05 Inhibits Harmful Microcystis sp. Front. Microbiol. 12:660351. doi: 10.3389/fmicb.2021.660351

INTRODUCTION

Blooms of toxic cyanobacteria are an increasing phenomenon in water bodies worldwide. *Microcystis*, the most predominant genus in cyanobloom, has been considered the leading producer of microcystins (MCs) (Harke et al., 2016). MCs have been intensively studied among cyanotoxins due to their toxicity, causing severe liver and kidney damages, tumor promotion, and gastroenteritis

(Falconer et al., 1983; Carmichael, 2001; Li et al., 2017). Accumulation of MCs in aquatic ecosystems increases public health concerns (Pham and Utsumi, 2018; Bi et al., 2019).

Microcystis is a unicellular microorganism and exhibits high phenotypic plasticity (Xiao et al., 2018). It forms large aggregated colonies in natural freshwater, involving extracellular polymeric substances (EPS). EPS not only regulate buoyancy but also provide protective functions against predator grazing and chemical stressors (Chen et al., 2019). Such characteristics promote global distribution and dominance of *Microcystis*.

Several approaches have been developed to prevent and control cyanobloom, such as nutrient management, artificial mixing and chemical control (Huisman et al., 2018). However, these strategies have faced several problems, including the persistence of toxic residues, time requirement and cost. Biological control using bacteriophage against the cyanobacteria is an attractive idea. Cyanobacterial viruses or cyanophages are abundant during peak-cyanobloom and play an important role in mediating host communities in the ecosystem (Yoshida-Takashima et al., 2012). Cyanobloom can be controlled through the lysis-inducing mortality by phages.

Phages exhibit diverse sizes, morphology, and genome. The vast majority of phages have smaller genomes at tens of kb, while phages with larger genomes are either jumbo phages (>200 kb) (Yuan and Gao, 2017) or megaphages (>500 kb) (Devoto et al., 2019). To date, more than 150 available genome databases of jumbo phages have been reported and exhibited various genomic features. Jumbo phages have been isolated from various environments and infected mostly gram-negative bacteria (Imam et al., 2019).

Genome sequences of jumbo phages are highly divergent. Besides structural components and genome replication proteins, jumbo phages harbor numerous hypothetical proteins and auxiliary metabolic genes (AMGs) that are absent in small phage genomes. The presence of AMGs is implicated in the interception and redirection of host metabolism (Thompson A.W. et al., 2011; Yuan and Gao, 2017). Multisubunit RNA polymerase (RNAP) encoded by jumbo phages cause independence of their replication from the host transcription (Lavysh et al., 2016; Yuan and Gao, 2017). Jumbo phages also harbor elongation factors to maintain the overall translation efficiency during infection (Al-Shayeb et al., 2020). In addition, translation termination elements in jumbo phage rescue ribosomes stalled on damaged transcripts and enhance the degradation of aberrant proteins (Al-Shayeb et al., 2020). Furthermore, AMGs in cyanophage genomes appear to contribute to photosynthesis and pentose phosphate pathways that increase dNTP synthesis for phage replication and supply substantial energy and carbon for phage production (Thompson L.R. et al., 2011; Zimmerman et al., 2020).

To date, eight cyanophages specific to the genus *Microcystis* have been reported (Jaskulska and Mankiewicz-Boczek, 2020). Only three cyanophage genomes (MaMV-DC, Ma-LMM01 and Mic1) have been sequenced and characterized, exhibiting genomes with less than 200 kb (Yoshida et al., 2008; Ou et al., 2015; Yang et al., 2020). All of them carry AMGs responsible for maintaining cyanophage genes and releases of their progeny. Genome comparative analyses indicated that they are phylogenetically distant from other bacteriophages and each other. Based on morphology, MaMV-DC and Ma-LMM01 are grouped in the family *Myoviridae*, while Mic1 belongs to *Siphoviridae*.

Microcystins-producing *Microcystis* is harmful to humans and animals. Many strategies have been used to prevent or reduce *Microcystis* blooms (Huisman et al., 2018). These methods have been successful; however, success is not guaranteed. The purpose of this study was to offer an alternative method using cyanophage as a bio-control against cyanotoxins-producing bacteria to facilitate water management. We isolated and evaluated a cyanophage against MCs-producing *Microcystis*. For the first time, infection kinetics and lysis-mediated MCs release on both planktonic and aggregated cells were investigated. Comprehensive biological characterization and genome analysis of cyanophage were performed. We also examined cyanophage properties, including the virion stability, growth kinetic and viral yield host range.

MATERIALS AND METHODS

Cyanophage Isolation and Plaque Formation

Cyanophages infecting *Microcystis* were isolated using a modified liquid bioassay as described by Chénard and Chan (2017). The *Microcystis* SG03 was previously isolated from the Songkhla Lake (Songkhla, Thailand) and used as the host. The host culture at exponential state (approximately 10^6 CFU/ml), was prepared in BG-11 broth (pH 7.5) and incubated under 25 μmol photon m^{-2}/s (cool fluorescent light), 12 light and 12 h dark cycle at 25°C for 5 days (Belcher and Swale, 1982). Hospital wastewater samples were collected from an aeration basin of activated sludge treatment in January 2020 from Songklanagarind Hospital, Songkhla Province, Thailand. Ten milliliters of the wastewater samples were centrifuged and the supernatant was filtered (0.22 μm pore-size, polyethersulfone membrane, Sartorius, United Kingdom). Five milliliters of the filtrates were added to six-well plates containing 1 ml of the host prepared as mentioned above, while sterile water was used as a negative control. Samples were incubated for up to 10 days under the same conditions described above. Clearance of the host culture indicated the activity of lytic phages. The cultures from the clear wells were collected and centrifuged at 8,000 × *g* for 2 min. The supernatants containing phage (phage lysates) were diluted (10^{-4}–10^{-20}) with TM buffer (50 mM Tris–HCl and 10 mM $MgSO_4 \cdot 7H_2O$, pH 7.8). An aliquot of 20 μl of the diluted phage lysates was mixed with 180 μl of the host culture in a 96-well plate and incubated under the same conditions described above. Clearance of the host culture was observed daily, and phage lysates were collected from the wells that were clear. This procedure was conducted for five rounds to obtain homogenous phage stock.

The plaque formation was observed using a conventional double-layer agar method. One-hundred microliter of serially diluted cyanophage lysate with TM buffer was mixed with 1 ml of the 10^6 CFU/ml host culture. Three milliliters of melted top

agar containing 0.5% low melted agarose (Bio-Rad) in BG-11 medium were added to the mixture and then overlaid onto a 1% BG-11 agar six-well plate (Thermo Scientific, United States), and incubated under the previously described conditions for 15 days. Homogenous plaques were observed daily. The host culture without cyanophage served as a negative control.

Cyanophage Purification and Amplification

A conventional cesium chloride (CsCl) step gradient was performed for cyanophage purification (Nasukawa et al., 2017). Twenty milliliters of the exponential host culture were inoculated with 20 ml of cyanophage lysate and incubated under the previously described conditions for 7 days. The mixture was centrifuged and filtered (0.45 μm pore-size, cellulose acetate filters, Sartorius, United Kingdom). The filtrate was precipitated with polyethylene glycol 6,000 (10%, wt/v) and sodium chloride (2M), followed by incubation for 24 h at 4°C. After centrifugation at 10,000 × *g* for 30 min, the pellet was resuspended in 2 ml of TM buffer. The CsCl step gradient was performed by orderly layering CsCl at ρ = 1.0, 0.82, and 0.66 from the tube's bottom. The cyanophage suspension was slowly layered on top of the gradient tube, and the tubes were loaded in a SW40Ti swing-out rotor (Beckman Coulter, Inc.). After centrifugation at 30,000 × *g*, 4°C for 3 h, a single visible band was collected and dialyzed with TM buffer 4°C for 3 h.

The cyanophage was propagated using a liquid medium method. Briefly, the exponential host culture (450 ml, 10^6 CFU/ml) was mixed with 50 ml of the purified cyanophage and subsequently incubated for 7 days under the previously described conditions. The mixture was centrifuged and filtered (0.45-μm pore-size, cellulose acetate filters). The cyanophage titers were determined using the conventional double-layer agar method, as described above. The phage lysate was kept at 4°C for further experiments.

Transmission Electron Microscopy

The cyanophage size and morphology were determined by negatively stained images. Cyanophage lysate was absorbed onto copper grids, stained with 2% uranium acetate, and observed at 80 kV using a JEOL, JEM-2010 transmission electron microscope.

Host Range Test and Efficiency of Phage Killing

The lytic activity of cyanophage was determined against 10 strains of MCs-producing *Microcystis* isolated from the Songkhla Lake. *Microcystis* culture was prepared as described above. One-hundred microliters of cyanophage (10^8 PFU/ml) were added to 96-well plates (Thermo Scientific, United States), containing 100 μl of *Microcystis* cultures (10^8 CFU/ml) (multiple of infectivity: MOI 1). The cultures without cyanophage served as negative controls. Plates were incubated under the conditions described above and observed daily for *Microcystis* cell lysis. The cultures without lysis after 14 days were considered as insusceptible hosts (Ou et al., 2013).

The efficiency of phage killing (EOK) was assessed and classified by modifying the efficiency of plating (EOP) described by Mirzaei and Nilsson (2015). In the EOK, the phage titer was estimated by the Most Probable Number (MPN) (infectious units/ml). Then, the MPN number was used in EOK instead of the plaque forming unit (PFU/ml) in the EOP. The MPN assay was performed using serial dilutions (Suttle and Chan, 1993; Jarvis et al., 2010; Chénard and Chan, 2017). The infectious phage unit was obtained by MPN interpretation. Briefly, cyanophages were serially diluted (10^{-4}–10^{-20}) with BG-11 in 96-well plates to obtain a final volume of 100 μl solution. One hundred microliters of cyanobacterial cultures (10^6 CFU/ml) were added into each well and incubated for 7 days under the conditions described above. The numbers and the dilution levels of clear wells were recorded and interpreted through an MPN calculation program (Jarvis et al., 2010), resulting in infectious phage unit. Three independent experiments were conducted. The average infectious phage unit (A) was determined and used for the EOK. The EOK was calculated as:

$$\text{Efficiency of phage killing (EOK)} = \frac{At}{Ah} \quad (1)$$

where *At* and *Ah* are the average infectious/killing units on target bacteria and a total number of infectious phage units on the bacterial host, respectively. The EOK values were classified as highly productive (≥0.5), medium productive (0.1 ≤ EOK < 0.5), low productive (0.001 < EOK < 0.1) or inefficient (≤0.001) (Mirzaei and Nilsson, 2015).

Clonal Relatedness of *Microcystis* and Measurement of MCs-Production

Clonal relatedness among the 10 *Microcystis* sp. was investigated by the highly iterated palindromic (HIP) PCR method described elsewhere (Wilson et al., 2005). DNA of all isolates was extracted using a NucleoSpin®Soil kit (MACHEREY-NAGEL, Germany). The HIP-targeted primer was HIP-CA (GCGATCGCGCA). PCR amplification was performed with a volume of 20 μl containing 5 μl buffer (dNTP, Mg^{2+}) (bioline, United Kingdom), 3 μl of primer (1 μM), 0.25 μl MyTaq polymerase (1 unit), 1 μl DNA template (20 ng/ml), and 7.75 μl deionized water. The PCR thermal cycling program included initial denaturation at 95°C for 7 min, followed by 30 cycles at 90°C for 1 min, annealing at 52°C for 1 min, and extension at 70°C for 1 min and a final extension at 70°C for 10 min. PCR products were observed by electrophoresis on 1% agarose gel in 0.5 TBE buffer [89 mM Tris (pH 7.6), 89 mM boric acid, 2 mM EDTA] at 60 volts for 3 h. The 1 kb DNA ladder (Solis BioDyne) was run in parallel. Bionumerics version 7.6 was used to construct a dendrogram.

Intracellular MCs (IMCs) and/or extracellular MCs (EMCs) from *Microcystis* cultures were measured. Briefly, eighty milliliters of *Microcystis* (10^6 CFU/ml) were cultured as previously described for 5 days. After centrifugation at 10,000 × *g* for 15 min, the supernatant and pellets were collected. The IMCs and EMCs were determined using the pellets and supernatant, respectively. To determine IMCs content, the pellets were suspended in 4 ml of methanol-water solution (50%, v/v) (Dai et al., 2009) and sonicated for 10 min followed by incubation

at 50°C for 20 min (Gkelis et al., 2015). The extracted toxins were filtered (0.22 μm pore-size polyethersulfone membrane, Sartorius, United Kingdom). The filtered IMCs and the supernatant containing EMCs were measured using a MCs-ADDA ELISA kit (Product No. 520011, Abraxis, United States) following the manufacturer's instructions. The measurements were duplicated.

One-Step Growth Curve

A one-step growth experiment was conducted to evaluate the latent period, burst time and burst size of cyanophage (Ou et al., 2013). Ten milliliters of the cyanophage (10^5 PFU/ml) were added to 90 mL of the log-phase host culture (10^6 cell/ml), and the mixture was incubated for 7 days at the conditions described above. The cyanophage titers were determined daily using the conventional double-layer agar method as described above. Three independent experiments were conducted. The latent period was taken as the time interval between viral inoculation and the beginning of the cyanophage production. The burst size was calculated as the number of liberated phage particles minus the unadsorbed cyanophage particles divided by the number of initial bacteria (Kropinski, 2018).

Phage Stability Under Environmental Stress

Salinity, pH and temperature stability tests were performed. To test phage viability under salinity stress, phage suspensions in TM buffer (pH 7.5) containing various sodium chloride concentrations (0.5, 5, 10, 20, 30, and 40 ppt) were investigated. The different pH values in TM buffer adjusted by 5M HCL and 5M NaOH were obtained to achieve pH 5, 7, 9, and 11. The phage in TM buffer (pH 7.5) was used as a control for salinity and pH stability tests. The phage viability in TM buffer (pH 7.5) was tested at 4, 25, 35, and 45°C. One microliter of the cyanophage (10^5 PFU/ml) was added to each solution (900 μl) and then incubated at 25°C for 12 and 24 h. Titers of survival cyanophage from each test were estimated using the MPN assay as described above. The experiments were triplicated.

Planktonic Cell Killing Assay

Microcystis killing by cyanophage was conducted in 96-well plates. One-hundred microliters of the *Microcystis* SG03 culture (10^6 CFU/ml) were added to different cyanophage concentrations to have the multiplicity of infection (MOI) of 0.001, 0.01, 0.1, 1, 10, and 100. The plates were incubated for 7 days under the previously described conditions. Bacterial density was measured daily using optical densitometry (LUMIstar® Omega, Germany) at 580 nm (Myers et al., 2013). The cyanophage titer was estimated on day 7 by the MPN assay as described above. The highest phage titer provided by specific MOIs indicates the optimal ratio between phage particles and host cells (the optimal MOI) (Gašić et al., 2011).

Microcystins concentrations during cyanophage infection were determined. Different cyanophage concentrations were mixed with 20 ml of the host culture (10^6 CFU/ml) to achieve MOI of 0.01, 1, and 100. After 3- and 5-day incubation periods, the mixtures were centrifuged at 10,000 × *g* for 5 min. The IMCs accumulated in *Microcystis* and lysis-mediated MCs release (LM-MCs) were measured using the cell pellet and supernatant, respectively, as described above. MCs were determined using an ELISA kit as described above. The experiments were conducted in triplicate.

Aggregated Cell Killing Assay

The ability of cyanophage killing aggregated *Microcystis* cells was evaluated through cell density, cell-bound exopolymers, and MCs. Aggregated cell formation was prepared in 6-well plates (Thermo Scientific, United States), by mixing 5 ml of *Microcystis* culture (5.8×10^8 CFU/ml) with $CaCl_2$ (a final concentration of 60 mM) and followed by incubation under the conditions described above for 2 days (Dervaux et al., 2015; Drugă et al., 2019). After the aggregation was observed, the medium and planktonic cells were carefully removed, leaving aggregated cells at the bottom of the wells. Cyanophage solutions in BG-11 medium were added into each well to achieve the MOI of 0.1, 1, 10, and 100. The cultures were incubated for 7 days, as described above. Planktonic cell culture and aggregated cells without cyanophage served as controls. The bacterial densities were measured daily using optical densitometry (LUMIstar® Omega, Germany) at 580 nm.

To estimate the amount of cell-bound exopolymers, 200 μl of samples from each well were collected, centrifuged (at 10,000 × *g* for 1 min) and resuspended in 200 μl PBS buffer (137 mM NaCl, 2.7 mM KCl, 10 mM Na_2HPO_4, and 1.8 mM KH_2PO_4). Two microliters of Alcian blue solution (1%, w/v) in acetic acid (3%, v/v) (pH 2.5) were added and incubated with shaking at 80 rpm for 20 min at 25°C. The remaining Alcian blue in the solution was measured spectrophotometrically at 606 nm, compared to non-aggregated cells without cyanophage. The reduction of Alcian blue dye indicated its adsorption on bacterial EPS (Vandevivere and Kirchman, 1993).

To determine IMCs and LM-MCs during cyanophage infection of aggregated cells at the MOI of 100, 20 ml of the host culture (10^8 CFU/ml) were mixed with cyanophage (10^{10} PFU/ml) and incubated. After 3 and 7 days of incubation, the cultures were centrifuged at 10,000 × *g* for 15 min. The IMCs accumulated in *Microcystis* and LM-MCs were measured using the cell pellet and supernatant, respectively, as described above. All the experiments were conducted in triplicate.

Scanning Electron Microscopy

The aggregated cells were inoculated with the phage at the MOI of 100. After 5 days of incubation, 20 ml of the cultures were collected, centrifuged, and the pellet was washed with PBS three times and fixed with 1 ml of 2.5% glutaraldehyde in 0.1 M PBS, pH 7.4, followed by an incubation at 25°C for 2 h. The pellets were dehydrated by a series of ice-cold ethanol (30, 50, 70, 80, 90, and 100%, respectively and 10 min for each concentration). The samples were air dried and coated by gold particles, followed by

observation under a scanning electron microscope (Quanta 400, Thermo Fisher Scientific).

Genome Extraction, DNA Sequencing and Analysis

Cyanophage genome was analyzed as described elsewhere (Higuera et al., 2013). A cyanophage lysate was concentrated through Amicon® Ultra-15 (Sigma, Germany). Two-hundred microliters of concentrated cyanophage were then treated with DNase I and RNase A (Thermo Scientific, United States) according to the manufacturer's instructions to remove host DNA and RNA. Then, three-hundred microliters of the cyanophage were mixed with 100 μl lysis buffer (1M Tris, pH 8.0, 0.5M EDTA, 10 % SDS and 10 mg/ml proteinase K) and incubated at 60°C for 1 h. An equal volume (approximately 400 μl) of the phenol:chloroform:isoamyl alcohol solution (24:24:1) was added to separate phage DNA. After centrifugation (10,000 × *g*, 10 min), two separate phases were formed. The upper phase solution containing phage DNA was collected. The DNA was precipitated using 0.3 volume of 3 M NaOA and 1 volume of isopropanol followed by incubation at −20°C for 2 h. The mixture was centrifuged (10,000 × *g*, 10 min), and then the DNA pellet was dissolved in 50 μl of sterile distilled water. The DNA quality was checked using electrophoresis (sharp single DNA band) and a NanoDrop spectrophotometer (A_{260}/A_{280} = 1.8–1.9) (MaestroGen Inc.) and kept at −20°C until use.

The whole-genome sequencing of cyanophage was performed with paired-end 150-bp reads on Illumina NovaSeq 6000 (Novogene Co., Ltd., Singapore). The reads quality was investigated using FASTQC (Brown et al., 2017) and trimmed with Trimmomatic 0.39 (Bolger et al., 2014). Resulting reads were *de novo* assembled into contigs using Spades 3.11.1 (Bankevich et al., 2012). The open reading frames (ORFs) were identified using GeneMarkS (Besemer et al., 2001) and PHASTER (Zhou et al., 2011). The annotation of ORFs was performed using Blastp (E-value cutoff = 10^{-3}) of NCBI server (Chénard et al., 2015).

The phylogenetic analysis of the major capsid protein was compared with other phages in the NCBI database using Mega-X software (version 10.1.6.). The inferred amino acid sequences' alignment was performed with ClustalX using default parameters, followed by manually refining the alignments with Geneious (version 2020.1.2). The maximum likelihood tree was constructed with RAxML rapid bootstrapping (100 replicates) and the Jones-Taylor-Thornton model.

Genome comparison of PhiMa05 was analyzed using EasyFig version 2.2.3 (Sullivan et al., 2011). Multiple genome alignment for analysis of the genomic synteny was performed using the progressiveMauve (Darling et al., 2010) plugin in Geneious software (version 2020.1.2). A full list of phage genomes can be found in a **Supplementary Table 2**.

Statistical Analysis

Data obtained were analyzed by ANOVA with the post hoc Tukey test using the SPSS statistical software version 17.0 for Windows EDU in order to investigate the significance of MCs production among different treatments of killing assay of *Microcystis* planktonic cells and aggregated cells at $P \leq 0.05$.

RESULTS AND DISCUSSION

Cyanophage Isolation and Plaque Forming Ability

The wastewater samples were collected to test the presence of cyanophage against MCs-producing *Microcystis* SG03. This strain, previously confirmed by 16s RNA sequences (accession number MT534586) synthesized the highest IMCs contents (3.19 pg/cell) among our harmful *Microcystis* collection. Since the wastewater environment provides complexity of microbial ecosystem, it has been used to isolate phage for multiple applications, including phages against *Klebsiella pneumoniae* and *Escherichia coli* as potential therapeutic and biocontrol agents (Olsen et al., 2020; Wintachai et al., 2020). Based on the clearance of liquid culture, cyanophage designated PhiMa05 was identified with an ability to lyse SG03 within 3 days after infection. The plaque assay displayed transparent and round plaques with a diameter of approximately 4 mm on the lawns of SG03 culture on day 6 (**Figure 1A**). The plaque size increased daily to approximately 20 mm in diameter on day 13. Our plaque assay method was modified by using 0.5% low melted agarose instead of 0.75% conventional agar to overcome the burden of plaque forming. The less agarose content attributed phage diffusion to the medium, promoting phage propagation (Yuan and Gao, 2017; Wang et al., 2019). Because of the difficulty of plaque forming on 0.75% top agar, PhiMa05 was suspected to be a large sized virion, specifically a jumbo phage. Jumbo phages have been less isolated because they are often eliminated during the size-exclusion process of isolation, and it is hard for them to form plaque under the conventional method (Lewis et al., 2020). The liquid bioassay approach provided a shorter detection period due to the preference of cyanobacterial growth conditions in the water. Thus, this method is a suitable alternative jumbo-cyanophage isolation method comparable to the gold standard, double agar overlay assay.

Phage PhiMa05 Morphology

A transmission electron microscopy (TEM) image of PhiMa05 revealed that virus particle exhibited tail phage with icosahedral head, a characteristic of the order *Caudovirales* (**Figure 1B**). The average length of the cyanophage from the top of the capsid to the end of the tail was 243 nm. The average icosahedral head width and height were 108 and 111 nm, respectively. The phage tail had a height of 127 nm and a width of 19 nm. With these morphological features, the PhiMa05 was characterized in the family of *Myoviriae*. Eight cyanophages specific to *Microcystis* sp. have been reported and belong to families: *Myoviridae* (2), *Podoviridae* (3), *Siphoviridae* (2), and Corticovirus-like particles (1) (Jaskulska and Mankiewicz-Boczek, 2020; Yang et al., 2020). Myoviruses exhibit an icosahedral capsid connected with a contractile tail, while siphoviruses have a long non-contractile tail, and podoviruses have a short non-contractile tail (Barylski et al., 2020). The corticovirus-like particles are tailless with

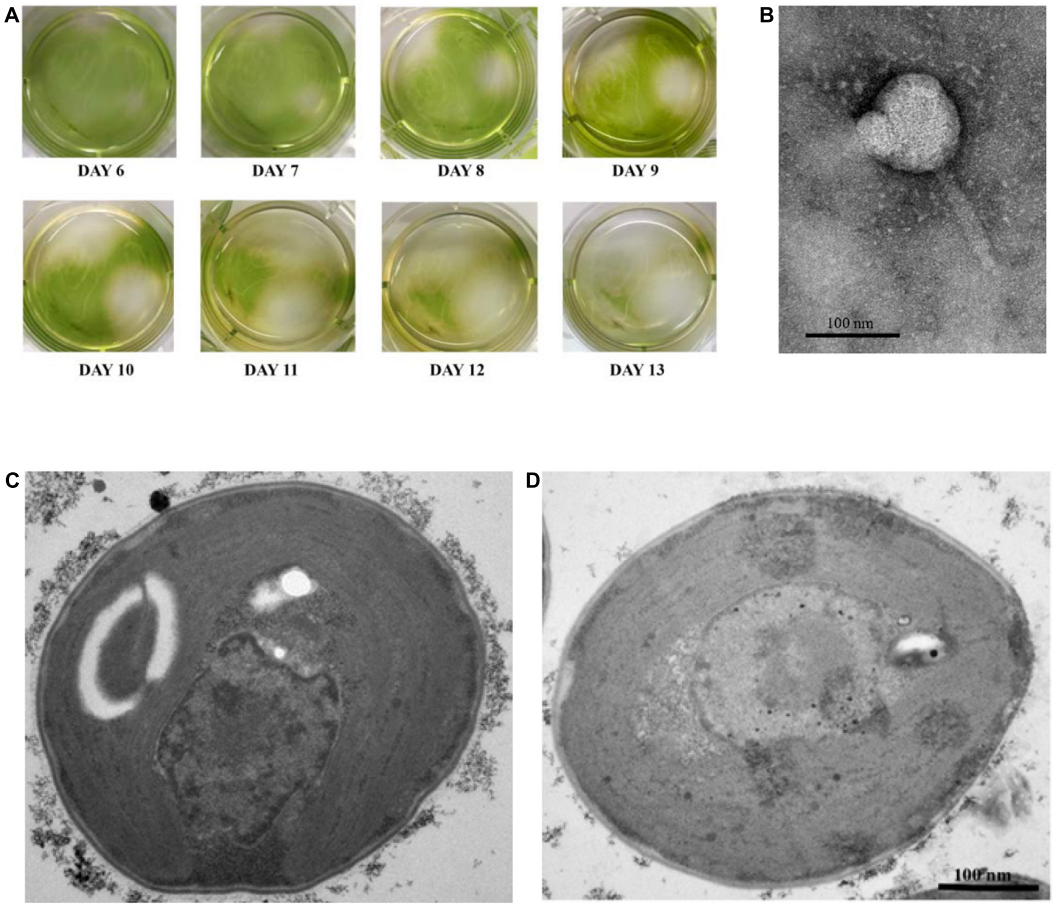

FIGURE 1 | (A) Plaques of cyanophage PhiMa05 on the lawn of SG03. TEM images of: **(B)** Cyanophage PhiMa05; **(C)** thin section of a healthy cell of *Microsystis* SG03; and **(D)** thin section of *Microsystis* SG03 2 days after incubation with PhiMa05.

an icosahedral capsid (Li et al., 2013). Two well-established myoviruses infecting *M. aeruginosa* are Ma-LMM01 and MaMV-DC isolated from a Japanese water reservoir and a Chinese freshwater lake (Yoshida et al., 2006; Ou et al., 2013). The heads of Ma-LMM01 and MaMV-DC had diameters of 86 and 70 nm, respectively, which are smaller than the PhiMa05 head. A healthy *Microcystis* cell is shown in **Figure 1C** in comparison with a thin section of the host cell after 2 days of incubation with PhiMa05 presented in **Figure 1D**, which revealed propagation of intracellular phage-like particles. This microscopic result suggests that PhiMa05 succeeded in entering hosts and propagation.

Host Range and Phage Stability

Host range and EOK were determined in 10 *Microcystis* strains. Both IMCs and EMCs productions after 5 days of inoculation were measured and only IMCs but not EMCs were detected in all strains (**Figure 2**). The clonal relatedness among the 10 isolates was investigated by HIP-PCR (Wilson et al., 2005), which has helped distinguish *Microcystis* genotypes (Jaiswal et al., 2013). The fingerprint patterns demonstrated high genetic variation. Two groups, A (n = 4) and B (n = 6), can be established (**Figure 2**). Members of group A showed less MCs production except for SH12. Cyanophage PhiMa05 can inhibit all group B members and the SH12. The result implies sharing receptors among these strains.

The EOK results agreed with the host range analysis. EOKs ranging from 0.62 to 1.00 were present after inoculating all group B members and SH12 with PhiMa05. This result indicates that the PhiMa05 infected toxic strains. Studies of host-specificity on freshwater cyanophage displayed that most of them are strain-specific, resulting from using only one host enrichment in the isolation process. Ma-LMM01 is a toxic strain-specific, whereas MaMV-DC is a non-toxic strain-specific (Yoshida et al., 2006; Ou et al., 2013). Our result indicates that PhiMa05 was also a narrow host range with toxin strain-specific rather than species-specific. The presence of these cyanophages in environments may affect the dynamic of toxic and non-toxic populations in cyanobacterial blooms.

As an alternative biological control agent, phage stability was determined under several stress conditions, including salinity, pH and temperature. PhiMa05 can withstand a wide range of salinity from 0.5 to 20 ppt after 12 and 24 h of incubations (**Supplementary Figure 1A**). The cyanophage viability decreased significantly when the concentrations of sodium chloride were

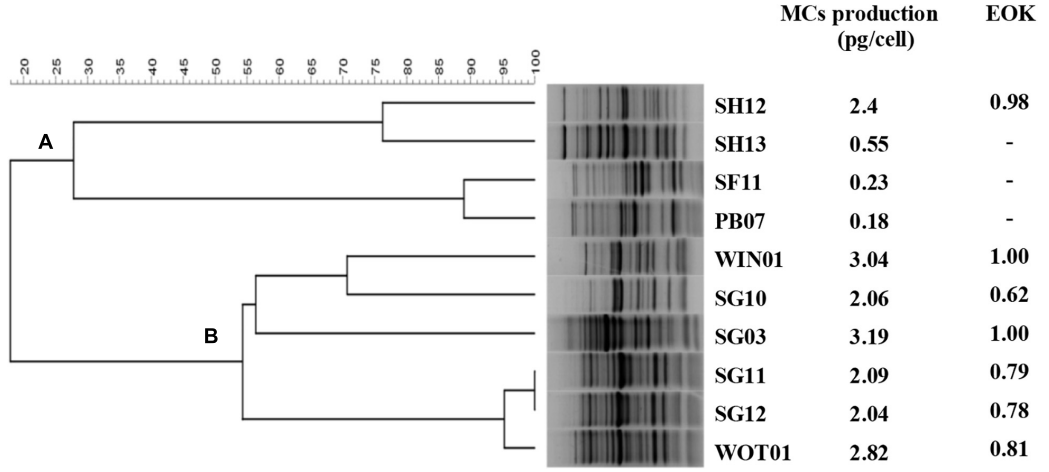

FIGURE 2 | Dendrogram for *Microcystis* strains created by HIP PCR. HIP PCR was performed in 10 *Microcystis* isolates, creating 2 groups: **(A)** and **(B)**.

at 30 and 40 ppt. PhiMa05 can also tolerate a wide range of pH. However, extreme pH conditions, pH 5 and 11, caused a significant decrease in the cyanophage viability (**Supplementary Figure 1B**). Additionally, the cyanophage PhiMa05 showed stability from 4°C to 35°C after 12 h and 24 h incubations. However, after exposure to 45°C for 24 h, there was a 23% reduction in phage viability (**Supplementary Figure 1C**). Our study is the first report of environmental stress on the stability of cyanophage. These tolerance characteristics suggest the strength of PhiMa05 in various environments. They could be an alternative biological method for inhibiting the growth of MCs-producing *Microcystis* and reducing the MCs accumulation in an aquatic environment.

One Step Growth Curve

To understand the growth kinetics of PhiMa05, the one-step growth curve experiment was performed with the cyanophage at the MOI of 0.01 (**Figure 3**). The cyanophage latent period was estimated to be 1 day followed by a log period of approximately 3 days. The burst size of PhiMa05 was around 127 phage particles/infected cell. A total lysis was observed 4 days after inoculation. Up to date, only two studies have reported one step growth curve for cyanophage. Ou et al. (2013) reported *Microcystis* phage MaMV-DC with 2 days of latent period and a burst size of approximately 80 phage particles/infected cell. Another *Microcystis* phage, Ma-LMM01, revealed a faster latent period (12 h) with a burst size of 120 progeny virions without complete host cell lysis (Yoshida et al., 2006).

Infection Dynamics in Planktonic Culture and Lysis-Mediated MCs Release

Lytic activity of PhiMa05 at various MOIs (0.001–100) was demonstrated in **Figure 4**. Cyanophage PhiMa05 inhibited the growth of *Microcystis* SG03 in a concentration-dependent manner. The higher PhiMa05 concentration resulted in a faster decrease in SG03 number. At the MOIs of 1, 10 and 100, PhiMa05 effectively inhibited the SG03 growth. At the MOI of 100, the bacterial host (SG03) density decreased dramatically after 2 days of incubation, and then the bacterial population entirely collapsed within 3 days. The bacterial host reduction at the MOIs of 10 and 1 was observed after 3 and 4 days of incubation, respectively. At lower MOIs (0.001, 0.01, and 0.1), *Microcystis* growth was significantly inhibited after 5 days of inoculation. Phage titers were determined 7 days after inoculation. The highest phage densities (8×10^{18} infectious unit/ml) were obtained from infection at the MOIs of 0.001-1 (**Supplementary Figure 2**). These MOIs were optimal for phage propagation.

Our results suggest that using a higher phage ratio was suitable for phage therapy. The lower MOIs may provide additional time for phage infection resulting in host adaptation and cope phage infection (Watkins et al., 2014). However, Morimoto et al. (2018) revealed that Ma-LMM01 infecting *Microcystis* does not induce the antiviral defense response during the phage amplification.

To monitor the MCs after PhiMa05 infection at the MOIs of 0.01, 1, and 100, IMCs and LM-MCs were investigated after 3 and 5 days of incubation in comparison with the control, uninfected culture (**Figure 5**). The IMCs in the SG03 inoculum was 0.17 μg/L (day 0). In the control culture, MCs production significantly increased to 0.44 μg/L and 0.62 μg/L after 3 days and 5 days of incubation, respectively ($p < 0.05$). Infecting SG03 with PhiMa05 at all MOIs led to a significant MCs reduction (**Figure 5**). Phage PhiMa05 inhibited MCs production in a concentration-dependent manner, agreeing with the bacterial growth inhibition results. At the MOI of 100, PhiMa05 presumably infected all host cells within a short latent period (1 day). Then, SG03 host cells were entirely lysed after 3 days of inoculation, releasing MCs (LM-MCs) in the culture. Therefore, only LM-MCs but not IMCs and the host cells were detected. The LM-MCs of infected cells on days 3 and 5 were equal but were significantly less than IMCs from the control ($p < 0.05$). The incomplete killing was observed when the host was infected with phages at lower MOIs. At the MOIs of 0.01 and 1, the IMCs production significantly decreased after 3 days of infection, whereas the

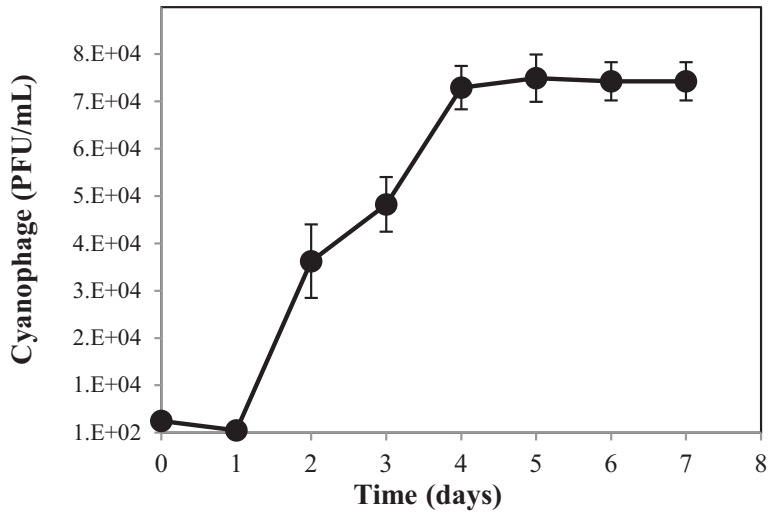

FIGURE 3 | One-step growth curve of cyanophage PhiMa05. Data are the mean of triplicate independent experiments with standard deviation.

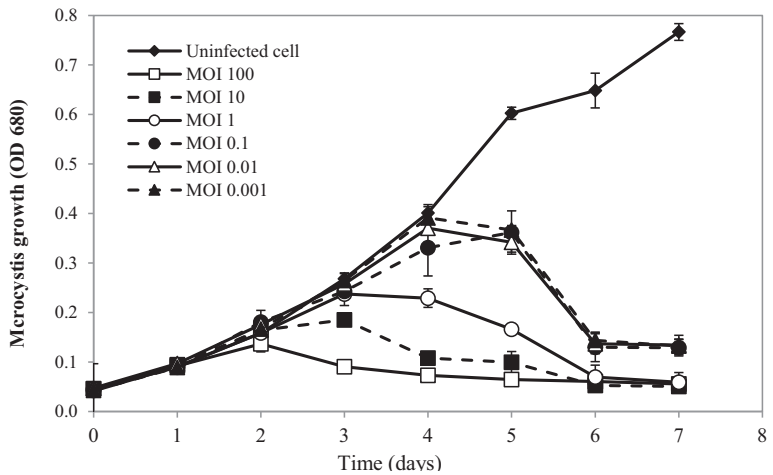

FIGURE 4 | Time killing assay of cyanophage PhiMa05 against *Microcystis* SG03. The bacterial cultures were infected with the cyanophage at MOIs of 0.001, 0.01, 0.1, 1, 10, and 100. Uninfected bacterial culture was used as a control. Independent experiments were conducted in triplicate and optical density at 680 nm was measured, averaged, and plotted. Error bars are standard deviations.

bacterial growth reduction was not observed (**Figure 4**). The total MCs productions were also reduced, implying that phages interfered with MCs production. The LM-MCs in the culture were detected after 3 and 5 days of infection, indicating the death of infected cells. Our results demonstrate that the cyanophage adversely affected the bacterial host population and suggest its functions in creating ecosystems' stability.

PhiMa05 Inhibitions of MCs Production and Aggregated Cells

In the natural ecosystem, divalent cations play a major role in *Microcystis* aggregation during blooming (Xu et al., 2016). The aggregation prolongs *Microcystis* in water bodies and enhances buoyancy (Drugă et al., 2019). At a laboratory scale, an aggregated form of SG03 was initiated by calcium addition (Drugă et al., 2019; Wei et al., 2019; Gu et al., 2020). The aggregated cells were infected by cyanophage PhiMa05 at different MOIs of 0.1, 1, 10, and 100. The density and cell-bound exopolymers of SG03 were determined daily within 7 days of infection. As shown in **Figure 6**, the aggregated SG03 cells were degraded by PhiMa05 in a concentration- and time-dependent manner. Reduction in cell density was seen after 3 days of infection. Within 7 days of infection, the aggregated cells were undetectable, indicating a total population collapse. At the MOI of 100, the bacterial density dramatically declined after 3 days of infection, and SG03 was entirely killed after 4 days of infection (**Figure 6A**).

Several studies have shown the involvement of exopolymer in cyanobacterial aggregated colonies (Boudarel et al., 2018; Liu et al., 2018; Bhatnagar and Bhatnagar, 2019). Here, exopolymer

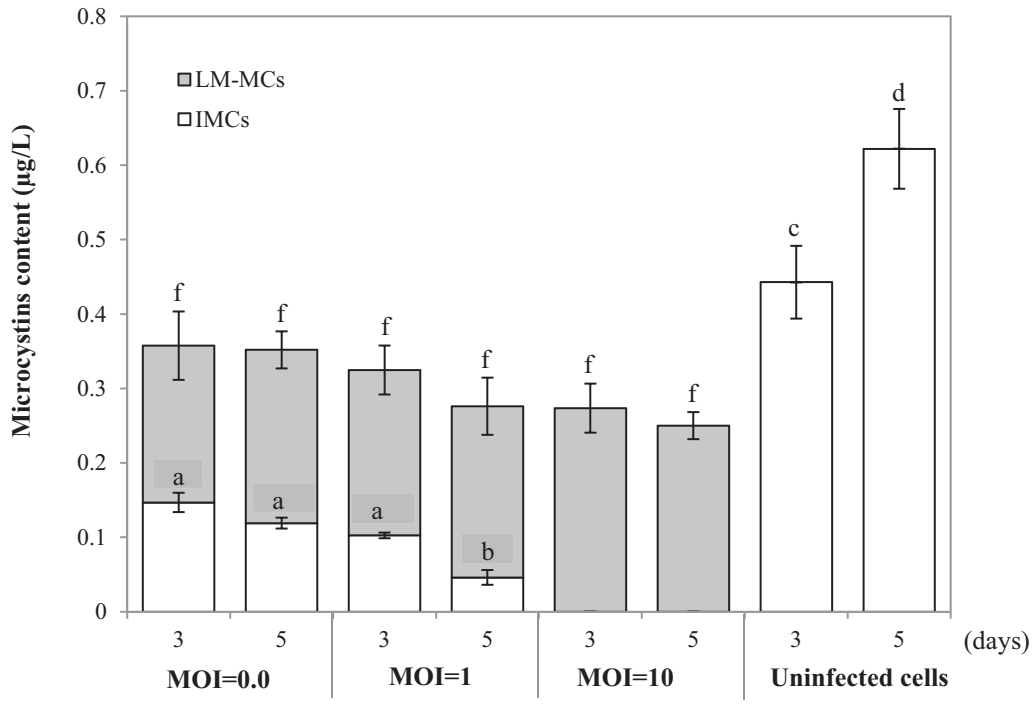

FIGURE 5 | Changes in accumulated microcystins (IMCs) and lysis-mediated microcystins (LM-MCs) on days 3 and 5 of the control and PhiMa05 infected culture of *Microcystis* SG03 at MOIs of 0.01, 1, and 100. Each data point is the mean from three independent experiments. Error bars show standard deviations. Different letters above bars show values that are significantly different ($p < 0.05$). Each value is compared within each category.

contents were determined through cell-bound exopolymers by measuring Alcian blue absorbed by aggregated cells (Vandevivere and Kirchman, 1993). After 2 days of infection at the MOIs of 10 and 100, bacterial clumps disaggregated, releasing dye (Alcian blue) residual to the culture. The disaggregation of bacterial clump was apparent after 3 days of infection with the MOIs of 1 and 0.1 (**Figure 6B**).

The MCs productions were determined in uninfected aggregated cells and bacterial aggregated colonies after cyanophage inoculation at the MOI of 100 (**Figure 7A**). In the beginning, the MCs content in the uninfected SG03 cells was 0.805 µg/L. After 3 and 7 days of incubation, IMCs but not LM-MCs were detected. On the other hand, LM-MCs and fewer IMCs were present with infected aggregated colonies indicating cyanobacterial death. Within 7 days of infection, PhiMa05 killed the entire aggregated colonies releasing LM-MCs without IMCs detection. Scanning electron microscopy (SEM) images revealed disaggregation and cell debris after 3 days of inoculation (**Figures 7B,C**). Our result indicates that after PhiMa05 attachment, aggregated cells were initially disrupted and then killed. The killing ability of phages against aggregated bacterial cells, including biofilm, has been demonstrated in other organisms such as *K. pneumoniae* and *Pseudomonas aeruginosa* (Wu et al., 2019; Oliveira et al., 2020; Wintachai et al., 2020). Our study is the first report of cyanophage activity against aggregated MCs-producing *Microcystis*.

Toxic cyanobacterial blooms are comprised of planktonic and aggregated cells. Our result showed that PhiMa05 is a good candidate for controlling toxic *Microcystis*, since conventional treatment processes are inefficient. The practical application of cyanophage to eliminate harmful cyanobloom was suggested by using high concentration cyanophages in a capsule (Mathieu et al., 2019). The phage will be released and infect surrounding cells. The limitations of this procedure involve environmental factors, including water flow and weather. The opportunity to use this approach in the water supply is more promising. Addition of cyanophages *in situ* could control toxic *Microcystis* without any modification to treatment facilities.

PhiMa05 Genome Features and Analysis

The cyanophage PhiMa05 contains a linear double-stranded DNA genome of 273,876 bp in length with a GC content of 54.2%. Three current *Microcystis* viral genomes databases are available, including Ma-LMM01, MaMV-DC and Mic1 (Yoshida et al., 2008; Ou et al., 2015; Yang et al., 2020). The Mic1 is grouped in *Siphoviridae*, while PhiMa05 shared morphological characteristics with Ma-LMM01 and MaMV-DC, members of *Myoviridae*. All of them contain genome sizes ranging from 92 to 169 kb, while the PhiMa05 genome is larger. PhiMa05 is the first jumbo myovirus infecting MC producing *Microcystis*. The annotation of the PhiMa05 sequence revealed the presence of 254 predicted ORFs. All the ORFs showed an ATG start codon. One hundred thirty-three ORFs were presented on the negative strand, with the remaining ORFs on the positive strand. Yuan and Gao (2017) demonstrated that jumbo phages have diverse origins and carry essential genes for the phage life cycle and extra

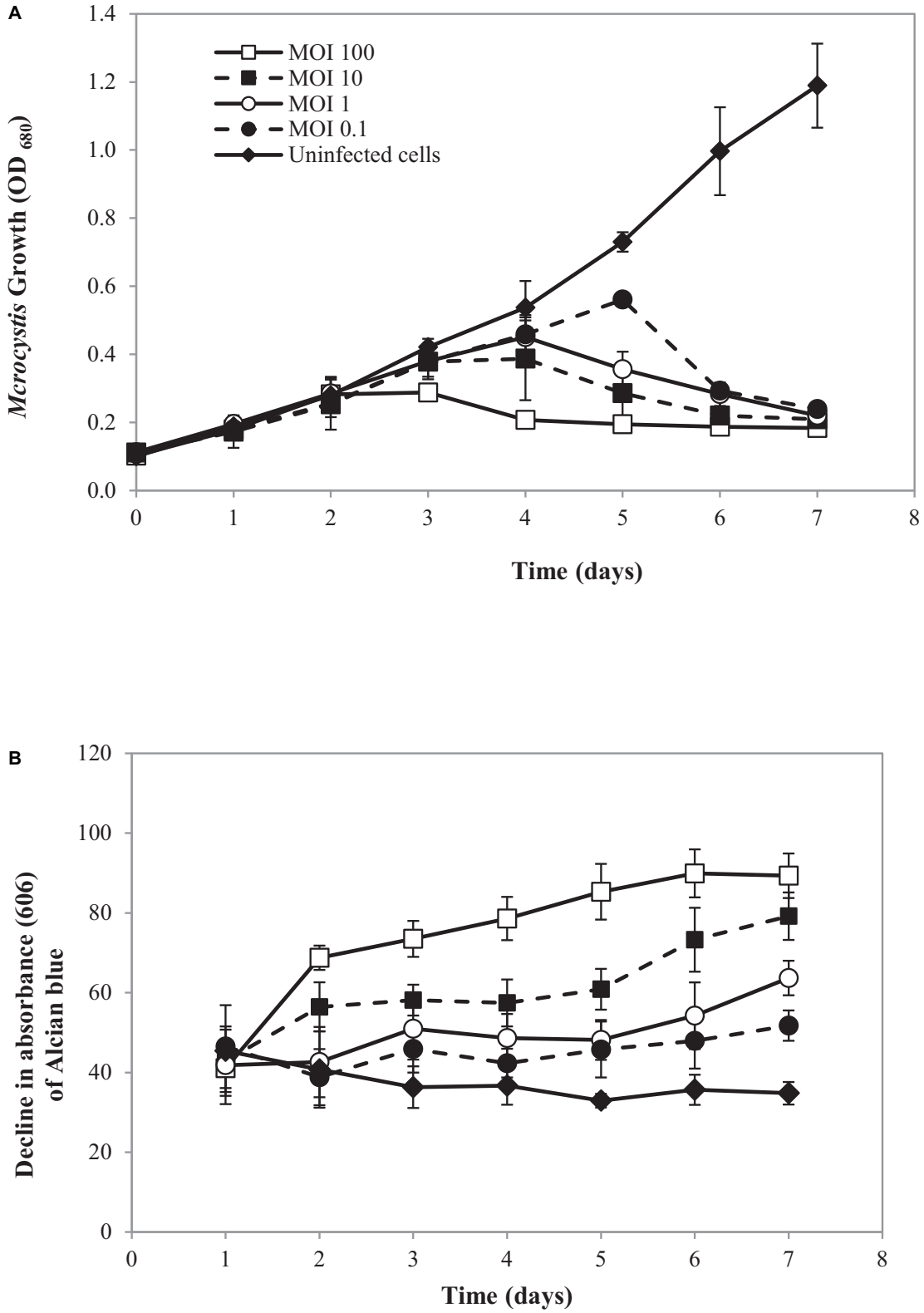

FIGURE 6 | Effect of cyanophage PhiMa05 on aggregated *Microcystis* SG03. The aggregated cells were infected with the cyanophage at MOIs of 0.1, 1, 10, and 100. **(A)** Time-kill assay of cyanophage PhiMa05 against aggregated *Microcystis* SG03. **(B)** Effect of phage on bacterial aggregation. The data show the means ± standard deviations based on triplicated experiments.

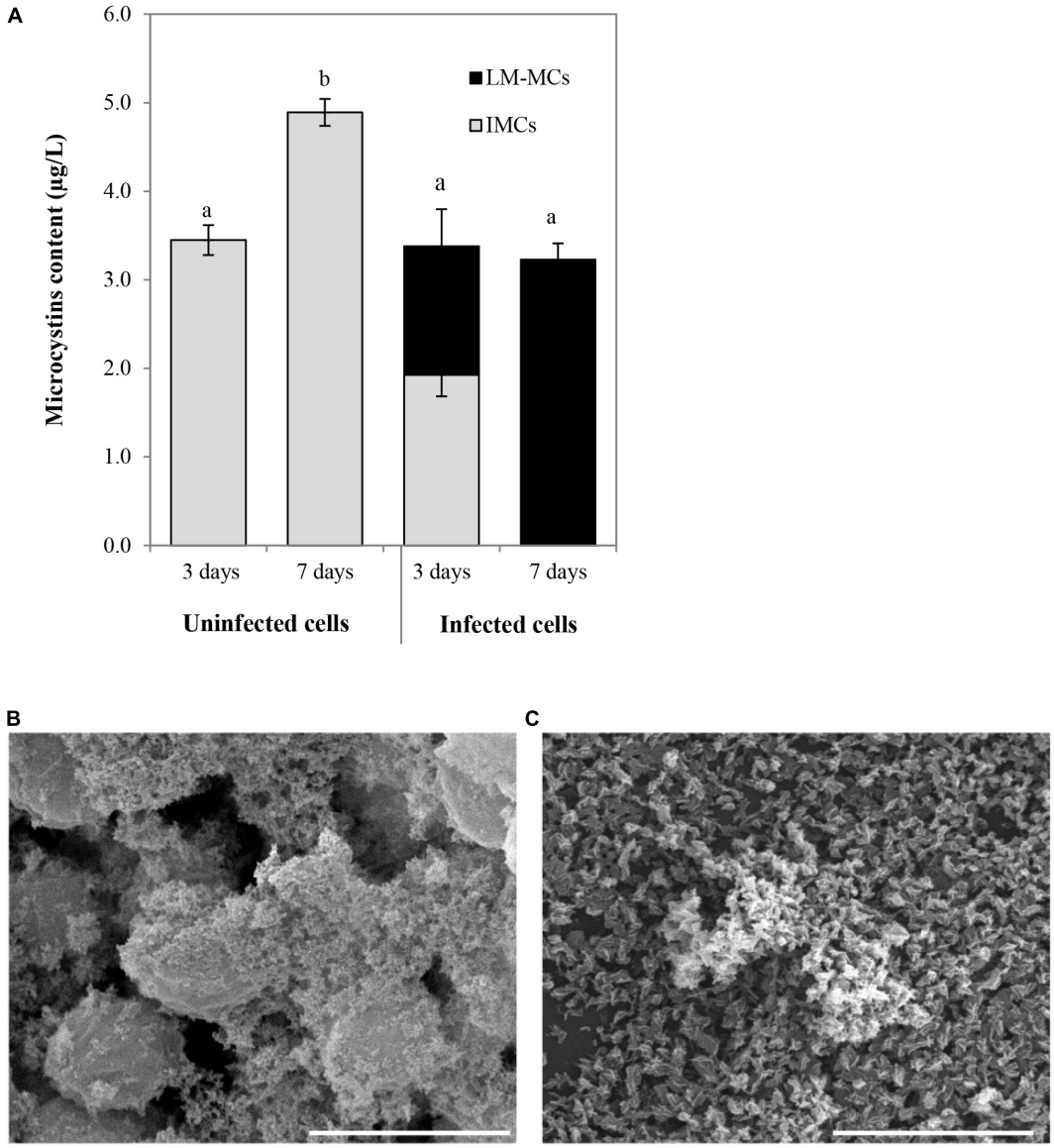

FIGURE 7 | (A) Changes in accumulated microcystins (IMCs) and lysis-mediated microcystins (LM-MCs) after PhiMa05 infecting aggregated *Microcystis* SG03 at MOI of 100 on days 3 and 7. Each data point is the mean value from three independent experiments ± standard deviation (*P* value < 0.05). **(B,C)** Scanning electron micrographs after the phage treatment at MOI of 100: **(B)** Uninfected bacterial aggregation, **(C)** PhiMa05 infecting aggregated cells. Scale bar = 5 μm.

genes obtained from their host during the evolutionary process (Yuan and Gao, 2017).

To search homologs of the PhiMa05 predicted proteins, ORFs were annotated with protein available in the NCBI database. Only 54 ORFs were identified as putative functional proteins, and 12 ORFs were assigned hypothetical proteins (**Supplementary Table 1**). A total of 16 known ORFs were homologous to protein from uncultured *Caudovirales* phage, and four ORFs show a degree of similarity to *Myoviridae* proteins (**Supplementary Table 1**). However, most of the putative proteins presented a lower percentage of similarity than other phages in the database. All predicted ORFs did not match with any proteins from the Ma-LMM01 and MaMV-DC. The genomes of cyanoviruses infecting freshwater cyanobacteria have displayed less homology to each other (Morimoto et al., 2020).

The putative functional genes of PhiMa05 were analyzed (**Supplementary Table 1**) and separated into 4 groups comprising AMGs, DNA replication and nucleotide metabolism, host cell lysis and structural proteins. The AMGs in cyanophage are derived from cyanobacterial hosts (Thompson A.W. et al., 2011). After infection, the host metabolism is shut off, and then phages boost and redirect host metabolism via AMGs (Thompson et al., 2016). The proteins encoded by AMGs are crucial for energy metabolism (photosynthesis, carbon metabolism, and phosphorus utilization), providing ATP

or reducing power for nucleotide biosynthesis and phage genome replication (Thompson A.W. et al., 2011; Enav et al., 2014; Puxty et al., 2015). Here, PhiMa05 possesses ORF228-encoded S-adenosylmethionine decarboxylase (*SpeD*), a key enzyme for maintaining the host PSII reaction center's activity during phage infection (Bograh et al., 1997; Sullivan et al., 2005). In addition, the photosynthetic electron transport as ferredoxin (ORF1) was identified in PhiMa05, as a function in redirection of the electron transport chain (Puxty et al., 2015) and so was the electron acceptor as ferredoxin-NADP reductase (ORF48) for the generation of NADPH during infection (Thompson et al., 2016). Several genes involving dNTP synthesis and energy production in the tricarboxylic acid cycle (TCA) have been reported in cyanophage genomes (Sullivan et al., 2010; Thompson L.R. et al., 2011). Here, phosphopantetheine adenylyltransferase (ORF34), isocitrate dehydrogenase (ORF56), and phosphoglucomutase (ORF204) involving in the TCA cycle were detected in PhiMa05. In contrast to most cyanophage, PhiMa05 lacked of carbon metabolic genes in the pentose phosphate pathway and the Calvin cycle. Only phosphoribosylpyrophosphate synthetase (ORF79) for dNTP biosynthesis existed (Hurwitz and U'Ren, 2016).

We identified 25 genes involved in DNA replication, recombination, and repair in PhiMa05 (**Table 1**). The nucleotide biosynthesis genes have been reported in T4-like cyanophage genomes, including ribonucleotide reductase (RNRs) (Hanson and Mathews, 1994; Gao et al., 2016). Lytic T4-like phages but not temperate phages present the RNRs (Chen and Lu, 2002). Here, the ORF58 of PhiMa05 was RNR-encoded genes, indicating that RNRs degrade the host DNA during cyanophage replication. The products of ORF60 and ORF208 were RNAP sigma subunits, which are essential inhibitors of the host RNAP (Bae et al., 2013). ORF11 was encoded for thioredoxin reductase (gp344), which has been predicted to be responsible for DNA metabolism and replication and structural proteins (Danis-Wlodarczyk et al., 2018). Morimoto et al. (2018) suggested that cyanophages use their genes in transcription and translation, keeping the host in a stable metabolic state. Therefore, host antiviral responses are less virulent, allowing cyanophage propagation.

We detected 2 genes (ORF134 and 191) encoding for peptidases involving host cell lysis in PhiMa05. The putative Zn-dependent peptidase (ORF134) was reported to cleave *N*-acetylmuramic acid of peptidoglycan resulting in cell wall lysis (Hermoso et al., 2007). Another protein, peptidase M15 (ORF191) was proposed as putative endolysins among *Myoviridae* members (Walmagh et al., 2012; Antonova et al., 2019). None of predicted proteins involving lysogeny functions was found in the PhiMa05 genome, including integrase, transposase, excisionase, repressor, and genome attachment site (CI and CII proteins) (Lamont et al., 1993; Golais et al., 2013;

TABLE 1 | Predicted ORFs of cyanophage PhiMa05 with similarity to genes of know function.

ORF	Putative proteins	Phage	*E*-value	Identity (%)	GenBank ID
8	Tryptophanyl-tRNA synthetase	*Myoviridae* sp.	1.00E-20	30	AXH72876.1
11	Putative RNA polymerase sigma subunit	*Bacillus* phage AP631	5.00E-21	37	AZF88386.1
36	Transcription antitermination protein	*Sinorhizobium* phage phi3LM21	4.00E-14	28	ATE84713.1
58	Ribonucleoside-diphosphate reductase	*Loktanella* phage pCB2051-A	9.00E-10	35	YP_007674964.1
60	RNA polymerase sigma factor	*Klebsiella* phage ST147-VIM1phi7.1	4.00E-82	50	YP_009882596.1
76	DNA polymerase IV	*Paracoccus* phage vB_PthS_Pthi1	9.00E-24	30	AZV00415.1
94	PcnB tRNA nucleotidyltransferase/poly(A) polymerase	Uncultured *Caudovirales* phage	8.80E-12	24	CAB4197116.1
104	Pentapeptide repeat	Uncultured *Caudovirales* phage	5.00E-27	40	CAB5225639.1
106	GTP-binding protein	*Klebsiella* phage ST512-KPC3phi13.3	6.00E-06	26	QBQ71826.1
112	Glycine-tRNA ligase beta subunit	*Yersinia* phage vB_YpM_Tongde	4.00E-06	46	QMP18904.1
132	DNA repair exonuclease SbcCD ATPase subunit	Phage 5P_2	8.00E-06	35	AZF90183.1
136	GIY-YIG nuclease superfamily protein	Vibrio phage 1.031.O._10N.261.46.F8	2.00E-07	35	AUR82991.1
144	MutT-like nucleotide pyrophosphohydrolase	*Streptomyces* phage Bmoc	1.00E-04	28	QJD50776.1
148	TopA topoisomerase IA	Uncultured *Caudovirales* phage	6.00E-123	37	CAB4197034.1
177	Leucine-tRNA ligase	*Staphylococcus* phage UPMK_1	3.00E-04	22	ATW69266.1
183	PurB Adenylosuccinate lyase	Uncultured *Caudovirales* phage	2.00E-74	36	CAB4177963.1
188	Threonine-tRNA ligase	*Vibrio* phage Va_90-11-286_p16	9.00E-10	26	QCW19681.1
189	FusA translation elongation factors (GTPases)	Uncultured *Caudovirales* phage	5.00E-25	38	CAB4196865.1
208	RNA polymerase sigma-W factor	crAssphage cr118_1	8.00E-15	30	QOR58402.1
211	LysU Lysyl-tRNA synthetase (class II)	Uncultured *Caudovirales* phage	3.00E-75	25	CAB4196783.1
221	Amidophosphoribosyltransferase	*Wolbachia* phage WO	6.00E-105	42	QHJ75434.1
222	Putative phosphoribosyl formylglycinamidine (FGAM) synthase II	*Microbacterium* phage Min1	3.00E-173	40	YP_001294830.1
224	Pentapeptide repeat family protein	*Caulobacter* phage RW	2.00E-20	40	QDH50377.1
242	RNA binding protein	*Streptomyces* phage Abt2graduatex2	4.00E-10	28	ATN93725.1
248	MerR family transcriptional regulator	*Streptococcus* phage Javan105	4.00E-07	32	QBX13757.1

Altamirano and Barr, 2019). This evidence suggested that PhiMa05 was a lytic phage.

ORF 198, 119, and 201 in PhiMa05 showed the best hits with structural proteins; capsid protein, and portal protein, respectively. An evolutionary analysis in bacteriophages has been based on the capsid protein and terminase large subunit sequence. Since the terminase was not found in the PhiMa05 genome, a phylogenetic tree based on the capsid sequence was generated (**Figure 8**). This protein sequence of PhiMa05 was closely related to deep-sea thermophilic bacteriophage D6E (40% sequence identity with 99% query coverage), unclassified *Myoviridae* (**Figure 8**), suggesting that the relationships among marine and freshwater cyanoviruses. This evidence agrees with Morimoto et al. (2020) that the cyanoviruses co-evolved independently with the host origin. Genome comparative analysis with other phages in the database indicated that PhiMa05 is unique as it shares ANI < 1%. Therefore, PhiMa05 is a new phage species. Genome alignment PhiMa05 with *Microcystis* cyanophages (Ma-LMM01, MaMV-DC, and Mic1) was shown in **Figure 9**. Three collinear blocks were shared among PhiMa05, Ma-LMM01 and MaMV-DC with different arrangements and lengths. No synteny

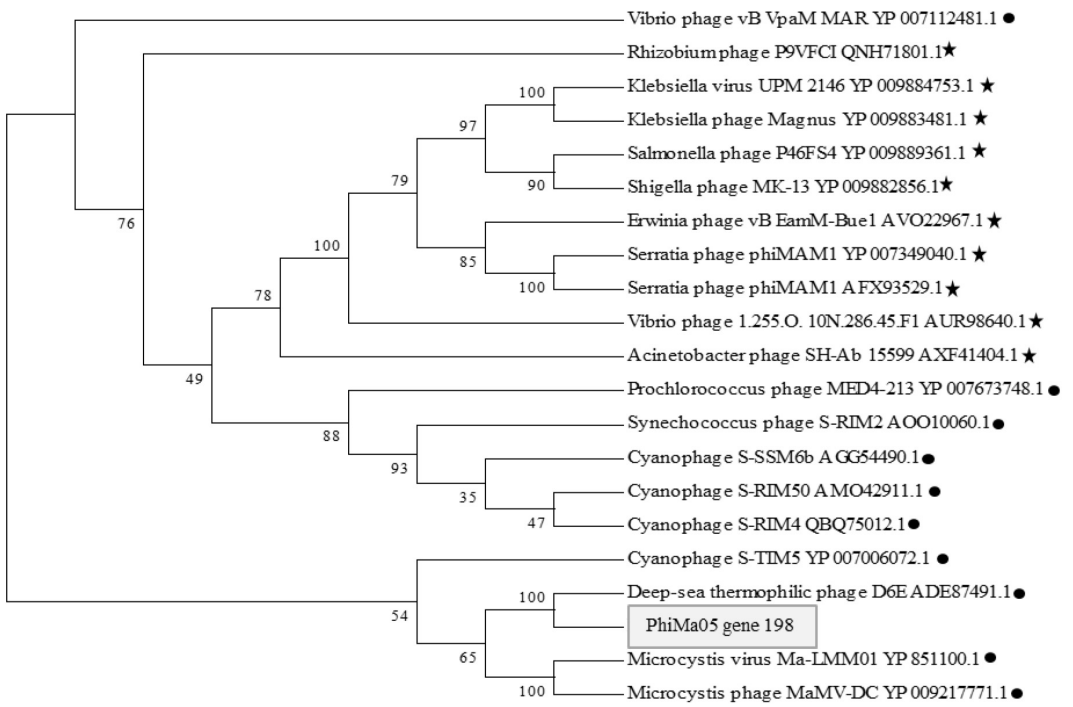

FIGURE 8 | Maximum likelihood amino acid tree of the PhiMa05 major capsid protein. Boostraps values are shown (100 replicate). Black circle and star represent phage family of *Myoviridae* and *Ackermannviridae*, respectively.

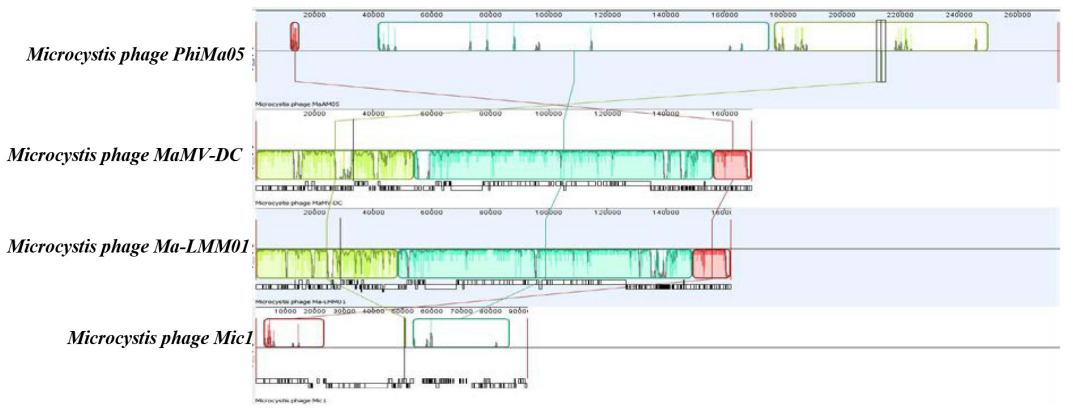

FIGURE 9 | Comparative genome analysis of phage PhiMa05 genome with *Microcystis* phages. The colored collinear blocks indicate homologous regions between genome sequences while the height of the similarity profile in the collinear blocks indicates average level of conservation in the regions of the genome sequence.

and very low sequence similarities were observed. Alignment with four jumbo phages revealed no shared collinear blocks and sequence similarities (**Supplementary Figure 3**). Interestingly, *g91* encoding the sheath protein of the contractile tail was not detected in the PhiMa05 genome. The *g91* has been proposed to be conserved among myovirus infecting *M. aeruginosa* (Jaskulska and Mankiewicz-Boczek, 2020). This finding indicates the evolutionary divergence of PhiMa05 apart from other reported phages.

CONCLUSION

Although viral infections have been considered a promising strategy for controlling harmful cyanobacterial populations, dynamics of toxin-release infection by cyanophage have not been reported. This study demonstrates the characteristics of myovirus PhiMa05 specific to MCs-producing *Microcystis* and its genome. The PhiMa05 lysed toxin-producing strains of *Microcystis*, with a large burst size, rapid killing, and high stability under various environmental stresses. Based on the infection experiments, lysis-mediated MCs were detected. PhiMa05 could kill both planktonic and aggregated cells and interfere with MCs productions. Applications of using PhiMa05 as a bio-control should be further investigated. The whole-genome sequence analysis suggests that PhiMa05 was a jumbo phage possessing several genes, including AMGs, structural proteins and other genes involving in phage DNA replication and host cell lysis. Based on the plaque formation assay and genome analysis, PhiMa05 was the virulent phage without any genes correlated to lysogenic phage, toxin, or antibiotic resistance. However, future studies are needed to explore (1) the transcriptional program of PhiMa05-host during infection and ecological roles, and (2) the safety of potential PhiMa05 applications because most of ORFs are putative and their functions are unknown.

DATA AVAILABILITY STATEMENT

The datasets presented in this study can be found in online repositories. The names of the repository/repositories and accession number(s) can be found below: NCBI, MW495066.1.

AUTHOR CONTRIBUTIONS

RP, OS, and AN contributed to the experimental design. AN performed the experiment and drafted the manuscript. KS and AN contributed to the bioinformatics analysis. RP contributed to the data analysis, manuscript discussion, and revision. EK and RP edited and approved the final content manuscript. All authors contributed to the article and approved the submitted version.

FUNDING

This work was supported by the Thailand Agricultural Research Development Agency (No. HRD6305063).

ACKNOWLEDGMENTS

The authors thank Microbiology Laboratory and Faculty of Science and Faculty of Environmental Management, Prince of Songkla University, Hat Yai, Thailand for chemical reagent and infrastructure support.

SUPPLEMENTARY MATERIAL

The Supplementary Material for this article can be found online at: https://www.frontiersin.org/articles/10.3389/fmicb.2021.660351/full#supplementary-material

REFERENCES

Al-Shayeb, B., Sachdeva, R., Chen, L.-X., Ward, F., Munk, P., Devoto, A., et al. (2020). Clades of huge phages from across Earth's ecosystems. *Nature* 578, 425–431.

Altamirano, F. L. G., and Barr, J. J. (2019). Phage therapy in the postantibiotic era. *Clin. Microbiol. Rev.* 32:e00066–18.

Antonova, N. P., Vasina, D. V., Lendel, A. M., Usachev, E. V., Makarov, V. V., Gintsburg, A. L., et al. (2019). Broad bactericidal activity of the Myoviridae bacteriophage Lysins LysAm24, LysECD7, and LysSi3 against gram-negative ESKAPE pathogens. *Viruses* 11:284. doi: 10.3390/v11030284

Bae, B., Davis, E., Brown, D., Campbell, E. A., Wigneshweraraj, S., and Darst, S. A. (2013). Phage T7 Gp2 inhibition of *Escherichia coli* RNA polymerase involves misappropriation of σ70 domain 1.1. *Proc. Natl. Acad. Sci.U.S.A.* 110, 19772–19777. doi: 10.1073/pnas.1314576110

Bankevich, A., Nurk, S., Antipov, D., Gurevich, A. A., Dvorkin, M., Kulikov, A. S., et al. (2012). SPAdes: a new genome assembly algorithm and its applications to single-cell sequencing. *J. Comput. Biol.* 19, 455–477. doi: 10.1089/cmb.2012.0021

Barylski, J., Enault, F., Dutilh, B. E., Schuller, M. B., Edwards, R. A., Gillis, A., et al. (2020). Analysis of spounaviruses as a case study for the overdue reclassification of tailed phages. *Syst. Biol.* 69, 110–123. doi: 10.1093/sysbio/syz036

Belcher, H., and Swale, E. (1982). *Culturing Algae. A Guide for Schools and Colleges*. Cambridge: Institute of Terrestrial Ecology.

Besemer, J., Lomsadze, A., and Borodovsky, M. (2001). GeneMarkS: a self-training method for prediction of gene starts in microbial genomes. Implications for finding sequence motifs in regulatory regions. *Nucleic Acids Res.* 29, 2607–2618. doi: 10.1093/nar/29.12.2607

Bhatnagar, M., and Bhatnagar, A. (2019). "Diversity of polysaccharides in cyanobacteria," in *Microbial Diversity in Ecosystem Sustainability and Biotechnological Applications*, eds T. Satyanarayana, B. Johri, and S. Das (Singapore: Springer), 447–496. doi: 10.1007/978-981-13-8315-1_15

Bi, X., Dai, W., Wang, X., Dong, S., Zhang, S., Zhang, D., et al. (2019). Microcystins distribution, bioaccumulation, and *Microcystis* genotype succession in a fish culture pond. *Sci. Total Environ.* 688, 380–388. doi: 10.1016/j.scitotenv.2019.06.156

Bograh, A., Gingras, Y., Tajmir-Riahi, H., and Carpentier, R. (1997). The effects of spermine and spermidine on the structure of photosystem II proteins in relation to inhibition of electron transport. *FEBS Lett.* 402, 41–44. doi: 10.1016/s0014-5793(96)01453-6

Bolger, A. M., Lohse, M., and Usadel, B. (2014). Trimmomatic: a flexible trimmer for Illumina sequence data. *Bioinformatics* 30, 2114–2120. doi: 10.1093/bioinformatics/btu170

Boudarel, H., Mathias, J.-D., Blaysat, B., and Grédiac, M. (2018). Towards standardized mechanical characterization of microbial biofilms: analysis and

critical review. *NPJ Biofilms Microbiomes* 4, 1–15. doi: 10.4324/9781315120119-1

Brown, J., Pirrung, M., and Mccue, L. A. (2017). FQC Dashboard: integrates FastQC results into a web-based, interactive, and extensible FASTQ quality control tool. *Bioinformatics* 33, 3137–3139. doi: 10.1093/bioinformatics/btx373

Carmichael, W. W. (2001). Health effects of toxin-producing cyanobacteria:"The CyanoHABs". *Hum. Ecol. Risk Assess.* 7, 1393–1407. doi: 10.1080/20018091095087

Chen, F., and Lu, J. (2002). Genomic sequence and evolution of marine cyanophage P60: a new insight on lytic and lysogenic phages. *Appl. Environ. Microbiol.* 68, 2589–2594. doi: 10.1128/aem.68.5.2589-2594.2002

Chen, M., Tian, L.-L., Ren, C.-Y., Xu, C.-Y., Wang, Y.-Y., and Li, L. (2019). Extracellular polysaccharide synthesis in a bloom-forming strain of Microcystis aeruginosa: implications for colonization and buoyancy. *Sci. Rep.* 9, 1–11.

Chénard, C., Chan, A., Vincent, W., and Suttle, C. (2015). Polar freshwater cyanophage S-EIV1 represents a new widespread evolutionary lineage of phages. *ISME J.* 9, 2046–2058. doi: 10.1038/ismej.2015.24

Chénard, C., and Chan, A. M. (2017). Isolation and purification of viruses infecting cyanobacteria using a liquid bioassay approach. *Bio Protocol* 8:e2691.

Dai, R., Liu, H., Qu, J., Zhao, X., and Hou, Y. (2009). Effects of amino acids on microcystin production of the Microcystis aeruginosa. *J. Hazard. Mater.* 161, 730–736. doi: 10.1016/j.jhazmat.2008.04.015

Danis-Wlodarczyk, K., Blasdel, B. G., Jang, H. B., Vandenheuvel, D., Noben, J.-P., Drulis-Kawa, Z., et al. (2018). Genomic, transcriptomic, and structural analysis of *Pseudomonas* virus PA5oct highlights the molecular complexity among Jumbo phages. *bioRxiv* [Preprint] bioRxiv: 406421,

Darling, A. E., Mau, B., and Perna, N. T. (2010). progressiveMauve: multiple genome alignment with gene gain, loss and rearrangement. *PLoS One* 5:e11147. doi: 10.1371/journal.pone.0011147

Dervaux, J., Mejean, A., and Brunet, P. (2015). Irreversible collective migration of cyanobacteria in eutrophic conditions. *PLoS One* 10:e0120906. doi: 10.1371/journal.pone.0120906

Devoto, A. E., Santini, J. M., Olm, M. R., Anantharaman, K., Munk, P., Tung, J., et al. (2019). Megaphages infect Prevotella and variants are widespread in gut microbiomes. *Nat. Microbiol.* 4, 693–700. doi: 10.1038/s41564-018-0338-9

Drugă, B., Buda, D.-M., Szekeres, E., Chiş, C., Chiş, I., and Sicora, C. (2019). The impact of cation concentration on Microcystis (cyanobacteria) scum formation. *Sci. Rep.* 9, 1–10.

Enav, H., Mandel-Gutfreund, Y., and Béjà, O. (2014). Comparative metagenomic analyses reveal viral-induced shifts of host metabolism towards nucleotide biosynthesis. *Microbiome* 2:9. doi: 10.1186/2049-2618-2-9

Falconer, I. R., Runnegar, M. T., and Beresford, A. M. (1983). Evidence of liver damage by toxin from a bloom of the blue-green alga, Microcystis aeruginosa. *Med. J. Aust.* 1, 511–514. doi: 10.5694/j.1326-5377.1983.tb136192.x

Gao, E.-B., Huang, Y., and Ning, D. (2016). Metabolic genes within cyanophage genomes: implications for diversity and evolution. *Genes* 7:80. doi: 10.3390/genes7100080

Gašić, K., Ivanović, M. M., Ignjatov, M., Calić, A., and Obradović, A. (2011). Isolation and characterization of Xanthomonas euvesicatoria bacteriophages. *J. Plant Pathol.* 2, 415–423.

Gkelis, S., Tussy, P. F., and Zaoutsos, N. (2015). Isolation and preliminary characterization of cyanobacteria strains from freshwaters of Greece. *Open Life Sci.* 10, 52–60.

Golais, F., Hollý, J., and Vítkovská, J. (2013). Coevolution of bacteria and their viruses. *Folia Microbiol.* 58, 177–186. doi: 10.1007/s12223-012-0195-5

Gu, P., Li, Q., Zhang, W., Zheng, Z., and Luo, X. (2020). Effects of different metal ions (Ca, Cu, Pb, Cd) on formation of cyanobacterial blooms. *Ecotoxicol. Environ. Safe.* 189:109976. doi: 10.1016/j.ecoenv.2019.109976

Hanson, E., and Mathews, C. K. (1994). Allosteric effectors are required for subunit association in T4 phage ribonucleotide reductase. *J. Biol. Chem.* 269, 30999–31005. doi: 10.1016/s0021-9258(18)47381-4

Harke, M. J., Steffen, M. M., Gobler, C. J., Otten, T. G., Wilhelm, S. W., Wood, S. A., et al. (2016). A review of the global ecology, genomics, and biogeography of the toxic cyanobacterium, Microcystis spp. *Harmful Algae* 54, 4–20. doi: 10.1016/j.hal.2015.12.007

Hermoso, J. A., García, J. L., and García, P. (2007). Taking aim on bacterial pathogens: from phage therapy to enzybiotics. *Curr. Opin. Microbiol.* 10, 461–472. doi: 10.1016/j.mib.2007.08.002

Higuera, G., Bastías, R., Tsertsvadze, G., Romero, J., and Espejo, R. T. (2013). Recently discovered *Vibrio anguillarum* phages can protect against experimentally induced vibriosis in Atlantic salmon, *Salmo salar*. *Aquaculture* 392, 128–133. doi: 10.1016/j.aquaculture.2013.02.013

Huisman, J., Codd, G. A., Paerl, H. W., Ibelings, B. W., Verspagen, J. M., and Visser, P. M. (2018). Cyanobacterial blooms. *Nat. Rev. Microbiol.* 16, 471–483.

Hurwitz, B. L., and U'Ren, J. M. (2016). Viral metabolic reprogramming in marine ecosystems. *Curr. Opin. Microbiol.* 31, 161–168. doi: 10.1016/j.mib.2016.04.002

Imam, M., Alrashid, B., Patel, F., Dowah, A. S., Brown, N., Millard, A. D., et al. (2019). vB_PaeM_MIJ3, a novel jumbo phage infecting *Pseudomonas aeruginosa*, possesses unusual genomic features. *Front. Microbiol.* 10:2772. doi: 10.3389/fmicb.2019.02772

Jaiswal, P., Prasanna, R., and Singh, P. K. (2013). Physiological characterization and molecular profiling of toxic and non-toxic isolates of Cyanobacterium Microcystis. *J. Environ. Biol.* 34:555.

Jarvis, B., Wilrich, C., and Wilrich, P. T. (2010). Reconsideration of the derivation of Most Probable Numbers, their standard deviations, confidence bounds and rarity values. *J. Appl. Microbiol.* 109, 1660–1667.

Jaskulska, A., and Mankiewicz-Boczek, J. (2020). Cyanophages specific to cyanobacteria from the genus *Microcystis*. *Ecohydrol. Hydrobiol.* 20, 83–90. doi: 10.1016/j.ecohyd.2019.06.001

Kropinski, A. M. (2018). "Practical advice on the one-step growth curve," in *Bacteriophages: Methods in Molecular Biology*, Vol. 1681, eds M. Clokie, A. Kropinski, and R. Lavigne (Berlin: Springer), 41–47. doi: 10.1007/978-1-4939-7343-9_3

Lamont, I., Richardson, H., Carter, D., and Egan, J. (1993). Genes for the establishment and maintenance of lysogeny by the temperate coliphage 186. *J. Bacteriol.* 175, 5286–5288. doi: 10.1128/jb.175.16.5286-5288.1993

Lavysh, D., Sokolova, M., Minakhin, L., Yakunina, M., Artamonova, T., Kozyavkin, S., et al. (2016). The genome of AR9, a giant transducing *Bacillus* phage encoding two multisubunit RNA polymerases. *Virology* 495, 185–196. doi: 10.1016/j.virol.2016.04.030

Lewis, R., Clooney, A. G., Stockdale, S. R., Buttimer, C., Draper, L. A., Ross, R. P., et al. (2020). Isolation of a novel jumbo bacteriophage effective against *Klebsiella aerogenes*. *Front. Med.* 7:67. doi: 10.3389/fmed.2020.00067

Li, J., Li, R., and Li, J. (2017). Current research scenario for microcystins biodegradation–a review on fundamental knowledge, application prospects and challenges. *Sci. Total Environ.* 595, 615–632. doi: 10.1016/j.scitotenv.2017.03.285

Li, S., Ou, T., and Zhang, Q. (2013). Two virus-like particles that cause lytic infections in freshwater cyanobacteria. *Virol. Sin.* 28, 303–305. doi: 10.1007/s12250-013-3339-0

Liu, L., Huang, Q., and Qin, B. (2018). Characteristics and roles of Microcystis extracellular polymeric substances (EPS) in cyanobacterial blooms: a short review. *J. Freshw. Ecol.* 33, 183–193. doi: 10.1080/02705060.2017.1391722

Mathieu, J., Yu, P., Zuo, P., Da Silva, M. L., and Alvarez, P. J. (2019). Going viral: emerging opportunities for phage-based bacterial control in water treatment and reuse. *Acc. Chem. Res.* 52, 849–857. doi: 10.1021/acs.accounts.8b00576

Mirzaei, M. K., and Nilsson, A. S. (2015). Isolation of phages for phage therapy: a comparison of spot tests and efficiency of plating analyses for determination of host range and efficacy. *PLoS One* 10:e0118557. doi: 10.1371/journal.pone.0118557

Morimoto, D., Kimura, S., Sako, Y., and Yoshida, T. (2018). Transcriptome analysis of a bloom-forming cyanobacterium *Microcystis aeruginosa* during Ma-LMM01 phage infection. *Front. Microbiol.* 9:2. doi: 10.3389/fmicb.2018.00002

Morimoto, D., Šulčius, S., and Yoshida, T. (2020). Viruses of freshwater bloom-forming cyanobacteria: genomic features, infection strategies and coexistence with the host. *Environ. Microbiol. Rep.* 12, 486–502. doi: 10.1111/1758-2229.12872

Myers, J. A., Curtis, B. S., and Curtis, W. R. (2013). Improving accuracy of cell and chromophore concentration measurements using optical density. *BMC Biophys.* 6:4. doi: 10.1186/2046-1682-6-4

Nasukawa, T., Uchiyama, J., Taharaguchi, S., Ota, S., Ujihara, T., Matsuzaki, S., et al. (2017). Virus purification by CsCl density gradient using general centrifugation. *Arch. virol.* 162, 3523–3528. doi: 10.1007/s00705-017-3513-z

Oliveira, V. C., Bim, F. L., Monteiro, R. M., Macedo, A. P., Santos, E. S., Silva-Lovato, C. H., et al. (2020). Identification and characterization of new

bacteriophages to control multidrug-resistant *Pseudomonas aeruginosa* biofilm on endotracheal tubes. *Front. Microbi.* 11:580779. doi: 10.3389/fmicb.2020.580779

Olsen, N. S., Forero-Junco, L., Kot, W., and Hansen, L. H. (2020). Exploring the remarkable diversity of culturable *Escherichia coli* phages in the Danish Wastewater Environment. *Viruses* 12:986. doi: 10.3390/v12090986

Ou, T., Gao, X.-C., Li, S.-H., and Zhang, Q.-Y. (2015). Genome analysis and gene nblA identification of Microcystis aeruginosa myovirus (MaMV-DC) reveal the evidence for horizontal gene transfer events between cyanomyovirus and host. *J. Gen. Virol.* 96, 3681–3697. doi: 10.1099/jgv.0.000290

Ou, T., Li, S., Liao, X., and Zhang, Q. (2013). Cultivation and characterization of the MaMV-DC cyanophage that infects bloom-forming cyanobacterium *Microcystis aeruginosa*. *Virol. Sin.* 28, 266–271. doi: 10.1007/s12250-013-3340-7

Pham, T.-L., and Utsumi, M. (2018). An overview of the accumulation of microcystins in aquatic ecosystems. *J. Environ. Manag.* 213, 520–529. doi: 10.1016/j.jenvman.2018.01.077

Puxty, R. J., Millard, A. D., Evans, D. J., and Scanlan, D. J. (2015). Shedding new light on viral photosynthesis. *Photosynth. Res.* 126, 71–97. doi: 10.1007/s11120-014-0057-x

Sullivan, M. B., Coleman, M. L., Weigele, P., Rohwer, F., and Chisholm, S. W. (2005). Three Prochlorococcus cyanophage genomes: signature features and ecological interpretations. *PLoS Biol.* 3:e144. doi: 10.1371/journal.pbio.0030144

Sullivan, M. B., Huang, K. H., Ignacio−Espinoza, J. C., Berlin, A. M., Kelly, L., Weigele, P. R., et al. (2010). Genomic analysis of oceanic cyanobacterial myoviruses compared with T4−like myoviruses from diverse hosts and environments. *Environ. Microbiol.* 12, 3035–3056. doi: 10.1111/j.1462-2920.2010.02280.x

Sullivan, M. J., Petty, N. K., and Beatson, S. A. (2011). Easyfig: a genome comparison visualizer. *Bioinformatics* 27, 1009–1010. doi: 10.1093/bioinformatics/btr039

Suttle, C. A., and Chan, A. M. (1993). Marine cyanophages infecting oceanic and coastal strains of Synechococcus: abundance, morphology, cross-infectivity and growth characteristics. *Mar. Ecol. Prog. Ser.* 92, 99–99. doi: 10.3354/meps092099

Thompson, A. W., Huang, K., Saito, M. A., and Chisholm, S. W. (2011). Transcriptome response of high-and low-light-adapted *Prochlorococcus* strains to changing iron availability. *ISME J.* 5, 1580–1594. doi: 10.1038/ismej.2011.49

Thompson, L. R., Zeng, Q., and Chisholm, S. W. (2016). Gene expression patterns during light and dark infection of Prochlorococcus by cyanophage. *PLoS One* 11:e0165375. doi: 10.1371/journal.pone.0165375

Thompson, L. R., Zeng, Q., Kelly, L., Huang, K. H., Singer, A. U., Stubbe, J., et al. (2011). Phage auxiliary metabolic genes and the redirection of cyanobacterial host carbon metabolism. *Proc. Natl. Acad. Sci.* 108, E757–E764.

Vandevivere, P., and Kirchman, D. L. (1993). Attachment stimulates exopolysaccharide synthesis by a bacterium. *Appl. Environ. Microbiol.* 59, 3280–3286. doi: 10.1128/aem.59.10.3280-3286.1993

Walmagh, M., Briers, Y., Dos Santos, S. B., Azeredo, J., and Lavigne, R. (2012). Characterization of modular bacteriophage endolysins from Myoviridae phages OBP, 201φ2-1 and PVP-SE1. *PLoS One* 7:e36991. doi: 10.1371/journal.pone.0036991

Wang, J., Bai, P., Li, Q., Lin, Y., Huo, D., Ke, F., et al. (2019). Interaction between cyanophage MaMV-DC and eight *Microcystis* strains, revealed by genetic defense systems. *Harmful Algae* 85:101699. doi: 10.1016/j.hal.2019.101699

Watkins, S. C., Smith, J. R., Hayes, P. K., and Watts, J. E. (2014). Characterisation of host growth after infection with a broad-range freshwater cyanopodophage. *PLoS One* 9:e87339. doi: 10.1371/journal.pone.0087339

Wei, K., Jung, S., Amano, Y., and Machida, M. (2019). Control of the buoyancy of Microcystis aeruginosa via colony formation induced by regulating extracellular polysaccharides and cationic ions. *SN Appl. Sci.* 1:1573.

Wilson, A. E., Sarnelle, O., Neilan, B. A., Salmon, T. P., Gehringer, M. M., and Hay, M. E. (2005). Genetic variation of the bloom-forming cyanobacterium *Microcystis aeruginosa* within and among lakes: implications for harmful algal blooms. *Appl. Environ. Microbiol.* 71, 6126–6133. doi: 10.1128/aem.71.10.6126-6133.2005

Wintachai, P., Naknaen, A., Thammaphet, J., Pomwised, R., Phaonakrop, N., Roytrakul, S., et al. (2020). Characterization of extended-spectrum-β-lactamase producing *Klebsiella pneumoniae* phage KP1801 and evaluation of therapeutic efficacy in vitro and in vivo. *Sci. Rep.* 10, 1–18.

Wu, Y. Q., He, P., and Wang, R. (2019). A novel polysaccharide depolymerase encoded by phage SH-KP152226 confers specific activities against multidrug resistant *Klebsiella pneumoniae* via biofilm degradation. *Front. Microbiol.* 10:2768. doi: 10.3389/fmicb.2019.02768

Xiao, M., Li, M., and Reynolds, C. S. (2018). Colony formation in the cyanobacterium *Microcystis*. *Biol. Rev.* 93, 1399–1420. doi: 10.1111/brv.12401

Xu, H., Lv, H., Liu, X., Wang, P., and Jiang, H. (2016). Electrolyte cations binding with extracellular polymeric substances enhanced *Microcystis* aggregation: implication for *Microcystis* bloom formation in eutrophic freshwater lakes. *Environ. Sci. Technol.* 50, 9034–9043. doi: 10.1021/acs.est.6b00129

Yang, F., Jin, H., Wang, X.-Q., Li, Q., Zhang, J.-T., Cui, N., et al. (2020). Genomic analysis of Mic1 reveals a novel freshwater long-tailed cyanophage. *Front. Microbiol.* 11:484. doi: 10.3389/fmicb.2020.00484

Yoshida, T., Nagasaki, K., Takashima, Y., Shirai, Y., Tomaru, Y., Takao, Y., et al. (2008). Ma-LMM01 infecting toxic *Microcystis aeruginosa* illuminates diverse cyanophage genome strategies. *J. Bacteriol.* 190, 1762–1772. doi: 10.1128/jb.01534-07

Yoshida, T., Takashima, Y., Tomaru, Y., Shirai, Y., Takao, Y., Hiroishi, S., et al. (2006). Isolation and characterization of a cyanophage infecting the toxic cyanobacterium Microcystis aeruginosa. *Appl. Environ. Microbiol.* 72, 1239–1247. doi: 10.1128/aem.72.2.1239-1247.2006

Yoshida-Takashima, Y., Yoshida, M., Ogata, H., Nagasaki, K., Hiroishi, S., and Yoshida, T. (2012). Cyanophage infection in the bloom-forming cyanobacteria *Microcystis aeruginosa* in surface freshwater. *Microb. Environ.* 27, 350–355. doi: 10.1264/jsme2.me12037

Yuan, Y., and Gao, M. (2017). Jumbo bacteriophages: an overview. *Front. Microbiol.* 8:403. doi: 10.3389/fmicb.2017.00403

Zhou, Y., Liang, Y., Lynch, K. H., Dennis, J. J., and Wishart, D. S. (2011). PHAST: a fast phage search tool. *Nucleic Acids Res.* 39, W347–W352.

Zimmerman, A. E., Howard-Varona, C., Needham, D. M., John, S. G., Worden, A. Z., Sullivan, M. B., et al. (2020). Metabolic and biogeochemical consequences of viral infection in aquatic ecosystems. *Nat. Rev. Microbiol.* 18, 21–34. doi: 10.1038/s41579-019-0270-x

Conflict of Interest: The authors declare that the research was conducted in the absence of any commercial or financial relationships that could be construed as a potential conflict of interest.

Copyright © 2021 Naknaen, Suttinun, Surachat, Khan and Pomwised. This is an open-access article distributed under the terms of the Creative Commons Attribution License (CC BY). The use, distribution or reproduction in other forums is permitted, provided the original author(s) and the copyright owner(s) are credited and that the original publication in this journal is cited, in accordance with accepted academic practice. No use, distribution or reproduction is permitted which does not comply with these terms.

frontiers in Microbiology

ORIGINAL RESEARCH
published: 22 April 2021
doi: 10.3389/fmicb.2021.674068

Combination Therapy of Phage vB_KpnM_P-KP2 and Gentamicin Combats Acute Pneumonia Caused by K47 Serotype *Klebsiella pneumoniae*

*Zijing Wang[1†], Ruopeng Cai[2†], Gang Wang[1†], Zhimin Guo[3†], Xiao Liu[1], Yuan Guan[1], Yalu Ji[1], Hao Zhang[1], Hengyu Xi[1], Rihong Zhao[1], Lanting Bi[1], Shanshan Liu[4], Li Yang[1], Xin Feng[1], Changjiang Sun[1], Liancheng Lei[1], Wenyu Han[1,5] and Jingmin Gu[1,5]**

[1] Key Laboratory of Zoonosis Research, Ministry of Education, College of Veterinary Medicine, Jilin University, Changchun, China, [2] College of Animal Science and Technology, Jilin Agricultural University, Changchun, China, [3] Department of Clinical Laboratory, The First Hospital of Jilin University, Changchun, China, [4] Department of Chinese Journal of Veterinary Science, Jilin University, Changchun, China, [5] Jiangsu Co-Innovation Center for the Prevention and Control of Important Animal Infectious Disease and Zoonose, Yangzhou University, Yangzhou, China

OPEN ACCESS

Edited by:
Shuai Le,
Army Medical University, China

Reviewed by:
Hang Yang,
Wuhan Institute of Virology, Chinese Academy of Sciences (CAS), China
Tang Fang,
Nanjing Agricultural University, China

***Correspondence:**
Jingmin Gu
jingmin0629@163.com

† These authors have contributed equally to this work

Specialty section:
This article was submitted to Virology, a section of the journal Frontiers in Microbiology

Received: *28 February 2021*
Accepted: *30 March 2021*
Published: *22 April 2021*

Citation:
Wang Z, Cai R, Wang G, Guo Z, Liu X, Guan Y, Ji Y, Zhang H, Xi H, Zhao R, Bi L, Liu S, Yang L, Feng X, Sun C, Lei L, Han W and Gu J (2021) Combination Therapy of Phage vB_KpnM_P-KP2 and Gentamicin Combats Acute Pneumonia Caused by K47 Serotype Klebsiella pneumoniae. Front. Microbiol. 12:674068. doi: 10.3389/fmicb.2021.674068

Klebsiella pneumoniae (*K. pneumoniae*) is an important nosocomial and community acquired opportunistic pathogen which causes various infections. The emergence of multi-drug resistant (MDR) *K. pneumoniae* and carbapenem-resistant hypervirulent *K. pneumoniae* (CR-hvKP) has brought more severe challenge to the treatment of *K. pneumoniae* infection. In this study, a novel bacteriophage that specifically infects *K. pneumoniae* was isolated and named as vB_KpnM_P-KP2 (abbreviated as P-KP2). The biological characteristics of P-KP2 and the bioinformatics of its genome were analyzed, and then the therapeutic effect of P-KP2 was tested by animal experiments. P-KP2 presents high lysis efficiency *in vitro*. The genome of P-KP2 shows homology with nine phages which belong to "*KP15 virus*" family and its genome comprises 172,138 bp and 264 ORFs. Besides, P-KP2 was comparable to gentamicin in the treatment of lethal pneumonia caused by *K. pneumoniae* W-KP2 (K47 serotype). Furthermore, the combined treatment of P-KP2 and gentamicin completely rescued the infected mice. Therefore, this study not only introduces a new member to the phage therapeutic library, but also serves as a reference for other phage-antibiotic combinations to combat MDR pathogens.

Keywords: bacteriophage, *Klebsiella pneumoniae*, genome sequencing, bioinformatics analysis, phage therapy

INTRODUCTION

As the second-ranked nosocomial infection-causing-pathogens, *Klebsiella pneumoniae* (*K. pneumoniae*) causes fatal systemic infections (Paczosa and Mecsas, 2016). The presence of at least 79 serotypes greatly increases the complexity of treatment for these bacterial infections (Hsu et al., 2013; Pan et al., 2015). What's more, the existing antibiotics have failed to cure clinical infections caused by multidrug-resistant (MDR) *K. pneumoniae*, such as

extended-spectrum β-lactamase (ESBL)-producing and carbapenemase [such as *K. pneumoniae* carbapenemases (KPC), metallo β-lactamases (MBL), and oxacillinase-48-type carbapenemases (OXA-48)]-producing strains (Navon-Venezia et al., 2017). In addition, the recent emergence of carbapenem-resistant hypervirulent *Klebsiella pneumoniae* (CR-hvKP) has further exacerbated the dilemma of antibiotic treatment, provoking the need for alternative therapies (Gu et al., 2018).

Bacteriophages (phages) are bacterial viruses that specifically recognize, infect, and replicate inside a host bacterium. It has been reported that there are more than 10^{31} phage particles in the biosphere. This massive phage diversity has a marked effect on the environment, ecology, and bacterial evolution (Davies et al., 2016). Owing to their specific bactericidal abilities, phages have been considered as therapeutic agents since the early 1920s. However, the development of this therapy has been hampered by the widespread use of antibiotics (Nobrega et al., 2015). Recently, due to the global emergence of multidrug-resistant bacteria, phage therapy has been experiencing a renaissance for its ability to combat their antibiotic-resistant host specifically. Until now, phage therapy have already been developed in various bacterial species including MDR *K. pneumoniae* and have made some achievements. Studies based on mice as animal models have shown that phages have good therapeutic effects on pneumonia (Anand et al., 2020), liver abscess (Lin et al., 2014), burn infection (Chadha et al., 2017), and bacteremia (Kaabi and Musafer, 2019) caused by *K. pneumoniae*. Not only that, phage therapy has also been applied in clinical practice. Medical workers have confirmed that multiple rounds of phage administration have a significant curative effect on refractory urinary tract infections triggered by MDR *K. pneumoniae* (Bao et al., 2020). Although phage therapy has great potential application prospects, both the phage resistance of bacteria and phage elimination by the immune system are the main challenges (Hodyra-Stefaniak et al., 2015; Hampton et al., 2020). However, the combination therapy of phage and antibiotics can effectively increase the sensitivity of target strains to antibiotics and reduce the probability of phage resistance mutations, thereby providing a development direction for controlling bacterial infections caused by MDR strains (Abedon, 2019).

In the present work, a novel myophage that specifically infects *K. pneumoniae* was isolated and named as vB_KpnM_P-KP2 (abbreviated as P-KP2). The biological characteristics of this phage such as morphology and one-step growth curve were measured. Besides, the genetic background of P-KP2 was revealed by bioinformatics analysis, and the powerful therapeutic effect of the phage combined with gentamicin on lung infection caused by *K. pneumoniae* W-KP2 (K47 serotype MDR *K. pneumoniae* strain) was also confirmed.

MATERIALS AND METHODS

Animals

Female C57BL/6J mice (18–20 g) were purchased from Liaoning Changsheng Biotechnology Co., Ltd. (Benxi, Liaoning, China). All animal experiments were performed in strict accordance with the Regulations for the Administration of Affairs Concerning Experimental Animals approved by the State Council of the People's Republic of China and the Animal Welfare and Research Ethics Committee at University.

Bacterial Strains and Culture Conditions

K. pneumoniae W-KP2 was isolated from sputum provided by Zhimin Guo and confirmed to be *K. pneumoniae* using 16S rRNA sequence analysis after PCR amplification with the universal primers (27F: AGAGTTTGATCCTGGCTCAG and 1429R: GGTTACCTTGTTACGACTT) (Sunagawa et al., 2009). The serotype of *K. pneumoniae* was identified by the universal primer (F: GGGTTTTTATCGGGTTGTAC and R: 5′-3′ TTCAGCTGGATTTGGTGG) according to the previous description (Pan et al., 2013). The minimum inhibitory concentration (MIC) of antibiotics listed in **Supplementary Table 1** for *K. pneumoniae* W-KP2 (0.5–0.63 MacFarland) was assessed using the VITEK® 2 Compact system with VITEK® 2 AST-GN 09 Card (bioMérieux, Marcy-l'Étoile, France) according to the manufacturer's instructions. The strain was routinely inoculated in lysogeny broth (LB) broth and then propagated on an orbital shaker (180 rpm/min).

Phage Isolation, Purification, and Host Spectrum Determination

Phage P-KP2 was isolated by using *K. pneumoniae* W-KP2 as the host strain from sewage samples collected from the Changchun sewer system (43°92′ N, 125°25′ E) (Changchun, Jilin Province, China) according to the previously described method (Ji et al., 2019). In brief, W-KP2 was incubated with sewage samples in LB broth at 37°C overnight. After 15 min of centrifugation (4°C, 10,000 × g) to remove the precipitate, the supernatant was filtered by 0.22-μm filters (Millipore, Billerica, MA, United States). Phage P-KP2 was purified by the double-layer agar plate method and then stored at 4°C or −80°C in glycerol (3:1 [*v*/*v*]). To determine its host spectrum, 5 μL of phage P-KP2 suspension was spot tested against 80 clinical *K. pneumoniae* strains preserved in the laboratory, by the double-layer agar plate method (Cai et al., 2019b).

Growth Characteristics of the Phage

To determine the titers of phage P-KP2 corresponding to different multiplicity of infection (MOI), the phage was added to fresh *K. pneumoniae* W-KP2 culture with final concentration of 2.0×10^7 CFU/mL ($OD_{600} \approx 0.4$) at different MOIs (phage/bacteria = 0.00000001, 0.0000001, 0.000001, 0.00001, 0.0001, 0.001, 0.01, 0.1, 1, 10, and 100). After the mixed culture was incubated for 5 h at 37°C (180 rpm), the phage titers were measured by the double-layer agar plate method after serial dilution (Gong et al., 2016).

To determine the one-step growth curve of P-KP2, the phage was added to W-KP2 culture (5.0×10^5 CFU/mL) at an MOI of 0.1. After 10 min of incubation at 37°C, the mixture was centrifuged at 12,000 × g for 5 min at 4°C. The pellet was resuspended in 10 mL of fresh LB broth followed by incubation at 37°C with shaking at 180 rpm. Cultures were collected

every 10 min for 180 min and were filtered by 0.22-μm filters (Millipore, Billerica, MA, United States). Finally, plaque assays were used to quantify the lysate titers at different time intervals (Gadagkar and Gopinathan, 1980).

Concentration and Purification of the Phage

Phage P-KP2 was concentrated and purified according to the previous description for morphological observation and genome extraction (Sambrook and Russell, 2006). Briefly, 100 μL of phage P-KP2 suspension (2.0×10^7 PFU/mL) was added to 1 L of *K. pneumoniae* W-KP2 ($OD_{600} \approx 0.4$). After shaking culture (180 rpm) for 4 h, the lysates were centrifuged for 20 min (4°C, 4,000 × g) to recover the supernatant, and DNase I and RNase A (1 μg/mL) were added. Followed by incubation at 25°C for 30 min, 1 M NaCl was then added to the supernatants (ice bath for 1 h). After the addition of polyethylene glycol 8000 (PEG8000) (10% [*w/v*]), the mixture was incubated in an ice bath overnight. Next, the phage particles were collected by centrifugation for 10 min (4°C, 10,000 × g) and resuspended in 2 mL SM buffer. The concentrated phage was purified by cesium chloride (CsCl) density gradient centrifugation (4°C, 35,000 × g, 3 h, CsCl gradient: 1.32, 1.45, 1.50, and 1.70 g/mL), and then the light blue phage band was carefully collected and subjected to dialysis before being stored at 4°C.

Morphological Observation of the Phage

After negative staining with phosphotungstic acid (PTA) (2% [*w/v*]), the morphology of the concentrated phage (2.5×10^{10} PFU/mL) was examined using a transmission electron microscope (TEM) (JEOL JEM-1200EXII, Japan Electronics and Optics Laboratory, Tokyo, Japan) at an acceleration voltage of 80 kV.

Sequencing and Bioinformatics Analysis of the Phage Genome

The genome was extracted from the concentrated and purified phage preparations using a viral genome extraction kit (Omega Bio-Tek Inc., Doraville, GA, United States) [Quality criteria for DNA samples: $OD_{260/280}$ = 1.8–2.0, $OD_{260/230}$ = 2.0–2.2, RIN = 6.0–8.0, ≥10 μg in total (≥100 ng/μL)]. Whole-genome sequencing was performed by using Illumina HiSeq 2500 sequencing. The genome sequences were assembled using Roche Newbler v.2.8 (Margulies et al., 2005). Potential open reading frames (ORFs) were identified using GeneMarkS (Georgia Institute of Technology, Atlanta, GA, United States) [parameter settings: (sequence type: phage; output format for gene prediction: LST; output options: gene nucleotide sequence)] (Besemer et al., 2001). The gene alignment and ORF annotation were performed using BLASTN (nucleotide collection database, Megablast) and BLASTP [non-redundant protein sequence database, PSI-BLAST (Threshold = 0.005)], respectively, from the National Center for Biotechnology Information (NCBI) (Altschul et al., 1997). The schematic of the phage genome with predicted ORFs was generated using CLC Main Workbench, version 8.0.1 (CLC Bio-Qiagen, Aarhus, Denmark). The circular view of the phage genome was illustrated using CGView[1] (Stothard and Wishart, 2005) and termini of the phage was identified by PhageTerm[2] (Garneau et al., 2017). Genome comparisons among P-KP2 and homologous phages were performed by Mauve 2.3.1 (Darling et al., 2004). After genes of terminase large subunit, major capsid protein and DNA polymerase were aligned by ClustalW, phylogenetic trees of phages were constructed using Neighbor-Joining Method (100 bootstrap replicates) by PHYLIP (version 3.697) (Shimada and Nishida, 2017). Additionally, domain analyses were performed by HHpred at MPI bioinformatics Toolkit[3] (Zimmermann et al., 2018).

Therapeutic Effects of P-KP2 and Gentamicin Against *K. pneumoniae* W-KP2

After *K. pneumoniae* W-KP2 was cultured to exponential growth phase (2.0×10^9 CFU/mL), the bacterial solution was concentrated by centrifugation and suspended in phosphate buffered saline (PBS) (adjust to 5.0×10^{10} CFU/mL). To determine the virulence of W-KP2, mice were anesthetized intraperitoneally with ketamine (100 mg/kg) and xylazine (10 mg/kg) followed by intranasal inoculation with 50 μL of W-KP2 suspension of different dilutions (5.0×10^5, 5.0×10^6, 5.0×10^7, 5.0×10^8, 1.0×10^9, or 2.5×10^9 CFU/mouse, n = 10 per group), and then the minimum bacterial dose that triggered 100% death within 7-days [minimum lethal dose (MLD)] was determined (Xia et al., 2016). Finally, all surviving mice were euthanized by intravenous injection of Fatal Plus (sodium pentobarbital) (100 mg/kg).

The therapeutic effects of phage P-KP2, gentamicin and phage-antibiotic combination in the treatment of acute pneumonia caused by *K. pneumoniae* W-KP2 were evaluated based on the mouse model. Mice were challenged intranasally with 2 × MLD (1.0×10^9 CFU/mouse) of W-KP2 in reference to our previous study (Cheng et al., 2017). At 1 h post infection, mice were treated intranasally with P-KP2 after concentration (1.0×10^7 PFU/mouse, 1.0×10^8 PFU/mouse or 1.0×10^9 PFU/mouse), gentamicin (1.5 mg/kg), or P-KP2 (1.0×10^9 PFU/mouse) in combination with gentamicin (gentamicin was administered intranasally at 30 min after P-KP2 administration), respectively. The untreated group was administered with PBS buffer after W-KP2 challenge. The survival rate, body weight and health status in each group were recorded within 7 days follow-up period.

Three mice selected randomly from each treatment group (n = 30 per group) at every time point were euthanized using Fatal Plus (sodium pentobarbital) (100 mg/kg) every 24 h (lasting for 7 days) after infection. Blood was collected from the tail vein of these mice and then the bacterial load was determined by plating after serial dilution. Their lungs were carefully removed and photographed. After fixation with 4% formalin, the left lungs were embedded with paraffin and stained with hematoxylin and eosin (H&E) (Feldman and Wolfe, 2014), followed by

[1]http://wishart.biology.ualberta.ca/cgview/

[2]https://sourceforge.net/projects/phageterm

[3]https://toolkit.tuebingen.mpg.de/#/tools/hhpred

histopathological analysis through a microscope (Olympus CX-41; Olympus America, Center Valley, PA, United States). After weighing, the right lung tissues were immediately lysed and homogenized, then the lung homogenates were serially diluted and bacterial loads were determined by plating. Simultaneously, the phage titers in lung tissues were detected using the double-layer agar plate method. For enzyme-linked immunosorbent assay, the supernatants of lung homogenates were obtained according to our previous method (4°C, 5,000 × g, 10 min) (Cai et al., 2019a). The concentrations of interleukin 1β (IL-1β), interleukin 6 (IL-6), tumor necrosis factor-α (TNF-α), and interferon-γ (IFN-γ) in the supernatants were measured by ELISA kits (eBioscience, San Diego, CA, United States) according to the manufacturer's instructions.

Statistical Analysis

Survival curve analyses were performed using log-rank (Mantel–Cox) test. While other statistical data presented in this study were processed by One-way analysis of variance (ANOVA). GraphPad Prism 6 (GraphPad Software, Inc., San Diego, CA, United States) was utilized for chart generation. $P < 0.05$ were considered statistically significant. Error bars represented standard error of the mean.

RESULTS

The Characteristics of *K. pneumoniae* W-KP2 and Phage P-KP2

Since sequencing result of W-KP2 *wzc* gene was consistent with K47 serotype reference sequences, *K. pneumoniae* W-KP2 was identified as belonging to the K47 serotype (**Supplementary Figure 1**), which was resistant to the antibiotics listed in **Supplementary Table 1**, except for gentamicin, indicating that it is a MDR strain that may lead to ineffective antibiotic treatment.

A *Klebsiella* phage named vB_KpnM_P-KP2 (abbreviated as P-KP2) was isolated using *K. pneumoniae* W-KP2 in this study, and the initial titer of phage P-KP2 obtained after phage enrichment was 2.0×10^7 PFU/mL. The phage formed small circular translucent plaques (diameter < 1 mm) on the lawns of *K. pneumoniae* W-KP2 (**Figure 1A**). P-KP2 showed a prolate head with icosahedral structure (105 ± 5 nm in length and 79 ± 3 nm in diameter) and a long contractile tail (100 ± 10 nm) with a baseplate as observed with TEM (**Figure 1B**), which indicated that it belongs to the family *Myoviridae*. Among the 80 *K. pneumoniae* strains tested, phage P-KP2 could form both spots and plaques on 10 of them, including W-KP2 (**Supplementary Table 2**).

Phage titer of P-KP2 after propagation was highest at MOI 0.000001 with a titer of 7.5×10^7 PFU/mL (**Figure 2A**). Besides, the latent period of this phage was 30 min, after which the number of viral particles was rapidly increased. The proliferation of P-KP2 took about another 30 min to reach the growth plateau phase with a burst size of 204 PFU/cell (**Figure 2B**).

Bioinformatics Analyses of P-KP2 Genome

The genome of phage P-KP2 is a linear double-stranded DNA that is comprised of 172,138 bp with a G + C content of 41.9%, and the termini of the phage genome is located at 38,590 bp (**Supplementary Figure 2**). Comparative analysis of the complete nucleotide sequence indicates that several phages

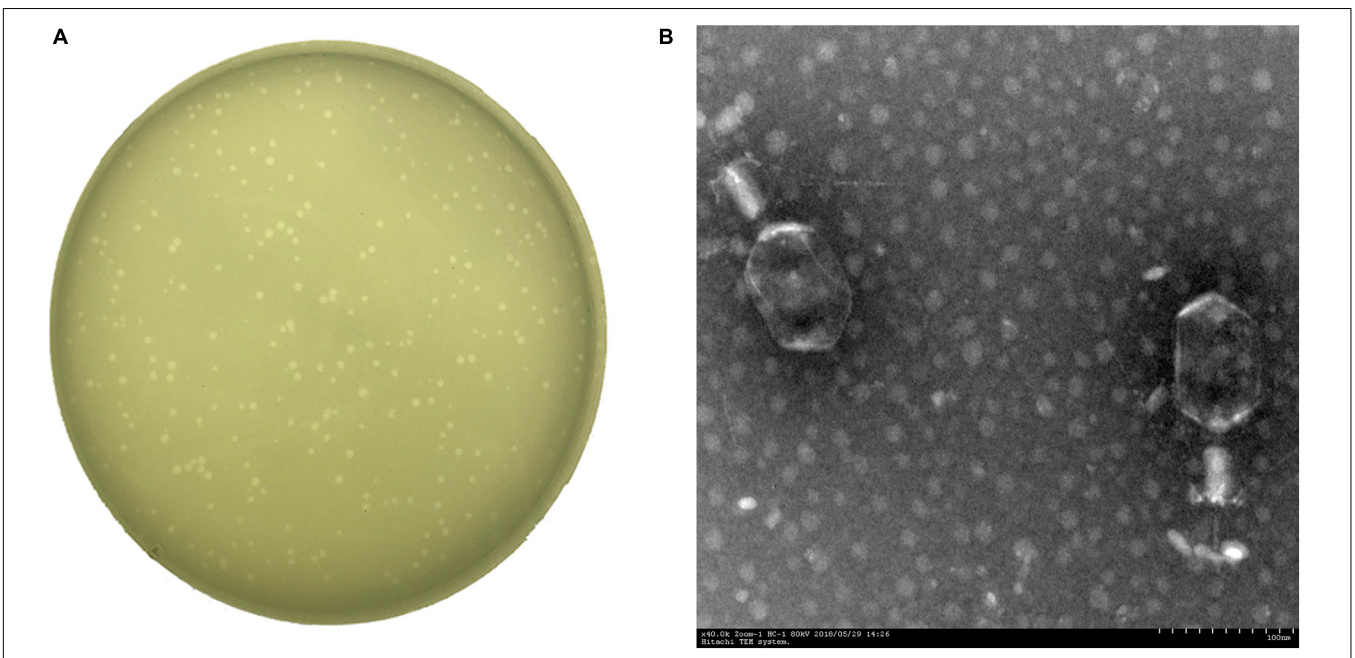

FIGURE 1 | The morphology of phage P-KP2. **(A)** The plaques formed by phage P-KP2 on the lawns of *K. pneumoniae* W-KP2. **(B)** The morphology of phage P-KP2 was determined by transmission electron microscopy (TEM). The scale bars represent 100 nm.

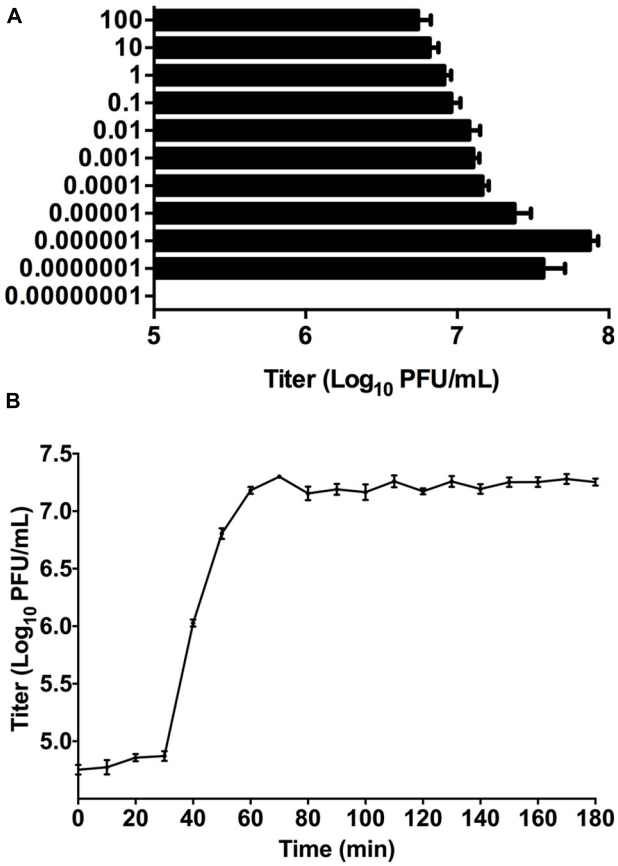

FIGURE 2 | The growth characteristics of P-KP2. **(A)** Titers of the phage under different MOI (phage/bacteria = 0.00000001, 0.0000001, 0.000001, 0.00001, 0.0001, 0.001, 0.01, 0.1, 1, 10, and 100), as indicated in the Y-axis. At the MOI of 0.000001, P-KP2 reached maximum titers. **(B)** One-step growth curve of P-KP2 was carried out at MOI = 0.1. Each data is shown as means ± SEM from three biological experiments.

show high similarity to P-KP2, including *Enterobacter* phage phiEap-3 (Zhao et al., 2019), *Klebsiella* phage Matisse (Provasek et al., 2015), *Klebsiella* phage KP27, *Klebsiella* phage KP15, *Klebsiella* phage PMBT1 (Koberg et al., 2017), *Klebsiella* phage KOX10, *Klebsiella* phage Miro (Mijalis et al., 2015), *Escherichia* phage phT4A (Pereira et al., 2017), and *Klebsiella* phage KOX8 (**Table 1**), which can be classified as a member of pseudo-T-even myophages which belong to "*KP15likevirus*" genus. Multiple genome alignment confirmed that these phages have parallel gene functional modules (**Figure 3**). Phylogenetic analyses of the large terminase subunits, major capsid proteins and DNA polymerases showed that P-KP2 has close evolutionary relationships with *Klebsiella* phage KP27 (**Figure 4**).

The complete genome of P-KP2 includes 264 predicted ORFs. Among all the ORFs, 120 are transcribed in one orientation, and 144 are transcribed in the opposite orientation; their arrangement at the whole-genome level was mapped (**Figure 5**). All predicted proteins were examined for similarity to known sequences deposited in the public databases of NCBI, and the obtained information was used to provide detailed annotations of the phage proteome. From **Figure 5** and **Supplementary Table 3**, it can be seen that 106 ORFs share apparent database matches with known functions and the rest 158 ORFs are assigned as hypothetical proteins. Aside lysogeny modules, morphogenesis modules (ORFs 9, 10, 43–46, 147–154, 235, 238–240, 242–252, 255–262, and 264) and DNA packaging modules (ORFs 253–254) can be clearly identified. However, many ORFs are widely distributed in the phage genome without forming an obvious module, ORFs that are associated with nucleotide metabolism and replication and ORFs that are related to metabolic correlation (**Figure 5**). The host lysis system of P-KP2 is composed of four parts, T holin lysis mediator (ORF48), spanin (ORF123 and ORF124), antiholin (ORF180), and endolysin (ORF197), which is consistent with the characteristics of the lysis modules of "*KP15likevirus*" genus (Zhao et al., 2019).

Most of the gene coding sites of P-KP2 show extremely high homology with their homologous phage, but there are some exceptions. Several loci (including ORFs 3, 20–21, 85, 135–136, and 206 of P-KP2) show different dissimilarity with homologous phages due to the deletion or insertion of a few bases. For example, P-KP2 gp85 (54,624–55,700 bp) has >98% coverage with homologous phages listed in **Table 1** at nucleotide level. However, P-KP2 ORF85 shows only 63–72% coverage with these phages. Actually, "C54409" and "T54410" in P-KP2 were inserted compared with homologous phages. Additionally, lacking one "C" between G11040 and C11041 compared with homologous phages, ORF20 and ORF21 were both predicted as parts of RNA ligase 2.

As a putative tail fiber protein, P-KP2 ORF46 shows less similarity with homologous phages either at the nucleotide or at the protein level (**Supplementary Figure 3**). HHPred analysis shows that ORF46 has some identity with tail spike of Enterobacteria phage Mu (976-1050 residues, PDB ID: 3VTN_A).

P-KP2 Shows Protective Effects Against *K. pneumoniae* Infection in a Mouse Model

The MLD of intranasal inoculation of *K. pneumoniae* W-KP2 was determined as 5.0×10^8 CFU/mouse. To monitor the therapeutic effect of phage P-KP2 on acute pneumonia caused by W-KP2, mice were infected with 2 × MLD (1.0×10^9 CFU/mouse). At the initial stage of infection (12 h), only a small amount of W-KP2 was colonized. However, without therapeutic intervention, the bacterial load in the lung raised to nearly 10^{10} CFU/g within 5 days (**Figure 6A**), and a considerable amount of bacteria entered the peripheral blood (6.7×10^6 CFU/mL) (**Figure 6B**). These untreated mice developed severe congestion and hemorrhage in the lung tissues as the disease progressed, most of the alveolar structures collapsed and partially disappeared, accompanied by fibrotic lesions (**Figure 7A** and **Supplementary Figure 6**). Besides, W-KP2 infection significantly induced the up-regulation of pro-inflammatory cytokines, such as IL-1β, IL-6, TNF-α, and IFN-γ in mice at 72 h after infection (**Figure 7B**). Accompanied by sustained weight loss and declining health status

TABLE 1 | Global genome comparison of P-KP2 with homologous phages.

	P-KP2	phiEap-3	Matisse	KP27	KP15
Host strain type	*Klebsiella pneumoniae*	*Enterobacter aerogenes*	*Klebsiella pneumoniae*	*Klebsiella pneumoniae*	*Klebsiella pneumoniae*
GenBank number	MT157285.1	KT321315.1	KT001918.1	HQ918180.1	GU295964.1
G + C content	41.9%	42.0%	41.8%	41.8%	41.8%
Genome size (bp)	172,138	175,814	176,081	174,413	174,436
Identity of P-KP2 BLASTN	100%	98%	99%	99%	99%
Query coverage of P-KP2	100%	97%	97%	94%	96%
	PMBT1	**KOX10**	**Miro**	**phT4A**	**KOX8**
Host strain type	*Klebsiella pneumoniae*	*Klebsiella oxytoca*	*Klebsiella pneumoniae*	*Escherichia coli*	*Klebsiella oxytoca*; *Klebsiella pneumoniae*
GenBank number	NC_042138.1	MN101223.1	KT001919.1	KX130727.1	MN101221.1
G + C content	41.9%	41.7%	41.8%	41.7%	41.9%
Genome size (bp)	175,206	168,074	176,055	170,698	131,200
Identity of P-KP2 BLASTN	99%	98%	97%	99%	99%
Query coverage of P-KP2	98%	91%	96%	90%	73%

(**Supplementary Figure 4**), all the mice of this group died within 5 days.

Phage P-KP2 had a concentration-dependent therapeutic effect on lung infection in mice. Neither 1.0×10^7 PFU/mouse nor 1.0×10^8 PFU/mouse of P-KP2 was able to eliminate bacteria from the lungs within 7 days (**Supplementary Figure 5A**). The phage titer in the lungs of mice treated with low concentration of phage (1.0×10^7 PFU/mouse) was lower than 10^4 PFU/g, and phages were completely exhausted within 3 days (**Supplementary Figure 5C**). Moreover, low concentration of phage (1.0×10^7 PFU/mouse) cannot stop bacterial proliferation and lung damage, leading to weight loss, poor health status and only 20% survival rate (**Supplementary Figures 4**, **5**D). When the therapeutic concentration was 1.0×10^9 PFU/mouse, the bacteria loads in the lungs were effectively reduced (**Figure 6A**) along with the increase of phage titers (**Figure 6C**). At the same time, the pneumonia symptoms of mice were significantly alleviated and the survival rate increased to 70% according to the results of 7 days monitoring, which was comparable to the therapeutic effect of gentamicin (**Figure 6D**). The lungs of gentamicin-treated and phage-treated mice showed mild congestion at 72 h post infection, but the texture remained tough and shiny. The histopathological changes of the two treatment groups had many similarities, both of which showed local capillary dilatation and a small amount of collapse in local alveolar walls, but most of the alveolar structures still in their normal morphology (**Figure 7A** and **Supplementary Figure 6**). In spite of P-KP2 (1.0×10^9 PFU/mouse) was less able to eliminate bacteria than gentamicin within 3 days of infection, phage treatment was more effective in eliminating residual bacteria from the lungs at the late stage of infection (**Figure 6A**). Unfortunately, we may not be able to obtain better phage treatment results because higher P-KP2 concentrations cannot be obtained. However, it is heartening that mice treated with both gentamicin and phage showed only transient respiratory symptoms and completely survived (**Figure 6D**). When P-KP2 was used in combination with gentamicin, the bacteria in the lungs was almost completely eliminated within 6 days (**Figure 6A**). Moreover, the lung tissue status of the dual treatment group never showed obvious pathological changes (**Figure 7A** and **Supplementary Figure 6**). Additionally, at 72 h after infection, the cytokine levels of the double-treated group were comparable to healthy mice, but both gentamicin-treated and phage-treated mice were slightly higher than that in the dual treatment group (**Figure 7B**). Therefore, for the lung infection in mice caused by W-KP2, the above results not only showed that P-KP2 had a good substitution effect on gentamicin, but also suggested that the combined effect of phage and gentamicin was far superior to that of a single administration.

DISCUSSION

According to the production of capsular polysaccharides (CPSs), *K. pneumoniae* can be divided into two major types: classic *K. pneumoniae* (cKP) and hypervirulent *K. pneumoniae* (hvKP). Unlike hvKP strains, which are prevalent in people with normal immunity, cKP strains are mainly found in populations with weakened immunity or immunodeficiency. Derived from the sputum, non-capsulated W-KP2 is a typical cKP strain. However, it is only sensitive to gentamicin in the drug sensitivity test including carbapenems, so it can be defined as a typical MDR *K. pneumoniae*. Although the virulence of W-KP2 could not be compared with the hypervirulent strains with capsules (especially K1 and K2 serotypes), high-dose (1.0×10^9 CFU/mouse) challenge through the respiratory tract still caused mice to die within 5 days. Even after 7 days of infection, residual strains could still be detected in gentamicin-treated mice. Therefore, once such MDR *K. pneumoniae* causes clinical infection, especially the immunodeficiency population as the target, it is likely that the lag of antibiotic treatment (appropriate antibiotics and doses need to be explored) will lead to delayed healing and even poor prognosis. What's more serious is that while medical workers are still struggling with hvKP and MDR-KP, CR-hvKP

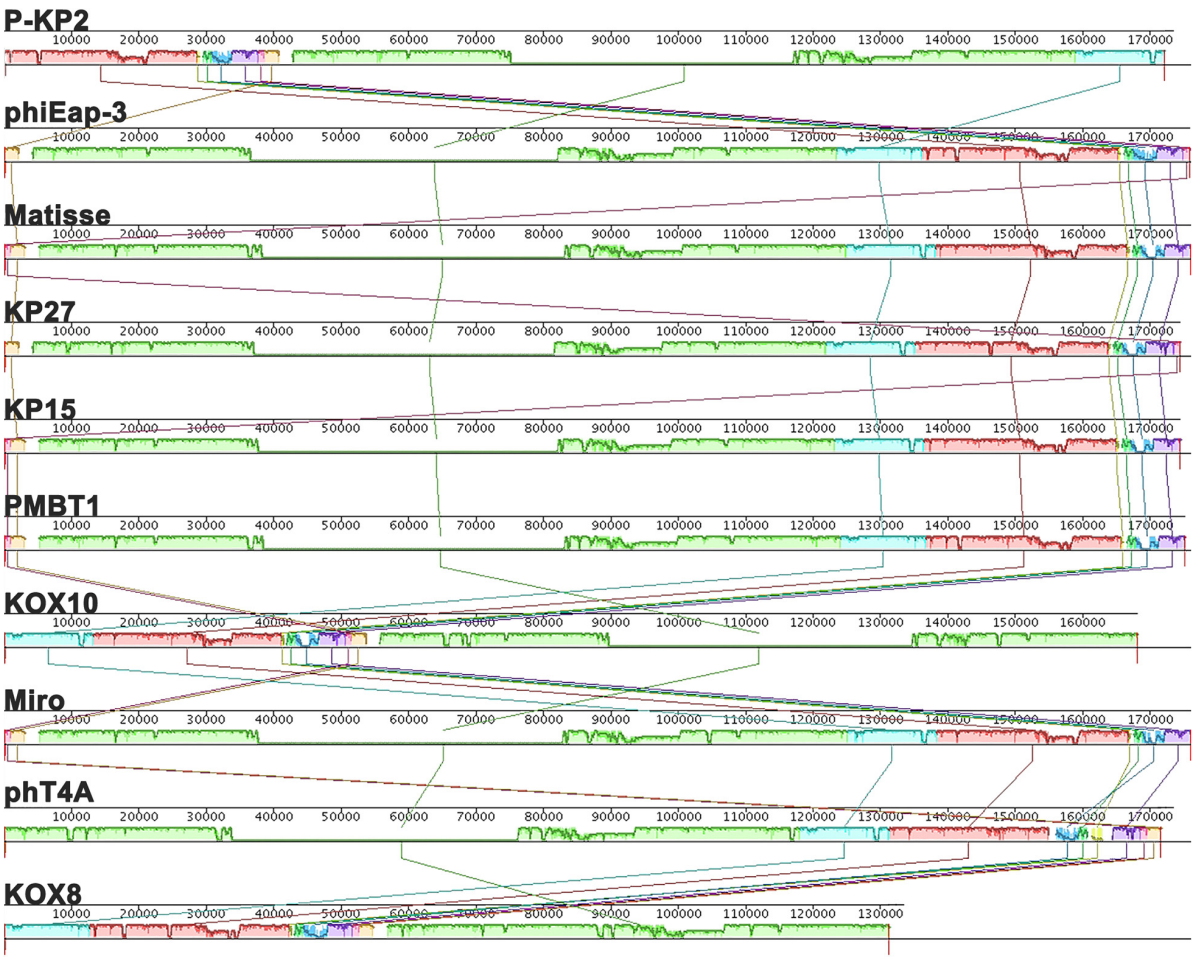

FIGURE 3 | Multiple genome alignments among P-KP2 and homologous phages. The graph was generated by Mauve software. To present the average conservation level in the genome sequence, the similarity of regions is indicated by the height of the bars. Fragment that are not aligned or specific to a particular genome are represented by white areas. Regions of homologous DNA shared by two or more genomes are defined as a local collinear blocks (LCBs), represented by boxes with the identical colors.

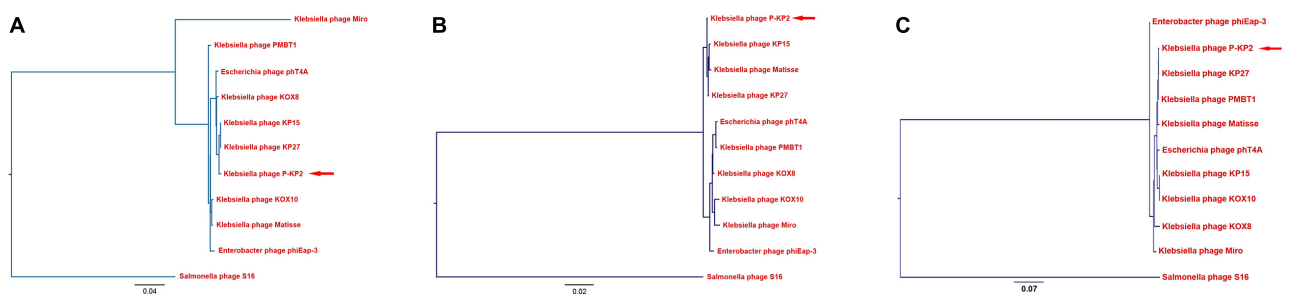

FIGURE 4 | Phylogenetic analyses of P-KP2 and homologous phages. **(A)** Phylogenetic tree based on terminase large subunit genes. **(B)** Phylogenetic tree based on genes of major capsid protein. **(C)** Phylogenetic tree based on genes of DNA polymerase. These sequences were compared using ClustalW, and the phylogenetic tree was generated by PHYLIP version 3.697 (Neighbor-Joining Method, 100 bootstrap replicates). Salmonella phage S16 was selected as the outgroup.

have quietly approached as a new threat, and this new type of strains are largely derived from the horizontal transfer of virulence plasmids or drug-resistant plasmids among strains that have existed for a long time in hospitals or communities. As confirmed by recent studies, some carbapenemase-producing strains, especially members of serotype K47, converted to CR-hvKP by obtaining pLVPK-like plasmids (Gu et al., 2018). It can be inferred that W-KP2 also has the possibility to evolve

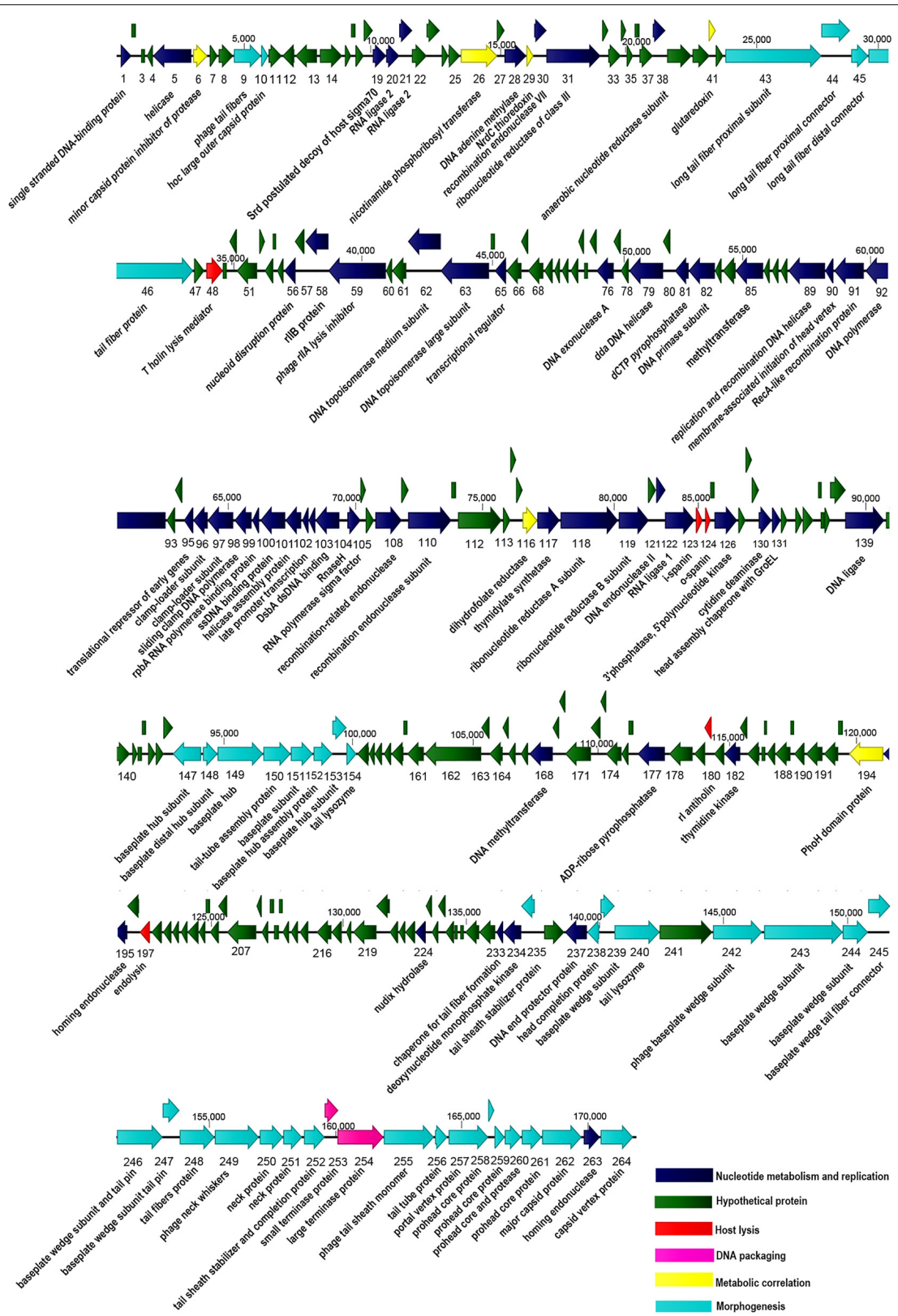

FIGURE 5 | Graphical representation of the phage P-KP2 genome. 264 ORFs and the direction of transcription are presented as arrows. Proposed modules are based on hypothetical functions predicted through bioinformatic analysis. The genome map was generated using CLC Main Workbench (version 8.0.1).

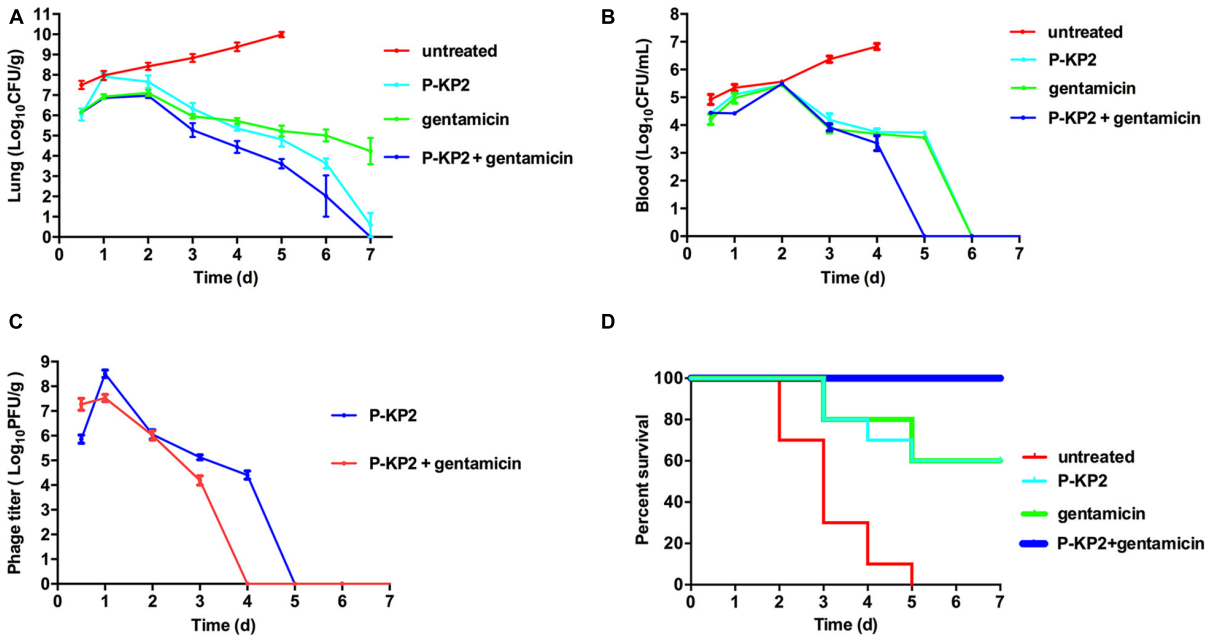

FIGURE 6 | Therapeutic effects of P-KP2 and gentamicin on *K. pneumoniae in vivo*. All the mice were challenged intranasally with 1.0×10^9 CFU/mouse of *K. pneumoniae* W-KP2. After 1 h post infection, they were intranasally treated with P-KP2 (1.0×10^9 PFU/mouse), gentamicin (1.5 mg/kg), or phage-antibiotic combination (gentamicin was administered intranasally at 30 min after P-KP2 administration), respectively. The untreated group was administered with PBS under the same conditions. **(A)** Bacterial loads in the lungs. At every 24 h (lasting for 7 days) after W-KP2 infection, the right lungs of the euthanized mice in each group were carefully separated, weighed and homogenized. Then the bacterial loads in the lung homogenates were detected after serial dilution ($n = 3$). **(B)** Bacterial loads in blood. Peripheral blood samples (10 μL) were obtained from the caudal veins of the anesthetized mice ($n = 3$). **(C)** Phage titers in the lungs. Phage titers of lung homogenates of each group were detected after serial dilution ($n = 3$). The above data represent the mean ± SEM of triplicate experiments. **(D)** Survival rates. Survival rates of W-KP2-infected mice in each group were determined. Each group contained ten mice. Statistical analysis was performed using the Kaplan-Meier method [$P < 0.0001$, log-rank (Mantel-Cox) test].

into CR-hvKP. Therefore, this study attempted to control the infection caused by W-KP2 *in vivo* through phage therapy and phage-antibiotic combination therapy and provided a solution to prevent such strains from evolving into CR-hvKP.

P-KP2 has extremely high sequence homology with *Enterobacter* phage phiEap-3 (Zhao et al., 2019) and *Escherichia* phage phT4A (Pereira et al., 2017). They all form small plaques with a diameter ≈ 1 mm, but their host spectrums are quite different. The host spectrums of phiEap-3 and phT4A are much wider than that of P-KP2, but they cannot lyse any *K. pneumoniae*. The host spectrum of phages largely depends on the three-dimensional structure of their receptor-binding proteins (RBPs), especially the C-terminus. With the functions of depolymerase or tail spike protein (TSP), most of RBPs are encoded in the tail fiber protein, and a few are located on the base plate or neck of the phage (Pires et al., 2016). In this study, P-KP2 ORF46, a putative tail fiber protein, had been predicted to be RBP of the phage due to its tail spike-like domain (976–1,050 residues, PDB ID: 3VTN_A), indicating that the protein may mediate specific binding of phage to the host outer membrane proteins (Tu et al., 2017). The C-terminus of ORF46 and its homologous proteins have low sequence conservation (**Supplementary Figure 3**), suggesting that gp46 may be originated from a later evolutionary stage in the process of horizontal gene exchange (Evseev et al., 2020). Besides, the unique C-terminus may determine the huge host spectrum difference between P-KP2 and its homologous phages. In fact, phage P-KP2 can specifically lyse K47 serotype *K. pneumoniae*. The reason for its narrow host spectrum may be that clinical isolates of this serotype are not common.

The high burst size of P-KP2 (204 PFU/cell) may depend on the multi-gene lysis system composed of T holin lysis mediator (ORF48), spanin (ORF123 and ORF124), antiholin (ORF180), and endolysin (ORF197). Antiholin can control the timing of host lysis by regulating holin, thereby gaining time for the replication and assembly of more progeny virions, resulting in a larger burst size of phages with multi-gene lysis systems (Cahill and Young, 2019). With such a high burst size and no harmful genes in the genome, P-KP2 has the potential to become a therapeutic agent for K47 serotype *K. pneumoniae* infection. In our study, P-KP2 treatment (1.0×10^9 PFU/mouse) alone significantly reduced inflammatory responses and pathological changes in mice with acute pneumonia *in vivo*. In addition, the survival rate of the group was comparable to that of treated with gentamicin, but it was significantly better in eliminating residual bacteria from lung tissue. Some recent studies have shown that the combined administration of phages and antibiotics is more effective than monotherapy in treating bacterial infections (Segall et al., 2019). Based on this, we attempted to treat acute pneumonia caused by W-KP2 with a combination of P-KP2

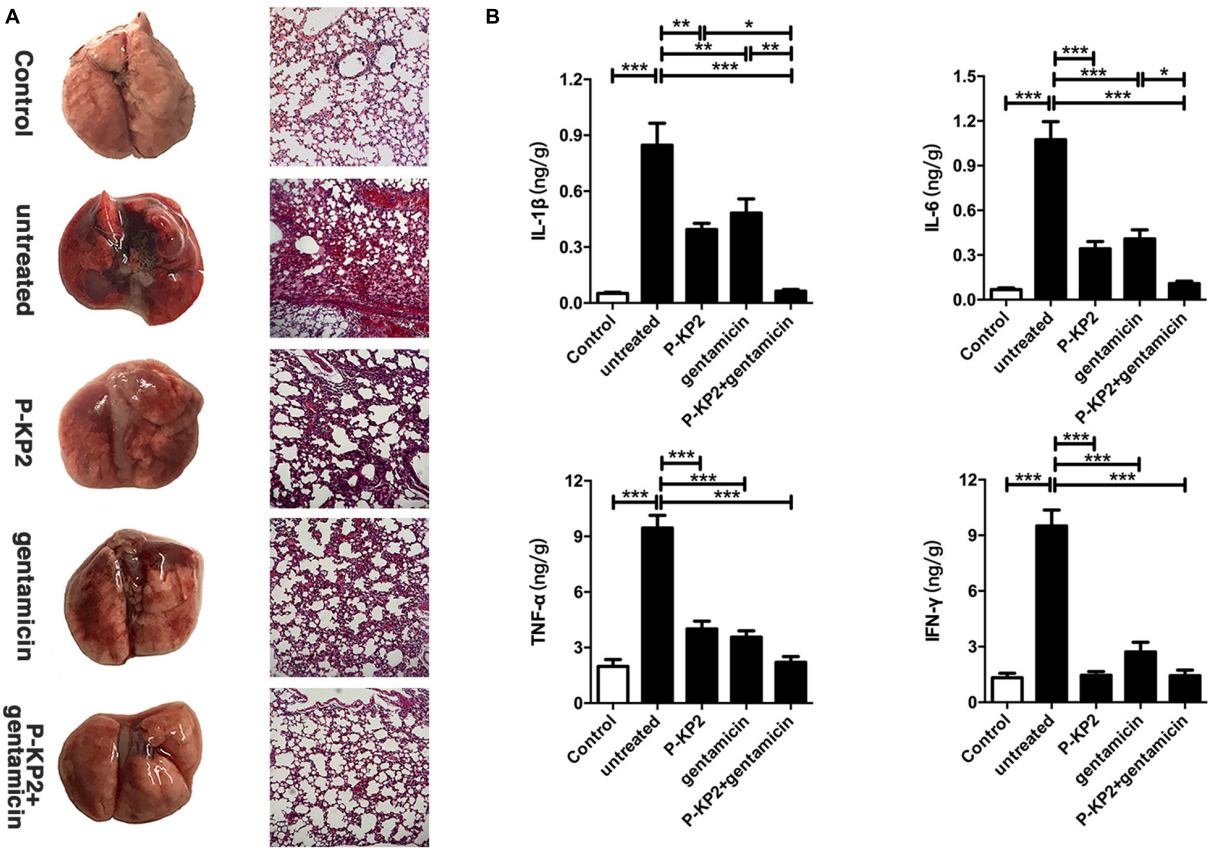

FIGURE 7 | Pathological changes and cytokine levels of mice in different groups. All the mice were challenged intranasally with 1.0×10^9 CFU/mouse of *K. pneumoniae* W-KP2. After 1 h post infection, they were intranasally treated with P-KP2 (1.0×10^9 PFU/mouse), gentamicin (1.5 mg/kg), or phage-antibiotic combination (gentamicin was administered intranasally at 30 min after P-KP2 administration), respectively. The untreated group was administered with PBS under the same conditions. **(A)** Pathological observation. At 72 h after W-KP2 infection, the lungs of the euthanized mice in each group were photographed after careful removal, and the sections of left lung tissues were stained with H&E (magnification, ×100). Lung tissue of healthy mice was served as a control. **(B)** Determination of cytokine levels. At 72 h after W-KP2 infection, cytokine levels (IL-1β, IL-6, TNF-α, and IFN-γ) in lung homogenates of mice treated with phage P-KP2, gentamicin, or phage-antibiotic combination were determined. Lung tissue homogenates of healthy mice were served as controls. *, **, and *** represent significant differences at $P < 0.05$, $P < 0.01$, and $P < 0.001$, respectively. Data represent the mean ± SEM of triplicate experiments.

and gentamicin. Encouragingly, not only did all the mice of the combined therapy group survive, but the pathological changes and inflammatory responses in the lungs were maintained at normal levels, possibly due to the effective inhibition of bacterial proliferation and complete elimination of residual bacteria by phage-antibiotic combination therapy. As an important reason for limiting the therapeutic effect of P-KP2 alone, this phage was easily eliminated by the immune system (**Supplementary Figure 5C**), and gentamicin seems to play a leading role in our combination therapy. However, phages specifically alter the surface structures of bacteria (polysaccharides, outer membrane proteins, etc.), thereby clearing the barriers for the infiltration of some antibiotics, indicating that phages have the effect of enhancing the sensitivity of bacteria to antibiotics (Segall et al., 2019). Therefore, the synergistic effect of phages on antibiotics is the key to the outstanding therapeutic effect of this combination therapy.

From the main way of treating bacterial infections worldwide, it will take time for us to get rid of dependence on antibiotics completely. However, both the combination of high-dose antibiotics and the treatment with new antibiotics may increase suffering and treatment costs for patients. Therefore, in the context of "weak" antibiotic efficacy, it is more realistic to seek ways to enhance the therapeutic effect of "low-grade" antibiotics. In summary, our study provided a clear case for phage-antibiotic combination against MDR *K. pneumoniae* infections and pointed out the direction to curb the emergence of more CR-hvKP, which has important theoretical significance and practical value.

CONCLUSION

The threat of MDR *K. pneumoniae* to public health in humans, especially in immunocompromised populations, and its evolution toward CR-hvKP have led to increased public recognition in the substitution or synergism of phage therapy for antibiotics. In this study, MDR *K. pneumoniae* W-KP2 was used as the host to isolate a novel myophage P-KP2 belonging to "*KP15 virus*" family, and then its biological characteristics

and genomics information were analyzed. Due to its high burst size and the absence of harmful genes, P-KP2 was analyzed as a candidate therapeutic agent against acute pneumonia caused by W-KP2. When administered with 1.0×10^9 PFU/mouse, the phage proliferated rapidly and completely eliminated the bacteria in the lungs within 7 days, which exceeded the therapeutic effect of gentamicin. More encouragingly, the combination of P-KP2 and gentamicin not only rescued all infected mice, but also effectively inhibited the development of inflammation. Therefore, as the first case of "*KP15 virus*" family phage to be applied for treatment, the processes of P-KP2 proliferation, promotion of bacterial elimination have been elucidated *in vivo*, which not only filled the gap in the phage library against K47 serotype *K. pneumoniae* infection, but also provided a theoretical basis for the subsequent phage-antibiotic combination therapies and blocking the occurrence of more CR-hvKP.

DATA AVAILABILITY STATEMENT

The completed genome sequence of Klebsiella phage P-KP2 has been deposited in the GenBank database under accession number MT157285.

ETHICS STATEMENT

The animal study was reviewed and approved by the Care and Use of Laboratory Animals of the Jilin University.

AUTHOR CONTRIBUTIONS

GW, ZG, YJ, XL, YG, HZ, HX, RZ, LB, SL, and LY assisted in carrying out the experiment. ZW and RC wrote the manuscript. XF, CS, LL, WH, and JG helped with the design of experimental ideas and the revision of manuscripts. All authors contributed to the article and approved the submitted version.

FUNDING

This work was financially supported through grants from the National Natural Science Foundation of China (Grant Nos. 32072824, 31872505, and U19A2038), the Natural Science Foundation of Jilin Province (Changchun, China; Grant No. 20200201120JC), the Jilin Province Science Foundation for Youths (Changchun, China; Grant No. 20190103106JH), the Achievement Transformation Project of the First Hospital of Jilin University (No. JDYYZH-1902025), the Shanghai Municipal Health Commission Scientific Research Project (Grant No. 20194Y0061), and the Fundamental Research Funds for the Central Universities.

SUPPLEMENTARY MATERIAL

The Supplementary Material for this article can be found online at: https://www.frontiersin.org/articles/10.3389/fmicb.2021.674068/full#supplementary-material

REFERENCES

Abedon, S. T. (2019). Phage-antibiotic combination treatments: antagonistic impacts of antibiotics on the pharmacodynamics of phage therapy? *Antibiotics (Basel)* 8:182. doi: 10.3390/antibiotics8040182

Altschul, S. F., Madden, T. L., Schaffer, A. A., Zhang, J., Zhang, Z., Miller, W., et al. (1997). Gapped BLAST and PSI-BLAST: a new generation of protein database search programs. *Nucleic Acids Res.* 25, 3389–3402. doi: 10.1093/nar/25.17.3389

Anand, T., Virmani, N., Kumar, S., Mohanty, A. K., Pavulraj, S., Bera, B. C., et al. (2020). Phage therapy for treatment of virulent *Klebsiella pneumoniae* infection in a mouse model. *J. Glob. Antimicrob. Resist.* 21, 34–41. doi: 10.1016/j.jgar.2019.09.018

Bao, J., Wu, N., Zeng, Y., Chen, L., Li, L., Yang, L., et al. (2020). Non-active antibiotic and bacteriophage synergism to successfully treat recurrent urinary tract infection caused by extensively drug-resistant *Klebsiella pneumoniae*. *Emerg. Microbes Infect.* 9, 771–774. doi: 10.1080/22221751.2020.1747950

Besemer, J., Lomsadze, A., and Borodovsky, M. (2001). GeneMarkS: a self-training method for prediction of gene starts in microbial genomes. Implications for finding sequence motifs in regulatory regions. *Nucleic Acids Res.* 29, 2607–2618. doi: 10.1093/nar/29.12.2607

Cahill, J., and Young, R. (2019). Phage lysis: multiple genes for multiple barriers. *Adv. Virus Res.* 103, 33–70. doi: 10.1016/bs.aivir.2018.09.003

Cai, R., Wang, G., Le, S., Wu, M., Cheng, M., Guo, Z., et al. (2019a). three capsular polysaccharide synthesis-related glucosyltransferases, gt-1, gt-2 and wcaj, are associated with virulence and phage sensitivity of *Klebsiella pneumoniae*. *Front. Microbiol.* 10:1189. doi: 10.3389/fmicb.2019.01189

Cai, R., Wang, Z., Wang, G., Zhang, H., Cheng, M., Guo, Z., et al. (2019b). Biological properties and genomics analysis of vB_KpnS_GH-K3, a *Klebsiella* phage with a putative depolymerase-like protein. *Virus Genes* 55, 696–706. doi: 10.1007/s11262-019-01681-z

Chadha, P., Katare, O. P., and Chhibber, S. (2017). Liposome loaded phage cocktail: enhanced therapeutic potential in resolving *Klebsiella pneumoniae* mediated burn wound infections. *Burns* 43, 1532–1543. doi: 10.1016/j.burns.2017.03.029

Cheng, M., Liang, J., Zhang, Y., Hu, L., Gong, P., Cai, R., et al. (2017). The Bacteriophage EF-P29 efficiently protects against lethal vancomycin-resistant enterococcus faecalis and alleviates gut microbiota imbalance in a murine bacteremia model. *Front. Microbiol.* 8:837. doi: 10.3389/fmicb.2017.00837

Darling, A. C., Mau, B., Blattner, F. R., and Perna, N. T. (2004). Mauve: multiple alignment of conserved genomic sequence with rearrangements. *Genome Res.* 14, 1394–1403. doi: 10.1101/gr.2289704

Davies, E. V., Winstanley, C., Fothergill, J. L., and James, C. E. (2016). The role of temperate bacteriophages in bacterial infection. *FEMS Microbiol. Lett.* 363:fnw015. doi: 10.1093/femsle/fnw015

Evseev, P. V., Lukianova, A. A., Shneider, M. M., Korzhenkov, A. A., Bugaeva, E. N., Kabanova, A. P., et al. (2020). Origin and evolution of studiervirinae bacteriophages infecting pectobacterium: horizontal transfer assists adaptation to new niches. *Microorganisms* 8:1707. doi: 10.3390/microorganisms8111707

Feldman, A. T., and Wolfe, D. (2014). Tissue processing and hematoxylin and eosin staining. *Methods Mol. Biol.* 1180, 31–43. doi: 10.1007/978-1-4939-1050-2_3

Gadagkar, R., and Gopinathan, K. P. (1980). Bacteriophage burst size during multiple infections. *J. Biosci.* 2, 253–259. doi: 10.1007/BF02703251

Garneau, J. R., Depardieu, F., Fortier, L. C., Bikard, D., and Monot, M. (2017). PhageTerm: a tool for fast and accurate determination of phage termini and packaging mechanism using next-generation sequencing data. *Sci. Rep.* 7:8292. doi: 10.1038/s41598-017-07910-5

Gong, P., Cheng, M., Li, X., Jiang, H., Yu, C., Kahaer, N., et al. (2016). Characterization of *Enterococcus faecium* bacteriophage IME-EFm5 and its endolysin LysEFm5. *Virology* 492, 11–20. doi: 10.1016/j.virol.2016.02.006

Gu, D., Dong, N., Zheng, Z., Lin, D., Huang, M., Wang, L., et al. (2018). A fatal outbreak of ST11 carbapenem-resistant hypervirulent *Klebsiella pneumoniae* in

a Chinese hospital: a molecular epidemiological study. *Lancet Infect. Dis.* 18, 37–46. doi: 10.1016/S1473-3099(17)30489-9

Hampton, H. G., Watson, B. N. J., and Fineran, P. C. (2020). The arms race between bacteria and their phage foes. *Nature* 577, 327–336. doi: 10.1038/s41586-019-1894-8

Hodyra-Stefaniak, K., Miernikiewicz, P., Drapala, J., Drab, M., Jonczyk-Matysiak, E., Lecion, D., et al. (2015). Mammalian host-versus-phage immune response determines phage fate in vivo. *Sci. Rep.* 5:14802. doi: 10.1038/sre14802

Hsu, C. R., Lin, T. L., Pan, Y. J., Hsieh, P. F., and Wang, J. T. (2013). Isolation of a bacteriophage specific for a new capsular type of *Klebsiella pneumoniae* and characterization of its polysaccharide depolymerase. *PLoS One* 8:e70092. doi: 10.1371/journal.pone.0070092

Ji, Y., Cheng, M., Zhai, S., Xi, H., Cai, R., Wang, Z., et al. (2019). Preventive effect of the phage VB-SavM-JYL01 on rabbit necrotizing pneumonia caused by *Staphylococcus aureus*. *Vet. Microbiol.* 229, 72–80. doi: 10.1016/j.vetmic.2018.12.021

Kaabi, S. A. G., and Musafer, H. K. (2019). An experimental mouse model for phage therapy of bacterial pathogens causing bacteremia. *Microb. Pathog.* 137:103770. doi: 10.1016/j.micpath.2019.103770

Koberg, S., Brinks, E., Fiedler, G., Husing, C., Cho, G. S., Hoeppner, M. P., et al. (2017). Genome sequence of *Klebsiella pneumoniae* bacteriophage PMBT1 isolated from raw sewage. *Genome Announc.* 5:e00914-16. doi: 10.1128/genomeA.00914-16

Lin, T. L., Hsieh, P. F., Huang, Y. T., Lee, W. C., Tsai, Y. T., Su, P. A., et al. (2014). Isolation of a bacteriophage and its depolymerase specific for K1 capsule of *Klebsiella pneumoniae*: implication in typing and treatment. *J. Infect. Dis.* 210, 1734–1744. doi: 10.1093/infdis/jiu332

Margulies, M., Egholm, M., Altman, W. E., Attiya, S., Bader, J. S., Bemben, L. A., et al. (2005). Genome sequencing in microfabricated high-density picolitre reactors. *Nature* 437, 376–380. doi: 10.1038/nature03959

Mijalis, E. M., Lessor, L. E., Cahill, J. L., Rasche, E. S., and Kuty Everett, G. F. (2015). Complete genome sequence of *Klebsiella pneumoniae* carbapenemase-producing K. pneumoniae myophage miro. *Genome Announc.* 3:e01137-15. doi: 10.1128/genomeA.01137-15

Navon-Venezia, S., Kondratyeva, K., and Carattoli, A. (2017). *Klebsiella pneumoniae*: a major worldwide source and shuttle for antibiotic resistance. *FEMS Microbiol. Rev.* 41, 252–275. doi: 10.1093/femsre/fux013

Nobrega, F. L., Costa, A. R., Kluskens, L. D., and Azeredo, J. (2015). Revisiting phage therapy: new applications for old resources. *Trends Microbiol.* 23, 185–191. doi: 10.1016/j.tim.2015.01.006

Paczosa, M. K., and Mecsas, J. (2016). *Klebsiella pneumoniae*: going on the offense with a strong defense. *Microbiol. Mol. Biol. Rev.* 80, 629–661. doi: 10.1128/mmbr.00078-15

Pan, Y. J., Lin, T. L., Chen, C. T., Chen, Y. Y., Hsieh, P. F., Hsu, C. R., et al. (2015). Genetic analysis of capsular polysaccharide synthesis gene clusters in 79 capsular types of *Klebsiella* spp. *Sci. Rep.* 5:15573. doi: 10.1038/srep15573

Pan, Y. J., Lin, T. L., Chen, Y. H., Hsu, C. R., Hsieh, P. F., Wu, M. C., et al. (2013). Capsular types of *Klebsiella pneumoniae* revisited by wzc sequencing. *PLoS One* 8:e80670. doi: 10.1371/journal.pone.0080670

Pereira, C., Moreirinha, C., Lewicka, M., Almeida, P., Clemente, C., Romalde, J. L., et al. (2017). Characterization and in vitro evaluation of new bacteriophages for the biocontrol of *Escherichia coli*. *Virus Res.* 227, 171–182. doi: 10.1016/j.virusres.2016.09.019

Pires, D. P., Oliveira, H., Melo, L. D., Sillankorva, S., and Azeredo, J. (2016). Bacteriophage-encoded depolymerases: their diversity and biotechnological applications. *Appl. Microbiol. Biotechnol.* 100, 2141–2151. doi: 10.1007/s00253-015-7247-0

Provasek, V. E., Lessor, L. E., Cahill, J. L., Rasche, E. S., and Kuty Everett, G. F. (2015). Complete genome sequence of carbapenemase-producing *Klebsiella pneumoniae* myophage matisse. *Genome Announc.* 3:e01136-15. doi: 10.1128/genomeA.01136-15

Sambrook, J., and Russell, D. W. (2006). Precipitation of Bacteriophage *Lambda* Particles from large-scale lysates. *CSH Protoc.* 2006:pdb.rot3966. doi: 10.1101/pdb.prot3966

Segall, A. M., Roach, D. R., and Strathdee, S. A. (2019). Stronger together? Perspectives on phage-antibiotic synergy in clinical applications of phage therapy. *Curr. Opin. Microbiol.* 51, 46–50. doi: 10.1016/j.mib.2019.03.005

Shimada, M. K., and Nishida, T. (2017). A modification of the PHYLIP program: a solution for the redundant cluster problem, and an implementation of an automatic bootstrapping on trees inferred from original data. *Mol. Phylogenet. Evol.* 109, 409–414. doi: 10.1016/j.ympev.2017.02.012

Stothard, P., and Wishart, D. S. (2005). Circular genome visualization and exploration using CGView. *Bioinformatics* 21, 537–539. doi: 10.1093/bioinformatics/bti054

Sunagawa, S., DeSantis, T. Z., Piceno, Y. M., Brodie, E. L., DeSalvo, M. K., Voolstra, C. R., et al. (2009). Bacterial diversity and White Plague Disease-associated community changes in the Caribbean coral *Montastraea faveolata*. *ISME J.* 3, 512–521. doi: 10.1038/ismej.2008.131

Tu, J., Park, T., Morado, D. R., Hughes, K. T., Molineux, I. J., and Liu, J. (2017). Dual host specificity of phage SP6 is facilitated by tailspike rotation. *Virology* 507, 206–215. doi: 10.1016/j.virol.2017.04.017

Xia, F., Li, X., Wang, B., Gong, P., Xiao, F., Yang, M., et al. (2016). Combination therapy of LysGH15 and apigenin as a new strategy for treating pneumonia caused by staphylococcus aureus. *Appl. Environ. Microbiol.* 82, 87–94. doi: 10.1128/AEM.02581-15

Zhao, J., Zhang, Z., Tian, C., Chen, X., Hu, L., Wei, X., et al. (2019). Characterizing the biology of lytic bacteriophage vb_eaem_phieap-3 infecting multidrug-resistant *Enterobacter aerogenes*. *Front. Microbiol.* 10:420. doi: 10.3389/fmicb.2019.00420

Zimmermann, L., Stephens, A., Nam, S. Z., Rau, D., Kubler, J., Lozajic, M., et al. (2018). A completely reimplemented MPI bioinformatics toolkit with a new HHpred server at its core. *J. Mol. Biol.* 430, 2237–2243. doi: 10.1016/j.jmb.2017.12.007

Conflict of Interest: The authors declare that the research was conducted in the absence of any commercial or financial relationships that could be construed as a potential conflict of interest.

Copyright © 2021 Wang, Cai, Wang, Guo, Liu, Guan, Ji, Zhang, Xi, Zhao, Bi, Liu, Yang, Feng, Sun, Lei, Han and Gu. This is an open-access article distributed under the terms of the Creative Commons Attribution License (CC BY). The use, distribution or reproduction in other forums is permitted, provided the original author(s) and the copyright owner(s) are credited and that the original publication in this journal is cited, in accordance with accepted academic practice. No use, distribution or reproduction is permitted which does not comply with these terms.

frontiers in Microbiology

ORIGINAL RESEARCH
published: 20 May 2021
doi: 10.3389/fmicb.2021.637490

Evolutionarily Stable Coevolution Between a Plastic Lytic Virus and Its Microbial Host

*Melinda Choua[1], Michael R. Heath[1] and Juan A. Bonachela[2]**

[1] Marine Population Modeling Group, Department of Mathematics and Statistics, University of Strathclyde, Scotland, United Kingdom, [2] Department of Ecology, Evolution and Natural Resources, Rutgers University, New Brunswick, NJ, United States

Hosts influence and are influenced by viral replication. Cell size, for example, is a fundamental trait for microbial hosts that can not only alter the probability of viral adsorption, but also constrain the host physiological processes that the virus relies on to replicate. This intrinsic connection can affect the fitness of both host and virus, and therefore their mutual evolution. Here, we study the coevolution of bacterial hosts and their viruses by considering the dependence of viral performance on the host physiological state (viral plasticity). To this end, we modified a standard host-lytic phage model to include viral plasticity, and compared the coevolutionary strategies emerging under different scenarios, including cases in which only the virus or the host evolve. For all cases, we also obtained the evolutionary prediction of the traditional version of the model, which assumes a non-plastic virus. Our results reveal that the presence of the virus leads to an increase in host size and growth rate in the long term, which benefits both interacting populations. Our results also show that viral plasticity and evolution influence the classic host quality-quantity trade-off. Poor nutrient environments lead to abundant low-quality hosts, which tends to increase viral infection time. Conversely, richer nutrient environments lead to fewer but high-quality hosts, which decrease viral infection time. Our results can contribute to advancing our understanding of the microbial response to changing environments. For instance, both cell size and viral-induced mortality are essential factors that determine the structure and dynamics of the marine microbial community, and therefore our study can improve predictions of how marine ecosystems respond to environmental change. Our study can also help devise more reliable strategies to use phage to, for example, fight bacterial infections.

Keywords: phage (bacteriophage), virus modeling, lysis, viral latency, *E. coli*, T phage, host-virus interactions

OPEN ACCESS

Edited by:
Xuesong He,
The Forsyth Institute, United States

Reviewed by:
Pradeep Ram Angia Sriram,
UMR 6023 Laboratoire Microorganismes Génome Et Environnement (LMGE), France
Kyle Edwards,
University of Hawaii at Manoa, United States
Jozsef Farkas,
University of Stirling, United Kingdom

****Correspondence:***
Juan A. Bonachela
juan.bonachela@rutgers.edu

Specialty section:
This article was submitted to Virology, a section of the journal Frontiers in Microbiology

Received: *03 December 2020*
Accepted: *09 April 2021*
Published: *20 May 2021*

Citation:
Choua M, Heath MR and Bonachela JA (2021) Evolutionarily Stable Coevolution Between a Plastic Lytic Virus and Its Microbial Host. Front. Microbiol. 12:637490. doi: 10.3389/fmicb.2021.637490

INTRODUCTION

Cell size is a key trait for microbial systems. Replication rates and physiological traits are generally correlated with cell size, both within and across species (Litchman et al., 2007). For virus-bacteria interactions, the size of the host is particularly important. In this paper, we focus on viral infections as an evolutionary selective pressure for host body size.

The adsorption of viruses to host cells depends on a combination of multiple factors. Host size influences the probability of host-virus encounter (Delbrück, 1940; Rabinovitch et al., 2002), and the density of host receptors to which the virus attaches (Schwartz, 1976; Berg and Purcell, 1977). In addition, the size of the host influences the surface-to-volume ratio, which triggers additional consequences e.g., increasing cell size decreases the diffusion flux per unit cell volume of external nutrient into the cell, but increases internal diffusion rates (Gallet et al., 2017). Both external and internal diffusion rates affect the mobility of intracellular resources used by the host. The latter, among other factors influenced by cell size such as resource uptake, affects the host physiological state. Here, we use growth rate as a proxy for host physiological state because it captures a diversity of intracellular indicators (Bremer and Dennis, 2008). In turn, the host physiological state influences the performance of the viral infection (Calendar and Abedon, 2005) and thus the dynamics of both viral and bacterial populations (Choua and Bonachela, 2019).

Viral infection starts when the virus encounters a host and becomes irreversibly attached onto a specific receptor at the host surface, with the frequency of successful encounters defining the adsorption rate (Calendar and Abedon, 2005). Once adsorbed, the virus perforates the cell's membrane and inserts its genome into the host cytoplasm, which triggers the biosynthesis of viral genome and proteins by the host machinery. The host machinery (ribosomes, ATP, etc.) is therefore monopolized by the virus to transcribe proteins that will constitute the viral offspring. The time between attachment and the assembly of the first virion defines the eclipse period, and the number of virions assembled per unit time is the maturation rate, both depending mainly on the host physiological state. The lytic cycle ends with the lysis of the host and the consequent release of virions into the environment (Abedon et al., 2003). The time between adsorption and host lysis, and number of virions released to the environment per infection, define the latent period and burst size, respectively. For a given host growth rate, longer latent periods typically lead to larger burst sizes (Abedon, 1989; Gnezda-Meijer et al., 2006; Wang, 2006).

Experimental work has shown that these key viral traits are not fixed, but change with the host physiological state (Rabinovitch et al., 2002; You et al., 2002; Birch et al., 2012; Golec et al., 2014): eclipse and latent periods decrease, and maturation rate and burst size increase, with host growth rate. Thus, intracellular changes in the host (effectively the phage's environment) lead to either active or passive responses by the virus, which are typically referred to as viral phenotypic plasticity (Abedon et al., 2001; Choua and Bonachela, 2019).

Viral plasticity has been shown to have important ecological and evolutionary implications for host-phage systems (Thyrhaug et al., 2003; Weitz and Dushoff, 2008; Wang and Goldenfeld, 2010; Edwards and Steward, 2018; Choua and Bonachela, 2019; Choua et al., 2020). It is yet to be determined, however, how viral plasticity affects the evolution of the host and, more specifically, the evolution of a trait so important for bacteria-virus interactions as host body size. Larger bacterial cell sizes lead to higher maximal growth rates (Gallet et al., 2017), but typically decrease uptake affinity (Wirtz, 2002) and render the host more susceptible to viral adsorption (Delbrück, 1940). Accounting for viral plasticity, a host with a higher growth rate will not only replicate faster but will also facilitate viral replication (i.e., the virus will release more virions in a shorter time) (Choua and Bonachela, 2019). This change, in turn, may alter the selection pressure on e.g., the viral latent period, as an increase in infection time enables the release of more virions but decreases the opportunities of subsequent infections by the new offspring (Choua and Bonachela, 2019). Here, we aim to understand from an evolutionary viewpoint how host and virus affect each other in different environments, with emphasis on how viral plasticity might affect their coevolution.

Bacteria-phage coevolution has previously been studied in the context of an "arms race" (Morgan and Koskella, 2011), e.g., using theoretical systems where the host evolves resistance by changing the receptors used by the virus for attachment at a fitness cost, and the phage responds to this resistance by adapting its tail fiber to overcome the receptor changes (Weitz et al., 2005; Menge and Weitz, 2009). These studies showed that, for example, coevolution maintains phenotypic and genetic diversity within microbial communities (Koskella and Brockhurst, 2014). However, none of these studies have considered how the presence of an inherently plastic virus affects this coevolution.

To fill this knowledge gap, here we use a standard host-lytic phage model that we modified to include viral plasticity. To implement coevolution, we used a numerical ecoevolutionary framework that focuses on host size and viral latent period as representative evolving traits. With this framework, we compare the traits that emerge under coevolution to those emerging when host evolves without virus, and to those obtained in previous work when host does not evolve but virus does (Choua and Bonachela, 2019). Theoretical studies like ours can help understand and predict the coevolutionary dynamics of host and phage, and therefore contribute to a wide variety of fields, from increasing the effectiveness and safety of phage therapy to improving the reliability of biogeochemical models, since bacterioplankton cell size plays a central role in the prediction of the response of marine ecosystems to climate change (Finkel et al., 2009).

MATERIALS AND METHODS

Model Description

To represent the ecological dynamics of the host- phage system, we used a well-known model that considers explicitly the delay between infection and lysis (Levin et al., 1977). This model has been ecologically validated by experiments, and proven to provide evolutionarily meaningful outcomes (Bonachela and Levin, 2014). The model keeps track of the dynamics of a generic nutrient (N), uninfected hosts cells (C), infected hosts (I) and extracellular viruses (V). The environmental conditions are set up to those of a chemostat, i.e., a well-stirred controlled environment in which the host and phage encounter each other randomly. Because we assume that, once a host is infected, its machinery is devoted to viral production, infected hosts do not replicate

and therefore the host's generation time does not constrain the viral latent period. We further consider that bacteria grow in the limited volume of the chemostat, and thus system-size effects can trigger competition for space, light, or other resources not explicitly modeled here that can limit/hinder population growth. This crowding effect can be implemented through a density-dependent term, in our case a quadratic loss term that only affects free hosts as uptake and growth stop at infection.

Thus, assuming that a host phenotype *i* is characterized solely by its size (i.e., all host types are phenotypically identical except for their size and consequently any trait related to it), and a viral phenoptype *j* is characterized by its latent period, the equations for the dynamics of the different phenotype populations and the nutrient are given by:

$$\frac{dN}{dt} = w\,(N_0 - N) - \frac{1}{Y}\sum_i \mu_i(N) C_i \quad (1)$$

$$\frac{dC_i(t)}{dt} = \mu_i\, C_i - k_i\, C_i \sum_j V_j - w\, C_i - \alpha\, C_i \sum_n C_n \quad (2)$$

$$\frac{dI_j(t)}{dt} = \sum_i k_i\, C_i V_j - \sum_i k_i C_{i\,t-L_j} V_{j\,t-L_j} e^{-wL_j} - w\, I_j \quad (3)$$

$$\frac{dV_j(t)}{dt} = B_{j\mu_i} \sum_i k_i C_{i\,t-L_j} V_{j\,t-L_j} e^{-wL_j} - \sum_i k_i C_i V_j - (m+w) V_j \quad (4)$$

(see definitions of symbols and units in **Table 1**). The first equation represents the dynamics of the concentration of the most limiting nutrient within the chemostat, with an inflow and outflow of nutrient (first term) and the nutrient uptake by all possible host phenotypes present in the chemostat at time t (second term). For the sake of concreteness, we assume that carbon is the most limiting nutrient. Note that we assume the yield factor *Y* (i.e., how much the host population can grow per unit of resource) to be the same for all host phenotypes. Equation (2) describes the growth of each host phenotype population, C_i, as a result of reproduction (first term), infection by the different viral phenotypes present in the chemostat at time *t* (second term), bacterial loss due to dilution (third term), and population growth slowdown due to crowding (fourth term). Equation (3) keeps track of the cells infected by viral phenotype *j* (equally, the number of intracellular viruses, as we consider that a host can be infected by only a single viral individual, i.e., there is no superinfection). The first term represents the new infected individuals resulting from the adsorption of that specific *j* viral phenotype. Infected cells disappear during dilution (last term) or due to the lysis of the cells that became infected exactly one latent period (L_j) in the past (second term, where e^{-wL_j} is the probability for infected cells to survive dilution during the latent period). The lysis of these infected cells releases new free phage for viral phenotype *j* (first term in Eq. (4), with *B* representing the burst size, see below). This pool of free phage then decreases due to phage adsorption (second term), and natural mortality and dilution (last term).

We assume that free hosts grow according to the classic Monod equation (Monod, 1949):

$$\mu_i(N) = \mu_{max}(r_i)N/(N + K_n(\mu_{max})) \quad (5)$$

where $\mu_{max}(r_i)$ is the maximum growth rate, and $K_n(\mu_{max})$ (half saturation constant for growth) is inversely correlated with the affinity of the uptake/growth machinery for this nutrient. As explained below, both traits depend on the host's cell size, r_i (Chien et al., 2012).

We use this model to represent host and phage coevolution by letting the host size and viral latent period evolve. We implement evolution using a genetic algorithm in which the phenotype with the highest probability to be selected for mutation (i.e., the one with the highest relative abundance in the system) generates a new mutant phenotype. A new host phenotype is identical to the parental cell except for its radius, chosen randomly from a normal distribution centered on the parental value and with a standard deviation of 0.1 microns. Similarly, a new viral phenotype is identical to the parent except for the value of the latent period, chosen randomly within a normal distribution centered on the parental value with a standard deviation of 10^{-3} days (narrowed to 10^{-4} days for the last 5,000 days of the simulation, when the algorithm is expected to have reached the vicinity of the evolutionary steady state). This leads to the addition of a new population every time a host mutant and/or a virus mutant join the system (Menge and Weitz, 2009; Choua and Bonachela, 2019). Note that, here, any viral phenotypes can infect any of the host phenotypes (i.e., generalist virus). Although phage are relatively specific (i.e., virus adsorbs to only a limited subset of the total bacteria), they have been shown to become generalist when coevolving with their host (Hall et al., 2011).

Host Trait Set

For most microorganisms, size is a master trait because it affects most aspects of their life cycle (Litchman et al., 2007). Although the metabolic theory of ecology states that the growth rate of microbes decreases with increasing body size (Brown et al., 2004), recent experimental data showed that maximal growth rates tend to increase with body size for organisms smaller than six microns (Gallet et al., 2017; Ward et al., 2017). These data revealed a key trade-off between rates of resource acquisition and the rate of internal metabolism (i.e., μ_{max}), which suggests different limiting factors for small and large organisms. For small cells such as bacteria, molecular transit time inside the cell can be the limiting factor whereas uptake rate limits larger cells (Gallet et al., 2017); also, the rate at which internal quotas are replenished by nutrient uptake limits smaller cells but nutrient conversion into biomass limits larger cells (Ward et al., 2017).

Here, we choose size as single trait characterizing the host, and use allometries to calculate the rest of trait values that are relevant for host dynamics. We specifically focus on *Escherichia coli* as host, but our approach can be generalized to any bacterium. Existing experimental work provides an allometric expression

TABLE 1 | Symbols for variables and parameters used 1in the model.

Symbol	Description	Units	Value	References
N	Dissolved inorganic nutrient concentration	mol l^{-1}	Ecological variable, Eq. 1	Levin et al., 1977, for the equations
C	Non-infected-host concentration	cell l^{-1}	Ecological variable, Eq. 2	
V	Free virus concentration	cell l^{-1}	Ecological variable, Eq. 3	
μ	Non-infected-host population growth rate	d^{-1}	Ecological variable, Eq. 4	Monod, 1949, for the equation
Host parameters/traits				
r	Equivalent spherical radius	μm	Evolutionary variable	Loferer-Krößbacher et al., 1998
μ_{max}	Maximum host population growth rate	d^{-1}	Eq. 6	Gallet et al., 2017
c, h	Parameters Eq. 6	—	c = 0.33 h = 3.8	Gallet et al., 2017
K_{ref}	Half-saturation constant for μ_{max} = 0	mol l^{-1}	3.05×10^{-8}	Wirtz, 2002
μ_{ref}	Asymptotic μ_{max} for $K_n \rightarrow \infty$	d^{-1}	32.4	Wirtz, 2002
K_n	Half-saturation constant for growth	mol	Eq. 7	Wirtz, 2002
Y	Yield parameter	cell mol^{-1}	9×10^{13}	Choua and Bonachela, 2019
$\mu_{max,\ experiment}$	Maximum growth rate in the experiment	d^{-1}	40.8	You et al., 2002
α	Parameter of crowding effect	l d^{-1} $cell^{-1}$	0–12 $\times 10^{-7}$	Sensitivity analysis
Viral parameters/traits				
D	Diffusion of viral particle	m^2 s^{-1}	4.3132×10^{-12}	Calculated using Stokes-Einstein expression
m	Viral decay rate	d^{-1}	0.09	De Paepe and Taddei, 2006
k	Adsorption rate	l $virus^{-1}$ d^{-1}	4π D $Conv_3$ r	Delbrück, 1940
E(μ)	Eclipse period	d	Eq. 8	Choua and Bonachela, 2019
M(μ)	Maturation rate	virions d^{-1}	Eq. 9	Choua and Bonachela, 2019
L	Latent period	d	Evolutionary variable	
B	Burst size	virions $cell^{-1}$	B = M (L-E)	Wang, 2006
Chemostat parameters				
w	Chemostat dilution rate	d^{-1}	1–30	Ranges set by Eq(7) and range for r
N_0	Dissolved inorganic nutrient supply concentration	mol l^{-1}	9×10^{-5}	Sensitivity analysis
Conversion constants				
$Conv_1$	Constant to convert from (ml) to (μm^3)	$\mu m^3 ml^{-1}$	10^{-12}	—
$Conv_2$	Constant to convert from ($hour^{-1}$) to (d^{-1})	hour d^{-1}	24	—
$Conv_3$	Constant to convert from (m^3 s^{-1}) to (l d^{-1})	l s d^{-1} m^{-3}	$86{,}400 \times 10^3$	—

linking the radius, r, of the bacterium (assumed spherical) and its maximum potential for growth, $\mu_{\max}$ (Gallet et al., 2017; Shestopaloff, 2016):

$$\mu_{max}(r_i) = Conv_2\ 10^{c\ log_{10}(4\pi Conv_1 r_i^3/3)+h} \quad (6)$$

(see **Table 1** for symbols and units) where the c and h parameters determine how steeply the maximum growth rate increases with r_i. In turn, the two Monod parameters are positively correlated with each other, which determines a relationship that can be mathematically expressed through the following function (Wirtz, 2002):

$$K_n(\mu_{max}) = K_{ref}\ e^{\mu_{max}(r_i)/[\mu_{ref}-\mu_{max}(r_i)]} \quad (7)$$

where μ_{ref} represents the asymptotic maximal growth rate for an infinitely high K_n and K_{ref} represents half-saturation constant at $\mu_{max} = 0$. Other forms for this relationship have previously been shown not to affect qualitatively the ecological predictions of this model (Choua et al., 2020). Note that Eq.(7) together with Eq.(6) entail that nutrient affinity declines as cell size increases.

Phage Trait Set and Plasticity

We focus here on the T-phage subfamily, which infects *E. coli* through receptors that occupy up to 75% of the cell surface (Nikaido and Vaara, 1985). The latter allows us to approximate, for simplicity, that all collisions lead effectively to adsorption (Delbrück, 1940; Schwartz, 1976; Berg and Purcell, 1977). Importantly, the size of the host affects the viral adsorption rate, which has been represented in the past using the linear function $k_i = 4r_i\pi D$ (Delbrück, 1940), where D is the diffusion coefficient of the phage.

Although the exact factors that determine the latent period, L_j, are unknown, evidence points to the so-called holin gene as the responsible of the timing of lysis (Young and Bläsi, 1995; Wang et al., 2000; Ramanculov and Young, 2001; White et al., 2011). This link between L_j and the holin gene justifies the characterization of phenotypes using the latent period as an evolving trait. Because this timing is typically smaller than the time needed to deplete the host resources involved in virion production (Rabinovitch et al., 1999; Wang, 2006), we assume that the burst size is only limited by the number of phage that has been assembled between the end of the eclipse period and lysis. This assumption is usually represented by the linear function $B = M(L-E)$ (Wang, 2006). We consider here that E and

M, respectively, the eclipse period and maturation rate, depend on the physiological state of the host (represented by the host growth rate, μ_i) through the following data-informed expressions (Choua and Bonachela, 2019):

$$E(\mu_i) = E_\infty + E_0 e^{-\alpha_E \mu_i / \mu_{\max,\ experiment}} \quad (8)$$

$$M(\mu_i) = \frac{M_\infty}{1 + e^{\alpha_M \left(\frac{\mu_i}{\mu_{\max,experiment}} - M_0 \right)}} \quad (9)$$

In short, E decreases and M increases with the host growth rate. Both functional forms show a plateau at high growth rates, which reflects the physiological limits of the host machinery to synthesizing proteins (Choua and Bonachela, 2019). E_∞ and E_0 determine E for very low growth rates, α_E determines the slope of the (decreasing) function, and $\mu_{\max,experiment}$ is the maximal growth rate that the host reached in the experimental data used to deduce Eqs. (8)–(9); M_∞ represents the upper plateau of the increasing sigmoid, α_M how steeply M reaches it, and M_0 the midpoint of the function. Finally, Eq. (8) shows a finite value for $\mu \to 0$, which represents the possibility of viral reproduction at very low host growth rates, observed experimentally (Golec et al., 2014). Alternatively, for such extreme conditions the virus may switch from lytic to temperate mode (e.g., lysogeny). Although such change in viral strategy can certainly influence the coevolution of the system, here we focused on obligate-lytic viruses since the main plastic traits above are linked to cell lysis. All together leads to the following plastic representation of the burst size for viral phenotype j infecting host i:

$$B_j(\mu_i) = M(\mu_i)(L - E(\mu_i)) \quad (10)$$

For each host phenotype i, the viral traits [i.e., $E(\mu_{ni})$, $M(\mu_{ni})$, and thus B_j] are adjusted at each integration step to follow updates in the host growth rate. In contrast, models that neglect viral plasticity use fixed values for E and M, obtained from experiments that standardly set optimal conditions for the host (Abedon et al., 2001). In consequence, the associated $E = E_{non}$ and $M = M_{non}$ reflect the performance of the host machinery at the maximum growth rate expected for the particular phenotype, i.e., at $\mu_i = \mu_{max}(r_i)$. These values are thus host-specific: because different host phenotypes/strains show different sizes and therefore different μ_{max}, E_{non} and M_{non} must follow accordingly. As we could not find values for E and M for all the different host sizes used in our simulations, we estimated those values as $E_{non}(r_i) = E[\mu_{\max}(r_i)]$ and $M_{non}(r_i) = M[\mu_{\max}(r_i)]$. In consequence, the burst size for the non-plastic virus follows here the expression:

$$B_{non} = M_{non}(r_i)(L - E_{non}(r_i)) \quad (11)$$

Parametrization and Analysis

We use Matlab® to integrate numerically these equations under different environmental conditions (i.e., different values of w and N_0) and, due to the limited amount of information available about the (broadly defined) crowding strength, we also vary the parameter α in a range commensurate with the rest of terms in Eq.(2). Specifically, we try $\alpha = 0$ (i.e., no crowding), $\alpha = 10^{-6}$ lcell^{-1}d^{-1}, and 10^{-7} lcell^{-1}d^{-1}.

Thus, during 10^4 simulated days (enough for the system to reach stationarity), multiple hosts compete for the common nutrient (bottom-up regulation) while experiencing the mortality exerted by the viral populations (top-down pressure), which in turn compete for the available hosts. In our system, host size can evolve between 0.3 to 1.1 μm, range that provides trait values usually observed for *E. coli* (i.e., host volume, μ_{max}, and K_n are compatible with experimental observations) (Schulze and Lipe, 1964; Loferer-Krößbacher et al., 1998; Füchslin et al., 2012). On the other hand, the viral latent period can evolve between a realistic maximal value for T-phage of 2 days and a certain minimal value. This minimal value is calculated based on the host phenotype that shows the highest growth rate (i.e., the smallest E) among all the host mutants, which ensures a minimal latent period bigger than any eclipse period in the system. The latter is necessary because we assume that any viral phenotype can infect any available host. We also consider that both host and virus mutate at similar times. Increasing the viral mutation rate to up to 5 times that of the host did not change the probability of coexistence nor the number of functional combination (results not shown), and therefore we set the less-computationally-expensive limit of equal timing for both host and viral mutations.

With this model and constraints, and starting from a pair of host-virus phenotypes with (L, r) randomly chosen within the ranges above, mutation and selection enable the stochastic exploration of the phenotypic space until, eventually, a combination of phenotype maximizing fitness for the host and virus emerges: the Evolutionary Stable Strategy (ESS) (L_{ESS}, r_{ESS}). Due to the stochastic character of the simulation, we run up to 500 replicates for each combination of w, N_0, and α, in order to find the ESS as the average of the trait values emerging over replicates. We further compare the emergent ESS for both plastic and non-plastic viruses, running for the latter the non-plastic version of the model (Eq. 11).

Out of the many replicates, we select the cases that show coexistence between host and virus at the end of the simulation, and reject those that lead to host and/or viral extinction. Moreover, in order to focus on the evolutionarily stable values of the evolving traits, we retain only the replicates for which a true dominant phenotype can be discerned. Specifically, we label as dominant the phenotype such that its abundance represents more than 75% of the total mutant community (i.e., both $C_{ESSst}/\sum_i C_{ist}$ and $V_{ESSst}/\sum_j V_{jst}$ above 0.75, where the subscript "st" refers to the stationary state obtained by averaging the 20 last days of the simulation).

We then analyze how these (L_{ESS},r_{ESS}) combinations vary as w, N_0, and α change. For each case, we compare the (L_{ESS},r_{ESS}) for the plastic case to those obtained for the non-plastic description of the system. Finally, we compare (i) the L_{ESS} emerging from coevolution to the analytical expression provided by Choua and Bonachela (2019) for a system where only the virus evolves; and (ii) the r_{ESS} emerging from coevolution to the ESS obtained in a system where bacteria evolve in the absence of viruses.

Note that extreme conditions deterministically result in a number of useable combinations (L_{ESS},r_{ESS}) that is lower than our original number of replicates. For example, at low dilution rates, virus and host cannot coexist as the associated low growth rate eventually leads to the extinction of the host (followed by the extinction of virus); at high dilution rates, viral mortality is very high and the viral population goes to extinction, which allows the host to thrive alone.

RESULTS

Host Evolving Without Virus

In a simple system where the virus and crowding effect are neglected (i.e., $V = \alpha = 0$), both the ecological and evolutionary dynamics of the host can be assessed analytically (see **Supplementary Appendix A**). The analytical results show that the ESS for the host presents a size that minimizes nutrient consumption, in agreement with classic competition theory (Tilman, 1982). On the other hand, in cases where the virus is absent but the crowding effect is considered (i.e., $V = 0$, $\alpha \neq 0$), the evolutionary stationary state of the host can be calculated numerically using the genetic algorithm described above. As the dilution rate increases, the emerging host size increases with the dilution rate and eventually saturates (see **Figure 1**). Because the dilution rate is positively correlated with nutrient concentration (see **Figure 2**), increasing w leads to bigger hosts in richer environments and, eventually, an emerging size is reached that maximizes host growth (see **Supplementary Appendix C**). As a consequence, for w values beyond a specific threshold, the host does not survive because growth (limited by its maximum value and nutrient availability) cannot overcome the increasing mortality due to dilution. Increasing crowding strength increases the emerging host size, which still ultimately saturates at the same value (see **Supplementary Appendix B**).

Coevolution of Host and Virus

The coevolution of host and virus allows for wide regions of coexistence. Both plastic and non-plastic versions of the model predict similar qualitative behavior for nutrient and host density as a function of the dilution rate (**Figure 2**). As the dilution rate increases, both cases show an increasing nutrient availability and a slightly negative correlation with host availability. Viral density, however, shows a negative trend in the non-plastic case, whereas it remains approximately constant for the plastic model. From a quantitative point of view, host availability is larger for the plastic version of the model. For low to mid dilution rates, hosts in the plastic model show a much lower growth than the non-plastic case, which results in a lower viral burst size (**Supplementary Figure 1**). The consequent decrease in viral density decreases top-down pressure on the host, which ultimately reaches densities higher than those of the non-plastic model. Thus, viral density is lower for the plastic case for mid-to-low dilution rates, but vice versa for high dilution. For the latter regime, the non-plastic case shows higher nutrient densities, but for both cases the nutrient concentration saturates to N_0 for high dilutions, which ultimately leads to similar growth rates and burst sizes but larger latent periods for the plastic case (**Supplementary Figure 1**). The emerging eclipse period is also longer for the latter case, whereas the maturation rate is smaller (**Supplementary Figure 2**).

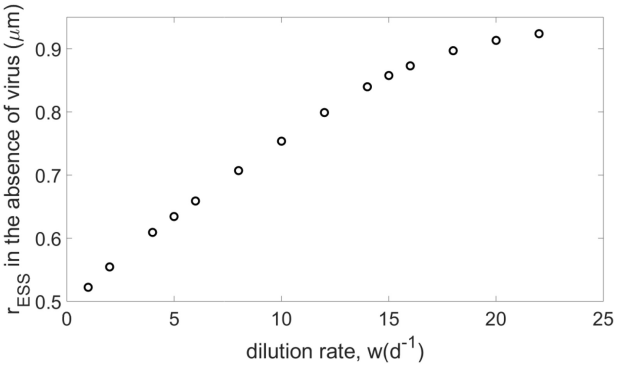

FIGURE 1 | Evolutionary stable strategies (ESS) when the host evolves in the absence of the virus, for $N_0 = 10^{-5} mol\ l^{-l}$ and $\alpha = 10^{-8} l\ cell^{-1}\ d^{-1}$, and different dilution rates.

As (**Supplementary Figure 3**) shows, the combinations (L_{ESS},r_{ESS}) emerging from different replicates for a given dilution rate are clustered around a clear mean value, indicating that only one true combination of host size and latent period results from each environment. For a better visualization, we show in **Figure 3** only the means for the evolving traits. The emergent host size and viral latent period show a negative correlation. For mid-to-low dilution rates, the same parametrization typically produces a smaller r_{ESS} for the plastic case than the non-plastic case, while L_{ESS} is smaller at lower dilution rates but becomes larger at higher dilution rates. At $w = 10\, d^{-1}$, r_{ESS} saturates to the host size that provides the highest growth for the fixed N_0 (see **Supplementary Appendix C**), showing that the system is limited by external factors (i.e., nutrient input). Increasing N_0 increases both L_{ESS} and r_{ESS}, as well as the saturation threshold (see **Supplementary Appendix C**). Note that coexistence is not reached for $w < 4\, d^{-1}$ or $w > 16\, d^{-1}$. In addition, the strength of the crowding effect tends to increase the emerging host size r_{ESS}, but barely affects the emerging latent period L_{ESS} (see **Supplementary Appendix B**).

Host size plays two distinct roles in our model: it affects (i) host quality by influencing μ_{max} [Eq.(6)], and (ii) the number of infections by influencing the adsorption rate. In order to separate the influence of those effects on the emerging traits, we also check the emerging ESSs when the adsorption rate is fixed (i.e., $k = 3 \cdot 10^{-9} l\ virus^{-1} d^{-1}$). Our results do not change qualitatively when using a fixed adsorption rate (not shown).

Comparison of Results for Coevolution Versus Single Evolution of Either Host or Virus

In order to understand the role of coevolution in the selection of the evolving traits (host size and viral latent period), we compare, respectively, the r_{ESS} and L_{ESS} emerging from coevolution with the emerging (i) r_{ESS} obtained when the host evolves alone and

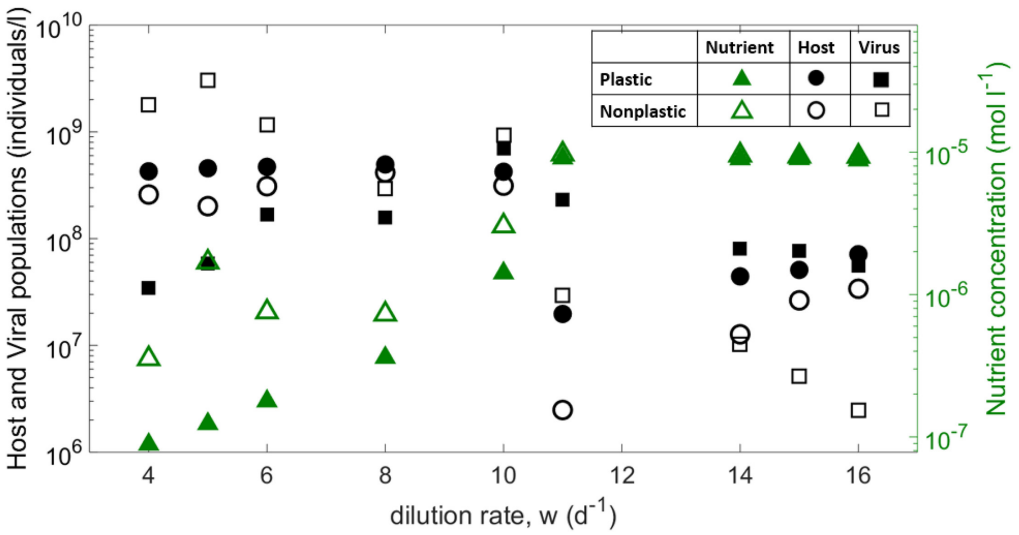

FIGURE 2 | Median across replicates for the host, viral and nutrient concentrations averaged over the last 20 days of each replicate, as a function of the dilution rate. Note that small dilution rate led to wide oscillations [e.g., for $w = 4\ d^{-1}$ in the plastic case N varies between10^{-8} and $10^{-5} mol\ l^{-1}$].

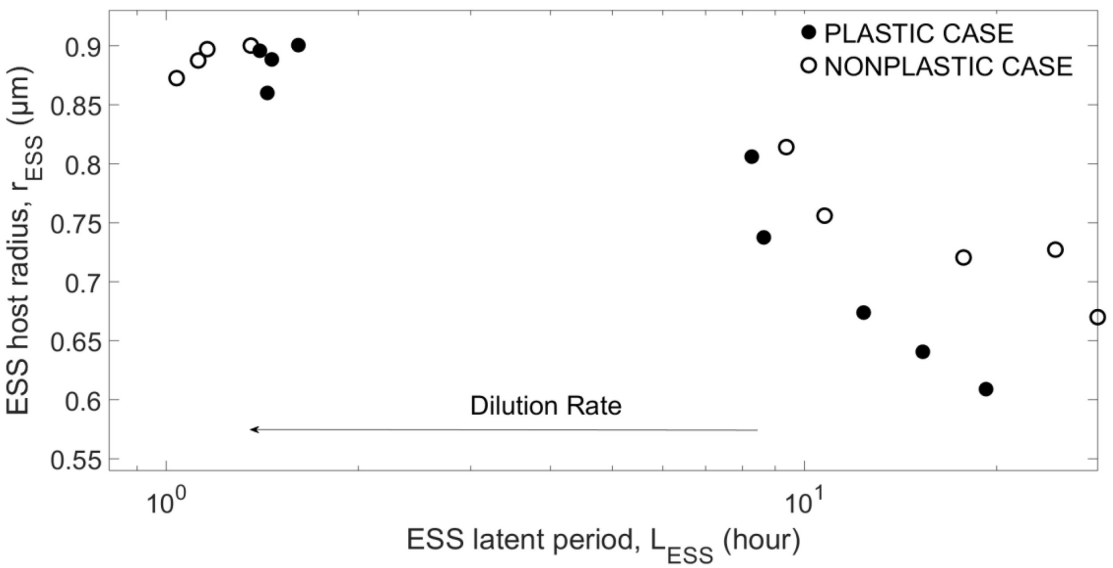

FIGURE 3 | Evolutionary stable strategies (ESS) for the host and virus obtained for $N_0 = 10^{-5} mol\ l^{-1}$ and $\alpha = 10x\ 10^{-9} l\ cell^{-1}\ d^{-1}$, and different dilution rates.

(ii) L_{ESS} obtained when the virus evolves with only one single host phenotype. For the latter, we use the expression $L_{ESS} = \frac{1}{w} + E(\mu)$, calculated analytically in Choua and Bonachela (2019).

Coevolution Versus Evolution of Host in the Absence of Virus

Figure 4 shows that, as the dilution rates increases, the r_{ESS} resulting from the plastic case departs from the virus-free case, resulting in a larger host. The r_{ESS} in the non-plastic case shows larger host sizes than the plastic cases for all dilution rates, although both plastic and non-plastic cases converge to a similar value at high dilution rates. For low dilution rates, the emergent host size in the case of the plastic virus is similar to that without the virus. **Supplementary Figure 4** shows that the resulting host growth rate follows a pattern similar to that described for host size. Host availability for the plastic case remains similar to the case without virus for most dilution rates, whereas the non-plastic virus keeps the host concentration lower than in the absence of the virus (**Supplementary Figure 5**).

Coevolution Versus Evolution of Virus

As **Figure 5** shows, coevolution leads to larger L_{ESS} than in the case of viral evolution with a fixed (i.e., non-evolving)

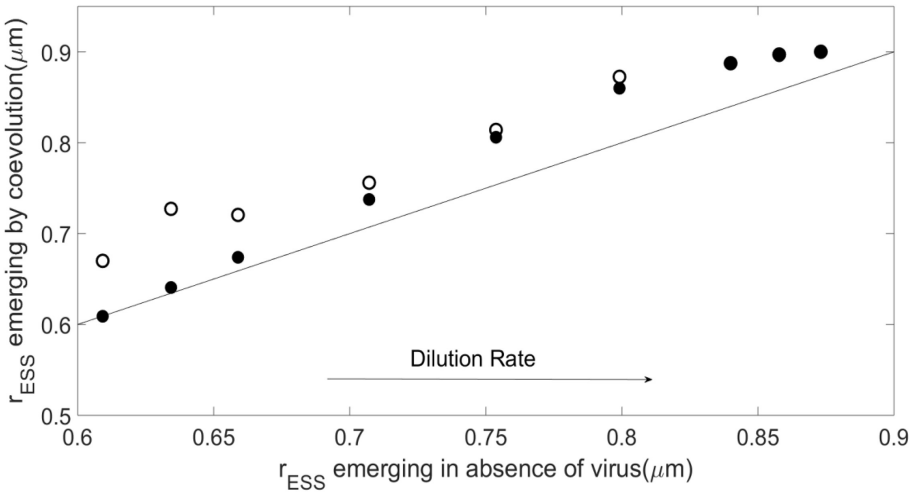

FIGURE 4 | Evolutionary stable strategies (ESS) for the host obtained when it coevolves with the virus as compared with the host ESS in the absence of the virus for $N_0 = 10^{-5} mol\ l^{-1}$ and $\alpha = 10^{-8} lcell^{-1}\ d^{-1}$, and different dilution rates. As in **Figure 3**, solid points represent the plastic case whereas empty points represent the non-plastic case, all above or on the 1:1 line.

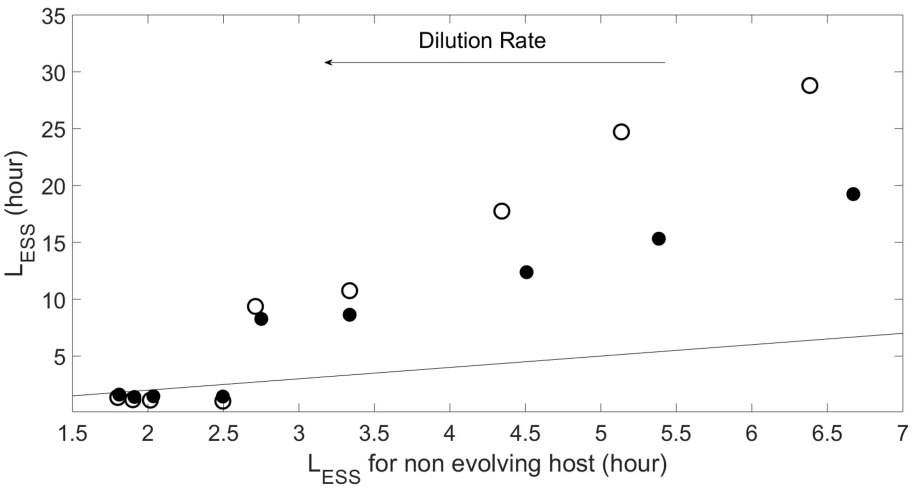

FIGURE 5 | Evolutionary stable strategy (ESS) for the virus obtained when host evolves at $N_0 = 10^{-5} mol\ l^{-1}$ and $\alpha = 10^{-8} lcell^{-1} d^{-1}$, and different dilution rates as compared to the viral ESS when the host does not evolve (i.e., $L = 1/w + E$). Symbols and line as in **Figure 4**.

host phenotype. This difference is more noticeable for the non-plastic case. Increasing the dilution rate (or strength of the crowding effect, see **Supplementary Appendix B**) reduces the difference between the with- and without-coevolution L_{ESS} for both plastic and non-plastic cases. In this regime the pattern actually inverts, the emergent latent period with coevolution becomes smaller than that with a non-evolving host, and the plastic case shows a L_{ESS} that is slightly larger than that of the non-plastic case.

DISCUSSION

Understanding the strategies that organisms use to survive under different ecological scenarios is key to understanding their role within their changeable ecosystem. Here, we studied the coevolution of a bacterial host and a phage. Viruses can impose a significant top-down pressure on their hosts, which may trigger different evolutionary responses in the latter. Our study can help understand which strategies are dominant for bacteria and viruses when coevolving under different scenarios, and the effect that viral plasticity (i.e., viral dependence on its host) has on these strategies. Typically, the virus drives the host to evolving defense mechanisms against phage infection, as repeatedly reported in the literature (Morgan and Koskella, 2011). In our case, the host evolves by changing its size, which has clear ecological implications: smaller hosts show a decreased rate of infection, but also a reduced maximal growth. The virus in turn can respond by adapting its infection time (i.e., latent

period), which comes with the trade-off of either releasing fewer virions (shorter time) or losing opportunities of infection for its offspring (longer time).

In the absence of the virus, the emerging host strategy (r_{ESS}) shows smaller sizes in environments with lower nutrient concentration, which result from lower dilution rates. This evolutionary strategy resonates with the fact that smaller microbes are better competitors when nutrient is scarce, like is the case for smaller phytoplankton (e.g., cyanobacteria) in oligotrophic waters (Mena et al., 2019).

For a same environment (i.e., for a fixed w), the phage pressure maintains the bacterial population to a lower level than in the absence of virus. Consequently, fewer bacteria compete for the nutrient and thus the host population grows faster, which ultimately results in larger emergent sizes. A logical expectation would be for the host to show, in the presence of the virus, a smaller size than in its absence, to avoid viral infection. Instead, the observed increase in host size indicates that the increase in metabolic rate associated to the larger size compensates for being a larger target for viral adsorption. This strategy also benefits the virus as it increases adsorption, and the improved host physiological state reduces latent period and increases burst size. Because a fixed adsorption rate did not alter our results, we conclude that the evolution of host size influences viral evolution mostly by altering host quality and, indirectly, host availability.

Increasing the dilution rate leads to larger host sizes (and therefore higher host quality) but lower host densities (i.e., lower host availability), which reveals a host quality-quantity trade-off. In nutrient-poor environments, the associated increased availability of the host with small size, which leads to small growth rates, i.e., low quality, tends to increase the latent period; this contrasts with past theory predicting that high host cell density favors phage with short latent period (Abedon, 1989). Thus, as we observe a decrease in the latent period even when the host availability decreases, we hypothesize that the lower host availability is compensated by the higher host quality, which appears to be the dominant factor in the selection of the latent period. This resonates with claims about the importance of host quality in determining the length of latent period when host density is high (Wang et al., 1996). Surprisingly, this quality-driven phenomenology is also shown by the non-plastic case. The reason is that, in spite of the viral traits being independent of the host growth rate in this case, evolutionary changes in host size determine viral trait values through their dependence on the maximum growth rate (e.g., Eq. 11), i.e., the non-plastic virus can produce more virions in a shorter time when host size increases. An important difference, thus, is that the latter occurs as a result of evolution, whereas viral plasticity is an ecological process.

Unexpectedly, the emerging latent period in the plastic case is shorter than in the non-plastic case for most dilution rates, and longer only for very high values of w. This result is in contrast with the definition of non-plastic virus we used here, as the latter shows the latent period expected at maximum growth rate (by definition the smaller possible value for L). **Supplementary Figure 1** also shows that the growth rates reached by the host with the non-plastic virus are larger than those reached in the presence of the plastic virus, which should lead to a shorter latent period. The fact that the eclipse period is, as expected attending to host growth rate, longer in the plastic case and the maturation rate smaller (**Supplementary Figure 2**) means that the plastic virus spends less time to assembling virions, and does so at a slower rate. We hypothesize that, because here the non-plastic virus shows fewer hosts but of higher quality than the plastic virus, the lower L value for the latter might result from the effect of host availability on the emerging latent period, compensating the effect of the smaller host growth rate. With an abundant host, the strategy of the plastic virus is to lyse hosts earlier even if the resulting burst size is smaller. On the other hand, the lower amount of available hosts and the roughly one-order-of-magnitude difference in burst size requires from the non-plastic virus a longer latent period, to avoid host "overexploitation" (i.e., a Tragedy of the Commons scenario in which the virus kills the host and hence itself).

When the dilution rate is high, the burst size and host availability for both cases equalize, the only determining factor is the difference between host maximum growth rate (for the non-plastic virus traits) and realized growth rate (for the plastic virus traits) and, as a consequence, the non-plastic virus shows a shorter latent period than the plastic one. The differences in L and B between plastic and non-plastic virus are, however, small because the host growth rate for the former is close to its maximum. The crowding effect is an additional factor that regulates the bacterial population. The decrease in population resulting from crowding actually allows the host to reach the highest size that maximizes its growth rate for lower dilution rates, which can again be due to the lower competition for nutrient (see above). For sufficiently high α, the bacterial population is entirely regulated by the crowding effect, which explains the similar emergent size in the presence or absence of the virus.

Finally, the virus adapts to the evolutionary response of the host showing a L_{ESS} larger than that obtained when the host does not evolve, for both plastic and non-plastic viruses. Therefore, we conclude that coevolution slows down viral infection, the more so for a non-plastic virus. This delay and differences between plastic and non-plastic cases are amplified in nutrient-poor environments (i.e., for small dilution rates), where the host grows far from its maximal rate and the importance of plasticity is more observable. Without further empirical information, however, we cannot hypothesize the mechanisms underlying these strategies.

Our framework has a few important limitations. Although coevolutionary branching is a possibility that has been observed in laboratory and natural populations (Koskella and Brockhurst, 2014), we focused here on situations in which a single, well-defined ESS emerging for each simulated environment (evidenced by the clustered points obtained from the different replicates, i.e., each cluster can be represented by a single, well-defined mean value). Diversification can occur, for example, when a mutant virus adsorbs to only a limited subset of the total bacteria, i.e., it is a specialist (Weitz et al., 2005). In our case, however, viral phenotypes are all generalists [i.e., any viral

mutant can infect any of the host phenotypes, shown to happen during coevolution (Hall et al., 2011)]. Although this "global" competition for hosts prevents a complete niche separation among viruses, we cannot exclude the possibility of evolutionary branching occurring in some of the discarded (surviving) replicates. Further, we discarded simulations in which either host or virus populations collapsed. The reason is that those simulations did not represent examples of "evolutionary suicide" but rather resulted from initial conditions for the traits that were outside the expected coexistence region of the parameter space [see (Choua et al., 2020)], and where evolution and/or plasticity did not reach the coexistence region before extinction. As a final remark, note that we have explored the role of one single environmental factor at a time: dilution rate, and nutrient input concentration (see **Supplementary Appendix**). Realistic conditions susceptible to be studied with our framework, from gut microbiome to phytoplankton populations, will necessitate of the inclusion of several abiotic (e.g., different nutrients) and biotic factors (e.g., grazers) varying simultaneously (Weitz et al., 2015; Pourtois et al., 2020).

CONCLUSION

Although pathogens typically have detrimental effects on their hosts, in some cases the evolution of parasitic organisms may benefit the host by increasing host fitness (Morgan and Koskella, 2011). In our system, coevolution translates into the presence of virus fostering the emergence of larger host sizes that show larger growth potential, which is also beneficial for the virus as larger host growth rates improve also viral replication. We observe as a result an increased coexistence between host and phage. Our results, therefore, reveal an important aspect of the interaction between host and phage that should be considered when devising treatments to use phage against bacterial infections in either medical or environmental management contexts. This is especially relevant given the variability in host growth rate and sizes that is expected from bacterial infections, as well as the rapid evolutionary response that both bacteria and virus can show. Further, the predicted shift in host size due to the presence of the virus can have a cascading effect at larger scale in e.g., marine food webs. Cell size is a key trait for phytoplankton that influences the response of the lower trophic levels of the marine food web to climate change and carbon export to the deep ocean, among others (Finkel et al., 2009). Phytoplankton size, for example, influences mortality due to grazing, and therefore energy export to higher trophic levels. However, the dependence of phytoplankton maximum growth rate on cell size is non-monotonic, with smaller species following an increasing trend (qualitatively similar to that used here for *E. coli*) but larger species showing a negative correlation with cell size (Marañón et al., 2013). Our conclusions could therefore apply to species such as cyanobacteria and chlorophytes. Importantly, our theoretical framework is still applicable since the expectation is that similar dependence of viral performance on host physiology occur generically. Thus, our model could be easily modified to adapt it to other species and, ultimately, help to understand the processes involved in and determining the phytoplankton community structure, which in turn influences key biogeochemical cycles such as that of carbon, nitrogen, and phosphorus.

DATA AVAILABILITY STATEMENT

The code used to obtain the data supporting the conclusions of this article will be made available by the authors under request.

AUTHOR CONTRIBUTIONS

JAB and MH designed the research. MC conducted the research. MC and JAB wrote the manuscript with input from MH. All authors contributed to the article and approved the submitted version.

FUNDING

All authors were supported by the Marine Alliance for Science and Technology for Scotland pooling initiative, funded by the Scottish Funding Council (HR09011) and contributing institutions. Results were obtained using the ARCHIE-West High Performance Computer (www.archie-west.ac.uk) based at the University of Strathclyde.

ACKNOWLEDGMENTS

The authors would like to thank Douglas Speirs for helpful discussions in early stages of this project.

SUPPLEMENTARY MATERIAL

The Supplementary Material for this article can be found online at: https://www.frontiersin.org/articles/10.3389/fmicb.2021.637490/full#supplementary-material

REFERENCES

Abedon, S. T. (1989). Selection for bacteriophage latent period length by bacterial density: a theoretical examination. *Microb. Ecol.* 18, 79–88. doi: 10.1007/bf02030117

Abedon, S. T., Herschler, T. D., and Stopar, D. (2001). Bacteriophage latent-period evolution as a response to resource availability. *Appl. Environ. Microbiol.* 67, 4233–4241. doi: 10.1128/AEM.67.9.4233-4241.2001

Abedon, S. T., Hyman, P., and Thomas, C. (2003). Experimental examination of bacteriophage latent-period evolution as a response to bacterial availability. *Appl. Environ. Microbiol.* 69, 7499–7506. doi: 10.1128/aem.69.12.7499-7506.2003

Berg, H. C., and Purcell, E. M. (1977). Physics of chemoreception. *Biophys. J.* 20, 193–219. doi: 10.1016/S0006-3495(77)85544-6

Birch, E. W., Ruggero, N. A., and Covert, M. W. (2012). Determining host metabolic limitations on viral replication via integrated modeling and

experimental perturbation. *PLoS Comput. Biol.* 8:e1002746. doi: 10.1371/journal.pcbi.1002746

Bonachela, J. A., and Levin, S. A. (2014). Evolutionary comparison between viral lysis rate and latent period. *J. Theor. Biol.* 345, 32–42. doi: 10.1016/j.jtbi.2013.12.006

Bremer, H., and Dennis, P. P. (2008). Modulation of chemical composition and other parameters of the cell at different exponential growth rates. *EcoSal Plus* 2008:1128. doi: 10.1128/Ecosal.5.2.3

Brown, J. H., Gillooly, J. F., Allen, A. P., Savage, V. M., and West, G. B. (2004). Toward a metabolic theory of ecology. *Ecology* 85, 1771–1789. doi: 10.1890/03-9000

Calendar, R. L., and Abedon, S. T. (2005). *The Bacteriophages*. Oxford: Oxford University Press.

Chien, A.-C., Hill, N. S., and Levin, P. A. (2012). Cell size control in bacteria. *Curr. Biol.* 22, R340–R349. doi: 10.1016/j.cub.2012.02.032

Choua, M., and Bonachela, J. A. (2019). Ecological and evolutionary consequences of viral plasticity. *Am. Natural.* 193, 346–358. doi: 10.1086/701668

Choua, M., Heath, M. R., Speirs, D. C., and Bonachela, J. A. (2020). The effect of viral plasticity on the persistence of host-virus systems. *J. Theoret. Biol.* 498:110263. doi: 10.1016/j.jtbi.2020.110263

De Paepe, M., and Taddei, F. (2006). Viruses' life history: towards a mechanistic basis of a trade-off between survival and reproduction among phages. *PLoS Biol.* 4:e193. doi: 10.1371/journal.pbio.0040193

Delbrück, M. (1940). Adsoprtion of bacteriophage under various physiological conditions of the host. *J. Gen. Physiol.* 23, 631–642. doi: 10.1085/jgp.23.5.631

Edwards, K. F., and Steward, G. F. (2018). Host traits drive viral life histories across phytoplankton viruses. *Am. Natural.* 191, 566–581. doi: 10.1086/696849

Finkel, Z. V., Beardall, J., Flynn, K. J., Antonietta, Q. T., Rees, A. V., and Raven, J. A. (2009). Phytoplankton in a changing world: cell size and elemental stoichiometry. *J. Plank. Res.* 32, 119–137. doi: 10.1093/plankt/fbp098

Füchslin, H. P., Schneider, C., and Egli, T. (2012). In glucose-limited continuous culture the minimum substrate concentration for growth, s(min), is crucial in the competition between the enterobacterium *Escherichia coli* and *Chelatobacter heintzii*, an environmentally abundant bacterium. *ISME J.* 6, 777–789. doi: 10.1038/ismej.2011.143

Gallet, R., Violle, C., Fromin, N., Jabbour-Zahab, R., Enquist, B. J., and Lenormand, T. (2017). The evolution of bacterial cell size: the internal diffusion-constraint hypothesis. *ISME J.* 11, 1559–1568. doi: 10.1038/ismej.2017.35

Gnezda-Meijer, K., Mahne, I., Poljsak-Prijatelj, M., and Stopar, D. (2006). Host physiological status determines phage-like particle distribution in the lysate. *FEMS Microb. Ecol.* 55, 136–145. doi: 10.1111/j.1574-6941.2005.00008.x

Golec, P., Karczewska-Golec, J., Łoś, M., and Węgrzyn, G. (2014). Bacteriophage T4 can produce progeny virions in extremely slowly growing *Escherichia coli* host: comparison of a mathematical model with the experimental data. *FEMS Microbiol. Lett.* 351, 156–161. doi: 10.1111/1574-6968.12372

Hall, A. R., Scanlan, P. D., and Buckling, A. (2011). Bacteria-phage coevolution and the emergence of generalist pathogens. *Am. Natural.* 177, 44–53. doi: 10.1086/657441

Koskella, B., and Brockhurst, M. A. (2014). Bacteria-phage coevolution as a driver of ecological and evolutionary processes in microbial communities. *FEMS Microbiol. Rev.* 38, 916–931. doi: 10.1111/1574-6976.12072

Levin, B. R., Stewart, F. M., and Chao, L. (1977). Resource-limited growth, competition, and predation: a model and experimental studies with bacteria and bacteriophage. *Am. Natural.* 111, 3–24. doi: 10.1086/283134

Litchman, E., Klausmeier, C. A., Schofield, O. M., and Falkowski, P. G. (2007). The role of functional traits and trade-offs in structuring phytoplankton communities: scaling from cellular to ecosystem level. *Ecol. Lett.* 10, 1170–1181. doi: 10.1111/j.1461-0248.2007.01117.x

Loferer-Krößbacher, M., Klima, J., and Psenner, R. (1998). Determination of bacterial cell dry mass by transmission electron microscopy and densitometric image analysis. *Appl. Environ. Microbiol.* 64, 688–694. doi: 10.1128/aem.64.2.688-694.1998

Marañón, E., Cermeño, P., López-Sandoval, D. C., Rodríguez-Ramos, T., Sobrino, C., Huete-Ortega, M., et al. (2013). Unimodal size scaling of phytoplankton growth and the size dependence of nutrient uptake and use. *Ecol. Lett.* 16, 371–379. doi: 10.1111/ele.12052

Mena, C., Reglero, P., Hidalgo, M., Sintes, E., Santiago, R., Martín, M., et al. (2019). Phytoplankton community structure is driven by stratification in the oligotrophic Mediterranean Sea. *Front. Microbiol.* 10:1698. doi: 10.3389/fmicb.2019.01698

Menge, D. N., and Weitz, J. S. (2009). Dangerous nutrients: evolution of phytoplankton resource uptake subject to virus attack. *J. Theor. Biol.* 257, 104–115. doi: 10.1016/j.jtbi.2008.10.032

Monod, J. (1949). The growth of bacterial cultures. *Annu. Rev. Microbiol.* 3, 371–394. doi: 10.1146/annurev.mi.03.100149.002103

Morgan, A. D., and Koskella, B. (2011). "6 – Coevolution of host and pathogen," in *Genetics and Evolution of Infectious Disease*, ed. M. Tibayrenc (London: Elsevier), 147–171.

Nikaido, H., and Vaara, M. (1985). Molecular basis of bacterial outer membrane permeability. *Microbiol. Rev.* 49, 1–32. doi: 10.1128/mmbr.49.1.1-32.1985

Pourtois, J., Tarnita, C., and Bonachela, J. A. (2020). Impact of lytic phages on phosphorus- versus nitrogen-limited marine microbes. *Front. Microbiol.* 11:221.

Rabinovitch, A., Fishov, I., Hadas, H., Einav, M., and Zaritsky, A. (2002). Bacteriophage T4 development in *Escherichia coli* is growth rate dependent. *J. Theor. Biol.* 216, 1–4. doi: 10.1006/jtbi.2002.2543

Rabinovitch, A., Hadas, H., Einav, M., Melamed, Z., and Zaritsky, A. (1999). Model for bacteriophage T4 development in *Escherichia coli*. *J. Bacteriol.* 181, 1677–1683.

Ramanculov, E., and Young, R. (2001). Genetic analysis of the T4 holin: timing and topology. *Gene* 265, 25–36. doi: 10.1016/s0378-1119(01)00365-1

Schulze, K. L., and Lipe, R. S. (1964). Relationship between substrate concentration, growth rate, and respiration rate of *Escherichia coli* in continuous culture. *Archiv. Mikrobiol.* 48, 1–20. doi: 10.1007/bf00406595

Schwartz, M. (1976). The adsorption of coliphage lambda to its host: effect of variations in the surface density of receptor and in phage-receptor affinity. *J. Mol. Biol.* 103, 521–536. doi: 10.1016/0022-2836(76)90215-1

Shestopaloff, Y. K. (2016). Interspecific allometric scaling of unicellular organisms as an evolutionary process of food chain creation. *arXiv* [Preprint]. arXiv:1611.09824.

Thyrhaug, R., Larsen, A., Thingstad, T. F., and Bratbak, G. (2003). Stable coexistence in marine algal host-virus systems. *Mar. Ecol. Progr. Ser.* 254:25451.

Tilman, D. (1982). Resource competition and community structure. *Monogr. Populat. Biol.* 17, 1–296.

Wang, I.-N. (2006). Lysis timing and bacteriophage fitness. *Genetics* 172, 17–26. doi: 10.1534/genetics.105.045922

Wang, I.-N., Dykhuizen, D., and Slobodkin, L. (1996). The evolution of phage lysis timing. *Evolut. Ecol.* 10, 545–558. doi: 10.1007/BF01237884

Wang, I.-N., Smith, D. L., and Young, R. (2000). Holins: the protein clocks of bacteriophage infections. *Annu. Rev. Microbiol.* 54, 799–825. doi: 10.1146/annurev.micro.54.1.799

Wang, Z., and Goldenfeld, N. (2010). Fixed points and limit cycles in the population dynamics of lysogenic viruses and their hosts. *Phys. Rev. E Statist. Nonlin. Soft Matter Phys.* 82(1 Pt 1):011918. doi: 10.1103/physreve.82.011918

Ward, B. A., Marañón, E., Sauterey, B., Rault, J., and Claessen, D. (2017). The size dependence of phytoplankton growth rates: a trade-off between nutrient uptake and metabolism. *Am. Natural.* 189, 170–177. doi: 10.1086/689992

Weitz, J. S., and Dushoff, J. (2008). Alternative stable states in host–phage dynamics. *Theoret. Ecol.* 1, 13–19. doi: 10.1007/s12080-007-0001-1

Weitz, J. S., Hartman, H., and Levin, S. A. (2005). Coevolutionary arms races between bacteria and bacteriophage. *Proc. Natl. Acad. Sci. U.S.A.* 102, 9535–9540. doi: 10.1073/pnas.0504062102

Weitz, J. S., Stock, C. A., Wilhelm, S. W., Bourouiba, L., Coleman, M. L., Buchan, A., et al. (2015). A multitrophic model to quantify the effects of marine viruses on microbial food webs and ecosystem processes. *ISME J.* 9, 1352–1364. doi: 10.1038/ismej.2014.220

White, R., Chiba, S., Pang, T., Dewey, J. S., Savva, C. G., Holzenburg, A., et al. (2011). Holin triggering in real time. *Proc. Natl. Acad. Sci. U.S.A.* 108:798. doi: 10.1073/pnas.1011921108

Wirtz, K. W. (2002). A generic model for changes in microbial kinetic coefficients. *J. Biotechnol.* 97, 147–162. doi: 10.1016/s0168-1656(02)00064-0

You, L., Suthers, P., and Yin, J. (2002). Effects of *Escherichia coli* physiology on growth of phage T7 in vivo and in silico. *J. Bacteriol.* 184, 1888–1894. doi: 10.1128/jb.184.7.1888-1894.2002

Young, R., and Bläsi, U. (1995). Holins: form and function in bacteriophage lysis. *FEMS Microbiol. Rev.* 17, 191–205. doi: 10.1016/0168-6445(94)00079-4

Conflict of Interest: The authors declare that the research was conducted in the absence of any commercial or financial relationships that could be construed as a potential conflict of interest.

Copyright © 2021 Choua, Heath and Bonachela. This is an open-access article distributed under the terms of the Creative Commons Attribution License (CC BY). The use, distribution or reproduction in other forums is permitted, provided the original author(s) and the copyright owner(s) are credited and that the original publication in this journal is cited, in accordance with accepted academic practice. No use, distribution or reproduction is permitted which does not comply with these terms.

frontiers in Microbiology

ORIGINAL RESEARCH
published: 20 May 2021
doi: 10.3389/fmicb.2021.613356

Safety and Efficacy of a Phage, kpssk3, in an *in vivo* Model of Carbapenem-Resistant Hypermucoviscous *Klebsiella pneumoniae* Bacteremia

*Yunlong Shi[1], Yuan Peng[2], Yixin Zhang[2], Yu Chen[1], Cheng Zhang[1], Xiaoqiang Luo[1], Yajie Chen[1], Zhiqiang Yuan[1], Jing Chen[1] and Yali Gong[1]**

[1] State Key Laboratory of Trauma, Burns and Combined Injury, Institute of Burn Research, Southwest Hospital, Third Military Medical University (Army Medical University), Chongqing, China, [2] Department of Plastic and Reconstructive Surgery, Shanghai Ninth People's Hospital, Shanghai Jiao Tong University School of Medicine, Shanghai, China

OPEN ACCESS

Edited by:
Robert Czajkowski,
University of Gdańsk, Poland

Reviewed by:
Zhiyong Zong,
Sichuan University, China
Balaji Veeraraghavan,
Christian Medical College and Hospital, India

***Correspondence:**
Yali Gong
yizhipengtmmu@163.com

Specialty section:
This article was submitted to Virology, a section of the journal Frontiers in Microbiology

Received: 02 October 2020
Accepted: 29 March 2021
Published: 20 May 2021

Citation:
Shi Y, Peng Y, Zhang Y, Chen Y, Zhang C, Luo X, Chen Y, Yuan Z, Chen J and Gong Y (2021) Safety and Efficacy of a Phage, kpssk3, in an in vivo Model of Carbapenem-Resistant Hypermucoviscous Klebsiella pneumoniae Bacteremia. Front. Microbiol. 12:613356. doi: 10.3389/fmicb.2021.613356

Antimicrobial resistance (AMR) is one of the most significant threats to global public health. As antibiotic failure is increasing, phages are gradually becoming important agents in the post-antibiotic era. In this study, the therapeutic effects and safety of kpssk3, a previously isolated phage infecting carbapenem-resistant hypermucoviscous *Klebsiella pneumoniae* (CR-HMKP), were evaluated in a mouse model of systemic CR-HMKP infection. The therapeutic efficacy experiment showed that intraperitoneal injection with a single dose of phage kpssk3 (1×10^7 PFU/mouse) 3 h post infection protected 100% of BALB/c mice against bacteremia induced by intraperitoneal challenge with a $2 \times LD_{100}$ dose of NY03, a CR-HMKP clinical isolate. In addition, mice were treated with antibiotics from three classes (polymyxin B, tigecycline, and ceftazidime/avibactam plus aztreonam), and the 7 days survival rates of the treated mice were 20, 20, and 90%, respectively. The safety test consisted of 2 parts: determining the cytotoxicity of kpssk3 and evaluating the short- and long-term impacts of phage therapy on the mouse gut microbiota. Phage kpssk3 was shown to not be cytotoxic to mammalian cells *in vitro* or *in vivo*. Fecal samples were collected from the phage-treated mice at 3 time points before (0 day) and after (3 and 10 days) phage therapy to study the change in the gut microbiome via high-throughput 16S rDNA sequence analysis, which revealed no notable alterations in the gut microbiota except for decreases in the Chao1 and ACE indexes.

Keywords: phage, *Klebsiella pneumoniae*, gut microbiota, hypermucoviscous, carbapenem-resistant

INTRODUCTION

Carbapenem-resistant *Klebsiella pneumoniae* (CRKP) has recently become one of the most important global public health challenges, causing treatment failures, high mortality rates, exorbitant healthcare expenses and prolonged hospital stays (Suay-Garcia and Perez-Gracia, 2019). In 2017, the World Health Organization (WHO) listed CRKP as a high-priority critical pathogen

due to the limited treatment options and urgent need for new drugs (Venter, 2019). Some traditional antibiotics, e.g., polymyxin and tigecycline, remain drugs of last resort against CRKP, but the optimization of dosage regimens, their high toxicity, low efficacy and increasing resistance are issues remaining to be addressed (Porreca et al., 2018). Ceftazidime/avibactam (CAZ/AVI) is an effective antimicrobial combination that was approved for clinical use in 2015 and provides a new alternative strategy to treat CRKP; however, CAZ/AVI resistance was reported even before this treatment was commercially available in China (Zhang et al., 2020). In addition, in 1986, a report from Taiwan first described a new *Klebsiella pneumoniae* (*K. pneumoniae*) strain with a high-virulence and hypermucoviscosity phenotype—i.e., hypervirulent *K. pneumoniae* (hvKP)—that could cause serious invasive infections, such as endophthalmitis, pyogenic liver abscess (PLA) and meningitis, in relatively young and healthy individuals (Gu et al., 2018). Even more concerningly, an increasing number of *K. pneumoniae* clinical isolates with a combination of carbapenem resistance and hypervirulence are being reported worldwide, which might cause a severe public health crisis (Chen and Kreiswirth, 2018).

Bacteriophages (phages) are viruses that can kill specific bacteria (Guo et al., 2020). Approximately one century ago, phages were discovered and used as antibacterial agents to combat infections. During World War II, phage therapy (PT) saved the lives of many soldiers (Myelnikov, 2018). Compared to antibiotic therapy, PT has many advantages, such as strict specificity toward target pathogens, the ability of phages to self-replicate, the ability to eradicate bacterial biofilms, low toxicity, and relatively few side effects, and is thus an alternative treatment modality for infectious diseases in the postantibiotic era. However, before PT can be introduced as a therapeutic approach for bacterial infection in humans, its efficacy and safety must be evaluated in an animal model. In previous work, using a CR-HMKP strain (NY03) isolated from blood samples of a patient with severe burns as the host, we isolated a T7-like lytic phage from hospital sewage (Shi et al., 2020). Here, based on this previous work, we evaluated the therapeutic efficacy and safety of this phage in a mouse model.

MATERIALS AND METHODS

Ethics Statement

All animal experiments in this study were approved by the Ethics Committee of Army Medical University (AMU), Chongqing, China. The BALB/c female mice (18–22 g, 6–8 weeks old) used in the study were purchased from the Experimental Animal Center of AMU and kept in a room maintained at 24 ± 3°C with free access to a standard rodent diet and sterile drinking water on a 12 h light/dark cycle. All mice were euthanized at the end of the experiments.

Bacterial Strain and Phage

Both the phage kpssk3 and the CRKP clinical isolate NY03 used in this study were previously characterized and analyzed (Shi et al., 2020). NY03 was screened by PCR for the presence of resistance genes, as previously described (Vergara et al., 2020). NY03 was grown in Luria–Bertani broth at 37°C. An endotoxin affinity column (ToxinEraser Endotoxin Removal Kit, Genscript, China) was used to remove endotoxin from the phage preparation, which reduced the endotoxin-to-phage ratio to less than 1 EU/10^9 PFU (Hietala et al., 2019).

Hospital Course of the Patient Infected With NY03

In 2017, a 15-years-old male patient with a severe electrical burn injury (total burn surface area = 75%) was hospitalized in a teaching hospital (Chongqing, China) for 50 days, during which he developed sepsis caused by CRKP (NY03). Specifically, on day 30 of hospitalization, culture of central blood revealed growth of a CRKP strain that was resistant to 14 antibiotics, including imipenem (IPM, MIC = 16 μg/ml), ertapenem (ETP, MIC = 8 μg/ml) and aztreonam (ATM, MIC = 64 μg/ml), and susceptible to polymyxin B (PMB, MIC = 1 μg/ml) and tigecycline (TGC, MIC = 1 μg/ml). However, CAZ/AVI was not commercially available in China at that time. The patient was treated with TGC and PMB; however, the CRKP strain was not eradicated from the circulatory system during the treatment course, and the patient's overall condition deteriorated progressively. Finally, on day 50, the patient died of multiple organ failure (MOF) caused by CRKP.

Antimicrobial Susceptibility Testing and Phenotype Detection

The susceptibility of NY03 to CAZ/AVI (Pfizer, Inc., United States) was tested by the broth microdilution method (BMD) according to the Clinical and Laboratory Standards Institute guidelines (28th edition) (Wang et al., 2020). NY03 carried a gene, bla_{GIM}, encoding an Ambler class B metallo-β-lactamase (MBL), which might confer resistance to CAZ/AVI. A checkerboard assay was performed as previously described to determine the synergistic antibacterial effects of the combination of CAZ/AVI with ATM (Solarbio Life Science, China) against NY03 (Ungphakorn et al., 2018). The combination interaction of the 2 antibiotics was evaluated by calculating and interpreting the fractional inhibitory concentration index (FICI) according to criteria described elsewhere (Ferrer-Espada et al., 2020). Additionally, a string test was conducted as described previously to assess the hypermucoviscosity phenotypes of NY03. The formation of a viscous string with a length of at least 5 mm when the NY03 bacterial colony was stretched with a loop on a blood agar plate was considered to indicate a positive string test (Khalil et al., 2019). The presence of virulence genes, including *rmpA*/*rmpA*2, *magA*, *iucA*, and *iroA*, was checked by PCR using previously described methods (Alsanie, 2020).

Cytotoxicity of kpssk3

First, the cytotoxicity of different concentrations of kpssk3 (1×10^8 PFU/ml and 1×10^9 PFU/ml) to HeLa cells was evaluated with a Cell Counting Kit-8 (CCK-8, Sigma, Japan) in accordance with the instructions (Aleksandrzak et al., 2019). Triton X-100 (2%) was used as the positive control, and PBS

buffer was used as the negative control. The absorbance (optical density, OD) at 450 nm (A_{450nm}) was measured in a microplate reader (Thermo Fisher Scientific, United States). For *in vivo* studies, 2 different doses of kpssk3 (10^8 PFU/mouse and 10^9 PFU/mouse) were injected into 10 mice (5 mice for each dose level) intraperitoneally (i.p.) twice daily for 5 days. During the experimental period, the health status of the mice was monitored based on the following symptoms: decreased physical activity, lethargy, hunched posture, unkempt fur, purulent periocular secretions, labored breathing, and death (Xia et al., 2016), and the body weight was recorded daily. Two randomly selected mice (1 for each dose level) were euthanized by cervical dislocation after 5 days, at which time the spleen, lungs, kidneys and liver were harvested for histopathological analysis.

Distribution of kpssk3 in the Blood of Healthy Mice

Twenty-seven healthy mice were injected i.p. with 1 ml of 10^8 PFU/ml kpssk3. At 6 min and at 1, 2, 3, 4, 5, 6, 7, and 8 h after injection, 3 mice were randomly selected and anesthetized by pentobarbital sodium (40 mg/kg, i.p.) (Ginosar et al., 2015). Cardiac puncture was then performed to collect approximately 1 ml of blood from the ventricle of each anesthetized mouse on which an open thoracotomy had been performed. The titer of kpssk3 in the blood was measured by the double-layer agar method as previously described (Fulgione et al., 2019). This experiment was repeated three times.

PT in a CR-HMKP-Induced Bacteremia Model

First, the absolute lethal dose (LD_{100}) of strain NY03 in mice was determined as described elsewhere (Cheng et al., 2017). The model of CR-HMKP-induced bacteremia was established by intraperitoneal injection of a 2 × LD_{100} dose of early log-phase NY03, which was followed 3 hours later by treatment with different antibacterial agents. Sixty mice were averagely divided into 6 groups and treated as follows:

(Group 1) Mice were infected i.p. with 0.1 ml of NY03 (2 × LD_{100}/mouse);
(Group 2) Mice were injected subcutaneously (s.c.) with 10 mg/kg PMB (Sangon, Shanghai, China) twice daily after bacterial challenge (Landersdorfer et al., 2018);
(Group 3) Mice were injected s.c. with 5 mg/kg TGC (Pfizer, Inc., United States) twice daily after bacterial challenge (Docobo-Perez et al., 2012);
(Group 4) Mice were treated with a single dose of kpssk3 (0.1 ml, 1 × 10^8 PFU/ml, i.p.). Simultaneously, we also collected feces from the mice of this group to study the changes in the mice gut microbiome during the treatment period (**Figure 1**);
(Group 5) Mice were treated with a single dose of kpssk3 (0.1 ml, 1 × 10^7 PFU/ml, i.p.);
(Group 6) Mice were treated with a combined regimen of CAZ/AVI (32 mg/kg every 8 h, s.c.) plus ATM (32 mg/kg every 8 h, s.c.) (Marshall et al., 2017);
(Group 7) Mice were treated with an equal amount of normal saline (0.1 ml, i.p.).

The survival rate in each group was recorded daily for 7 days. For PT, phage resistance is one major limitation, so the phage cross-streak assay was performed *in vitro* to screen phage-resistant mutant (Guo et al., 2017).

PT's Influence on the Mouse Gut Microbiota

We evaluated the therapeutic effects of kpssk3 in a CR-HMKP-induced bacteremia model in the previous step, and simultaneously collected fresh feces from the mice in group 4 three times in a sterile manner to study the alterations in the mouse gut microbiome after PT (**Figure 1**). The fecal samples (approximately 1 g) were harvested by gently massaging the abdomens of the mice and were immediately frozen at −80°C. The mice in group 4 were housed in 10 numbered cages (1–10). The first 10 fecal samples were collected before infection with NY03 and designated ipB (1–10). The second set of fecal samples was collected 3 days after phage treatment and designated ipA (1–10). The third set of fecal samples was collected after 7 more days, i.e., 10 days after kpssk3 treatment, and designated ipD (1–10). After 10 days, one surviving mouse was randomly selected from group 4 and euthanized for histopathological analysis; the remaining mice in group 4 were sacrificed to determine the presence of kpssk3 and NY03 in the blood collected using the cardiac puncture method and different organs (heart, liver, spleen, lungs, kidneys and brain). Blood and organs homogenized in 2 ml of normal saline were then streaked onto Columbia blood agar base plates containing 5% defibrinated sheep blood and incubated for 12 h at 37°C. The presence of kpssk3 was detected using the double-layer agar method.

16S rDNA Sequencing and Data Analysis

After microbial DNA was extracted from the 30 fecal samples using HiPure Soil DNA Kits (Magen, Guangzhou, China) according to the specifications, the V3 and V4 regions of 16S rDNA were amplified by PCR as previously described (Guo et al., 2017; Lv et al., 2020). The PCR products extracted from the 2% agarose gel were then purified, quantified, and sequenced (paired-end, 2 × 250 bp) on the Illumina MiSeq platform. Raw reads were filtered with FASTP[1] to obtain clean reads, which were further merged as raw tags with software FLASH (version 1.2.11) (Magoc and Salzberg, 2011). Raw tags were filtered with QIIME 1.9.1 software to obtain clean tags (Caporaso et al., 2010), and chimeric tags were then removed with UCHIME (version 8.1) to obtain effective tags. The UPARSE pipeline was used to identify operational taxonomic units (OTUs) with a sequence similarity of ≥ 97% (Edgar, 2013), and Venn analysis was performed using R Project 3.4.1 to identify the unique and common OTUs. Alpha diversity and beta diversity analyses were then carried out. The alpha diversity reflects the species diversity in a single sample and is evaluated using the Chao1, ACE, Simpson, and Shannon indexes, which were calculated with QIIME (version

[1]https://github.com/OpenGene/fastp

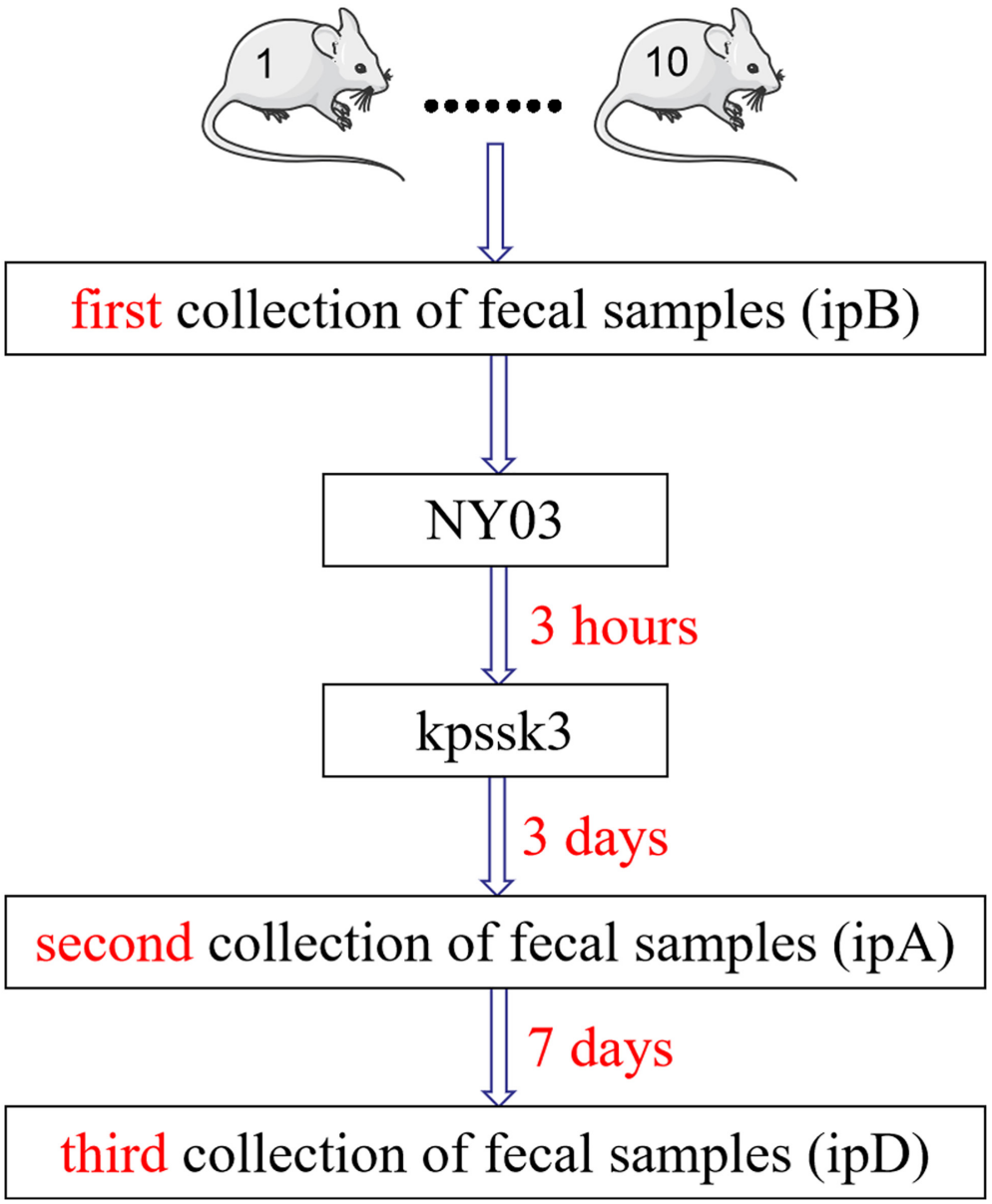

FIGURE 1 | Diagrammatic sketch of the fecal sample collection process.

1.9.1). The Chao1 and ACE indices are used to estimate the species richness of each group, which is proportional to the richness of each community, while the Simpson and Shannon indices demonstrate the species diversity, higher values of which indicate lower and greater species diversity, respectively. Alpha index comparison (*p*-value) was performed with the Wilcoxon rank sum test (between 2 groups) or Kruskal-Wallis test (among 3 groups) in R Project. Beta diversity is an important component of biological diversity, measuring compositional change across temporal and spatial scales. Beta diversity analysis was used to compare the composition of the microbial community among the different samples (Feng et al., 2019). Principal coordinates analysis (PCoA) and Adonis (all called PERMANOVA) tests were performed via R Project. $P < 0.05$ was considered statistically significant.

RESULTS

Antimicrobial Susceptibility Testing and Phenotype Detection

Antibiotic resistance genes, including bla_{TEM}, bla_{KPC}, bla_{GIM}, bla_{OXA-48}, bla_{ACT}, $bla_{CTX-M-9}$, $bla_{CTX-M-10}$, $bla_{CTX-M-14}$, bla_{DHA}, and bla_{SHV}, were detected in NY03 by PCR. As expected, NY03 was resistant to CAZ/AVI with an MIC value of 32 mg/L. **Table 1** showed the MICs of antibiotics alone and in combination.

The combination of CAZ/AVI and ATM revealed a synergistic antibacterial effect against NY03 *in vitro* (FICI = 0.16). Regarding the identification of the hypermucoviscosity phenotype, NY03 generated a viscous filament of 6 cm in length when stretched with a loop (**Figure 2**), demonstrating that this NY03 colony with a positive string test possessed a hypermucoviscous phenotype and was thus considered carbapenem-resistant hypermucoviscous *K. pneumoniae* (CR-HMKP). However, NY03 was negative for the tested virulence genes.

Cytotoxicity of kpssk3

To evaluate cell viability after treatment with different concentrations of kpssk3, a CCK-8 assay was carried out. As shown in **Figure 3**, compared to PBS treatment, treatment with 10^8 PFU/ml or a higher concentration (10^9 PFU/ml) of kpssk3 had no significant suppressive effect on HeLa cells. For histological examination, the isolated tissue samples from the spleen, lungs, kidneys and liver were stained with hematoxylin and eosin and analyzed under a microscope to determine any pathological changes in the different organs of the mice. As seen in **Figure 4**, compared to those in the control mice, these 4 organs in the mice treated with different doses of kpssk3 by intraperitoneal injection showed no notable histological changes. In addition, all mice treated with kpssk3 remained alive and healthy during the entire experimental period, without showing any signs of toxicity or any changes in body weight.

Distribution of kpssk3 in the Blood of Healthy Mice

As shown in **Figures 5**, **6** min after intraperitoneal injection, kpssk3 was rapidly diffused into the systemic circulation and reached a titer of 10^5 PFU/ml. During the first 4 h, the blood phage level remained high (approximately 10^6 PFU/ml) but was approximately two orders of magnitude lower than the injected concentration. Over the subsequent 4 h, the number of active phages in the blood rapidly decreased, completely disappearing by the 8th hour.

Therapeutic Efficacy of kpssk3 Against Bacteremia in Mice

Intraperitoneal injection of 1×10^7 CFU/mouse of NY03 caused a 100% mortality rate within 1.5 days; therefore, the mouse model of bacteremia was established by infection with 0.1 ml of a log-phase (OD600 = 0.6) bacterial inoculum containing 2×10^7 CFU of NY03. In group 1, intraperitoneal administration of 0.1 ml of NY03 bacterial suspension (2×10^7 CFU/mouse) caused 100% mortality within 8 h. In group 2, the survival rate at the end of the first day was 50% (5/10) and decreased further to 20% (2/10) by the third day, with 2 mice surviving after PMB treatment. In group 3, the survival rate of the mice on day 7 was 20% (2/10); however, treatment with CAZ/AVI plus ATM raised the survival rate of the mice in group 6–90% (9/10). By contrast, 100% of mice infected i.p. with 2×10^7 CFU of NY03 and treated with 10^7 PFU kpssk3 survived and remained healthy during this entire period. Treatment with 10^6 PFU kpssk3 protected 80% of mice against bacteremia. No death was observed 7 days after administration of normal saline to mice in group 7. **Figure 6**, generated with GraphPad Prism (version 6.0), shows the survival rates for groups 2, 3, 4, 5, and 6. By the end of the experiment, no bacteria or phages were found in the blood or organs of the 9 sacrificed mice in group 4. As shown in **Figure 4** "Group 4," histopathological examination of the spleen, lung, kidney and liver removed from the phage-rescued mouse revealed no notable histological changes (**Figure 4**). And the phage-resistant strain, named NY03r, was obtained by cross-streak method after incubation for about 24 h. NY03r had a same antibiogram with the parent strain (NY03), however, the viscous filament formed by NY03r (approximately 1.5 cm) was much shorter than the one formed by NY03 (**Figure 2**).

TABLE 1 | Results of MIC and AST of CAZ/AVI single dosing and combined with ATM against NY03.

MIC (mg/L) single dosing		MIC (mg/L) combined dosing		FIC value
ATM	**CAZ-AVI**	**ATM**	**CAZ-AVI**	
64	32	8	1	0.16

Alpha Diversity and Beta Diversity

The total number of OTUs was 3,270 in the ipB group, 3,574 in the ipA group, and 2,786 in the ipD group, and 1,762 OTUs were shared by the 3 groups (**Figure 7**). Regarding alpha diversity analysis, the Chao 1, ACE, Shannon, and Simpson indexes of each group are listed in **Table 2** and shown with box plots (**Supplementary Figure 1**). The Chao1 and ACE indexes, which reflect the species richness of samples, were the highest in the ipB group and lowest in the ipD group, and the differences between the 2 groups were statistically significant (Chao1 $P < 0.05$; ACE $P < 0.05$) (**Table 3**). The Chao1 and ACE indexes in the ipA group were lower than those in the ipB group, but the differences were not significant ($P > 0.05$). The Simpson and Shannon indexes, which reflect the species diversity of samples, did not differ among the 3 groups ($P > 0.05$) (**Table 3**). Regarding beta diversity analysis, PCoA based on the weighted UniFrac and Bray-Curtis distances revealed that there was no clear separation of the gut microbiome among the ipB, ipA and ipD groups (**Supplementary Figure 2**). The Adonis test based on the weighted UniFrac or Bray-Curtis distances did not show a significant difference in the gut microbiome between the groups (**Table 3**). Additionally, we analyzed the microbial composition of each group at different classification levels, including phylum, class, order, family and genus, and selected the top 10 abundant species in each level to generate species relative abundance bar plots (**Supplementary Figure 3**). The Wilcoxon rank sum test and Kruskal-Wallis test showed no statistically significant differences in the microbial community structure among the 3 groups (**Supplementary Table 1**).

DISCUSSION

CRKP, which is often associated with the lack of available effective antibiotics, increased mortality and exorbitant medical

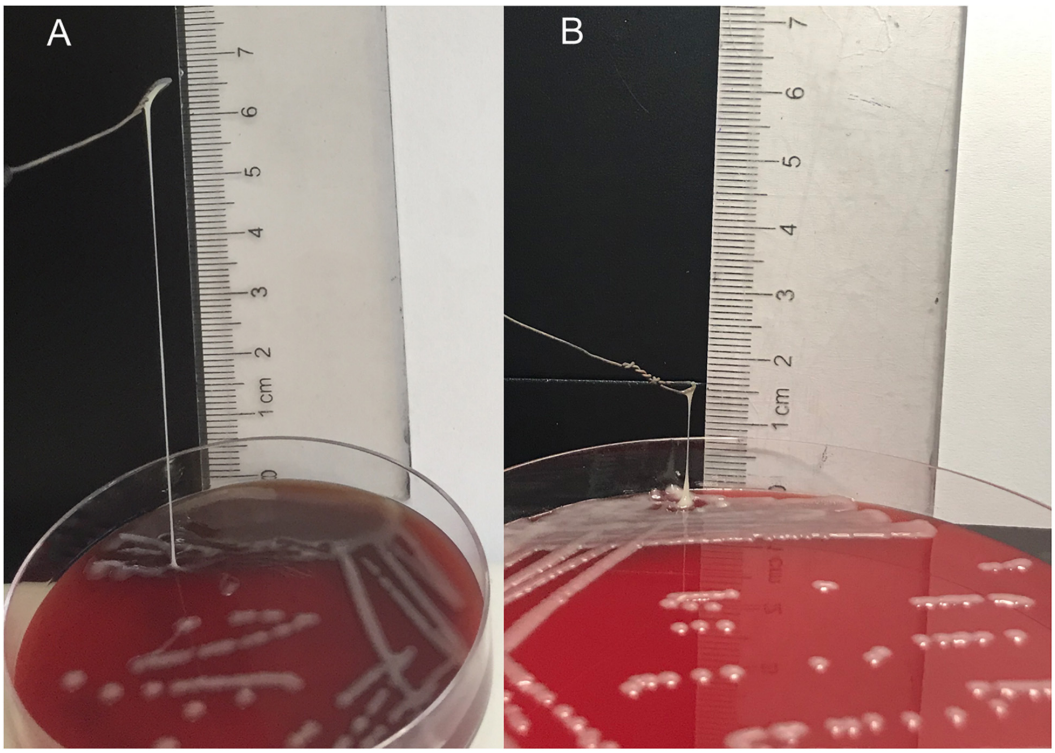

FIGURE 2 | String test of NY03 **(A)** and NY03r **(B).**

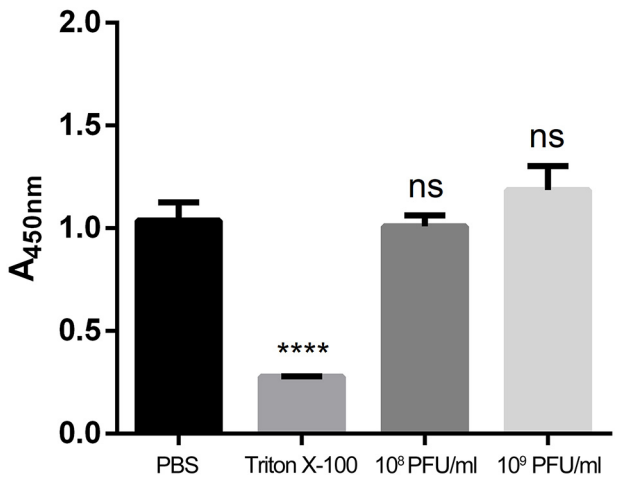

FIGURE 3 | Cell viability evaluation by a CCK-8 assay (****$P < 0.001$).

expenses, is an extremely dangerous clinical pathogen. The emergence of and continuing increase in hvKP, which is generally associated with community-acquired invasive infections and the hypermucoviscosity phenotype, constitutes another global threat. Clearly, the combination of hypervirulence and resistance in *K. pneumoniae* clinical isolates may worsen the situation even further (Lai et al., 2019). PT provides us with a promising alternative strategy and new hope in combating hard-to-treat infections. The present study evaluated the therapeutic effects and safety of kpssk3 PT as a treatment for CR-HMKP infection in a mouse model.

The clinical isolate NY03 exhibited the hypermucoviscous phenotype, which is generally considered the hallmark of hypervirulence (Chen et al., 2020). However, large knowledge gaps regarding the relationship between the expression of the capsule, hypermucoviscosity and hypervirulence still exist (Walker et al., 2019). Additionally, there is no consensus definition of hvKP, despite the numerous studies over the past few decades (Cubero et al., 2019). Genomic background and clinical features should be considered when estimating the virulence of a *K. pneumoniae* strain with a positive string test (Catalan-Najera et al., 2017). The tested virulence genes (*rmpA*/*rmpA2*, *magA*, *iucA*, and *iroA*) were not detected in NY03. The mouse lethality assay showed that the LD_{100} of NY03 was 10^7 CFU, a high inoculation dose compared with that of hvKP strains. Additionally, no invasive infection, such as PLA, lung abscess, endophthalmitis, meningitis or necrotizing fasciitis, was found in the patient who developed sepsis caused by NY03. Therefore, NY03 was considered a low virulent CR-HMKP strain.

To investigate phage kpssk3 as a therapeutic choice, we sought to obtain basic pharmacokinetic data about its distribution in and clearance from the blood of healthy mice. Phages can be delivered via many different administration routes, among which intraperitoneal injection has been proven to be a highly efficient method to introduce phages into the circulatory system (Dabrowska et al., 2005). In this study, active phages were

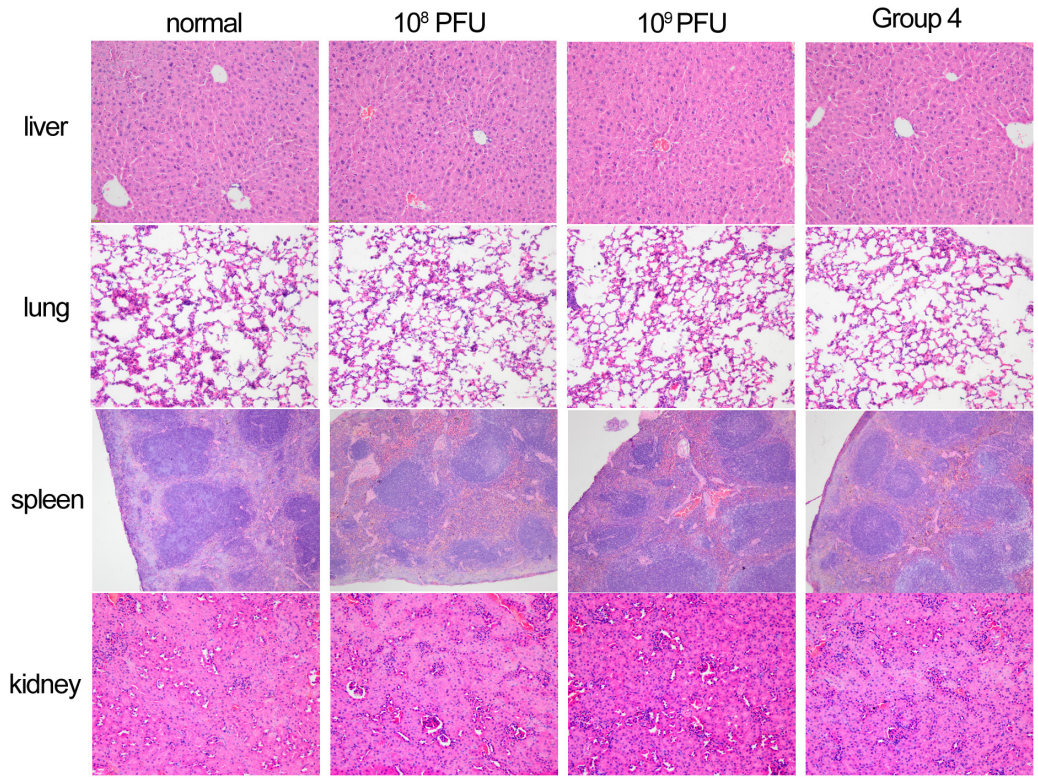

FIGURE 4 | Histopathology of spleen, lung, kidney and liver tissues from normal mouse, mice used to detect the toxicity of different doses of kpssk3 (10^8 PFU/mouse and 10^9 PFU/mouse), and phage-rescued mouse.

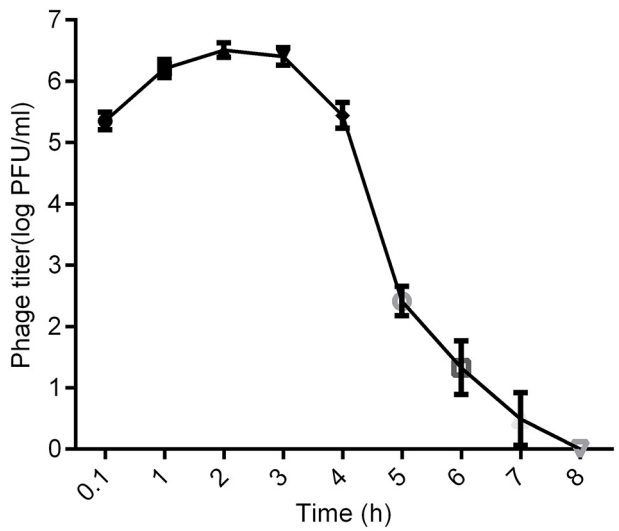

FIGURE 5 | Distribution of kpssk3 in the blood of healthy mice at different time points after intraperitoneal injection with 1 ml of 10^8 PFU/ml kpssk3.

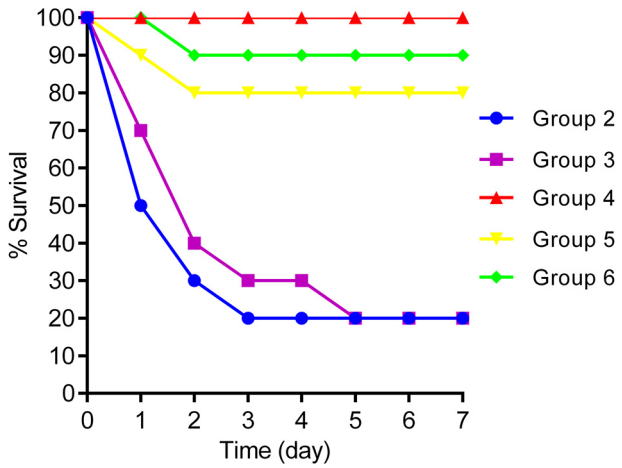

FIGURE 6 | Survival rates for groups 2, 3, 4, 5, and 6.

detected in blood 6 min after intraperitoneal administration of kpssk3. The phage titer in the blood peaked within the first hour and remained relatively high for 4 h, which made kpssk3 very applicable for treatment of systemic infections. However, the maximum phage concentration in the blood was approximately 100-fold lower than the injected phage concentration, and no phage was detected in the blood only 8 h after intraperitoneal delivery. Phage kpssk3 was expected to be diluted in blood and cleared by the mononuclear phagocyte

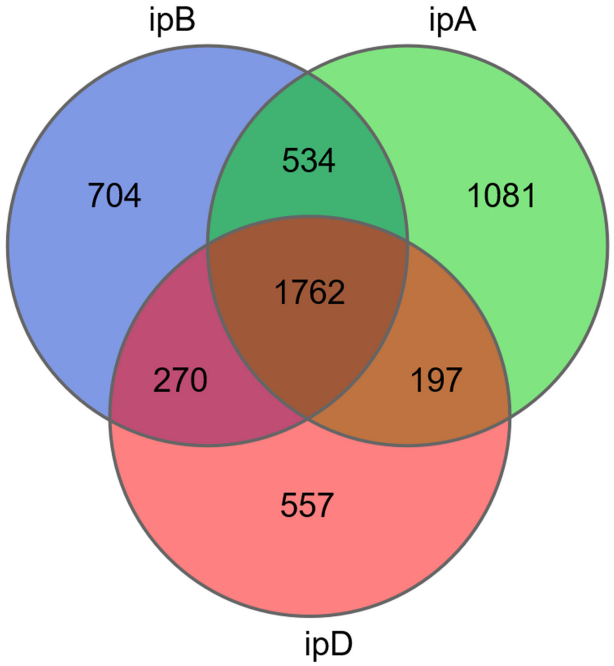

FIGURE 7 | Venn diagram of OTUs in the 3 groups. The different colored circles represent different groups.

TABLE 2 | The mean values of different alpha diversity indices (Chao1, ACE, Shannon, Simpson) in the three groups.

	ipB	ipA	ipD
Chao1	3668.1131	3301.8437	3192.2723
ACE	3648.6512	3264.6104	3206.5178
Shannon	7.0432	7.6565	7.2710
Simpson	0.9670	0.9776	0.9745

system (MPS) after entering the systemic circulation (Dabrowska, 2019). The short life of phages (e.g., kpssk3) in blood has historically been considered an important limitation for PT (Barr, 2017). To change the fate of phages *in vivo*, some experimental attempts (e.g., serial passage technique) have been made to obtain long-circulating phage mutants with an enhanced capability to escape capture by the MPS (Singla et al., 2016), which was favorable in improving the therapeutic potential of PT. However, whether these phage mutants persisting in the circulation can cause adverse effects is unclear. Considering this possibility, short-circulating phages can better prevent the potential side effects of PT.

Notably, the peak blood kpssk3 concentration, approximately 10^6 PFU/ml, made achieving the inundation threshold (the minimum phage concentration that can reduce the number of sensitive bacteria), which was equal to 10^7 PFU/ml or higher according to different calculations, difficult (Abedon, 2017). Thus, the phage (kpssk3) must first undergo self-replication, and the titer must then exceed the inundation threshold, based on which the PT in a passive mode can occur and decrease the bacterial population (Cairns et al., 2009). To achieve the optimal therapeutic effect, kpssk3 should be administered at a sufficiently high dose and applied more directly to infections, rather than relying on the concentration of kpssk3 to reach the "killing titer" by replication *in vivo*. In addition, much more research is required to better understand the pharmacological properties of kpssk3, such as its immunogenicity, its distribution in various organs, its ability to cross the blood-brain barrier and placental barrier, and its vertical transmission characteristics.

Regarding the effects of kpssk3, more effective protection of mice from lethal bacteremia was observed in the kpssk3 treatment group than in the PMB or TGC treatment groups, and both kpssk3 and NY03 were fully cleared 7 days later. In addition, the CAZ/AVI plus ATM treatment protocol was used for 7 days, and 90% of mice systemically infected with CR-HMKP survived. On the other hand, the antibiotic treatment protocols used in this study may need to be optimized for the selection of antibiotics, dosage, combination therapy and the prevention of side effects. Regarding the safety of kpssk3 PT, kpssk3 had no cytotoxic effect on mammalian cells and a lower impact on the gut microbiota. Many studies have demonstrated that the gut microbiota plays significant roles in human health (Ahlawat et al., 2020). Introduction of phages into the blood is followed by rapid extravasation of the phages from the bloodstream into internal organs and other tissues, including the gastrointestinal tract (Barr, 2017). Therefore, we are concerned about the short- and long-term impacts of kpssk3 treatment on the gut microbiota, despite its high specificity. Based on 16S rDNA analysis, only the Chao1 and ACE indexes were significantly decreased 10 days after kpssk3 PT, possibly because of the emergence of slight gut microbiota dysbiosis induced by PT. In addition, the possibility that NY03 impacted the gut microbiota cannot be ruled out.

TABLE 3 | Alpha and beta diversity statistical analysis.

Group	α diversity analysis (*p*-value)				β diversity analysis (*p*-value)	
	Chao1	ACE	Shannon	Simpson	Bray–Curtis	Weighted UniFrac
ipB-ipA	0.11	0.14	0.53	0.58	0.54	0.44
ipA-ipD	0.52	0.91	0.97	0.91	0.41	0.33
ipB-ipD	0.01	0.01	0.63	0.68	0.69	0.97
ipB-ipA-ipD	0.04	0.07	0.78	0.82	0.61	0.59

Alpha diversity indices comparison by Wilcoxon rank sum test or Kruskal-Wallis test; beta diversity indices comparison by Adonis test based on the weighted UniFrac or Bray-Curtis distances.

Whether this change is restored after 10 days requires further study. Obviously, we need to remain vigilant about the potential side effects and long-term effects of PT.

In summary, treatment with phage kpssk3 increased the survival rate of mice with CR-HMKP-induced bacteremia to 100%, and no serious side effects or signs of toxicity were observed in the *in vivo* test. There were also no significant changes in gut microbiome of mice during the treatment period. Based on these results, kpssk3 PT could be considered an effective alternative for CR-HMKP bacteremia due to its considerable therapeutic effect and lack of side effects.

DATA AVAILABILITY STATEMENT

The data presented in the study are deposited in the NCBI SRA repository, accession number PRJNA723119 (https://www.ncbi.nlm.nih.gov/Traces/study1/?acc=PRJNA723119).

ETHICS STATEMENT

The animal study was reviewed and approved by the Ethics Committee of Army Medical University.

AUTHOR CONTRIBUTIONS

YLG and YXZ conceived and designed the experiments. YLS, YP, and YC performed the experiments. YJC and ZQY analyzed the data. CZ, XQL and JC contributed reagents and materials. YLS wrote the paper. All authors contributed toward revising the paper and agreed to be accountable for all aspects of the work.

FUNDING

This work was funded by the National Natural Science Foundation of China (Nos. 81571896 and 81772073), the Foundation of State Key Laboratory of Trauma, Burns and combined injury (No. SKLZZ201708), and the Technological Innovation Plan in Major Fields of Southwest Hospital, Key Projects (No. SWH2016ZDCX2001).

ACKNOWLEDGMENTS

We would like to thank Yin Chang (Beijing Normal University, School of Foreign Languages and Literature) for English language editing.

SUPPLEMENTARY MATERIAL

The Supplementary Material for this article can be found online at: https://www.frontiersin.org/articles/10.3389/fmicb.2021.613356/full#supplementary-material

Supplementary Figure 1 | Box plot of the alpha diversity indexes (Chao1, ACE, Shannon, and Simpson).

Supplementary Figure 2 | Principal coordinates analysis (PCoA) plot based on Bray-Curtis **(A)** and weighted UniFrac distances **(B)**. Each point represents the microbial community structure of an individual fecal sample.

Supplementary Figure 3 | Relative abundance of species at different classification levels (phylum, class, order, family, genus). The abscissa shows grouping information, and the ordinate shows the relative abundance.

REFERENCES

Abedon, S. T. (2017). Active bacteriophage biocontrol and therapy on sub-millimeter scales towards removal of unwanted bacteria from foods and microbiomes. *AIMS Microbiol.* 3, 649–688. doi: 10.3934/microbiol.2017.3.649

Ahlawat, S., Asha, and Sharma, K. K. (2020). Gut-organ axis: a microbial outreach and networking. *Lett. Appl. Microbiol.* [Epub ahead of print]. doi: 10.1111/lam.13333

Aleksandrzak, M., Jedrzejczak-Silicka, M., Sielicki, K., Piotrowska, K., and Mijowska, E. (2019). Size-dependent *in vitro* biocompatibility and uptake process of polymeric carbon nitride. *ACS Appl. Mater. Interfaces* 11, 47739–47749. doi: 10.1021/acsami.9b17427

Alsanie, W. F. (2020). Molecular diversity and profile analysis of virulence-associated genes in some *Klebsiella pneumoniae* isolates. *Pract. Lab. Med.* 19:e152. doi: 10.1016/j.plabm.2020.e00152

Barr, J. J. (2017). A bacteriophages journey through the human body. *Immunol. Rev.* 279, 106–122. doi: 10.1111/imr.12565

Cairns, B. J., Timms, A. R., Jansen, V. A., Connerton, I. F., and Payne, R. J. (2009). Quantitative models of *in vitro* bacteriophage-host dynamics and their application to phage therapy. *PLoS Pathog.* 5:e1000253. doi: 10.1371/journal.ppat.1000253

Caporaso, J. G., Kuczynski, J., Stombaugh, J., Bittinger, K., Bushman, F. D., Costello, E. K., et al. (2010). QIIME allows analysis of high-throughput community sequencing data. *Nat. Methods* 7, 335–336. doi: 10.1038/nmeth.f.303

Catalan-Najera, J. C., Garza-Ramos, U., and Barrios-Camacho, H. (2017). Hypervirulence and hypermucoviscosity: Two different but complementary *Klebsiella* spp. phenotypes? *Virulence* 8, 1111–1123. doi: 10.1080/21505594.2017.1317412

Chen, L., and Kreiswirth, B. N. (2018). Convergence of carbapenem-resistance and hypervirulence in *Klebsiella pneumoniae*. *Lancet Infect. Dis.* 18, 2–3. doi: 10.1016/S1473-3099(17)30517-0

Chen, Y., Marimuthu, K., Teo, J., Venkatachalam, I., Cherng, B., De Wang, L., et al. (2020). Acquisition of plasmid with carbapenem-resistance gene blaKPC2 in Hypervirulent *Klebsiella pneumoniae*, Singapore. *Emerg. Infect. Dis.* 26, 549–559. doi: 10.3201/eid2603.191230

Cheng, M., Liang, J., Zhang, Y., Hu, L., Gong, P., Cai, R., et al. (2017). The Bacteriophage EF-P29 efficiently protects against lethal vancomycin-resistant *Enterococcus faecalis* and alleviates gut microbiota imbalance in a Murine Bacteremia model. *Front. Microbiol.* 8:837. doi: 10.3389/fmicb.2017.00837

Cubero, M., Marti, S., Dominguez, M. A., Gonzalez-Diaz, A., Berbel, D., and Ardanuy, C. (2019). Hypervirulent *Klebsiella pneumoniae* serotype K1 clinical isolates form robust biofilms at the air-liquid interface. *PLoS One* 14:e222628. doi: 10.1371/journal.pone.0222628

Dabrowska, K. (2019). Phage therapy: What factors shape phage pharmacokinetics and bioavailability? Systematic and critical review. *Med. Res. Rev.* 39, 2000–2025. doi: 10.1002/med.21572

Dabrowska, K., Switala-Jelen, K., Opolski, A., Weber-Dabrowska, B., and Gorski, A. (2005). Bacteriophage penetration in vertebrates. *J. Appl. Microbiol.* 98, 7–13. doi: 10.1111/j.1365-2672.2004.02422.x

Docobo-Perez, F., Nordmann, P., Dominguez-Herrera, J., Lopez-Rojas, R., Smani, Y., Poirel, L., et al. (2012). Efficacies of colistin and tigecycline in mice with experimental pneumonia due to NDM-1-producing strains of *Klebsiella*

pneumoniae and *Escherichia coli*. *Int. J. Antimicrob. Agents* 39, 251–254. doi: 10.1016/j.ijantimicag.2011.10.012

Edgar, R. C. (2013). UPARSE: highly accurate OTU sequences from microbial amplicon reads. *Nat. Methods* 10, 996–998. doi: 10.1038/nmeth.2604

Feng, Y., Huang, Y., Wang, Y., Wang, P., and Wang, F. (2019). Severe burn injury alters intestinal microbiota composition and impairs intestinal barrier in mice. *Burns Trauma* 7:20. doi: 10.1186/s41038-019-0156-1

Ferrer-Espada, R., Sanchez-Gomez, S., Pitts, B., Stewart, P. S., and Martinez-de-Tejada, G. (2020). Permeability enhancers sensitize beta-lactamase-expressing *Enterobacteriaceae* and *Pseudomonas aeruginosa* to beta-lactamase inhibitors, thereby restoring their beta-lactam susceptibility. *Int. J. Antimicrob. Agents* 56:105986. doi: 10.1016/j.ijantimicag.2020.105986

Fulgione, A., Ianniello, F., Papaianni, M., Contaldi, F., Sgamma, T., Giannini, C., et al. (2019). Biomimetic hydroxyapatite nanocrystals are an active carrier for *Salmonella* bacteriophages. *Int. J. Nanomedicine* 14, 2219–2232. doi: 10.2147/IJN.S190188

Ginosar, Y., Nachmanson, N. C., Shapiro, J., Weissman, C., and Abramovitch, R. (2015). Inhaled carbon dioxide causes dose-dependent paradoxical bradypnea in animals anesthetized with pentobarbital, but not with isoflurane or ketamine. *Respir. Physiol. Neurobiol.* 217, 1–7. doi: 10.1016/j.resp.2015.06.003

Gu, D., Dong, N., Zheng, Z., Lin, D., Huang, M., Wang, L., et al. (2018). A fatal outbreak of ST11 carbapenem-resistant hypervirulent *Klebsiella pneumoniae* in a Chinese hospital: a molecular epidemiological study. *Lancet Infect. Dis.* 18, 37–46. doi: 10.1016/S1473-3099(17)30489-9

Guo, M., Wu, F., Hao, G., Qi, Q., Li, R., Li, N., et al. (2017). *Bacillus subtilis* improves immunity and disease resistance in rabbits. *Front. Immunol.* 8:354. doi: 10.3389/fimmu.2017.00354

Guo, Z., Lin, H., Ji, X., Yan, G., Lei, L., Han, W., et al. (2020). Therapeutic applications of lytic phages in human medicine. *Microb. Pathog.* 142:104048. doi: 10.1016/j.micpath.2020.104048

Hietala, V., Horsma-Heikkinen, J., Carron, A., Skurnik, M., and Kiljunen, S. (2019). The removal of endo- and enterotoxins from bacteriophage preparations. *Front. Microbiol.* 10:1674. doi: 10.3389/fmicb.2019.01674

Khalil, M., Hager, R., Abd-El, R. F., Mahmoud, E. E., Samir, T., Moawad, S. S., et al. (2019). A study of the virulence traits of carbapenem-resistant *Klebsiella pneumoniae* isolates in a *Galleria mellonella* model. *Microb. Drug Resist.* 25, 1063–1071. doi: 10.1089/mdr.2018.0270

Lai, Y. C., Lu, M. C., and Hsueh, P. R. (2019). Hypervirulence and carbapenem resistance: two distinct evolutionary directions that led high-risk *Klebsiella pneumoniae* clones to epidemic success. *Expert Rev. Mol. Diagn.* 19, 825–837. doi: 10.1080/14737159.2019.1649145

Landersdorfer, C. B., Wang, J., Wirth, V., Chen, K., Kaye, K. S., Tsuji, B. T., et al. (2018). Pharmacokinetics/pharmacodynamics of systemically administered polymyxin B against *Klebsiella pneumoniae* in mouse thigh and lung infection models. *J. Antimicrob. Chemother.* 73, 462–468. doi: 10.1093/jac/dkx409

Lv, X., Li, S., Yu, Y., Xiang, J., and Li, F. (2020). The immune function of a novel crustin with an atypical WAP domain in regulating intestinal microbiota homeostasis in *Litopenaeus vannamei*. *Dev. Comp. Immunol.* 111:103756. doi: 10.1016/j.dci.2020.103756

Magoc, T., and Salzberg, S. L. (2011). FLASH: fast length adjustment of short reads to improve genome assemblies. *Bioinformatics* 27, 2957–2963. doi: 10.1093/bioinformatics/btr507

Marshall, S., Hujer, A. M., Rojas, L. J., Papp-Wallace, K. M., Humphries, R. M., Spellberg, B., et al. (2017). Can Ceftazidime-Avibactam and Aztreonam Overcome beta-Lactam Resistance Conferred by Metallo-beta-Lactamases in *Enterobacteriaceae*? *Antimicrob. Agents Chemother.* 61:e02243-16. doi: 10.1128/AAC.02243-16

Myelnikov, D. (2018). An alternative cure: the adoption and survival of Bacteriophage therapy in the USSR, 1922–1955. *J. Hist. Med. Allied Sci.* 73, 385–411. doi: 10.1093/jhmas/jry024

Porreca, A. M., Sullivan, K. V., and Gallagher, J. C. (2018). The epidemiology, evolution, and treatment of KPC-producing organisms. *Curr. Infect. Dis. Rep.* 20:13. doi: 10.1007/s11908-018-0617-x

Shi, Y., Chen, Y., Yang, Z., Zhang, Y., You, B., Liu, X., et al. (2020). Characterization and genome sequencing of a novel T7-like lytic phage, kpssk3, infecting carbapenem-resistant *Klebsiella pneumoniae*. *Arch. Virol.* 165, 97–104. doi: 10.1007/s00705-019-04447-y

Singla, S., Harjai, K., Raza, K., Wadhwa, S., Katare, O. P., and Chhibber, S. (2016). Phospholipid vesicles encapsulated bacteriophage: a novel approach to enhance phage biodistribution. *J. Virol. Methods* 236, 68–76. doi: 10.1016/j.jviromet.2016.07.002

Suay-Garcia, B., and Perez-Gracia, M. T. (2019). Present and future of carbapenem-resistant *Enterobacteriaceae* (CRE) infections. *Antibiotics* 8:12. doi: 10.3390/antibiotics8030122

Ungphakorn, W., Lagerback, P., Nielsen, E. I., and Tangden, T. (2018). Automated time-lapse microscopy a novel method for screening of antibiotic combination effects against multidrug-resistant Gram-negative bacteria. *Clin. Microbiol. Infect.* 24, 777–778. doi: 10.1016/j.cmi.2017.10.029

Venter, H. (2019). Reversing resistance to counter antimicrobial resistance in the World Health Organisation's critical priority of most dangerous pathogens. *Biosci. Rep.* 39:BSR20180474. doi: 10.1042/BSR20180474

Vergara, A., Moreno-Morales, J., Roca, I., Pitart, C., Kostyanev, T., Rodriguez-Bano, J., et al. (2020). A comparative study between real-time PCR and loop-mediated isothermal amplification to detect carbapenemase and/or ESBL genes in *Enterobacteriaceae* directly from bronchoalveolar lavage fluid samples. *J. Antimicrob. Chemother.* 75, 1453–1457. doi: 10.1093/jac/dkaa031

Walker, K. A., Miner, T. A., Palacios, M., Trzilova, D., Frederick, D. R., Broberg, C. A., et al. (2019). A *Klebsiella pneumoniae* regulatory mutant has reduced capsule expression but retains hypermucoviscosity. *mBio* 10:e00089-19. doi: 10.1128/mBio.00089-19

Wang, Q., Zhang, F., Wang, Z., Chen, H., Wang, X., Zhang, Y., et al. (2020). Evaluation of the Etest and disk diffusion method for detection of the activity of ceftazidime-avibactam against *Enterobacterales* and *Pseudomonas aeruginosa* in China. *BMC Microbiol.* 20:187. doi: 10.1186/s12866-020-01870-z

Xia, F., Li, X., Wang, B., Gong, P., Xiao, F., Yang, M., et al. (2016). Combination therapy of LysGH15 and apigenin as a new strategy for treating pneumonia caused by *Staphylococcus aureus*. *Appl. Environ. Microbiol.* 82, 87–94. doi: 10.1128/AEM.02581-15

Zhang, P., Shi, Q., Hu, H., Hong, B., Wu, X., Du, X., et al. (2020). Emergence of ceftazidime/avibactam resistance in carbapenem-resistant *Klebsiella pneumoniae* in China. *Clin. Microbiol. Infect.* 26, 121–124. doi: 10.1016/j.cmi.2019.08.020

Conflict of Interest: The authors declare that the research was conducted in the absence of any commercial or financial relationships that could be construed as a potential conflict of interest.

Copyright © 2021 Shi, Peng, Zhang, Chen, Zhang, Luo, Chen, Yuan, Chen and Gong. This is an open-access article distributed under the terms of the Creative Commons Attribution License (CC BY). The use, distribution or reproduction in other forums is permitted, provided the original author(s) and the copyright owner(s) are credited and that the original publication in this journal is cited, in accordance with accepted academic practice. No use, distribution or reproduction is permitted which does not comply with these terms.

frontiers in Microbiology

ORIGINAL RESEARCH
published: 25 May 2021
doi: 10.3389/fmicb.2021.670799

Characterization of a Novel Bacteriophage swi2 Harboring Two Lysins Can Naturally Lyse *Escherichia coli*

*Bingrui Sui†, Xin Qi†, Xiaoxue Wang, Huiying Ren, Wenhua Liu and Can Zhang**

College of Veterinary Medicine, Qingdao Agricultural University, Shandong, China

The novel virulent *Siphoviridae* bacteriophage swi2 was isolated from a pig farm, and its biological characteristics, genome architecture, and infection-related properties were characterized. Phage swi2 has a high titer of 1.01×10^{12} PFU/mL with good tolerance to UV rays and remains stable in the pH range of 6–10 and at temperatures less than 50°C. One-step growth analysis revealed that phage swi2 had a 25 min latent period with a large burst size (1,000 PFU/cell). The biological characteristics indicated that swi2 had good host infectivity and effective lytic activities. The genome of phage swi2 is composed of 47,611 bp with a G + C content of 46.50%. Eighty-nine orfs were predicted, and only 18 of them have known functions. No virulence genes or drug resistance genes were found in the genome. Genome sequence comparison of phage swi2 showed that there were a total of 10 homologous phages in the database with low similarity (less than 92.51% nucleotide identity and 66% query coverage). The predicted host lysis-related genes of phage swi2 consist of one *holin*, two *endolysins*, and *Rz/Rz1* equivalents. Antibacterial activity assays showed that both endolysins could naturally reduce the host *Escherichia coli* 51 titers by -1 log unit both *in vitro* and *in vivo*, EDTA showed no obvious synergistic action, and holin had no lytic effects on the host cell. These results provide necessary information for the development of antibiotic alternatives for the treatment of multidrug-resistant *Escherichia coli* infection.

Keywords: bacteriophage swi2, biological and genomic character, endolysin, holing, antibacterial activity

OPEN ACCESS

Edited by:
Shuai Le,
Army Medical University, China

Reviewed by:
Josefina Leon-Felix,
Consejo Nacional de Ciencia y Tecnología (CONACYT), Mexico
Xiaohong Wang,
Huazhong Agricultural University, China

***Correspondence:**
Can Zhang
cleverflame@163.com

†These authors share first authorship

Specialty section:
This article was submitted to Virology, a section of the journal Frontiers in Microbiology

Received: *22 February 2021*
Accepted: *22 April 2021*
Published: *25 May 2021*

Citation:
Sui B, Qi X, Wang X, Ren H, Liu W and Zhang C (2021) Characterization of a Novel Bacteriophage swi2 Harboring Two Lysins Can Naturally Lyse Escherichia coli. Front. Microbiol. 12:670799. doi: 10.3389/fmicb.2021.670799

INTRODUCTION

Escherichia coli (*E. coli*) is widely distributed in the environment as one of the most important opportunistic pathogens and can cause colibacillosis of swine, which seriously threatens animal health globally, especially in high-density breeding farms (Tran et al., 2018). *E. coli* mainly infects 1–2-week-old piglets and causes white scour, yellow scour or porcine edema disease with clinical symptoms of diarrhea, which leads to very large economic losses (Sun et al., 2019). Antibiotics are currently used to treat colibacillosis in piglets. However, the development of antibiotics can hardly keep up with the rapid emergence of antagonistic bacteria in recent years (Lee et al., 2018). Therefore, new antibacterial agents have been encouraged for the control of pathogens, and bacteriophages or their endolysins are among the most promising candidates (Guenther et al., 2017). It has been reported that phages are the most abundant and diverse life forms on earth, and

although some of them have been sequenced and reported, there is still much work to do in the process of phage therapy. In the past decade, phages and their enzymes have become a hot topic in the field of developing antibiotic substitutes, and there have been many successful phage therapy reports regarding the prevention and treatment of bacterial infections, suggesting that phages are good candidates as antibiotic alternatives (Vahedi et al., 2018). A bacteriophage (phage) with a broad host range, efficient proliferation, a high lysis titer and stable physical is more dominant in the prevention and control of colibacillosis. In this way, it can avoid the failure of prevention and control in the process of phage preparation to prevent and control bacterial infections based on the mismatch between the lysis range and the host bacteria (Alemayehu et al., 2012). Endolysin (lysin), a phage enzyme, has a broader lysis spectrum than its original phage. To date, most of the reported endolysins have shown good bactericidal activity against gram-positive bacteria but have shown less activity against gram-negative bacteria due to the outer membrane barrier, and the endolysins generally require the help of membrane permeating agent (Young, 2013). Recently, limited lysins have been reported that show bactericidal activity against gram-negative bacteria, it showed that the ability of lysins to pass bacterial outer membrane is mediated by the naturally occurring sequence of two ends (residues 1–20) carrying positively charged or hydrophobic residues (Plotka et al., 2019; Lai et al., 2020; Wang et al., 2020).

In the current study, an enterophage was isolated from a pig farm which showed a very high titer. Its biological characteristics, genomic architecture and infection-related properties were analyzed and found it was a new phage with a good tolerance to physical and chemical factors with a large burst size and a short incubation period. Interestingly, the proteins encoded by two functional *lysin* genes of phage swi2 had natural antibacterial activity in gram-negative bacteria. This special ability of phage swi2 and its lysins makes the clinical treatment of pathogenetic and drug-resistant *E. coli* possible.

MATERIALS AND METHODS

Samples and Bacteria Strains

Samples of sewage were collected from pig farms in Shandong, China. A total of 79 *E. coli* clinical isolates with different resistances to antibiotic were selected as strains for host range testin this study (**Supplementary Table 1**). All *E. coli* strains were cultured in Luria-Bertani (LB) culture at 37°C overnight and stored at 4°C until used.

Phage Isolation

The *E. coli* 51 strain was used as the host cell in this study for phage isolation. Sewage samples were performed using a standard enrichment method to propagate the phages, and the phages were isolated using the conventional double-layer agar plate method as described before (Zhang et al., 2013). Briefly, the sewage sample was cultured with 500 μL of *E. coli* 51 in 50 mL of LB at 37°C overnight. Then, the mixture was centrifuged at 12,000 × *g* for 30 min to collect the supernatant, and the supernatant was filtered through a 0.22 μm filter. One hundred microliters of supernatant and 100 μL of *E. coli* 51 were mixed and incubated for 5 min at room temperature, added to 3 mL of melted 0.7% soft agar, plated on an LB agar plate, and cultured at 37°C for 6 h. A single plaque was selected and purified four times, and the purified phage was stored at -80°C in 30% glycerol until use.

Electron Microscopy of Phage swi2

For morphological observation, 10 μL of purified phage suspension (10^{10} PFU/mL) was dropped onto a carbon-coated grid, negatively stained with 2% uranyl acetate for 5 min and observed by transmission electron microscopy (HT7700, Hitachi, Japan) at an accelerating voltage of 80 kV. The size of the phage particles was determined from at least 10 measurements.

Host Range and EOP Analysis

The host range of phage swi2 was determined by a spot test with 79 clinical isolates. In brief, 5 μL of purified phage swi2 was spotted onto freshly seeded lawns of each bacterial strain, left to dry, and then incubated at 37°C for 6 h. Additionally, the efficiency of plating (EOP) was calculated by the spot test as described in a previous report (Chen et al., 2013). Briefly, 10 μL of different dilutions (10^{10}–10^{13}) of phage swi2 were spotted onto freshly seeded lawns of the clinical isolates and incubated for 6 h at 37°C. The EOP values were determined by calculating the ratio of PFUs of each phage-susceptible strain to the PFUs obtained with *E. coli* 51. Moreover, the phage swi2 titer was determined by *SYBR Green I*-based quantitative PCR. Briefly, *lysin1-SYBR*-specific primers for the real-time quantitative PCR system were designed (**Supplementary Table 2**), amplification was performed according to the kit's instructions. And the recombinant plasmid pColdTF-lysin1-SYBR was constructed after correct identification. The copy number of the recombinant plasmid was determined, and the plasmid was diluted by 10 times ratio to obtain the standard substance and establish the standard curve, then the titer of phage swi2 was tested. The experiments were repeated three times.

Stability of Phage swi2

The thermal stability, ultraviolet light, and pH sensitivity of phage swi2 were determined as previously reported (Jamal et al., 2015). In brief, for thermal stability tests, aliquots of phage swi2 were incubated at 40, 50, 60, 70, and 80°C for 1 h, and samples were taken at 20 min intervals. For the ultraviolet stability tests, aliquots of phage swi2 were incubated at 37°C (at a distance of 40 cm away from a UV lamp) for 1 h, and samples were taken at 10 min intervals. For the pH stability tests, aliquots of phage swi2 were incubated at 37°C in the pH range from 1–14 for 1–3 h, and samples were taken at 1 h intervals. The phage titer of each sample was determined by the double-layer agar plate method. Each assay was repeated three times.

MOI Assay of Phage swi2

The multiplicity of infection (MOI) refers to the ratio of phage to host bacteria during the processes for infection. The host cell *E. coli* 51 was selected and cultured to the logarithmic growth

phase, diluted to 10^7 CFU/mL, and then coincubated with phage swi2 at different MOIs (0.001, 0.01, 0.1, 1, 10, 100, and 1,000) for 4 h at 37°C. An *E. coli* 51 culture without phage swi2 was used as the control. The phage titers of swi2 were tested by the double-layer agar plate method, and the most optimal MOI was determined.

One-Step Growth of Phage swi2

The latent period and burst size of phage swi2 were determined by one-step growth analysis as described previously (Yang et al., 2019). In brief, the host bacterial strain (10^9 CFU) and phage swi2 suspension (10^{10} PFU) were mixed at an MOI of 10, incubated at 37°C for 5 min, and then centrifuged at 13,000 × *g* for 30 s to remove the unabsorbed phage particles. The precipitate was washed with LB twice and resuspended in 7 mL of LB, followed by further incubation at 37°C for 4 h. Samples were collected every 5 min in the first hour, every 10 min in the second hour, and every 30 min in the last 2 h. The phage titer was determined by the double-layer agar plate method. The experiment was repeated three times.

Sequencing and Genomic Analysis of Phage swi2

The genome of phage swi2 was extracted with the TIANamp Virus DNA/RNA kit (Tiangen Biotech Beijing Co., Ltd.) and sequenced on an Illumina HiSeq platform. Contigs were assembled using the *de novo* assembly algorithm Newbler version 3.0 with default parameters (Bao et al., 2014). Open Reading Frames (*orfs*) were predicted using GeneMark[1] and the RAST website[2] (Park et al., 2012). Potential tRNA genes were identified with tRNA-scan-SE[3] (Lowe and Chan, 2016). Resistance genes and virulence genes were identified using the Antibiotic Resistance Genes Database[4] and Comprehensive Antibiotic Resistance Database[5]. The transmembrane area of the *holin* gene was predicted by TMHMM[6]. The domain of *lysin* genes was analyzed by CD-search in NCBI[7]. Phylogenetic analyses of phage swi2 were performed in the NCBI GenBank database based on the genome sequence or large terminase subunit sequences, and phylogenetic trees were constructed using the neighbor-joining method with the default parameters in MEGA 7.0 software (Kumar et al., 2016). The genome sequence of swi2 was deposited in GenBank under accession number MT768060.

Antibacterial Activity Assay of Lytic System-Associated Proteins

Predicted *lysin* genes *orf 50* (*lysin1*), *orf 51* (*lysin2*), and *holin* gene (*orf 49*) were amplified from extracted phage swi2 genomic DNA by PCR using the designed primers (**Supplementary Table 2**) to construct recombined plasmids pColdTF-holin, pColdTF-lysin1, and pColdTF-lysin2, and plasmids were transferred into *E. coli* BL21 to express proteins. One hundred microliters of *E. coli* BL21 carrying the recombinant plasmid was cultured to the logarithmic growth period in LB broth at 37°C and induced with 1 mM IPTG at 16°C for 12 h. Then, the cultures were processed and sonicated to collect expressed proteins as previously reported (Zhang et al., 2015). The soluble expressed proteins were purified by Ni-affinity chromatography (CoWin Biosciences). The antibacterial activities of the proteins lysin1, lysin2, and holin against *E. coli* BL21 were tested both *in vivo* and *in vitro*. The antibacterial activities were evaluated by bacterial turbidity changes and bacterial log reductions. Briefly, for the antibacterial activity assay *in vivo*, *E. coli* BL21 carrying different plasmids was cultured to the logarithmic stage in LB at 37°C

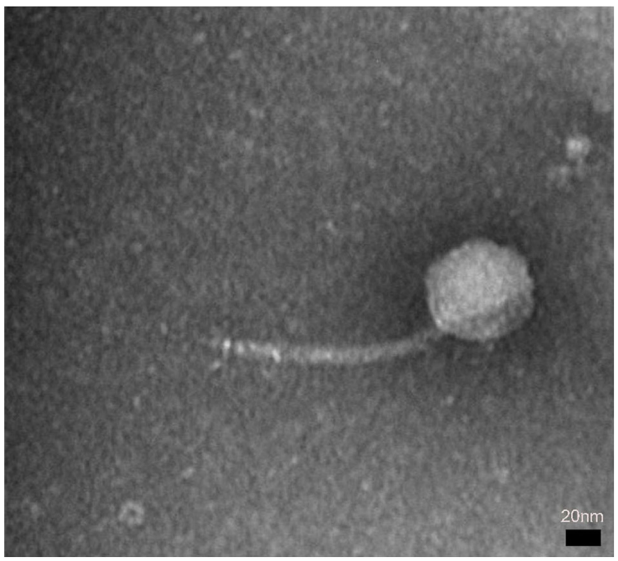

FIGURE 1 | The morphology of phage swi2. Phage swi2 was negatively stained with 2% uranyl acetate and observed by transmission electron microscopy (TEM) at an accelerating voltage of 80 kV. The scale bars represent 20 nm.

TABLE 1 | The titer and EOP of phage swi2 in host bacteria.

Strain numbers	Strain name	Titer phage swi2 (PFU/mL)	The efficiency of plating (EOP)
1	*E. coli* 21	1.7×10^{10}	0.02
2	*E. coli* 24	1.4×10^{12}	1.39
3	*E. coli* 30	2.3×10^{13}	22.77
4	*E. coli* 38	1.4×10^{13}	13.86
5	*E. coli* 42	1.3×10^{13}	12.87
6	*E. coli* 45	1.1×10^{13}	10.89
7	*E. coli* 46	1.1×10^{12}	1.09
8	*E. coli* 48	8.0×10^{11}	0.79
9	*E. coli* 49	1.0×10^{11}	0.10
10	*E. coli* 51	1.01×10^{12}	1.00
11	*E. coli* 54	7.0×10^{11}	0.69

[1]http://topaz.gatech.edu/GeneMark/
[2]https://rast.nmpdr.org/
[3]http://lowelab.ucsc.edu/tRNAscan-SE/
[4]http://ardb.cbcb.umd.edu/
[5]http://arpcard.mcmaster.ca
[6]http://www.cbs.dtu.dk/services/TMHMM-2.0/
[7]https://www.ncbi.nlm.nih.gov/Structure/cdd/wrpsb.cgi

and induced with 1 mM IPTG for 16 h. The absorbance of the cultures at OD_{600} was measured at 0, 4, and 16 h in a 96-well plate. Additionally, colony counts of the cultures were carried out at 16 h. *E. coli* BL21 carried different plasmids without IPTG induction, and *E. coli* BL21 carrying the pColdTF plasmid with or without IPTG induction was used as a control. For the antibacterial activity assay *in vitro*, 100 μL of purified proteins (2 μM final concentration) was mixed with 100 μL of *E. coli* BL21 (10^6 CFU/mL) in a 96-well plate with or without EDTA (2 μM final concentration) and incubated at 37°C for 4 h. The absorbance at OD_{600} was measured each hour and colony counts were carried out after 4 h. Trigger factor (TF) protein expressed by the pColdTF plasmid was used as the control. All the experiments were repeated three times.

RESULTS

Morphological Characterization of Phage swi2

A novel phage, swi2, targeting *E. coli* was isolated from a pig farm. The phage swi2 was observed under transmission electron microscopy (HT7700, Hitachi, Japan), which showed that it had a regular icosahedral head (80 nm in diameter) and an inextensible tail 140 nm in length (**Figure 1**). According to the current guidelines of the International Committee on Taxonomy of Viruses (ICTV), phage swi2 belongs to the family *Siphoviridae,* order *Caudovirales*.

Biological Characterization of Phage swi2

The *E. coli* 51 strain was selected as the host cell to test the biological characterization of phage swi2. Phage swi2, after propagation at an MOI of 10, showed a high titer of 1.01×10^{12} PFU/mL. Furthermore, the efficiency of plating (EOP) of swi2 was tested to confirm the extremely high titer, which showed a titer range from 1.7×10^{10} PFU/mL to 2.3×10^{13} PFU/mL in different host strains (**Table 1**). Quantitative fluorescent PCR was also used to test the phage swi2 titer, the results showed that the copy number of recombinant plasmid pColdTF-lysin1-SYBR was 6.15×10^{13} copies/mL and established the standard curve $y = -3.086x + 42.852$, then the titer of phage swi2 showed similar results (**Supplementary Figure 1**). In addition, phage swi2 tolerated UV light well (**Figure 2A**) and remained stable in the pH range of 6–10 (**Figure 2B**) and at a temperature less than 50°C for at least 1 h (**Figure 2C**). A one-step growth test showed that the latent period of swi2 was approximately 25 min, after which there was

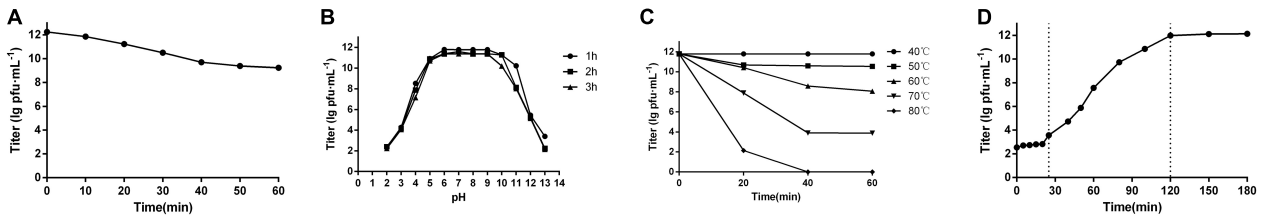

FIGURE 2 | Biological characteristics of phage swi2. **(A)** UV stability, **(B)** pH stability, **(C)** thermal stability, and **(D)** one-step growth curve. Data are expressed as the means. Phage swi2 showed good physical and chemical tolerance, and had a very high titer and burst size in *E. coli 51* with a short latent period.

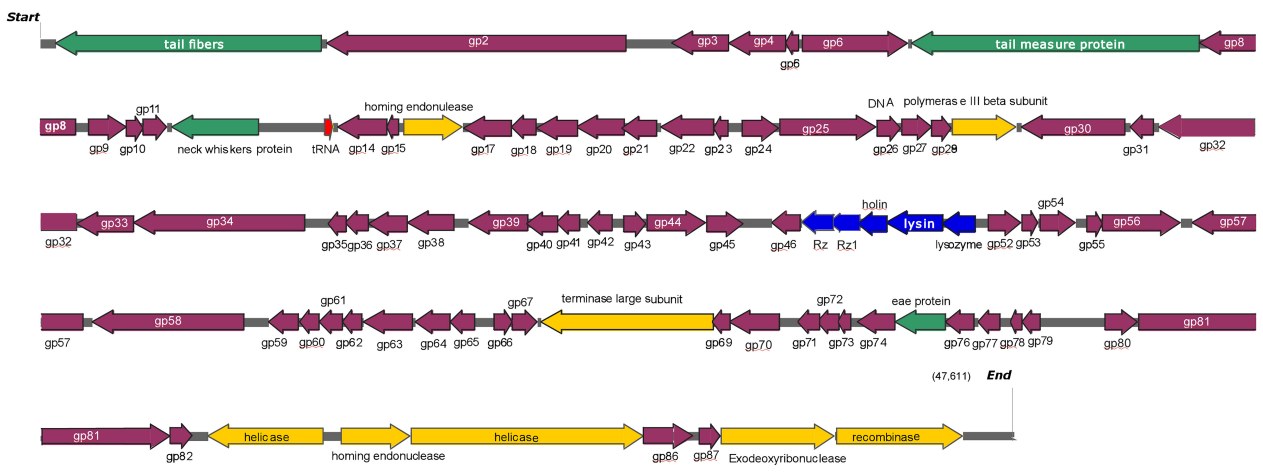

FIGURE 3 | Detailed phage swi2 genome annotation. The arrow represents the direction of transcription. Different colors represent orfs with different predictive functions. The structural proteins are represented in green, the cleavage-related proteins are represented in blue, the proteins associated with transcription are represented in yellow, tRNA is represented in red and the hypothetical proteins are represented in purple.

a rapid increase in the number of released viral particles until approximately 95 min, and the burst size was as high as 1,000 PFU/cell (**Figure 2D**).

Genomic Characterization of Phage swi2

The genome of phage swi2 was sequenced and analyzed. The phage swi2 genome contains 47,611 bp with a 46.50% G + C content. Eighty-nine *orfs* were predicted, 31 of which were positive-stranded, while the others were negative-stranded. Only 18 of 89 *orfs* were annotated as functional genes, including four structure-related genes, eight genes of transcription and replication, five lysis-related genes, and one $tRNA^{Met}$ gene. No virulence genes or drug resistance genes were found in the genome. Detailed phage swi2 genome annotation showed that the *orfs* related to transcription and replication were mainly concentrated in the downstream part of the whole genome, while the structurally related *orfs* were scattered throughout the whole genome sequence (**Figure 3**).

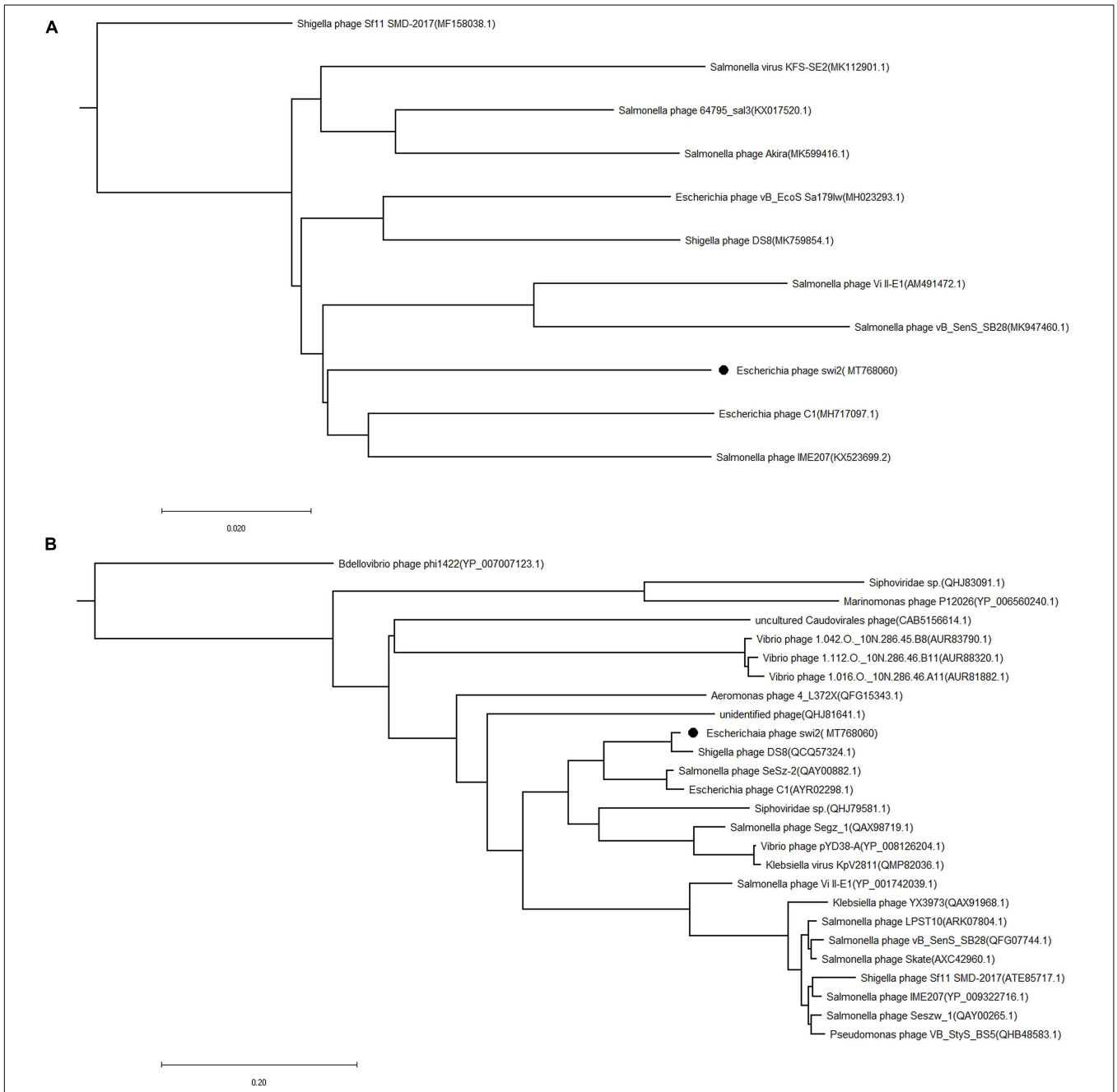

FIGURE 4 | Phylogenetic analysis of the phage swi2. The sequences of **(A)** the whole genome and **(B)** the terminase large subunit were compared in the NCBI GenBank database, and the phylogenetic tree was generated using the neighbor-joining method with default parameters in MEGA 7.0. • Represents phage swi2.

The lysis cassette of swi2 was composed of the genes holin (*orf 49*), lysin1 *(orf 50)*, lysin2 (*orf 51*), and *Rz/Rz1* equivalents (*orf 47* and *orf 48*). *Rz/Rz1* equivalents consist of a type II integral membrane protein and an outer membrane lipoprotein, which can destroy the outer membrane after lysin destroys the peptidoglycan of the host cell (Summer et al., 2007; Catalao et al., 2013; Young, 2014). In this study, phage swi2 employed two components spanning *Rz* and *Rz1* and might play a role in the final step of gram-negative host lysis. *Orf 49*, downstream of the *Rz/Rz1* equivalents, was predicted as the *holin* gene and had 96.2% amino acid sequence identity with that of *Salmonella phage Skate* as found in the GenBank database. Structural analysis showed that there were two transmembrane domains and belonged to the type II holin (data not shown).

Most phages lyse bacteria through the holin-lysin mechanism. Lysin, expressed at the late stage of the phage, is essential for the release of progeny phages. Based on the enzymatic activity, lysins can be classified into five types (Oliveira et al., 2014). Two *lysin* genes (*orf 50* and *orf 51*) were predicted in phage swi2, and their enzymatic activities were analyzed. Lysin1 has the activity of glycoside hydrolase, and lysin2 has the activity of muraminidase, both of which hydrolyze β-1, four glycosidic bonds in murein.

Generally, lysins for gram-positive bacteria are modular with an N-terminal catalytic domain (CD) and a C-terminal cell wall binding domain (CBD). However, phages infecting gram-negative bacteria express lysins that are, in general, single domain structures with a few exceptions (Young, 2014). In this study, a CD search was used to analyze the conserved domains of lysin1 and lysin2, and no CD or CBD domain was found (data not shown).

Phylogenetic and Genomic Analysis of Phage swi2

The phylogenetic tree of phage swi2 was constructed based on the genomic sequence and amino acid sequence of the terminase large subunit (encoded by *orf 68*). The homology comparison results showed that the terminase large subunit is highly conserved in phages, which means it was a good candidate to determine the homology relationship. Based on the terminase large subunit, 25 homologous phages were classified into two groups (**Figure 4B**). The phage swi2 had the highest homology with *Shigella phage DS8* (QCQ57324.1) and was the farthest from *Shigella phage Bdellovibrio phage phi1422* (YP_007007123.1) of the other group. All of the homologous phages had no classification in genera degree.

Compared with the terminase large subunit, the phylogenetic tree based on the whole genomic sequence of phage swi2 showed a significant difference. There was low homology between swi2 and the phages registered in the NCBI database. A total of 10 phages in the database had homology with swi2. The highest relationship with phage swi2 was *Escherichia* phage C1 (AYR02298.1), with only a 66% coverage rate and 92.51% identity, followed by *Salmonella* phage IME207 (YP_009322716.1), with a 53% coverage rate and 92.10% identity. Phage swi2 had the most remote relationship with *Shigella phage Sf11 SMD-2017* (ATE85717.1) (**Figure 4A**). Similarly, all phages were not classified to genera. Phages with ≥40% protein homologs were grouped into the same genus (Wittmann et al., 2015). Therefore, we suggest that phage swi2 and 10 homologous phages in the database should be classified into a new genus.

Expression and Antibacterial Activity of Lysis-Related Genes

Holin, *lysin1,* and *lysin2* were amplified by PCR to construct recombinant plasmids for expression in *E. coli* BL21. The expressed proteins were purified by affinity chromatography. SDS-PAGE results showed that the recombined proteins were all soluble and expressed in *E. coli* BL21 with masses of 61 kDa (holin), 69 kDa (lysin1), and 62 kDa (lysin2) (**Figure 5**). Holin had a low expression level and showed no antibacterial activity in both *in vitro* and *in vivo* tests ($P > 0.05$; **Figure 6**).

Lysin1 and lysin2 were also soluble when expressed in *E. coli* BL21. The activity measurement results *in vivo* showed that lysin1 or lysin2 expression in *E. coli* BL21 led to an -1 log titer reduction at 16 h and showed antibacterial activity ($0.01 < P < 0.05$). In an *in vitro* test, proteins lysin1 and lysin2 showed natural antibacterial activities against *E. coli* BL21 ($0.01 < P < 0.05$), and compared with the control group, lysin1 and lysin2 reduced the titer of *E. coli* BL21 by -1 log unit in 4 h (**Figure 7**). It has been reported that EDTA can penetrate the outer membrane of gram-negative bacteria to help lysins have better cleavage effects (Oliveira et al., 2014). In this study, the coeffect of lysin1 or lysin2 with EDTA was also tested. There was no significant difference between groups with or without EDTA. The results of the antibacterial activity assay showed that lysin1 and lysin2 of

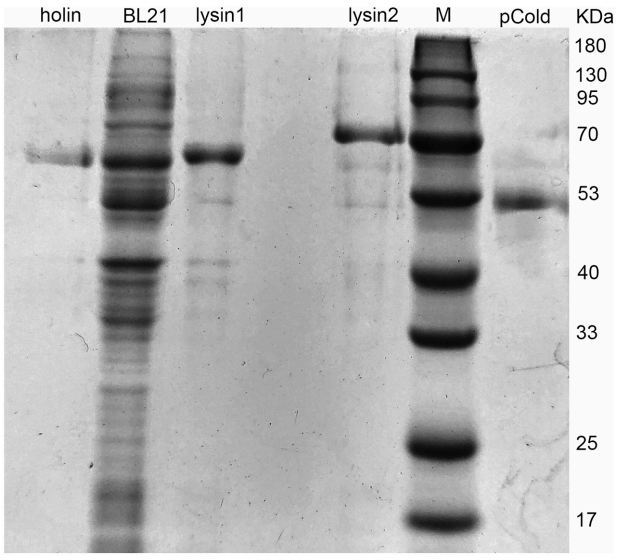

FIGURE 5 | Protein expression of holin, lysin1, and lysin2. *E. coli* BL21 harboring the recombinant plasmids (pColdTF-holin, pColdTF-lysin1, pColdTF-lyisn2) were induced with 1 mM IPTG at 16°C for 16 h. After ultrasonic purification, the expressed proteins in the supernatant were collected and detected by SDS-PAGE.

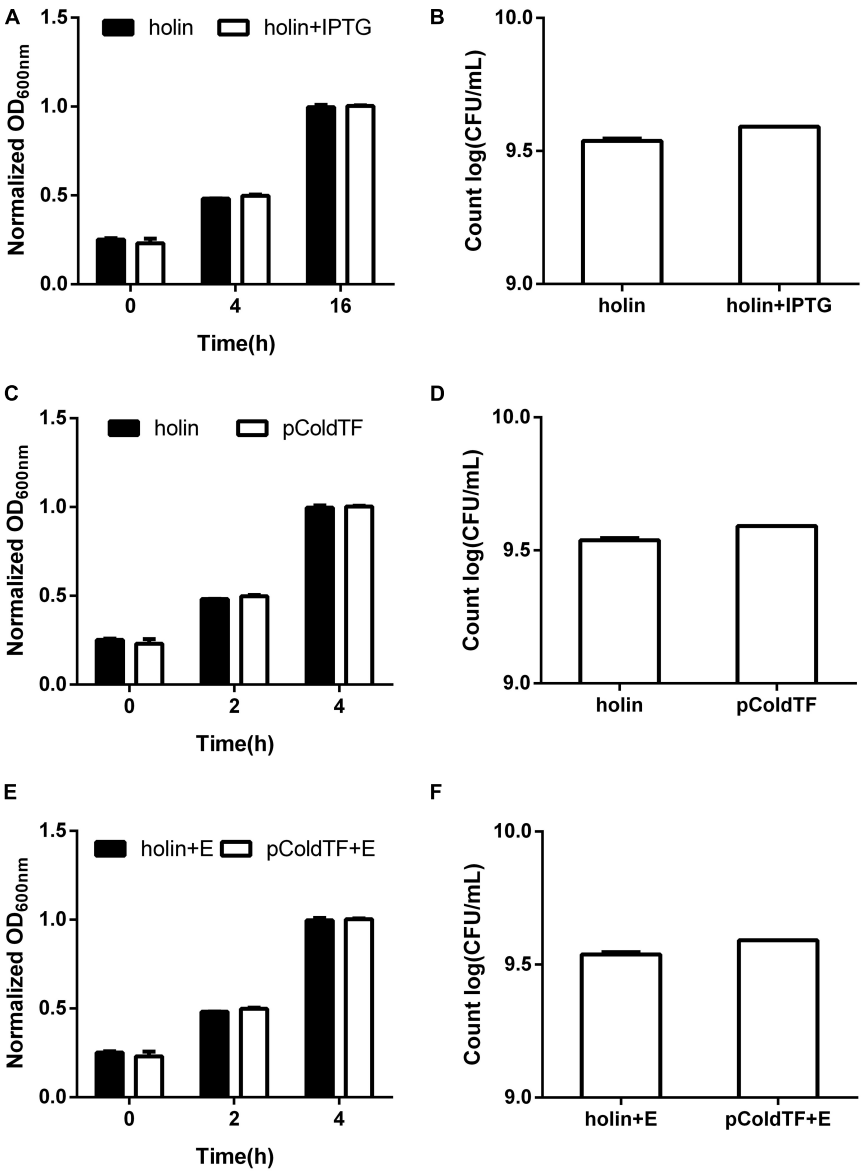

FIGURE 6 | Lytic activity assay of the holin protein. *E. coli* BL21 carrying the pColdTF-holin plasmid was cultured in LB at 16°C. **(A)** The turbidity was detected at 0, 4, and 16 h with or without IPTG inducement, and **(B)** colony counts were performed at 16 h. The antibacterial activities of holin against *E. coli* BL21 were tested *in vitro* for the **(C)** absorbance at OD_{600} within 4 h and **(D)** colony count at 4 h. Similarly, the antibacterial activity of holin with EDTA against *E. coli* BL21 was determined by the **(E)** absorbance at OD_{600} within 4 h and **(F)** colony count at 4 h. The pColdTF protein with the same concentration was used as a control. Holin showed no lytic activity in any of the tests ($P > 0.05$).

phage swi2 could naturally lyse gram-negative bacteria *in vitro* and *in vivo*.

DISCUSSION

Colibacillosis is an important infectious disease that endangers the world pig industry. Currently, the prevalence of drug-resistant bacteria makes *E. coli* infections difficult to control by antibiotics, and new alternatives are urgently needed to treat this crisis. Phages and their lysins showed great therapeutic potential due to their capacity to induce immediate lysis of the target bacterium with no effects on the normal flora structure (Sillankorva et al., 2011). In the last decade, there have been numerous reports of phages successfully preventing and treating pathogenic bacteria (Vieira et al., 2012; Zhang et al., 2013; Waters et al., 2017). In this study, a novel virulent enterophage, swi2, was isolated, and its genomic and biological characteristics were investigated.

Phage swi2 had good tolerance to physical and chemical factors, such as UV stability, pH stability, and temperature stability. The phage swi2 had a 10^{12} titer and 10^3 burst size

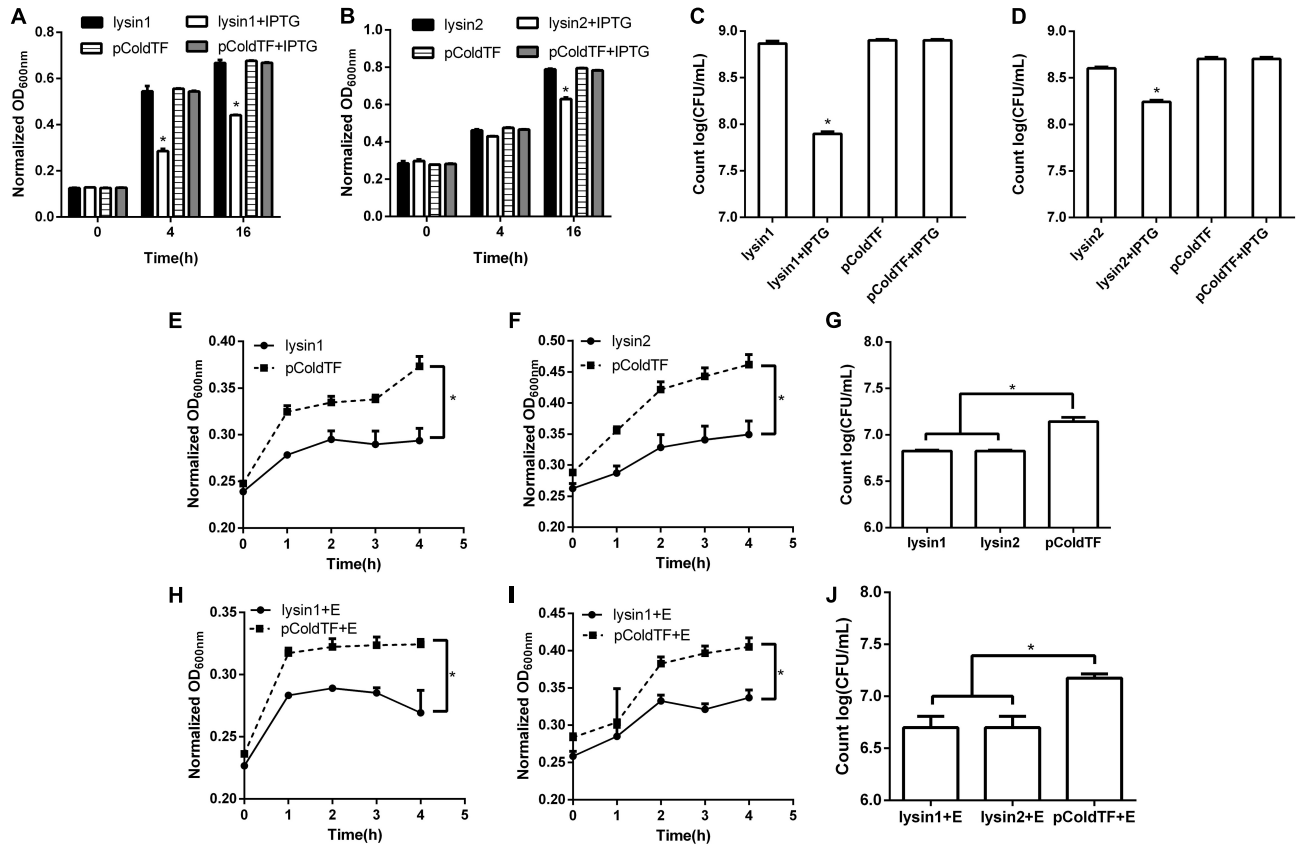

FIGURE 7 | Lytic activity assay of lysin1 and lysin2. *E. coli* BL21 carrying the pColdTF-lysin1 or pColdTF-lysin2 plasmid was cultured in LB and induced with IPTG at 16°C to express proteins. The turbidities of **(A)** lysin1 and **(B)** lysin2 were detected by absorbance at OD_{600} at 0, 4, and 16 h, and colony counts were performed for **(C)** lysin1 and **(D)** lysin2 at 16 h. Lysin1 and lysin2 reduced titers by -1 log unit at 16 h and showed natural antimicrobial activities ($0.01 < P < 0.05$). The antibacterial activities against *E. coli* BL21 tested *in vitro* for the **(E)** lysin1 and **(F)** lysin2 absorbance at OD_{600} within 4 h; also, **(G)** *E. coli* BL21 colonies were counted at 4 h. Similarly, the antibacterial activities of lysin1 and lysin2 with EDTA on *E. coli* BL21 *in vitro* were determined by **(H)** lysin1 and **(I)** lysin2 absorbance at OD_{600} within 4 h; also, **(J)** *E. coli* BL21 colonies were counted at 4 h. The pColdTF protein was used as a control. Lysin1 and lysin2 reduced the titer of *E. coli* BL21 by -1 log unit at 4 h with or without EDTA and showed natural antimicrobial activity ($0.01 < P < 0.05$).

in *E. coli* 51 with a short incubation period, which indicated good host infectivity and effective lytic activities. One phage had different titers and burst sizes in different hosts for the protein-synthesizing machinery of the host bacteria. To further confirm this result, we determined the titer of phage swi2 in all susceptible host bacteria with a spot test and quantitative fluorescent PCR. The EOP results showed that phage swi2 had a generally high titer in most host bacterial strains (10^{10}–10^{13} PFU). In general, the phage titer and burst size were associated with the incubation period and the proportion of protein synthesis machinery of the host cell (Choi et al., 2010). The larger the size of the host cell and the longer the incubation period of the phage tend to result in a larger burst size. For example, The phage SA has 30 min incubation period with 1,000 PFU/cell burst size; the phage MS2 has 45 min latent period with 2,000 PFU/cell burst size; the Avian-pathogenic *E. coli* phage has 24 h incubation period and 2.4×10^4 PFU/mL burst size (Horiuchi and Adelberg, 1965; Hamza et al., 2016; Fakhouri et al., 2019). In this study, phage swi2 has a short incubation period of 25 min with a high to 1,000 PFU/cell burst size, which indicates that swi2 has potential development value for clinical application.

The homological relationship of phage swi2 was analyzed based on the genome sequence and the amino acid sequence of the terminase large subunit. The terminase large subunit showed high conservation in the phylogenetic tree, which was consistent with previous reports (Daudén et al., 2013). However, the phylogenetic tree based on the genomic sequence of phage swi2 showed low homology with all 10 phages registered in the NCBI database. None of these phages were characterized or classified, which showed that swi2 is a new phage and is different from that of previous reports.

Phage swi2 was found to have one *holin* gene and two *lysin* genes, and it was speculated that phage swi2 lyses host bacteria through the holin-lysin system. However, lytic activity tests showed that holin had no lytic activity, while both lysins had intracellular and extracellular lytic activities. This showed that holin in phage swi2 was not essential in the process of phages lysing host bacteria, and multiple lysins can participate in the lysis process at the same time, which is consistent with

previous reports (Catalao et al., 2011). Additionally, *Rz/Rz1* equivalents may play a role in the process of releasing progeny, which could destroy the outer membrane after lysin destroys the peptidoglycan of the host cell. The plaque of phage swi2 is very small, which may also be related to the inactivated holin. Interestingly, two functional *lysin* genes were found in the phage swi2, and both lysozymes showed strong activity to naturally lyse gram-negative bacteria without EDTA. To date, there have been few reports of lysozymes with natural lytic activities on gram-negative bacteria, and most of them have a positively charged hydrophobic amino acid at the N-terminus (Vázquez et al., 2018; Wang et al., 2020). In this study, amino acid sequence analysis of lysin1 and lysin2 showed a similar character: there were hydrophobic and positively charged amino acids at the N-terminus (data not shown).

In conclusion, the novel virulent *Siphoviridae* phage swi2 isolated in this study produced a very high titer and burst size with a short incubation period, it had low homology with phages registered in the NCBI database, and its lysins could naturally lyse gram-negative bacteria. These results provide necessary information for the development of antibiotic alternatives for the treatment of multidrug-resistant *Escherichia coli* infection.

DATA AVAILABILITY STATEMENT

The datasets presented in this study can be found in online repositories. The names of the repository/repositories and accession number(s) can be found below: NCBI Genbank MT768059 and MT768060.

AUTHOR CONTRIBUTIONS

BS and XQ performed the experiments, analyzed the data, and wrote this manuscript. XW, HR, and WL performed the experiments. CZ designed the experiments and revised the manuscript. All authors contributed to the article and approved the submitted version.

FUNDING

This work was supported by the National Key R&D Program of China (2018YFD0501403) and the Shandong Key Research and Development Program (2019GNC106108).

SUPPLEMENTARY MATERIAL

The Supplementary Material for this article can be found online at: https://www.frontiersin.org/articles/10.3389/fmicb.2021.670799/full#supplementary-material

REFERENCES

Alemayehu, D., Casey, P. G., McAuliffe, O., Guinane, C. M., Martin, J. G., Shanahan, F., et al. (2012). Bacteriophages phiMR299-2 and phiNH-4 can eliminate *Pseudomonas aeruginosa* in the murine lung and on cystic fibrosis lung airway cells. *mBio* 3:e00029-12. doi: 10.1128/mBio.00029-12

Bao, E., Jiang, T., and Girke, T. (2014). AlignGraph: algorithm for secondary de novo genome assembly guided by closely related references. *Bioinformatics* 30, i319–i328. doi: 10.1093/bioinformatics/btu291

Catalao, M. J., Gil, F., Moniz-Pereira, J., Sao-Jose, C., and Pimentel, M. (2013). Diversity in bacterial lysis systems: bacteriophages show the way. *FEMS Microbiol. Rev.* 37, 554–571. doi: 10.1111/1574-6976.12006

Catalao, M. J., Milho, C., Gil, F., Moniz-Pereira, J., and Pimentel, M. (2011). A second endolysin gene is fully embedded in-frame with the lysA gene of mycobacteriophage Ms6. *PLoS One* 6:e20515. doi: 10.1371/journal.pone.0020515

Chen, L. K., Liu, Y. L., Hu, A., Chang, K. C., Lin, N. T., Lai, M. J., et al. (2013). Potential of bacteriophage ΦAB2 as an environmental biocontrol agent for the control of multidrug-resistant *Acinetobacter baumannii*. *BMC Microbiol.* 13:154. doi: 10.1186/1471-2180-13-154

Choi, C., Kuatsjah, E., Wu, E., and Yuan, S. (2010). The effect of cell size on the burst size of T4 bacteriophage infections of *Escherichia coli* B23. *J. Exp. Microbiol. Immunol.* 14, 85–91.

Daudén, M., Martiñ-Benito, J., Sánchez-Ferrero, J. C., Pulido-Cid, M., Valpuesta, J. M., and Carrascosa, J. L. (2013). Large terminase conformational change induced by connector binding in bacteriophage T7. *J. Biol. Chem.* 288, 16998–17007. doi: 10.1074/jbc.M112.448951

Fakhouri, H., Juneidi, O., Mohtaseb, H. A., Ishnaiwer, M., and Al-Razem, F. (2019). Isolation and Characterization of a Bacteriophage That Hosts on Avian-pathogenic *Escherichia coli* (APEC). *Int. J. Poult. Sci.* 18, 223–230. doi: 10.3923/ijps.2019.223.230

Guenther, S., Falgenhauer, L., Semmler, T., Imirzalioglu, C., Chakraborty, T., Roesler, U., et al. (2017). Environmental emission of multiresistant *Escherichia coli* carrying the colistin resistance gene mcr-1 from German swine farms. *J. Antimicrob. Chemother.* 72, 1289–1292. doi: 10.1093/jac/dkw585

Hamza, A., Perveen, S., Abbas, Z., and Ur Rehman, S. (2016). The lytic SA phage demonstrate bactericidal activity against mastitis causing *Staphylococcus aureus*. *Open Life Sci.* 11, 39–45. doi: 10.1515/biol-2016-0005

Horiuchi, K., and Adelberg, E. A. (1965). Growth of male-specific bacteriophage in *Proteus mirabilis* harboring F-Genotes derived from *Escherichia coli*. *J. Bacteriol.* 89, 1231–1236.

Jamal, M., Hussain, T., Das, C. R., and Andleeb, S. (2015). Characterization of Siphoviridae phage Z and studying its efficacy against multidrug-resistant *Klebsiella pneumoniae* planktonic cells and biofilm. *J. Med. Microbiol.* 64, 454–462. doi: 10.1099/jmm.0.000040

Kumar, S., Stecher, G., and Tamura, K. (2016). MEGA7 molecular evolutionary genetics analysis version 7.0 for bigger datasets. *Mol. Biol. Evol.* 33, 1870–1874. doi: 10.1093/molbev/msw054

Lai, W. C. B., Chen, X., Ho, M. K. Y., Xia, J., and Leung, S. S. Y. (2020). Bacteriophage-derived endolysins to target gram-negative bacteria. *Int. J. Pharm.* 589:119833. doi: 10.1016/j.ijpharm.2020.119833

Lee, D. S., Lee, S.-J., and Choe, H.-S. (2018). Community-acquired urinary tract infection by *Escherichia coli* in the era of antibiotic resistance. *Biomed. Res. Int.* 2018:7656752. doi: 10.1155/2018/7656752

Lowe, T. M., and Chan, P. P. (2016). tRNAscan-SE On-line integrating search and context for analysis of transfer RNA genes. *Nucleic Acids Res.* 44, W54–W57. doi: 10.1093/nar/gkw413

Oliveira, H., Thiagarajan, V., Walmagh, M., Sillankorva, S., Lavigne, R., Neves-Petersen, M. T., et al. (2014). A thermostable *Salmonella* Phage endolysin, Lys68, with broad bactericidal properties against gram-negative pathogens in presence of weak acids. *PLoS One* 9:e108376. doi: 10.1371/journal.pone.0108376

Park, M., Lee, J. H., Shin, H., Kim, M., Choi, J., Kang, D. H., et al. (2012). Characterization and comparative genomic analysis of a novel bacteriophage, SFP10, simultaneously inhibiting both *Salmonella enterica* and *Escherichia coli* O157:H7. *Appl. Environ. Microbiol.* 78, 58–69. doi: 10.1128/AEM.06231-11

Plotka, M., Kapusta, M., Dorawa, S., Kaczorowska, A. K., and Kaczorowski, T. (2019). Ts2631 endolysin from the extremophilic *Thermus scotoductus* bacteriophage vB Tsc2631 as an antimicrobial agent against gram-negative multidrug-resistant bacteria. *Viruses* 11:657. doi: 10.3390/v11070657

Sillankorva, S., Oliveira, D., Moura, A., Henriques, M., Faustino, A., Nicolau, A., et al. (2011). Efficacy of a broad host range lytic bacteriophage against *E. coli* adhered to urothelium. *Curr. Microbiol.* 62, 1128–1132. doi: 10.1007/s00284-010-9834-8

Summer, E. J., Berry, J., Tran, T. A., Niu, L., Struck, D. K., and Young, R. (2007). Rz/Rz1 lysis gene equivalents in phages of gram-negative hosts. *J. Mol. Biol.* 373, 1098–1112. doi: 10.1016/j.jmb.2007.08.045

Sun, J., Du, L., Li, X., Zhong, H., Ding, Y., Liu, Z., et al. (2019). Identification of the core bacteria in rectums of diarrheic and non-diarrheic piglets. *Sci. Rep.* 9:18675. doi: 10.1038/s41598-019-55328-y

Tran, T. H. T., Everaert, N., and Bindelle, J. (2018). Review on the effects of potential prebiotics on controlling intestinal enteropathogens *Salmonella* and *Escherichia coli* in pig production. *J. Anim. Physiol. Anim. Nut.* 102, 17–32. doi: 10.1111/jpn.12666

Vahedi, A., Soltan Dallal, M. M., Douraghi, M., Nikkhahi, F., Rajabi, Z., Yousefi, M., et al. (2018). Isolation and identification of specific bacteriophage against enteropathogenic *Escherichia coli* (EPEC) and in vitro and in vivo characterization of bacteriophage. *FEMS Microbiol. Lett.* 365:fny136. doi: 10.1093/femsle/fny136

Vázquez, R., García, E., and García, P. (2018). Phage lysins for fighting bacterial respiratory a new generation of antimicrobials. *Front. Immunol.* 9:2252. doi: 10.3389/fimmu.2018.02252

Vieira, A., Silva, Y. J., Cunha, A., Gomes, N. C., Ackermann, H. W., and Almeida, A. (2012). Phage therapy to control multidrug-resistant *Pseudomonas aeruginosa* skin infections: in vitro and ex vivo experiments. *Eur. J. Clin. Microbiol. Infect. Dis.* 31, 3241–3249. doi: 10.1007/s10096-012-1691-x

Wang, F., Ji, X., Li, Q., Zhang, G., Peng, J., Hai, J., et al. (2020). TSPphg Lysin from the extremophilic thermus bacteriophage TSP4 as a potential antimicrobial agent against both gram-negative and gram-positive pathogenic bacteria. *Viruses* 12:192. doi: 10.3390/v12020192

Waters, E. M., Neill, D. R., Kaman, B., Sahota, J. S., Clokie, M. R. J., Winstanley, C., et al. (2017). Phage therapy is highly effective against chronic lung infections with *Pseudomonas aeruginosa*. *Thorax.* 72, 666–667. doi: 10.1136/thoraxjnl-2016-209265

Wittmann, J., Klumpp, J., Moreno Switt, A. I., Yagubi, A., Ackermann, H. W., Wiedmann, M., et al. (2015). Taxonomic reassessment of N4-like viruses using comparative genomics and proteomics suggests a new subfamily–"Enquartavirinae". *Arch. Virol.* 160, 3053–3062. doi: 10.1007/s00705-015-2609-6

Yang, Z., Liu, X., Shi, Y., Yin, S., Shen, W., Chen, J., et al. (2019). Characterization and genome annotation of a newly detected bacteriophage infecting multidrug-resistant *Acinetobacter baumannii*. *Arch. Virol.* 164, 1527–1533. doi: 10.1007/s00705-019-04213-0

Young, R. (2013). Phage lysis: do we have the hole story yet? *Curr. Opin. Microbiol.* 16, 790–797. doi: 10.1016/j.mib.2013.08.008

Young, R. (2014). Phage lysis: three steps, three choices, one outcome. *J. Microbiol.* 52, 243–258. doi: 10.1007/s12275-014-4087-z

Zhang, C., Li, W., Liu, W., Zou, L., Yan, C., Lu, K., et al. (2013). T4-like phage Bp7, a potential antimicrobial agent for controlling drug-resistant *Escherichia coli* in chickens. *Appl. Environ. Microbiol.* 79, 5559–5565. doi: 10.1128/AEM.01505-13

Zhang, C., Wang, Y., Sun, H., and Ren, H. (2015). Multiple-site mutations of phage Bp7 endolysin improves its activities against target bacteria. *Virol. Sin.* 30, 386–395. doi: 10.1007/s12250-015-3618-z

Conflict of Interest: The authors declare that the research was conducted in the absence of any commercial or financial relationships that could be construed as a potential conflict of interest.

Copyright © 2021 Sui, Qi, Wang, Ren, Liu and Zhang. This is an open-access article distributed under the terms of the Creative Commons Attribution License (CC BY). The use, distribution or reproduction in other forums is permitted, provided the original author(s) and the copyright owner(s) are credited and that the original publication in this journal is cited, in accordance with accepted academic practice. No use, distribution or reproduction is permitted which does not comply with these terms.

frontiers in Microbiology

ORIGINAL RESEARCH
published: 02 June 2021
doi: 10.3389/fmicb.2021.692512

A Bacteriophage DNA Mimic Protein Employs a Non-specific Strategy to Inhibit the Bacterial RNA Polymerase

Zhihao Wang[1,2†], Hongliang Wang[3†], Nancy Mulvenna[2], Maximo Sanz-Hernandez[2], Peipei Zhang[1], Yanqing Li[1], Jia Ma[1], Yawen Wang[1], Steve Matthews[2], Sivaramesh Wigneshweraraj[2] and Bing Liu[1,4]**

[1] BioBank, The First Affiliated Hospital of Xi'an Jiaotong University, Xi'an, China, [2] MRC Centre for Molecular Bacteriology and Infection, Imperial College London, London, United Kingdom, [3] Department of Pathogen Biology and Immunology, School of Basic Medical Sciences, Xi'an Jiaotong University, Xi'an, China, [4] Instrument Analysis Centre of Xi'an Jiaotong University, Xi'an, China

DNA mimicry by proteins is a strategy that employed by some proteins to occupy the binding sites of the DNA-binding proteins and deny further access to these sites by DNA. Such proteins have been found in bacteriophage, eukaryotic virus, prokaryotic, and eukaryotic cells to imitate non-coding functions of DNA. Here, we report another phage protein Gp44 from bacteriophage SPO1 of *Bacillus subtilis*, employing mimicry as part of unusual strategy to inhibit host RNA polymerase. Consisting of three simple domains, Gp44 contains a DNA binding motif, a flexible DNA mimic domain and a random-coiled domain. Gp44 is able to anchor to host genome and interact bacterial RNA polymerase *via* the β and β′ subunit, resulting in bacterial growth inhibition. Our findings represent a non-specific strategy that SPO1 phage uses to target different bacterial transcription machinery regardless of the structural variations of RNA polymerases. This feature may have potential applications like generation of genetic engineered phages with Gp44 gene incorporated used in phage therapy to target a range of bacterial hosts.

Keywords: bacteriophage, RNA polymerase, DNA binding ability, intrinsic disordered protein, DNA mimic protein

OPEN ACCESS

Edited by:
Shuai Le,
Army Medical University, China

Reviewed by:
Lichun He,
Innovation Academy for Precision Measurement Science and Technology Chinese Academy of Sciences (CAS), China
Kaifeng Hu,
Chengdu University of Traditional Chinese Medicine, China

***Correspondence:**
Sivaramesh Wigneshweraraj
s.r.wig@imperial.ac.uk
Bing Liu
bliu2018@xjtu.edu.cn

† These authors have contributed equally to this work

Specialty section:
This article was submitted to Virology, a section of the journal Frontiers in Microbiology

Received: *08 April 2021*
Accepted: *30 April 2021*
Published: *02 June 2021*

Citation:
Wang Z, Wang H, Mulvenna N, Sanz-Hernandez M, Zhang P, Li Y, Ma J, Wang Y, Matthews S, Wigneshweraraj S and Liu B (2021) A Bacteriophage DNA Mimic Protein Employs a Non-specific Strategy to Inhibit the Bacterial RNA Polymerase. Front. Microbiol. 12:692512. doi: 10.3389/fmicb.2021.692512

INTRODUCTION

Bacteriophages, or bacterial viruses, have evolved distinct mechanisms to take over various host biological processes for effective reproduction. Phage enters the host *via* specific receptors on the surface of bacteria, which limits its host range (Koskella and Meaden, 2013). After entering the host, phage produces many proteins that interact with bacterial key enzymes to inhibit or modify related biological activities (Salmond and Fineran, 2015). RNA polymerase is the predominant target for the phage to utilize the bacterial transcription machinery in the early stage of invasion and to inhibit the host RNA polymerase activity in the later stages (Krupp, 1988). The majority of the bacterial transcription studies are carried out on *Escherichia coli*, and studies on prototypical lytic phage of T7 and T4 of Gram-negative model bacterium—*E. coli* and their RNA polymerase (RNAP) inhibitory proteins, Gp0.7, Gp2, and Gp5.7 (T7) and AsiA (T4) shed lights on how phages modulate

host RNAP activity (Lambert et al., 2004; Severinova and Severinov, 2006; Bae et al., 2013; Tabib-Salazar et al., 2017, 2018, 2019). Understanding the molecular mechanisms of phage antibacterial proteins and their interactions with RNAP has inspired research into new antibacterial compounds or treatments for Gram-negative bacteria (Sunderland et al., 2017).

Different from the core *E. coli* RNAP complex which consists of two α subunits and single β, β′, and ω subunits ($\alpha_2\beta\beta'\omega$), *Bacillus subtilis* has a $\alpha_2\beta\beta'\delta\omega_1\omega_2$ subunit composition (Wiedermannova et al., 2014). As a result, the study of Gram-positive bacterial phages has been lagging behind its counterpart for a long time and in need of revamp to stimulate the search for new antibacterial approaches (Pires et al., 2016). SPO1 is a lytic phage that infects *B. subtilis* (Stewart, 2018). A cluster of genes in the SPO1 genome, called the host takeover module, which are expressed early during the infection process, encode proteins associated with modulation and/or inhibition of bacterial processes for efficient takeover of the bacterial cell for the production of viral progeny (Stewart et al., 1998; Mulvenna et al., 2019; Zhang et al., 2019; Wang et al., 2020). The expression of SPO1 genes are temporally coordinated and products of host takeover genes *gp44*, *gp50*, and *gp51* have been previously reported to be essential for the transition from early to middle gene expression and complete shutoff of host DNA, RNA, and protein synthesis (Sampath and Stewart, 2004). The expression of recombinant Gp44, a 27 kDa negatively charged protein, in either *B. subtilis* or *E. coli*, results in inhibition of host DNA, RNA and protein synthesis and eventual demise of the bacterial cell (Wei and Stewart, 1993). As RNA synthesis was found to be most affected by expression of Gp44, Gp44 was considered to be an RNAP interacting protein. Moreover, the central region of Gp44 shows remarkable sequence resemblance to the RNAP binding region of σ^{54}—the nitrogen-limitation sigma factor (Tintut et al., 1994). Gp44 was reported to act as a competitor of the DNA interaction with the β subunit (Wei and Stewart, 1995). Gp44 is an also very acidic protein, therefore it is conceivable that it can adopt biophysical features of DNA to compete.

DNA mimicry by proteins is a strategy often used by viruses, prokaryotic and eukaryotic cells to inhibit or interfere with the activity of DNA interacting proteins (Bochkareva et al., 2005; Hegde et al., 2005; Wang et al., 2008). DNA mimic proteins (DMPs) often function by directly occupy the DNA binding cavity of the cognate substrate proteins to inhibit their DNA binding activity (Putnam and Tainer, 2005; Dryden, 2006; Dryden and Tock, 2006). For effective DNA mimicry, DMPs must display a conformation resembling DNA and have a localized negative charge distribution. While DNA also carries genetic information in all cellular forms of life and some viruses, DMP does not contain any genetic information. Furthermore, although DNA double helix structure has a degree of flexibility (Levitt, 1982), DMPs reported so far do not have DNA-like structural flexibility but rather rigid secondary or tertiary protein structure features (Tucker et al., 2014).

Here, we have used multidimensional nuclear magnetic resonance (NMR) spectroscopy and molecular dynamics to elucidate structural features of Gp44. It contains a DNA binding motif, a DNA mimic domain and a random-coiled domain—a combination never found in any known mimic proteins to our knowledge (Wang et al., 2014). And we proposed a new model in which Gp44 interacts with β and β′ subunit of RNAP to interfere with bacterial RNAP activity during SPO1 development.

MATERIALS AND METHODS

Protein Expression and Purification

SPO1 gene 44 and the truncated constructs were PCR amplified from SPO1 genomic DNA using pET EK/LIC primers for ligation independent cloning and cloned into pET-46 EK/LIC for adding N terminal His-tag and pDE2 vector for C-terminal His-tag or tag free constructs. Three Gp44 constructs: (1–55), (1–122), and full length (1–237) were made by nickel affinity purification from *E. coli* strain BL21(DE3). The culture of BL21(DE3) cells contains pET-46 Gp44 construct, was grown at 37°C to OD_{600} of ∼0.6 and induced by 1 μM of IPTG. The cells were left to continue growing at 37°C for 4 h before harvesting. The cell pellet was re-suspended in binding buffer (50 mM NaH_2PO_4, pH 8.0, 0.3 M NaCl, and 5 mM DTT) containing cocktail of protease inhibitors and lysed by sonication. The cleared cell lysate was loaded onto a His-Trap HP column (GE Healthcare Life Sciences), which was connected to AKTA pure chromatograph machine. The purified protein was eluted over a 50 ml gradient of 0–100% Elution buffer (Binding buffer + 1 M imidazole pH 8.0) according to manufacturer's instructions. The purified protein was dialyzed into storage buffer (50 mM NaH_2PO_4, pH 6.8, 250 mM NaCl, 1 mM DTT) and concentrated for NMR studies. Expression and purification of β and β′ subunits were using pDE1 vector and followed the same protocol described above. Expression and purification of recombinant *B. subtilis* RNA polymerase followed the protocol described by Yang and Lewis (2008).

Pull-Down Assays

For His-tag protein pull down assay, the Ni-NTA column was first equilibrated with five column volumes of lysis buffer (10 mM imidazole) then the His-tagged protein was applied into the column. The column was subsequently washed with five column volumes of lysis buffer before applying supernatant of *B. subtilis* (strain 168) cell lysate which was harvested at 0.8 of OD_{600}. The column was washed with 10 column volumes of lysis buffer before samples were eluted with 50 μl of Laemmli 2x concentrate SDS Sample Buffer. Samples were then boiled for 5 min prior to analysis by SDS-PAGE.

NMR Structure Determination

Nuclear magnetic resonance spectra were collected at 310K on Bruker DRX600 and DRX800 spectrometers equipped with cryo-probes. Spectral assignments were completed using our in-house, semi-automated assignment algorithms and standard triple-resonance assignment methodology. H_α and H_β assignments were obtained using HBHA (CBCACO)NH and the full side-chain assignments were extended using 3D HCCH-TOCSY and (H)CCH-TOCSY experiment. Three-dimensional ^{1}H-^{15}N/^{13}C NOESY-HSQC (mixing time 100 ms at 800 MHz) experiments

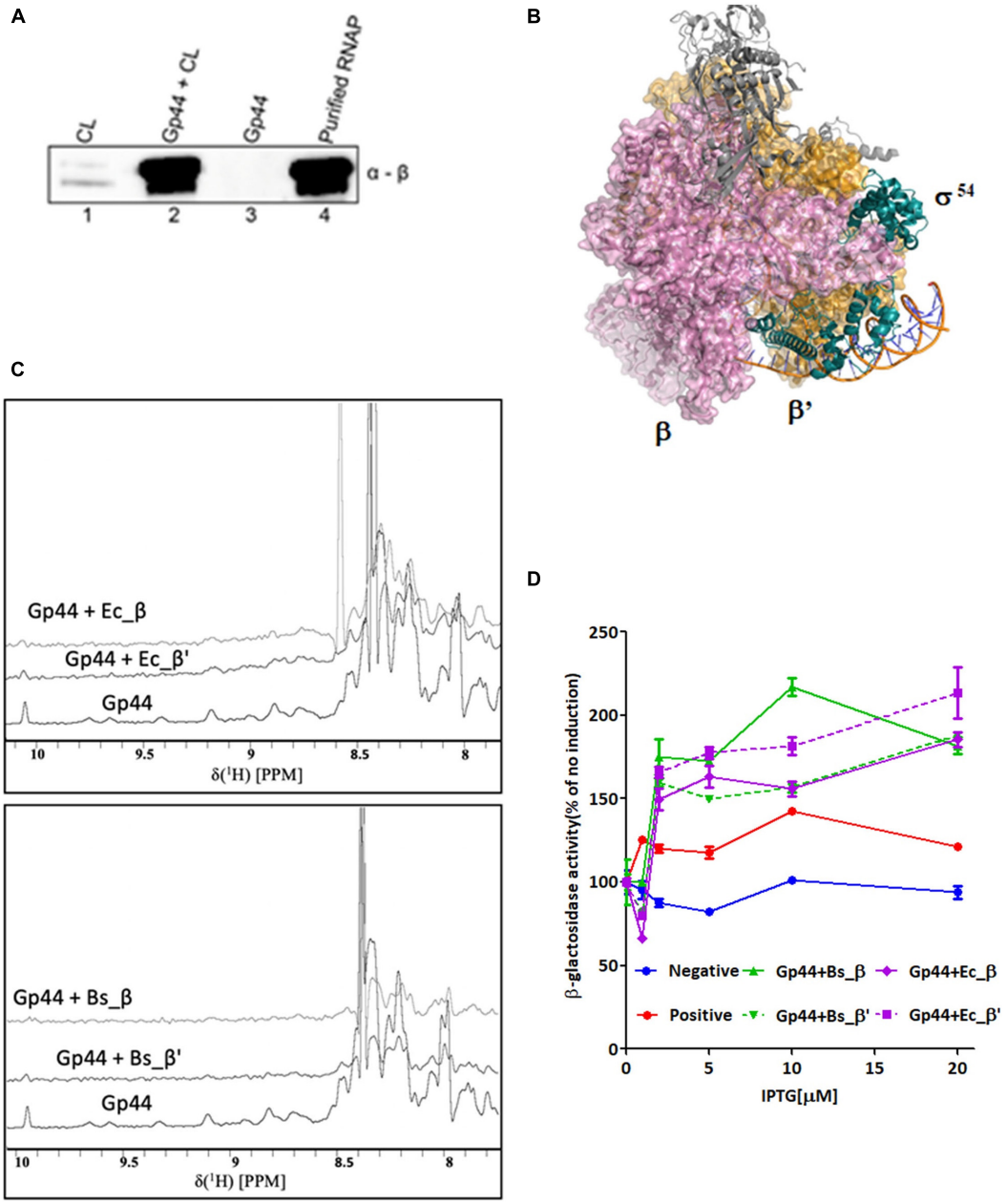

FIGURE 1 | Gp44 interacts with β and β′ subunits of *B. subtilis* and *E. coli* RNAP. **(A)** Images of SDS-PAGE gel (left panel) and immunoblotting with anti RNAP β subunit antibody (right panel) showing results of the pull-down assay with His-tagged Gp44 and whole-cell extracts (WCL) of *B. subtilis*. **(B)** Complex structure of RNAP-σ^{54} holoenzyme initial transcribing complex in which σ^{54} interacts with RNAP *via*β and β′ subunits (PDB ID: 6GFW. σ^{54}, β and β′ subunits are labeled respectively.) **(C)** ^{1}H NMR spectra showing peak broadening effect when adding β and β′ subunits of *B. subtilis* and *E. coli* to Gp44. **(D)** BTH assay shows Gp44 interacts with β and β′ subunits of *E. coli* and *B. subtilis*.

provided the distance restraints used in the final structure calculation. The ARIA protocol was used for completion of the NOE assignment and structure calculation. The frequency window tolerance for assigning NOEs was ±0.025 ppm and ±0.03 ppm for direct and indirect proton dimensions and ±0.6 ppm for both nitrogen and carbon dimensions. The ARIA parameters p, Tv, and Nv were set to default values. 110 dihedral angle restraints derived from TALOS were also implemented. The 10 lowest energy structures had no NOE violations greater than 0.5 Å and dihedral angle violations greater than 5°. The structural statistics are shown in **Supplementary Table 1**.

NMR Titration

One equivalent of β or β′ subunit of either *E. coli* or *B. subtilis* was added the unlabeled full length Gp44 to perform the 1D titration. Maximal twofolds of protein were added to Gp44 in

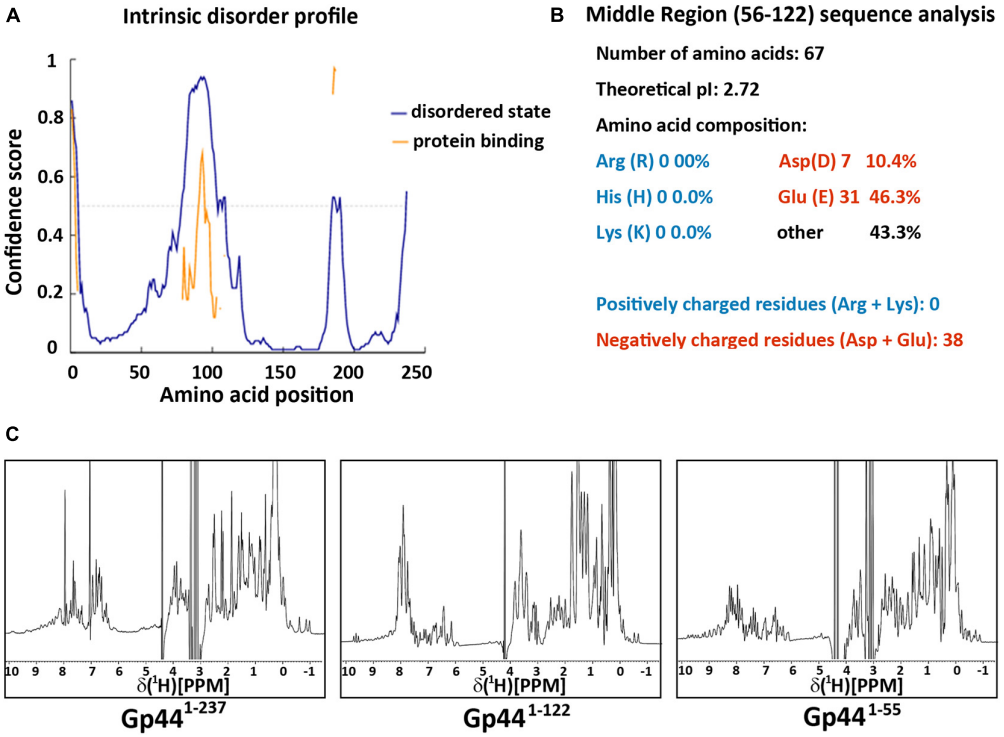

FIGURE 2 | Gp44 has three distinctive domains. **(A)** Intrinsic disorder profile predicted by DISOPRED. Blue line stands for the likelihood of protein in the natural disordered state and yellow line indicates the possibility of protein binding **(B)** Primary structure analysis of the middle disorder domain (56–122), including its ultra-low pI and extreme negative charged amino composition. **(C)** 1D ^{1}H spectra of three Gp44 constructs. From left to right: ($Gp44^{1-237}$), ($Gp44^{1-122}$), and ($Gp44^{1-55}$).

order to reach the end of the reaction. For the DNA titration, double stranded DNA fragments was added to ^{15}N labeled Gp44 constructs according to stoichiometric ratio to perform NMR titration. Maximal fivefold dsDNA was added to Gp44 in order to reach the end of the reaction.

ITC

Isothermal titration calorimetry (ITC) experiments were performed on a MicroCal PEAQ-ITC Instrument (Microcal) at 25°C using the dialysis buffer described above. β or β′ subunit 30 μM in the cell was titrated with 300 μM Gp44 in the syringe *via* 19 injections with 2 μL each at 120 s interval. The raw data were integrated, normalized for the molar concentration and analyzed using MicroCal PEAQ-ITC Analysis Software.

Bacterial Growth Attenuation Assays

Start cultures were grown at 37°C, shaking at 700 rpm. for 6–7 h in a plate incubator by directly inoculating a colony from a freshly transformed Luria agar plate into 200 μl of Luria broth (LB) medium containing 100 μg carbenicillin ml^{-1} into a 96-well microtiter plate (Corning). The start cultures were diluted 1:100 in a final volume of 200 μl of fresh LB medium containing 100 μg carbenicillin ml^{-1} and incubated at 30°C, shaking at 500 rpm. The expression of Gp44 constructs was induced at OD_{600} of ∼0.2–0.25 by adding 0.1 μm of isopropeyl-β-D-thiogalactoside (IPTG) for *E. coli* strains DH5α and ATCC35218. The experimental growth curves were also performed in 96-well microtiter plates in a Cytation3 multi-well plate reader (BioTek). At least three biological and technical replicates were performed for each growth curve.

Bacterial Two-Hybrid Assay

Bacterial two-hybrid assay was performed as previously described (Rao et al., 2009) with minor modifications. Briefly, GP44 (or mutant) and RNAP subunit were first subcloned into pAC and pRB constructs, respectively. KS1 reporter strains cells were then co-transformed with the indicated pAC and pBR derived plasmids and grown in LB containing 100 μg/ml carbenicillin, 35 μg/ml chloramphenicol and 50 μg/ml kanamycin. pAC and pRB empty vectors were used as negative control, while pAC-β flap and pRBL28 co-transformation were used as positive control. When the OD_{600} of the culture reached 0.3, cells were treated with indicated concentrations of isopropeyl-β-D-thiogalactoside (IPTG) for 1 h followed by 50 μM Fluorescein di-β-D-galactopyranoside (FDG) for another 1 h. β-galactosidase activity was assayed by measuring the fluorescence intensity of fluorescein with Cytation 3 plate reader equipped with 485 ± 20 nm excitation and 520 ± 25 nm emission filters.

Molecular Dynamics Simulation

Two homologous conserved fragments were extracted from $Gp44^{56-122}$ using RADAR (Li et al., 2015). The initial

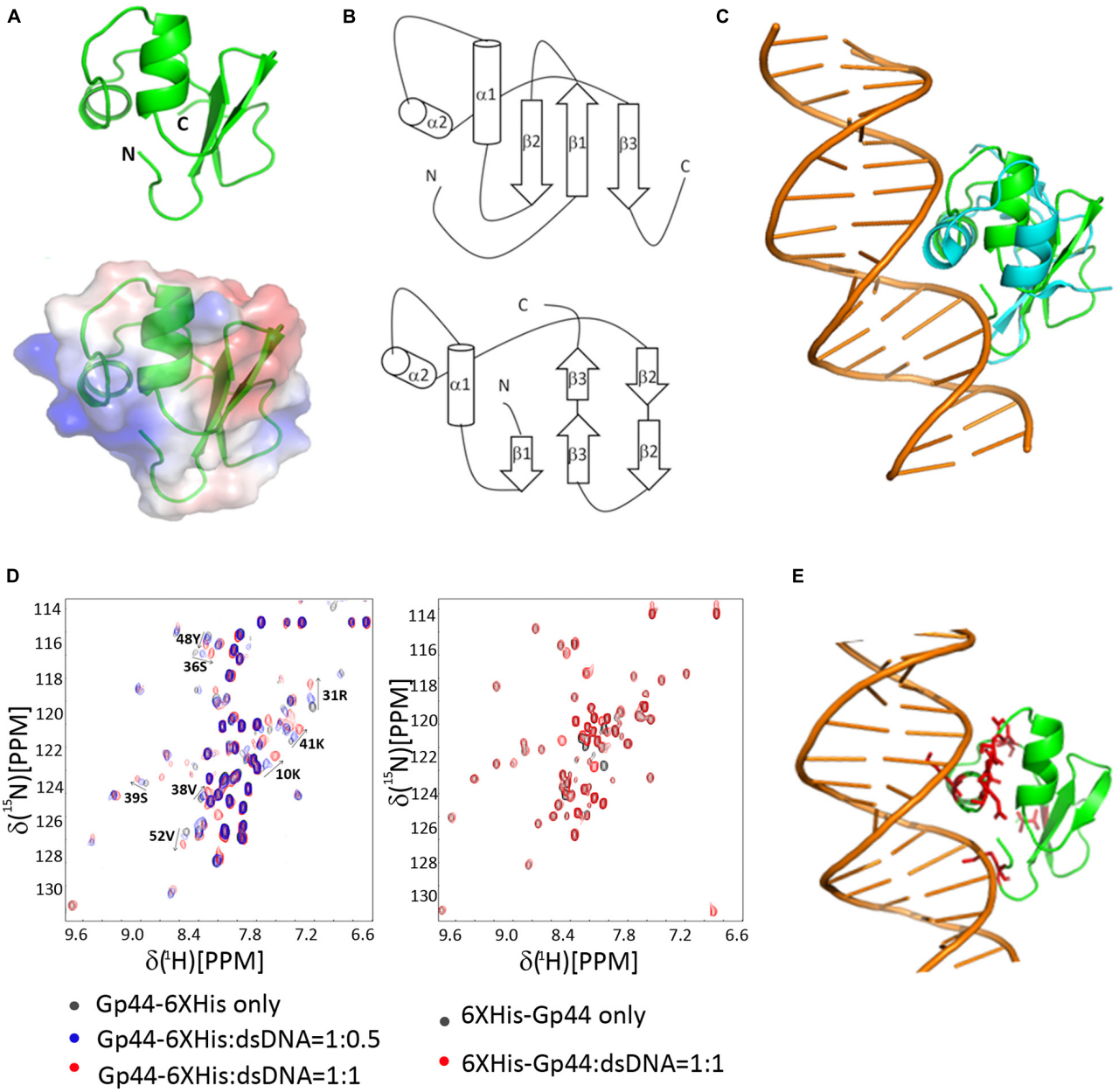

FIGURE 3 | NMR-derived three-dimensional structure of Gp44NT and DNA interaction **(A)** A cartoon representation of Gp44NT structure (top), and basic electrostatic surface distribution (bottom), calculated using the vacuum electrostatics program in Pymol, version 0.99rc6. Red represents residues with negatively charged sidechain and blue indicate positively charged amino acids. **(B)** Topologies of Gp44NT (top) and Xis (bottom). **(C)** Superimposed Gp44_NT (green) and Xis/DNA complex (cyan, PDB ID: 2OG0, DNA major and minor grooves included). **(D)** Left: Overlay of 2D ^{1}H–^{15}N HSQC spectra of Gp44NT-His with and without dsDNA. Black: no dsDNA; Blue: 0.5 equivalent of dsDNA added and Red: 1 equivalent of dsDNA added. Spectra recorded at pH 6.5, 298K. Right: Overlay of 2D ^{1}H–^{15}N HSQC spectra of His-Gp44$^{1-55}$ with and without dsDNA. Black: no dsDNA and Red: 1 equivalent of dsDNA added. Spectra recorded at pH 6.5, 298K. **(E)** A model of Gp44NT/dsDNA interaction created by using Xis/DNA complex structure (PDB ID: 2IEF). Peaks experience most chemical shift perturbation is highlighted in red.

disordered 3D structures of the fragments were obtained from I-TASSER, and the starting structures were chosen after energy minimization. The fragments were solvated with water, in cubic box and Na^{+} and Cl^{-} ions were added to balance the charges. An improved CHARMM36 force field which was optimized to simulate both ordered and disordered proteins (Huang et al., 2017) were employed to model the protein molecules. MD simulations were performed using GROMACS 4.6.7 molecular dynamic engine (Hess et al., 2008). The fragments were constrained, and their energy minimization were carried out, followed by the 1 ns equilibration at NVT and NPT ensembles at 300K and 1 bar, respectively. The fragments

were then simulated for 500 ns each, with protein snapshot saved every 500 ps (running parameters are summarized in **Supplementary Table 3**).

Protein Identification by Mass Spectroscopy

Identification was done locally at instrument analysis center. Samples were digested with trypsin and desalted by a C18 ZipTip. Peptides were analyzed by Q-Exactive plus mass spectrometer (Thermo Fisher Scientific) coupled with an UltiMate 3000 RSLCnano system. Database search were performed by MaxQuant.

RESULTS

Gp44 Interacts With β and β′ Subunits of Both *Escherichia coli* and *Bacillus subtilis* RNAP

To demonstrate Gp44 directly interacts with RNAP, we first expressed recombinant Gp44 fused with Histidine tag (His-tag) in *E. coli*. A pull-down assay using whole-cell extracts of exponentially growing *B. subtilis* cells expressing His-tagged Gp44 revealed a band around 120 kDa, which can be recognized by antibody against β subunit of *B. subtilis* RNAP and mass spectroscopy results confirmed that sample contains both β and β′ subunit (**Figure 1A**). To further localize the subunit(s) that Gp44 interacts with, we analyzed into the RNAP interacting region of σ^{54}, which interacts with both β and β′ subunits (**Figure 1B**) and postulated that Gp44 might target the β and β′ subunits. We thus used 1D ^{1}H NMR titration and a bacterial two-hybrid assay (BTH) to verify the hypothesis. In the NMR experiment, we successfully expressed and purified four recombinant subunits (β and β′ subunits of *E. coli* and *B. subtilis*) and titrated with Gp44 separately. After addition of any of the four subunits, all ^{1}H spectra of Gp44 demonstrated peak broadening effects, suggesting a productive interaction (**Figure 1C**). Furthermore, we used ITC to determine the binding affinities (**Supplementary Figure 1A**). The K_Ds for the two interactions were determined at 3.46 ± 0.27 μM for Gp44-β and 4.08 ± 0.31 μM for Gp44-β′, respectively. These values were consistent with the peak broadening observed in the NMR titration experiments as both fell into the intermediate NMR timescale. Meanwhile, BTH assay results confirmed the NMR results, showing increases of β-glactosidase activity after IPTG induction of Gp44 and RNAP subunit expression (**Figure 1D**).

While RNAP of *E. coli* has five subunits—$\alpha_2\beta\beta'\omega$, that of *B. subtilis* has seven subunits $\alpha_2\beta\beta'\delta\omega_1\omega_2$ representing Gram-positive bacteria (Weiss and Shaw, 2015). As Gp44 is able to interact with both RNAP subunits regardless of structural variations suggests the possible existence of a new RNAP inhibitory mechanism.

Domain Organization of Gp44

To understand the mechanism of Gp44 inhibition further, we employed various structural and biophysical tools for analysis. Despite its resemblance to σ^{54} in the central region (amino acids 56–122 of Gp44 to 44–113 of σ^{54}) (**Supplementary Figure 1B**), the overall amino acid sequence of Gp44 only shares similarity among *Bacillus* phages in BLAST analyses. No homologous structures have been deposited in Protein Data Bank (PDB) and 3D structural prediction servers failed to produce meaningful predictions. As there are clusters of continuous negatively charged amino acids in its sequence, it is conceivable that Gp44 may not form regular secondary structure due to electrostatic repulsion in these regions. To assess the intrinsic disorder in this region, we use DISOPRED server (Ward et al., 2004) to identify regions in Gp44 that have increased propensity to be disordered. As shown in **Figure 2A**, the middle of Gp44 ranging from residue 56–122 ($Gp44^{56-122}$) has a very high possibility of being disordered. Strikingly, this region consisted primarily of negatively charged amino acids where either aspartate or glutamate making up 57% of amino acids in this region (**Figure 2B**), which is more extreme than its counterpart in σ^{54} which carries 22% negatively charged amino acids. Notably, no positively charged amino acid residues (arginine, histidine, and lysine) were present in this region. Nevertheless, the percentage of charged amino acids in the rest of the sequence is also high in the rest of the sequence.

To identify the existence of any folded globular regions, we expressed and purified N-terminal histidine tagged (His-tagged) full length and truncated constructs of Gp44 and examined their foldedness by NMR. Dispersion in the ^{1}H NMR spectrum of full-length Gp44 revealed the clear presence of a folded domain as well as unstructured region (**Figure 2C**). The spectrum of a C-terminally truncated construct ($Gp44^{1-122}$) shows the folded domain is still present with only unstructured residues removed. After further removing central acidic region, the final construct ($Gp44^{1-55}$) is fully folded and feasible for NMR structure determination.

Our full length recombinant Gp44, either tag free or carboxy-terminal (CT) His-tagged, fully inhibits the growth of both *E. coli* and *B. subtilis* as reported by Wei et al., suggesting the recombinant protein used in our NMR experiments is its natural functional state. As the presence of a functional protein ensures the comprehensive structural study of Gp44 based on the initial NMR structural analysis, we are able to divide it into three distinctive domains—a folded NT domain, a negatively charged middle domain and an unstructured CT domain.

Amino Acid Residues 1–55 of Gp44 Interact With Double-Stranded DNA

We determined its solution structure of $Gp44^{1-55}$ using standard multidimensional NMR spectroscopy (PDB ID: 6L6V and BMRB ID: 36290). A notable feature in the solution structure of $Gp44^{1-55}$ is that surface-exposed positively and negatively charged residues are located on opposite sides of the protein (**Figure 3A**). This type of charge distribution, especially with the positively charged residues on an α helix (α2 in $Gp44^{1-55}$) resembles the charge distribution seen in a helix-turn-helix DNA binding motif. Indeed, a search for protein structure similarities using PDBefold (Krissinel and Henrick, 2005) revealed that the

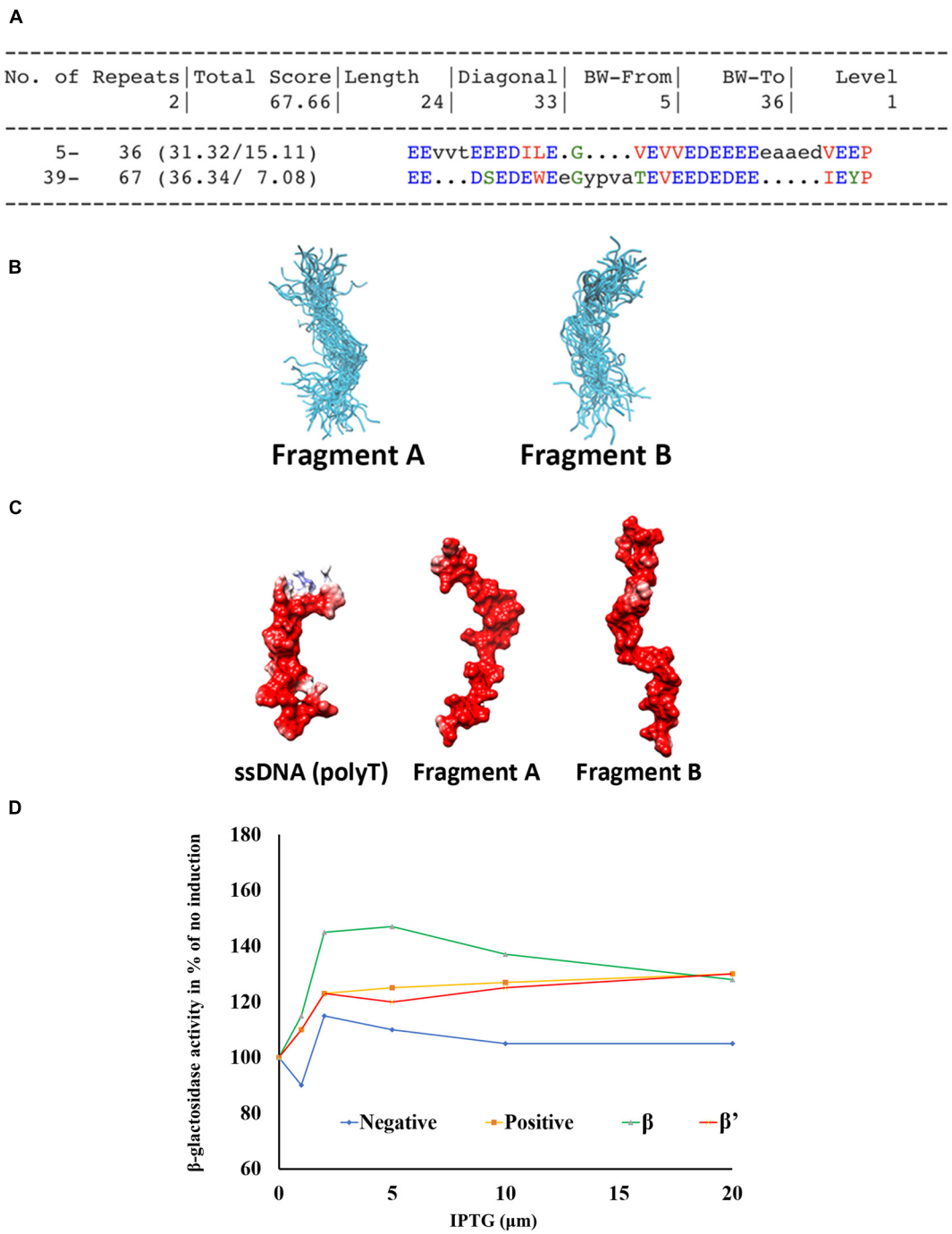

FIGURE 4 | Domain 56–122 of Gp44 mimics single strand DNA. **(A)** Two conserved repeats (Fragment A and B) of Gp44$^{56-122}$ were extracted using RADAR. **(B)** The cartoon representation of the ensembles of disordered conformations populated by fragments A and B during the simulation. **(C)** The negatively charged and highly flexible nature of fragment A and B is comparable to that of single-stranded DNA—poly-Thymidine (Left). **(D)** BTH assay shows Gp44$^{56-122}$ interacts with β and β′ subunits *of B. subtilis*.

overall structure of Gp44$^{1-55}$ exhibits a statistically significant similarity to an unusual DNA binding motif found in bacteriophage Lamda Xis protein—a DNA binding excisionase (Abbani et al., 2007). Xis adopts an unusual winged-helix structure in which two α helices are packed against two extended strands and similar positioning of α1 and α2 also found in Gp44$^{1-55}$ (**Figure 3B**). In Xis, the four-residue linker between the two-stranded anti-parallel beta-sheet is called the "wing" (**Figure 3B**). Although the wing is "missing" in Gp44$^{1-55}$, the N terminal region of Gp44$^{1-55}$ bends back to α2 forming a loop to

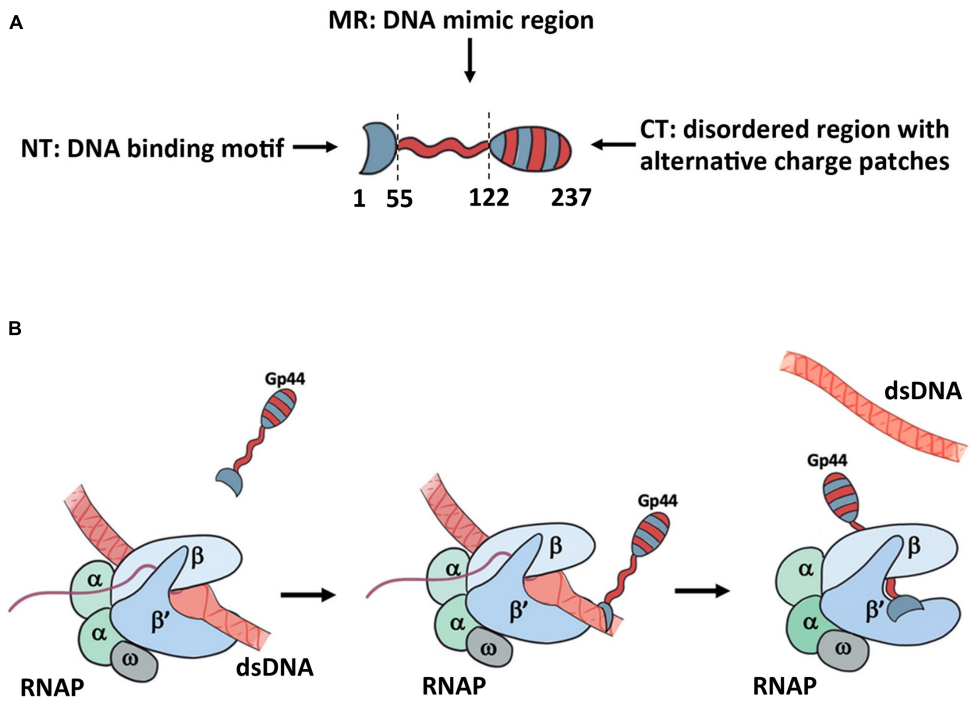

FIGURE 5 | Proposed model for the mechanism of action for Gp44. **(A)** the domain arrangement of Gp44 in cartoon. Red stands for negatively charged and blue stands for positively charged patch. **(B)** Proposed model for Gp44/DNA/RNAP interaction. While the exact mechanism of how Gp44 replaces DNA remains unclear, it could explain previous observations, including causing premature of mRNAs.

potentially mimic the Xis wing. When Xis interacts with DNA, α2 inserts into the major groove, while the wing contacts the adjacent minor groove and phosphodiester backbone. The overlay of Xis and $Gp44^{1-55}$ with DNA suggests that $Gp44^{1-55}$ could interact with DNA in a similar manner to Xis (**Figure 3C**).

To determine whether $Gp44^{1-55}$ can indeed interact with DNA, we performed NMR titration experiments with two different double-stranded DNA probes containing strong promoters recognized by the *E. coli* or *B. subtilis* RNAP (**Supplementary Table 2**). Results revealed that $Gp44^{1-55}$ binds double stranded DNA without displaying any preference for either DNA probe (**Figure 3D**). Overall, we conclude that the amino terminal region of Gp44 constitutes a DNA binding motif and build a Gp44NT/DNA complex model based on the published Xis/DNA complex structure and our NMR data (**Figure 3E**). Another interesting observation is that N-terminal (NT) His-tag block $Gp44^{1-55}$ interaction with dsDNA (**Figure 3D**), perhaps by occluding the positive charged patch on Gp44 and inhibiting the interaction. Consistent with this, NT His-tagged Gp44 does not inhibit bacterial growth, indicating DNA binding is crucial for the function of Gp44 (**Supplementary Figure 2**).

Domain 56–122 Mimics Single Strand DNA

As the central region of Gp44 is predicted as disordered with significant negative charge and the equivalent region in σ^{54} (44–113) is mostly undefined random coiled yet contacting both β and β′ in the crystal structure of σ^{54}-RNAP holoenzyme (Tabib-Salazar et al., 2019), we chose molecular dynamics to simulate this region to see is any interesting conformations are sampled and stable within the ensemble. First, we were able to extract two similarly conserved fragments from this region using RADAR (Li et al., 2015; **Figure 4A**) for use in simulations. These two fragments were simulated for 500 ns each under the updated CHARMM36 force field, optimized for both ordered and disordered proteins (Huang et al., 2017). The two fragments retain their random coil configuration throughout the simulations, not forming any secondary structure elements at any stage. The repulsion between sidechains of the highly charged segments prevents the formation of tertiary contacts. A representation of the ensembles of disordered conformations populated by fragments A and B during the simulations is shown in **Figure 4B**. The negatively charged and highly flexible nature of these fragments is comparable to that of single-stranded DNA (poly-thymidine) (**Figure 4C**), potentially suggesting that, in addition to DNA binding, DNA mimicry, is involved in the mode of action of Gp44. Flexibility is one of the interesting features for Gp44 as all previous reported DMPs do not have DNA-like flexibility due to rigid tertiary structure of proteins. Our attempts to express recombinant $Gp44^{55-122}$ to conduct *in vitro* assays also failed, but BTH assays showed that this region alone is able to interact with β and β' subunit of *B. subtilis* (**Figure 4D**). Interestingly, $Gp44^{1-122}$ still has inhibitory effects although not as potent as the full length Gp44 in the growth attenuation assays (**Supplementary Figure 2**). These observations suggest that the

construct with just a DNA binding motif which docks Gp44 on host genome and a DNA mimic region which binds to RNAP is capable of inhibiting host growth.

Gp44CT Is Required for Optimal RNAP Inhibition

Our 1D NMR analysis shows that the C-terminal region does not possess any folded domains. Compared to the full length Gp44 NMR spectrum, line widths of folded domain peaks at 0.5 ppm increases and the relative intensity of these peaks compared with unstructured peaks decreases for $Gp44^{1-122}$ despite being a shorter construct, suggesting the C-terminus may alleviate aggregation. This region possesses both positive and negative charges in mosaicking blocks, which may play a role in preventing self-tangling (Weiss and Shaw, 2015) keeping the DNA mimic domain accessible (**Figure 2C**). The inhibitory effect of Gp44ΔCT ($Gp44^{1-122}$) is also affected (**Supplementary Figure 2**), suggesting it is also required for optimal inhibition of the host transcription by this phage protein. Consistent with this, we observed less response of domain 56–122 compared to full length Gp44 in the BTH assay (**Figure 4D**), also indicating that C-terminal is required for its optimal function.

DISCUSSION

Gp44 has some interesting features. First, its NT DNA binding motif resembles the fold adopted by Lamda phage protein Xis, which is part of the excision complex essential for the excision of prophage from the host genome *via* site-specific recombination. $Gp44^{1-55}$ has a further simplified structure at DNA minor grove interactive part and perhaps as a consequence, it gives up any sequence specificity. Importantly, DNA binding is essential for the inhibitory effect on host cell growth, possibly because the DNA binding property increases the chance to encounter RNAP. The middle section $Gp44^{56-122}$ also has some unique features. It is extremely negatively charged, and it is likely that this region would be susceptible to be interacting with various nucleic acids binding protein in the bacterium. The DNA mimicry is provided by a flexible disordered domain that possesses the ability to adopt and resemble a single strand DNA-like conformation. Although the unstructured C-terminal domain remains largely uncharacterized, it is also essential for inhibition of the host transcription, possibly by preventing self-entanglement.

With a NT DNA binding motif, a DNA mimic domain and the CT putative self-protection domain, Gp44 has an unusual domain organization (**Figure 5A**). Our growth attenuation assays show that none of these domains is able to inhibit the host growth alone and removal of any domain from Gp44 abolishes or decrease its ability to kill the bacteria (**Figure 5A**). Thus, we proposed a model for mechanism of action on inhibition of host RNA synthesis by Gp44 inspired by σ^{54} (**Figure 5B**). In our model, Gp44 first docked to host dsDNA, waiting for the arrival of transcribing host RNAP. When RNAP contacts the Gp44 during the transcriptional elongation, Gp44 slips into the transcription bubble with its DNA mimic region interacting with β and β subunit. Once Gp44 occupied RNAP, its CT stops Gp44 slipping away and results in a lockdown on RNAP, causing mRNA premature as described in previous studies. Our proposed model is supported by the broad range bacterial inhibition capability. Potentially, Gp44 might work as the universal inhibitory for many if not all bacteria. With further optimization, it could be even incorporated into existing bacteriophages to enhance their anti-bacteria activity thus used in phage therapy.

DATA AVAILABILITY STATEMENT

The datasets presented in this study can be found in online repositories. The names of the repository/repositories and accession number(s) can be found below: http://www.wwpdb.org/, 6L6V.

AUTHOR CONTRIBUTIONS

SW and BL designed the research. BL, NM, ZW, HW, MS-H, JM, and YW performed the research. SW, SM, and BL wrote the manuscript. All authors contributed to the article and approved the submitted version.

FUNDING

This work was supported by the National Natural Science Foundation of China 81871662 (HW); Young Talent Award of Xi'an Jiaotong University (BL and HW); and Innovation Capability Support Program of Shaanxi (No.2018PT-28, 2017KTPT-04).

ACKNOWLEDGMENTS

We would like to thank High Performance Computer Cluster of the First Affiliated Hospital for structure calculation. We would also like to thank Jing Lin for the artwork in figures.

SUPPLEMENTARY MATERIAL

The Supplementary Material for this article can be found online at: https://www.frontiersin.org/articles/10.3389/fmicb.2021.692512/full#supplementary-material

REFERENCES

Abbani, M. A., Papagiannis, C. V., Sam, M. D., Cascio, D., Johnson, R. C., and Clubb, R. T. (2007). Structure of the cooperative Xis-DNA complex reveals a micronucleoprotein filament that regulates phage lambda intasome assembly. *Proc. Natl. Acad. Sci. U.S.A.* 104, 2109–2114. doi: 10.1073/pnas.0607820104

Bae, B., Davis, E., Brown, D., Campbell, E. A., Wigneshweraraj, S., and Darst, S. A. (2013). Phage T7 Gp2 inhibition of *Escherichia coli* RNA polymerase involves

misappropriation of sigma70 domain 1.1. *Proc. Natl. Acad. Sci. U.S.A.* 110, 19772–19777. doi: 10.1073/pnas.1314576110

Bochkareva, E., Kaustov, L., Ayed, A., Yi, G. S., Lu, Y., Pineda-Lucena, A., et al. (2005). Single-stranded DNA mimicry in the p53 transactivation domain interaction with replication protein A. *Proc. Natl. Acad. Sci. U.S.A.* 102, 15412–15417. doi: 10.1073/pnas.0504614102

Dryden, D. T. (2006). DNA mimicry by proteins and the control of enzymatic activity on DNA. *Trends Biotechnol.* 24, 378–382. doi: 10.1016/j.tibtech.2006.06.004

Dryden, D. T., and Tock, M. R. (2006). DNA mimicry by proteins. *Biochem. Soc. Trans.* 34, 317–319. doi: 10.1042/bst0340317

Hegde, S. S., Vetting, M. W., Roderick, S. L., Mitchenall, L. A., Maxwell, A. M., Takiff, H. E., et al. (2005). A fluoroquinolone resistance protein from mycobacterium tuberculosis that mimics DNA. *Abstr. Pap. Am. Chem. Sci.* 230, U538–U539.

Hess, B., Kutzner, C., van der Spoel, D., and Lindahl, E. (2008). GROMACS 4: algorithms for highly efficient, load-balanced, and scalable molecular simulation. *J. Chem. Theory Comput.* 4, 435–447. doi: 10.1021/ct700301q

Huang, J., Rauscher, S., Nawrocki, G., Ran, T., Feig, M., de Groot, B. L., et al. (2017). CHARMM36m: an improved force field for folded and intrinsically disordered proteins. *Nat. Methods* 14, 71–73. doi: 10.1038/nmeth.4067

Koskella, B., and Meaden, S. (2013). Understanding bacteriophage specificity in natural microbial communities. *Viruses* 5, 806–823. doi: 10.3390/v5030806

Krissinel, E., and Henrick, K. (2005). Multiple alignment of protein structures in three dimensions. *Lect. Notes Comput. Sci.* 3695, 67–78. doi: 10.1007/11560500_7

Krupp, G. (1988). RNA synthesis: strategies for the use of bacteriophage RNA polymerases. *Gene* 72, 75–89. doi: 10.1016/0378-1119(88)90129-1

Lambert, L. J., Wei, Y., Schirf, V., Demeler, B., and Werner, M. H. (2004). T4 AsiA blocks DNA recognition by remodeling sigma70 region 4. *EMBO J.* 23, 2952–2962. doi: 10.1038/sj.emboj.7600312

Levitt, M. (1982). Computer-simulation of DNA double-helix dynamics. *Cold Spring Harb. Symp.* 47, 251–262. doi: 10.1101/sqb.1983.047.01.030

Li, W., Cowley, A., Uludag, M., Gur, T., McWilliam, H., Squizzato, S., et al. (2015). The EMBL-EBI bioinformatics web and programmatic tools framework. *Nucleic Acids Res.* 43, W580–W584.

Mulvenna, N., Hantke, I., Burchell, L., Nicod, S., Bell, D., Turgay, K., et al. (2019). Xenogeneic modulation of the ClpCP protease of *Bacillus subtilis* by a phage-encoded adaptor-like protein. *J. Biol. Chem.* 294, 17501–17511. doi: 10.1074/jbc.ra119.010007

Pires, D. P., Cleto, S., Sillankorva, S., Azeredo, J., and Lu, T. K. (2016). Genetically engineered phages: a review of advances over the last decade. *Microbiol. Mol. Biol. Rev.* 80, 523–543. doi: 10.1128/mmbr.00069-15

Putnam, C. D., and Tainer, J. A. (2005). Protein mimicry of DNA and pathway regulation. *DNA Repair.* 4, 1410–1420. doi: 10.1016/j.dnarep.2005.08.007

Rao, X., Deighan, P., Hua, Z., Hu, X., Wang, J., Luo, M., et al. (2009). A regulator from *Chlamydia trachomatis* modulates the activity of RNA polymerase through direct interaction with the beta subunit and the primary sigma subunit. *Genes Dev.* 23, 1818–1829. doi: 10.1101/gad.1784009

Salmond, G. P., and Fineran, P. C. (2015). A century of the phage: past, present and future. *Nat. Rev. Microbiol.* 13, 777–786.

Sampath, A., and Stewart, C. R. (2004). Roles of genes 44, 50, and 51 in regulating gene expression and host takeover during infection of *Bacillus subtilis* by bacteriophage SPO1. *J. Bacteriol.* 186, 1785–1792. doi: 10.1128/jb.186.6.1785-1792.2004

Severinova, E., and Severinov, K. (2006). Localization of the *Escherichia coli* RNA polymerase beta' subunit residue phosphorylated by bacteriophage T7 kinase Gp0.7. *J. Bacteriol.* 188, 3470–3476. doi: 10.1128/jb.188.10.3470-3476.2006

Stewart, C. R. (2018). Analysis of host-takeover during SPO1 infection of *Bacillus subtilis*. *Methods Mol. Biol.* 1681, 31–39. doi: 10.1007/978-1-4939-7343-9_2

Stewart, C. R., Gaslightwala, I., Hinata, K., Krolikowski, K. A., Needleman, D. S., Peng, A. S., et al. (1998). Genes and regulatory sites of the "host-takeover module" in the terminal redundancy of *Bacillus subtilis* bacteriophage SPO1. *Virology* 246, 329–340. doi: 10.1006/viro.1998.9197

Sunderland, K. S., Yang, M., and Mao, C. (2017). Phage-enabled nanomedicine: from probes to therapeutics in precision medicine. *Angew. Chem. Int. Edn. Engl.* 56, 1964–1992. doi: 10.1002/anie.201606181

Tabib-Salazar, A., Liu, B., Barker, D., Burchell, L., Qimron, U., Matthews, S. J., et al. (2018). T7 phage factor required for managing RpoS in *Escherichia coli*. *Proc. Natl. Acad. Sci. U.S.A.* 115, E5353–E5362.

Tabib-Salazar, A., Liu, B., Shadrin, A., Burchell, L., Wang, Z., Wang, Z., et al. (2017). Full shut-off of *Escherichia coli* RNA-polymerase by T7 phage requires a small phage-encoded DNA-binding protein. *Nucleic Acids Res.* 45, 7697–7707. doi: 10.1093/nar/gkx370

Tabib-Salazar, A., Mulvenna, N., Severinov, K., Matthews, S. J., and Wigneshweraraj, S. (2019). Xenogeneic regulation of the bacterial transcription machinery. *J. Mol. Biol.* 431, 4078–4092. doi: 10.1016/j.jmb.2019.02.008

Tintut, Y., Wong, C., Jiang, Y., Hsieh, M., and Gralla, J. D. (1994). RNA polymerase binding using a strongly acidic hydrophobic-repeat region of sigma 54. *Proc. Natl. Acad. Sci. U.S.A.* 91, 2120–2124. doi: 10.1073/pnas.91.6.2120

Tucker, A. T., Bobay, B. G., Banse, A. V., Olson, A. L., Soderblom, E. J., Moseley, M. A., et al. (2014). A DNA mimic: the structure and mechanism of action for the anti-repressor protein AbbA. *J. Mol. Biol.* 426, 1911–1924. doi: 10.1016/j.jmb.2014.02.010

Wang, H. C., Ho, C. H., Hsu, K. C., Yang, J. M., and Wang, A. H. J. (2014). DNA mimic proteins: functions, structures, and bioinformatic analysis. *Biochemistry* 53, 2865–2874. doi: 10.1021/bi5002689

Wang, H. C., Wang, H. C., Ko, T. P., Lee, Y. M., Leu, J. H., Ho, C. H., et al. (2008). White spot syndrome virus protein ICP11: a histone-binding DNA mimic that disrupts nucleosome assembly. *Proc. Natl. Acad. Sci. U.S.A.* 105, 20758–20763. doi: 10.1073/pnas.0811233106

Wang, Z., Liang, Y., Liu, H., Wang, Y., Wang, H., and Liu, B. (2020). Resonance assignments of bacteriophage SPO1 Gp49 protein. *Biomol. NMR Assign.* 14, 111–114. doi: 10.1007/s12104-020-09929-8

Ward, J. J., McGuffin, L. J., Bryson, K., Buxton, B. F., and Jones, D. T. (2004). The DISOPRED server for the prediction of protein disorder. *Bioinformatics* 20, 2138–2139. doi: 10.1093/bioinformatics/bth195

Wei, P., and Stewart, C. R. (1993). A cytotoxic early gene of *Bacillus subtilis* bacteriophage SPO1. *J. Bacteriol.* 175, 7887–7900. doi: 10.1128/jb.175.24.7887-7900.1993

Wei, P., and Stewart, C. R. (1995). Genes that protect against the host-killing activity of the E3 Protein of *Bacillus-subtilis* Bacteriophage Spo1. *J. Bacteriol.* 177, 2933–2937. doi: 10.1128/jb.177.10.2933-2937.1995

Weiss, A., and Shaw, L. N. (2015). Small things considered: the small accessory subunits of RNA polymerase in Gram-positive bacteria. *FEMS Microbiol. Rev.* 39, 541–554. doi: 10.1093/femsre/fuv005

Wiedermannova, J., Sudzinova, P., Koval, T., Rabatinova, A., Sanderova, H., Ramaniuk, O., et al. (2014). Characterization of HelD, an interacting partner of RNA polymerase from *Bacillus subtilis*. *Nucleic Acids Res.* 42, 5151–5163. doi: 10.1093/nar/gku113

Yang, X., and Lewis, P. J. (2008). Overproduction and purification of recombinant *Bacillus subtilis* RNA polymerase. *Protein Expr. Purif.* 59, 86–93. doi: 10.1016/j.pep.2008.01.006

Zhang, P., Wang, Z., Zhao, S., Wang, Y., Matthews, S., and Liu, B. (2019). (1)H, (13)C and (15)N NMR assignments of *Bacillus subtilis* bacteriophage SPO1 protein Gp46. *Biomol. NMR Assign.* 13, 245–247. doi: 10.1007/s12104-019-09885-y

Conflict of Interest: The authors declare that the research was conducted in the absence of any commercial or financial relationships that could be construed as a potential conflict of interest.

Copyright © 2021 Wang, Wang, Mulvenna, Sanz-Hernandez, Zhang, Li, Ma, Wang, Matthews, Wigneshweraraj and Liu. This is an open-access article distributed under the terms of the Creative Commons Attribution License (CC BY). The use, distribution or reproduction in other forums is permitted, provided the original author(s) and the copyright owner(s) are credited and that the original publication in this journal is cited, in accordance with accepted academic practice. No use, distribution or reproduction is permitted which does not comply with these terms.

Advantages of publishing in Frontiers

OPEN ACCESS
Articles are free to read for greatest visibility and readership

FAST PUBLICATION
Around 90 days from submission to decision

HIGH QUALITY PEER-REVIEW
Rigorous, collaborative, and constructive peer-review

TRANSPARENT PEER-REVIEW
Editors and reviewers acknowledged by name on published articles

Frontiers
Avenue du Tribunal-Fédéral 34
1005 Lausanne | Switzerland

Visit us: www.frontiersin.org
Contact us: frontiersin.org/about/contact

REPRODUCIBILITY OF RESEARCH
Support open data and methods to enhance research reproducibility

DIGITAL PUBLISHING
Articles designed for optimal readership across devices

FOLLOW US
@frontiersin

IMPACT METRICS
Advanced article metrics track visibility across digital media

EXTENSIVE PROMOTION
Marketing and promotion of impactful research

LOOP RESEARCH NETWORK
Our network increases your article's readership